

## Cele mai relevante publicații pentru realizările profesionale



1. **Bogdan-Constantin Neagu**, Ovidiu Ivanov, Gheorghe Grigoras, Mihai Gavrilas, A New Vision on the Prosumers Energy Surplus Trading Considering Smart Peer-to-Peer Contracts. *Mathematics*, 2020, 8, 235. Accession Number: WOS:000519234000090 (Q1) IF 2.258.
2. **Bogdan-Constantin Neagu**, Ovidiu Ivanov, Gheorghe Grigoras, Mihai Gavrilas, Marcel Istrate, New Market Model with Social and Commercial Tiers for Improved Prosumer Trading in Microgrids. *Sustainability* 2020, 12, 7265, WOS:000584284700001. (Q2) IF 3.251.
3. Ovidiu Ivanov; **Bogdan-Constantin Neagu**; Gheorghe Grigoras; Scarlatache, Florina; Gavrilas, Mihai, A Metaheuristic Algorithm for Flexible Energy Storage Management in Residential Electricity Distribution Grids. *Mathematics* 2021, 9, 2375. WOS:000628360103201, (Q1) IF 2.258.
4. Jasim, Ali M., Basil H. Jasim, **Bogdan-Constantin Neagu**, and Bilal Naji Alhasnawi. "Efficient optimization algorithm-based demand-side management program for smart grid residential load." *Axioms* 12, no. 1 (2022): 33 WOS:000916714000001 (Q2) IF 2.000.
5. Gheorghe Grigoras, **Bogdan-Constantin Neagu**, An Advanced Decision Support Platform in Energy Management to Increase Energy Efficiency for Small and Medium Enterprises, *Applied Sciences*, 2020, 10, 3505. Accession Number: WOS:000541440000166, (Q2) IF 2.679
6. **Bogdan-Constantin Neagu**, Gheorghe Grigoras, and Florina Scarlatache. "Engineering Applications of Blockchain Based Crowdsourcing Concept in Active Distribution Grids." In *Smart Grid 3.0: Computational and Communication Technologies*, pp. 57-76. Cham: Springer International Publishing, 2023, 2021, ISBN: 978-3-030-62190-2.
7. Ovidiu Ivanov, **Bogdan-Constantin Neagu**, Gheorghe Grigoras, Mihai Gavrilas, *Optimal Capacitor Bank Allocation in Electricity Distribution Networks Using Metaheuristic Algorithms*. *Energies* 2019, 12, 4239, Accession Number: WOS:000504898500017
8. Gheorghe Grigoras, **Bogdan-Constantin Neagu**, Mihai Gavrilas, Ion Triștiu, Constantin Bulac, Optimal Phase Load Balancing in Low Voltage Distribution Networks using a Smart Meter Data-based Algorithm, *Mathematics*, 2020, 8, 549. Accession Number: WOS:000531824100089 (Q1) IF 2.258.
9. Banu, Ioan Viorel, Fadila Barkat, Marcel Istrate, Josep M. Guerrero, George Culea, Petru Livinti, Justina G. Motas, Bogdan Neagu, and Dragos Andrioaia. "Passive anti-Islanding protection for Three-Phase Grid-Connected photovoltaic power systems." *International Journal of Electrical Power & Energy Systems* 148 (2023): 108946. WOS:001009658800001 (Q1) IF 2.258.
10. Grigoraș, Gheorghe, Maria Simona Raboaca, Catalin Dumitrescu, Daniela Lucia Manea, Traian Candin Mihaltan, Violeta-Carolina Niculescu, and **Bogdan Constantin Neagu**. "Contributions to power grid system analysis based on clustering techniques." *Sensors* 23, no. 4 (2023): 1895, WOS:000942301200001 (Q2) IF 3.900.

Candidat conf. dr. ing. Bogdan-Constantin Neagu  
Data 25 septembrie 2023



Article

# A New Vision on the Prosumers Energy Surplus Trading Considering Smart Peer-to-Peer Contracts

Bogdan-Constantin Neagu , Ovidiu Ivanov, Gheorghe Grigoras  and Mihai Gavrilas

Department of Power Engineering; Gheorghe Asachi Technical University of Iasi, Iasi 705000, Romania; ovidiuivanov@tuiasi.ro (O.I.); mgavril@tuiasi.ro (M.G.)

\* Correspondence: bogdan.neagu@tuiasi.ro (B.-C.N.); ggrigor@tuiasi.ro (G.G.)

Received: 31 December 2019; Accepted: 9 February 2020; Published: 12 February 2020



**Abstract:** A growing number of households benefit from government subsidies to install renewable generation facilities such as PV panels, used to gain independence from the grid and provide cheap energy. In the Romanian electricity market, these prosumers can sell their generation surplus only at regulated prices, back to the grid. A way to increase the number of prosumers is to allow them to make higher profit by selling this surplus back into the local network. This would also be an advantage for the consumers, who could pay less for electricity exempt from network tariffs and benefit from lower prices resulting from the competition between prosumers. One way of enabling this type of trade is to use peer-to-peer contracts traded in local markets, run at microgrid ( $\mu$ G) level. This paper presents a new trading platform based on smart peer-to-peer (P2P) contracts for prosumers energy surplus trading in a real local microgrid. Several trading scenarios are proposed, which give the possibility to perform trading based on participants' locations, instantaneous active power demand, maximum daily energy demand, and the principle of first come first served implemented in an anonymous blockchain trading ledger. The developed scheme is tested on a low-voltage (LV) microgrid model to check its feasibility of deployment in a real network. A comparative analysis between the proposed scenarios, regarding traded quantities and financial benefits is performed.

**Keywords:** microgrids; prosumers; local trading; peer-to-peer contracts; blockchain technology

## 1. Introduction

In distribution systems, intelligent networks (known as 'smart grids') are implemented for encouraging energy savings and the integration of distributed generation sources, to help distribution utilities choose the optimal investment plans, achieve optimal operation of their systems, and to increase system efficiency. Other issues that need to be taken into consideration are the proliferation of prosumers and the creation of new consumer services. These research directions are in agreement with the European Union (EU) priorities, stated in the European Commission (EC) Communication published in 28 November 2018: renewable technologies, which must be the core of the new energy systems, smart grids, better energy efficiency, and low-carbon technologies. The fight against climate change is one of the five main topics of the EU extensive strategy for smart, sustainable and inclusive growth.

A microgrid can be defined as a LV network with loads, distributed energy resources (DER), and energy storage systems (ESS) connected to it, which can be operated in standalone or grid connected mode. The capacity of the DER considered in  $\mu$ G is in relatively small scale, but without universal agreement. It is mentioned as smaller than 100 kW by Huang et al. [1]. One of the main concepts in the active distribution network (ADN) is demand side management (DSM). Demand response (DR) as one of subcategories of DSM is defined by the EC as "voluntary changes by end-consumers of their usual electricity use patterns—in response to market signals". It is a shift of electricity usage in response to price signals or certain requests [2].

The existing energy management systems (EMS) available to operators will soon seem archaic with the increasing integration of small-scale renewable energy sources (SSRES), distributed generation (DG), ESS, electric vehicles, and DR programs. With the increased penetration of DER into the electricity distribution network (EDN), the power flow no longer remains unidirectional and power system control becomes increasingly complex. With their distributed control,  $\mu$ Gs provide a novel alternative and can help transform the existing burdened power system into a smart grid. As a first step towards these goals, in the EU, the implementation of smart metering systems is finished in some countries and is in various levels of development in others [3]. The spread of smart metering allows the creation of the  $\mu$ G energy markets (micro-markets:  $\mu$ M), which enable small-scale participants such as consumers (residential buildings) and prosumers (defined as consumers with excess of produced power) to locally exchange the energy surplus [4].

In addition to the metering functions, smart meters provide a wide range of applications: two-way communication between the smart meters mounted at consumer/prosumers sites and concentrators (management platforms or traders), secure data transmission between the participants, remotely controlled connections on the  $\mu$ Gs and specify the limitation of consumers/prosumers, and differentiated time-of-use tariffs [5]. The blockchain concept, as a rising technology, proposes new challenges for the  $\mu$ G based on the decentralized or community energy market, which ensures clear and favorable applications that allow consumers to be prosumers in a secured way [6]. The application of blockchain for  $\mu$ M has recently earned the consideration of the researchers worldwide.

Through bilateral prosumer-consumer contracts, consumers can obtain electricity at significantly lower price offers than from traditional suppliers. If a blockchain trading system is used, transactions are distributed and encrypted for data validation and local storage at the  $\mu$ G level. Each member of the network automatically verifies, confirms, and saves the authenticity of the transaction data. Furthermore, third-party trading agents are not needed, because the trading process is performed by participants, who become witnesses and guarantees for every transaction.

The massive implementation of active  $\mu$ Gs will be a critical challenge for electrical grids that will require new management and control strategies. Aggregators and  $\mu$ Gs, in a certain manner, may look similar because they were both introduced as aggregation element, which allows a coherent operation of a number of DERs, ESSs and flexible loads. In reality, there is a substantial difference between these two actors. In fact,  $\mu$ G perform the optimal management and control of resources based on geographical contiguity. On the contrary, this characteristic is not required in aggregators and the affiliated resources can be delocalized through the territory.

In Romania, by the provisions of Order 228 of 28 December 2018 proposed by ANRE (Regulation National Agency in Energy Domain) regarding prosumers, consumers who wish to trade the energy produced from renewable sources such as photovoltaic (PV), biomass, wind, cogeneration, etc. on the free market, and taking into account the current economic and technical context from the energy industry regarding the increase of investments in the small sources of distributed generation, it is expected that the need to develop new technological platforms for monitoring, management, and advanced analysis of the energy market will extend to the level of  $\mu$ G and of individual consumers, with the modernization of technical infrastructures and their transformation into smart  $\mu$ G.

According to the aforementioned regulations, the electricity suppliers bound by contracts with prosumers are required to buy the electricity at the weighted average day-ahead market price from the previous year. Thus, the prosumer can sell on the market its electricity generation surplus, while the advantage for the supplier is the exemption from the payment of the distribution network tariff. This trading system is the most basic, limiting the options of both parties, prosumers who want to sell and consumers who want to buy electricity at lower prices.

By not allowing prosumers to set custom selling prices, it does not account for differences in generation costs and installed capacity. The incentive of increasing local generation is not present. Consumers cannot buy electricity directly from the prosumers, and thus do not the freedom to choose specific prosumers for trading.

The aim of this paper is to provide an innovative electricity trading system implementing a new vision for local electricity trading between prosumers and consumers in  $\mu$ Gs. In electricity markets, trading is based usually on the minimum selling price principle. However, the electricity quantities traded in  $\mu$ Gs are much smaller, with narrower differences between selling prices. Thus, other criteria can become equally relevant, such as traded quantity or distance between seller and buyer. On the other hand, blockchain trading is based on the principle of first come, first served (FCFS), regardless of quantity and price. Based on these considerations, the prosumer electricity surplus trading (PEST) algorithm proposed in this paper offers several transaction priority scenarios, prosumer-driven and consumer-driven. In the prosumer-driven scenarios, the local generators with surplus to sell choose their trading parties (consumers), based on four principles: minimum distance, maximum instantaneous demand, maximum daily demand, and blockchain trading. In the consumer-driven scenario, consumers use the blockchain trading system to place buying offers, which are fulfilled by selling offers in the ascending order of prices. The term “smart” from the title coincide with the mode of transaction priority scenarios, where the peers sign according to its own advantage.

The remainder of the paper is structured as follows. Section 2 presents a literature review on the proposed problem highlighting the advantages of the proposed PEST methodology. Section 3 describes the proposed PEST algorithm for prosumer-consumer trading in  $\mu$ G. In Section 4, a case study is performed, with a comparison between the proposed trading strategies, outlining their particularities. The paper ends with Section 5 and references.

## 2. Literature Review

The latest trends in academic or industrial research describe several PEST solutions via P2P contracts with or without blockchain technologies. The P2P concept represents a process in which the prosumers trade energy in exchange for a deposit with the consumer [7]. Prosumers use P2P contracts for selling their generation surplus to local consumers, instead of selling it back to the grid.

In active distribution networks, the P2P trading process is structured as a four-layer architectural business model, from which three dimensions are used for secured energy exchange: bidding between prosumers and consumers for certain energy quantities through smart contracts, the selection of the offers to be fulfilled, energy delivery, and finally payment settling. In the aforementioned trading procedure, selling and buying offers are posted in a ledger secured by the blockchain technology. Offers are verified by the system administrator and accepted by parties by signing the P2P contracts. The energy demand can be met by any prosumer, and energy exchange in lieu of digital money takes place [8].

If a  $\mu$ M is established in the  $\mu$ G, small-scale prosumers and consumers have a market platform to trade energy generated locally within their community. In this way, energy losses are reduced, because the consumption of energy is in close proximity to the source. This helps to promote the sustainable and efficient utilization of local resources, because the market participants in a  $\mu$ M do not compulsorily need to be physically connected. Multiple energy producers, prosumers, and consumers can be added to form a local (or virtual) community and the control can be maintained through local (virtual)  $\mu$ Gs. Blockchain is a secure system for transactions, which also provides distributed applications to convey an understanding of each block and data on the system [9]. Even though in literature it exists an important number of research papers regarding the  $\mu$ M on the one hand and blockchain technology on the other hand, their aggregation is still lacking [10].

Several P2P transaction mechanisms are known from the literature as follows: based on transaction zoning in [11], based on total share of SSRES between neighbourhoods for energy bills saving in [7,12], and also on the provision of ancillary services and voltage regulation service [13]. P2P energy trading schemes are also proposed for local community or  $\mu$ G which already have implemented the blockchain technologies [14]. In [15], to secure the transactions of the PEST by P2P contracts, a specific blockchain technology is developed. Other authors propose double auction mechanism. The maximization of social welfare in the PEST can use auction-based mechanism [16,17]. The author from [18] uses an

optimum pricing scheme for local electricity trading in  $\mu$ Gs considering four particular priorities. In other words, the prosumers become the new actors in local electricity power market, considered as  $\mu$ M [19,20]. A different formulation of the PEST optimization follows a hierarchical framework considering the future energy price uncertainty in [21], information and communication technologies (ICT) in [22], and multi-layer architecture model in [23,24]. Paper [25] proposes a comprehensive analysis regarding the P2P communication architectures and highlights the performance of common protocols evaluated in accordance with IEEE 1547.3-2007.

In study [26], a P2P index optimization process was proposed. Here, a compromise regarding the balancing between the demand and generation in the LV network are identified. An incentive mechanism for PEST is presented in [27]. In the aforementioned paper, the authors consider three prices for prosumers profit maximization. Moreover, in [20,21,28], the authors proposed an evolutionary game theory-based approach for a dynamic modelling of the consumers (as buyers), in order to select the prosumers (as sellers). Thus, the evolutionary game theory was used for a dynamic modelling of the buyers for selecting sellers. The particular approach from [29] consider a Model Productive Control (MPC) method, for transactions only between two SSRES (prosumers), to avoid selling the surplus electricity production to classical traders or suppliers. This work considers the direct transactions without P2P contracts and blockchain technologies. Another category of the published papers regards the transactions of the PEST in the context of transactive energy in  $\mu$ Gs [30–32]. The authors in [33] the transactions consider different preference of prices.

To highlight the newness and the originality of our proposed approach, in Table 1, a brief description of the literature paper is presented, considering the five proposed trading objectives (four prosumer-driven and one consumer-driven) and the P2P contracts. The four prosumer-driven are S1: path of supply length, S2: instantaneous power demand, S3: daily energy consumption-based clustering, and S4: blockchain technologies. In addition, the consumer-driven scenario is S5—minimum price for consumers. It should be mentioned that many papers are the same with the References [7,11–18,20–23,25–33] presented in Table 1.

**Table 1.** A comparative state of the art between our method and the literature.

References	Path of Supply (S1)	Instantaneous Power Demand (S2)	Daily Energy Consumption (S3)	Blockchain Technologies (S4)	Minimum Price for Consumers (S5)	P2P Contracts
[7,17]	no	no	no	no	yes	yes
[11,12,25]	yes	no	no	no	no	yes
[13]	no	no	yes	yes	no	yes
[14,15]	no	no	yes	yes	yes	yes
[16,23]	yes	no	no	yes	no	yes
[18]	no	no	yes	no	no	no
[20,26]	no	no	yes	no	no	yes
[21,22,30]	no	no	no	no	yes	no
[27]	no	no	no	yes	yes	no
[28]	no	no	yes	no	yes	yes
[29]	no	yes	no	no	no	yes
[31]	no	yes	no	yes	no	no
[32,33]	no	no	no	no	yes	yes
Proposed approach	yes	yes	yes	yes	yes	yes

A previous work of the authors, in [34], proposes only at principle level a particular approach for prosumers energy trading in  $\mu$ Gs as an efficient P2P exchange based on the blockchain technology. Specifically, the algorithm solves a mathematical model for the latest challenges regarding both the ADN and the newest type of electricity market participants (prosumers) using virtual or crypto price as the transaction currency. In other words, this work emphasizes the capabilities and plausible benefits

of P2P contracts for energy trading in local  $\mu$ Gs from both prosumers and consumers perspectives. Taking into account that the Smart Meters are able to perform automatic energy transfer from the prosumers to the  $\mu$ G, the energy exchanged between the  $\mu$ Gs peers, the utilities will be reduced, through the minimization of active power losses. In the aforementioned context, the proposed algorithm implemented in the MATLAB environment is developed as a final energy market transaction platform for both the prosumers and traders.

### 3. A New Vision for Prosumer Energy Surplus Trading Algorithm

As described in the previous sections, an increasing number of consumers from LV EDN are using SSRES such as PV panels and wind turbines to gain energy independence by reducing the electricity need from the classic grid. This trend is driven by incentives provided by governments, such as subsidies for installing equipment or legislative provisions that allow them to sell the generation surplus back to the grid or to other consumers, thus becoming prosumers. The trading model that gives prosumers the ability to sell the surplus generation to the grid uses often-regulated tariffs, which results in low profits. The financial gain of the prosumers can increase if they get the possibility to sell energy to the consumers from their vicinity, at negotiated prices, via new trading tools, such as P2P contracts. Furthermore, to ensure equal access and transaction anonymity, the blockchain technology can be implemented to secure prosumer-consumer transactions.

The paper presents an algorithm for electricity transactions between prosumers and consumers belonging to the same local network or  $\mu$ G, using P2P contracts and, optionally, the blockchain technology.

In this section, prosumers and consumers' selection process, P2P pricing methodology, and the surplus trading mathematical model will be explained in detail.

The trading model implemented in the algorithm uses the following assumptions:

- Transactions are settled by the local non-profit  $\mu$ G manager or aggregator using the consumer or prosumer merit order derived from the priority mechanism agreed for trading and data from the metering system.
- The prosumer-consumer acquisition priority rules are the same for the entire  $\mu$ G.
- To be able to acquire electricity from a prosumer  $P_k$ , a consumer  $C_j$  must have previously signed a P2P contract that includes the bilateral trading agreement, price, and other supplemental information, such as trading priority.
- By default, any prosumer and prosumers in the  $\mu$ G have signed bilateral P2P trading contracts. In other words, any prosumer who has a generation surplus can theoretically sell electricity to any consumer in the microgrid. This setting is changeable to exclude any consumer from the trading process.
- When a consumer is awarded a P2P contract, the power supplied by the prosumer will try to match the entire load of the consumer, within the limit of the available surplus, as in Equation (1). This setting is changeable to allow specified quantity requirements for each consumer.

$$P_{trade,k,j,h} = \begin{cases} P_{j,h}, & \text{if } P_{surplus,k,h} \geq P_{j,h} \\ P_{surplus,k,h}, & \text{otherwise} \end{cases} \quad (1)$$

where  $P_{trade,k,j,h}$  is the power traded at hour  $h$  ( $h = 1, \dots, nh$ ), to consumer  $j$  ( $j = 1, \dots, nc$ ) by prosumer  $k$  ( $k = 1, \dots, np$ );  $P_{j,h}$  is the own consumption of prosumer  $k$  at hour  $h$ , and  $P_{surplus,k,h}$  is the power surplus at hour  $h$  of the prosumer  $k$ .

- The selling price of a prosumer is considered fixed for all trading intervals of a day. This assumption is made because only PV panels are used at this point as generation sources, and no storage capabilities are present in the  $\mu$ G. Thus, the local generation does not cover evening peak load or low consumption night hours, which would favor the application of differentiated tariffs.

- The consumers in the network are generally one-phase, supplied through a four-wire three-phase network. Prosumers are supplying their surplus generation in the  $\mu\text{G}$  using a three-phase balanced connection point, as required by technical regulations for LV distribution systems [35].
- When transactions take place between certain prosumers and consumers, the prosumers will deliver and the consumer will receive electricity from the same grid.
- If the surplus exceeds the local demand traded via P2P contracts, the  $\mu\text{G}$  market administrator will sell the untraded electricity back to the grid, at regulated tariffs.

The main input data needed by the algorithm refers to the consumption and local generation available in the  $\mu\text{G}$ . For this, two matrices are provided: matrix  $C = C(h, j) \in \mathbb{R}^{nh \times nc}$  for consumptions and matrix  $G = G(h, k) \in \mathbb{R}^{nh \times np}$  for generation. Generation will be available for prosumers for which, at the same hour  $h$  and prosumer  $k$ ,  $G(h, k) > C(h, k)$ , and the surplus available for trading follows as:

$$S(h, k) = G(h, k) - C(h, k) \tag{22}$$

computed into a matrix  $S = S(h, k) \in \mathbb{R}^{nh \times np}$ .

Also, for prosumers, the daily selling price is provided as a matrix  $PR = PR(h, k) \in \mathbb{R}^{nh \times np}$ , where any element  $PR(h, k)$  represents the selling price for a generic prosumer  $k$  at hour  $h$ .

This surplus will be sold to local consumers if P2P contracts exist, or to the grid. The local transactions are governed by a priority of supply mechanism agreed at the  $\mu\text{G}$  level, which describes the order in which any consumer  $C_j$  can acquire electricity from any prosumer  $P_k$ . In the algorithm, the complete list of priorities is encoded in a matrix  $M_x = M_x(k, j) \in \mathbb{Z}^{np \times nc}$ . A generic element  $M_x(k, j)$  denotes the merit order of consumer  $j$  in the priority list of prosumer  $k$ , for the trading scenario  $x$ .

The trading algorithm proposed in the paper offers improved flexibility by considering two trading paradigms: consumer-driven, where the minimum price for consumers is sought, as in any traditional electricity market, and prosumer-driven, where the aim is to incentivize prosumer offers.

In the prosumer-driven scenarios, trading is performed to prioritize the selling of the generation surplus to consumers. The prosumer selling price is not considered, and the selling offers are fulfilled using the FCFS principle [34]. When trading is consumer-driven, the fulfillment of the consumer needs is sought first, and the prosumers with the lowest selling prices are prioritized for trading, as shown in Figure 1.

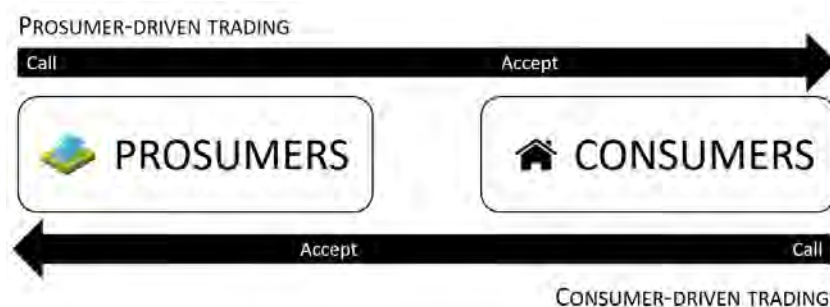


Figure 1. Trading scenarios used in the algorithm.

Five scenarios for assigning consumer priorities for P2P trading are available:

- Prosumer-driven
  - Scenario 1: Path of supply length
  - Scenario 2: Instantaneous power demand
  - Scenario 3: Daily energy consumption-based clustering
  - Scenario 4: Blockchain offers
- Consumer-driven:
  - Scenario 5: Minimum price for consumers

In each scenario, when the primary priorities are equal, a second dissociation criterion is applied. A description of these scenarios follows.

### 3.1. Trading Priority Based on the Length of the Supply Path—Scenario 1 (Prosumer-Driven)

- Consumer-driven:
  - Scenario 5: Minimum price for consumers

In each scenario, when the primary priorities are equal, a second dissociation criterion is applied. A description of these scenarios follows.

3.1. Trading Priority Based on the Length of the Supply Path—Scenario 1 (Prosumer-Driven)

If this criterion is used, the prosumers will sell their electricity surplus to consumers using as ranking criterion the minimal network length between the generation and consumption locations. The consumer(s) with minimal network length from a given prosumer will be awarded first its available surplus, followed by other consumers in the ascending order of the connection distance. If two consumers are located at equal network lengths from a prosumer, the one with the higher power request will be preferred:

$$\text{Priority level 1 } \min(L_{j,k}) \text{ Priority level 2 } \max(P_{h,j}) \tag{3}$$

This prioritization approach is modelling the true load flows occurring in an EDN, where the energy generated locally would predominantly supply the consumptions located at the closest locations, following the shortest path. Thus, the consumers most likely to physically receive the surplus are preferred for trading in this case.

3.2. Trading Priority Based on Consumer Hourly Demand—Scenario 2 (Prosumer-Driven)

In this scenario, the prosumers will sell their electricity surplus to consumers ranked in descending order of their trading offer or instantaneous consumption measured in the trading hour. If two consumers have equal power trading requirements at the same time, the one located closer to the seller prosumer will be preferred:

$$\text{Priority level 1 } \max(P_{h,j}) \text{ Priority level 2 } \min(L_{j,k}) \tag{4}$$

This prioritization is favoring for trading the consumers with the highest instantaneous demand, reducing the number of contracts fulfilled simultaneously by one prosumer. The use of this prioritization procedure minimizes the number of financial settlements required in each trading interval and in a day. In most cases, if a consumer is accepted for trading, its financial saving resulting from the lower electricity prices offered by prosumers, compared with standard regulated prices, is maximized. Larger profits can act as an incentive for consumers with high demand to be involved in the retail electricity market operated at microgrid level.

3.3. Trading Priority Based on Consumer Daily Demand—Scenario 3

In this scenario, the trading priority considers the total electricity demand of the consumers over 24 h. The consumers prioritized for receiving the prosumers’ surplus will be those with the highest daily demand. For this purpose, the Ward hierarchical clustering method was applied.

The Ward method is an agglomerative hierarchical method that first assigns each observation to its own cluster and then groups adjacent clusters so that minimum variance within a cluster is obtained. The distance between two clusters *a* and *b* is computed with:

$$d_{ab} = \frac{\|\bar{c}_a - \bar{c}_b\|^2}{\frac{1}{n_a} + \frac{1}{n_b}} \tag{5}$$

where:  $d_{ab}$  refers to the distance between cluster *a* and cluster *b*,  $\bar{c}_X$  is the mean of cluster *X*,  $\| \cdot \|$  is the Euclidean length, and  $n_x$  is number of elements grouped in cluster *X*.



The minimum variance criterion used by the Ward method is grouping the consumers in clusters of similar demand level and pattern over 24 h. In the algorithm, a maximum of five priority levels were considered for grouping, and within the same priority level, the criterion of the maximum instantaneous hourly demand was applied:

$$\text{Priority level 1 } \max(W_j) \text{ Priority level 2 } \max(P_{h,j}) \tag{6}$$

3.4. Trading Priority Based on the Blockchain Technology—Scenario 4

The blockchain technology allows secure anonymous transactions that are fulfilled on the FCFS principle. This means that prosumers or the market administrator cannot choose the trading partners, and buying offers are fulfilled regardless of quantity and price, based only on the time of placement in the trading system.

The algorithm simulates this scenario by assigning randomly generated priorities for each consumer and prosumer, at each trading interval. In addition, as a rule, no two consumers can have equal trading priorities, as the time index of each offer is unique in the blockchain system. Thus, no second ranking criterion is required in this case.

3.5. Trading Priority Based on the Minimum Price for Consumers—Scenario 5

A standard market procedure is to accept trading offers based on the minimum selling price. This approach is modeled in the last scenario implemented in the algorithm, where consumers will acquire the electricity from prosumers in the ascending order of the selling process. The consumer offers will be fulfilled in the sequence taken from the blockchain system ledger, on the FCFS principle. If two prosumers have the same price offer, the highest traded quantity will be preferred.

$$\text{Priority level 1 } \min(PR_{k,h}) \text{ Priority level 2 } \max(P_{k,j}) \tag{7}$$

Scenarios 1 and 2 require the knowledge of the length of the supply paths from each prosumer to each consumer. Based on these distances, the priority matrix  $M_1 = M_1(k, j) \in z^{np \times nc}$  is determined, where a generic element  $M_1(k, j)$  denotes the trading priority of consumer  $j$  for prosumer  $k$ . Priorities are positive integer numbers. Lower distances between prosumer  $k$  and consumer  $j$  result in higher trading priority between the two peers. The highest priority level is 1.

Similarly, Scenario 3 requires the priority matrix  $M_2 = M_2(k, j) \in z^{np \times nc}$  where each element  $M_2(k, j)$  denotes the trading priority of consumer  $j$  for prosumer  $k$  determined by the Ward clustering of consumers according to the daily energy demand. Higher demand is equivalent with higher priority.

Scenarios 4 and 5 use the priority matrix  $M_3 = M_3(k, j, h) \in z^{np \times nc \times nh}$ , where each element  $M_3(k, j, h)$  is the priority of consumer  $j$  for prosumer  $k$  at hour  $h$ , determined by the time index at which consumer  $j$  inputs its purchasing offer for hour  $h$ . An earlier time index is equivalent with higher priority. In all priority matrices, the highest priority level is 1. A higher value denotes a lower priority.

For the prosumer-driven scenarios, the surplus is computed using Equation (2) for each prosumer. Then, for each hour and prosumer, if the surplus exists, it is distributed to the consumers using one of the priorities from Scn<sub>1</sub> ÷ Scn<sub>4</sub>. For the consumer-driven scenario (Scn<sub>5</sub>), at each hour  $h$  where surplus exists, it is distributed amongst the consumers using the priority determined by the blockchain system, prioritizing the prosumers with the lowest prices.

The results are stored in an acquisition matrix  $A = A(h, j, k) \in z^{nh \times nc \times np}$ , where each element  $A(h, j, k)$  represents the electricity sold at hour  $h$  to consumer  $j$  by prosumer  $k$ . Similarly, the financial settlement matrix  $F = F(h, j, k) \in z^{nh \times nc \times np}$  is computed, where each element  $F(h, j, k)$  represents the payment made by consumer  $j$  to prosumer  $k$  at hour  $h$ . The mathematical model used in determining the hourly surplus sold by prosumers to local consumers via a P2P contract is presented in Algorithm 1. Algorithm 1 uses Subroutine 1, Subroutine 2 and Subroutine 3.

**Algorithm 1: The proposed trading algorithm**


---

**Step 1.** Specify trading scenario: 1—network length; 2—instantaneous demand; 3—daily demand; 4—blockchain trading; 5—prosumer minimum price with blockchain.

**Step 2.** Load input data: the consumer load profile matrix  $C$ , the prosumer generation matrix  $G$ , the supply path lengths of the network, the prosumer price matrix  $PR$ .

**Step 3.** According to the selected scenario, compute priority matrices  $M_1, M_2, M_3$ .

**Step 4.** Initialize the acquisition matrix  $A$  and financial settlement matrix  $F$ .

**Step 5.** Initialize the unsold surplus  $us = 0$ .

**Step 6.** Trading:

for prosumer-driven scenarios

for each hour  $h, h = 1..24$

for each prosumer  $k, k = 1, \dots, np$

compute surplus  $S(h, k)$ ;

if  $S(h, k) > 0$

srp =  $S(h, k)$ ;

find  $ix$ , the row index corresponding to prosumer  $k$  in matrix  $M_1$

case Scenario 1—*network length*

build a temporary consumer priority matrix MTC with two rows:

row 1: line  $ix$  from matrix  $M_1$ ;

row 2: line  $h$  from matrix  $C$ ;

$(MTC, A, F, srp) = \text{Subroutine 1}(MTC, A, F, srp, h, ix, nc)$ .

case Scenario 2—*instantaneous demand*

build a temporary consumer priority matrix MTC with two rows:

row 1: line  $h$  from matrix  $C$ ;

row 2: line  $ix$  from matrix  $M_1$ ;

$(MTC, A, F, srp) = \text{Subroutine 2}(MTC, A, F, srp, h, ix, nc)$

case Scenario 3—*daily demand*

build a temporary consumer priority matrix MTC with two rows:

row 1: line  $ix$  from matrix  $M_2$ ;

row 2: line  $h$  from matrix  $C$ ;

$(MTC, A, F, srp) = \text{Subroutine 1}(MTC, A, F, srp, h, ix, nc)$

case Scenario 4—*blockchain trading*

build a temporary consumer priority matrix MTC with two rows:

row 1: line  $ix$  from matrix  $M_3$ ;

row 2: line  $h$  from matrix  $C$ ;

$(MTC, A, F, srp) = \text{Subroutine 1}(MTC, A, F, srp, h, ix, nc)$

Update line  $h$  from  $C$  using the modified matrix MTC

Update the unsold surplus:  $us = us + srp$ ;

for consumer-driven scenarios—prosumer minimum price with blockchain

for each hour  $h, h = 1, \dots, 24$

compute the total surplus for hour  $h$ ,  $srph$ ;

if  $srph > 0$

build a temporary consumer priority matrix MTC with two rows:

row 1: line  $h$  from matrix  $M_3$ ;

row 2: line  $h$  from matrix  $C$ ;

build a temporary prosumer priority matrix MTP with two rows:

row 1: line  $h$  from matrix  $PR$ ;

row 2: line  $h$  from matrix  $S$ ;

$(MTC, MTP, A, F, srp) = \text{Subroutine 3}(MTC, MTP, A, F, h)$

**Step 7.** Compute the hourly and total electricity sold by prosumers to each consumer and the electricity traded hourly and daily by all prosumers, using matrices  $A$  and  $F$ .

---

---

**Subroutine 1**

---

*Step 1.* Read input data: the priority matrix MTC, acquisition matrix A, the financial settlement matrix F, the surplus to be distributed between consumers  $srp$ , the current prosumer index  $ix$ , the current hour  $h$ .

*Step 2.* Transpose matrix MTC into matrix MC.

*Step 3.* Sort matrix MC ascending by column 1, and for equal values in column 1, sort descending the corresponding values in column 2.

*Step 4.* Distribute the surplus  $srp$ :

set initial consumer index:  $k = 0$ ;

while  $srp > 0$  or  $(k < nc)$

$k = k + 1$ ;

if the consumer has a P2P contract

subtract the available surplus from its trading offer  $MC(k, 2) = MC(k, 2) - srp$ ;

if the surplus exceeds the consumer contract quantity:  $MC(k, 2) < 0$

update remaining surplus:  $srp = -MC(k, 2)$ ;

the contract from consumer  $k$  is fulfilled:  $MC(k, 2) = 0$ ;

else

the contract from consumer  $k$  is partially fulfilled and the surplus is depleted:  $srp = 0$ ;

update matrix MTC for by subtracting from the served consumer demand the fulfilled contract;

update acquisition matrix A for hour  $h$  according to the served consumer  $k$ , serving prosumer  $ix$  and traded quantity

---

**Subroutine 2**

---

*Step 1.* Read input data: the priority matrix MTC, the acquisition matrix A, the financial settlement matrix F, the surplus to be distributed between consumers  $srp$ , the current prosumer index  $ix$ , the number of consumers  $nc$ , the current hour  $h$ .

*Step 2.* Transpose matrix MTC into matrix MC.

*Step 3.* Sort matrix MC descending by column 1, and for equal values in column 1, sort ascending the corresponding values in column 2.

*Step 4.* Distribute the surplus  $srp$ :

set initial consumer index:  $k = 0$ ;

while  $srp > 0$  or  $(k < nc)$

$k = k + 1$ ;

if the consumer has a P2P contract

subtract the available surplus from its trading offer  $MC(k, 1) = MC(k, 1) - srp$ ;

if the surplus exceeds the consumer contract quantity:  $MC(k, 1) < 0$

update remaining surplus:  $srp = -MC(k, 1)$ ;

the contract from consumer  $k$  is fulfilled:  $MC(k, 1) = 0$ ;

else

the contract from consumer  $k$  is partially fulfilled and the surplus is depleted:  $srp = 0$ ;

update matrix MTC for by subtracting from the served consumer demand the fulfilled contract;

update acquisition matrix A and financial settlement matrix F for hour  $h$  according to the served consumer  $k$ , serving prosumer  $ix$  and traded quantity.

---

**Subroutine 3**

*Step 1.* Read input data: the priority matrix for consumers MTC, the priority matrix for prosumers MTP, the acquisition matrix A, the financial settlement matrix F, hour h.

*Step 2.* Transpose matrix MTC into matrix MC, and matrix MTP into matrix MP

*Step 3.* Sort matrix MC in ascending order of consumer priority (column 1). Keep original consumer order in vector idxk.

*Step 4.* Sort matrix MT ascending by column 1, and for equal values in column 1, sort descending the corresponding values in column 2. Keep original prosumer order in vector idxp.

*Step 5.* Compute the total surplus and consumption (st, ct).

*Step 6.* Distribute the surplus srp:

set initial consumer index: kc = 0 and prosumer index kp = 0;

while (st > 0) & (ct > 0)

increase consumer index: kc = kc + 1;

read consumption to be traded c\_crt = MC (kc, 2);

if c\_crt > 0, if consumption exists

while (c\_crt > 0) & (st > 0)

increase consumer index: kp = kp + 1;

read prosumer surplus p\_crt = MP (kp, 2);

if p\_crt > 0

subtract the surplus from the consumption

c\_crt = c\_crt - p\_crt;

if the surplus exceeds the consumer contract quantity: c\_crt < 0

update remaining surplus: t\_crt = c\_crt; p\_crt = - c\_crt;

the contract from consumer k is fulfilled c\_crt = 0;

else

the contract from consumer k is partially fulfilled and the surplus is depleted: p\_crt = 0;

compute traded consumption

ctz = abs (t\_crt - abs (c\_crt));

update transposed consumption and generation priority matrices

MC (kc, 2) = c\_crt;

MP (kp, 2) = p\_crt;

update consumption and generation priority matrices

MTC (2, idxc (kc)) = MC (kc, 2); MTP (2, idxp (kp)) = MP (kp, 2);

identify price pr = MP (kp, 1);

update st and ct;

update acquisition matrix A and financial settlement matrix F.

**4. Results**

The proposed algorithm was tested on a real 0.4 kV EDN from the northeastern Romania. The network, whose one-line diagram is given in Figure 2, supplies 27 one-phase residential consumers using four-wire three-phase overhead lines, mounted on concrete poles. The distance between poles is of 40 m in average.

This network is modeling a  $\mu$ G in which the prosumers located at buses 6, 7, 15, 21, and 27 want to sell their electricity surplus to other consumers. The case study considers that all the consumers in the  $\mu$ G are integrated in the local  $\mu$ M and can receive electricity from the prosumers through P2P contracts. The consumption and generation of the consumers and prosumers are modelled as 24-h profiles taken from the Smart Metering system installed in the  $\mu$ G. The consumption and generation profiles are provided in Table A1 and A2 from Appendix A. Table 2 presents the electricity surplus available for trading in the considered interval, for all the prosumers. This surplus will be distributed between the consumers or/and prosumers using one of the priority scenarios built in the proposed algorithm, as presented in the previous section.

The proposed algorithm was tested on a real 0.4 kV EDN from the northeastern Romania. The network, whose one-line diagram is given in Figure 2, supplies 27 one-phase residential consumers using four-wire three-phase overhead lines, mounted on concrete poles. The distance between poles is of 40 m on average.

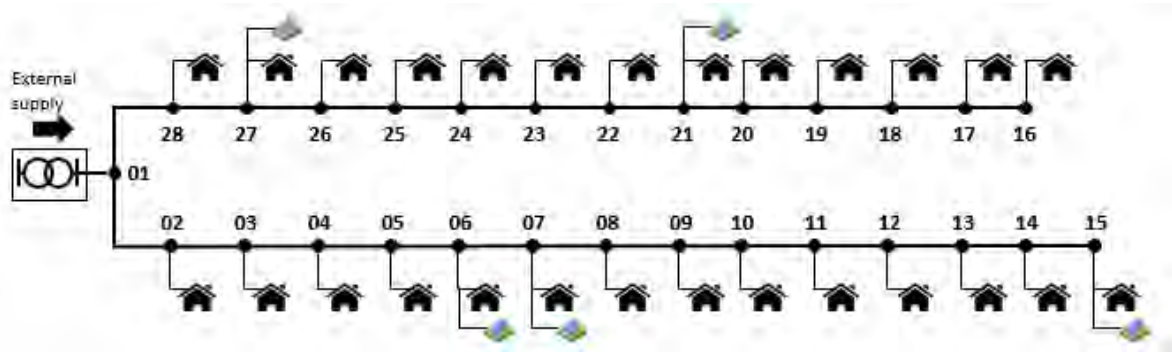


Figure 2. The 28-bus LV distribution network used in the case study.

Table 2. Local generation and consumption in the  $\mu M$  and prosumer selling price, in  $\text{MU/kWh}$ .

Bus	Bus with Prosumers	Total Surplus	Total Consumption
h06	0	1.95	1.59
h07	0	1.59	0
h08	0	1.59	0
h09	0	1.59	0
h10	0	1.59	0
h11	0	1.59	0
h12	0	1.59	0
h13	0	1.59	0
h14	0	1.59	0
h15	0	1.59	0
h16	0	1.59	0
h17	0	1.59	0
h18	0	1.59	0
h19	0	1.59	0
h20	0	1.59	0
h21	0	1.59	0
h22	0	1.59	0
h23	0	1.59	0
h24	0	1.59	0
h25	0	1.59	0
h26	0	1.59	0
h27	0	1.59	0
h28	0	1.59	0
total	0	43.77	30.97

The electricity price is considered constant for each prosumer over the trading interval, and is also given in Table 2. The regulated price at which consumers can buy electricity from the classic market operator has an average level of  $0.72 \text{ MU/kWh}$ , including taxes. On the other hand, the regulated price at which prosumers can sell electricity back to the grid is set at  $0.235 \text{ MU/kWh}$  for 2018 [36,37]. Thus, the selling prices for the local prosumers were set in the  $[0.40, 0.55] \text{ MU/kWh}$  interval. As it can be seen from Table 2 and Figure 3, the local generation amounts to  $22.8\%$  from the consumption, in the  $06:00\text{--}18:00$  interval, and the hourly surplus does not exceed the demand in any trading interval.

The electricity price is considered constant for each prosumer over the trading interval, and is also given in Table 2. The regulated price at which consumers can buy electricity from the classic market operator has an average level of  $0.72 \text{ MU/kWh}$ , including taxes. On the other hand, the regulated price at which prosumers can sell electricity back to the grid is set at  $0.235 \text{ MU/kWh}$  for 2018 [36,37]. Thus, the selling prices for the local prosumers were set in the  $[0.40, 0.55] \text{ MU/kWh}$  interval. As it can be seen from Table 2 and Figure 3, the local generation amounts to  $22.8\%$  from the consumption, in the  $06:00\text{--}18:00$  interval, and the hourly surplus does not exceed the demand in any trading interval. This means that all the local generation will be sold in the local  $\mu M$ , through P2P contracts. The generation surplus from Table 2 will be distributed to the consumers with different priorities, according to each scenario. Table 3 presents the priorities computed according to the distance between prosumers and consumers (Scenario 1) and daily energy demand (Scenario 3). For Scenario 1, the priorities are straightforward, the consumers close to the prosumer having maximum trading priority. For instance, if prosumer 21 is used as reference, consumers 22 and 20 will have maximum trading priority, while consumer 14 or prosumer 15 (in case of deficit) will be the last in the priority list. In all scenarios, consumers or prosumers marked with X in Table 3 are excluded from trading. Bus 1 has no load, and each prosumer cannot sell to itself, because it is considered that it is selling on the market its surplus.

	h16	0	0.41	1.32	0.82	0.56	3.12	26.19
	h17	0	0	1.06	0	0	1.06	32.15
	h18	0	0	1.16	1.17	0	2.33	30.75
	total	10.90	9.99	24.17	18.90	11.51	75.48	330.52
Mathematics 2020, 8, 235	Selling price	0.43	0.40	0.48	0.55	0.43	-	-

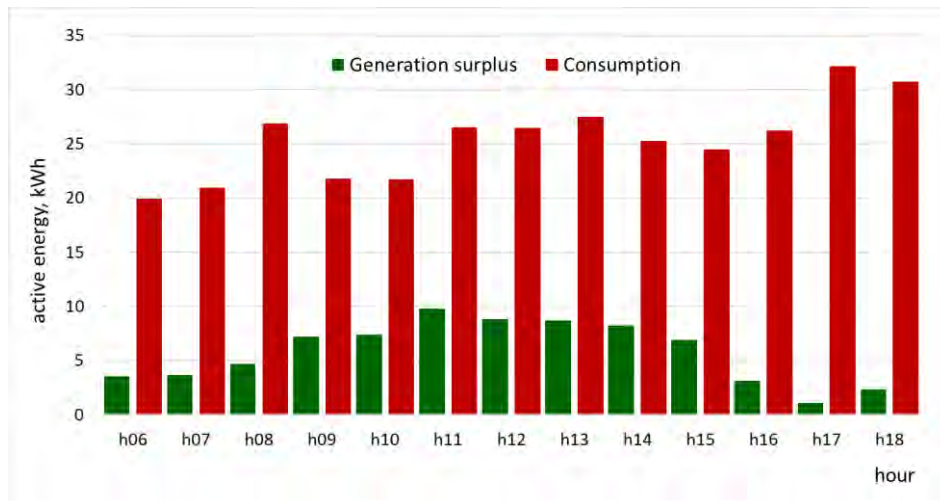


Figure 3. Local generation and consumption, in kWh.

Table 3. Consumer trading priorities for Scenarios 1 and 3.

The priorities for Scenario 2 are computed in the same manner, but using the hourly demand values indicated in Table A1 from Appendix A as ranking criterion, instead of distance.

For Scenario 3 (daily consumption), the Ward clustering method was run for the consumptions from Appendix A. The dendrogram and the clusters obtained after grouping are presented in Figures 4 and 5, which show multiple consumers belonging to the same priority group (with consumers/prosumers).

Cons.	Scenario 1	Scenario 2	Scenario 3	Scenario 3	Scenario 3	Scenario 3	Scenario 3	Scenario 3	Scenario 3	Scenario 3
1	X	X	X	X	X	X	X	X	X	X
2	4	5	13	8	2	4	4	4	4	4
3	3	4	12	9	3	3	3	3	3	3
4	2	3	11	10	4	5	5	5	5	5
5	1	2	10	11	5	2	2	2	2	2
6	X	1	9	12	6	X	1	1	1	1
7	1	X	8	13	7	1	X	1	1	1
8	2	1	7	14	8	3	3	3	3	3
9	3	2	6	15	9	3	3	3	3	3
10	4	3	5	16	10	1	1	1	1	1
11	5	4	4	17	11	3	3	3	3	3
12	6	5	3	18	12	4	4	4	4	4
13	7	6	2	19	13	4	4	4	4	4
14	8	7	1	20	14	3	3	3	3	3
15	9	8	X	21	15	1	1	X	1	1
16	17	18	26	5	11	2	2	2	2	2
17	16	17	25	4	10	4	4	4	4	4
18	15	16	24	3	9	4	4	4	4	4
19	14	15	23	2	8	5	5	5	5	5
20	13	14	22	1	7	3	3	3	3	3
21	12	13	21	X	6	2	2	2	X	2
22	11	12	20	1	5	4	4	4	4	4
23	10	11	19	2	4	4	4	4	4	4
24	9	10	18	3	3	3	3	3	3	3
25	8	9	17	4	2	4	4	4	4	4
26	7	8	16	5	1	3	3	3	3	3
27	6	7	15	6	X	4	4	4	4	X
28	5	6	14	7	1	5	5	5	5	5

The priorities for Scenario 2 are computed in the same manner, but using the hourly demand values indicated in Table A1 from Appendix A as ranking criterion, instead of distance.

For Scenario 3 (daily consumption), the Ward clustering method was run for the consumptions from Appendix A. The dendrogram and the clusters obtained after grouping are presented in Figures 4 and 5, which show multiple consumers belonging to the same priority group (with consumers/prosumers).

prosumers, thus all prosumers will sell their surplus to consumers via P2P contracts. However, the prioritization of the consumers for trading will change in each scenario, together with the financial settlements between parties.

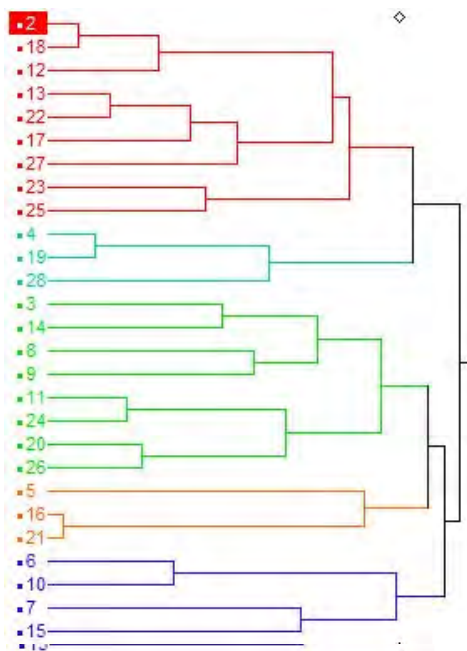


Figure 4. The dendrogram of the consumer grouping procedure using the Ward method.

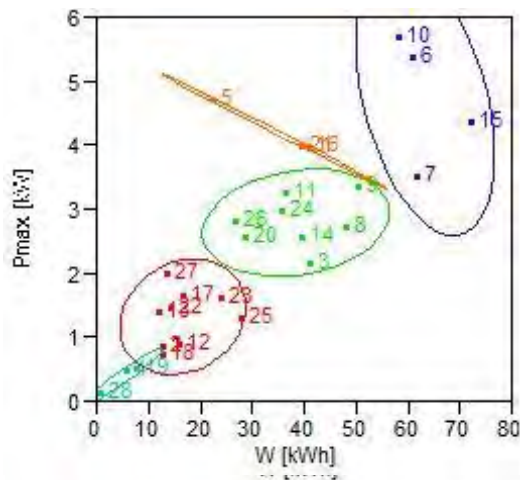


Figure 5. The consumer clusters obtained using the Ward method.

The first three scenarios use the same priority for all trading intervals. On the other hand, Scenarios 4 and 5 modelling the blockchain trading, priority require different priorities for each consumer and oriented scenario (Scn5), the prosumers will sell the same quantities, as is indicated in Table 4.

Scenarios 1-4, prosumer-oriented, do not take into account prosumer prices. The prosumer priority order is preset, to take into account the incentivization of specific prosumers, based on criteria particular to each  $\mu G$ , such as connection, generation, technology, common, or remuneration maximization of the social welfare. For convenience, the results presented in the following subparagraphs use the bus index as prioritization index, but the algorithm does not consider any user-preferred priority.

Scenario 5, consumer-oriented, uses FC as principle for consumers as a primary trading prioritization tool, and the consumer has the benefit of selecting available prosumer offers with the lowest price.

On the other hand, the quantities purchased by consumers are different in accordance with each proposed scenario. These values can be viewed in Table 5. For the first scenario (Scn1), the quantities

Table 4. The results for the total quantities of surplus for the prosumers, in kWh.

Scenarios/Bus	Scn1	Scn2	Scn3	Scn4	Scn5
Bus 6	10,899	10,899	10,899	10,899	10,899
Bus 7	9,998	9,998	9,998	9,998	9,998
Bus 13	24,170	24,170	24,170	24,170	24,170
Bus 15	24,170	24,170	24,170	24,170	24,170
Bus 21	18,903	18,903	18,903	18,903	18,903
Bus 27	11,511	11,511	11,511	11,511	11,511

The main reasons for creating  $\mu$ M are to promote generation from small-scale renewable sources, and to lower consumer electricity prices. Next, a comparative study regarding the advantages of each prosumer-oriented scenario is presented. The main focus is on the financial savings of the consumers and market flexibility, in terms of the number of served contracts.

In these scenarios, because the prosumer price is not relevant, all the consumers are integrated into the local  $\mu$ M and the hourly total consumption always exceeds the available surplus from the prosumers, thus all prosumers will sell their surplus to consumers via P2P contracts. However, the prioritization of the consumers for trading will change in each scenario, together with the financial settlements between parties.

Regardless of the first four prosumers-oriented scenarios (Scn<sub>1</sub> – Scn<sub>4</sub>) and the unique consumer-oriented scenario (Scn<sub>5</sub>), the prosumers will sell the same quantities, as is indicated in Table 4.

**Table 4.** The results for the total quantities of surplus of the prosumers, in kWh.

Scenarios/Bus	Scn <sub>1</sub>	Scn <sub>2</sub>	Scn <sub>3</sub>	Scn <sub>4</sub>	Scn <sub>5</sub>
Bus 6	10.899	10.899	10.899	10.899	10.899
Bus 7	9.998	9.998	9.998	9.998	9.998
Bus 15	24.170	24.170	24.170	24.170	24.170
Bus 21	18.903	18.903	18.903	18.903	18.903
Bus 27	11.511	11.511	11.511	11.511	11.511

On the other hand, the quantities purchased by consumers are different in accordance with each proposed scenario. These values can be viewed in Table 5. For the first scenario (Scn<sub>1</sub>), the quantities traded by prosumers to consumers are shown in Figure 6. It can be seen that the consumers geographically close from prosumers locations purchase the higher quantities. For example, the prosumer P7 sells energy to consumer C8, prosumer P15 to consumer C14, and the prosumer P21 to consumer C20. Similar results are obtained for Scenario 2 (Scn<sub>2</sub>) where the prioritization is made according to the instantaneous power required by consumers. In this scenario, the consumers with the highest demand are preferred in the same manner, in each trading interval (C10, C9, C8, C5), as seen in Figure 6 and Table 5.

**Table 5.** The electricity quantities purchased by the consumers, in kWh.

Scn./Cons.	C2	C3	C4	C5	C6	C7	C8	C9	C10
Scn1	0.136	0.000	0.000	8.532	0.000	0.000	12.287	0.077	0.000
Scn2	0.000	1.588	0.000	7.951	0.000	0.000	8.781	15.973	21.325
Scn3	0.000	0.000	0.000	13.134	1.310	0.116	1.141	6.088	35.305
Scn4	1.678	7.109	0.378	1.489	0.000	0.000	7.430	3.927	5.133
Scn5	1.678	7.109	0.378	1.489	0.000	0.000	7.430	3.927	5.133
Scn./Cons.	C11	C12	C13	C14	C15	C16	C17	C18	C19
Scn1	1.615	2.036	2.546	17.973	0.000	0.000	0.000	0.000	0.963
Scn2	2.232	0.000	0.000	0.000	0.000	6.964	0.000	0.000	0.000
Scn3	0.000	0.000	0.000	0.000	0.000	14.654	0.000	0.000	0.000
Scn4	4.340	3.885	0.206	7.460	0.000	8.814	1.625	1.407	0.315
Scn5	4.340	3.885	0.206	7.460	0.000	8.814	1.625	1.407	0.315
Scn./Cons.	C20	C21	C22	C23	C24	C25	C26	C27	C28
Scn1	9.949	0.000	3.597	3.654	0.740	6.919	4.191	0.000	0.265
Scn2	1.805	0.000	0.000	0.000	6.882	0.000	1.980	0.000	0.000
Scn3	0.000	0.000	0.000	0.000	3.733	0.000	0.000	0.000	0.000
Scn4	2.822	0.000	1.901	3.500	7.187	3.612	1.264	0.000	0.001
Scn5	2.822	0.000	1.901	3.500	7.187	3.612	1.264	0.000	0.001



geographical proximity from consumers locations to higher quantities. For example, the prosumer P7 sells energy to consumer C8, prosumer P15 to consumer C14, and the prosumer P21 to consumer C20. Similar results are obtained for Scenario 2 (Scn2) where the prioritization is made according to the instantaneous power required by consumers. In this scenario, the consumers with the highest demand are preferred in the same manner, in each trading interval (C10, C9, C8, C5), as seen in Figure 6 and Table 5.

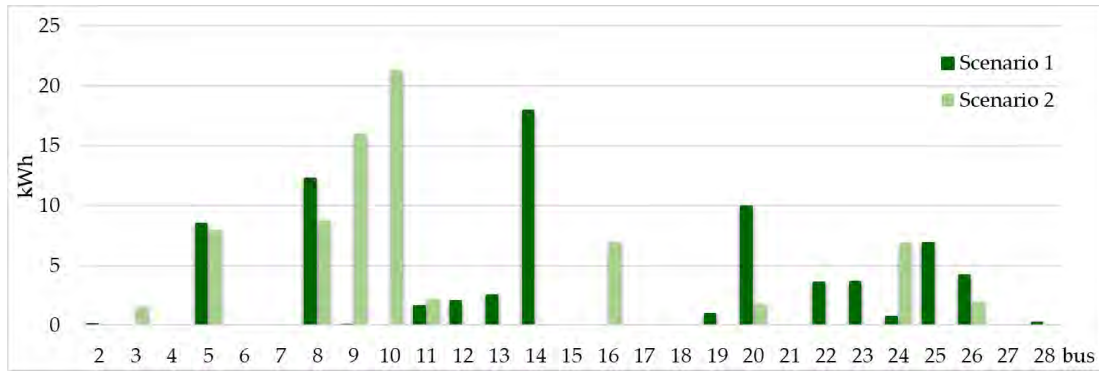


Figure 6: The electricity quantities purchased by the consumers in first and second scenario, in kWh.

For Scenario 3, where consumers are allocated in five priority clusters according to the daily electricity demand (Figure 5), it is observed that cluster I already contains three prosumers (P6, P7 and P21) and one consumer (C10). Cluster II has a prosumer (P21) and two consumers (C5 and C16) and cluster III comprises of eight peers, and the last two clusters group the rest of the peers. From Figure 8, it can be observed that the traded quantities resulting from applying the mathematical model proposed for the last two scenarios. The differences between Scn2 and Scn3 are seen in the purchase price of the surplus according to the type of P2P contract concluded between prosumers and the rest of the participants in the network.

Scn/Cons.	C1	C2	C3	C4	C5	C6	C7	C8	C9	C10
Scn1	0.136	0.000	0.000	8.532	0.000	0.000	0.000	12.287	0.077	0.000
Scn2	0.000	1.588	0.000	7.951	0.000	0.000	0.000	8.781	12.973	21.325
Scn3	0.000	0.000	0.000	12.134	1.310	0.116	0.141	7.460	3.927	5.133
Scn4	1.678	7.109	0.378	1.489	0.000	0.000	0.000	7.430	3.927	5.133
Scn5	0.778	7.109	0.378	1.489	0.000	0.000	0.000	7.430	3.927	5.133

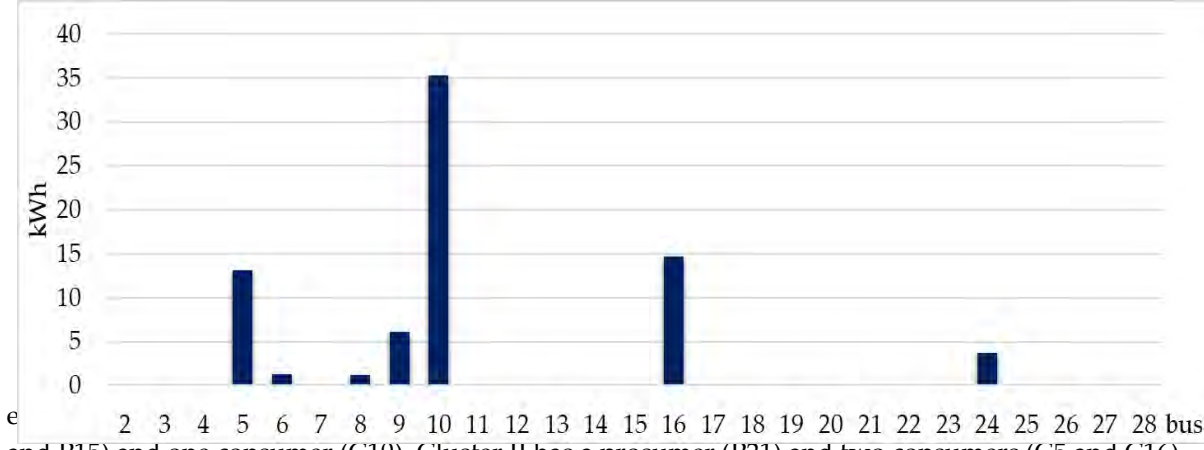


Figure 7: The electricity quantities achieved of the consumers in third scenario, in kWh.

From Figure 7, it can be observed that the peers from the first two clusters have priority for trading, and the remaining surplus is sold to other consumers from cluster III respectively. Consumers depending on the P2P contracts already signed, it is observed that the only ones who do not receive are presented in Tables 6–10. Moreover, the last four columns from the aforementioned tables contain the surplus of electricity are prosumers, the consumer from bus 28, which has an insignificant total quantity purchased by each consumer, the price paid by consumer(s) to prosumers for this quantity through P2P contracts, the regulated price that should have been paid by consumers to the classical supplier at 0.72 MU/kWh, and also by prosumers to the grid aggregator with a regulated price of 0.223 MU/kWh. The last columns present the financial advantages for all the transaction participants (see Table A1, Appendix A).

Figure 8 shows the similarities in traded quantities, resulting from applying the mathematical model proposed for the last two scenarios. The differences between Scn2 and Scn3 are seen in the purchase price of the surplus according to the type of P2P contract concluded between prosumers and the rest of the participants in the network.

For all five scenarios, the daily electricity quantities, from prosumers purchased by consumers are presented in Tables 6–10. Moreover, the last four columns from the aforementioned tables contain

Bus	P6	P7	P15	P21	P27	Total kWh	P2P Price	Total Cost/Revenue for Cj	Total Cost/Revenue for Pk
2	0.000	0.000	0.000	0.000	0.136	0.136	0.058	0.098	0.030
5	8.532	0.000	0.000	0.000	0.000	8.532	3.629	6.143	1.903
8	2.366	9.921	0.000	0.000	0.000	12.287	4.986	8.847	2.740
9	0.000	0.077	0.000	0.000	0.000	0.077	0.031	0.055	0.017
11	0.000	0.000	1.615	0.000	0.000	1.615	0.775	1.163	0.360
12	0.000	0.000	2.036	0.000	0.000	2.036	0.977	1.466	0.454
13	0.000	0.000	2.546	0.000	0.000	2.546	1.222	1.833	0.568
14	0.000	0.000	17.973	0.000	0.000	17.973	8.627	12.941	4.008
19	0.000	0.000	0.000	0.963	0.000	0.963	0.529	0.692	0.215

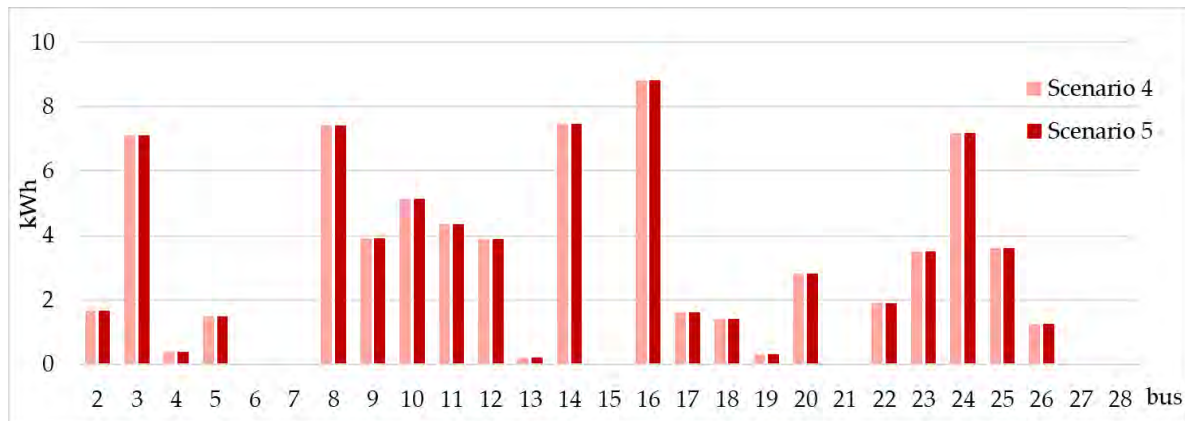


Figure 8. The electricity quantities achieved of the consumers in four and five scenarios, in kWh.

For example, in Figure 9 the prosumers financial benefits were presented, with the price paid for the consumers to each prosumer through the smart considered P2P contracts compared to the regulated price received. The Active Energy Surplus plus directly into the P2P. Total Cost/Revenue

The benefits of using the local market are also present for the consumers. In Figure 10, the differences between the regulated price that would be paid by consumers and the P2P price used in trading with the prosumers are presented, which is always lower for the equal quantities traded in Scenarios 4 and 5, the differences in financial settlements resulting from the blockchain merit order, but with different prosumer-consumer trading prices are presented in Figure 11.

Bus	P6	P7	P15	P21	P27	Total kWh	P2P Price	Total Cost/Revenue for Cj	Total Cost/Revenue for Pk
2	0.000	0.000	0.000	0.000	0.000	0.000	0.000	0.000	0.000
3	8.532	0.000	0.000	0.000	0.000	8.532	3.669	6.143	1.803
5	2.366	9.921	0.000	0.000	0.000	12.287	4.986	8.847	2.740
8	0.000	0.077	0.000	0.000	0.000	0.077	0.031	0.055	0.017
9	0.000	0.000	1.615	0.000	0.000	1.615	0.775	1.163	0.360
12	0.000	0.000	2.036	0.000	0.000	2.036	0.977	1.466	0.454
13	0.000	0.000	0.000	0.000	0.000	0.000	0.000	0.000	0.000
14	0.000	0.000	17.973	0.000	0.000	17.973	8.627	12.941	4.008
16	0.000	0.000	0.000	0.963	0.000	0.963	0.529	0.693	0.215
19	0.000	0.000	0.000	0.000	0.000	0.000	0.000	0.000	0.000
20	0.000	0.000	0.000	2.949	0.000	2.949	3.472	7.164	0.199
22	0.000	0.000	0.000	1.588	5.970	0.000	1.588	1.390	0.360
23	0.000	0.000	0.000	0.000	0.000	0.000	0.000	0.000	0.000
24	0.000	2.050	1.950	0.000	6.541	1.590	0.000	7.231	1.703
25	0.000	0.000	5.088	3.607	7.400	0.000	0.000	6.323	1.968
26	0.000	10.000	7.000	3.869	0.000	3.446	9.191	11.508	3.565
28	0.000	0.000	4.000	1.867	0.000	3.304	1.912	15.351	4.709
28	0.000	0.000	1.062	1.190	0.000	0.265	2.239	1.607	0.498

Table 6. The prosumers energy surplus trading (kWh) and prices (MU/kWh) in Scenario 4.

Bus	P6	P7	P15	P21	P27	Total kWh	P2P Price	Total Cost/Revenue for Cj	Total Cost/Revenue for Pk
16	0.000	2.281	1.302	1.726	1.655	6.964	3.198	5.014	1.553
24	1.116	0.000	1.880	2.376	1.510	6.882	3.339	4.955	1.535
26	0.000	0.000	0.000	0.000	0.000	0.000	0.000	0.000	0.000

Table 7. The prosumers energy surplus trading (kWh) and prices (MU/kWh) in Scenario 5.

Bus	P6	P7	P15	P21	P27	Total kWh	P2P Price	Total Cost/Revenue for Cj	Total Cost/Revenue for Pk
3	0.000	0.000	0.000	1.588	0.000	0.000	0.000	0.000	0.000
5	2.295	2.105	1.957	0.000	1.595	7.951	3.454	5.725	1.773
8	0.000	0.000	0.000	0.000	0.000	0.000	0.000	0.000	0.000
9	0.000	0.356	0.151	0.185	0.443	0.973	0.473	1.050	0.302
10	0.000	0.000	5.091	5.608	2.381	13.110	0.586	19.354	2.925
11	0.000	0.000	0.106	1.102	0.000	1.342	0.756	1.607	0.298
16	0.000	0.381	0.132	0.000	0.000	0.655	0.198	0.814	0.253
20	0.000	0.000	0.000	0.000	1.805	1.141	0.993	1.300	0.403
24	1.116	0.000	1.880	2.376	1.510	6.882	3.339	4.955	1.535
26	0.000	0.000	0.012	3.301	2.775	6.088	3.014	4.383	1.358
26	10.899	8.954	12.399	2.491	0.563	35.305	1.980	1.425	0.441
16	0.000	0.986	6.345	4.595	2.728	14.654	7.140	10.551	3.268
24	0.000	0.000	0.000	1.811	1.922	3.733	1.822	2.688	0.832

**Table 8.** The prosumers energy surplus trading (kWh) and prices (MU/kWh) in Scenario 3.

Bus	The Active Energy Surplus, in kWh					Total kWh	P2P Price	Total Cost/Revenue	
	P6	P7	P15	P21	P27			for Cj	for Pk
5	0.000	0.058	5.091	5.604	2.381	13.134	6.573	9.456	2.929
6	0.000	0.000	0.208	1.102	0.000	1.310	0.706	0.943	0.292
7	0.000	0.000	0.116	0.000	0.000	0.116	0.056	0.084	0.026
8	0.000	0.000	0.000	0.000	1.141	1.141	0.491	0.822	0.255
9	0.000	0.000	0.012	3.301	2.775	6.088	3.014	4.383	1.358
10	10.899	8.954	12.399	2.491	0.563	35.305	15.831	25.420	7.873
16	0.000	0.986	6.345	4.595	2.728	14.654	7.140	10.551	3.268
24	0.000	0.000	0.000	1.811	1.922	3.733	1.822	2.688	0.832

**Table 9.** The prosumers energy surplus trading (kWh) and prices (MU/kWh) in Scenario 4.

Bus	The Active Energy Surplus, in kWh					Total kWh	P2P Price	Total Cost/Revenue	
	P6	P7	P15	P21	P27			for Cj	for Pk
2	0.860	0.000	0.000	0.176	0.641	1.678	0.743	1.208	0.374
3	0.000	1.154	2.962	1.394	1.599	7.109	3.338	5.118	1.585
4	0.378	0.000	0.000	0.000	0.000	0.378	0.163	0.272	0.084
5	0.000	0.000	0.181	0.749	0.559	1.489	0.739	1.072	0.332
8	0.244	1.048	0.603	2.761	2.773	7.430	3.525	5.350	1.657
9	0.000	0.002	2.046	0.773	1.106	3.927	1.884	2.827	0.876
10	2.295	1.356	0.122	1.361	0.000	5.133	2.336	3.695	1.145
11	1.845	0.745	1.130	0.620	0.000	4.340	1.975	3.125	0.968
12	0.000	0.645	2.572	0.668	0.000	3.885	1.860	2.797	0.866
13	0.150	0.056	0.000	0.000	0.000	0.206	0.087	0.148	0.046
14	1.116	0.691	2.141	2.140	1.372	7.460	3.551	5.371	1.664
16	1.917	1.632	1.634	3.631	0.000	8.814	4.259	6.346	1.966
17	0.000	1.331	0.294	0.000	0.000	1.625	0.674	1.170	0.362
18	0.000	0.263	1.144	0.000	0.000	1.407	0.654	1.013	0.314
19	0.000	0.298	0.017	0.000	0.000	0.315	0.127	0.227	0.070
20	0.000	0.000	1.100	1.722	0.000	2.822	1.475	2.032	0.629
22	0.412	0.000	1.136	0.000	0.353	1.901	0.874	1.369	0.424
23	0.000	0.410	3.090	0.000	0.000	3.500	1.647	2.520	0.781
24	0.000	0.000	2.430	1.649	3.108	7.187	3.410	5.174	1.603
25	0.742	0.368	1.242	1.260	0.000	3.612	1.755	2.601	0.805
26	0.940	0.000	0.324	0.000	0.000	1.264	0.560	0.910	0.282

To highlight the prosumer/consumer advantages using the proposed PEST algorithm, from Tables 6–10 can be seen the benefits registered by each participant in the trading process, regardless of the chosen prioritization scenario.

For example, in Figure 9 the prosumers financial benefits were presented, with the price paid for the consumers to each prosumer through the smart considered P2P contracts compared to the regulated price received if they injected the surplus directly into the  $\mu G$ .

The benefits of using the local market are also present for the consumers. In Figure 10, the differences between the regulated price that would be paid by consumers and the P2P price used in trading with the prosumers are presented, which is always lower. For the equal quantities traded in Scenarios 4 and 5, the differences in financial settlements resulting from the blockchain merit order, but with different prosumer-consumer trading prices are presented in Figure 11.

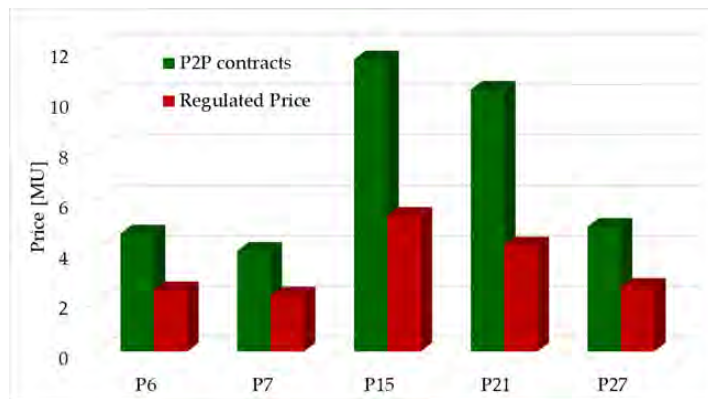


Figure 9. The difference between P2P and regulated prices obtained by the prosumers in the P2P market.

Table 10. The prosumers energy surplus trading (kWh) and prices (MU/kWh) in Scenario 5.

Bus	The Active Energy Surplus, in kWh					Total kWh	P2P Price	Total Cost for Cj	Revenue for Pk
	P6	P7	P15	P21	P27				
2	0.000	0.860	0.000	0.817	0.000	1.678	0.794	1.208	0.374
3	0.889	0.000	2.610	2.430	1.179	7.109	3.479	5.118	1.585
4	0.000	0.378	0.000	0.000	0.000	0.378	0.151	0.272	0.084
5	0.000	0.000	0.930	0.559	0.000	1.489	0.754	1.072	0.332
8	0.000	0.108	0.546	4.988	0.503	7.430	3.810	3.350	1.657
9	0.000	0.000	0.000	0.000	0.000	0.000	0.000	0.000	0.876
10	0.000	0.000	0.000	0.000	0.000	0.000	0.000	0.000	1.145
11	0.000	0.000	0.000	0.000	0.000	0.000	0.000	0.000	0.968
12	0.000	0.000	0.000	0.000	0.000	0.000	0.000	0.000	0.866
13	0.000	0.000	0.000	0.000	0.000	0.000	0.000	0.000	0.046
14	0.000	0.000	0.000	0.000	0.000	0.000	0.000	0.000	1.664
15	0.000	0.000	0.000	0.000	0.000	0.000	0.000	0.000	1.966
16	0.000	0.000	0.000	0.000	0.000	0.000	0.000	0.000	0.362
17	0.000	0.000	0.000	0.000	0.000	0.000	0.000	0.000	0.314
18	0.000	0.000	0.000	0.000	0.000	0.000	0.000	0.000	0.070
19	0.000	0.000	0.000	0.000	0.000	0.000	0.000	0.000	0.629
20	0.000	0.000	0.000	0.000	0.000	0.000	0.000	0.000	0.424
22	0.000	0.000	0.000	0.000	0.000	0.000	0.000	0.000	0.781
24	0.000	0.000	0.000	0.000	0.000	0.000	0.000	0.000	1.603
25	0.000	0.000	0.000	0.000	0.000	0.000	0.000	0.000	0.805
26	0.000	0.940	0.324	0.000	0.000	1.264	0.532	0.910	0.282

Figure 9. The difference between P2P and regulated prices obtained by the prosumers in the P2P market.

Figure 11. The difference between P2P prices obtained by the consumers in the P2P market, for Scenario 4 and 5.

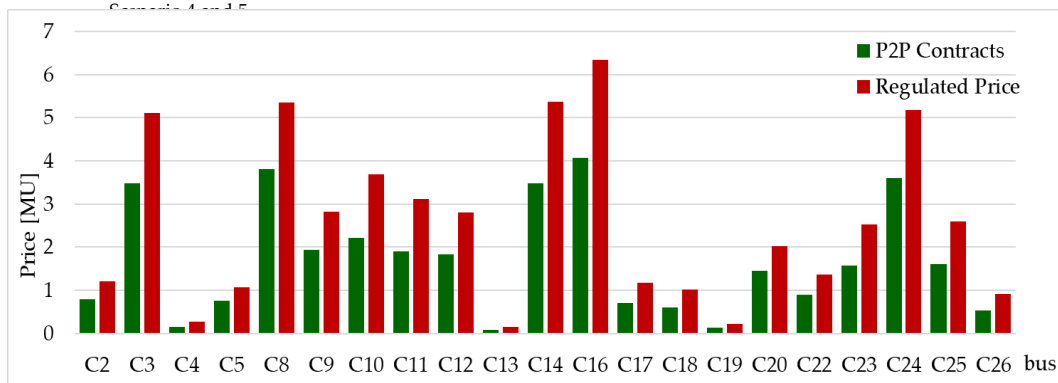
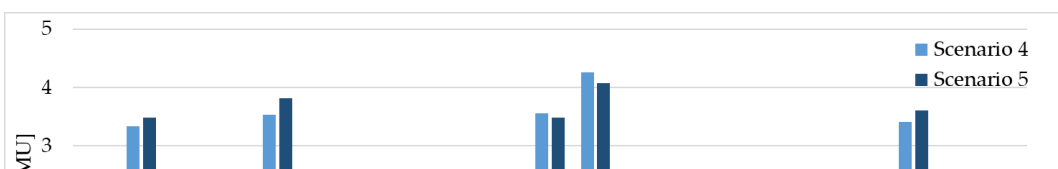
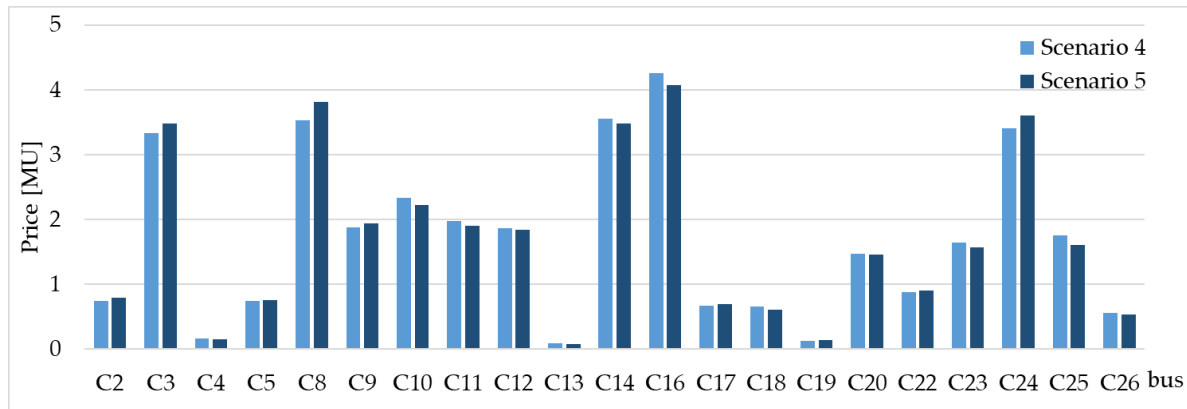


Figure 10. The difference between P2P and regulated prices obtained by the consumers in the P2P market for scenario 5.





**Figure 10.** The difference between P2P and regulated prices obtained by the consumers in the P2P market, for scenario 5. *Mathematics* 2020, 8, 235 20 of 27



**Figure 11.** The difference between P2P prices obtained by the consumers in the P2P market, for Scenario 4 and 5.

## 5. Discussion

As the results presented in the study case show, both the consumers and the prosumers can obtain significant profits from the implementation of a local  $\mu M$  in which prosumers sell directly to the prosumers. In this market, prosumer can sell electricity to prosumers at prices lower than the regulated tariff established for residential consumers, but higher than the price at which they can sell back to the grid their generation surplus. As in Figure 9, the daily profits for prosumers can vary from 1.8 to 6.2 MU (1 MU = 1 Romanian leu or 0.21 EUR), and for consumers from 1.8 to 6.2 MU.

For consumers, the daily financial gain can amount to up to 2.2 MU (consumer C16). The consumer's total demand for the considered day is of 23.84 kWh, amounting to an electricity bill of 17.16 MU, which means that the daily saving of the consumer is of 12.8%, in the scenario with the maximum number of consumers involved in trading. Our proposed mechanism was tested also for the cases when the PV generation of the prosumers is small. In these cases, if it is a surplus, the most convenient turned out to be Scenario 4 based on the blockchain technologies, which consider both quantities and price (from P2P contracts).

For a technical consideration, it should be noted that the trading results presented in the paper do not account for the energy losses in the LV distribution network, because they have the same influence on all the scenarios considered in the algorithm. In the physical network, prosumers would inject the surplus in the local network, and the consumers would draw power in the same manner. The difference is only in the financial settlement performed in the  $\mu M$ . The losses need to be settled at the market level, but this is a separate mechanism that needs future research. In Table 11, the number of consumers which benefits from the trading process are presented. It can be seen that only three consumers are commonly to the five considered scenarios. For the three consumers in Figures 12–14 the purchased energy and the costs of consumers, and the revenue of prosumers.

**Table 11.** The prosumers energy surplus trading (kWh) and prices (MU/kWh).

No. of Scenarios	No. of Consumers	Diff. of Common Consumers
Scn1	16	13
Scn2	10	7
Scn3	8	5
Scn4	21	18
Scn5	23	20

Scenarios	Consumers	Consumers
Scn1	16	13
Scn2	10	7
Scn3	8	5
Scn4	21	18
Scn5	23	20

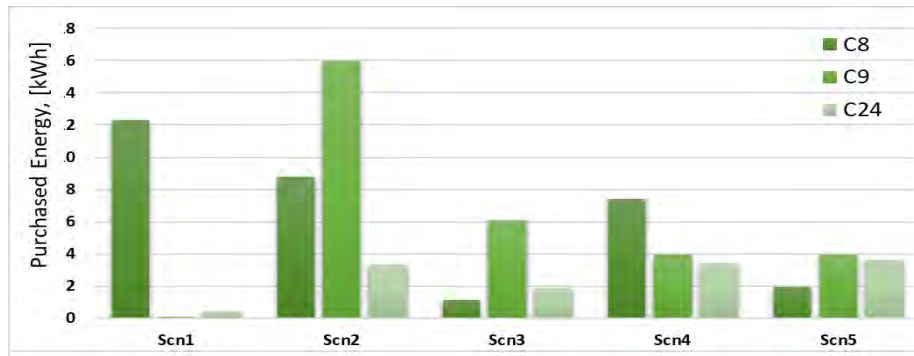


Figure 12. The purchased energy for the three common consumers, in all scenarios.

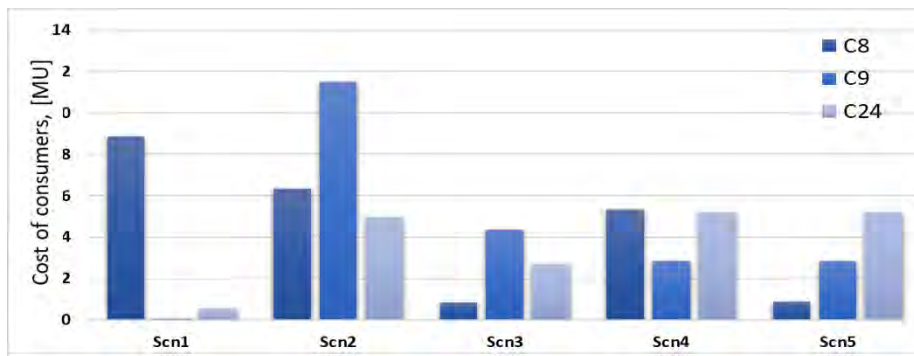


Figure 13. The cost for the three common consumers, in all scenarios.

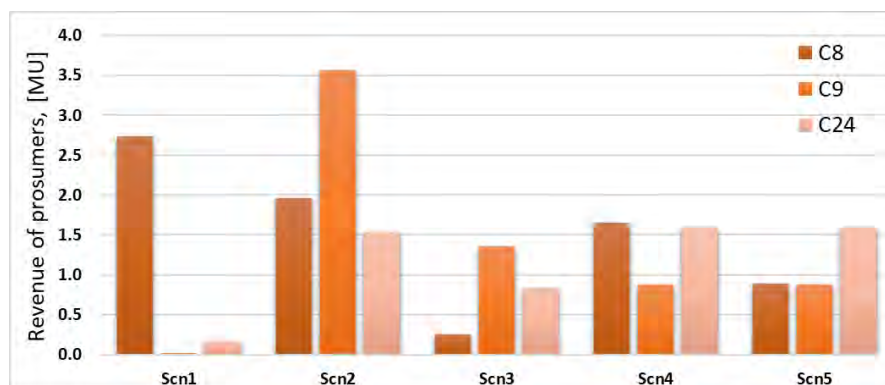


Figure 14. The revenue of prosumers considering the three common consumers, in all scenarios.

Considering the obtained results from Tables 5–10 and Figures 7 and 12, Figures 13 and 14, it is emphasized that the third scenario is the least favorable for the participants. In this scenario, the distribution network operators win due to an optimization of power flows between the prosumers and the consumers with high power demand.

The time granularity and period of day was considered. Our study was conducted only hourly trading for a day, but the mechanism can be easily used for other periods. A complete transaction depends on the proposed mechanism, taking into account the contracts of the prosumers, consumers power demand, proposed transactions, and the proposed algorithm. The proposed algorithm is only the first step in developing a platform for consumers and prosumers in microgrids, and is aimed to serve as a simulation tool for developing alternatives for the current regulation framework regarding prosumer activity in the Romanian electricity market. However, future research will extend its capabilities for other trading scenarios.

However, future research will extend its capabilities for other trading scenarios.

## 6. Patents

National Patent Application “Innovative method of decision-making assistance aimed at streamlining the management of prosumer activity”, Romania, 2019, in press.

## 6. Patents

National Patent Application “Innovative method of decision-making assistance aimed at streamlining the management of prosumer activity”, Romania, 2019, in press.

**Author Contributions:** Conceptualization, B.-C.N., O.I. and G.G.; methodology, B.-C.N. and O.I.; software, B.-C.N. and O.I.; validation, O.I. and B.-C.N.; formal analysis, M.G.; investigation, O.I. and G.G.; data curation, O.I.; writing—original draft preparation, B.-C.N. and O.I.; writing—O.I., G.G. and M.G.; supervision, M.G. All authors have read and agreed to the published version of the manuscript.

**Funding:** This research received no external funding.

**Acknowledgments:** This paper was realized with the support of national project PNIII-1.2.PDI-PFC-C1-2018, as COMPETE project no.9PFE/2018, financed by the Romanian Government.

**Conflicts of Interest:** The authors declare no conflict of interest.

## Nomenclature

a, b, X	Clusters
A	The acquisition matrix
A(h,j,k)	The electricity sold at hour h to consumer j by prosumer k
ANRE	Regulation National Agency in Energy Domain
C	Matrix of consumptions
C <sub>j</sub>	Consumer j
c <sub>t</sub>	Total consumption
$\bar{c}_X$	The mean of cluster X
d <sub>ab</sub>	the distance between cluster A and cluster B
DER	Distributed Energy Resources
DG	Distributed Generation
DR	Demand Response
DSM	Demand Side Management
EC	European Commission
EDN	Electricity Distribution Network
ESS	Energy Storage System
EU	European Union
F	The financial settlement matrix
F(h,j,k)	The payment made by consumer j to prosumer k at hour h
FCFS	First Come—First Served
G	Matrix of generations
ICT	Information and Communication Technologies
ix	index
h	The current hour (h, . . . , 1, . . . , H)
j	The index for consumers
k	The index for prosumers
l	The consumer (l, . . . , 1, . . . , n <sub>c</sub> )
p	The number of priority matrix.
L <sub>j,k</sub>	The length between consumer j and prosumer k
LV	Low Voltage
M <sub>p</sub>	Matrix of priorities, (p, . . . , 1, . . . , 3)
MC	The Transposed Temporary Consumer Priority Matrix
MP	The Transposed Temporary Prosumer Priority Matrix
MPC	Model Productive Control
MTC	Temporary Consumer Priority Matrix
MTP	Temporary Prosumer Priority Matrix
MU	Monetary unit

MV	Medium Voltage
nc	total number of consumers ( $j, \dots, 1, \dots, nc$ )
nh	total number of hour ( $h, \dots, 1, \dots, nh$ )
np	total number of prosumers ( $k, \dots, 1, \dots, np$ )
nx	number of elements grouped in cluster X
P2P	Peer-to-Peer
PEST	Prosumers Energy Surplus Trading
$P_{h,j}$	Maximum active power at hour h, of consumers j
Pk	Prosumer k
PR	Vector of prices
$P_{surplus}$	Power surplus of prosumers
$P_{trade}$	Power traded by prosumers
PV	Photovoltaic
S	Matrix of surplus
Scny	Scenarios ( $y, \dots, 1, \dots, 5$ )
srp	Surplus
srph	Total surplus for hour h
SSRES	Small-Scale Renewable Energy Sources
st	Total surplus
us	Unsold surplus
$W_j$	The total active energy for consumer j, in kWh
$\mu G$	Micro-grid
$\mu M$	Micro-market
$\mathbb{R}$	Set of reals
$z$	Set of integers

**Appendix A**

**Table A1.** Active load curve for the 28-bus network, in kW.

-	C2	C3	C4	C5	C6	C7	C8	C9	C10
h1	0.616	2.010	0.273	0.000	1.370	2.418	1.152	1.936	0.310
h2	0.608	1.908	0.078	0.020	1.520	2.210	1.664	1.368	0.678
h3	0.557	2.004	0.048	0.260	1.910	2.149	2.056	1.376	0.300
h4	0.522	2.010	0.306	0.040	1.770	2.151	2.048	2.048	0.640
h5	0.522	1.902	0.063	0.050	1.990	2.192	1.816	1.528	0.360
h6	0.571	2.004	0.165	0.250	2.070	2.299	1.168	2.992	0.468
h7	0.529	1.836	0.213	0.125	2.280	2.364	0.720	3.352	0.748
h8	0.592	1.236	0.060	4.710	2.530	2.543	1.704	2.240	3.208
h9	0.562	1.302	0.312	1.290	1.850	2.382	1.976	2.112	2.815
h10	0.616	1.200	0.258	0.525	1.850	2.549	1.944	2.192	1.483
h11	0.860	1.188	0.243	2.985	1.460	2.426	1.904	2.232	4.538
h12	0.535	1.146	0.423	1.895	1.180	2.414	1.872	2.144	3.295
h13	0.641	1.140	0.198	4.595	1.650	2.450	2.456	2.048	3.650
h14	0.322	1.374	0.378	0.930	1.950	2.418	2.632	2.176	5.230
h15	0.181	1.944	0.321	0.260	1.810	2.444	1.896	2.256	4.293
h16	0.214	1.542	0.207	0.535	2.640	2.467	2.072	2.328	3.895
h17	0.781	2.148	0.495	2.125	2.810	2.553	2.080	2.288	3.028
h18	0.764	1.902	0.282	1.025	2.720	2.757	2.016	2.336	1.980
h19	0.426	1.968	0.336	0.140	3.580	3.042	2.720	2.464	1.768
h20	0.426	1.968	0.336	0.140	3.580	3.042	2.720	2.464	1.768
h21	0.496	1.956	0.207	0.210	5.310	3.515	2.672	3.136	3.033
h22	0.561	1.986	0.405	0.480	5.390	3.248	2.488	1.312	5.695
h23	0.554	1.872	0.246	0.195	4.750	3.075	2.432	1.336	4.033
h24	0.578	1.986	0.045	0.100	3.170	2.713	2.088	1.184	1.180



Table A1. Cont.

-	C2	C3	C4	C5	C6	C7	C8	C9	C10
-	C11	C12	C13	C14	C15	C16	C17	C18	C19
h1	0.230	0.585	0.142	0.910	2.783	2.220	0.210	0.360	0.345
h2	0.220	0.765	0.078	0.920	2.411	1.320	0.000	0.525	0.286
h3	0.200	0.585	0.352	0.925	2.548	0.942	0.000	0.534	0.243
h4	0.200	0.675	0.440	1.225	2.313	0.972	0.045	0.636	0.213
h5	0.200	0.660	0.062	1.345	2.288	0.954	0.000	0.444	0.237
h6	1.240	0.570	1.416	1.290	2.426	1.044	0.115	0.462	0.242
h7	1.400	0.900	0.482	1.325	3.239	1.374	0.075	0.477	0.281
h8	1.440	0.630	0.182	1.520	3.798	3.984	0.475	0.450	0.287
h9	1.170	0.765	0.502	1.430	3.097	2.184	0.380	0.504	0.278
h10	1.130	0.645	1.046	1.120	4.371	1.986	0.495	0.579	0.268
h11	1.390	0.555	0.150	1.170	2.994	1.986	1.130	0.573	0.285
h12	1.740	0.630	1.032	1.265	3.763	2.844	0.630	0.498	0.315
h13	1.760	0.615	0.056	1.760	2.999	1.566	0.420	0.600	0.301
h14	1.200	0.570	0.056	2.000	2.759	0.930	0.980	0.540	0.329
h15	0.280	0.750	0.236	1.840	3.807	0.798	0.955	0.357	0.312
h16	0.460	0.555	1.024	1.815	3.317	1.152	0.965	0.423	0.350
h17	3.180	0.825	0.232	2.015	3.214	1.944	0.970	0.588	0.366
h18	2.570	0.780	0.890	2.365	2.940	2.046	0.960	0.570	0.468
h19	2.890	0.780	0.458	2.480	3.445	2.460	1.450	0.678	0.443
h20	2.890	0.780	0.458	2.480	3.445	2.460	1.450	0.678	0.443
h21	3.210	0.630	0.864	2.580	3.278	1.884	1.385	0.753	0.454
h22	3.260	0.570	1.326	2.365	2.475	1.374	1.660	0.621	0.482
h23	2.815	0.720	0.376	2.060	2.073	1.380	1.235	0.750	0.509
h24	1.780	0.570	0.200	1.495	2.769	1.158	0.880	0.390	0.328
-	C20	C21	C22	C23	C24	C25	C26	C27	C28
h1	1.010	0.973	0.636	0.790	0.049	1.266	0.384	0.248	0.006
h2	1.100	1.013	0.484	0.780	0.056	1.194	0.384	0.296	0.000
h3	0.990	0.733	0.448	0.730	0.749	1.056	0.388	0.260	0.000
h4	1.090	0.453	0.460	0.920	1.148	1.032	0.392	0.292	0.000
h5	1.070	0.680	0.520	0.800	1.148	1.014	0.400	0.208	0.000
h6	1.450	0.773	0.512	1.340	1.148	1.020	0.396	0.356	0.048
h7	2.260	0.980	0.428	0.960	1.946	1.122	0.376	0.700	0.035
h8	0.610	1.560	0.368	0.270	1.393	1.116	0.352	0.336	0.038
h9	0.310	1.580	0.408	0.420	1.596	1.110	0.356	0.144	0.000
h10	0.400	1.347	0.408	1.000	2.975	1.110	0.360	0.128	0.001
h11	0.310	1.713	0.668	0.930	1.519	1.242	0.620	0.204	0.019
h12	0.500	1.913	0.412	1.050	2.492	1.260	0.344	0.320	0.127
h13	0.760	3.127	0.344	1.020	1.974	1.266	0.324	0.476	0.014
h14	0.630	2.560	0.428	0.970	1.974	1.260	0.332	0.384	0.005
h15	1.260	1.433	1.068	1.010	2.240	1.206	0.940	0.456	0.061
h16	1.170	2.013	0.424	1.110	2.296	1.134	2.500	0.352	0.022
h17	1.620	4.000	0.448	1.540	1.778	1.140	2.544	2.000	0.020
h18	1.620	1.067	0.468	1.630	1.939	1.260	2.820	0.876	0.057
h19	1.620	1.907	0.436	1.570	1.750	1.296	2.104	1.824	0.000
h20	1.620	1.907	0.436	1.570	1.750	1.296	2.104	1.824	0.000
h21	2.440	2.473	1.092	1.280	1.106	1.212	2.144	0.728	0.102
h22	2.570	2.253	1.484	1.110	1.092	1.194	2.084	0.688	0.103
h23	1.450	1.933	1.364	0.710	1.092	1.194	2.248	0.256	0.133
h24	1.010	1.260	0.880	0.840	0.763	1.176	2.008	0.324	0.036

**Table A2.** Generation load curve of the five prosumers, in kW.

-	C11		C12	C13	C14
h1	P6	P7	P15	P21	P27
h2	0.000	0.000	0.000	0.000	0.000
h3	0.000	0.000	0.000	0.000	0.000
h4	0.000	0.000	0.000	0.000	0.000
h5	0.000	0.000	0.000	0.000	0.000
h6	0.000	0.000	0.000	0.000	0.000
h7	2.070	2.299	4.375	2.361	0.356
h8	2.280	2.627	4.824	2.785	0.700
h9	2.530	3.247	5.385	3.286	1.004
h10	2.592	3.438	5.325	3.329	1.581
h11	2.966	3.642	5.673	3.639	1.735
h12	3.346	3.826	5.769	3.751	1.859
h13	3.509	3.639	5.643	3.735	1.915
h14	3.945	3.863	5.825	3.812	1.984
h15	3.297	3.803	5.704	3.742	1.756
h16	2.994	3.492	5.353	3.461	1.562
h17	2.640	2.877	4.642	2.832	0.915
h18	2.810	2.553	4.276	4.000	2.000
h19	2.720	2.757	4.101	2.237	0.876
h20	0.000	0.000	0.000	0.000	0.000
h21	0.000	0.000	0.000	0.000	0.000
h22	0.000	0.000	0.000	0.000	0.000
h23	0.000	0.000	0.000	0.000	0.000
h24	0.000	0.000	0.000	0.000	0.000

## References

- Huang, J.; Jiang, C.; Xu, R. A review on distributed energy resources and MicroGrid. *Renew. Sustain. Energy Rev.* **2008**, *12*, 2472–2483.
- Pudjianto, D.; Ramsay, C.; Strbac, G. Virtual power plant and system integration of distributed energy resources. *IET Renew. Power Gener.* **2007**, *1*, 10–16. [[CrossRef](#)]
- Hierzinger, R.; Albu, M.; van Elburg, H.; Scott, A.; Lazicki, A.; Penttinen, L.; Puente, F.; Saele, H. *European Smart Metering Landscape Report 2012—Update May 2013*; ÖSTERREICHISCHE ENERGIEAGENTUR—AUSTRIAN ENERGY AGENCY: Vienna, Austria, 2013.
- Kohlhepp, P.; Harb, H.; Wolisz, H.; Waczowicz, S.; Müller, D.; Hagenmeyer, V. Large-scale grid integration of residential thermal energy storages as demand-side flexibility resource: A review of international field studies. In *Renewable and Sustainable Energy Reviews*; Elsevier: Amsterdam, The Netherlands, 2019; Volume 101, pp. 527–547.
- Piti, A.; Verticale, G.; Rottondi, C.; Capone, A.; Lo Schiavo, L. The role of smart meters in enabling real-time energy services for households: The Italian case. *Energies* **2017**, *10*, 199. [[CrossRef](#)]
- Mengelkamp, E.; Notheisen, B.; Beer, C.; Dauer, D.; Weinhardt, C. A blockchain-based smart grid: Towards sustainable local energy markets. *Comput. Sci.-Res. Dev.* **2018**, *33*, 207–214. [[CrossRef](#)]
- Zhang, C.; Wu, J.; Cheng, M.; Zhou, Y.; Long, C. A Bidding System for Peer-to-Peer Energy Trading in a Grid connected Microgrid. *Energy Procedia* **2016**, *103*, 147–152. [[CrossRef](#)]
- Espe, E.; Potdar, V.; Chang, E. Prosumer Communities and Relationships in Smart Grids: A Literature Review, Evolution and Future Directions. *Energies* **2018**, *11*, 2528. [[CrossRef](#)]
- Andoni, M.; Robu, V.; Flynn, D.; Abram, S.; Geach, D.; Jenkins, D.; McCallum, P.; Peacock, A. Blockchain technology in the energy sector: A systematic review of challenges and opportunities. *Renew. Sustain. Energy Rev.* **2019**, *100*, 143–174. [[CrossRef](#)]
- Wu, J.; Tran, N. Application of blockchain technology in sustainable energy systems: An overview. *Sustainability* **2018**, *10*, 3067. [[CrossRef](#)]
- Kim, H.J.; Song, Y.H.; Kim, S.W.; Yoon, Y.T. Implementation of peer-to-peer energy auction based on transaction zoning considering network constraints. *J. Int. Counc. Electr. Eng.* **2019**, *9*, 53–60. [[CrossRef](#)]

12. Liu, T.; Tan, X.; Sun, B.; Wu, Y.; Guan, X.; Tsang, D.H.K. Energy Management of Cooperative Microgrids with P2P Energy Sharing in Distribution Networks. In Proceedings of the IEEE International Conference on Smart Grid Communications (SmartGridComm), Miami, FL, USA, 2–5 November 2015; pp. 410–415.
13. Di Silvestre, M.L.; Gallo, P.; Ippolito, M.G.; Musca, R.; Sanseverino, E.R.; Tran, Q.T.T.; Zizzo, G. Ancillary Services in the Energy Blockchain for Microgrids. *IEEE Trans. Ind. Appl.* **2019**, *55*, 7310–7319. [[CrossRef](#)]
14. Wang, N.; Xu, W.; Xu, Z.; Shao, W. Peer-to-Peer Energy Trading among Microgrids with Multidimensional Willingness. *Energies* **2018**, *11*, 3312. [[CrossRef](#)]
15. Kang, J.; Yu, R.; Huang, X.; Maharjan, S.; Zhang, Y.; Hossain, E. Enabling localized peer-to-peer electricity trading among plug-in hybrid electric vehicles using consortium blockchains. *IEEE Trans. Ind. Inform.* **2017**, *13*, 3154–3164. [[CrossRef](#)]
16. Thakur, S.; Hayes, B.P.; Breslin, J.G. Distributed Double Auction for Peer to Peer Energy Trade Using Blockchains. In Proceedings of the 2018 5th International Symposium on Environment-Friendly Energies and Applications (EFEA), Rome, Italy, 24–26 September 2018; pp. 1–8.
17. Khorasany, M.; Mishra, Y.; Ledwich, G. Design of auction-based approach for market clearing in peer-to-peer market platform. *J. Eng.* **2019**, *2019*, 4813–4818. [[CrossRef](#)]
18. Islam, S.N. A New Pricing Scheme for Intra-Microgrid and Inter-Microgrid Local Energy Trading. *Electronics* **2019**, *8*, 898. [[CrossRef](#)]
19. Leal-Arcas, R.; Lesniewska, F.; Proedrou, F. Prosumers as New Energy Actors. In *Africa-EU Renewable Energy Research and Innovation Symposium*; Springer: Berlin/Heidelberg, Germany, 2018; pp. 139–151.
20. Zhang, C.; Wu, J.; Zhou, Y.; Cheng, M.; Long, C. Peer-to-Peer energy trading in a Microgrid. *Appl. Energy* **2018**, *220*, 1–12. [[CrossRef](#)]
21. El Rahi, G.; Etesami, S.R.; Saad, W.; Mandayam, N.B.; Poor, H.V. Managing Price Uncertainty in Prosumer-Centric Energy Trading: A Prospect-Theoretic Stackelberg Game Approach. *IEEE Trans. Smart Grid* **2019**, *10*, 702–713. [[CrossRef](#)]
22. Bremdal, B.A.; Olivella, P.; Rajasekharan, J. EMPOWER: A network market approach for local energy trade. In *IEEE Manchester PowerTech*; IEEE: Piscataway, NJ, USA, 2017; pp. 1–6.
23. Cali, U.; Fifield, A. Towards the decentralized revolution in energy systems using blockchain technology. *Int. J. Smart Grid Clean Energy* **2019**, *8*, 245–256.
24. Uslar, M.; Rohjans, S.; Neureiter, C.; Pröbstl Andrén, F.; Velasquez, J.; Steinbrink, C.; Efthymiou, V.; Migliavacca, G.; Horsmanheimo, S.; Brunner, H.; et al. Applying the Smart Grid Architecture Model for Designing and Validating System-of-Systems in the Power and Energy Domain: A European Perspective. *Energies* **2019**, *12*, 258. [[CrossRef](#)]
25. Jogunola, O.; Ikpehai, A.; Anoh, K.; Adebisi, B.; Hammoudeh, M.; Gacanin, H.; Harris, G. Comparative Analysis of P2P Architectures for Energy Trading and Sharing. *Energies* **2018**, *11*, 62. [[CrossRef](#)]
26. Long, C.; Wu, J.; Zhang, C.; Cheng, M.; Al-Wakeel, A. Feasibility of peer-to-peer energy trading in low voltage electrical distribution networks. *Energy Procedia* **2017**, *105*, 2227–2232. [[CrossRef](#)]
27. Yu, Q.; Meeuw, A.; Wortmann, F. Design and implementation of a blockchain multi-energy system. *Energy Inform.* **2018**, *1*, 17. [[CrossRef](#)]
28. Paudel, A.; Chaudhari, K.; Long, C.; Gooi, H.B. Peer-to-Peer Energy Trading in a Prosumer-Based Community Microgrid: A Game-Theoretic Model. *IEEE Trans. Ind. Electron.* **2018**, *66*, 6087–6097. [[CrossRef](#)]
29. Aldaouab, I.; Daniels, M.; Ordóñez, R. MPC for Optimized Energy Exchange between Two Renewable-Energy Prosumers. *Appl. Sci.* **2019**, *9*, 3709. [[CrossRef](#)]
30. Hou, P.; Yang, G.; Hu, J.; Douglass, P.J.; Xue, Y. An Interactive Transactive Energy Mechanism Integrating Grid Operators, Aggregators and Prosumers. *arXiv* **2019**, arXiv:1912.07139.
31. Amanbek, Y.; Tabarak, Y.; Nunna, H.K.; Doolla, S. Decentralized Transactive Energy Management System for Distribution Systems with Prosumer Microgrids. In Proceedings of the 19th International Carpathian Control Conference (ICCC), Szilvasvarad, Hungary, 28–31 May 2018; pp. 553–558.
32. Nizami, M.S.H.; Hossain, M.J.; Amin, B.M.R.; Kashif, M.; Fernandez, E.; Mahmud, K. Transactive Energy Trading of Residential Prosumers Using Battery Energy Storage Systems. In Proceedings of the 2019 IEEE Milan PowerTech, Milan, Italy, 23–27 June 2019; pp. 1–6.
33. Le Cadre, H.; Jacquot, P.; Wan, C.; Alasseur, C. Peer-to-Peer Electricity Market Analysis: From Variational to Generalized Nash Equilibrium. *Eur. J. Oper. Res.* **2020**, *282*, 753–771. [[CrossRef](#)]

34. Neagu, B.C.; Grigoras, G.; Ivanov, O. An Efficient Peer-to-Peer Based Blockchain Approach for Prosumers Energy Trading in Microgrids. In Proceedings of the International Conference on Modern Power Systems (MPS), Cluj Napoca, Romania, 21–23 May 2019; pp. 1–4.
35. Barrero-González, F.; Pires, V.F.; Sousa, J.L.; Martins, J.F.; Milanés-Montero, M.I.; González-Romera, E.; Romero-Cadaval, E. Photovoltaic Power Converter Management in Unbalanced Low Voltage Networks with Ancillary Services Support. *Energies* **2019**, *12*, 972. [[CrossRef](#)]
36. All You Need to Know to Become a prosumer. Available online: <https://energyindustryreview.com/renewables/all-you-need-to-know-to-become-a-prosumer/> (accessed on 18 December 2019).
37. National Regulatory Authority for Energy. *The 228 Order for the Approval of the Technical Norm Technical Conditions for Connection to the Public Electrical Networks of the Prosumers*; National Regulatory Authority for Energy: Bucharest, Romania, 2018.



© 2020 by the authors. Licensee MDPI, Basel, Switzerland. This article is an open access article distributed under the terms and conditions of the Creative Commons Attribution (CC BY) license (<http://creativecommons.org/licenses/by/4.0/>).

Article

# New Market Model with Social and Commercial Tiers for Improved Prosumer Trading in Microgrids

Bogdan-Constantin Neagu <sup>\*</sup>, Ovidiu Ivanov , Gheorghe Grigoras , Mihai Gavrilas and Dumitru-Marcel Istrate

Department of Power Engineering, Gheorghe Asachi Technical University of Iasi, 700050 Iasi, Romania; ovidiuivanov@tuiasi.ro (O.I.); ggrigor@tuiasi.ro (G.G.); mgavril@tuiasi.ro (M.G.); mistrate@tuiasi.ro (D.-M.I.)

\* Correspondence: bogdan.neagu@tuiasi.ro; Tel.: +40-232-70-11-10

Received: 13 August 2020; Accepted: 2 September 2020; Published: 4 September 2020



**Abstract:** In the deregulated electricity markets, trading prices are determined by the offer-demand mechanism, and retail consumers can negotiate tariffs with their supplier of choice. For classic wholesale suppliers, the tariffs are determined by the prices of transactions performed on the wholesale market. In parallel with becoming eligible for participating in the market, the consumers use increasingly local generation sources based mostly on renewable electricity generation equipment such as Photovoltaic (PV) panels, and become prosumers. They want to be able to sell back to the market the generation surplus, in order to obtain the maximum benefits from their initial investment. This paper proposes a two-tier local market model oriented for prosumers and consumers connected in microgrids, based on the blockchain technologies and other technologies and concepts such as smart grids, crowdsourcing and energy poverty. Its goals are to improve the possibilities of local prosumers to sell electricity to local consumers and to increase their profitability, compared to the trading model often used in developing markets, of selling the surplus back to the grid via aggregators. The research aims to contribute to the sustainable development of the electricity sector using new and renewable sources of energy, state-of the art technologies and smart contracts, leading to prosumer proliferation and electricity cost reduction for consumers.

**Keywords:** local electricity market; smart grids; energy crowdsourcing; renewable energy sources; prosumers; blockchain technology; energy poverty; smart contracts

## 1. Introduction

The European Commission's strategic framework envisages an improved and modernized European energy market, aimed at creating secure, sustainable, accessible and decentralized energy networks in response to the global challenge of greenhouse gas emissions [1]. In the context of the next generation of digital energy networks, and in the presence of multiple decentralized microgrids, managing the energy generation from various and complementary sources will result in gaining more flexibility in meeting demand and lowering costs for the community. The adoption of a decentralized electricity distribution network, in which ordinary consumers can also be energy producers, named 'prosumers', and can sell their surplus generation to the network, thus getting involved in market transactions inside a community represents an alternative to current traditional networks. It is expected that an increasing number of end-users will want to become active in the electricity sector, which will lead to a large number of transactions. A possible tool for enabling the creation of such microgrid-level markets is the blockchain technology which could provide secure and reliable means of communication and data management between the end-users [2].

Blockchain technology was created as a solution to the problem of mistrust and data security. The first steps in the development of the technology were taken in 1991, when Stuart Haber and

W. Scott Stornetta first spoke about a cryptographically secure blockchain [3]. In 1993, together with Dave Bayer, they integrated optimal Merkle type trees in the concept [4]. Following the financial crisis of 2008, the concept of blockchain as a distributed database was developed, proposing a solution to change the way monetary transactions are carried out through various financial institutions. With the help of a peer-to-peer (P2P) communications network and a distributed data server, a blockchain database can be autonomous [5].

In the recent years, billions of dollars have been invested in research on blockchain technology in an attempt to make the most of its potential and understand how appropriate it is in the different economic domains [6]. But not all domains are fully ready to assimilate the blockchain technology. In each particular case, the current technological opportunities must be analyzed, as well as the challenges that the end-users face and how a new decentralized architecture could create value for them. The electricity industry is an extremely suitable candidate for blockchain technology-based innovation, with its complex supply chain that requires transparency and improved data processing and its highly transactional trading market that would gain advantage from faster settlement. The transparency and immutability of the blockchain can empower end-users of this industry and consumers.

A blockchain system is primarily based on a decentralized ledger of transactions that take place in a network. This network consists of nodes owned by independent entities that use a cryptographic protocol to validate the transactions that are entered in the ledger and to ensure that the entered data cannot be altered or changed. It is immutable, secure and completely transparent. Fully decentralized and replicated to node level, blockchain networks are harder to penetrate and manipulate by dangerous entities.

The blockchain system, coupled with other innovative technologies such as smart grids, big data mining and remote sensing, has the potential to provide solutions to various challenges in the energy sector and to contribute to the achievement of energy efficiency objectives, including to compensate for the funding gap for various projects in the field [7]. The technologies regarding blockchain-based platforms will lead to fundamental changes that will require the involvement of the distribution and supply companies, manufacturers of equipment, regulators and, last but not least, end-users [8,9].

A review of renewable and sustainable energy published in [6] provides a thorough analysis of more than 140 blockchain research projects and startups in the energy sector, from countries belonging all around the world. The electricity sector has a high potential to implement the blockchain technology as part of addressing several challenges [7,10,11]:

- Climate change. The need to integrate in existing electricity distribution systems renewable energy sources (RES) has led to the development of technologies such as PV panels and wind turbines, whose costs are constantly decreasing. The consumers who choose to install such generation sources become prosumers, which presents a challenge for the current structure of electricity networks. They can create technical difficulties for the Distribution Network Operators (DNOs) in ensuring the energy balance. However, electricity generation at the household level (classically with PV panels on the roof) is a great opportunity for the development of blockchain technology-based architectures, because it capitalizes on the distributed nature of electricity generation with unprecedented efficiency.
- The development of technologies that allow the transition to active distribution networks. The technological solutions refer to the communications and networking components, inverters, bidirectional smart metering systems, energy storage solutions. This evolution allows greater control at network level. Electricity becomes a controllable, storable and easily quantifiable product, suitable for trading through smart contracts.
- The creation of energy communities managed by local energy production cooperatives formed by community members. The microgrids which integrate the blockchain technology can represent a solution for connecting the poorest consumers to cleaner and cheaper energy, but also for energy savings and more responsible and accessible consumption. In some EU member states, European Federation of Renewable Energy Cooperatives (REScoop) have explicitly set social goals, such as

reducing energy poverty. They meet those objectives by developing solidarity schemes aimed at lowering the energy bills of vulnerable members, providing them with services and training in reducing consumption. They also use the gains from RES energy generation to increase the living standards of vulnerable and low-income households.

- Simplifying the architecture of the current trading models. The implementation of a blockchain-based prosumer network leads to the elimination of a large number of intermediaries in the electricity trading process.

Among the technical advantages of this technology can be underlined the following: better management of power generation, fewer hours of supply interruption, secure energy transactions, increased distributed generation. The main economic advantages refer to protecting the identities of the traders, creating a distributed economy, reducing the tax burdens, data protection and control, and compensation for producers [12,13].

Another concept that can be associated with local electricity trading in microgrids is the mitigation of energy poverty. 'Energy poverty' can be defined as the lack of access to clean, renewable, affordable energy, which leads to costly energy bills [14]. The concept lies at the intersection of energy sustainability and social issues mitigation, being characterized by three realities: high energy prices, low or stagnating incomes, and energy inefficient homes in urgent need of renovations.

The mitigation of energy poverty can be achieved using crowdsourcing, a concept first introduced in 2005 by James Surowiecki [15], which can be defined as utilizing contributions from peers and the collective wisdom of the crowd to alleviate a problem. It can also be an effective approach to enable the crowd to provide a service in a community within a limited geographical area by using smart metering [16].

In Romania, according to Order 228/28.12.2018 published by ANRE (Romanian Energy Regulatory Authority), the prosumers can trade electricity generated from renewable sources such as photovoltaics (PV), biomass, wind, cogeneration. The suppliers are bound to buy the surplus at the weighted average day-ahead market price from the previous year [17], with the advantage of the exemption from the payment of the distribution network tariff. This trading system is the most basic, limiting the options of both parties [18]. More advanced trading models should be considered to increase the benefits of the prosumers and consumers who trade electricity in a local market organized at the microgrid or community level.

Usually, in classic wholesale electricity markets, electricity is traded using bilateral contracts with negotiated prices, for long periods (years, months, weeks). This trading manner helps to reduce the prices for the buyers, and provides stability and predictability for the producers. For shorter trading intervals, such as in the day-ahead (SPOT) markets, the merit order price setting mechanism is preferred, which ensures maximum benefits for producers when the demand is high and can lead to higher prices for suppliers and end-users.

On the other hand, the electricity quantities traded in local grids by prosumers are much smaller, and the trading intervals need to be smaller, because of renewable generation uncertainty. At the same time, the generation from prosumers needs to be incentivized to promote the proliferation of renewable electricity. Thus, a market model for microgrids should take into consideration creating advantages simultaneously for prosumers and consumers.

In this regard, the paper presents a new trading approach for prosumers that uses the blockchain technology for creating a local market at microgrid level, forecasts for consumer buy offers, obtained using technologies such as remote sensing tools, and the energy crowdsourcing concept for energy poverty mitigation. The proposed model takes as reference the trading model for excess prosumer generation used in Romania and applicable to developing markets, which consists in selling back the available electricity at fixed tariffs back to the grid. The authors propose a diversification of the trading methods and settlement procedures by creating a local trading mechanism intended to provide flexible market model that can be adapted to specific microgrid conditions and rules agreed at the community level. The proposed market model has two trading levels. The primary level is

intended for main trading. The secondary, two-tier market is designed by the authors for increasing the prosumer profitability and lowering consumer electricity cost while accommodating particular scenarios that can arise in real conditions. The considered scenarios are: mitigating energy poverty for vulnerable consumers, selling remaining prosumer surplus to consumers who do not participate in the primary market but have bilateral contracts with certain prosumers, allowing occasional access to the market in exchange for a tariff, and reducing the effect of erroneous consumer buy offers caused by inaccurate forecasts or temporary unusual consumption patterns. The primary market model offers two trading alternatives: ‘first-come-first-served’ (FCFS), and merit-order (MO). The secondary market proposes two tiers with three trading methodologies, which can be optionally used, in number and order, according to the specific needs of particular microgrids: energy poverty mitigation, tariff access and invite access. The proposed alternatives are tested in a case study, on an existing low voltage (LV) electricity distribution network from Romania which has microgrid characteristics, in order to assess the effects of the chosen trading methods on the profits achieved by prosumers and consumers.

The proposed market model provides flexible tools for incentivizing the sustainable development of local communities based on environment protection and economic and social inequality mitigation through the use of modern technology tools, by encouraging local trading of electricity generated from renewable, clean primary sources.

The results of the case study show that by using the local trading mechanisms designed for the primary and secondary markets, the prosumers can sell more electricity, at lower prices for the community and better individual profit. If the benefits are consistent, this can lead to the increase of distributed generation sources in microgrids, thus a more sustainable development of the electricity generation sector.

By lowering consumer prices, the sustainable economic and social development of communities is also encouraged. Not least, these goals are envisioned to be achieved by obtaining in parallel the modernization of the electricity distribution infrastructure, by using smart grid communication and energy management tools and involving digital instruments (specialized trading software and blockchain).

The remainder of the paper is structured as follows. Section 2 presents a literature review regarding the research proposed in the paper. Section 3 describes the proposed market model for microgrids. In Section 4 are presented the results of the case study, with a comparison between the proposed trading strategies, outlining their particularities. The paper ends with the sections dedicated for discussions and references, and annexes.

## 2. Literature Review

Recent studies have considered combining the operation of small-scale renewable energy sources (SSRES) in distribution networks and deregulated electricity markets. The range of these studies is covering unit commitment [19] and economic dispatch problems [20], in addition to scheduling of SSRES [21], and the uncertainty of renewable generation [22]. The main trends and approaches currently described in the literature are briefly summarized in the following paragraphs.

As it was presented in the introduction section, in Europe there are currently over 3400 green energy cooperatives (REScoop). In accordance with [23–26], the REScoop notion is defined in EU directives as “local energy communities”, according to data from the Federation of Green Energy Cooperatives in Europe. More than one million European citizens are participating in REScoops to invest together in the transition from fossil fuels to clean primary energy resources and energy efficiency. In Romania, starting in 2020, the first established REScoop proposes that future members who generate energy (prosumers) will be able to sell the surplus to other members, rather than to an aggregator, following the concept of ‘prosumer-friendly’ [27].

In another perspective, paper [28] considers a P2P electricity trading method using a private Ethereum blockchain ledger where all bids are encrypted for anonymity and peer matching is done by a functional encryption-based contract.



Regarding the energy crowdsourcing in prosumer-enabled electrical networks, a small number of published papers is available in the literature [16,29]. The existing studies consider a two-stage algorithm for minimizing the cost of generation and the energy losses by prior rescheduling of user loads and SSRES.

In other work, a particular local energy market model was considered in [30], which integrates different P2P energy trading platforms based on unidirectional market clearing price (MCP) for a microgrid. Moreover, the settlement considers an MCP or P2P mechanism.

The future active distribution network (ADN) is a P2P community based on active energy agent (AEA) users [31]. The maximization of social welfare in local prosumer generation trading with an auction-based mechanism is used in [32]. The same first author considers that in a microgrid the energy flows in a transactive way and the transactions are based on bilateral contracts between peers [33]. Another concept of prosumer surplus trading based on the transactive energy concept is proposed in the literature [34–37]. Paper [34] uses a Stackelberg game-based method for solving the transactive energy problem, in which the DNO and the SSRES aggregators are participating simultaneously in the Local Electricity Market (LEM) and Wholesale Electricity Market (WEM). A comprehensive cost–benefit model for prosumer load sharing was proposed in [35], using game theory and considering non-cooperative game models of the microgrids for prosumers energy surplus. In the same context, a particular social welfare-based concept on transactive energy or demand response (DR) is applied in [36,37] using negotiated prices.

Another way to trade surplus are DR programs, whereby the LEM operators play a vital role in managing the exchange of data, to ensure the notification flow between balancing authorities, service companies and end-users. First, the microgrid operator assesses the electricity consumption patterns based on the structure of variable electricity tariffs and prices to establish trading plans. They also sign bilateral P2P contracts with end-users to take direct control of specific energy assets [38]. This information is aggregated to create commitment portfolios—load reduction schedules that are provided to network operators in exchange for compensation commensurate with the size of the capacity involved [39]. In the event of a system emergency or demand, the DSO shall request the aggregator to reduce or increase a portion of the contracted portfolio. For this reason, the aggregator receives additional compensation which can take the form of tariff reductions, incentive payments and invoice credits.

Using online platforms [40–46], the consumers can become prosumers who create and distribute their own information about the energy generation. Some authors proposed a demurrage mechanism (DM) and Home Energy Management (HEM) for prosumers' energy surplus in an LEM based on blockchain [41]. A particular P2P business model for 48 residential prosumers with PV panels installed in a Swedish village is proposed in [42]. This article identifies some new potential opportunities for optimizing the LEM and its variables for the best gain, taking into account that a significant influence is represented by the integration of energy demand, generation supply, and LEM rules. The aforementioned study can be used to provide information for regulatory bodies to create a fair, useful and cost-effective P2P electricity trading framework for prosumers. Another comprehensive platform for prosumers' digitalization was recommended in [43], and market simulations are developed in [44,45] for consumers integration in microgrids. In the same manner, a virtual platform was proposed in [46] for efficient management of multiple energy prosumers (MEP).

The presence of decentralized energy sources demands the analysis of the problem of continuity of energy supply to operators whose activities significantly depend on electricity. There are EU countries where power outages amount to about 20 min per year, but in other cases the average power outages range from 450 to 500 min [47]. Prosumers' microinstallations ensure the business continuity for producers in such countries and negotiated surplus trading increases social welfare [48]. Because the SSRES efficiency depends on atmospheric conditions and regional climate, even minor temporary changes in weather conditions can cause significant variability in power generation at different time and space scales. Methodologies based on the remote sensing of atmospheric conditions are the primary

source of information for the development of numerical forecasting models that support the planning and operation of power systems in the presence of intermittent energy sources [49]. For local trading of such electricity surplus, the LEM operators consider the blockchain concept [11,12,16,28,29,40,41,48] or direct bilateral contracts [50,51]. These market models aim to provide secure and affordable energy supply for the end user, which is essential for the functioning of an economy in which energy poverty is reduced and the needs of vulnerable social groups are taken into account [52–54]. Social welfare is obtained by the authors in [53], where the smart P2P contracts are considered as a distributed optimization problem, solved with a virtual aggregator based on the Alternating Direction Method of Multipliers (ADMM). All the LEM actions can be completed by the peers who do not necessarily trust each other through an agreement algorithm which defines the speed of the transactions. One of the most used algorithms is the Proof-of-Work (PoW) [55]. Nonetheless, previous articles about energy sustainability have paid limited attention to prosumer engagement, management and administration. For example, according to [56,57] each of the providers can have a proper trading platform with specific architecture for sustainable planning of the local microgrid or region.

From other perspectives, the prosumer surplus trading process based on the specific transactive energy microgrids are examined by the researchers in [58–60]. The prosumers' aggregation to one group with the same interest based on virtual microgrids is analyzed by the authors in [61] for bill cost reduction as a particular energy poverty mitigation or social welfare. The aforementioned problem can be solved in smart buildings by using ADMM for energy sharing between the players, as is shown in [62,63].

In [64] remarkable directions for cost-effective use of digital cryptocurrencies in smart grid dynamic management are thoroughly explained to cover the challenging viewpoints of blockchain technology. The LEM is favorable for prosumers because the participation of the before-mentioned players is concrete in the purchase of energy surplus, but the revenues from the surplus traded are proportional between sellers [65]. Common consumers do not produce electricity and are only active in the purchasing process [66]. The load flexibility can change the trading offers. Other perspectives consider peak loads in the prosumer's vicinity with smart P2P subscribed capacity prices in [67], or the crowdsourcing concept for surplus energy planning or sharing, as is used in [68], or considering the indispensable local energy storage systems [69].

The main concepts taken from the literature and discussed above are compared with the market model proposed in the paper, in Table 1. In addition, the last column considers the type of settlement used in the market.

The objective of the local market is to enable an overlay social network of smart devices that facilitates the communication and trading process between players from LEM, prosumers, consumers and microgrid. They should share a common goal, such as optimal energy management, taking into account that the solution with local energy storage systems (as is battery banks) is too expensive [70,71], and without technical possibility for energy poverty mitigation.

**Table 1.** A comparison between the proposed model and the literature state-of-the-art survey.

Reference No.	Blockchain	P2P Contracts	Energy Crowdsourcing	REScoop	Energy Poverty	Settlement Procedure
[16,29]	Yes	Yes	Yes	No	No	Negotiated
[28]	Yes	Yes	No	Yes	No	Negotiated
[24,25,44,49,57]	No	No	No	Yes	No	Negotiated
[26,27]	Yes	No	No	Yes	No	Negotiated
[30–32,35,38,42,56,60,65]	No	Yes	No	No	No	Negotiated or MCP

Table 1. Cont.

Reference No.	Blockchain	P2P Contracts	Energy Crowdsourcing	REScoop	Energy Poverty	Settlement Procedure
[33,34,36,37,43,45]	No	No	No	No	No	Negotiated
[39,46,50,51,69,71]	No	Yes	No	Yes	No	Negotiated or MCP
[40,41,54,58,59]	Yes	Yes	No	No	No	Negotiated
[53]	Yes	Yes	No	No	Yes	Negotiated
[48,55,64]	Yes	No	No	No	No	Negotiated
[61,66]	No	No	No	No	Yes	Negotiated or MCP
[62,63]	No	Yes	No	No	Yes	Negotiated
[68]	No	Yes	Yes	No	No	Negotiated
Proposed model	Yes	Yes	Yes	Yes	Yes	Negotiated and MCP

### 3. Materials and Methods

In LV electricity distribution networks or local microgrids, there is an increasingly larger number of residential consumers who are opting to install local generation resources to gain independence from the grid. The predominant choice is the use of PV panels systems that are easier to install at household residences and provide energy by converting the solar irradiation into electricity. This trend is incentivized by the subsidies offered by governments worldwide. As the number of individual houses adopting this technology increases, new opportunities arise regarding the trading models used for selling the excess generation. Residences become prosumers, entities capable of consuming, producing and selling electricity. The prosumers will use their own generated electricity mainly to cover their individual consumption and when the generation exceeds this amount, they will sell the surplus to the grid. The simplest method of surplus trading is to sell the entire available quantity back to the supplier, though an aggregator entity, at a regulated price. However, this is the least profitable approach, as the regulated prices are usually low [72], and the benefits can be seen only by the suppliers/network operators, and the prosumers. New trading methods for microgrids are currently envisioned in the literature, aiming to create local electricity markets that would provide benefits for all the players involved (aggregators, prosumers and consumers). A main requirement for implementing such initiatives is the conversion of the classic electricity distribution infrastructures into intelligent or smart grids, capable of real-time communication between the supply and consumer buses, and centralized operation management and data processing at microgrid level.

In line with these trends, previous research efforts by the authors, published in [40], proposed an algorithm for prosumer surplus transactions at the microgrid level, using P2P contracts and blockchain technology. The market mechanism considers trading priorities set at central level and based on consumer or prosumer prices, or custom priorities determined by the prosumer–consumer geographical distances and the ‘first-come-first-served’ (FCFS) principle.

This paper extends the previous research considering an improved and extended market model, with two trading phases (primary and secondary). The basic flowchart of the proposed market model is depicted in Figure 1.

The primary market includes the blockchain approach from [40] and adds a supplementary trading method based on the merit order used in wholesale markets. These methods can be used as alternatives for trading.

A second market segment, with two tiers, is proposed to help the prosumers and consumers to better manage the sell and buy offers that can be affected by errors. Crowdsourcing and energy poverty mitigation are used for this purpose.

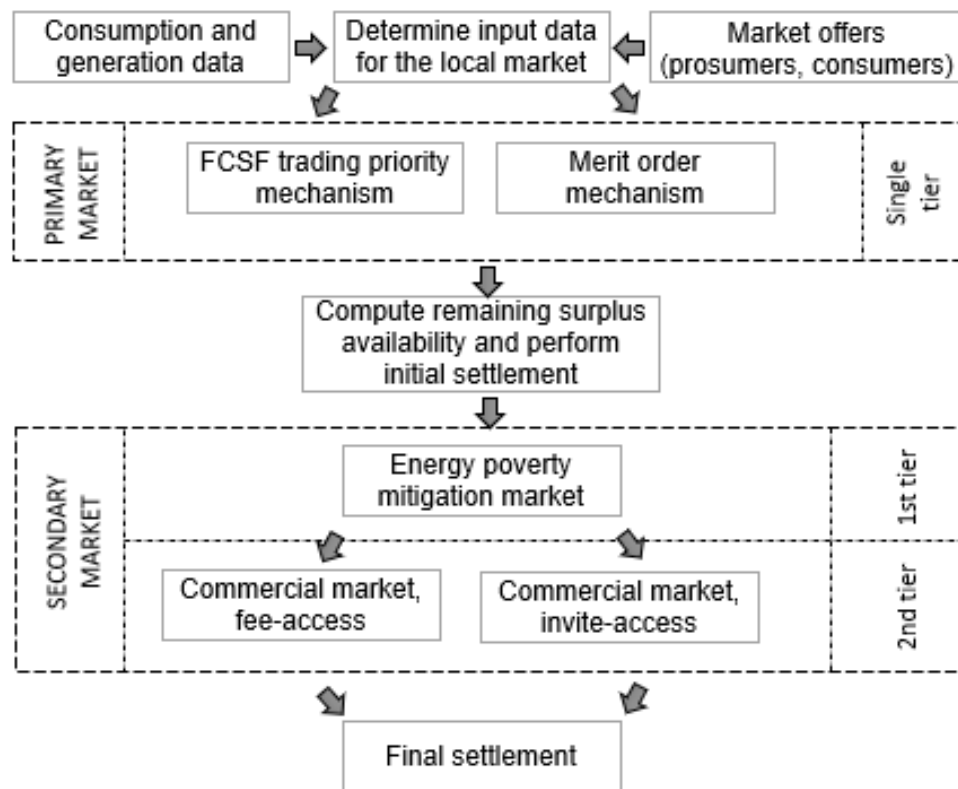


Figure 1. The basic diagram of the proposed market algorithm.

The sell offers are the result of the surplus that the prosumers can generate but cannot use locally. The newly proposed algorithm provides market mechanisms designed to alleviate these problems.

The buy offers placed by the consumers in the local market are usually the result of forecasts made with variable precision. In the case of trading electricity obtained from PV panels, the forecasts must consider weather data obtained with technologies such as remote sensing and big data mining.

The following general assumptions are made:  
 • The prosumer and consumer selling and buying offers are managed by the local non-profit aggregator using two possible market mechanisms integrated in a blockchain trading system: mismatches between the needed and traded quantities.

In the Romanian market model, when the electricity acquired from the local market is less than the demand, the consumers would buy the rest at higher prices from the national grid, and the generators would be forced to sell any surplus to the aggregator at a lower price.

A secondary market with a two-tier trading mechanism for minimizing the imbalance between the offers placed in the blockchain system and the actual traded quantities.

On the other hand, if trading is performed in a local market, when the consumers forecasts are higher than the actual demand, the buyers would be forced to sell the excess quantities to the aggregator if sufficient and cheap storage facilities are not available.

The primary market can use two alternative price-setting methods based on blockchain technology: the 'first-come-first-served' (FCFS) method or the merit-order method used in traditional day-ahead markets.

The newly proposed algorithm provides market mechanisms designed to alleviate these problems.

The following general assumptions are made:

- The secondary market provides two optional trading tiers:
  - The energy poverty mitigation tier, aimed at low-income consumers who otherwise could not afford to participate in the market.
  - The commercial tier, with two options, aimed for expanding the market through crowdsourcing with two types of consumers: those participating occasionally, in exchange for a fee, and consumers who do not participate directly with offers but are represented (invited) in the market by other consumers.
- For the invite option of the commercial tier, any consumer  $G_i$  can acquire electricity from the second market layer only if has signed previously a P2P contract with a specific prosumer  $P_i$ .
- The selling price of a prosumer or consumer can vary hourly, but in the paper is set constant for all trading intervals. This approach is modelling the practice used for traditional differentiated tariffs where the peak and night prices are outside the hours when PV panels can generate electricity, and the case where no storage capabilities are installed in the network. Electricity is

- The energy poverty mitigation tier, aimed at low-income consumers who otherwise could not afford to participate in the market.
- The commercial tier, with two options, aimed for expanding the market through crowdsourcing, with two types of consumers: those participating occasionally, in exchange for a fee, and consumers who do not participate directly with offers but are represented (invited) in the market by other consumers.
- For the invite option of the commercial tier, any consumer  $C_i$  can acquire electricity from the second market layer only if has signed previously a P2P contract with a specific prosumer  $P_j$ .
- The selling price of a prosumer or consumer can vary hourly, but in the paper is set constant for all trading intervals. This approach is modelling the practice used for traditional differentiated tariffs where the peak and night prices are outside the hours when PV panels can generate electricity, and the case where no storage capabilities are installed in the network. Electricity is sold on the market for the surplus intervals, and settlement is performed at the end of each trading interval.
- If the local surplus exceeds the demand traded in the market, the surplus will be sold to the aggregator/market administrator, at regulated tariffs.
- The secondary two-tier market components are optional, but the case study considers all the available options, in order to better demonstrate the advantages of the proposed trading algorithm.

### 3.1. Input Data for the Local Market

The input data required for trading consist of the quantities and prices associated with the consumption and local generation measured in the market. This information is provided in six matrices:  $C = C(h, i) \in \mathbb{R}^{nh \times NCM}$ ,  $CO = CO(h, i) \in \mathbb{R}^{nh \times NCM}$  and  $PCO = PCO(h, i) \in \mathbb{R}^{nh \times NCM}$  for consumption quantity, offers and price offers, and  $G = G(h, j) \in \mathbb{R}^{nh \times NPM}$ ,  $GO = GO(h, j) \in \mathbb{R}^{nh \times NPM}$ ,  $PGO = PGO(h, j) \in \mathbb{R}^{nh \times NPM}$  for generation quantity, offers and price offers, where  $NCM$  and  $NPM$  are the number of consumers and prosumers participating at hour  $h$  in the market. It is considered that generally  $NCM < NC$  and  $NPM < NP$ ,  $NC$  and  $NP$  being the number of consumers and prosumers connected in the microgrid.

Trading in the primary market can occur at any hour  $h$  when there are consumer buying offers placed in the blockchain system (1), and there is generation surplus offered for selling (2).

$$\sum_{i=1}^{NCM} CO(h, i) > 0 \quad (1)$$

$$\sum_{j=1}^{NPM} GO(h, j) > 0 \quad (2)$$

Surplus occurs when the local generation of a prosumer exceeds its individual consumption (3) and the surplus is traded in the market (4).

$$S(h, j) = G(h, j) - C(h, j), \quad j = 1..NPM \quad (3)$$

$$S(h, j) \Rightarrow GO(h, j) \quad (4)$$

The consumer quantity offers for the primary market use two types of representation:

- as actual consumption value measured in [W], when the price is set according to the blockchain priority model, as in [40];
- as a multiple of 100 W for the price setting according to the day-ahead merit order model used in wholesale markets.

The prosumers can choose to sell their surplus directly to the aggregator for a fixed regulated tariff, or in the primary local market. In the paper, it is considered that all the available surplus is traded through sell offers placed in the market blockchain system.

The secondary market is activated at any hour  $h$  when at least one of the following conditions is fulfilled:

- The sum of the buy offers is lower than the aggregated offers placed by the prosumers, i.e., the prosumers need to sell the remaining surplus:

$$\sum_{i=1}^{NCM} CO(h, i) < \sum_{j=1}^{NPM} GO(h, j) \tag{5}$$

- The buy offer of a consumer  $i$  is greater than the actual consumption because of the forecast error or representation model used in the market (multiple of 100 kW).

Sustainability 2020, 12, x FOR PEER REVIEW 10 of 43  
 $CO(h, i) > TCO(h, i), i = 1..NCM \tag{6}$

where  $TCO(h, i)$  is the quantity of electricity actually traded by the consumer  $i$  at hour  $h$ , which can be equal to or less than the offer placed on the market.

### 3.3.2. The Primary Market

This market segment is the main trading tool for the prosumers and consumers in the microgrid. As outlined previously, two alternatives are provided for determining the consumer and prosumer trading priority: 'first-come-first-served' and merit order. Both methods use the consumer (buy) and prosumer (sell) offers placed in a centralized secure and anonymous blockchain system established at the microgrid or market level. The blockchain system is preferred because it guarantees trading fairness, all players being unaware of the offers placed by others, thus minimizing the risk of market manipulation.

Another assumption used in the paper is that, by means of an automated system comprising smart metering, two-way communication and continuous monitoring at the microgrid level, the algorithm has immediate access to measured and forecasted data at consumer and prosumer buses. For examining the possible effects on trading, two consumer offer mechanisms are considered:

- Consumers place on the market buy offers for the entire consumption at hour  $h$ , in order to minimize their electricity bill by attempting to buy the maximum quantity of electricity from the local market, at lower prices, rather than from the main grid, at higher prices.
- Consumers place on the market buy offers determined by forecast techniques using big data analysis or remote sensing techniques.

The first type of offer is used in the FCFS trading method, where a generic consumer  $i$  places fixed-price-per-kWh and variable quantity offers, the trading order being determined by the time tag of the offer. The quantities for these offers are determined in the settlement phase, based on consumption measurements taken from the microgrid. The flowchart of this trading method is given in Figure 2.

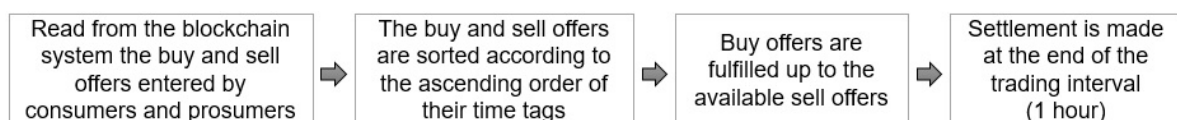


**Figure 2.** The basic diagram of the primary market first-come-first-served trading mechanism.

The second type of offer is used in the merit order trading mechanism. The buy offer prices and quantities are placed in the blockchain system by the consumers before the trading interval. Quantities are given as multiples of 100 W and prices are given for each kWh. The flowchart of this trading method is given in Figure 3. The trading order and price are determined by the standard merit-order price method, provided in Figure 4, where the trading price is determined as the market clearing price (MCP).

For both methods, the prosumer sell offers are given as the full available surplus  $S(i, h)$ , in kWh.

Quantities are given as multiples of 100 W and prices are given for each kWh. The flowchart of this trading method is given in Figure 3. The trading order and price are determined by the standard merit-order method, provided in Figure 4, where the trading price is determined as the market clearing price (MCP).

For both methods, the prosumer sell offers are given as the full available surplus  $S(i, h)$ , in kWh.

The maximum amount of traded electricity  $TC$  is determined by the minimum between the aggregated buy and sell offers:

$$TC = \min \left( \sum_{i=1}^{NCM} CO(h, i), \sum_{j=1}^{NPM} GO(h, j) \right) \quad (7)$$

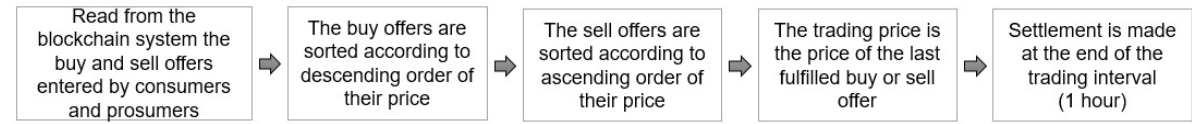


Figure 3. The basic flowchart of the primary market merit-order trading mechanism. 11 of 43

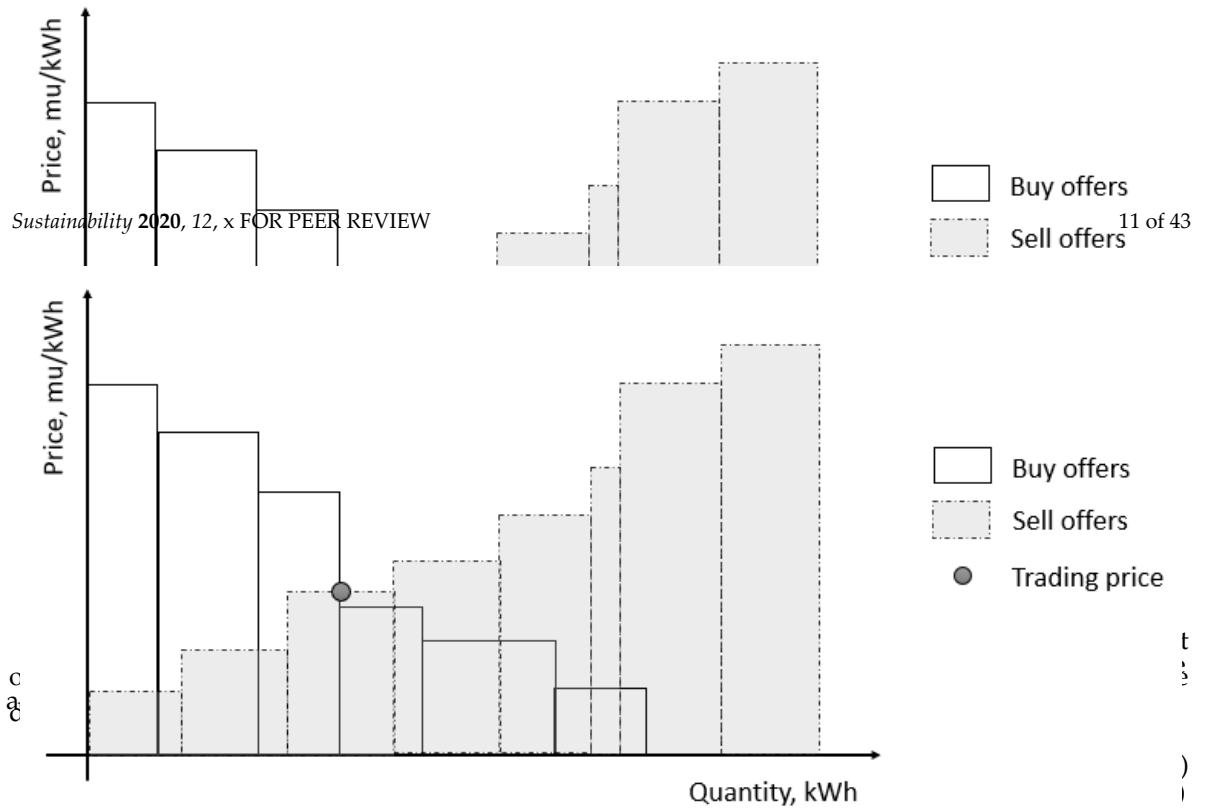
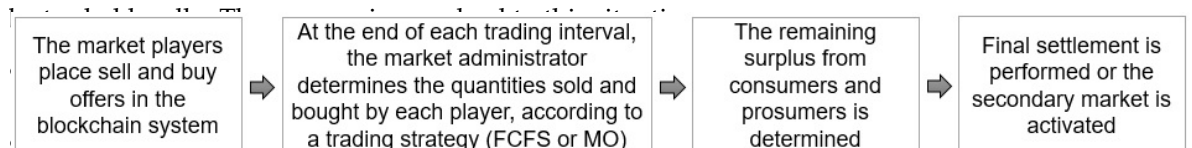


Figure 4. The merit-order trading mechanism. 11 of 43

The settlement price of each transaction is given by the amount of the remaining surplus from consumers and prosumers. The market administrator determines the quantities sold and bought by each player, according to a trading strategy (FCFS or MO). The trading price is determined by the market clearing price (MCP).

$$TP(h, t) = C(h, t) \cdot P(h, t) \quad (8)$$

Figure 5. The flowchart of the primary market trading algorithm. 11 of 43



offers are the  $S(h, i)$  quantities. This leads to  $S(h, i)$  fractions that cannot be fulfilled. The trading mechanisms used in the primary market can lead to electricity quantities that cannot be traded locally. Three scenarios can lead to this situation:

- At given hours the total local generation available in the market (sell offers) exceed the total consumption (buy offers).
- If the merit-order method is used, the buy offers are given as multiples of 100 W, while the sell offers are the  $S(h, i)$  quantities. This leads to  $S(h, i)$  fractions that cannot be fulfilled.
- The consumers place in the market buy offers that exceed their real consumption, following forecast errors or significant accidental deviations from the daily demand pattern.

- At given hours, the total local generation available in the market (sell offers) exceed the total consumption (buy offers).
- If the merit-order method is used, the buy offers are given as multiples of 100 W, while the sell offers are the  $S(h,i)$  quantities. This leads to  $S(h,i)$  fractions that cannot be fulfilled.
- The consumers place in the market buy offers that exceed their real consumption, following forecast errors or significant accidental deviations from the daily demand pattern.

All these quantities can amount to an important value over longer time periods. If they are not traded in the local market, the prosumers would sell at minimum price to the aggregator, while the consumers would buy electricity at standard, high tariffs.

The algorithm proposed in the paper offers the possibility of extending the primary market with a two-tier secondary market, in order to make prosumer and consumer surplus quantities available for trading in the local network.

### 3.3. The Secondary Market—The Energy Poverty Tier

The local market is profitable mostly to consumers with high demand, who can better benefit from the energy cost reduction obtained from the difference between the grid tariffs and the price per kWh offered by the local producers. These consumers are also usually those who have the financial resources to install the physical and software infrastructure required to access the market.

On the other hand, amongst the consumers connected in a microgrid can exist a number of low-income consumers, who in traditional networks would be classified as belonging to vulnerable categories and suffer from energy poverty. The paper proposes an optional secondary market tier in which the surplus that cannot be traded in the primary market would be automatically allocated in the initial settlement phase (see Figure 1) to such vulnerable consumers who, in normal conditions, would not be able to access the local market.

The surplus can come from both prosumers and consumers, as summarized in the previous subsection. In all the cases, the electricity quantities will result from the mismatch between the quantities offered for trading (higher)— $CO(h,i)$  or  $GO(h,j)$ —and actual traded quantity, determined by the existing (lower) generation availability  $TC(h,j)$  or realized consumption  $TC(h,i)$ :

$$\begin{aligned} TC(h,i) &= CO(h,i) - TC(h,i), \quad i = 1 \dots NCM, \quad \text{for consumers} \\ TC(h,j) &= GO(h,j) - TC(h,j), \quad j = 1 \dots NPM, \quad \text{for prosumers} \end{aligned} \quad (9)$$

Thus, consumers who were buyers in the primary market can act as sellers in the secondary market, together with the prosumers.

The quantities sold to vulnerable consumers in the secondary market are determined using the merit-order method where the buyers' prices are set as 0 mu/kWh (mu is the monetary units) and the quantities are ranked in descending order. The cost for traded kWh can be set using as reference the price obtained by the seller in the primary market, the original price offer placed by the seller in the primary market or an agreed fixed tariff, according to the policy agreed in the local market.

This trading scheme offers two benefits. The vulnerable consumers from the microgrid will see social welfare increase by the reduction of their electricity bill, which will be proportional to their consumption in the trading hours interval and the market price. On the other hand, the prosumers with remaining generation surplus and the consumers who have surplus to sell after the initial settlement of the primary market can sell electricity at higher prices than the tariff used by the aggregator.

The flowchart of the first tier of the secondary market is presented in Figure 6.

Since the demand of the vulnerable consumers selected for the energy poverty tier is expected to be low, the remaining surplus after the settlement of the first tier can be further traded in a second tier reserved for commercial trading.



The flowchart of the first tier of the secondary market is presented in Figure 6.

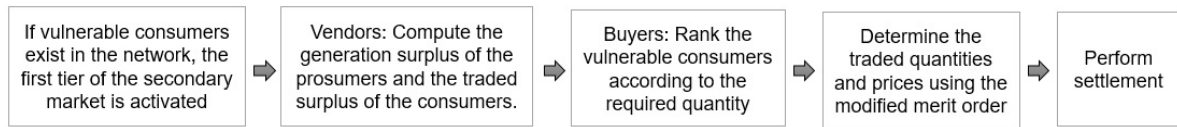


Figure 6. The flowchart of the second inclusion tier of the secondary market.

3.4. The Secondary Market – The Commercial Tier

Since the demand of the vulnerable consumers selected for the energy poverty tier is expected to be low, the remaining surplus after the settlement of the first tier can be further traded in a second tier reserved for commercial trading.

Several consumer categories are envisioned. Some consumers would not trade continuously and would seek only occasional access to the market, buying the local generation surplus to supply automated receptors such as greenhouse irrigation systems in given hours of preset days. Other types of occasional consumers would benefit from the price difference when trading on the local market, but the initial investment for the infrastructure required to get access to the market would be prohibitive.

The trading model considers the merit-order priority method described in Figure 5 for the primary market, but where the consumers offer to buy from the market their entire surplus from the primary market, but where the consumers offer to buy from the market their entire surplus from the secondary market to gain priority access for the surplus remaining after the settlement of the primary market offers. The trading model considers the merit-order priority method described in Figure 5 for the primary market, but where the consumers offer to buy from the market their entire surplus from the secondary market to gain priority access for the surplus remaining after the settlement of the primary market offers. The trading model considers the merit-order priority method described in Figure 5 for the primary market, but where the consumers offer to buy from the market their entire surplus from the secondary market to gain priority access for the surplus remaining after the settlement of the primary market offers.

- Option 1: Fee access.
- Option 2: Invite access.

In the fee-access model, the consumers who need only occasional access to the market can submit offers in the secondary market to gain priority access for the surplus remaining after the settlement of the primary market offers.

The trading model considers the merit-order priority method described in Figure 5 for the primary market, but where the consumers offer to buy from the market their entire surplus from the secondary market to gain priority access for the surplus remaining after the settlement of the primary market offers. The trading model considers the merit-order priority method described in Figure 5 for the primary market, but where the consumers offer to buy from the market their entire surplus from the secondary market to gain priority access for the surplus remaining after the settlement of the primary market offers. The trading model considers the merit-order priority method described in Figure 5 for the primary market, but where the consumers offer to buy from the market their entire surplus from the secondary market to gain priority access for the surplus remaining after the settlement of the primary market offers.

$$TP(h, i) = C(h, i); (PCO(h, i), PGO(h, i), or MCP(h)); (1 + f\%)$$

$$TP(h, i) = C(h, i); (PCO(h, i), PGO(h, i), or MCP(h)); (1 + f\%)$$

The basic flowchart of the fee-access secondary market model is given in Figure 7.

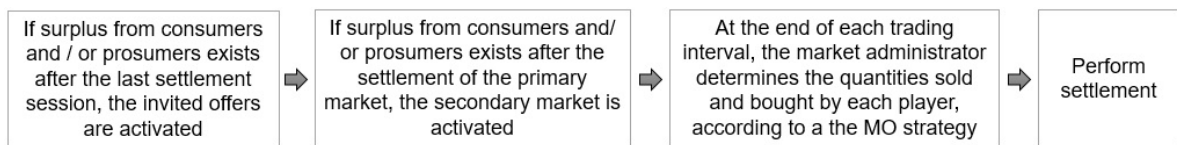


Figure 7. The flowchart of the secondary market fee-access model.

In the invite-access model, existing market players can act as sub-contractors for other consumers from the microgrid. Certain prosumers or consumers can still have surplus quantities unsold after the previous settlement sessions have been completed. In order to get the lowest price for the remaining quantities, they can occasionally sell the surplus from the microgrid to which the remaining quantities will be sold. The transactions are based on P2P or P2C contracts existing between the two entities and identified in the market administrator responsible for the final settlement at market level. The price is agreed between the parties, on the one hand the buyer offers the flowchart of the secondary market invite-access model is provided in Figure 8.

The flowchart of the secondary market invite-access model is provided in Figure 8.

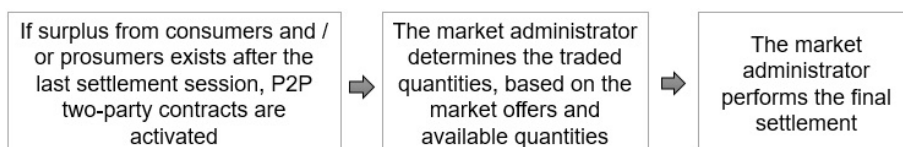


Figure 8. The flowchart of the secondary market invite-access model.

It should be noted that the secondary market models are optional and their order of activation

The flowchart of the secondary market invite-access model is provided in Figure 8.

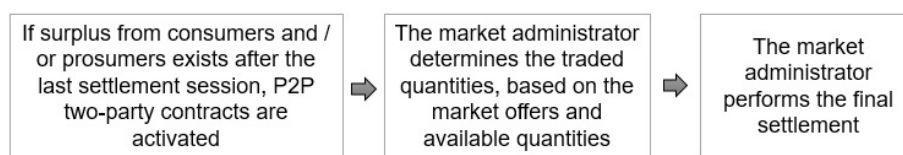


Figure 8. The flowchart of the secondary market invite-access model.

It should be noted that the secondary market models are optional, and their order of activation can be changed according to the priorities of a specific microgrid. Instances can exist where the energy poverty mitigation tier is absent or one or both segments of the secondary commercial tier are used.

#### 4. Results

The new market was tested on an LV distribution network from Romania, with 28 buses and two four-wire three-phase bundled feeders, with an average distance between the connection points of 40 m. The network supplies only single-phase residential consumers, some of whom also have PV generation capabilities. The load and generation profiles used in the study are considered as daily 24-hour measured values, as provided from the smart metering infrastructure existing in the LV microgrid. The 24-hour load profiles for the network buses are presented in Table A1 in Appendix A.

Each bus, except bus 1, which is a branching point, has one residence connected. The prosumers are located at buses 3, 6, 7, 10, 15, 25 and 27, as shown in the one-line diagram from Figure 9. Their 24-hour generation profiles were modeled using representative data for this type of generation and are provided in Appendix A, Table A2. The prosumers will use the generated electricity primarily for supplying their own hourly demand, and wish to sell the remaining surplus to the consumers participating in the local market set up at microgrid level and managed by a non-profit aggregator. From Table 2 and Figure 10, it is seen that generation occurs only in the 06:00–18:00 interval, when solar energy is available. The surplus is maximized in the 10:00–13:00 interval and minimized towards the evening time, when the peak load hours are near.

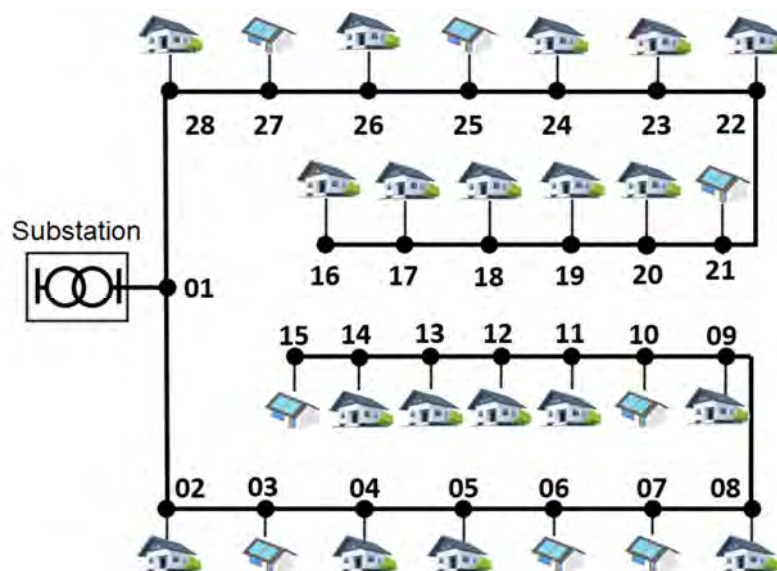


Figure 9. The low voltage (LV) microgrid used in the case study.

Table 2. The prosumers’ electricity surplus, in kWh.

Hour	P27	P21	P7	P15	P6	P3	P10	P25	Total
h6	0.000	1.588	0.000	1.948	0.000	1.208	2.496	3.052	10.292
h7	0.000	1.805	0.263	1.585	0.000	1.806	2.616	3.487	11.562
h8	0.668	1.726	0.704	1.586	0.000	2.879	0.714	3.826	12.103
h9	1.437	1.749	1.056	2.228	0.741	2.836	1.279	3.956	15.282
h10	1.607	2.292	1.093	1.302	1.116	3.251	2.794	4.232	17.687
h11	1.655	2.038	1.400	2.775	1.886	3.372	0.000	4.175	17.301
h12	1.595	1.822	1.225	1.880	2.328	3.392	0.980	4.060	17.282

Figure 9. The low voltage (LV) microgrid used in the case study.

Table 2. The prosumers' electricity surplus, in kWh.

Hour	P27	P21	P7	P15	P6	P3	P10	P25	Total
h6	0.000	1.588	0.000	1.948	0.000	1.208	2.496	3.052	10.292
h7	0.000	1.805	0.263	1.585	0.000	1.806	2.616	3.487	11.562
h8	0.668	1.726	0.704	1.586	0.000	2.879	0.714	3.826	12.103
h9	0.000	1.584	0.000	2.228	0.000	2.838	1.279	3.956	15.282
h10	0.668	1.805	0.263	1.585	0.000	1.806	2.616	3.487	11.562
h11	1.655	1.726	0.704	1.586	0.000	2.879	0.714	3.826	17.301
h12	1.607	1.805	0.263	1.585	0.000	1.806	2.616	3.487	17.282
h13	1.508	1.726	0.704	1.586	0.000	2.879	0.714	3.826	17.282
h14	1.372	1.805	0.263	1.585	0.000	1.806	2.616	3.487	15.623
h15	1.106	1.726	0.704	1.586	0.000	2.879	0.714	3.826	12.945
h16	0.363	1.805	0.263	1.585	0.000	1.806	2.616	3.487	8.439
h17	0.000	1.584	0.000	2.228	0.000	2.838	1.279	3.956	10.896
h18	0.000	1.805	0.263	1.585	0.000	1.806	2.616	3.487	12.065
Total	11.904	19.997	2.169	10.896	32.203	12.065	47.629	167.905	167.905

It is considered that they wish to sell the entire surplus on the market to maximize their revenue. The quantities offered, derived from Tables A1 and A2, are presented in Table 2 and Figure 10, where it can be seen that surplus exists for trading in all hourly intervals from 06:00 to 18:00, but there are prosumers who cannot trade electricity at some hours (for example, P27 or P6).

For all quantity offers, the consumers and the prosumers must also provide in the blockchain system of the primary market the desired price offers, which are given in Tables A4 and A5 in Appendix A. These values were set between 0.39 and 0.6 mu/kWh for consumers, and in the 0.4–0.55 mu/kWh range for prosumers. The higher maximum prices for consumers were chosen taking into account the merit-order method, in which the offers with the highest prices are prioritized. Furthermore, both the prosumers' and consumers' price offers were set higher than the regulated tariff to incentivize the trading in the local market.

If the market would not be present, the total electricity surplus quantity (167.97 kWh) would be traded by the aggregator back in the grid, at a regulated tariff. Using the reference value of 0.251 mu/kWh applied in the case study, the total surplus value would be 42.16 mu/day.

For demonstrating the advantages and disadvantages of each trading priority method used in the market, FCFS and MO, the case study results are provided as comparisons between these alternatives.

From the 27 consumers existing in the microgrid, the case study considers that only 11 are participating in the primary market as buyers (from buses 5, 8, 9, 11, 12, 14, 16, 19, 20, 24, 26), chosen mainly demand used in the FCFS offers. This can happen because of two reasons: the forecast error and the standardized offer type (multiple of 100 W) used by the MO method. On the other hand, the offers placed by the consumers in the market are identical for both trading methods, and equal to the forecasted values, in multiples of 100 kW, as discussed in Section 3.2. For the forecasted offers, the available surplus (Figure 10), because one of the main objectives of the local market is to enable prosumers to sell the entire surplus locally, and offers given as multiples of 100 W would impede the achievement of this goal.

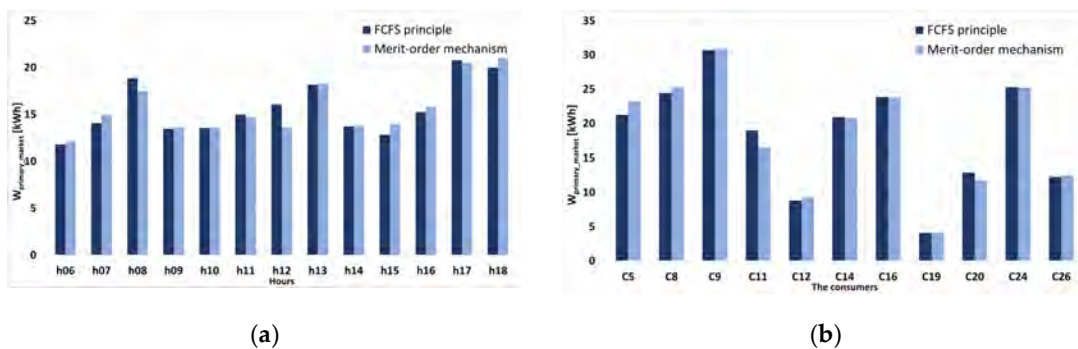


Figure 11. The buyer quantity offers in the primary market: (a) hourly (b) for each consumer.

The traded quantities and revenues/costs for each prosumer/consumer and hourly interval are given in Figures 12 and 13 and Tables 3–6.

The data from Tables 3–6 show some interesting results regarding the hourly and daily offers and traded quantities for the consumers and prosumers.

The sellers who place offers in the primary market are the prosumers with generation surplus. It is considered that they wish to sell the entire surplus on the market to maximize their revenue. The quantities offered, derived from Tables A1 and A2, are presented in Table 2 and Figure 10, where it can be seen that surplus exists for trading in all hourly intervals from 06:00 to 18:00, but there are prosumers who cannot trade electricity at some hours (for example, P27 or P6).

For all quantity offers, the consumers and the prosumers must also provide in the blockchain system of the primary market the desired price offers, which are given in Tables A4 and A5 in Appendix A. These values were set between 0.39 and 0.6 mu/kWh for consumers, and in the 0.4–0.55 mu/kWh range for prosumers. The higher maximum prices for consumers were chosen taking into account the merit-order method, in which the offers with the highest prices are prioritized. Furthermore, both the prosumers' and consumers' price offers were set higher than the regulated tariff to incentivize the trading in the local market.

If the market would not be present, the total electricity surplus quantity (167.97 kWh) would be traded by the aggregator back in the grid, at a regulated tariff. Using the reference value of 0.251 mu/kWh applied in Romania [73,74], the total revenue of the prosumers would be of 42.16 mu/day.

For demonstrating the advantages and disadvantages of each trading priority method used in the market, FCFS and MO, the case study results are provided as comparisons between these alternatives.

As it can be seen from Figure 11, there are hours when the MO offers differ from the total demand used in the FCFS offers. This can happen because of two reasons: the forecast error and the standardized offer type (multiple of 100 W) used by the MO method. On the other hand, the offers placed by the consumers in the market are identical for both trading methods, and equal to the available surplus (Figure 10), because one of the main objectives of the local market is to enable prosumers to sell the entire surplus locally, and offers given as multiples of 100 W would impede the achievement of this goal.

The traded quantities and revenues/costs for each prosumer/consumer and hourly interval are given in Tables 17 and 18 and Tables 3–6

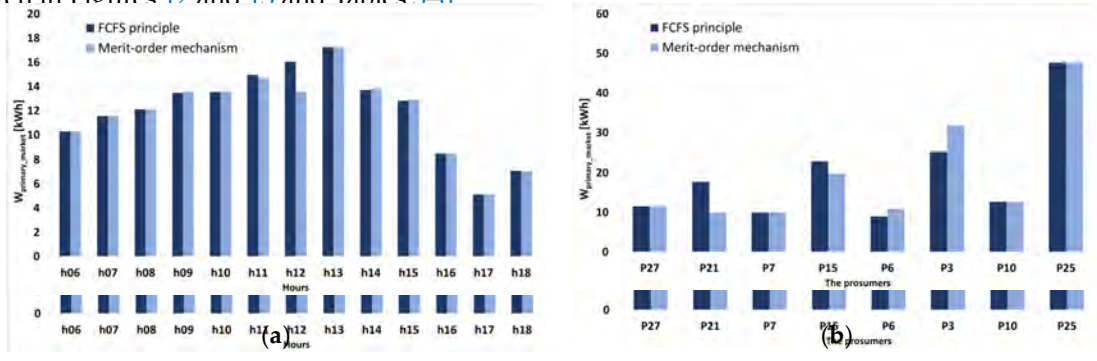


Figure 12. The traded quantities of the sellers in the primary market: (a) hourly; (b) for each prosumer.

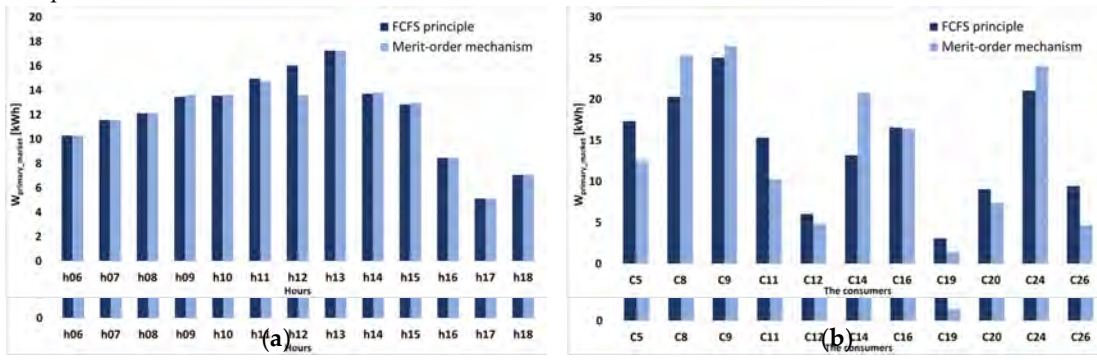


Figure 13. The traded quantities of the buyers in the primary market: (a) hourly; (b) for each consumer.

Table 9. The daily offer, traded and remaining quantities for each buyer in the primary market, kWh.

Consumer	C5	C8	C9	C11	C12	C14	C16	C19	C20	C24	C26	Total
Consumption	27.95	24.44	20.70	18.06	8.76	20.00	23.81	4.98	12.00	25.07	10.26	202.41

The data from Tables 3–6 show some interesting results regarding the hourly and daily offers and traded quantities for the consumers and prosumers.

The local generation surplus (167.97 kW) is insufficient to supply all the consumer needs (203.43 kWh). From Table 3, it is seen that, for the chosen consumption, local generation and primary market offers, when using the FCFS trading priority, the consumers can trade quantities lower than their consumption, and will need to buy the rest from the grid, at higher tariffs. If the MO trading priority is used, Table 4 shows that the hourly buy offers placed by the consumers are usually not fully fulfilled, but the traded quantities exceed the consumption. This leads to a surplus with the consumers, which will be traded to the grid, at regulated tariffs, or sold in the secondary market.

For prosumers, there are trading intervals where the surplus exceeds the traded prosumer offer and traded consumer quantities which are equal (for example, at *h11*, as seen from Tables 4 and 6). This suggests that the prosumer will not be able to sell their entire surplus because of lack of demand. Additionally, applying the FCFS and MO trading priorities in fulfilling the market offers has different effects on the traded quantities, both hourly and for individual prosumers or consumers. If the FCFS trading priority is used, the total quantity traded by the prosumers is larger (Table 5) because the prosumer surplus offers can be matched more closely by the consumer offers. This means that if the MO trading priority is used, it is expected to have more surplus unsold to the local consumers, thus reducing the profitability of the prosumers. In this case, they would have to sell extra surplus to the grid in exchange for the regulated tariff, which is lower than the local consumer offers. As it can be seen from Table 6, the generation surplus remaining after the primary market is concentrated in the 09:00–14:00 interval, while the evening and morning intervals see the highest deficit in local generation (Table 4).

**Table 3.** The daily offer, traded and remaining quantities for each buyer in the primary market, kWh.

Consumer	C5	C8	C9	C11	C12	C14	C16	C19	C20	C24	C26	Total
Consumption (offers FCFS)	21.25	24.44	30.70	18.96	8.79	20.92	23.84	4.08	12.90	25.27	12.26	203.41
offers MO	23.2	25.30	30.9	16.50	9.30	20.80	23.8	4.10	11.80	25.20	12.50	203.40
traded FCFS	17.32	20.29	25.07	15.33	6.04	13.20	16.54	3.08	9.05	21.04	9.44	156.40
traded MO	12.55	25.30	26.42	10.30	4.85	20.80	16.36	1.40	7.40	24.02	4.70	154.10
rem. FCFS	3.93	4.15	5.62	3.64	2.75	7.72	7.30	1.01	3.85	4.23	2.82	47.01
rem. MO	10.65	0	4.48	6.20	4.45	0	7.44	2.70	4.40	1.18	7.80	49.30

**Table 4.** The hourly offer, traded and remaining quantities in the primary market for all buyers, kWh.

Hour	h06	h07	h08	h09	h10	h11	h12	h13	h14	h15	h16	h17	h18	Total
Consumption (offer FCFS)	11.8	14.06	18.87	13.47	13.55	14.96	16.04	18.16	13.7	12.83	15.23	20.77	19.99	203.43
offer MO	12.1	14.9	17.5	13.6	13.6	14.7	13.6	18.3	13.8	14	15.8	20.5	21	203.40
traded FCFS	10.29	11.56	12.1	13.47	13.55	14.96	16.04	17.25	13.7	12.83	8.46	5.12	7.07	156.40
traded MO	10.29	11.56	12.1	13.6	13.6	14.7	13.6	17.25	13.8	12.95	8.46	5.12	7.07	154.10
rem. FCFS	1.51	2.5	6.77	0	0	0	0	0.91	0	0	6.77	15.65	12.92	47.03
rem. MO	1.81	3.34	5.40	0	0	0	0	1.05	0	1.05	7.34	15.38	13.93	49.30

**Table 5.** The daily offer, traded and remaining quantities for each seller in the primary market, kWh.

Prosumer	P27	P21	P7	P15	P6	P3	P10	P25	Total
surplus	11.51	18.90	10.00	24.17	10.90	32.20	12.67	47.63	167.97
traded FCFS	11.51	17.72	9.88	22.87	8.92	25.20	12.67	47.63	156.40
traded MO	11.51	9.89	10.00	19.80	10.90	31.71	12.67	47.63	154.10
rem. FCFS	0	1.18	0.11	1.30	1.98	7.00	0	0	11.58
rem. MO	0	9.02	0	4.37	0	0.49	0	0	13.88

**Table 6.** The hourly offer, traded and remaining quantities in the primary market, for all sellers, kWh.

Hour	h06	h07	h08	h09	h10	h11	h12	h13	h14	h15	h16	h17	h18	Total
Surplus	10.29	11.56	12.10	15.28	17.69	17.30	17.28	17.25	15.62	12.95	8.46	5.12	7.07	167.97
traded FCFS	10.29	11.56	12.10	13.47	13.55	14.96	16.04	17.25	13.70	12.83	8.46	5.12	7.07	156.40
traded MO	10.29	11.56	12.10	13.60	13.60	14.70	13.60	17.25	13.80	12.95	8.46	5.12	7.07	154.10
rem. FCFS	0	0	0	1.82	4.14	2.35	1.24	0	1.92	0.11	0	0	0	11.58
rem. MO	0	0	0	1.68	4.09	2.60	3.68	0	1.82	0	0	0	0	13.88

The profitability of the FCFS and MO trading priorities can be assessed from Figure 14 and Tables 7 and 8 for the buyers and Figure 15 and Tables 9 and 10 for the sellers. The market model offers the possibility of performing financial settlement in three assumptions for the prices: using the market clearing price (MCP), the consumer offers (COP) and the prosumer offers (POP), because different microgrids can pursue different objectives when establishing the local market. For example, using POP with MO in the primary market can be an advantage for the generating consumers, who will buy electricity at lower prices from the local prosumers. Instead of paying the standard residential tariff. Using the COP favors the prosumers with lower prices in generation scenarios. They sell electricity at higher clearing prices. Using the COP will be an advantage for the prosumers, who will be able to obtain settlement prices larger than their initial offers. The sellers/vendors with the highest cost/revenue can be considered as making the most profit because quantities are bought by consumers at a price lower than the standard residential tariff, while the sell offers are settled by the vendors at a price higher than the resell tariff to the grid.

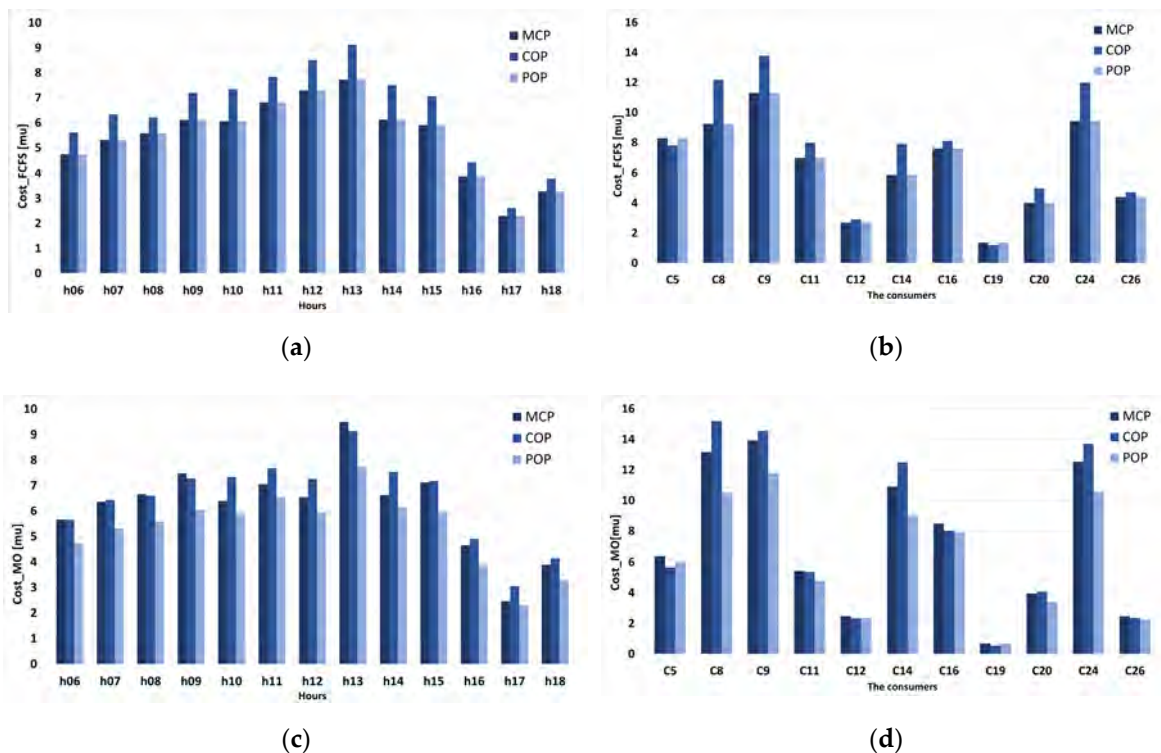


**Figure 14.** The primary market cost for buyers: (a) The hourly values, first-come-first-serve (FCFS); (b) The values for each consumer, FCFS; (c) The hourly values, MO; (d) The values for each consumer, MO.

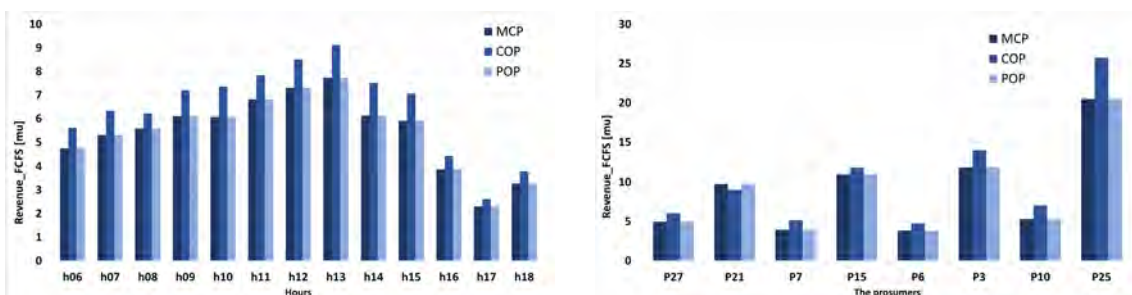


**Figure 14.** The primary market cost for buyers: (a) The hourly values, first-come-first-serve (FCFS); (b) The values for each consumer, FCFS; (c) The hourly values, MO; (d) The values for each consumer, MO.

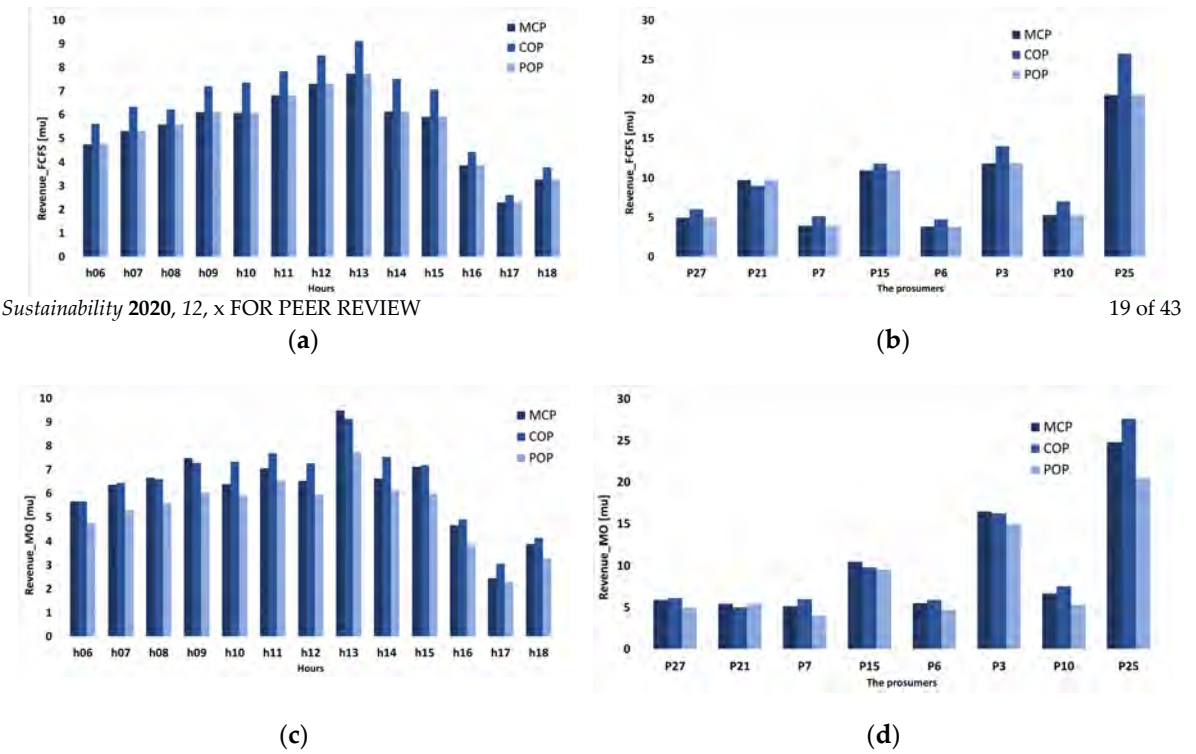


**Figure 15.** The primary market revenue for sellers: (a) The hourly values, FCFS; (b) The values for each prosumer, FCFS; (c) The hourly values, MO; (d) The values for each prosumer, MO.

For the scenario considered in the case study, Figures 14 and 15 show that the highest revenues are obtained by prosumers when the consumer offer prices (COP) are used for settlement. If the FCFS trading priority is used, the MCP and POP settlements give the same results, because the methodology from [49] uses as settlement price the prosumer offers, and the MCP and POP trading priorities would result the same, as the buy offer price is not relevant and thus considered 0 €/MWh for all buyers. For the MO trading priority, the MCP settlement results in higher trading prices than POP, because the trading price for all sellers and buyers is determined by the price unrestricted merit order used in wholesale markets (Figure 4).

As it can be seen from Tables 7-11, the players who get the most advantage from the local market are C8, C9, C24, the consumers without generation capability that have the highest demand, and P15, P3, P25, the prosumers with the largest daily surplus.

		Table 7. The daily cost for each buyer in the primary market, mu.															
		Table 8. The daily revenue for each seller in the primary market, mu.															
		Table 9. The daily revenue for each seller in the primary market, mu.															
		Table 10. The hourly revenue in the primary market for all sellers, mu.															
Consumers	FCFS	MCP	4.95	9.79	5.95	10.98	3.83	11.85	5.32	20.48	71.11					Total	71.11
		COP	6.02	9.04	7.15	11.86	4.74	13.95	7.04	25.74	82.54	C24	5.4	C26	4.39	Total	83.54
		POP	4.95	9.75	5.95	10.98	3.83	11.85	5.32	20.48	71.11					Total	71.11
Consumers	MO	MCP	8.28	9.23	11.30	6.96	2.70	5.87	7.59	1.36	4.00					Total	4.39
		COP	12.15	8.83	7.44	7.97	13.50	7.51	8.04	12.67	24.78	C8	10.93	C24	4.72	Total	83.54
		POP	8.28	9.23	11.30	6.96	2.70	5.87	7.59	1.36	4.00					Total	4.39
Consumers	MO	MCP	6.40	13.13	13.51	5.44	2.45	10.69	8.49	0.62	20.48					Total	2.46
		COP	5.65	15.18	14.53	5.36	2.33	12.48	8.01	0.55	4.07	C8	13.69	C24	2.35	Total	84.20
		POP	6.40	13.13	13.51	5.44	2.45	10.69	8.49	0.62	20.48					Total	2.46
		Table 10. The hourly revenue in the primary market for all sellers, mu.															
Consumers	FCFS	MCP	4.74	5.31	5.58	6.11	6.06	6.81	7.30	7.73	6.12	5.90	3.87	2.30	3.28	Total	71.11
		COP	5.60	6.33	6.21	7.20	7.35	7.84	8.51	9.12	7.51	7.06	4.42	2.61	3.79	Total	83.54
		POP	4.74	5.31	5.58	6.11	6.06	6.81	7.30	7.73	6.12	5.90	3.87	2.30	3.28	Total	71.11
Consumers	MO	MCP	5.66	6.36	6.66	7.48	6.39	7.06	6.53	9.49	6.62	7.12	4.65	2.46	3.89	Total	80.36
		COP	5.66	6.43	6.60	7.28	7.33	7.68	7.26	9.13	7.53	7.18	4.90	3.05	4.15	Total	84.20
		POP	4.74	5.31	5.58	6.04	5.90	6.52	5.94	7.73	6.13	5.95	3.87	2.30	3.28	Total	69.28

For the scenario considered in the case study, Figures 14 and 15 show that the highest revenues are obtained by prosumers when the consumer offer prices (COP) are used for settlement. If the FCFS trading priority is used, the MCP and POP settlements give the same results, because the

**Table 8.** The hourly cost in the primary market for all buyers, mu.

Consumers		h06	h07	h08	h09	h10	h11	h12	h13	h14	h15	h16	h17	h18	Total
FCFS	MCP	4.74	5.31	5.58	6.11	6.06	6.81	7.30	7.73	6.12	5.90	3.87	2.30	3.28	71.11
	COP	5.60	6.33	6.21	7.20	7.35	7.84	8.51	9.12	7.51	7.06	4.42	2.61	3.79	83.54
	POP	4.74	5.31	5.58	6.11	6.06	6.81	7.30	7.73	6.12	5.90	3.87	2.30	3.28	71.11
MO	MCP	5.66	6.36	6.66	7.48	6.39	7.06	6.53	9.49	6.62	7.12	4.65	2.46	3.89	80.36
	COP	5.66	6.43	6.60	7.28	7.33	7.68	7.26	9.13	7.53	7.18	4.90	3.05	4.15	84.20
	POP	4.74	5.31	5.58	6.04	5.90	6.52	5.94	7.73	6.13	5.95	3.87	2.30	3.28	69.28

**Table 9.** The daily revenue for each seller in the primary market, mu.

Prosumers		P27	P21	P7	P15	P6	P3	P10	P25	Total
FCFS	MCP	4.95	9.75	3.95	10.98	3.83	11.85	5.32	20.48	71.11
	COP	6.02	9.04	5.15	11.86	4.74	13.95	7.04	25.74	83.54
	POP	4.95	9.75	3.95	10.98	3.83	11.85	5.32	20.48	71.11
MO	MCP	5.88	5.44	5.13	10.50	5.51	16.44	6.67	24.78	80.36
	COP	6.11	4.98	6.00	9.80	5.90	16.25	7.54	27.61	84.20
	POP	4.95	5.44	4.00	9.51	4.69	14.90	5.32	20.48	69.28

**Table 10.** The hourly revenue in the primary market for all sellers, mu.

Prosumers		h06	h07	h08	h09	h10	h11	h12	h13	h14	h15	h16	h17	h18	Total
FCFS	MCP	4.74	5.31	5.58	6.11	6.06	6.81	7.30	7.73	6.12	5.90	3.87	2.30	3.28	71.11
	COP	5.60	6.33	6.21	7.20	7.35	7.84	8.51	9.12	7.51	7.06	4.42	2.61	3.79	83.54
	POP	4.74	5.31	5.58	6.11	6.06	6.81	7.30	7.73	6.12	5.90	3.87	2.30	3.28	71.11
MO	MCP	5.66	6.36	6.66	7.48	6.39	7.06	6.53	9.49	6.62	7.12	4.65	2.46	3.89	80.36
	COP	5.66	6.43	6.60	7.28	7.33	7.68	7.26	9.13	7.53	7.18	4.90	3.05	4.15	84.20
	POP	4.74	5.31	5.58	6.04	5.90	6.52	5.94	7.73	6.13	5.95	3.87	2.30	3.28	69.28

#### 4.2. The Secondary Market—The Energy Poverty Mitigation Tier

The proposed local market model uses in the secondary market an optional energy poverty mitigation tier, designed to include a category of consumers that can usually will not be able to trade on the market because of their low income or other social vulnerabilities. The microgrid community can decide to assist these consumers by supporting the reduction of their electricity bill. The simplest way to achieve this goal is to automatically allocate the prosumer surplus available after the settlement of the primary market to cover the demand of such consumers. In the data used for the case study, a single consumer, C28, fulfills the requirements of a vulnerable consumer. As seen in Table A1, its total daily consumption amounts to 3.31 kWh, with 1.79 kWh in the 06:00–18:00 interval.

Since the two trading priority methods (FCFS and MO) give in the primary market different results regarding the trading participants and quantities at each hour, a similar behavior is propagated in the secondary market. Thus, the trading results will be presented in the same manner as for the primary market, as a comparison between the cases in which the primary market uses the FCFS or the MO in determining the priorities of the traded quantities. It is considered that the secondary market uses the same price offers entered in the blockchain system for the primary market.

According to the data from Tables 3 and 5, after the settlement of the primary market, prosumers P21, P7, P15, P6, P3, P25 have unsold surplus if the FCFS trading priority is used. No consumers can participate in the secondary market, because they cannot have surplus after trading. If the MO priority is used, the prosumers with available surplus are P21, P15, P3, and also there are consumers which have placed in the primary market offers exceeding their real consumption, and can become sellers on the secondary market (C5, C9, C11, C12, C16, C19, C20, C24, and C26). The hours in which the sellers are having surplus after the primary market are presented in Appendix B, Tables A6 and A7.



participate in the secondary market, because they cannot have surplus after trading. If the MO priority is used, the prosumers with available surplus are P21, P15, P3, and also there are consumers which have placed in the primary market offers exceeding their real consumption, and can become sellers on the secondary market (C5, C9, C11, C12, C16, C19, C20, C24, and C26). The hours in which the sellers are having surplus after the primary market are presented in Appendix B, Tables A6 and A7. The only entity buying in this market is C28, and its hourly buy offer match its entire consumption. (See Table A1). However, these are total quantities, and each seller can trade different surplus quantities in each hour. This will lead to the necessity of prioritization of the sell offers and subsequent settlement between C28 and possibly multiple sellers. The quantities traded hourly are presented in Appendix B, Tables A8 and A9. The sell offers and traded quantities are given in Figures 16 and 17. Tables 11–14 summarize the daily and hourly offers and quantities traded by buyers and sellers. Tables 11–14 summarize the daily and hourly offers and quantities traded by buyers and sellers.

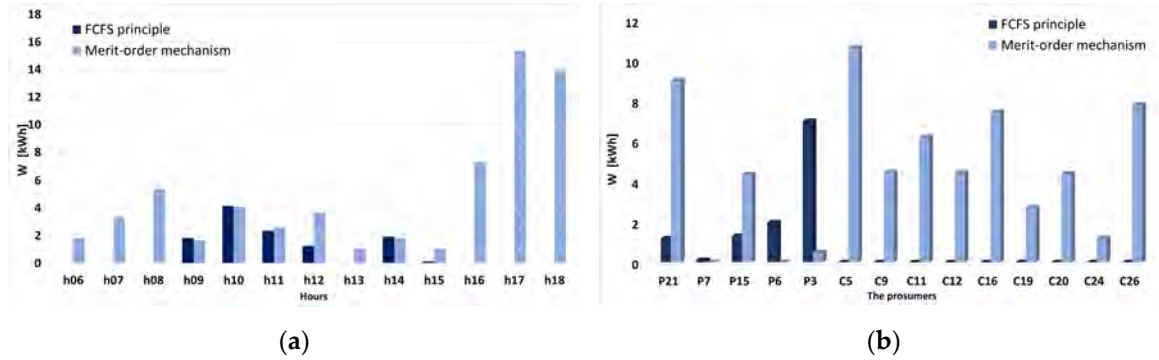


**Figure 16.** The sell offers of the vendors in the energy poverty mitigation market: (a) hourly; (b) for each prosumer/consumer.

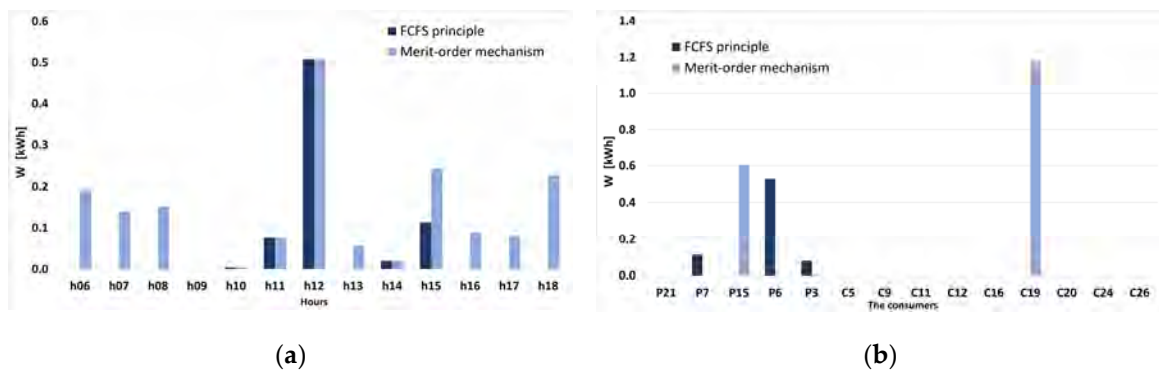


**Figure 17.** The traded quantities of the vendors in the energy poverty mitigation market: (a) hourly; (b) for each prosumer.

**Table 11.** The daily traded quantities for consumer C28 in the energy poverty mitigation market, kWh.

Consumer	Consumer	C28
Consumption (offers FCFS)	Consumption (offers FCFS)	1.79
offers MO	offers MO	1.79
traded FCFS	traded FCFS	0.72
traded MO	traded MO	1.79
rem. FCFS	traded MO	1.79
rem. MO	rem. FCFS	1.07
	rem. MO	0

**Table 12.** The hourly traded quantities in the poverty mitigation market for consumer C28, kWh.

Hour	h06	h07	h08	h09	h10	h11	h12	h13	h14	h15	h16	h17	h18	Total
Consumption (offer FCFS)	0.19	0.14	0.15	0	0	0.08	0.51	0.06	0.02	0.24	0.09	0.08	0.23	1.79
offer MO	0.19	0.14	0.15	0	0	0.08	0.51	0.06	0.02	0.24	0.09	0.08	0.23	1.79
traded FCFS	0	0	0	0	0	0.08	0.51	0	0.02	0.11	0	0	0	0.72
traded MO	0.19	0.14	0.15	0	0	0.08	0.51	0.06	0.02	0.24	0.09	0.08	0.23	1.79
rem. FCFS	0.19	0.14	0.15	0	0	0	0	0.06	0	0.13	0.09	0.08	0.23	1.07
rem. MO	0	0	0	0	0	0	0	0	0	0	0	0	0	0

**Table 13.** The daily traded quantities for each vendor in the energy poverty mitigation market, kWh.

**Table 12.** The hourly traded quantities in the poverty mitigation market for consumer C28, kWh.

Hour	h06	h07	h08	h09	h10	h11	h12	h13	h14	h15	h16	h17	h18	Total
Consumption (offer FCFS)	0.19	0.14	0.15	0	0	0.08	0.51	0.06	0.02	0.24	0.09	0.08	0.23	1.79
offer MO	0.19	0.14	0.15	0	0	0.08	0.51	0.06	0.02	0.24	0.09	0.08	0.23	1.79
traded FCFS	0	0	0	0	0	0.08	0.51	0	0.02	0.11	0	0	0	0.72
traded MO	0.19	0.14	0.15	0	0	0.08	0.51	0.06	0.02	0.24	0.09	0.08	0.23	1.79
rem. FCFS	0.19	0.14	0.15	0	0	0	0	0.06	0	0.13	0.09	0.08	0.23	1.07
rem. MO	0	0	0	0	0	0	0	0	0	0	0	0	0	0

**Table 13.** The daily traded quantities for each vendor in the energy poverty mitigation market, kWh.

Vendor	P21	P7	P15	P6	P3	C5	C9	C11	C12	C16	C19	C20	C24	C26	Total
surplus FCFS	1.18	0.11	1.30	1.98	7.00	0	0	0	0	0	0	0	0	0	11.58
surplus MO	9.02	0	4.37	0	0.49	10.65	4.48	6.20	4.46	7.44	2.70	4.40	1.18	7.80	63.18
traded FCFS	0	0.11	0	0.53	0.08	0	0	0	0	0	0	0	0	0	0.72
traded MO	0	0	0.60	0	0.00	0	0	0	0	0	1.18	0	0	0	1.79
rem. FCFS	1.18	0.00	1.30	1.45	6.92	0	0	0	0	0	0	0	0	0	10.86
rem. MO	9.02	0.00	3.76	0	0.49	10.65	4.48	6.20	4.46	7.44	1.52	4.40	1.18	7.80	61.39

**Table 14.** The hourly traded quantities in the energy poverty mitigation market for all vendors, kWh.

Hour	h06	h07	h08	h09	h10	h11	h12	h13	h14	h15	h16	h17	h18	Total
surplus FCFS	0	0	0	1.82	4.14	2.35	1.24	0	1.92	0.11	0	0	0	11.58
surplus MO	1.81	3.34	5.40	1.68	4.09	2.60	3.68	1.05	1.82	1.06	7.34	15.38	13.94	63.18
traded-FCFS	0	0	0	0	0.00	0.08	0.51	0	0.02	0.11	0	0	0	0.72
traded-MO	0.19	0.14	0.15	0.00	0.00	0.08	0.51	0.06	0.02	0.24	0.09	0.08	0.23	1.79
rem. FCFS	0	0	0	1.82	4.14	2.27	0.73	0	1.90	0	0	0	0	10.86
rem. MO	1.62	3.20	5.25	1.68	4.08	2.53	3.17	0.99	1.80	0.81	7.25	15.30	13.71	61.39

Figures 16 and 17 and Tables 11–14 reveal significantly different trading scenarios on the energy poverty mitigation market when the two trading priority methods (FCFS and MO) are used in the primary market. For FCFS, 3 out of 5 prosumers will trade electricity with C28, while if MO were to be used, only P15 and P3 will sell electricity, the rest of the buying offer being fulfilled by just one consumer, C19. Also, if the secondary market is activated, the available surplus rises when MO is used from 13.88 kWh in the primary market to 63.18 kWh, due to the presence of the consumers who need to sell the surplus generated by the forecast error or offer quantity rounding. In the absence of the secondary market, these two quantities would be sold back to the grid at minimal price. Thus, in addition to allowing prosumer to sell more surplus, the secondary market offers a mechanism for minimizing the effect of consumption forecast errors at the consumer side when the MO trading priority method is used. However, the prosumer and consumer surplus to be sold back to the grid remain high, at 13.27 kWh and 48.12 kWh respectively (Table 13).

The costs of the consumer C28 and revenues of the vendors in the energy poverty market tier are given in Tables 15–18 and Figures 18 and 19. The financial settlement is performed in this case using as reference only the vendor price offer, similar to POP from Tables 7–10, because with just one vulnerable consumer trading in the market, the COP is viable only if the consumer would buy at a fixed tariff, and MCP results are the same as POP when COP is not specified.

The results show that the vendor revenues are lower than in the primary market, because of the smaller traded quantities, but they can become significant if they are averaged over longer periods (months, years). The consumer C28 will pay less in the local market than when buying electricity from the grid, and the MO trading priority maximizes its earnings and the number of hourly intervals in which trading can be made. A more profitability analysis will follow in the Discussions section, for all the trading segments considered in the market algorithm.

The costs of the consumer C28 and revenues of the vendors in the energy poverty market tier are given in Tables 15–18 and Figures 18 and 19. The financial settlement is performed in this case using as reference only the vendor price offer, similar to POP from Tables 7–10, because with just one vulnerable consumer trading in the market, the COP is viable only if the consumer would buy at a fixed tariff, and MCP results are the same as POP when COP is not specified. 23 of 43

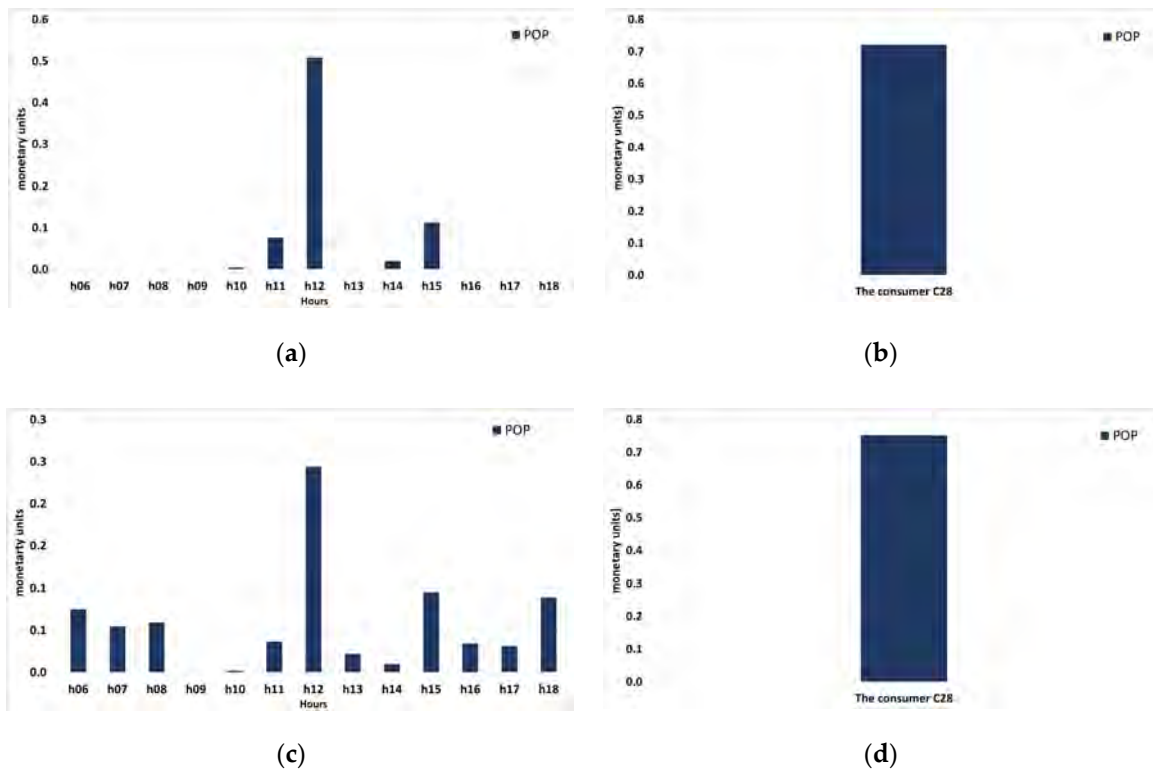


**Figure 18.** The energy poverty mitigation market costs for buyers: (a) hourly values, FCFS; (b) daily values for each consumer, FCFS; (c) hourly values, MO; (d) daily values for each consumer, MO. 23 of 43

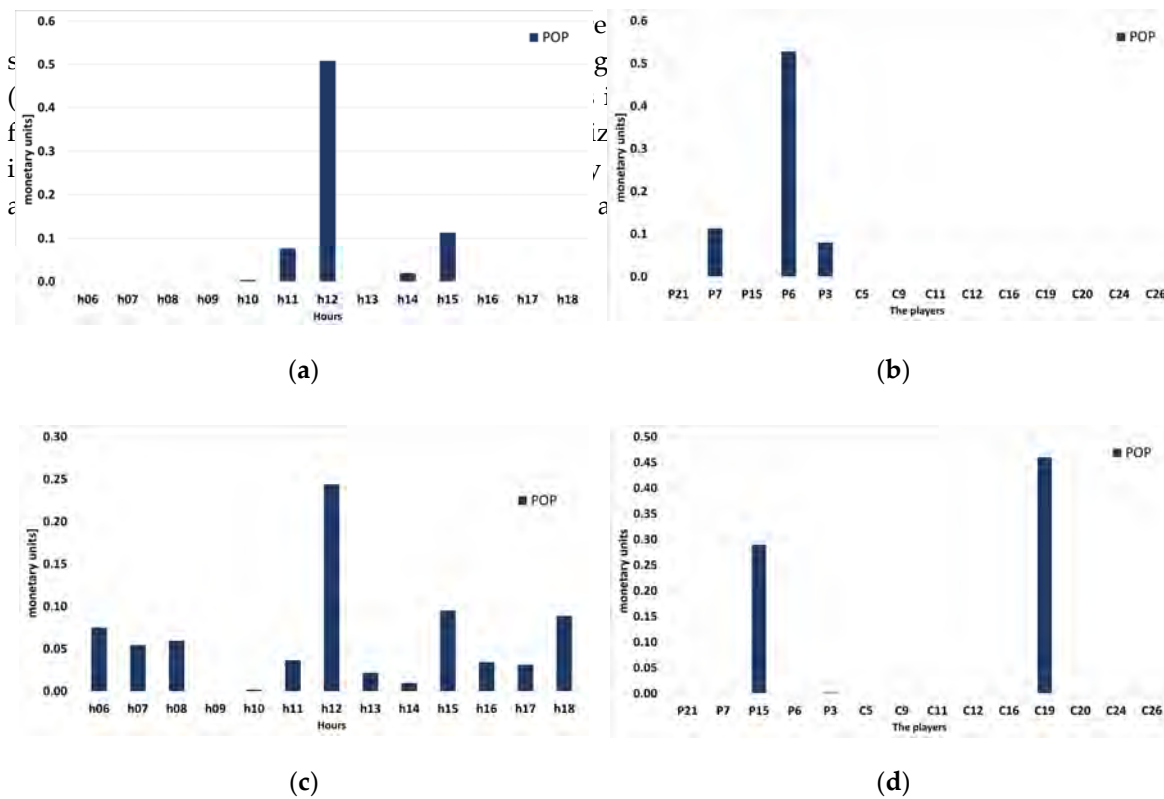


**Figure 19.** The energy poverty mitigation market revenue for vendors: (a) hourly values, FCFS; (b) daily values for each consumer, FCFS; (c) hourly values, MO; (d) daily values for each consumer, MO.

**Table 15.** The daily cost for each consumer in the energy poverty mitigation market, mu.

Consumers		C28
FCFS	POP	0.72
MO	POP	0.75

**Table 15.** The daily cost for each consumer in the energy poverty mitigation market, mu.

Consumers		C28
FCFS	POP	0.72
MO	POP	0.75

**Table 16.** The hourly cost for all buyers in the energy poverty mitigation market, mu.

Consumers		h06	h07	h08	h09	h10	h11	h12	h13	h14	h15	h16	h17	h18	Total
FCFS	POP	0	0	0	0	0.00	0.08	0.51	0	0.02	0.11	0	0	0	0.72
MO	POP	0.07	0.05	0.06	0	0.00	0.04	0.24	0.02	0.01	0.10	0.03	0.03	0.09	0.75

**Table 17.** The daily revenue for each vendor in the energy poverty mitigation market, mu.

Vendors		P21	P7	P15	P6	P3	C5	C9	C11	C12	C16	C19	C20	C24	C26	Total
FCFS	POP	0	0.11	0	0.53	0.08	0	0	0	0	0	0	0	0	0	0.72
MO	POP	0	0	0.29	0	0.00	0	0	0	0	0	0.46	0	0	0	0.75

**Table 18.** The hourly revenue in the energy poverty mitigation market for all vendors, mu.

Prosumers		h06	h07	h08	h09	h10	h11	h12	h13	h14	h15	h16	h17	h18	Total
FCFS	POP	0	0	0	0	0.00	0.08	0.51	0	0.02	0.11	0	0	0	0.72
MO	POP	0.07	0.05	0.06	0	0.00	0.04	0.24	0.02	0.01	0.10	0.03	0.03	0.09	0.75

#### 4.3. The Secondary Market—The Commercial Tariff Access Tier

As seen previously, the vendors can remain after the primary market with surplus available for selling. Both prosumers and consumers can become sellers on the secondary market. The energy poverty mitigation tier can help to reduce the surplus, but, if the vulnerable consumers have low demand and are in low numbers, the quantities still remaining after the settlement can be significant. For the demand-generation balance and the set of offers used in the case study, the total primary market surplus is of 63.18 kWh and reduces only to 61.39 kWh after the energy poverty mitigation market, if the MO trading method is used. For the FCFS method, the remaining surplus decreases from to 11.58 kWh to 10.86 kW. For further reducing the quantity sold to the grid, the local market model uses the second tier of the secondary market, operated according to the MO trading priority method used in the primary market, but with different market participants.

The sellers that can enter this market segment are the same as for the energy poverty mitigation market: prosumers with remaining surplus and consumers whose offers placed in the blockchain system of the primary market exceed their actual demand, thus becoming surplus. The buyers are consumers from the same microgrid who did not participate in the primary market, but are ready to occasionally buy surplus from the secondary market when it is available, at market prices. In exchange for this facility, they pay an extra fee, according to the formula from Equation (10). The quantities are determined automatically in the settlement phase of the energy poverty market or at the end of the primary market, if the EP tier is not used. The sell price offers are the offer prices entered by prosumers in the blockchain system of the primary market. For consumers the buy prices are: C13–0.47 mu/kWh, C17–0.30 mu/kWh, C18–0.42 mu/kWh, lower than the average offers from the primary market, in order to minimize the effect of the added tariffs. The fulfilment priority for the buy and sell offers is determined using the MO strategy from Figure 4, and the actual quantities and financial exchanges between sellers and buyers are settled as in the primary market.

Using as reference the trading data from Table 13, the sellers participating in the market are P21, P15, P6 and P3, if the FCFS method is used in the primary market, and P21, P15, P3, C5, C9, C11, C12, C16, C19, C20, C24, and C26. The buyers are three consumers that did not participate in the primary market, namely C13, C17 and C18. The fee applied for all the consumers is a 10% increase of the final

market, if the MO trading method is used. For the FCFS method, the remaining surplus decreases from 11.58 kWh to 10.86 kWh. For further reducing the quantity sold to the grid, the local market model uses the second tier of the secondary market, operated according to the MO trading priority method used in the primary market, but with different market participants.

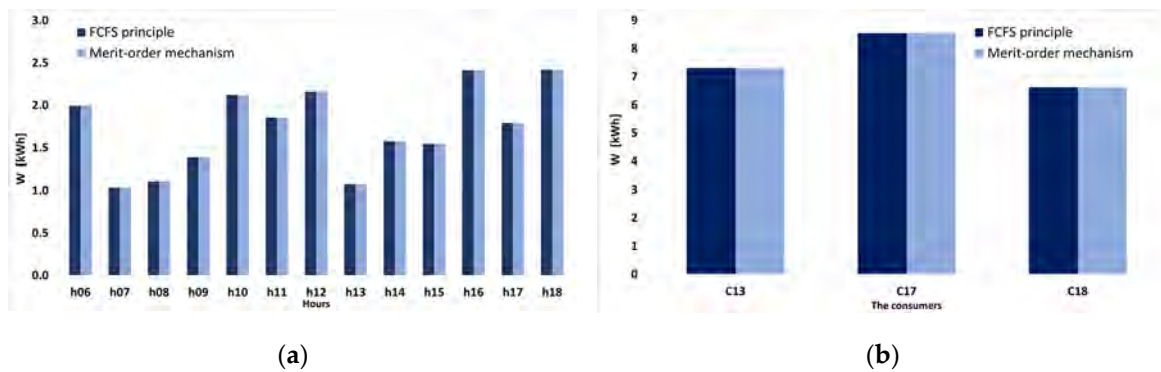
The sellers that can enter this market segment are the same as for the energy poverty mitigation market: prosumers with remaining surplus and consumers whose offers placed in the blockchain system of the primary market exceed their actual demand, thus becoming surplus. The buyers are consumers from the same microgrid who did not participate in the primary market, but are ready to the financial settlement, all three price alternatives will be considered: MCP, COP and POP, similar to occasionally buy surplus from the secondary market when it is available, at market prices. In the primary market. The quantities offered and actually traded by each vendor and buyer in the two primary market methodologies (FCFS and MO) are given in Appendix C, Tables A10–A14.

The results show that the use of the MO in the primary market leads to higher quantities traded in the end of the primary market, if the EP tier is not used. The sell price offers are the offer prices the tariff-access market tier, while if the FCFS priority is chosen, prosumer surplus is lower. The hourly results for the market and the daily quantities traded by the prosumers and the consumers are summarized, as for the previous market tiers, in Figures 20–23 and Tables 19–22.

The results from Tables 19–22 show that the tariff-access consumers are able to acquire 7.67 kWh buy and sell offers is determined using the MO strategy from Figure 4, and the actual quantities and for the FCFS primary market trading priority, exclusively from prosumer surplus. 21.28 kWh are bought for the MO trading priority method, mainly from consumer surplus, as it can be seen in Table 21.

Using as reference the trading data from Table 13, the sellers participating in the market are P21, P15, P6 and P3, if the FCFS method is used in the primary market, and P21, P15, P3, C5, C9, C11, C12, C16, C19, C20, C24, and C26. The buyers are three consumers that did not participate in the primary commercial market tiers, the prosumers lower their unsold surplus to only 3.19 kWh (FCFS) or 4.7 kWh (MO), while the consumer surplus remains high, at 35.94 kWh. The prosumer surplus is available buy price, and it is charged by the market administrator. For evaluating all the possibilities regarding mainly in the 09:00–14:00 interval, while the consumer surplus can be accessed outside this interval, the financial settlement, all three price alternatives will be considered: MCP, COP and POP, similar to the primary market. The quantities offered and actually traded by each vendor and buyer in the two primary market methodologies (FCFS and MO) are given in Appendix C, Tables A10–A14.

The results show that the use of the MO in the primary market leads to higher quantities traded the lower price offers used for the tariff-access consumers, the COP settlement option is the best choice in the tariff-access market tier, while if the FCFS priority is chosen, prosumer surplus is lower. For the consumers, incurring the lowest costs (see Table 25). For the FCFS trading priority method, hourly results for the market and the daily quantities traded by the prosumers and the consumers MCP and POP give the same results, which suggests that the merit order clearing price is determined by higher vendor price offers (Table 26).



Sustainability 2020, 12, x FOR PEER REVIEW 25 of 43

Figure 20. The buy quantities offered in the secondary tariff-access market (a) hourly (b) for each consumer.

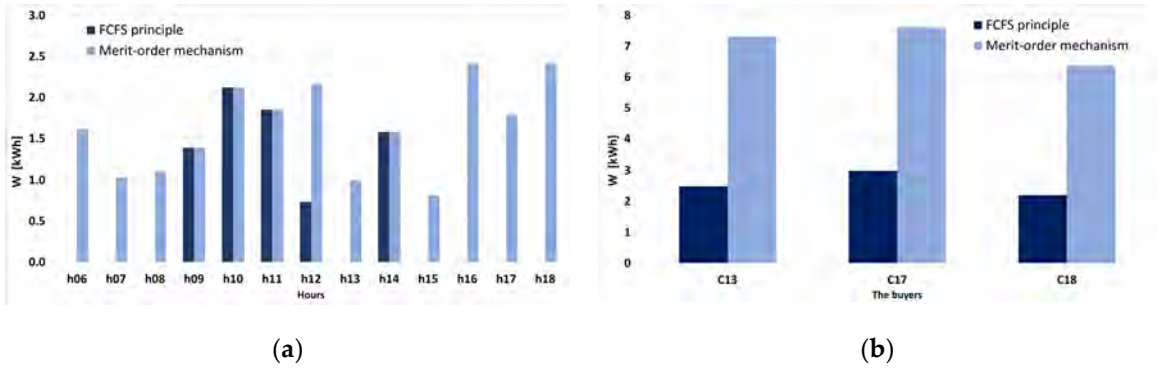
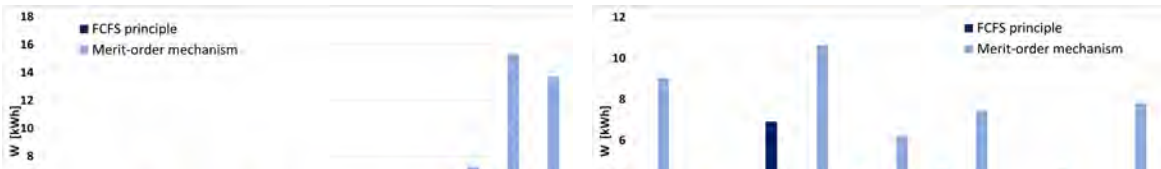


Figure 21. The buyer quantities traded in the secondary tariff-access market (a) hourly (b) for each consumer.







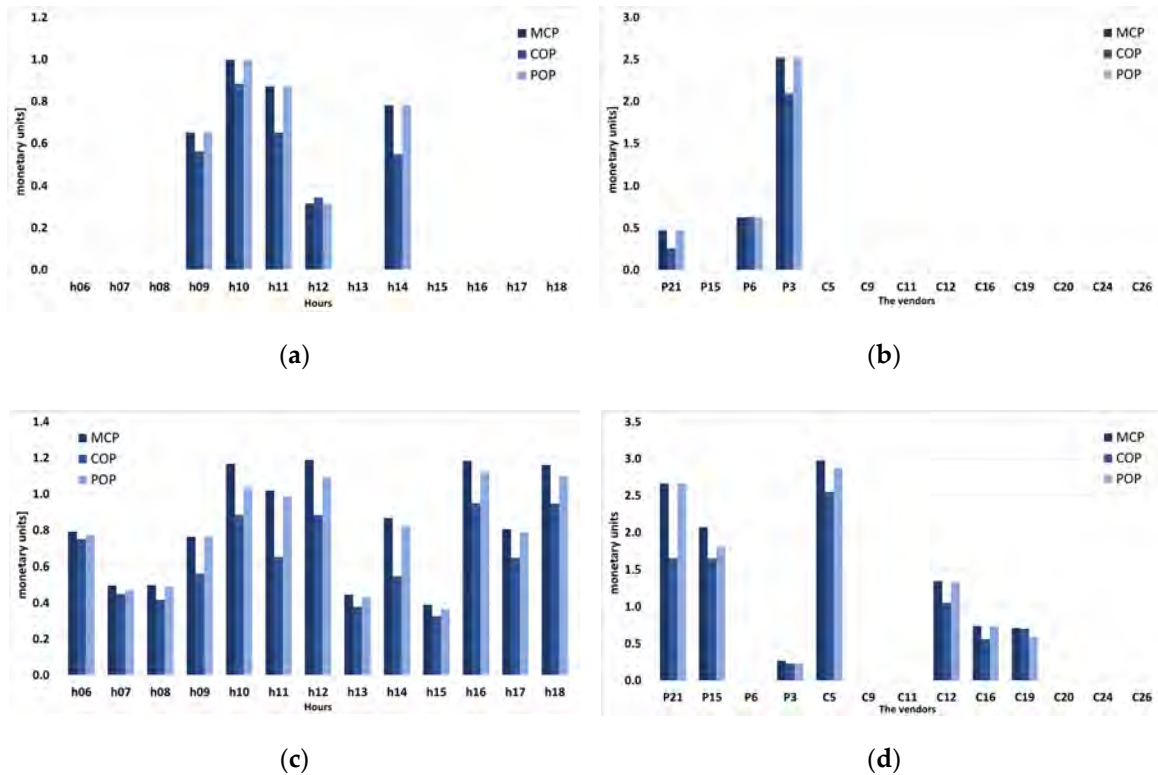


Figure 25. The tariff-access market revenue for vendors: (a) hourly values, FCFS; (b) daily values for each consumer, FCFS; (c) hourly values, MO; (d) daily values for each consumer, MO.

Table 23. The daily cost for each consumer in the tariff-access market,  $\mu$ .  
 Because of the larger quantities bought by the three consumers, the fee-access tier is more profitable for consumers plus vendors compared to the energy providers. In addition, considering the lower MCP price offers used for the tariff-access consumers, the COP settlement option is the best choice for the consumer, incurring the lowest costs (see Table 25). For the FCFS trading priority method, MCP and POP have the same results, which suggests that the merit order clearing price is determined by the higher vendor price offers (Table 26).

MO	COP	POP	Total	Total +10% Fee
MCP	3.43	2.28	2.67	8.39
COP	3.37	2.84	3.02	10.23
POP	3.37	2.84	3.02	11.26

4.4. The Secondary Market – The Commercial Incentive Access Tier

An alternative proposed in the local market model for the tariff-access secondary market is an invite-access market tier. This solution, while it has lower impact on the surplus reduction at market level, is viable for individual producers and consumers which are in the situation of frequently having unsold surplus after the final settlement. The invite-access strategy proposes that long-term P2P contracts can be established between seller-buyer pairs, stipulating that the buyer can automatically access the unsold surplus of the seller when it is available. In this case, the settlement is not performed at market level, but only for the two parties involved, and it can be considered that the buyer is an 'invited guest' in the local market.

Table 24. The hourly cost for all buyers in the tariff-access market,  $\mu$ .  
 The market diagram from Figure 1 considers the invite-access market as an alternative to the tariff-access market, but this approach is not mandatory, as the energy mitigation market, the tariff-access market and the invite-access market can be used in any desired order or number in the architecture of the local market.

Table 25. The daily revenue for each vendor in the tariff-access market,  $\mu$ .  
 Considering the layout from Figure 1 and the data from Tables 20, A2, A7 and A13, the evolution of the surplus of producer P21 in the MO primary market priority case is the one seen in Table 27. The producer is able to sell 4.842 kWh on the tariff-access market.  
 On the other hand, if the consumer has a P2P contract with consumer C22 who did not participate in the primary market, and the tariff access option is not activated, then it would be possible to sell in the invite-access market almost the same quantity, as can be seen in Table 28.



**Table 26.** The hourly revenue in the tariff-access market for all vendors, mu.

Prosumers		h06	h07	h08	h09	h10	h11	h12	h13	h14	h15	h16	h17	h18	Total
FCFS	MCP	0	0	0	0.65	1.00	0.87	0.32	0	0.78	0	0	0	0	3.61
	COP	0	0	0	0.56	0.88	0.65	0.34	0	0.55	0	0	0	0	2.99
	POP	0	0	0	0.65	1.00	0.87	0.32	0	0.78	0	0	0	0	3.61
MO	MCP	0.79	0.50	0.50	0.76	1.17	1.02	1.19	0.45	0.87	0.39	1.18	0.81	1.16	10.77
	COP	0.75	0.45	0.42	0.56	0.88	0.65	0.88	0.38	0.55	0.33	0.95	0.65	0.95	8.39
	POP	0.77	0.47	0.49	0.76	1.04	0.99	1.09	0.43	0.82	0.37	1.12	0.79	1.10	10.23

#### 4.4. The Secondary Market—The Commercial Invite Access Tier

An alternative proposed in the local market model for the tariff-access secondary market is an invite-access market tier. This solution, while it has lower impact on the surplus reduction at market level, is viable for individual prosumers and consumers which are in the situation of frequently having unsold surplus after the final settlement. The invite-access strategy proposes that long-term P2P contracts can be established between seller–buyer pairs, stipulating that the buyer can automatically access the unsold surplus of the seller when it is available. In this case, the settlement is not performed at market level, but only for the two parties involved, and it can be considered that the buyer is an ‘invited guest’ in the local market.

The market diagram from Figure 1 considers the invite-access market as an alternative to the tariff-access market, but this approach is not mandatory, as the energy mitigation market, the tariff-access market and the invite-access market can be used in any desired order or number in the architecture of the local market.

Considering the layout from Figure 1 and the data from Tables 2, A2, A7 and A13, the evolution of the surplus of prosumer P21 in the MO primary market priority case is the one seen in Table 27. The prosumer is able to sell 4.844 kWh on the tariff-access market.

**Table 27.** The surplus of prosumer P21 in the primary and secondary markets (energy poverty mitigation and tariff-access), kWh.

Hour	Initial Generation	Surplus			
		Initial	After the Primary Market	After the Secondary Market, 1st Tier	After the Secondary Market, 2nd Tier (Tariff-Access)
h01	2.361	1.588	0	0	0
h02	2.785	1.805	0	0	0
h03	3.286	1.726	0	0	0
h04	3.329	1.749	1.682	1.682	0.296
h05	3.639	2.292	2.292	2.292	1.963
h06	3.751	2.038	2.038	2.038	0.672
h07	3.735	1.822	1.822	1.822	1.014
h08	3.812	0.685	0	0	0
h09	3.742	1.182	1.182	1.182	0.227
h10	3.461	2.028	0	0	0
h11	2.832	0.819	0	0	0
h12	2.403	0	0	0	0
h13	2.237	1.17	0	0	0
Total	41.373	18.904	9.016	9.016	4.172

On the other hand, if the prosumer has a P2P contract with consumer C22 who did not participate in the primary market, and the tariff access option is not activated, then it would be possible to sell in the invite-access market almost the same quantity, as can be seen in Table 28. Furthermore, a scenario can be imagined in which the invite market is activated first, followed by the tariff-access market, in which case prosumer P21 would be able to sell their entire surplus in the local blockchain market.

Thus, if the market model is optimally configured, it can lead to the maximization of the local trading, thus minimizing the surplus sold to the grid at regulated tariffs.

**Table 28.** Comparison between the quantities sold by prosumer P21 in the tariff- and invite-access markets, kWh.

Hour	Surplus, P21	Consumption, C22	Electricity Sold in the Tariff-Access Market	Electricity Sold to C22 in the Invite-Access Market
h06	0	1.340	0	0
h07	0	0.960	0	0
h08	0	0.270	0	0
h09	1.682	0.420	1.386	0.420
h10	2.292	1.000	0.329	1.000
h11	2.038	0.930	1.366	0.930
h12	1.822	1.050	0.808	1.050
h13	0	1.020	0	0
h14	1.182	0.970	0.955	0.970
h15	0	1.010	0	0
h16	0	1.110	0	0
h17	0	1.540	0	0
h18	0	1.630	0	0
Total	9.016	13.250	4.844	4.370

## 5. Discussion

The results presented in the case study show that the secondary market has a positive effect regarding the surplus quantities sold by the prosumers in the local market. A key aspect that still needs to be discussed is the profitability of the local market, with its two components. Using Tables 3, 5, 11, 13, 19 and 21 for quantities, the influence of the primary and secondary markets on the quantities sold by the prosumers and consumers back to the grid is determined in Tables 29 and 30.

**Table 29.** The evolution of the electricity quantities bought from the grid in the time interval 06:00–18:00, before and after trading on each market segment, kWh.

Trading Priority in PM	Initial Consumption (No Market)	Traded in PM	Consumer Surplus for SM	Consumption Bought from the Grid after PM	Traded in SM1	Traded in SM2	Consumption Bought from the Grid after SM
FCFS	203.41	156.4	0	47.01	0.72	7.67	38.62
MO	203.41	154.1	49.31	98.62	1.79	21.28	75.55

**Table 30.** The evolution of the surplus quantities sold to the grid in the hourly interval 06:00–18:00, after trading on each market segment, kWh.

Market Player Type	PM Trading Priority	Initial Surplus	Traded in PM	Surplus after PM	Traded in SM1	Traded in SM2	Surplus after SM
prosumers	FCFS	167.97	156.4	11.58	0.72	7.67	3.18
	MO	167.97	154.1	13.88	0.6	9.1	4.17
consumers	FCFS	0	0	0	0	0	0
	MO	0	0	49.31	1.18	12.68	35.45

Table 29 shows that the offer quantities used in the MO trading priority determine a 49.3 kWh surplus at the consumers, which represents electricity traded but not consumed. This represents a high value, at 25% of the total consumption, and is mainly determined by hourly demand forecast errors. In the absence of the secondary market, the entire quantity would be sold to the grid, and the price mismatch between the buy price on the market (high) and sell price to the grid (low) would represent a cost increase for the consumers. Thus, accurate demand forecasts could reduce the costs for the consumers participating in the market. Additionally, it can be seen that the FCFS trading priority results in lower quantities sold back to the grid, as consumer surplus is absent.

Table 30 shows that the secondary market makes a significant contribution to reducing the prosumer surplus from 11.58/13.88 kWh to 3.18/4.17 kWh. Here, it can be seen that while the bulk of the surplus is sold on the primary market, the secondary market allows an important increase of local generation sold locally. The primary market helps prosumers to sell the majority of their surplus in the local market, and the supplementary market tiers allow consumers to mitigate forecast errors by acting as sellers, and also reduce the share of surplus prosumer generation sold back to the grid. These trading options can have, depending on local conditions, positive effects in increasing the number of prosumers in the microgrid and reducing the electricity acquired by the consumers from the grid, at higher prices and taxes. In other words, social and environmental sustainability can be improved.

The reduction of local generation quantities sold back to the grid has positive financial effects for both prosumers and consumers. In the absence of the local market, the prosumers would sell any surplus to the grid at the regulated price. The market allows them to obtain better prices, which are still attractive for consumers as long as they do not exceed the tariff paid for the electricity imported from the grid. On the other hand, by participating in the local market, the consumers have the chance of paying less for electricity. From Tables 7, 9, 15, 17, 23 and 25, the costs and revenues for the sellers and vendors on each market segment can be summarized in Tables 31 and 32, for the 06:00–18:00 interval of the analyzed day.

**Table 31.** Comparison between the costs of the consumers in each market segment and for each settlement price, mu.

Trading Priority in PM	Settlement Price	PM	SM1	SM2	SM	Total PM + SM
FCFS	MCP	71.11	0	3.98	3.98	75.09
	COP	83.54	0	3.29	3.29	86.83
	POP	71.11	0.72	3.98	4.7	75.81
MO	MCP	80.36	0	11.85	11.85	92.21
	COP	84.2	0	9.23	9.23	93.43
	POP	69.28	0.75	11.26	12.01	81.29

**Table 32.** Comparison between the vendor revenues on all market segments, mu.

Sellers	Revenue without Local Market	PM Trading Priority	Settlement Price	PM	SM1	SM2	SM	Total PM + SM	Total PM + SM + Grid	
prosumers	42.16	FCFS	MCP	71.11	0	3.61	3.61	74.72	75.52	
			COP	83.54	0	2.99	2.99	86.53	87.33	
			POP	71.11	0.72	3.61	4.33	75.44	76.24	
		MO	MCP	80.36	0	5	5	85.36	86.41	
			COP	84.2	0	3.53	3.53	87.73	88.78	
			POP	69.28	0.29	4.7	4.99	74.27	75.32	
	consumers	12.38	FCFS	MCP	0	0	0	0	0	12.38
				COP	0	0	0	0	0	12.38
				POP	0	0	0	0	0	12.38
MO			MCP	0	0	5.77	5.77	5.77	14.67	
			COP	0	0	4.86	4.86	4.86	13.76	
			POP	0	0.46	5.53	5.99	5.99	14.89	

Table 31 shows that the highest costs for the consumers occur when the COP settlement is used, while the POP settlement offers the best buy prices from the market. In Table 32, it can be seen that the prosumer revenues can double when the primary and secondary markets are used, with the highest profits being achieved on the primary market. The secondary market is, however, useful for the consumers who need to sell surplus remaining from the primary market, increasing their daily revenue by up to 200% (14.89 mu, compared to 12.38 mu).

Using the traded quantities and factoring the costs and revenues presented above, a comparison can be made between the daily electricity costs for the aggregated network demand in the 06:00–18:00

interval. Table 33 shows that the combined effect of the primary and secondary markets can decrease the cost by up to 26% when the FCFS trading prioritization is used. For MO prioritization, because of the significant consumer surplus in the primary market, the cost increases when MCP or COP settlement is used, but the effect of the secondary market is to compensate a fraction of the increase.

**Table 33.** Comparison between the influence of the primary secondary market on the electricity costs for the microgrid, time interval 06:00–18:00, mu.

PM Trading Priority	Settlement Price	Cost with Regulated Tariff	Cost with PM	Cost with PM and SM	% Reduction PM	% Reduction PM + SM
FCFS	MCP	136.89	102.75	101.08	24.94	26.16
	COP	136.89	115.18	112.82	15.86	17.59
	POP	136.89	102.75	101.80	24.94	25.64
MO	MCP	136.89	146.73	137.29	−7.19	−0.29
	COP	136.89	150.57	139.42	−9.99	−1.84
	POP	136.89	135.65	126.15	0.91	7.85

It is important to note that the results presented in the paper are highly dependent on the input data used for the case study. The profits of the prosumers and the cost reductions for the consumers are affected by the quantities and prices offered in the market by both parties and can vary significantly from the results presented in the paper. Also, depending on local constraints, the trading tiers of the secondary market can be used only partially and in a different order. The case study presents a scenario of a complete market trading sequence to show the capabilities of the proposed model.

The results presented in Tables 29–33 use for the commercial tier of the secondary market only the tariff-access option.

## 6. Conclusions

The paper proposes a new local market for active microgrids, designed to maximize the surplus sold by the prosumers to the local consumers. The local market requires smart grid features in the microgrid and a blockchain ledger for submitting buy and sell offers. Trading is performed in two phases, first on a primary market, followed by a two-tier secondary market. The case study shows that the secondary market can help the prosumers to sell more surplus to the local consumers, increasing their profitability. The advantages of the local market can be discussed from several perspectives:

- The reduction of electricity quantities traded back to the grid (at lower prices) for prosumers;
- The reduction of electricity costs for consumers, brought by acquiring cheaper electricity from the local prosumers;
- The increase of profits for prosumers, by selling larger quantities to local consumers, at higher prices than the regulated tariff used to sell back to the grid. This can also be seen as an incentive for increasing sustainable electricity generation from renewable resources;
- The energy poverty mitigation for some consumers, an aspect regarding economic and social sustainability.

However, as main disadvantages, accurate demand forecasts are necessary for the consumers if the MO trading method is used, for optimal market benefits. Furthermore, the implementation of the proposed market model is dependent on several prerequisites: the implementation of smart grid capabilities in the microgrid, the creation of adequate regulations by regional or national authorities, and the development of residential renewable electricity generation, all these being in incipient development stages across the world.

The proposed algorithm is a comprehensive tool of the trading process for consumers and prosumers in microgrids, considering the current regulation framework regarding prosumer activity in the Romanian electricity market, and future research directions considered by the authors aim to extend its capabilities for social inclusion, analyzing the influence of storage capabilities on local

market trading dynamics and profitability, and considering new trading options, by comparison with similar real local market models, as they become available in the literature.

## 7. Patents

National Patent Application “Innovative method of decision-making assistance aimed at streamlining the management of prosumer activity”, Romania, 2020, in press.

**Author Contributions:** Conceptualization, B.-C.N., O.I. and G.G.; methodology, B.-C.N. and O.I.; software, B.-C.N. and O.I.; validation, O.I. and B.-C.N.; formal analysis, M.G. and D.-M.I.; investigation, O.I. and G.G.; data curation, O.I.; writing—original draft preparation, B.-C.N. and O.I.; writing—O.I., G.G., D.-M.I. and M.G.; supervision, M.G. and D.-M.I. All the figures and tables used in the paper were created by the authors. All authors have read and agreed to the published version of the manuscript.

**Funding:** This research was funded by “Gheorghe Asachi” Technical University of Iasi, Romania, through the support of national project PNIII-1.2.PDI-PFC-C1-2018, as COMPETE project no. 9PFE/2018, financed by the Romanian Government.

**Acknowledgments:** The authors would like to express their gratitude to Maria Carmen Loghin, the Vice Rector of the “Gheorghe Asachi” Technical University of Iasi for his technical support, supporting logistics and open access of this journal publication.

**Conflicts of Interest:** The authors declare no conflict of interest.

## Abbreviations

ADMM	Alternating Direction Method of Multipliers
ADN	Active Distribution Network
AEA	Active Energy Agent
ANRE	Romanian Energy Regulatory Authority
C	Consumers/Consumption Quantity
CO	Consumption Offers
COP	Consumer Offers Price
DM	Demurrage Mechanism
DNOs	Distribution Network Operators
DR	Demand Response
EU	European Union
f%	fee added to the price resulting from trading mechanism
FCFS	First-Come-First-Served
G	Generation Quantity
GO	Generation Offers
HEM	Home Energy Management
kWh	kilowatt-hours
LEM	Local Electricity Market
LV	Low Voltage
MCP	Market Clearing Price
MEP	Multiple Energy Prosumers
MO	Merit-order
mu	Monetary units
NC	Total Number of Consumers
NCM	Number of Consumers participating in the Market
NP	Total Number of Prosumers
NPM	Number of Prosumers participating in the Market
P	Prosumer/Price
P2P	Peer-to-Peer
PCO	Price of Consumption Offers
PGO	Price of Generation Offers
PM	Primary Market
POP	Prosumer Offers Price

PoW	Proof-of-Work
PV	Photovoltaic
REScoop	European Federation of Renewable Energy Cooperatives
S	Surplus
SM	Secondary Market
SSRES	Small-Scale Renewable Energy Sources
TC	The Maximum Amount of Traded Electricity by Consumers
TP	Transaction of Prosumers
TCO	The Quantity of Electricity Actually Traded
WEM	Wholesale Electricity Market

## Appendix A. Input Data for the Primary Market

**Table A1.** The hourly demand profiles for the entire microgrid, in kW (27 consumers).

Hour	C2	C3	C4	C5	C6	C7	C8	C9	C10
h1	0.616	2.010	0.273	0.000	1.370	2.418	1.152	1.936	0.310
h2	0.608	1.908	0.078	0.020	1.520	2.210	1.664	1.368	0.678
h3	0.557	2.004	0.048	0.260	1.910	2.149	2.056	1.376	0.300
h4	0.522	2.010	0.306	0.040	1.770	2.151	2.048	2.048	0.640
h5	0.522	1.902	0.063	0.050	1.990	2.192	1.816	1.528	0.360
h6	0.571	2.004	0.165	0.250	2.070	2.299	1.168	2.992	0.468
h7	0.529	1.836	0.213	0.125	2.280	2.364	0.720	3.352	0.748
h8	0.592	1.236	0.060	4.710	2.530	2.543	1.704	2.240	3.208
h9	0.562	1.302	0.312	1.290	1.850	2.382	1.976	2.112	2.815
h10	0.616	1.200	0.258	0.525	1.850	2.549	1.944	2.192	1.483
h11	0.860	1.188	0.243	2.985	1.460	2.426	1.904	2.232	4.538
h12	0.535	1.146	0.423	1.895	1.180	2.414	1.872	2.144	3.295
h13	0.641	1.140	0.198	4.595	1.650	2.450	2.456	2.048	3.650
h14	0.322	1.374	0.378	0.930	1.950	2.418	2.632	2.176	5.230
h15	0.181	1.944	0.321	0.260	1.810	2.444	1.896	2.256	4.293
h16	0.214	1.542	0.207	0.535	2.640	2.467	2.072	2.328	3.895
h17	0.781	2.148	0.495	2.125	2.810	2.553	2.080	2.288	3.028
h18	0.764	1.902	0.282	1.025	2.720	2.757	2.016	2.336	1.980
h19	0.426	1.968	0.336	0.140	3.580	3.042	2.720	2.464	1.768
h20	0.426	1.968	0.336	0.140	3.580	3.042	2.720	2.464	1.768
h21	0.496	1.956	0.207	0.210	5.310	3.515	2.672	3.136	3.033
h22	0.561	1.986	0.405	0.480	5.390	3.248	2.488	1.312	5.695
h23	0.554	1.872	0.246	0.195	4.750	3.075	2.432	1.336	4.033
h24	0.578	1.986	0.045	0.100	3.170	2.713	2.088	1.184	1.180
h06–18	7.168	19.962	3.555	21.250	26.800	32.066	24.440	30.696	38.631
Hour	C11	C12	C13	C14	C15	C16	C17	C18	C19
h1	0.230	0.585	0.142	0.910	2.783	2.220	0.210	0.360	0.345
h2	0.220	0.765	0.078	0.920	2.411	1.320	0.000	0.525	0.286
h3	0.200	0.585	0.352	0.925	2.548	0.942	0.000	0.534	0.243
h4	0.200	0.675	0.440	1.225	2.313	0.972	0.045	0.636	0.213
h5	0.200	0.660	0.062	1.345	2.288	0.954	0.000	0.444	0.237
h6	1.240	0.570	1.416	1.290	2.426	1.044	0.115	0.462	0.242
h7	1.400	0.900	0.482	1.325	3.239	1.374	0.075	0.477	0.281
h8	1.440	0.630	0.182	1.520	3.798	3.984	0.475	0.450	0.287
h9	1.170	0.765	0.502	1.430	3.097	2.184	0.380	0.504	0.278
h10	1.130	0.645	1.046	1.120	4.371	1.986	0.495	0.579	0.268

Table A1. Cont.

Hour	C11	C12	C13	C14	C15	C16	C17	C18	C19
h11	1.390	0.555	0.150	1.170	2.994	1.986	1.130	0.573	0.285
h12	1.740	0.630	1.032	1.265	3.763	2.844	0.630	0.498	0.315
h13	1.760	0.615	0.056	1.760	2.999	1.566	0.420	0.600	0.301
h14	1.200	0.570	0.056	2.000	2.759	0.930	0.980	0.540	0.329
h15	0.280	0.750	0.236	1.840	3.807	0.798	0.955	0.357	0.312
h16	0.460	0.555	1.024	1.815	3.317	1.152	0.965	0.423	0.350
h17	3.180	0.825	0.232	2.015	3.214	1.944	0.970	0.588	0.366
h18	2.570	0.780	0.890	2.365	2.940	2.046	0.960	0.570	0.468
h19	2.890	0.780	0.458	2.480	3.445	2.460	1.450	0.678	0.443
h20	2.890	0.780	0.458	2.480	3.445	2.460	1.450	0.678	0.443
h21	3.210	0.630	0.864	2.580	3.278	1.884	1.385	0.753	0.454
h22	3.260	0.570	1.326	2.365	2.475	1.374	1.660	0.621	0.482
h23	2.815	0.720	0.376	2.060	2.073	1.380	1.235	0.750	0.509
h24	1.780	0.570	0.200	1.495	2.769	1.158	0.880	0.390	0.328
h06–18	18.960	8.790	7.304	20.915	42.724	23.838	8.550	6.621	4.082
Hour	C20	C21	C22	C23	C24	C25	C26	C27	C28
h1	0.973	0.636	0.790	0.049	1.266	0.384	0.248	0.024	0.973
h2	1.013	0.484	0.780	0.056	1.194	0.384	0.296	0.000	1.013
h3	0.733	0.448	0.730	0.749	1.056	0.388	0.260	0.000	0.733
h4	0.453	0.460	0.920	1.148	1.032	0.392	0.292	0.000	0.453
h5	0.680	0.520	0.800	1.148	1.014	0.400	0.208	0.000	0.680
h6	0.773	0.512	1.340	1.148	1.020	0.396	0.356	0.192	0.773
h7	0.980	0.428	0.960	1.946	1.122	0.376	0.700	0.140	0.980
h8	1.560	0.368	0.270	1.393	1.116	0.352	0.336	0.152	1.560
h9	1.580	0.408	0.420	1.596	1.110	0.356	0.144	0.000	1.580
h10	1.347	0.408	1.000	2.975	1.110	0.360	0.128	0.004	1.347
h11	1.713	0.668	0.930	1.519	1.242	0.620	0.204	0.076	1.713
h12	1.913	0.412	1.050	2.492	1.260	0.344	0.320	0.508	1.913
h13	3.127	0.344	1.020	1.974	1.266	0.324	0.476	0.056	3.127
h14	2.560	0.428	0.970	1.974	1.260	0.332	0.384	0.020	2.560
h15	1.433	1.068	1.010	2.240	1.206	0.940	0.456	0.244	1.433
h16	2.013	0.424	1.110	2.296	1.134	2.500	0.352	0.088	2.013
h17	4.000	0.448	1.540	1.778	1.140	2.544	2.000	0.080	4.000
h18	1.067	0.468	1.630	1.939	1.260	2.820	0.876	0.228	1.067
h19	1.907	0.436	1.570	1.750	1.296	2.104	1.824	0.000	1.907
h20	1.907	0.436	1.570	1.750	1.296	2.104	1.824	0.000	1.907
h21	2.473	1.092	1.280	1.106	1.212	2.144	0.728	0.408	2.473
h22	2.253	1.484	1.110	1.092	1.194	2.084	0.688	0.412	2.253
h23	1.933	1.364	0.710	1.092	1.194	2.248	0.256	0.532	1.933
h24	1.260	0.880	0.840	0.763	1.176	2.008	0.324	0.144	1.260
h06–18	12.900	24.066	6.384	13.250	25.270	15.246	12.264	6.732	1.788

Table A2. The hourly generation profiles for the prosumers in the microgrid, in kW (8 prosumers).

Hour	P27	P21	P7	P15	P6	P3	P10	P25
h1	0	0	0	0	0	0	0	0
h2	0	0	0	0	0	0	0	0
h3	0	0	0	0	0	0	0	0
h4	0	0	0	0	0	0	0	0
h5	0	0	0	0	0	0	0	0
h6	0.249	2.361	2.183	4.374	2.011	2.212	1.965	4.072

Table A2. Cont.

Hour	P27	P21	P7	P15	P6	P3	P10	P25
h7	0.518	2.785	2.627	4.824	2.132	2.642	2.364	4.609
h8	1.004	3.286	3.247	5.384	2.357	3.115	2.922	4.942
h9	1.581	3.329	3.438	5.325	2.592	3.139	3.094	5.066
h10	1.735	3.639	3.642	5.673	2.966	3.451	3.278	5.342
h11	1.859	3.751	3.826	5.769	3.346	3.561	3.443	5.417
h12	1.915	3.735	3.639	5.643	3.509	3.539	3.275	5.320
h13	1.984	3.812	3.863	5.825	3.945	3.603	3.477	5.506
h14	1.756	3.742	3.803	5.704	3.297	3.553	3.423	5.474
h15	1.562	3.461	3.492	5.353	2.994	3.276	3.143	4.908
h16	0.915	2.832	2.877	4.642	2.541	2.675	2.589	4.343
h17	0.495	2.403	2.305	4.276	2.352	2.283	2.075	4.017
h18	0.308	2.237	2.105	4.101	1.791	2.123	1.895	3.859
h19	0	0	0	0	0	0	0	0
h20	0	0	0	0	0	0	0	0
h21	0	0	0	0	0	0	0	0
h22	0	0	0	0	0	0	0	0
h23	0	0	0	0	0	0	0	0
h24	0	0	0	0	0	0	0	0

Table A3. The forecasted quantity offers of the buyers (consumers) for the primary market, MO trading priority, in kWh (11 consumers).

Trading Interval	C5	C8	C9	C11	C12	C14	C16	C19	C20	C24	C26
h6	0.30	1.10	3.20	1.30	0.60	1.20	2.00	0.20	0.50	1.20	0.50
h7	0.40	0.80	3.40	1.40	0.80	1.30	2.00	0.30	2.10	2.00	0.40
h8	4.10	1.70	2.10	1.30	0.60	1.40	3.50	0.30	0.60	1.50	0.40
h9	1.50	2.00	2.20	1.00	0.80	1.50	2.00	0.20	0.40	1.60	0.40
h10	0.80	1.90	2.10	1.00	0.80	1.10	2.00	0.30	0.40	2.80	0.40
h11	3.20	1.90	2.20	0.90	0.60	1.20	2.00	0.30	0.30	1.50	0.60
h12	2.00	2.00	2.10	0.00	0.60	1.30	2.00	0.30	0.50	2.40	0.40
h13	4.70	2.50	2.00	1.50	0.70	1.80	1.80	0.30	0.70	2.00	0.30
h14	1.10	2.40	2.20	1.20	0.70	2.00	1.00	0.30	0.60	2.00	0.30
h15	0.60	2.10	2.20	0.70	0.80	1.80	1.00	0.30	1.30	2.20	1.00
h16	0.60	2.20	2.30	0.70	0.70	1.90	1.00	0.40	1.20	2.30	2.50
h17	2.60	2.40	2.40	2.50	0.70	2.10	1.50	0.40	1.60	1.80	2.50
h18	1.30	2.30	2.50	3.00	0.90	2.20	2.00	0.50	1.60	1.90	2.80

Table A4. The offer prices submitted by the buyers (consumers) in the primary market, in mu/kWh.

Trading Interval	C5	C8	C9	C11	C12	C14	C16	C19	C20	C24	C26
h6–h18	0.45	0.6	0.55	0.52	0.48	0.6	0.49	0.39	0.55	0.57	0.5

Table A5. The offer prices submitted by the sellers (prosumers) in the primary market, in mu/kWh.

Trading Interval	P27	P21	P7	P15	P6	P3	P10	P25
h6–h18	0.43	0.55	0.4	0.48	0.43	0.47	0.42	0.43



## Appendix B. Data for the Energy Poverty Mitigation Market

**Table A6.** The sell offer quantities for the energy poverty mitigation tier (kWh), FCFS trading priority.

Hour	P21	P7	P15	P6	P3	Total
h06	0	0	0	0	0	0
h07	0	0	0	0	0	0
h08	0	0	0	0	0	0
h09	0	0	0	0	1.815	1.815
h10	0	0	1.302	0	2.840	4.142
h11	0	0	0	0	2.345	2.345
h12	0	0	0	1.241	0	1.241
h13	0	0	0	0	0	0
h14	1.182	0	0	0.739	0	1.921
h15	0	0.113	0	0	0	0.113
h16	0	0	0	0	0	0
h17	0	0	0	0	0	0
h18	0	0	0	0	0	0
Total	1.182	0.113	1.302	1.980	7.000	11.576

**Table A7.** The sell offer quantities for the energy poverty mitigation tier, MO trading priority, in kWh.

Hour	P21	P15	P3	C5	C9	C11	C12	C16	C19	C20	C24	C26	Total
h06	0	0	0	0.300	0	0	0.600	0.708	0.200	0	0	0	1.808
h07	0	0	0	0.400	0	0	0.800	1.838	0.300	0	0	0	3.338
h08	0	0	0	4.100	0	0	0.600	0.397	0.300	0	0	0	5.397
h09	1.682	0	0	0	0	0	0	0	0	0	0	0	1.682
h10	2.292	1.302	0.493	0	0	0	0	0	0	0	0	0	4.087
h11	2.038	0.563	0	0	0	0	0	0	0	0	0	0	2.601
h12	1.822	1.860	0	0	0	0	0	0	0	0	0	0	3.682
h13	0	0	0	0.746	0	0	0	0	0.3	0	0	0	1.046
h14	1.182	0.641	0	0	0	0	0	0	0	0	0	0	1.823
h15	0	0	0	0.600	0	0	0.155	0	0.300	0	0	0	1.055
h16	0	0	0	0.600	0.241	0.700	0.700	1	0.400	1.200	0	2.500	7.341
h17	0	0	0	2.600	2.400	2.500	0.700	1.5	0.400	1.600	1.181	2.500	15.381
h18	0	0	0	1.300	1.835	3.000	0.900	2	0.500	1.600	0	2.800	13.935
Total	9.016	4.366	0.493	10.646	4.476	6.200	4.455	7.443	2.700	4.400	1.181	7.800	63.176

**Table A8.** The sell quantities traded in the energy poverty mitigation tier, FCFS priority, in kWh.

Hour	P21	P7	P15	P6	P3	Total
h06	0	0	0	0	0	0
h07	0	0	0	0	0	0
h08	0	0	0	0	0	0
h09	0	0	0	0	0	0
h10	0	0	0	0	0.004	0.004
h11	0	0	0	0	0.076	0.076
h12	0	0	0	0.508	0	0.508
h13	0	0	0	0	0	0
h14	0	0	0	0.020	0	0.020
h15	0	0.113	0	0	0	0.113
h16	0	0	0	0	0	0
h17	0	0	0	0	0	0
h18	0	0	0	0	0	0
Total	0	0.113	0	0.528	0.08	0.721

**Table A9.** The sell quantities traded in the energy poverty mitigation tier, MO priority, in kWh.

Hour	P21	P15	P3	C5	C9	C11	C12	C16	C19	C20	C24	C26	Total
h06	0	0	0	0	0	0	0	0	0.192	0	0	0	0.192
h07	0	0	0	0	0	0	0	0	0.140	0	0	0	0.140
h08	0	0	0	0	0	0	0	0	0.152	0	0	0	0.152
h09	0	0	0	0	0	0	0	0	0	0	0	0	0
h10	0	0	0.004	0	0	0	0	0	0	0	0	0	0.004
h11	0	0.076	0	0	0	0	0	0	0	0	0	0	0.076
h12	0	0.508	0	0	0	0	0	0	0	0	0	0	0.508
h13	0	0	0	0	0	0	0	0	0.056	0	0	0	0.056
h14	0	0.020	0	0	0	0	0	0	0	0	0	0	0.020
h15	0	0	0	0	0	0	0	0	0.244	0	0	0	0.244
h16	0	0	0	0	0	0	0	0	0.088	0	0	0	0.088
h17	0	0	0	0	0	0	0	0	0.080	0	0	0	0.080
h18	0	0	0	0	0	0	0	0	0.228	0	0	0	0.228
Total	0	0.604	0.004	0	0	0	0	0	1.180	0	0	0	1.788

**Appendix C. Data for the Commercial Secondary Market, Fee-Access Method****Table A10.** The sell offer quantities for the commercial fee-access tier, FCFS trading priority, in kWh.

Hour	P21	P15	P6	P3	Total
h06	0	0	0	0	0
h07	0	0	0	0	0
h08	0	0	0	0	0
h09	0	0	0	1.815	1.815
h10	0	1.302	0	2.836	4.138
h11	0	0	0	2.269	2.269
h12	0	0	0.733	0	0.733
h13	0	0	0	0	0
h14	1.182	0	0.719	0	1.901
h15	0	0	0	0	0
h16	0	0	0	0	0
h17	0	0	0	0	0
h18	0	0	0	0	0
Total	1.182	1.302	1.452	6.920	10.855

**Table A11.** The sell offer quantities for the commercial fee-access tier, MO trading priority, in kWh.

Vendor	P21	P15	P3	C5	C9	C11	C12	C16	C19	C20	C24	C26	Total
h06	0	0	0	0.300	0	0	0.600	0.708	0.008	0	0	0	1.616
h07	0	0	0	0.400	0	0	0.800	1.838	0.160	0	0	0	3.198
h08	0	0	0	4.100	0	0	0.600	0.397	0.148	0	0	0	5.245
h09	1.682	0	0	0	0	0	0	0	0	0	0	0	1.682
h10	2.292	1.302	0.489	0	0	0	0	0	0	0	0	0	4.083
h11	2.038	0.487	0	0	0	0	0	0	0	0	0	0	2.525
h12	1.822	1.352	0	0	0	0	0	0	0	0	0	0	3.174
h13	0	0	0	0.746	0	0	0	0	0.244	0	0	0	0.990
h14	1.182	0.621	0	0	0	0	0	0	0	0	0	0	1.803
h15	0	0	0	0.600	0	0	0.155	0	0.056	0	0	0	0.811
h16	0	0	0	0.600	0.241	0.700	0.700	1.000	0.312	1.200	0	2.500	7.253
h17	0	0	0	2.600	2.400	2.500	0.700	1.500	0.320	1.600	1.181	2.500	15.301
h18	0	0	0	1.300	1.835	3.000	0.900	2.000	0.272	1.600	0	2.800	13.707
Total	9.016	3.762	0.489	10.646	4.476	6.200	4.455	7.443	1.520	4.400	1.181	7.800	61.388

**Table A12.** The sell quantities traded in the commercial fee-access tier, FCFS trading priority.

Hour	21	15	6	3	Total
h06	0	0	0	0	0
h07	0	0	0	0	0
h08	0	0	0	0	0
h09	0	0	0	1.386	1.386
h10	0	0	0	2.120	2.120
h11	0	0	0	1.853	1.853
h12	0	0	0.733	0	0.733
h13	0	0	0	0	0
h14	0.858	0	0.719	0	1.576
h15	0	0	0	0	0
h16	0	0	0	0	0
h17	0	0	0	0	0
h18	0	0	0	0	0
Total	0.858	0	1.452	5.359	7.668

**Table A13.** The sell quantities traded in the commercial fee-access tier, MO trading priority, in kWh.

Hour	P21	P15	P3	C5	C9	C11	C12	C16	C19	C20	C24	C26	Total
h06	0	0	0	0.300	0	0	0.600	0.708	0.008	0	0	0	1.616
h07	0	0	0	0.400	0	0	0.474	0	0.160	0	0	0	1.034
h08	0	0	0	0.959	0	0	0	0	0.148	0	0	0	1.107
h09	1.386	0	0	0	0	0	0	0	0	0	0	0	1.386
h10	0.329	1.302	0.489	0	0	0	0	0	0	0	0	0	2.120
h11	1.366	0.487	0	0	0	0	0	0	0	0	0	0	1.853
h12	0.808	1.352	0	0	0	0	0	0	0	0	0	0	2.160
h13	0	0	0	0.746	0	0	0	0	0.244	0	0	0	0.990
h14	0.955	0.621	0	0	0	0	0	0	0	0	0	0	1.576
h15	0	0	0	0.600	0	0	0.155	0	0.056	0	0	0	0.811
h16	0	0	0	0.600	0	0	0.700	0.8	0.312	0	0	0	2.412
h17	0	0	0	1.470	0	0	0	0	0.320	0	0	0	1.790
h18	0	0	0	1.300	0	0	0.848	0	0.272	0	0	0	2.420
Total	4.844	3.762	0.489	6.375	0	0	2.777	1.508	1.520	0	0	0	21.275

**Table A14.** The buy quantities traded in the commercial fee-access tier, MO trading priority, in kWh.

Hour	C13	C17	C18	Total
h06	0	0	0	0
h07	0	0	0	0
h08	0	0	0	0
h09	0.502	0.380	0.504	1.386
h10	1.046	0.495	0.579	2.120
h11	0.150	1.130	0.573	1.853
h12	0.733	0	0	0.733
h13	0	0	0	0
h14	0.056	0.980	0.540	1.576
h15	0	0	0	0
h16	0	0	0	0
h17	0	0	0	0
h18	0	0	0	0
Total	2.487	2.985	2.196	7.668

**Table A15.** The buy quantities traded in the commercial fee-access tier, MO trading priority, in kWh.

Hour	C13	C17	C18	Total
h06	1.416	0	0.200	1.616
h07	0.482	0.075	0.477	1.034
h08	0.182	0.475	0.450	1.107
h09	0.502	0.380	0.504	1.386
h10	1.046	0.495	0.579	2.120
h11	0.150	1.130	0.573	1.853
h12	1.032	0.630	0.498	2.160
h13	0.056	0.334	0.600	0.990
h14	0.056	0.980	0.540	1.576
h15	0.236	0.218	0.357	0.811
h16	1.024	0.965	0.423	2.412
h17	0.232	0.970	0.588	1.790
h18	0.890	0.960	0.570	2.420
Total	7.304	7.612	6.359	21.275

## References

1. Agora-Energiewende, European Energy Transition 2030: The Big Picture. Available online: [https://www.agora-energiewende.de/fileadmin2/Projekte/2019/EU\\_Big\\_Picture/153\\_EU-Big-Pic\\_WEB.pdf](https://www.agora-energiewende.de/fileadmin2/Projekte/2019/EU_Big_Picture/153_EU-Big-Pic_WEB.pdf) (accessed on 1 August 2020).
2. Saevelect, What Is eDREAM? Available online: <https://www.todaysoftmag.ro/article/2469/tehnologia-blockchain> (accessed on 1 August 2020).
3. Haber, S.; Scott Stornetta, W. How to time-stamp a digital document. *J. Cryptol.* **1991**, *3*, 99–111. [CrossRef]
4. Bayer, D.; Haber, S.; Scott Stornetta, W. *Improving the Efficiency and Reliability of Digital Time-Stamping*; Capocelli, R., de Santis, A., Vaccaro, U., Eds.; Sequences II; Springer: New York, NY, USA, 1993.
5. Toth, L.A. Blockchain Technology, Today Software Magazine. Available online: <https://www.todaysoftmag.ro/article/2469/tehnologia-blockchain> (accessed on 1 August 2020).
6. Tradesilvania. Why Use Blockchain Technology? Available online: <https://tradesilvania.com/ro/> (accessed on 1 August 2020).
7. Stratulat, A.M. Blockchain: A New Paradigm for the Energy System. Available online: <https://medium.com/@adrianmihaistratulat/blockchain-o-noua-paradigma-pentru-sistemul-energetic-ac95761b12a2> (accessed on 1 August 2020).
8. Unlimited Energy for Energy Communities from Renewable Sources. Available online: <http://fiiprosumator.ro/static/brosura-greenpeace-energie-fara-limite.pdf> (accessed on 1 August 2020).
9. Unguru, M. Blockchain technology: Opportunities for the energy sector. *Euro Infor* **2018**, *2*, 53–58.
10. NewsEnergy, Blockchain Technology and Renewables, the Next “Power Couple”. Available online: <https://newsenergy.ro/tehnologia-blockchain-si-regenerabilele-urmatorul-power-couple/> (accessed on 1 August 2020).
11. Andoni, M.; Robu, V.; Flynn, D.; Abram, S.; Geach, D.; Jenkins, D.; McCallum, P.; Peacock, A. Blockchain technology in the energy sector: A systematic review of challenges and opportunities. *Renew. Sustain. Energy Rev.* **2019**, *100*, 143–174. [CrossRef]
12. Mika, B.; Goudz, A. Blockchain-technology in the energy industry: Blockchain as a driver of the energy revolution? With focus on the situation in Germany. *Energy Syst.* **2020**. [CrossRef]
13. PwC Global Power & Utilities, Blockchain an Opportunity for Energy Producers and Consumers? Available online: <https://www.pwc.com/gx/en/industries/assets/pwc-blockchain-opportunity-for-energy-producers-and-consumers.pdf> (accessed on 1 August 2020).
14. Maxim, A.; Mihai, C.; Apostoaie, C.-M.; Popescu, C.; Istrate, C.; Bostan, I. Implications and Measurement of Energy Poverty across the European Union. *Sustainability* **2016**, *8*, 483. [CrossRef]
15. Surowiecki, J. *The Wisdom of Crowds*; Anchor: San Diego, CA, USA, 2005.
16. Wang, S.; Taha, A.F.; Wang, J.; Kvaternik, K.; Hahn, A. Energy crowdsourcing and peer-to-peer energy trading in blockchain-enabled smart grids. *IEEE Trans. Syst. Man Cybern. B Cybern.* **2019**, *49*, 1612–1623. [CrossRef]

17. National Regulatory Authority for Energy. *The 228 Order for the Approval of the Technical Norm Technical Conditions for Connection to the Public Electrical Networks of the Prosumers*; National Regulatory Authority for Energy: Bucharest, Romania, 2018.
18. Neagu, B.C.; Grigoras, G.; Ivanov, O. An Efficient Peer-to-Peer Based Blockchain Approach for Prosumers Energy Trading in Microgrids. In Proceedings of the International Conference on Modern Power Systems (MPS), Cluj Napoca, Romania, 21–23 May 2019; pp. 1–4.
19. Mohan, V.; Bu, S.; Jisma, M.; Rijinal, V.C.; Thirumala, K.; Thomas, M.S.; Xu, Z. Realistic energy commitments in peer-to-peer transactive market with risk adjusted prosumer welfare maximization. *Int. J. Electr. Power Energy Syst.* **2020**, *124*, 106377. [[CrossRef](#)]
20. De La Nieta, A.A.S.; Gibescu, M.; Wang, X.; Song, M.; Jensen, E.; Saleem, A.; Bremdal, B.; Ilieva, I. Local economic dispatch with local renewable generation and flexible load management. In Proceedings of the International Conference on Smart Energy Systems and Technologies (SEST), Sevilla, Spain, 10–12 September 2018; pp. 1–6.
21. Ottesen, S.Ø.; Tomasgard, A.; Fleten, S.-E. Prosumer bidding and scheduling in electricity markets. *Energy* **2016**, *94*, 828–843. [[CrossRef](#)]
22. Ferruzzi, G.; Cervone, G.; Delle Monache, L.; Graditi, G.; Jacobone, F. Optimal bidding in a Day-Ahead energy market for Micro Grid under uncertainty in renewable energy production. *Energy* **2016**, *106*, 194–202. [[CrossRef](#)]
23. Gregg, J.S.; Nyborg, S.; Hansen, M.; Schwanitz, V.J.; Wierling, A.; Zeiss, J.P.; Delvaux, S.; Saenz, V.; Polo-Alvarez, L.; Candelise, C.; et al. Collective action and social innovation in the energy sector: A mobilization model perspective. *Energies* **2020**, *13*, 651. [[CrossRef](#)]
24. Candelise, C.; Ruggieri, G. Status and evolution of the community energy sector in Italy. *Energies* **2020**, *13*, 1888. [[CrossRef](#)]
25. Marinakis, V.; Doukas, H.; Koasidis, K.; Albuflasa, H. From intelligent energy management to value economy through a digital energy currency: Bahrain city case study. *Sensors* **2020**, *20*, 1456. [[CrossRef](#)] [[PubMed](#)]
26. Horstink, L.; Wittmayer, J.M.; Ng, K.; Luz, G.P.; Marín-González, E.; Gähns, S.; Campos, I.; Holstenkamp, L.; Oxenaar, S.; Brown, D. Collective renewable energy prosumers and the promises of the energy union: Taking stock. *Energies* **2020**, *13*, 421. [[CrossRef](#)]
27. The First Green Energy Cooperative in Romania Will “Open Its Doors” Soon, Including for Prosumers. Available online: <https://newsenergy.ro/prima-cooperativa-de-energie-verde-din-romania-isi-va-deschide-portile-in-curand-inclusiv-pentru-prosumatori/> (accessed on 1 August 2020).
28. Son, Y.-B.; Im, J.-H.; Kwon, H.-Y.; Jeon, S.-Y.; Lee, M.-K. Privacy-preserving peer-to-peer energy trading in blockchain-enabled smart grids using functional encryption. *Energies* **2020**, *13*, 1321. [[CrossRef](#)]
29. Wang, S.; Taha, A.F.; Wang, J. Blockchain-assisted crowdsourced energy systems. In Proceedings of the IEEE Power & Energy Society General Meeting (PESGM), Porto, Portugal, 9–11 September 2018; pp. 1–5.
30. Morstyn, T.; Teytelboym, A.; Hepburn, C.; McCulloch, M.D. Integrating P2P Energy Trading with Probabilistic Distribution Locational Marginal Pricing. *IEEE Trans. Smart Grid* **2019**, *11*, 3095–3106. [[CrossRef](#)]
31. Fu, M.; Xu, Z.; Wang, N.; Lyu, X.; Xu, W. “Peer-to-Peer Plus” electricity transaction within community of active energy agents regarding distribution network constraints. *Energies* **2020**, *13*, 2408. [[CrossRef](#)]
32. Khorasany, M.; Mishra, Y.; Ledwich, G. Design of auction-based approach for market clearing in peer-to-peer market platform. *J. Eng.* **2019**, 4813–4818. [[CrossRef](#)]
33. Khorasany, M.; Azuatalam, D.; Glasgow, R.; Liebman, A.; Razzaghi, R. Transactive energy market for energy management in microgrids: The monash microgrid case study. *Energies* **2020**, *13*, 2010. [[CrossRef](#)]
34. Haghifam, S.; Zare, K.; Abapour, M.; Muñoz-Delgado, G.; Contreras, J. A stackelberg game-based approach for transactive energy management in smart distribution networks. *Energies* **2020**, *13*, 3621. [[CrossRef](#)]
35. Liu, Z.; Gao, J.; Yu, H.; Wang, X. Operation mechanism and strategies for transactive electricity market with multi-microgrid in grid-connected mode. *IEEE Access* **2020**, *8*, 79594–79603. [[CrossRef](#)]
36. Hwang, Y.M.; Sim, I.; Sun, Y.G.; Lee, H.-J.; Kim, J.Y. Game-theory modeling for social welfare maximization in smart grids. *Energies* **2018**, *11*, 2315. [[CrossRef](#)]
37. Singh, P.; Talwariya, A.; Kolhe, M. Demand response management in the presence of renewable energy sources using Stackelberg game theory. *IOP Conf. Ser. Mater. Sci. Eng.* **2019**, *605*, 012004. [[CrossRef](#)]

38. Arun, S.L.; Selvan, M.P. Prosumer based demand response for profitable power exchange between end-user and utility. In Proceedings of the 2018 20th National Power Systems Conference (NPSC), Iruchirappalli, India, 14–16 December 2018; pp. 1–6.
39. Liu, T.; Tan, X.; Sun, B.; Wu, Y.; Guan, X.; Tsang, D.H. Energy management of cooperative microgrids with p2p energy sharing in distribution networks. In Proceedings of the 2015 IEEE International Conference on Smart Grid Communications (SmartGridComm), Miami, FL, USA, 2–5 November 2015; pp. 410–415.
40. Neagu, B.-C.; Ivanov, O.; Grigoras, G.; Gavrilas, M. A new vision on the prosumers energy surplus trading considering smart peer-to-peer contracts. *Mathematics* **2020**, *8*, 235. [[CrossRef](#)]
41. Yahaya, A.S.; Javaid, N.; Alzahrani, F.A.; Rehman, A.; Ullah, I.; Shahid, A.; Shafiq, M. Blockchain based sustainable local energy trading considering home energy management and demurrage mechanism. *Sustainability* **2020**, *12*, 3385. [[CrossRef](#)]
42. Lovati, M.; Zhang, X.; Huang, P.; Olsmats, C.; Maturi, L. Optimal simulation of three peer to peer (p2p) business models for individual pv prosumers in a local electricity market using agent-based modelling. *Buildings* **2020**, *10*, 138. [[CrossRef](#)]
43. Martín, D.; Bordel, B.; Alcarria, R.; Sánchez-Picot, Á.; de Rivera, D.S.; Robles, T. Prosumerization Approach to Semantic Ambient Intelligence Platforms. In Proceedings of the International Conference on Ubiquitous Computing and Ambient Intelligence, Philadelphia, PA, USA, 7–10 November 2017; pp. 109–120.
44. Parag, Y. Beyond energy efficiency: A prosumer market as an integrated platform for consumer engagement with the energy system. *Eur. Counc. Energy Effic. Econ. Summer Study* **2015**, *1*, 15–23.
45. Bytschkow, D.; Capone, A.; Mayer, J.; Kramer, M.; Lickleder, T. An OPC UA-based Energy Management Platform for Multi-Energy Prosumers in Districts. In Proceedings of the 2019 IEEE PES Innovative Smart Grid Technologies Europe (ISGT-Europe), Bucharest, Romania, 29 September–2 October 2019; pp. 1–5.
46. Mamounakis, I.; Vergados, D.J.; Makris, P.; Varvarigos, E.; Mavridis, T. A virtual microgrid platform for the efficient orchestration of multiple energy prosumers. In Proceedings of the 19th Panhellenic Conference on Informatics (PCI'15), Athens, Greece, 1–3 October 2015.
47. Küfeoğlu, S.; Lehtonen, M. Comparison of different models for estimating the residential sector customer interruption costs. *Electr. Power Syst. Res.* **2015**, *122*, 50–55. [[CrossRef](#)]
48. Samuel, O.; Almogren, A.; Javaid, A.; Zuair, M.; Ullah, I.; Javaid, N. Leveraging blockchain technology for secure energy trading and least-cost evaluation of decentralized contributions to electrification in Sub-Saharan Africa. *Entropy* **2020**, *22*, 226. [[CrossRef](#)]
49. Engeland, K.; Borga, M.; Creutin, J.-D.; François, B.; Ramos, M.-H.; Vidal, J.-P. Space-time variability of climate variables and intermittent renewable electricity production—A review. *Renew. Sustain. Energy Rev.* **2017**, *79*, 600–617. [[CrossRef](#)]
50. Etukudor, C.; Couraud, B.; Robu, V.; Früh, W.-G.; Flynn, D.; Okereke, C. Automated negotiation for peer-to-peer electricity trading in local energy markets. *Energies* **2020**, *13*, 920. [[CrossRef](#)]
51. Narayanan, A.; Haapaniemi, J.; Kaipia, T.; Partanen, J. Economic impacts of power-based tariffs on peer-to-peer electricity exchange in community microgrids. In Proceedings of the International Conference on the European Energy Market, EEM, Lodz, Poland, 27–29 June 2018.
52. Kuzemko, C.; Lawrence, A.; Watson, M. New directions in the international political economy of energy. *Rev. Int. Polit. Econ.* **2019**, *26*, 1–24. [[CrossRef](#)]
53. Van Leeuwen, G.; AlSkaif, T.; Gibescu, M.; van Sark, W. An integrated blockchain-based energy management platform with bilateral trading for microgrid communities. *Appl. Energy* **2020**, *263*, 114613. [[CrossRef](#)]
54. Huang, H.; Nie, S.; Lin, J.; Wang, Y.; Dong, J. Optimization of peer-to-peer power trading in a microgrid with distributed PV and battery energy storage systems. *Sustainability* **2020**, *12*, 923. [[CrossRef](#)]
55. Ghaemi, S.; Khazaei, H.; Musilek, P. ChainFaaS: An open blockchain-based serverless platform. *IEEE Access* **2020**, *8*, 131760–131778. [[CrossRef](#)]
56. Anthony, B.; Petersen, S.A.; Ahlers, D.; Krogstie, J.; Livik, K. Big data-oriented energy prosumption service in smart community districts: A multi-case study perspective. *Energy Inform.* **2019**, *2*, 36. [[CrossRef](#)]
57. Cornélusse, B.; Savelli, I.; Paoletti, S.; Giannitrapani, A.; Vicino, A. A community microgrid architecture with an internal local market. *Appl. Energy* **2019**, *242*, 547–560. [[CrossRef](#)]
58. Eisele, S.; Eghtesad, T.; Campanelli, K.; Agrawal, P.; Laszka, A.; Dubey, A. Safe and private forward-trading platform for transactive microgrids. *arXiv* **2019**, arXiv:1910.12579.

59. Laszka, A.; Eisele, S.; Dubey, A.; Karsai, G.; Kvaternik, K. TRANSAX: A blockchain-based decentralized forward-trading energy exchanged for transactive microgrids. In Proceedings of the 24th International Conference on Parallel and Distributed Systems (ICPADS), Singapore, Singapore, 11–13 December 2018; pp. 918–927.
60. Li, S.; Lian, J.; Conejo, A.; Zhang, W. Transactive energy system: Market-Based coordination of distributed energy resources. *arXiv* **2019**, arXiv:1908.03641.
61. Vergados, D.J.; Mamounakis, I.; Makris, P.; Varvarigos, E. Prosumer clustering into virtual microgrids for cost reduction in renewable energy trading markets. *Sustain. Energy Grids Netw.* **2016**, *7*, 90–103. [[CrossRef](#)]
62. Cui, S.; Wang, Y.; Xiao, J. Peer-to-Peer energy sharing among smart energy buildings by distributed transaction. *IEEE Trans. Smart Grid* **2019**, *6*, 6491–6501. [[CrossRef](#)]
63. Cui, S.; Wang, Y.; Shi, Y.; Xiao, J. A new and fair Peer-to-Peer energy sharing framework for energy buildings. *IEEE Trans. Smart Grid* **2020**, *11*, 3817–3826. [[CrossRef](#)]
64. Ghorbanian, M.; Dolatabadi, S.H.; Siano, P.; Kouveliotis-Lysikatos, I.; Hatziargyriou, N.D. Methods for flexible management of blockchain-based cryptocurrencies in electricity markets and smart grids. *IEEE Trans. Smart Grid* **2020**, *11*, 4227–4235. [[CrossRef](#)]
65. Praça, I.; Ramos, S.; Andrade, R.; da Silva, A.S.; Sica, E.T. Analysis and simulation of local energy markets. In Proceedings of the 2019 16th International Conference on the European Energy Market (EEM), Ljubljana, Slovenia, 18–20 September 2019; pp. 1–5.
66. Neves, D.; Scott, I.; Silva, C.A. Peer-to-peer energy trading potential: An assessment for the residential sector under different technology and tariff availabilities. *Energy* **2020**, *205*, 118023. [[CrossRef](#)]
67. Almenning, O.M.; Bjarghov, S.; Farahmand, H. Reducing Neighborhood Peak Loads with implicit Peer-to-Peer energy trading under Subscribed Capacity tariffs. In Proceedings of the 2019 International Conference on Smart Energy Systems and Technologies (SEST), Porto, Portugal, 9–11 September 2019; pp. 1–6.
68. Liang, B.; Liu, W.; Sun, L.; He, Z.; Hou, B. An aggregated model for energy management considering crowdsourcing behaviors of distributed energy resources. *IEEE Access* **2020**, *7*, 145757–145766. [[CrossRef](#)]
69. Zepter, J.M.; Lüth, A.; Del Granado, P.C.; Egging, R. Prosumer integration in wholesale electricity markets: Synergies of peer-to-peer trade and residential storage. *Energy Build.* **2019**, *184*, 163–176. [[CrossRef](#)]
70. Neagu, B.C.; Gavrilas, M.; Pentiu, R.D.; Hopulele, E. Optimal Placement of Energy Storage Systems in Microgrids Using a PSO based Approach. In Proceedings of the 2019 IEEE PES Innovative Smart Grid Technologies Europe (ISGT-Europe), Bucharest, Romania, 29 September–2 October 2019; pp. 1–5. [[CrossRef](#)]
71. Faraji, J.; Ketabi, A.; Hashemi-Dezaki, H. Optimization of the scheduling and operation of prosumers considering the loss of life costs of battery storage systems. *J. Energy Storage* **2020**, *31*, 101655. [[CrossRef](#)]
72. All You Need to Know to Become A Prosumer. Available online: <https://energyindustryreview.com/renewables/all-you-need-to-know-to-become-a-prosumer/> (accessed on 4 August 2020).
73. Neagu, B.C.; Grigoras, G. A Fair Load Sharing Approach Based on Microgrid Clusters and Transactive Energy Concept. In Proceedings of the 12th International Conference on Electronics, Computers and Artificial Intelligence (ECAI 2020), Bucharest, Romania, 25–27 June 2020; pp. 1–5.
74. Electricity Market Monitoring Report—April 2020. Available online: <https://www.anre.ro/en/electric-energy/legislation/electricity-market-monitoring/2020> (accessed on 4 August 2020).



## Article

# A Metaheuristic Algorithm for Flexible Energy Storage Management in Residential Electricity Distribution Grids

Ovidiu Ivanov , Bogdan-Constantin Neagu , Gheorghe Grigoras , Florina Scarlatache  and Mihai Gavrilas

Power Engineering Department, Gheorghe Asachi Technical University of Iasi, 700050 Iasi, Romania; bogdan.neagu@tuiasi.ro (B.-C.N.); ggrigor@tuiasi.ro (G.G.); flr\_rotaru@yahoo.com (F.S.); mgavril@tuiasi.ro (M.G.)  
\* Correspondence: ovidiuivanov@tuiasi.ro

**Abstract:** The global climate change mitigation efforts have increased the efforts of national governments to incentivize local households in adopting PV panels for local electricity generation. Since PV generation is available during the daytime, at off-peak hours, the optimal management of such installations often considers local storage that can defer the use of local generation to a later time. The energy stored in batteries located in optimal places in the network can be used by the utility to improve the operation conditions in the network. This paper proposes a metaheuristic approach based on a genetic algorithm that considers three different scenarios of using energy storage for reducing the energy losses in the network. Two cases consider the battery placement and operation under the direct control of the network operator, with single and multiple bus and phase placement locations. Here, the aim was to maximize the benefit for the whole network. The third case considers selfish prosumer battery management, where the storage owner uses the batteries only for their own benefit. The optimal design of the genetic algorithm and of the solution encoding allows for a comparative study of the results, highlighting the important strengths and weaknesses of each scenario. A case study is performed in a real distribution system.



**Citation:** Ivanov, O.; Neagu, B.-C.; Grigoras, G.; Scarlatache, F.; Gavrilas, M. A Metaheuristic Algorithm for Flexible Energy Storage Management in Residential Electricity Distribution Grids. *Mathematics* **2021**, *9*, 2375. <https://doi.org/10.3390/math9192375>

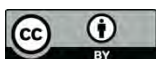
Academic Editor: Petr Stodola

Received: 2 September 2021

Accepted: 23 September 2021

Published: 24 September 2021

**Publisher's Note:** MDPI stays neutral with regard to jurisdictional claims in published maps and institutional affiliations.



**Copyright:** © 2021 by the authors. Licensee MDPI, Basel, Switzerland. This article is an open access article distributed under the terms and conditions of the Creative Commons Attribution (CC BY) license (<https://creativecommons.org/licenses/by/4.0/>).

**Keywords:** residential electricity distribution networks; renewable generation sources; energy storage; optimization; multipurpose algorithm; genetic algorithms

## 1. Introduction

The transition from the old vertically integrated, government-owned electricity trading model to the deregulated market has brought in many parts of the world the supply–demand balance as the main factor in establishing the price for electricity sold to the end consumers. On the wholesale market, which determines the prices offered by the suppliers to their clients, the short-term trading price can vary significantly between minimal values in off-peak intervals and maximal prices in high demand hours, which usually coincide with the peak demand hours of residential demand and network loading. In Romania, this market behavior is more significant, since more than half of the electricity is traded daily in the day-ahead market, for example, for 10 August 2021, there was a price variation from 77 EUR/MWh at 04.00 to 212 EUR/MWh at 21.00 [1].

On the other hand, in the last few decades, the developed countries have seen a shift in consumption from heavy industrial branches to an energy-efficient knowledge-based economy and a steady increase in the residential electricity demand [2]. At the same time, the growing concerns related to global warming have prompted international organizations and national governments to take concrete actions regarding the reduction in fossil fuel consumption and growth incentivization of the renewable electricity generation sector. The latest revision of the EU climate targets specify raising the share of renewable energy to 40% of the total electricity consumption by 2030 and reducing the GHG emissions by 55% by 2030, from the 1990 levels, with the aim of eliminating them by 2050 [3]. For the final consumers, these ambitious goals translate into the proliferation of small-scale



clean electricity generation, especially in the residential sector. National governments are currently offering incentive packages to encourage individual residences to become prosumers, entities that consume and produce electricity at the same time [4].

The low-voltage (LV) electricity distribution networks (EDN), where the vast majority of these residential consumers are located, have the distinction that they supply one-phase consumers using a three-phase four-wire main feeder configuration. This generates the problem that, in most cases, the load is unbalanced between the three phases, leading to increased active energy losses and poor voltage quality. The presence of prosumers, which need to inject their unused generation surplus back into the network outside the control of the distribution network operator (DNO) can further impact the secure and efficient operation of the supply infrastructure. It follows that an adequate prosumer surplus management is required for the optimal operation of LV EDNs [5]. One method of achieving this goal is to use storage in the EDN.

It is usually considered that the prosumers generate electricity mainly for their own use, but they have to manage their surplus. If they use PV panels as a means to generate electricity, it is often the case that the hours that generation occurs do not coincide with the hours of maximum consumer and EDN load. In this case, the surplus can be injected back into the network or stored for later use.

In Romania, the current regulations issued by the Romanian Energy Regulatory Authority (RERA) specify that prosumers must sell back to the grid all surplus at regulated prices, computed as the average day-ahead market price for the previous year [6]. For 2020, this resulted in an actual price of 40 EUR/MWh, much lower than the day-ahead market price. Thus, storage can be used to replace the expensive energy used in peak demand hours with local generation, eliminating the need to sell back to the grid at low prices. Since storage systems are not yet subsidized, they are accessible for a relatively small number of prosumers. Community storage can also be used [7].

This paper proposes an algorithm for flexible energy storage management in residential low-voltage electricity distribution grids (ESMRG) that considers the optimization of storage placement in the network from the perspectives of prosumer and DNO gain.

The main contributions of the paper are:

- The conceptualization of the mathematical model for three storage management approaches;
- The adaptation of the general GA structure using common encoding for the three proposed scenarios;
- The validation of the proposed algorithm in a case study that uses a real LV EDN from Romania; and
- Discussions regarding the possible advantages and disadvantages of each storage solution.

The remaining sections of the paper are organized as follows. Section 2 discusses the state-of-the-art in the problem of storage management in EDNs and the use of metaheuristic methods in this type of optimization; Section 3 presents the adaptation of the basic GA to the problem of storage management as developed by the authors; and Section 4 provides the results of the case study. The paper ends with a discussion and main conclusions.

## 2. Related Literature

Prosumer surplus management is a key factor for the safe and efficient operation of EDNs. It is of importance for the prosumers who seek to maximize their advantage in terms of energy cost savings, and also for the network operator, who seeks to minimize the potential negative effect of the presence of the prosumers with unpredictable power injections in the grid. The latest research shows the need to better understand the effect of prosumer presence in LV distribution grids and their interaction with the DNO. Such a study was performed in [8] for Denmark and in [9] for the United States. The uncertainty of renewable generation patterns is also a factor requiring attention. In [10], this issue was studied by comparing the efficiency of several short-term forecasting methods. Based

on such data, the prosumer–network interaction was modeled in [11] as a profit model of DNO concurrent with a utility model of the PV prosumers, where the operator wants to maximize its profit and the prosumers adjust their energy consumption and sharing according to the feed-in time-varying prices. Energy sharing between prosumers and its advantages and challenges were thoroughly reviewed in [12]. The authors of [13] analyzed the possibility of DNO strategies that use price-based demand side management (DSM) schemes for incentivizing the demand reduction. Another approach, developed in [14], considered the possibility of optimally managing prosumers that are acting independently, only in their self-interest, to maintain the voltage stability in the network within acceptable limits. The uncertainty of PV generation was managed in [10] by using a combination of load profiling and demand response techniques, and in [15] by creating energy hubs of prosumer communities. Prosumer management is more challenging for the network operator in islanded networks, a problem that was approached in [16].

Energy storage is used by prosumers to defer self-generated electricity consumption in order to avoid paying for electricity at high, peak-load tariffs. In [17], the authors analyzed the possibility of coordinating the operation of a PV prosumer with storage battery, with the goal of integrating it into the grid. At the level of an entire building, [18] proposed the management of HVAC systems by prosumers in cooperation with the grid operator and using storage to minimize the energy cost. The study in [19] proposed specific billing mechanisms to encourage selfish prosumers to combine energy exchange between households and to utilize their energy storage systems for minimizing the electricity cost. In [20], the same goal was pursued, but also encouraged the creation of “energy coalitions” between prosumers. Such coalitions can then use storage to participate in the wholesale market [21]. The optimal size of PV and power/energy capacities of the battery were also investigated in [22,23].

The research presented above concentrates on the optimization of prosumer operation and improving their goals. However, a second party directly interested in the behavior of the prosumer is the network operator. The accomplishment of the goals pursued by the prosumer must be correlated with the technical and economic interests of the DNO, which are directly influenced by the presence of the prosumer, as modeled in [24]. The intermittent nature of prosumer generation can negatively influence the energy losses [25] or bus voltage levels [26]. Current research suggests the optimization of the power injected to the grid by prosumers by using storage, resulting in over-voltage [27], generation–demand balance [28], or power loss [29] mitigation.

The latest trends regarding the use of storage for prosumer management is the implementation of community-shared storage, which can reduce the investment costs for prosumers and give network operators supplementary tools for optimizing the state of the distribution network [7,30,31].

Regarding the computational effort, the study carried out in [32] concluded that prosumer scheduling in microgrids is a NP-hard problem, for which optimization algorithms will find approximate solutions. It follows that, if the prosumer management is formulated as an optimization problem, the computational-intensive classical algorithms could be successfully replaced with other methods with marginal performance decrease. The literature survey from above lists several methods used for prosumer management problems: game theory [11,14,19,20], clustering [13], neural networks, random forest [10], mixed integer linear optimization [15,22,31], genetic algorithm [23], linear programming [21], alternating direction method of multipliers [18,30], dynamic programming [24], optimal power flow [26], and the proof-of-stake blockchain trading algorithm [29].

The classic optimization methods rely on deterministic analytical algorithms and converge to the optimal solution [33,34]. However, they are computationally intensive and are not suitable for problems with discrete search spaces. For problems belonging to this category, heuristic algorithms have been proven to be more flexible and efficient, with the drawback of decreased performance when the complexity of the problem increases [35].

Considering the particularities of the problem solved in the paper, a metaheuristic approach was chosen by the authors for implementing the optimization of storage placement in the LV distribution networks. Metaheuristic algorithms such as the genetic algorithm, particle swarm optimization, differential evolution, whale algorithm, and fireworks algorithm are nature-inspired optimization techniques that have proven their performance in problems regarding the optimization of operation conditions in electrical networks. Recently, they have been applied for integrating electric vehicles and distributed generation into smart grids [36], optimal reconfiguration of distribution networks [37], optimal power flow analysis in DC distribution networks [38], reliability improvement [39], and optimal consumption planning [40]. In this paper, a genetic algorithm was used to determine the optimal buses and phases of connection for a fixed number of storage units (batteries) with the aim of reducing the energy losses over a time interval of 24 h. The GA was preferred because, as the following subsection of the paper will describe in detail, it allows for simple and efficient modeling of the mentioned storage use scenarios, which is the same as using the same basic approach in solving three different problems with minimal modifications to a base case. This is an advantage offered by the metaheuristic approach, which retains its simplicity and flexibility with minimal performance cost.

To further develop the research performed in the literature and described above, the study assumed that storage could be installed in the network using two assumptions:

- In the standard approach, where the individual prosumers acquire storage batteries together with the PV system, and employ them mainly to defer the use of surplus generated during the daytime for the peak load hours, in order to lower their daily costs of electricity.
- In a novel approach, when the storage system is installed in the network at the initiative of the DNO, with the main aim of improving the operation conditions of the EDN. In this case, storage can be seen as
  - individual batteries placed in different locations in the network; and
  - a single community storage system [7].

The proposed algorithm investigates the advantages and disadvantages of each of the three proposed approaches, in terms of reducing the active energy losses in the EDN over a time interval of 24 h.

### 3. Materials and Methods

The genetic algorithm (GA) is a well-known metaheuristic belonging to the class of population-based evolutionary algorithms. Like many metaheuristics, it is inspired from natural behaviors and patterns, in this case the Darwinian natural selection. The algorithm mimics the continuous adaptation of a species to its environment by means of the ‘survival of the fittest’ principle. In the natural world, populations of variable sizes survive by reproduction and adaptation, with the most powerful or intelligent individuals being favored to pass their strong genes on to the next generation. The GA uses a mathematical representation of this process, and its application in solving NP-hard problems has been successful in a multitude of research and industry fields such as scheduling, multimedia content processing, network optimization, engineering, data mining, IoT, and blockchain [41–43].

The authors chose the GA to implement the energy storage management in residential electricity distribution grid (ESMRG) algorithm because of its specific technique of manipulating the elements of an individual from the population to obtain the optimal solution. The following subsections describe the basic structure of the GA and the implementation chosen by the authors for the ESMRG algorithm.

#### 3.1. The Genetic Algorithm

The mathematical model of the GA considers a (usually) fixed size population where each member is hierarchized by using a numerical value called ‘fitness function’, which measures the performance in solving an optimization problem. Each member from the

### 3.1. The Genetic Algorithm

The mathematical model of the GA considers a (usually) fixed size population where each member is hierarchized by using a numerical value called ‘fitness function’, which measures the performance in solving an optimization problem. Each member from the population is called a ‘chromosome’, and its elements are ‘genes’. The genes encode the parameters of a solution and each of them constitutes a search direction (dimension) for the algorithm. Thus, the GA can be considered as a parallel search algorithm.

Based on the values of their fitness functions, the chromosomes from the initial population are subjected to an iterative process in which their genetic structure is subjected to change through crossover (reproduction, gene exchange from parents to siblings) and mutation (random small changes in gene values). In each iteration (‘generation’), the chromosomes that are favored for reproduction are chosen using a selection procedure.

The literature lists various procedures for the selection and crossover operators [44] that must be chosen according to the specificities of the solved problem. To improve convergence, elitism techniques can be used to propagate the best known solution from the current generation to the next. The basic flowchart of the GA is presented in Figure 1.

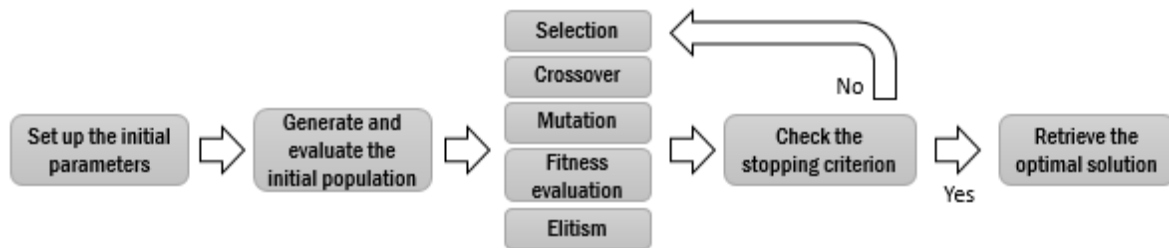


Figure 1. The basic genetic algorithm.

### 3.2. The Energy Storage Management Problem

The problem studied in the paper can be formulated as follows: given a low-voltage residential electricity distribution network in which a number of prosumers are active and can generate a surplus of electricity that otherwise would be injected back in the grid, find the optimal position of a number of storage devices (batteries) of known, fixed capacity, so that the active energy losses resulting from the operation of the network over a given time interval will be minimized.

- The implementation chosen by the authors considered the following assumptions:
- the LV network is operated in a three-phase, four-wire configuration and supplies one-phase residential consumers;
  - the demand pattern is unbalanced in space due to the uneven distribution of the consumers (as number and power demand, as connection on the phases), and unbalanced in time because of the normal demand variation of each consumer;
  - the prosumers connected in the network use PV panels for generating electricity, primarily for their own consumption;
  - to avoid injecting the prosumer surplus back into the grid, a number of equal capacity storage batteries will be placed in the network and so that the energy losses computed in the literature, surplus management is performed centered on maximizing the well-being of the prosumers.
  - One of the main objectives proposed in this paper is the consideration of the optimization of storage management paper is the consideration of the DNO priorities, mainly the installed at the network by the prosumers, together with the PV system and used to reduce the peak load of the network by the prosumers, together with the PV system will contribute to reducing the peak load of the network and peak load expenses, the prosumer will contribute to the grid with the stored energy, in the DNO network. In this case, the batteries are managed by the prosumer using their own home energy management system and the benefits for the DNO are minimal and indirect, often in the form of lower loss due to unoptimized power flow reduction in prosumer buses. In this scenario, the main beneficiary is the prosumer.

and discharge of the stored energy will be minimized.

In contrast, this paper investigates the benefits that can arise for the DNO if the storage system is developed independently from the prosumers. One way to achieve this goal is the use of a community storage system [7,30], in which a limited number of batteries is used across the entire network, charged during night time, at low-cost tariff, and discharged when needed. In this case, through optimal placement and sizing, the DNO can derive improved benefits in terms of loss reduction. The paper proposes a new hybrid approach that capitalizes on the advantages of both sides. Considering a fixed number of one-phase storage batteries managed by the DNO, with a nominal storage capacity compatible with equipment used generally by individual prosumers, the ESMRG algorithm needs to find the optimal placement of storage to buses and connection phase (a, b, or c), with the goal of minimizing the active energy losses. The storage can be installed at a single bus or at independent buses for each battery. The first case can be considered as a low-investment case, since all the batteries are grouped, and the second is the high-optimality case, with the best potential of reducing the energy losses. In both cases, it is considered that the initial investment and the management for the batteries is governed by the DNO, which will choose the bus(es) and connection phase for each battery. The efficiency of the two approaches was compared with the case when the storage management is performed by the prosumers, and the connection phase of the battery is limited by the prosumer connection phase and bus.

The optimization problem can be formulated mathematically as find the bus and phase connection for each storage system,  $s = 1, \dots, NSS$ :

$$[\{b_1, ph_1\}, \{b_2, ph_2\}, \dots, \{b_{NSS}, ph_{NSS}\}] \quad (1)$$

Therefore, the following objective function will be minimized:

$$\min(F) = \min(\Delta W_{tot}) = \sum_{h=1}^H \sum_{b=1}^{NB} \Delta P_h^b \cdot \Delta t_h \quad (2)$$

where  $\Delta W_{tot}$  represents the total energy losses, and  $\Delta P_h^b$  are the hourly active power losses for each branch  $b = 1, \dots, NB$ , computed as:

$$\sum_{b=1}^{NB} \Delta P_h^b = \sum_{b=1}^{NB} [R^b \cdot (I_h^b)^2 + K_h^b] \quad (3)$$

where  $R^b$  is the branch resistance;  $I_h^b$  is the branch current flow on branch  $b$  at hour  $h$ ; and  $K_h^b$  is the loss increase factor accounting for the supplementary current flow on the neutral wire due to the phase load unbalance on branch  $b$  at hour  $h$  [45].

The formulations in Equations (1)–(3) are subjected to a set of technical restrictions:

- The voltage magnitude  $U_h^n$  must not exceed the allowable upper and lower limits in each bus  $n = 1, \dots, NN$  and in each hour  $h$  in the interval of analysis  $h = 1, \dots, H$ :

$$U_{\min}^n \leq U_h^n \leq U_{\max}^n \quad (4)$$

- The current flow  $I_h^b$  must be lower than the allowable ampacity ( $I_{\max}$ ) on all branches from the EDN,  $b = 1, \dots, NB$  and in each hour  $h$  in the interval of analysis  $h = 1, \dots, H$ :

$$I_h^b \leq I_{\max}^b \quad (5)$$

- The state of charge (SOC) limits for the storage batteries should not exceed the technical limits for all the batteries  $s = 1, \dots, NSS$ , in each hour  $h$  in the interval of analysis  $h = 1, \dots, H$ :

$$SOC_{\min} \leq SOC_h^s \leq SOC_{\max} \quad (6)$$

$$SOC_{min} \leq SOC_h \leq SOC_{max} \tag{6}$$

3.3. The Adaptation of the Genetic Algorithm for the Storage Management Problem

As stated in Section 3.2, the goal of the ESMRG algorithm is to find the optimal bus and phase of connection for a given number of storage devices with the aim of minimizing the active energy losses. For that purpose, the structure of the chromosome was chosen in such a way as to encode in a straightforward manner the principle illustrated by Expression (1). Thus, the individuals used by the GA use the structure from Figure 2. The chromosome is divided in two parts of equal length. The first part encodes the buses, while the analogue elements from the second part specify the phases of connection for each battery installed in the EDN. The chromosome from Figure 2 can be decrypted as follows: there are NSS batteries in the network; a battery will be placed in bus 14, in phase a, and another in bus 38, in phase c.

1	...	NSS	1	...	NSS
$b_1$	...	$b_{NSS}$	$ph_1$	...	$ph_{NSS}$
14	...	38	1	...	3

Figure 2. A chromosome for the ESMRG algorithm.

This structure can be adapted to describe all three scenarios compared in this study. The following assumptions and constraints must be considered:

• For DNO priority:

- Scenario 1 (all the batteries should be installed at the same bus): All the values from  $b_1$  to  $b_{NSS}$  must be positive integers and equal; in the range  $(1, NN)$  (the number of buses in the EDN); the values from  $ph_1$  to  $ph_{NSS}$  can have the value 1, 2, or 3, denoting the phases a, b, or c:

$$SC1: \begin{cases} b_i \in \mathbb{Z}, b_i \in [1, NN], \forall i = 1 \dots NSS \\ ph_i \in \mathbb{Z}, ph_i \in [1, 3] \end{cases} \tag{7}$$

- Scenario 2 (the batteries can be installed at different buses and phases): All the values from  $b_1$  to  $b_{NSS}$  must be positive integers, in the range  $(1, NN)$ ; the values from  $ph_1$  to  $ph_{NSS}$  can have the value 1, 2, or 3, denoting the phases a, b, or c.

$$SC2: \begin{cases} b_i \in \mathbb{Z}, b_i \in [1, NN] \\ ph_i \in \mathbb{Z}, ph_i \in [1, 3] \end{cases} \tag{8}$$

• For prosumer priority:

- Scenario 3 (all the batteries should be installed at different buses and phases): All the values from  $b_1$  to  $b_{NSS}$  must be positive integers, denoting prosumers (because a more prosumer can be connected at a given bus) or prosumers that have a subset of the smaller subset of the total bus range  $ph_i$  (the values from  $ph_1$  to  $ph_{NSS}$  can be 1, 2, or 3, denoting the phases a, b, or c, chosen by the prosumers for storage installation).

$$SC3: \begin{cases} b_i \in \mathbb{Z}, b_i \in [PS_{1,NPS}, PS_{NPS}], \\ ph_i \in \mathbb{Z}, ph_i \in [1, 3], \forall i = 1 \dots NSS \end{cases} \tag{9}$$

This approach shows the flexibility of the GA chromosome structure, which allows for the simultaneous encoding of three problems with distinctive limitations inside the same algorithm.

The computation of the energy losses, which is the objective function of the problem, is part of the fitness function calculation for the GA. The standard tool used for this purpose is a classical load flow calculation, which would be the same regardless of the algorithm, classic or metaheuristic, used to find the optimal solution. The load flow method used in

The computation of the energy losses, which is the objective function of the problem, is part of the fitness function calculation for the GA. The standard tool used for this purpose is a classical load flow calculation, which would be the same regardless of the algorithm, classic or metaheuristic, used to find the optimal solution. The load flow method used in the paper is described by Equations (1)–(6). The GA is simply a mechanism of generating possible solutions encoded as vectors, employing a specific methodology. In this regard, any metaheuristic could be used in the same manner. However, the GA was chosen by the authors over other metaheuristics because, as Equations (7)–(9) show, all the elements from a solution are integer numbers, bounded in specified intervals. This is the ideal case for the crossover and mutation procedures used by the GA. At the same time, the integer encoding would create validation problems for other methods such as the well-known particle swarm optimization, fireworks algorithm, honey bees mating algorithm, etc. that use multiplication with random sub-unit numbers to change the values of individual elements from a solution. The GA eliminates the need to perform additional computation with random sub-unit numbers to change the values of individual elements from a solution. The GA eliminates the need for the genetic operators (selection, crossover, mutation). Based on preliminary testing, its for management selection is (selection was used for GA selection). Based on the preliminary crossover, was performed for the reproduction step of GA. Based on the limitations (7)–(9), the crossover is performed as the modified (the step for crossover over limitations (7)–(9)), the second half of the chromosome is modified. The phases are crossed over. Then, applied on the second half of the chromosome following the phases are used. Then, based on the result and scenario, one of the following procedures was used:

- For scenario 1: the connection buses for the offspring chromosomes, which must be the same for all the batteries, use as in Figure 3a), and random probability from the buses
- For Scenario 2 and 3: the crossover (as for Figure 3a) applied using the same random mask as for the phases (as in Figure 3b).

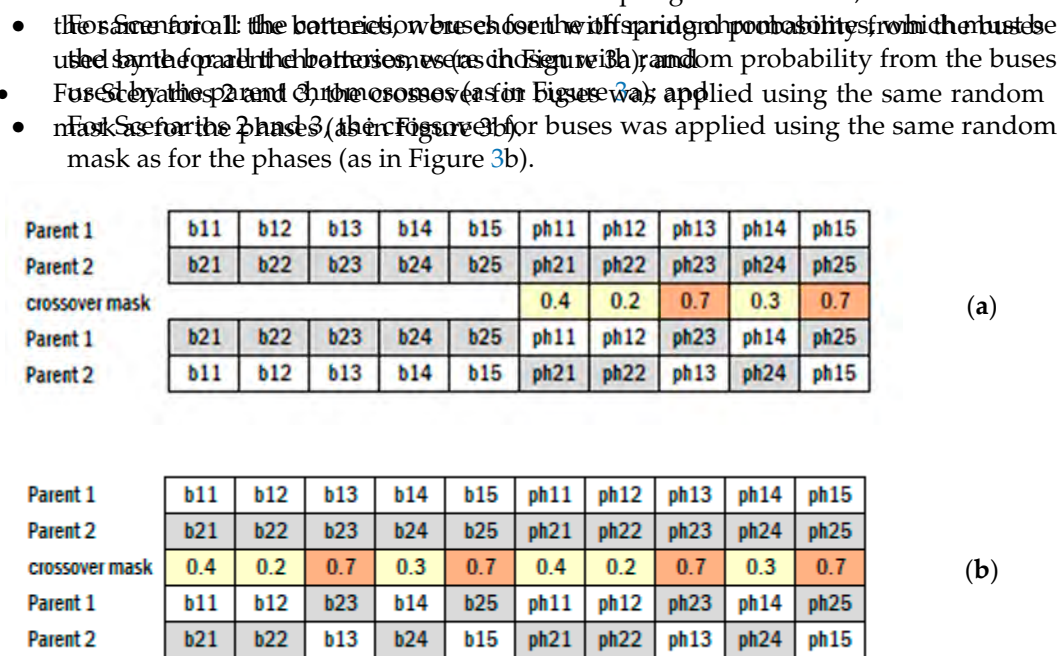


Figure 3. The uniform crossover procedure modified for the ESMRG algorithm: (a) Scenario 1; (b) Scenarios 2 and 3.

The mutation was performed by randomly selecting and altering a gene on the entire length of the chromosome, but particularized for each scenario:

- For Scenario 1: a phase gene can be mutated to any value 1, 2, or 3; but if a bus gene is selected from the mutation, then the entire first half of the chromosome is selected to be mutated.
- For Scenario 2: any phase gene can be randomly mutated to any value 1, 2, or 3, and any bus gene can be mutated to any value describing a valid bus number; and
- For Scenario 3: the mutation is first performed on the buses by randomly replacing a prosumer with another from the available pool; then, its corresponding phase is replaced accordingly in the second half of the chromosome.

These assumptions ensure that for each scenario, its constraints are always fulfilled and that the chromosomes resulting from crossover and mutations are always valid, reducing the computational effort and the number of solutions evaluated by the algorithm, thus increasing the speed of convergence toward the optimal solution. Using a more randomized

4. Results

The ESMRG algorithm was tested on a real LV EDN from northern Romania for which the consumption data were measured for a complete 24 h during the local Smart Metering day for each user. The general data for the network and its topology are provided in Figure 4 and Table 1.

4. Results

In the network, there are eight active prosumer buses depicted in black in Figure 4 that use PV panels and generate electricity during daytime in the 06:00–18:00 h interval. The electricity not used for local consumption constitutes the surplus that can be injected back in the grid or stored in batteries for later use, if storage capabilities exist. This surplus is represented, for each prosumer, in Figure 5.

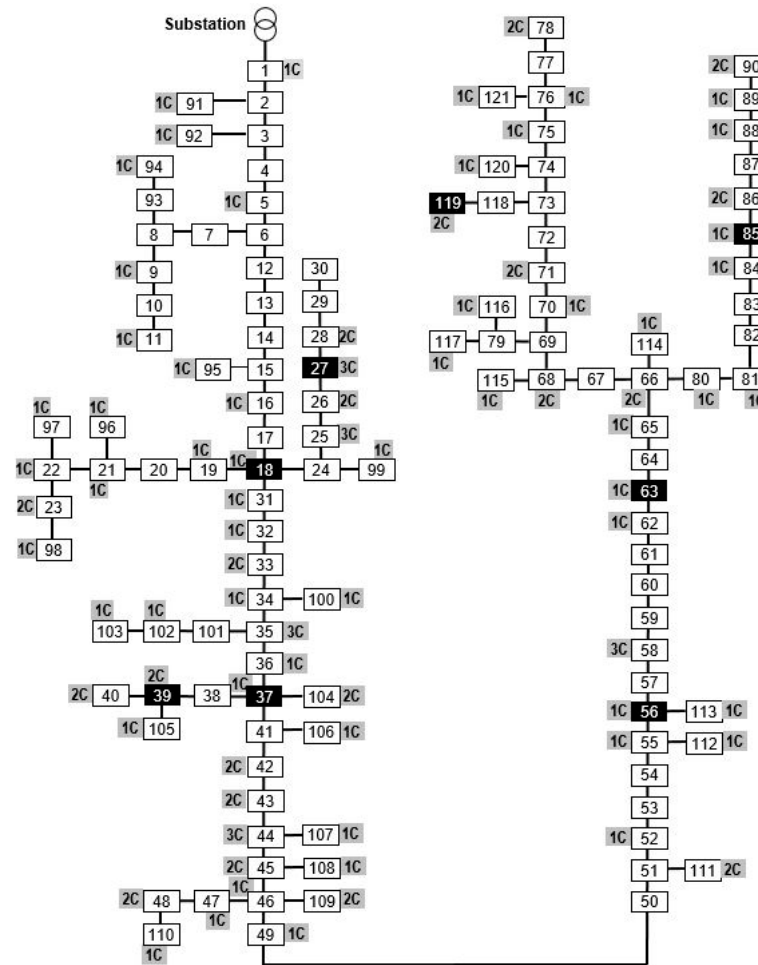


Figure 4. The EDN used in the study.

Table 1. Summary data for the network used in the case study.

Number of buses	121
Number of consumers	113
Total load (24 h/06:00–18:00)	219.85/76.01 kW
Total prosumer generation	122.00 kW
Total prosumer surplus	75.38 kW
Network type	Overhead, classic
Total/main feeder length	4840/2240 m

In the network, there are eight active prosumer buses depicted in black in Figure 4 that use PV panels and generate electricity during daytime in the 06:00–18:00 h interval. The electricity not used for local consumption constitutes the surplus that can be injected back in the grid or stored in batteries for later use, if storage capabilities exist. This surplus is represented, for each prosumer, in Figure 5.



Number of consumers	113	10 of 17
Total load (24 h/06:00–18:00)	219.85/76.01 kW	
Total prosumer generation	122.00 kW	
Total prosumer surplus	75.38 kW	
Network type	Overhead, classic	
Total/main feeder length	4840/2240 m	

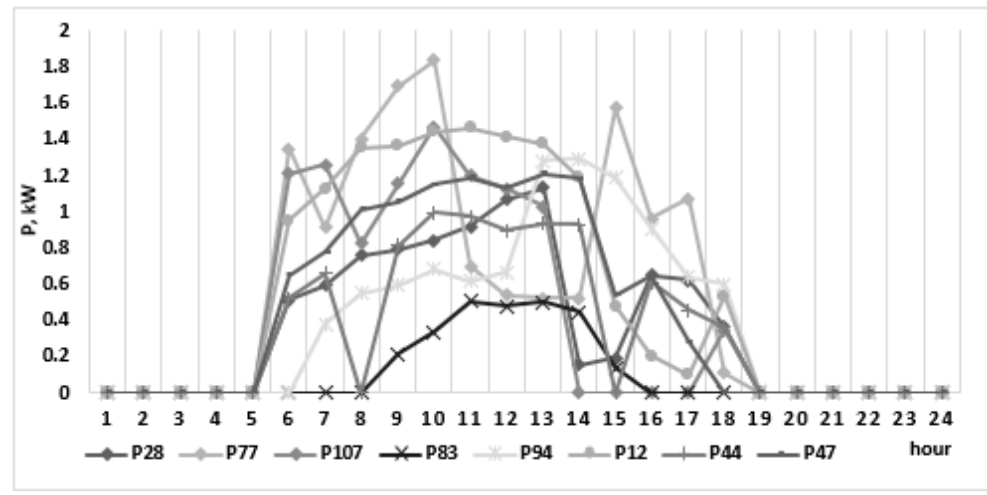


Figure 5. The hourly surplus of each prosumer.

On the other hand, the charge and discharge of the batteries influence the power demand from the grid at the buses where the batteries are located. For reference, the aggregated hourly consumption in each phase is presented in Figure 6, which shows that the load is highly unbalanced, with phase B having the lowest loading. With an optimal placement, the batteries can be used to balance the load and reduce the active energy losses in the network.

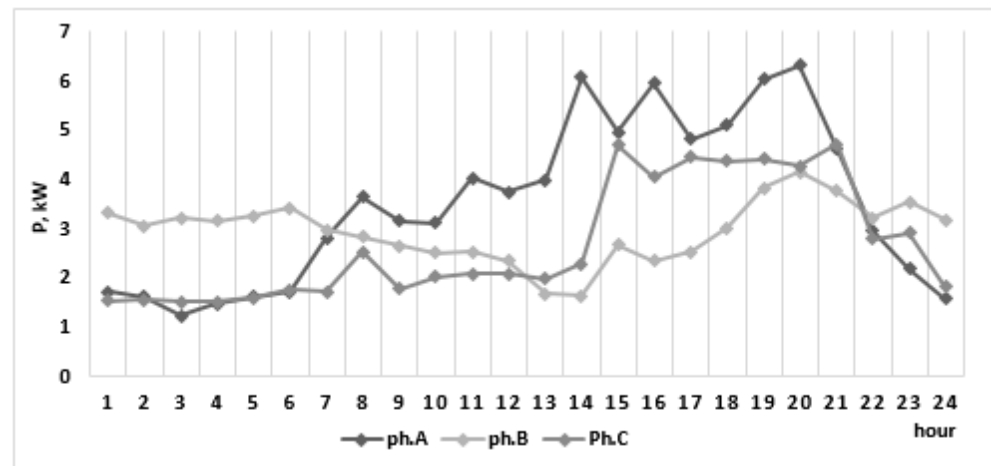


Figure 6. The hourly consumption in the network.

4.1. The Reference Case

The presence of storage in the network has the potential to reduce the energy losses in several ways. First, in the battery charging phase, the energy stored at the prosumers will not be injected in the network and the power flow on the branches adjacent to the respective bus will not increase. Depending on the operating scenario, the total losses in the network will also be affected (will increase or will decrease, according to the location of the prosumer buses). In the discharging phase, if this operation occurs at peak load, the total load of the network will be reduced, also reducing the energy losses. The loss reduction will depend on the placement of the batteries in the network at specific buses and connection phases. To analyze the effect of each storage placement solution, the losses obtained in each case were compared in this paper with the reference active losses value obtained when the consumption used the pattern from Figure 6 and the entire surplus from Figure 5 was injected back in the grid. In this case, the losses computed by a load flow algorithm amounted to 8.74 kWh in the interval 0:00–24:00, 6.90 kWh in the interval

total load of the network will be reduced, also reducing the energy losses. The loss reduction will depend on the placement of the batteries in the network at specific buses and connection phases. To analyze the effect of each storage placement solution, the losses obtained in each case were compared in this paper with the reference active losses value obtained when the consumption used the pattern from Figure 6 and the entire surplus from Figure 5 was injected back in the grid. In this case, the losses computed by a load flow algorithm amounted to 8.74 kWh in the interval 0:00–24:00, 6.90 kWh in the interval 06:00–24:00 and 5.04 kWh between 18:01–24:00 (Figure 7). These intervals were delimited considering as an initial assumption in the study that the prosumers begin to generate electricity at 06:00 and the batteries will begin to discharge at 18:01.

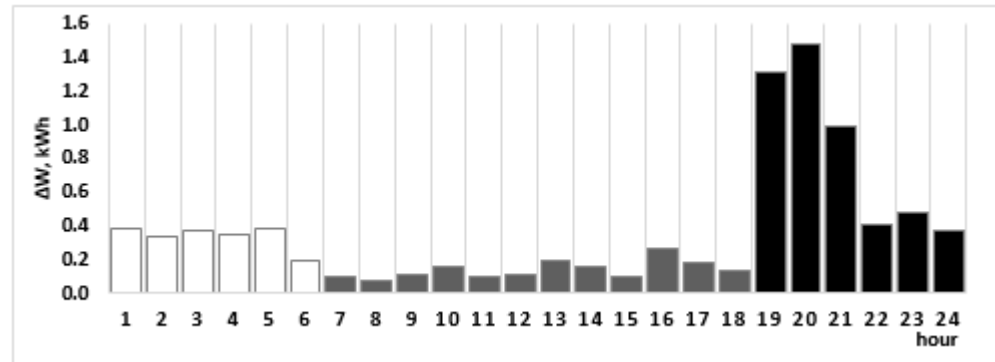


Figure 7. The active energy losses in the reference case.

Starting from this case, the three scenarios were run and the optimal solutions were determined for each case. The algorithm used each time for 100 generations and 100 individuals in the population, with a crossover rate of 0.9 and a mutation rate of 0.1. The solutions are presented in Table 2. The first part of the chromosomes for Scenarios 1 and 2 uses bus codes, while Scenario 3 uses prosumer codes, taken from the input data provided in the Supplementary Materials. The correspondent bus numbers are given for Scenario 3 in round brackets. Furthermore, the losses are given for the entire 24 h period. For Scenarios 1 and 2, it was considered that the batteries were loaded at 95% at the beginning of the interval of analysis. For Scenario 3, the batteries start at the minimum loading limit (20%) and can be charged up to the maximum limit of 95% from the prosumer surplus. The hour at which the batteries begin to discharge is at the beginning of the peak load time from Figure 7 (18:01–19:00). Five batteries with a maximum 4 kWh storage capacity each were considered for placement.

Table 2. The solutions obtained using the ESMRG algorithm.

Scenario	Solution										ΔW, kWh		
Scenario 1	85	85	85	85	85	85	85	1	1	31	12	2	6.63
Scenario 2	85	119	119	85	85	56	56	1	2	2	1	1	5.62
Scenario 3	107 (85)	83 (63)	107 (85)	94 (119)	44 (37)	1	2	1	2	3			7.61
Scenario 3	107 (85)	83 (63)	107 (85)	94 (119)	44 (37)	1	2	1	2	3			7.61

4.2. Scenario 1—Batteries Installed at the Same Bus

For this scenario, an interesting fact occurred. The algorithm chose bus 85 for installation, which is located near the far end of the network and has the highest demand in the interval of discharge 18:01–24:00 (6.81 kWh). For this case, taking into account the imposed min 20%–max 95% charging limits, a maximum of three batteries can be discharged in bus 85, which were placed by the algorithm in phase a, where the entire bus consumption is measured. Two batteries will be discharged down to the lowest limit of 20%; one will be discharged partially, while the remaining two will not be used at all, as presented in Figure 8. For reference purposes, this figure also contains the battery loading level an hour before the discharging begins.

For reference purposes, this figure also contains the battery loading level an hour before the discharging begins.

The total hourly load from Figure 6 will change starting from 18:01 only in phase a, resulting in a more balanced operation of the network at peak load hours. Consequently, the energy losses saw an important reduction from 8.74 kWh in the reference case to 6.63 kWh. This reduction of 2.11 kWh was concentrated in the (18:01–24:00) interval, as depicted in Figure 9 and was the highest in the peak interval 18:01–20:00 (h19 and h20 from Figure 8).

The total hourly load from Figure 6 will change starting from 18:01 only in phase a, resulting in a more balanced operation of the network at peak load hours. Consequently, the energy losses saw an important reduction from 8.74 kWh in the reference case to 6.63 kWh. This reduction of 2.11 kWh was concentrated in the (18:01–24:00) interval, as depicted in Figure 9 and was the highest in the peak interval 18:01–20:00 (h19 and h20 from Figure 8).

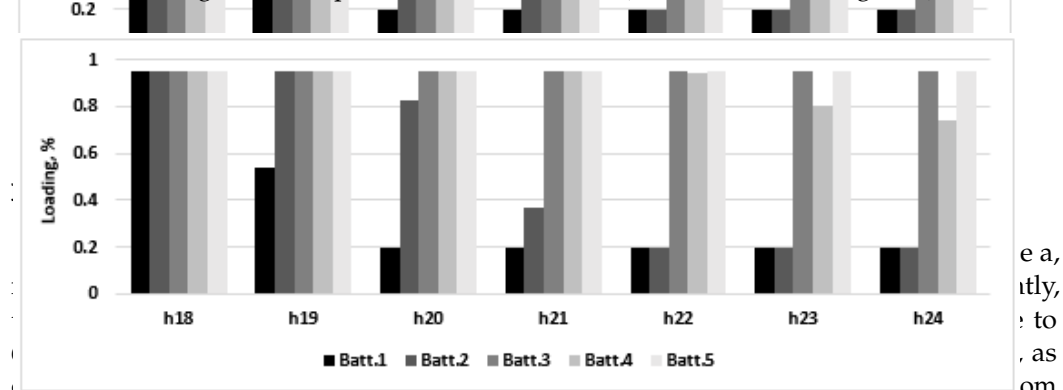


Figure 8. The discharge pattern for the batteries, Scenario 1.

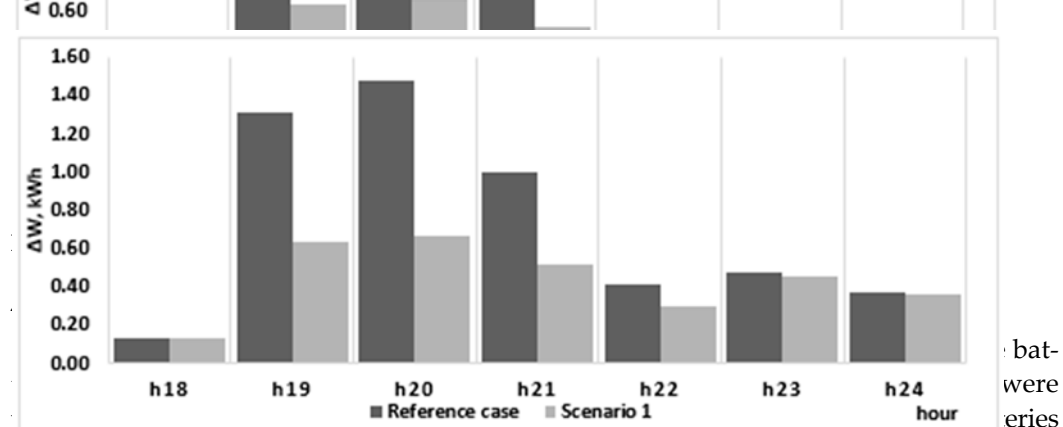


Figure 9. The energy loss reduction at peak hours, Scenario 1.

Scenario 2—Batteries Can Be Installed at Different Buses and Phases. In this case, as Table 2 shows, the algorithm chose three buses for installing the batteries: 85, 56 (in phase a, batteries 1–4, 5) and 119 (in phase b, batteries 2–3). All three were prosumer buses with high load and located near the far end of the network. The batteries all discharged differently. Those located in phase a discharged faster and were almost depleted at the end of the day. The batteries installed in phase b discharged later and slower, according to the load of the bus in the same time interval. This behavior can be seen in Figure 10. Battery 3 retained half of its load due to insufficient consumption in bus 119.

Because of the higher amount of energy used from the batteries, the energy loss reduction was much higher, with the total energy loss in 24 h only being 5.62 kWh, a significant improvement compared to Scenario 1. The loss reduction in the interval 18:01–24:00 is presented in Figure 11, and amounted to 3.02 kWh, the highest value achieved in the three scenarios considered in the paper. By optimally distributing the use of storage on different buses and phases, the effect is maximized.

Because of the higher amount of energy used from the batteries, the energy loss reduction was much higher, with the total energy loss in 24 h only being 5.62 kWh, a significant improvement compared to Scenario 1. The loss reduction in the interval 18:01–24:00 is presented in Figure 11, and amounted to 3.02 kWh, the highest value achieved in the three scenarios considered in the paper. By optimally distributing the use of storage on different buses and phases, the effect is maximized.

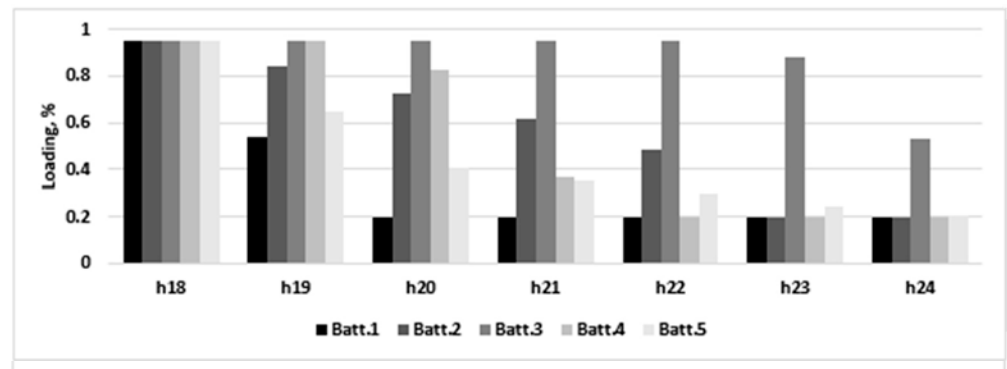


Figure 10. The discharge pattern for the batteries, Scenario 2.  
 Figure 10. The discharge pattern for the batteries, Scenario 2.

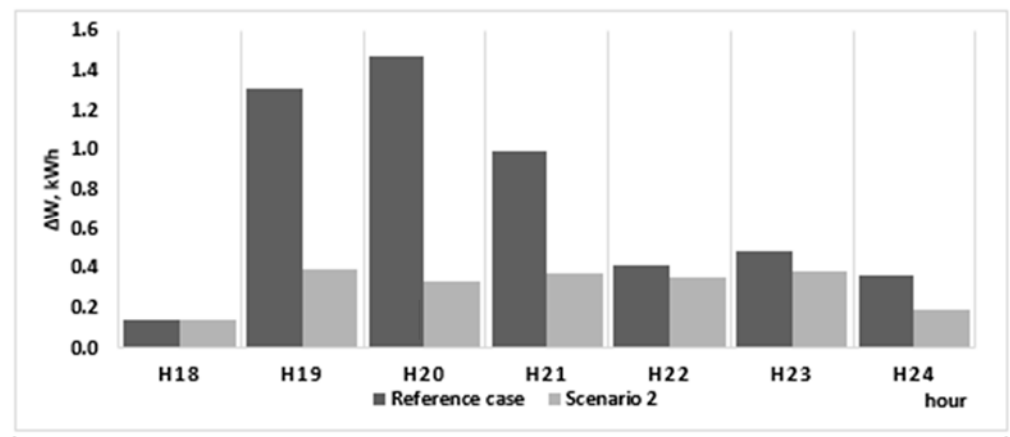


Figure 11. The energy loss reduction at peak hours, Scenario 2.  
 Figure 11. The energy loss reduction at peak hours, Scenario 2.

#### 4.4. Scenario 3 = Batteries Can Be Installed Only in Prosumer Buses

This scenario illustrates another set of operating conditions that can occur in the network. The results from Table 2 show that in Scenario 2, the batteries were placed in prosumer buses located at significant distance from the MV/LV substation, while the batteries are considered to be charged. This placement scheme could also be considered as a valid solution for Scenario 3. However, here, the assumption is that the batteries start at the minimum level of charge and are charged during the day by each prosumer using its surplus, and the charging sequence changes the hourly loss profile during the daytime. Thus, the optimal solution changes. The battery discharge pattern is modified as in Figure 12, supplemented with the charge pattern from Figure 13 (hours 06:00–17:59). The corresponding loss patterns in the same intervals are presented in Figures 14 and 15.

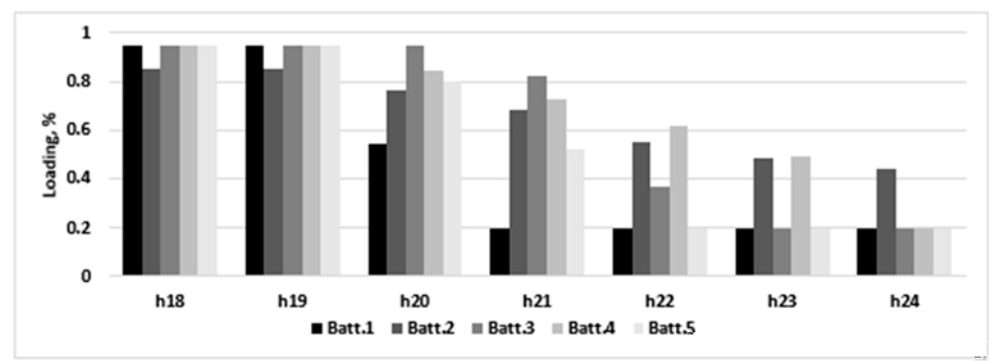


Figure 12. The discharge pattern for the batteries, Scenario 3.  
 Figure 12. The discharge pattern for the batteries, Scenario 3.

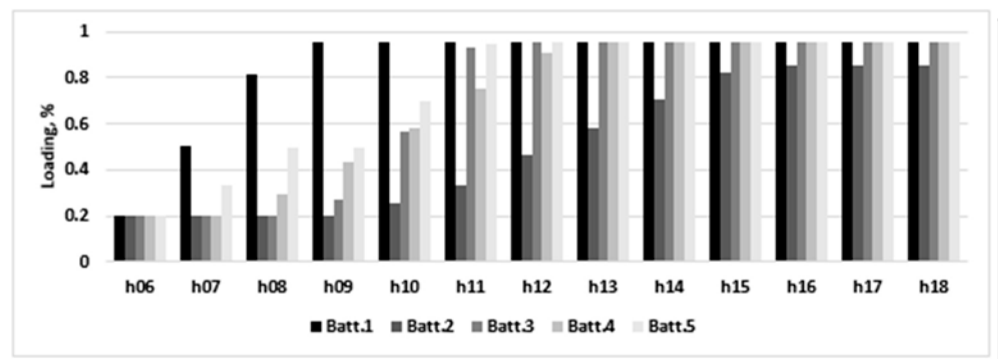


Figure 13. The charge pattern for the batteries, Scenario 3.

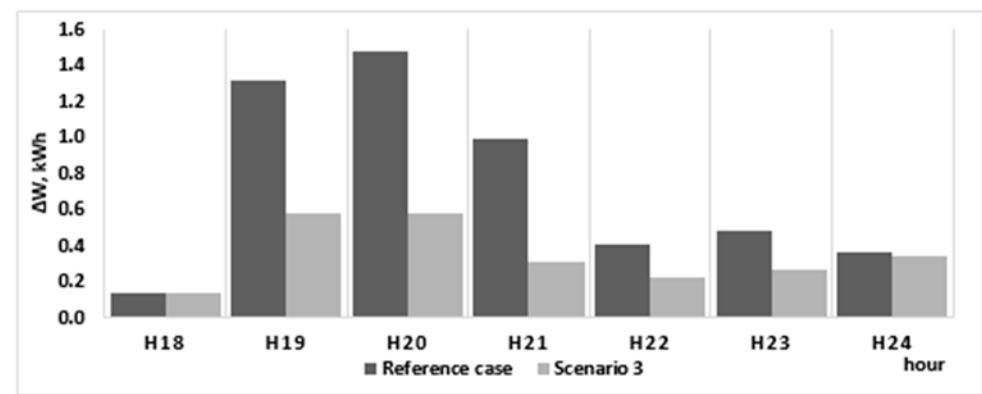


Figure 14. The energy loss pattern at battery discharging hours, Scenario 3.

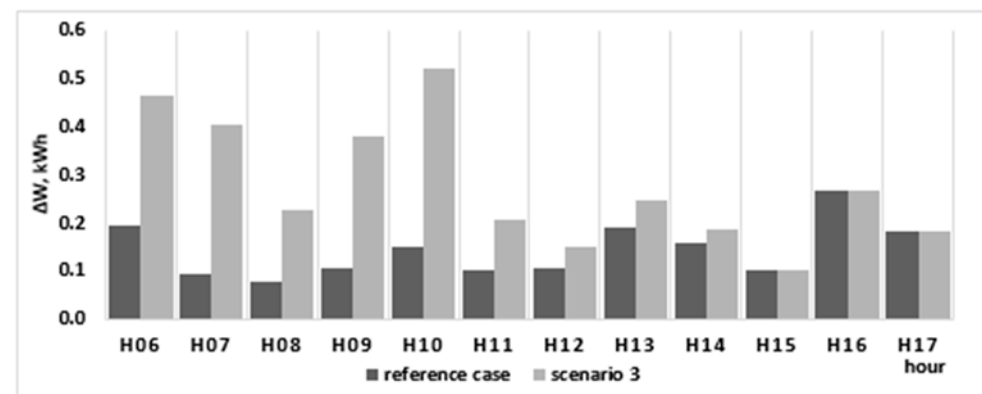


Figure 15. The energy loss pattern at battery charging hours, Scenario 3.

As Figure 15 shows, the increase in losses during the charge of the batteries is responsible for the high loss difference from Scenarios 2 and 3. The energy used to charge the batteries would be otherwise injected in the grid, replacing an equivalent supply from the substation. A high quantity of energy imported from the grid, which needs to supply consumption near the far end of the network, is likely to create equivalently high losses, accounting for the increase seen between hours 06:00 and 14:00, as seen in Figure 15. The loss reduction at peak time is of 2.74 kWh, comparable with the values obtained in the previous scenarios, but the increase in the 06:00–17:30 interval was 1.04 kWh. Another aspect, emphasized by Figure 13, is the fact that if the batteries are managed by the prosumer, they cannot not used to their maximum capacity, depending on their available surplus. This was the case of battery 2, which did not reach the maximum allowed loading of 95%.

## 5. Discussion

The authors proposed an algorithm capable of managing one-phase storage batteries installed in a three-phase low-voltage distribution network. Three scenarios were considered for optimization, and each of them shows possible situations that can occur in the operation of this type of network and storage, in real conditions.

In Scenario 1, where all the batteries need to be concentrated in one bus, the network operator is able to manage the batteries with minimal cost, but its options can be limited in reducing the energy losses. The electricity consumption was, in this case, lower than the available storage capacity, which is used sub-optimally. Two batteries were installed, but not discharged in the peak load interval. The operator will need to sustain minimal investment costs for storage installation, but will also obtain sub-optimal loss reduction.

Scenario 2 is the optimal case from the technical standpoint, because the loss reduction is maximal. However, the investment cost will increase for the network operator, because it will need to install and remotely manage batteries in three separate locations.

Scenario 3 shows that, even if the management of the batteries is outside the control of the DNO, the presence of storage can still provide energy loss reduction, although it can be significantly lower compared to the previous scenarios.

The genetic algorithm has been proven to be an efficient tool for computing the different formulations of the storage management problem. By properly choosing a chromosome structure that can be adapted to simulate these scenarios, it eliminates the need to build and solve each problem separately and can provide the necessary results for quick and meaningful comparison of the specificities encountered in each analyzed scenario.

Another aspect to be mentioned is the initial assumption for Scenarios 1 and 2, where the batteries were fully loaded at the beginning of the study. In real operation conditions, they would need to be charged at no-load night hours. As the loss profile from Scenario 3 shows, the charge could significantly impact the total daily losses. However, different strategies used for this purpose can result in significant differences (fast charge vs. low charge). A pertinent analysis should also take into account the price of electricity at night time, and the load profile of the network in the charging interval. These problems require an in-depth study and will be addressed in future research derived from this paper.

Other future research includes the possibility of combining storage technologies with reactive power compensation devices and substation transformer tap management, which would allow for further reduction in energy losses and bus voltage level improvement. It is expected that the impact of these measures would provide even more insights regarding the optimal use of storage in low-voltage distribution networks.

The results obtained in the paper show the necessity of the optimal use of storage in low-voltage unbalanced distribution networks. The problem is the cost of the batteries for the network operator, but, given the EU initiatives sustaining renewable electricity generation, it is foreseeable that these costs could be partially mitigated, but this also depends on local energy policies put forward by national governments.

## 6. Conclusions

The paper takes a new approach in prosumer surplus management, tested on a low-voltage electricity distribution network. Compared with the approach in which storage is owned and managed by the individual prosumers for their own benefit, which is preferred in the literature, the algorithm proposed by the authors considered two supplementary scenarios in which one-phase storage is used by the network manager to reduce the energy losses in three-phase, four-wire feeders. The community storage and the optimal distributed storage case were investigated, highlighting their strengths and weaknesses. Using the flexibility of the genetic algorithm approach, the three scenarios were modeled within the same chromosome structure, making the results easier to compare and evaluate, a feature that is a key factor for industry application.

**Supplementary Materials:** The following are available online at <https://www.mdpi.com/article/10.3390/math9192375/s1>, Table S1: the consumer and prosumer data used in the study.

**Author Contributions:** Conceptualization, M.G., B.-C.N., G.G. and O.I.; Methodology, O.I. and G.G.; Software, M.G., F.S. and O.I.; Validation, B.-C.N.; Formal analysis, M.G.; Data curation, B.-C.N. and F.S.; Writing—original draft preparation, O.I.; Writing—review and editing, B.-C.N. and F.S. All authors have read and agreed to the published version of the manuscript.

**Funding:** This research and the APC were funded by a publications grant of the “Gheorghe Asachi” Technical University of Iasi; project number GI/P19/2021.

**Conflicts of Interest:** The authors declare no conflict of interest.

## References

- OPCOM—the Romanian Gas and Electricity Market Operator. Available online: [https://www.opcom.ro/pp/grafice\\_ip/raportPIPSiVolumTranzactionat.php?lang=en](https://www.opcom.ro/pp/grafice_ip/raportPIPSiVolumTranzactionat.php?lang=en) (accessed on 10 August 2021).
- Kahouli, B. The causality link between energy electricity consumption, CO<sub>2</sub> emissions, R&D stocks and economic growth in Mediterranean countries (MCs). *Energy* **2018**, *145*, 388–399.
- Communication from the Commission to the European Parliament, the Council, the European Economic and Social Committee and the Committee of the Regions ‘Fit for 55’: Delivering the EU’s 2030 Climate Target on the Way to Climate Neutrality COM/2021/550 Final. Available online: <https://eur-lex.europa.eu/legal-content/EN/TXT/?uri=CELEX%3A52021DC0550> (accessed on 2 August 2021).
- Parag, Y.; Sovacool, B.K. Electricity market design for the prosumer era. *Nat. Energy* **2016**, *1*, 1–6. [CrossRef]
- Bellekom, S.; Arentsen, M.; van Gorkum, K. Prosumption and the distribution and supply of electricity. *Energy Sustain. Soc.* **2016**, *6*, 22. [CrossRef]
- Romanian Energy Regulatory Authority. The 228 Order for the Approval of the Technical Norm Technical Conditions for Connection to the Public Electrical Networks of the Prosumers. Available online: <https://www.anre.ro/ro/legislatie/prosumatori> (accessed on 2 August 2021).
- Van der Stelt, S.; AlSkaif, T.; van Sark, W. Techno-economic analysis of household and community energy storage for residential prosumers with smart appliances. *Appl. Energy* **2018**, *209*, 266–276. [CrossRef]
- Gram-Hanssen, K.; Hansen, A.R.; Mechlenborg, M. Danish PV prosumers’ time-shifting of energy-consuming everyday practices. *Sustainability* **2020**, *12*, 4121. [CrossRef]
- Li, X.; Lim, M.K.; Ni, D.; Zhong, B.; Xiao, Z.; Hao, H. Sustainability or continuous damage: A behavior study of prosumers’ electricity consumption after installing household distributed energy resources. *J. Clean. Prod.* **2020**, *264*, 121471. [CrossRef]
- Ruiz-Abellón, M.C.; Fernández-Jiménez, L.A.; Guillamón, A.; Falces, A.; García-Garre, A.; Gabaldón, A. Integration of demand response and short-term forecasting for the management of prosumers’ demand and generation. *Energies* **2020**, *13*, 11. [CrossRef]
- Liu, N.; Yu, X.; Wang, C.; Wang, J. Energy sharing management for microgrids with PV prosumers: A Stackelberg game approach. *IEEE Trans. Ind. Inform.* **2017**, *13*, 1088–1098. [CrossRef]
- Zafar, R.; Mahmood, A.; Razzaq, S.; Ali, W.; Naeem, U.; Shehzad, K. Prosumer based energy management and sharing in smart grid. *Renew. Sustain. Energy Rev.* **2018**, *82*, 1675–1684. [CrossRef]
- Venzelou, V.; Makrides, G.; Efthymiou, V.; Georgioudis, G.E. Methodology for deploying cost-optimum price-based demand side management for residential prosumers. *Renew. Energy* **2020**, *153*, 228–240. [CrossRef]
- Ghosh, A.; Aggarwal, V. Penalty based control mechanism for strategic prosumers in a distribution network. *Energies* **2020**, *13*, 452. [CrossRef]
- Ma, L.; Liu, N.; Zhang, J.; Wang, L. Real-time rolling horizon energy management for the energy-hub-coordinated prosumer community from a cooperative perspective. *IEEE Trans. Power Syst.* **2018**, *34*, 1227–1242. [CrossRef]
- Lim, S.Y.; Lee, T.W. Implementation of prosumer management system for small microGrid. *J. Korea Inst. Inf. Electron. Commun. Technol.* **2020**, *13*, 590–596.
- Barbosa, M.A.; Gül, K.; Bratcu, A.I.; Munteanu, I. Management of a photovoltaic-battery-based microgrid in a prosumer context. In Proceedings of the 6th International Symposium on Electrical and Electronics Engineering (ISEEE), Galati, Romania, 18–20 October 2019; IEEE: New York, NY, USA, 2019.
- Yang, Q.; Wang, H. Distributed energy trading management for renewable prosumers with HVAC and energy storage. *Energy Rep.* **2021**, *7*, 2512–2525. [CrossRef]
- Pilz, M.; Al-Fagih, L. Selfish energy sharing in prosumer communities: A demand-side management concept. In Proceedings of the IEEE International Conference on Communications, Control, and Computing Technologies for Smart Grids (SmartGridComm), Beijing, China, 21–23 October 2019; IEEE: New York, NY, USA, 2019.
- Han, L.; Morstyn, T.; McCulloch, M. Incentivizing prosumer coalitions with energy management using cooperative game theory. *IEEE Trans. Power Syst.* **2018**, *34*, 303–313. [CrossRef]
- Dolatabadi, M.; Siano, P. A scalable privacy preserving distributed parallel optimization for a large-scale aggregation of prosumers with residential PV-battery systems. *IEEE Access* **2020**, *8*, 210950–210960. [CrossRef]

22. Achiluzzi, E.; Kobikrishna, K.; Sivabalan, A.; Sabillon, C.; Venkatesh, B. Optimal Asset planning for prosumers considering energy storage and photovoltaic (PV) units: A stochastic approach. *Energies* **2020**, *13*, 1813. [[CrossRef](#)]
23. Korjani, S.; Serpi, A.; Damiano, A. A genetic algorithm approach for sizing integrated PV-BESS systems for prosumers. In Proceedings of the 2nd IEEE International Conference on Industrial Electronics for Sustainable Energy Systems (IESES), Cagliari, Italy, 1–3 September 2020; IEEE: New York, NY, USA, 2020.
24. Guo, Z.; Wei, W.; Chen, L.; Wang, Z.; Catalão, J.P.; Mei, S. Optimal energy management of a residential prosumer: A robust data-driven dynamic programming approach. *IEEE Syst. J.* **2020**, 1–10. [[CrossRef](#)]
25. Azim, M.I.; Tushar, W.; Saha, T.K. Investigating the impact of P2P trading on power losses in grid-connected networks with prosumers. *Appl. Energy* **2020**, *263*, 114687. [[CrossRef](#)]
26. Petrou, K.; Procopiou, A.T.; Gutierrez-Lagos, L.; Liu, M.Z.; Ochoa, L.F.; Langstaff, T.; Theunissen, J. Ensuring distribution network integrity using dynamic operating limits for prosumers. *IEEE Trans. Smart Grid.* **2021**, *12*, 3877–3888. [[CrossRef](#)]
27. Nousedil, A.I.; Christoforidis, G.C.; Papagiannis, G.K. Active power management in low voltage networks with high photovoltaics penetration based on prosumers' self-consumption. *Appl. Energy* **2018**, *229*, 614–624. [[CrossRef](#)]
28. Qi, M.; Yang, H.; Wang, D.; Luo, Y.; Zhang, S.; Liao, S. Prosumers peer-to-peer transaction decision considering network constraints. In Proceedings of the IEEE 3rd Conference on Energy Internet and Energy System Integration (EI2), Changsha, China, 8–12 November 2019; IEEE: New York, NY, USA, 2019.
29. Yang, J.; Paudel, A.; Gooi, H.B. Compensation for power loss by a Proof-of-Stake consortium blockchain microgrid. *IEEE Trans. Ind. Inform.* **2020**, *17*, 3253–3262. [[CrossRef](#)]
30. Wu, C.; Zhou, D.; Lin, X.; Wei, F.; Chen, C.; Ma, Y.; Dawoud, S.M. A novel energy cooperation framework for community energy storage systems and prosumers. *Int. J. Electr. Power Energy Syst.* **2022**, *134*, 107428. [[CrossRef](#)]
31. El-Batawy, S.A.; Morsi, W.G. Optimal design of community battery energy storage systems with prosumers owning electric vehicles. *IEEE Trans. Ind. Inform.* **2017**, *14*, 1920–1931. [[CrossRef](#)]
32. Shin, I. Approximation algorithm-based prosumer scheduling for microgrids. *Energies* **2020**, *13*, 5853. [[CrossRef](#)]
33. Ali, Z.M.; Diaaeldin, I.M.; Aleem, S.H.E.A.; El-Rafei, A.; Abdelaziz, A.Y.; Jurado, F. Scenario-Based network reconfiguration and renewable energy resources integration in large-scale distribution systems considering parameters uncertainty. *Mathematics* **2021**, *9*, 26. [[CrossRef](#)]
34. Pirouzi, S.; Aghaei, J.; Niknam, T.; Shafie-Khah, M.; Vahidinasab, V.; Catalão, J.P.S. Two alternative robust optimization models for flexible power management of electric vehicles in distribution networks. *Energy* **2017**, *141*, 635–652. [[CrossRef](#)]
35. Lin, M.H.; Tsai, J.F.; Yu, C.S. A review of deterministic optimization methods in engineering and management. *Math. Probl. Eng.* **2012**, *2012*, 756023. [[CrossRef](#)]
36. Adetunji, K.E.; Hofsajer, I.W.; Abu-Mahfouz, A.M.; Cheng, L. A Review of metaheuristic techniques for optimal integration of electrical units in distribution networks. *IEEE Access* **2021**, *9*, 5046–5068. [[CrossRef](#)]
37. Djebedjian, B.; Abdel-Gawad, H.A.; Ezzeldin, R.M. Global performance of metaheuristic optimization tools for water distribution networks. *Ain Shams Eng. J.* **2021**, *12*, 223–239. [[CrossRef](#)]
38. Grisales-Noreña, L.F.; González-Rivera, O.D.; Ocampo-Toro, J.A.; Ramos-Paja, C.A.; Rodríguez-Cabal, M.A. Metaheuristic optimization methods for optimal power flow analysis in DC distribution networks. *Trans. Energy Syst. Eng. Appl.* **2020**, *1*, 13–31. [[CrossRef](#)]
39. Kahouli, O.; Alsaiif, H.; Bouteraa, Y.; Ali, N.B.; Chaabene, M. Power System reconfiguration in distribution network for improving reliability using genetic algorithm and particle swarm optimization. *Appl. Sci.* **2021**, *11*, 3092. [[CrossRef](#)]
40. Ionescu, L.-M.; Bizon, N.; Mazare, A.-G.; Belu, N. Reducing the cost of electricity by optimizing real-time consumer planning using a new genetic algorithm-based strategy. *Mathematics* **2020**, *8*, 1144. [[CrossRef](#)]
41. Katoch, S.; Chauhan, S.S.; Kumar, V. A review on genetic algorithm: Past, present, and future. *Multimed. Tools Appl.* **2021**, *80*, 8091–8126. [[CrossRef](#)] [[PubMed](#)]
42. Lambora, A.; Gupta, K.; Chopra, K. Genetic algorithm—A literature review. In Proceedings of the 2019 International Conference on Machine Learning, Big Data, Cloud and Parallel Computing (COMITCon), Faridabad, India, 14–16 February 2019; IEEE: Piscataway, NJ, USA, 2019.
43. Alam, T.; Qamar, S.; Dixit, A.; Benaïda, M. Genetic algorithm: Reviews, implementations, and applications. *Int. J. Eng. Pedagog.* **2020**, *10*, 57–77. [[CrossRef](#)]
44. Mirjalili, S. Genetic algorithm. In *Evolutionary Algorithms and Neural Networks*; Springer: Berlin/Heidelberg, Germany, 2019; pp. 43–55.
45. The National Regulatory Authority for Energy (ANRE) Order no. 26/2016 Approving the Technical Energy Rule on Determining Own Technological Consumption in Public Electricity Networks—NTE 013/16/00. Available online: <http://www.anre.ro> (accessed on 10 August 2021).



## Article

# Efficient Optimization Algorithm-Based Demand-Side Management Program for Smart Grid Residential Load

Ali M. Jasim <sup>1,2,\*</sup> , Basil H. Jasim <sup>1</sup> , Bogdan-Constantin Neagu <sup>3,\*</sup>  and Bilal Naji Alhasnawi <sup>4</sup> <sup>1</sup> Electrical Engineering Department, University of Basrah, Basrah 61001, Iraq<sup>2</sup> Department of Communications Engineering, Iraq University College, Basrah 61001, Iraq<sup>3</sup> Power Engineering Department, Gheorghe Asachi Technical University of Iasi, 700050 Iasi, Romania<sup>4</sup> Department of Computer Technical Engineering, College of Information Technology, Imam Ja'afar Al-Sadiq University, Baghdad 66002, Iraq

\* Correspondence: e.alim.j.92@gmail.com (A.M.J.); bogdan.neagu@tuiasi.ro (B.-C.N.)

**Abstract:** Incorporating demand-side management (DSM) into residential energy guarantees dynamic electricity management in the residential domain by allowing consumers to make early-informed decisions about their energy consumption. As a result, power companies can reduce peak demanded power and adjust load patterns rather than having to build new production and transmission units. Consequently, reliability is enhanced, net operating costs are reduced, and carbon emissions are mitigated. DSM can be enhanced by incorporating a variety of optimization techniques to handle large-scale appliances with a wide range of power ratings. In this study, recent efficient algorithms such as the binary orientation search algorithm (BOSA), cockroach swarm optimization (CSO), and the sparrow search algorithm (SSA) were applied to DSM methodology for a residential community with a primary focus on decreasing peak energy consumption. Algorithm-based optimal DSM will ultimately increase the efficiency of the smart grid while simultaneously lowering the cost of electricity consumption. The proposed DSM methodology makes use of a load-shifting technique in this regard. In the proposed system, on-site renewable energy resources are used to avoid peaking of power plants and reduce electricity costs. The energy Internet-based ThingSpeak platform is adopted for real-time monitoring of overall energy expenditure and peak consumption. Peak demand, electricity cost, computation time, and robustness tests are compared to the genetic algorithm (GA). According to simulation results, the algorithms produce extremely similar results, but BOSA has a lower standard deviation (0.8) compared to the other algorithms (1.7 for SSA and 1.3 for CSOA), making it more robust and superior, in addition to minimizing cost (5438.98 cents of USD (mean value) and 16.3% savings).

**Keywords:** demand-side management; energy management; smart grid; sparrow search algorithm; binary orientation search algorithm; cockroach optimization algorithm; load shifting

**MSC:** 68Wxx

**Citation:** Jasim, A.M.; Jasim, B.H.; Neagu, B.-C.; Alhasnawi, B.N. Efficient Optimization Algorithm-Based Demand-Side Management Program for Smart Grid Residential Load. *Axioms* **2023**, *12*, 33. <https://doi.org/10.3390/axioms12010033>

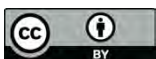
Academic Editors: José R. Cardoso and Rooney R. A. Coelho

Received: 6 December 2022

Revised: 19 December 2022

Accepted: 20 December 2022

Published: 27 December 2022



**Copyright:** © 2022 by the authors. Licensee MDPI, Basel, Switzerland. This article is an open access article distributed under the terms and conditions of the Creative Commons Attribution (CC BY) license (<https://creativecommons.org/licenses/by/4.0/>).

## 1. Introduction

Smart grid (SG) technology is regarded an innovation with the potential to improve the electricity grid in the 21st century. Owing to its distributed generation, universal control, digital two-way communication, and self-monitoring characteristics, the SG has acquired considerable appeal. Using contemporary information and communication technology, the SG can regulate the production of energy, electricity grid distribution, and transportation and develop intelligent monitoring systems. In addition, the SG is capable of managing the power market, controlling decentralized energy resources, and reconstructing infrastructure. Converting the traditional grid to an SG can enable a new era of DSM. DSM can be used to improve grid efficiency, reduce the expense of generation, possibly reduce load pressure, improve system reliability and sustainability, and maximize system capacity

without modifying the power system's physical infrastructure. The concurrently realized objectives of the incorporation of SG and DSM are (i) to minimize carbon emissions in order to combat global warming and (ii) to reduce electricity costs through demand management. By lowering carbon emissions and electricity costs, the combination of DSM and SG can ease the transition of citizens to smart, sustainable, and economic communities [1,2].

Because SGs can be grid-connected or islanded and because the Internet of Things (IoT) is a technique to connect people and things in any place at any time with anyone and anything through any electrical network or service, SGs serve as primary building blocks for an Energy Internet (EI). With the installation of smart meters in residential areas, real-time energy consumption monitoring is possible using EI. EI is hailed as a game-changing network of intelligent grids. It is considered a general IoT application for the energy and power sectors. The EI is made up of a variety of components and techniques, which can be divided into three classes: (i) communication systems, (ii) control algorithms, and (iii) power systems. Electricity generators and users (prosumers) are interconnected with renewable energy resources (RERs), electric loads, and storage systems, opening up infinite opportunities for energy sharing and giving rise to the EI concept. The Energy Internet is a game-changing innovation because it facilitates two-way flows of electricity and data in real time. This change is expected to be caused by the ongoing shift to renewable energy and the improvement of green technologies, such as SGs, storage systems, vehicle-to-grid systems, etc. [3–8].

SG technology facilitates grid connection and RER management and distribution. RERs are intermittent, posing a challenge for the grid. RERs increase the size of abrupt power output deficits due to adverse weather conditions, requiring the grid operator to maintain a higher level of backup power. This may be easily accomplished by reducing energy usage with DSM technology. Thus, load control methodologies must be used. A DSM system ought to be able to communicate with the controllable loads and the main controller [9,10]. The domain of optimal demanded power consumption criteria can be quite broad. Criteria could include increasing distributed production penetration, minimizing peak load demand, and enhancing economic gains by offering customers incentives to reduce demand during peak times [11,12].

The SG is distinguished by its dynamic pricing structures. Dynamic pricing schemes such as time of use (ToU), real-time pricing (RTP), and critical peak pricing (CPP) are frequently used in DSM methodologies, with the main difference being in price levels during operation times. Under RTP, the price changes every hour of the day. Under ToU, prices are fixed in advance (often up to one year in advance), and a variable pricing structure is designed for shoulder, on-peak, off-peak, and low-peak hours. Under CPP, the price of electricity is generally the same throughout the whole year, except during essential peak periods, when it reaches its maximum value. Price adjustments affect only the energy cost outcomes (not energy usage). The utility provides a pricing indication to smart home energy controllers. The energy management controller creates a schedule based on the user's load demand and the price signal. When any dynamic pricing scheme is combined with DSM strategies, the cost of electricity is calculated by the user's energy consumption estimations. Generally, the price can be increased if consumer demand is higher than supply. This growth in electricity pricing impacts all users of the power system. DSM governs the price of electricity in an energy market by lowering the peak demand. To this end, all residential loads are divided into shiftable and non-shiftable categories [13]. During peak hours, DSM techniques modify the demand patterns of customers in order to achieve the desired change in the load shape by shifting shiftable appliances to a more cost-effective time [14]. Therefore, DSM concentrates on energy-saving technology solutions, bill tariffs, and economic incentives instead of improving the grid's transmission and distribution grids or adding more power plants. Moreover, higher consumption demand can cause the load factor deteriorate (average load divided by the peak value), making the system unstable. This can be fixed by rescheduling the distribution system's peak load periods using the proper objective and DSM methodology. The load profile curve can be altered

load factor deteriorate (average load divided by the peak value), making the system stable. This can be fixed by rescheduling the distribution system's peak load periods using the proper objective and DSM methodology. The load profile curve can be altered using six DSM techniques: (1) peak clipping, (2) load shifting, (3) valley filling, (4) strategic load growth, (5) strategic conservation, and (6) load shape flexibility. Figure 1 shows the DSM strategies [15,16].

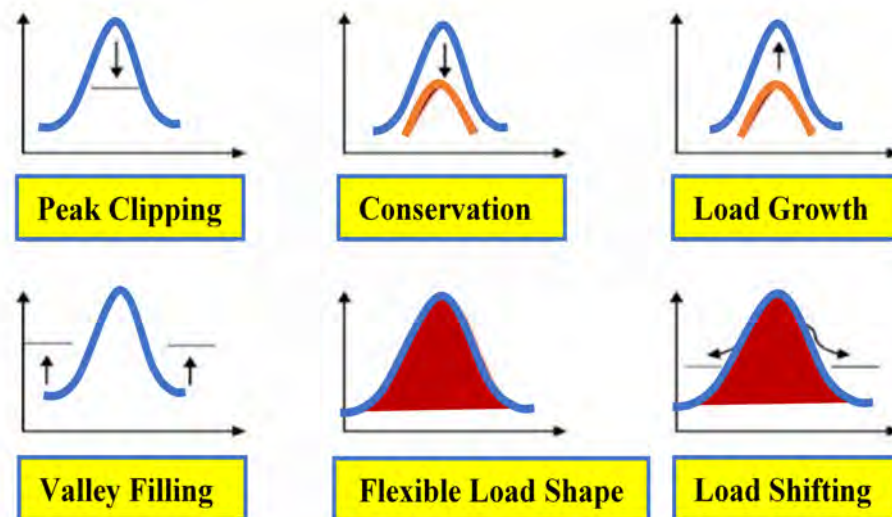


Figure 1. Techniques of DSM methodology.

Peak clipping is the practice of removing peaks above a predetermined consumption point. During peak clipping, loads are controlled directly to reduce the pressure of demand during the peak period. This causes a disruption in consumer comfort and compromises the level of consumer satisfaction with the service they receive. To increase electric loads during off-peak hours, valley filling necessitates the use of energy storage units [17]. The primary goal of load shifting is to move on-peak loads to off-peaks periods, thereby lowering the peak demand for energy. By reducing demand directly at the customer location, load profiles can be improved through strategic conservation goals. When there is a high level of demand, strategic load growth enables people to respond more quickly. The load shape greatly affects a smart grid's reliability. [18]. In SG management, load control strategies are referred to as flexible loads because they allow for individual participation. Different DSM techniques can be used in a variety of situations, depending on the implementation of the optimizing algorithm.

In this paper, a cost-effective model for residential appliance scheduling is presented. Our appliance-scheduling model seeks to optimize the operational time frame of electrical appliances using the load-shifting technique. The energy generated from SG REERs is considered alongside grid-generated energy in the model. This model simulates TOU pricing and makes use of CSO, SSA, and BSOA to generate optimal schedules. The adopted algorithms are evaluated based on their simple implementation, recentness, and fast convergence. The results show that the proposed model is effective in scheduling the electrical appliances in a residence, which benefits consumers by significantly lowering their electricity bills.

The remainder of the paper is divided into the following sections: Section 2 presents the related work. Section 3 explains the problem statement. The proposed system's overall architecture is discussed in Section 4. The problem statement is presented in Section 5. The proposed DSM methodology is described in Section 6. Section 7 describes the adopted optimization methodology. Section 8 discusses the problem formulation. The adopted optimization algorithm is described in Section 8. The simulation findings are displayed and discussed in Section 9. The paper concludes with Section 9.

2. Related Work

In order to reduce energy consumption, peak demand, and carbon emissions, many different methods have been developed to address energy management issues. In this context, the models proposed in [19–22] employ stationary techniques to reduce consumers'

electricity costs and user discomfort. In contrast, [23] presented interactions between interested consumers using a game of repeated energy scheduling, proving that static approaches provide inferior value in terms of both comfort and cost. In comparison, the authors defined non-static DSM techniques in which consumers can choose from a variety of options according to their energy usage and comfort requirements. The DSM architecture is described in detail in [24], in which the proposed design integrates green energy into the power system in order to reduce users' monitoring costs.

The authors of [25] scheduled power and time-shiftable appliances using an integer linear programming (ILP) technique. The authors of [26] proposed a Mixed-Integer Linear Programming (MILP)-based strategy for appliance scheduling to shift loads from peak to non-peak hours in order to reduce peak load and electricity demand costs. In [27], a cost-effective optimization-based model was proposed to control energy use in residences using linear programming (LP) in order to minimize overall cost and the peak-to-average ratio (PAR). An MILP formulation was proposed in [28] to schedule various types of appliances in order to minimize the user's electricity bill. Although dynamic programming (DP) and MILP have been considered to minimize the total cost of running a household and the PAR of electricity use, respectively [29,30], they require a great deal of computing time to implement.

In reference [31], an evolutionary algorithm-based (binary particle swarm optimization (BPSO), cuckoo search (CS), and genetic algorithm (GA)) DSM model was proposed to schedule residential users' appliances, resulting in reduced electricity bills and peaks. In [32], a DSM strategy based on monotonic optimization was presented; the optimal usage of renewable energy was demonstrated by mathematical modeling of a central renewable energy source. Sahar et al. [33] proposed a novel hybrid strategy combining GA, BPSO, and ant colony optimization (ACO) techniques for cost minimization and PAR reduction, taking user comfort into account when pricing ToU services. The authors of [34] proposed a system for managing residential energy demand within the confines of the user's budget. The authors used GA to solve an optimization conundrum with the aim of maximizing user convenience while minimizing energy consumption. The authors of [35] showed how to use RTP to schedule residential loads. To achieve the best electricity use, the authors used fractional programming. Simulated results indicate that the price of electricity was reduced. In [36], the authors came up with a way to shift the electricity load. They used a distributed algorithm to this end. Game theory was used to solve a residential load-scheduling problem. The newton method was also used to speed up the convergence rate of the Nash equilibrium. In [37], a strategy for avoiding distribution system overload was proposed, as well as an algorithm for checking the priority of an appliance and to shut it down to prevent distribution system overload. Overloading of the distribution system is avoided through proper load shedding. The authors of [38] proposed a scheme for scheduling appliances using the optimal stopping rule (OSR), which is a mathematical optimization technique used to indicate the lowest price, allowing the user to schedule their appliance during that time period. This lowers the cost of electricity consumption. In [39], a stochastic cost-minimization problem was proposed, along with renewable energy. The problem of cost minimization was solved using the Lyapunov optimization technique. The authors of [40] proposed a strategy for integrating renewable energy into the power system in order to increase the network's efficiency; users can reduce their monitoring costs by selling/purchasing grid energy. DSM studies were proposed by the authors of [41,42] using GA, PSO, and hybrid particle swarm optimization (HPSO) [43]. A number of engineering applications of artificial intelligence techniques were discussed in [44,45]. In [46], the grey wolf and crow search optimization algorithm was used to create a home appliance scheduling framework. Given the existence of real-time price signals, the proposed method analyzes the cost of electricity savings, user comfort, and PAR reduction for home appliances. To optimize energy usage in homes, in [47], researchers looked into a generic DSM model equipped with a power management controller. Optimization of electricity load scheduling for multiple residents and appliances using a Ladson generalized

bender algorithm was investigated in [48]. In addition, the authors of [49] used a non-dominated sorted GA to schedule home appliances while minimizing the associated energy costs. However, this method is computationally expensive and does not prioritize the convenience of end users.

To assure the lowest energy cost and the highest user comfort, the authors of [50] presented the grey wolf accretive satisfaction algorithm for DSM. In [51], a candidate solution updating algorithm (CSUA) was presented. The goal was to minimize the time a user must wait for PAR and an appliance while still providing that user with the desired level of comfort. By combining the modified and enhanced differential evolution with grey wolf optimization, a model for energy management was proposed and implemented with the goal of reducing peak energy usage and electricity costs [52]. The authors of [53] proposed a strategy for DSM based on load clipping and shifting. This strategy was simulated in MATLAB/Simulink and optimized with an artificial neural network (ANN) algorithm.

In this study, we implemented a smart grid Internet energy-based residential optimal demand management controller using the load-shifting technique. Our implemented model uses BOSA, SSA, and CSO algorithms. Notably, the use of these algorithms for DSM programs has not been mentioned in any previous studies to date, and this is the first study in which these algorithms have been applied in DSM. These optimization algorithms are compared to GA in terms of peak demand, electricity cost, robustness, and computation time tests. The Energy Internet is used to monitor meaningful findings by adopting the ThingSpeak platform. Moreover, adopting on-site RERs decreases peak power plants and reduces electricity costs in the proposed system. Furthermore, a ToU tariff scheme is adopted for electricity bill estimation. The simulation outcomes prove the effectiveness of the energy-optimization controller based on the preceding algorithms. The following are the highlights of the paper contributions:

1. For the first time, an optimal SG residential load-shifting DSM technique based on recent efficient optimization algorithms (BOSA, SSA, and CSO) is been proposed. The proposed DSM model is implemented using ToU dynamic pricing to establish prices in advance, as well as shoulder, on-off-peaks, and low-peak pricing while creating an interactive demand management market in which each consumer plays a role in reducing energy costs.
2. In-home demand consumption can be regulated by integrating applications for embedded systems and the Internet of Things. The model proposed in this study allows for continuous monitoring of the load, as well as scheduling of the load. Adopting EI and the ThingSpeak platform, total energy expenditures and peak energy consumption can be tracked from anywhere in real time.
3. To guarantee the achievement of minimum values of energy consumption, reduced electricity bills, and improved load factor using the load-shifting technique, the adopted algorithms are also compared in term of their robustness (code-tested for 20 times running). Computational speed tests are also performed to determine which algorithm offers the fastest and most effective processing.
4. In order to test the performance and effects of DSM on metrics such as peak consumption and bill electrification with and without DSM, the proposed algorithm-based optimal DSM is compared to the unscheduling load profile and to a DSM program with a commonly used algorithm (GA) for computation and evaluation of the optimal solutions.
5. The proposed optimization algorithm-based DSM program in SG is used to solve the problem of centralized optimization. In particular, each residential load has a local DSM controller and flexible appliances. By optimizing individual scheduling, the energy demand is decreased. The proposed algorithms are simple in construction, require few control parameters, and achieve a high rate of convergence, thereby avoiding getting stuck in local optima.

### 3. Problem Statement

Modern-world concerns include greenhouse gas emissions from fossil fuel electricity generation, requiring electrical researchers, engineers, and policymakers to optimize grid electricity consumption and renewable energy use. Residential loads frequently contribute significantly to both daily and seasonal peak demand, causing the power grid to be oversized to accommodate peak-period energy usage. DSM allows for more decentralized and efficient operation of appliances through the use of intelligent control strategies, mitigating problems with the current scenario from the perspective of the end user. Numerous other advantages motivate the use DSM; for example, it reduces spending and helps avoid power outages, guarantees a steady and long-lasting flow of power, helps to mitigate environmental concerns by decreasing the need for new conventional power plants, and aids the grid in reducing voltage problems. Without demand management, more power plants will be needed to increase the energy output of the SG and keep up with increasing energy demand. Under optimal DSM, its depth-enhancing benefits are maximized. In our work, an optimal DSM program is proposed to optimally shift the time of shiftable loads and modify the total load of the utility, thereby reducing anticipated peak loads and accomplishing the aforementioned goals. Heuristic algorithms should generally be discovered to find the most appropriate solutions for problems involving global optimization. The chosen algorithms (BSOA, SSA, and CSO) are evaluated based on their simple implementation, recentness (BSOA [54]), and significant advantages, such as their low number of parameters, fast convergence, and immunity to getting “stuck” in a local optimum (SSA [55]). CSO is simple and efficient and has successfully solved global optimization problems [56]. Here, the competency and robustness of the adopted algorithm-based methodology are confirmed. This study paves the way for real-time load monitoring. By using EI and the optimal DSM on the ThingSpeak platform, total energy costs and peak energy use can be tracked in real time from anywhere.

### 4. The Proposed System Structure

Appliances in a residential building should be scheduled in accordance with the ToU pricing model. An automated system must ensure that the workload is properly distributed. Residential energy management (EM) depends heavily on automated appliances, especially in the context of an SG. Below, we present an explanation of the infrastructure and concept of load scheduling in an energy management system.

#### 4.1. Model Representation and Concept

Figure 2 shows an illustration of the model’s structure, which serves as the basis for the development of optimization algorithms. An integrated power utility is focused on serving a diverse range of loads. To meet peak demand, the optimization program gives preference to residential load appliances that can use power during peak times. This is achieved by shifting schedulable appliances to off-peak hours. As a result, the load-side management system contributes to reducing the energy that is acquired from the utility company.

Smart meters, data centers, a communication network, and data incorporation into application platforms are some of the components of the residential building network. Figure 2 shows a smart meter, which is located between a home or building’s local area and utility, and is responsible for transmitting the aggregated demand for electricity to the utility. Smart meters can tell users when and how to use energy, and they can change their habits based on price patterns from the grid. Then, the utility calculates and provides a pricing pattern (e.g., time of use), which is used for load scheduling according to the collected customer data. A distribution board plays a crucial role in any electrical grid. It is used to divide a main power supply into several separate circuits. This board is necessary to separate shiftable appliances from non-shiftable appliances. The smart scheduler (SS) is an EM architecture-integrated device responsible for the scheduling and decision making of smart home appliances. Optimal performance is achieved by combining SS and the appliances. The main power contactor serves as an automatic power switch to transmit elec-

a pricing pattern (e.g., time of use), and the distribution board plays a crucial role in any electrical grid. It is used to divide a main power supply into several separate circuits. This board is necessary to separate shiftable appliances from non-shiftable appliances. The smart scheduler (SS) is an EM architecture-integrated device responsible for the scheduling and decision making of smart home appliances. Optimal performance is achieved by combining SS and the appliances. The main power contactor serves as an automatic power switch to transmit electrical power signals from the utility or microgrid (MG) or SG resources to appliances with the help of low-power relay devices and the distribution board. Lastly, through the smart meter, the adoption of the Energy Internet enables the user to continue real-time monitoring of total energy expenses and peak energy consumption via the ThingSpeak platform.

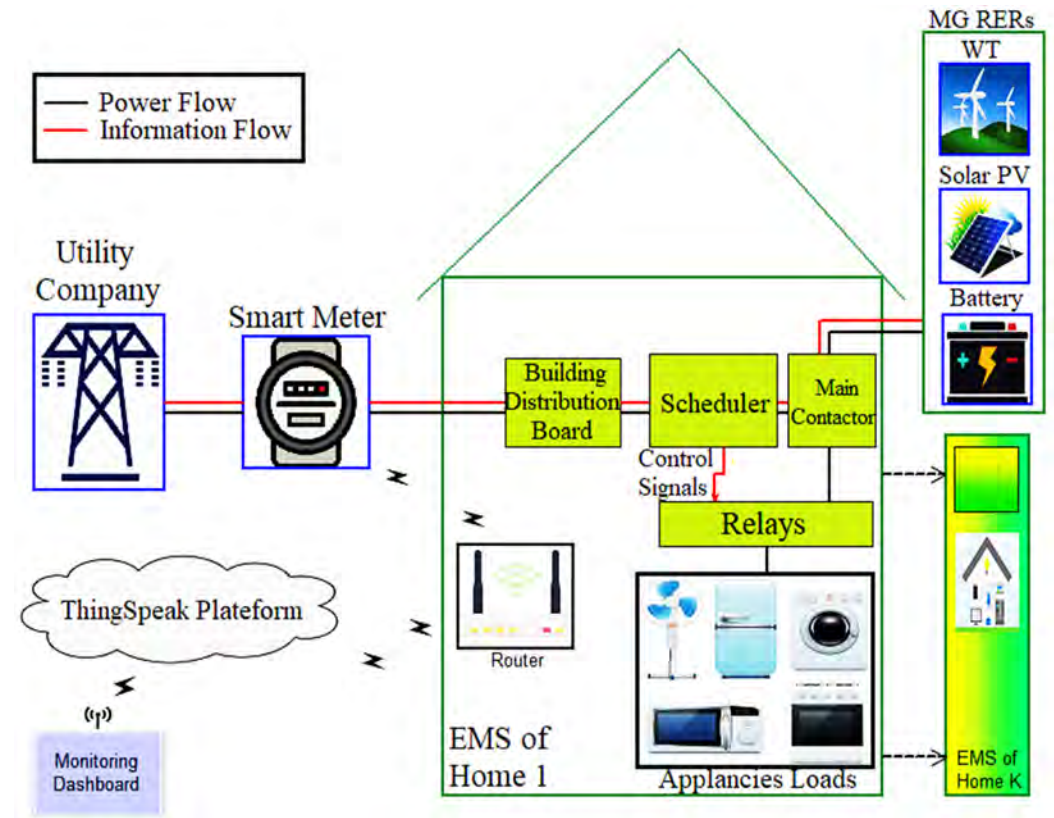


Figure 2. Graphical representation of the proposed model.

This work applies an intelligent approach that generates appliance usage patterns based on electricity price tariffs without human intervention. In order to better comprehend energy consumers, we divided them into two main categories: traditional consumers and intelligent consumers. Because traditional homeowners are not concerned with price, they do not include EM architecture in their homes or buildings. EM architecture is not used in traditional homes or buildings, unlike in the homes of smart users, who adopt an EM architecture. The EM system consists of the electrical grid, home appliances, and the display, as shown in Figure 2.

#### 4.2. Energy Management System

The home has a smart appliance scheduling and decision-making device, known as a smart scheduler, which is implemented into the EM architecture. SS works in tandem with the appliances. The EMS architecture is depicted in Figure 2. A smart meter sends out energy price signals, as well as a collection of energy-hungry appliances. The SS calculates household appliance ON/OFF schedules in the most efficient way. With a smart meter, the SS receives a signal from the main grid about prices and modifies the user’s hourly load demand level in line with the pricing signal. First, the SS moves or shifts the maximum level of electricity usage by each appliance from peak times to off-peak times. The, the SS calculates the cost of electricity for each hour.

#### 4.3. Energy Internet

We used a simulation test to monitor the energy demand of the SG according to the Energy Internet approach over the cloud platform to regulate smart home appliances. We

We used a simulation test to monitor the energy demand of the SG according to the Energy Internet approach over the cloud platform to regulate smart home appliances. We authors created a ThingSpeak platform interface with an effective and simple user interface (UI) that allows homeowners to access and monitor the consumption energy cost and peak energy through cloud-based home energy management. Figure 3 shows an Internet web page that users can access using an Internet browser after entering their username and password as uniform resource locator (URL) login credentials.

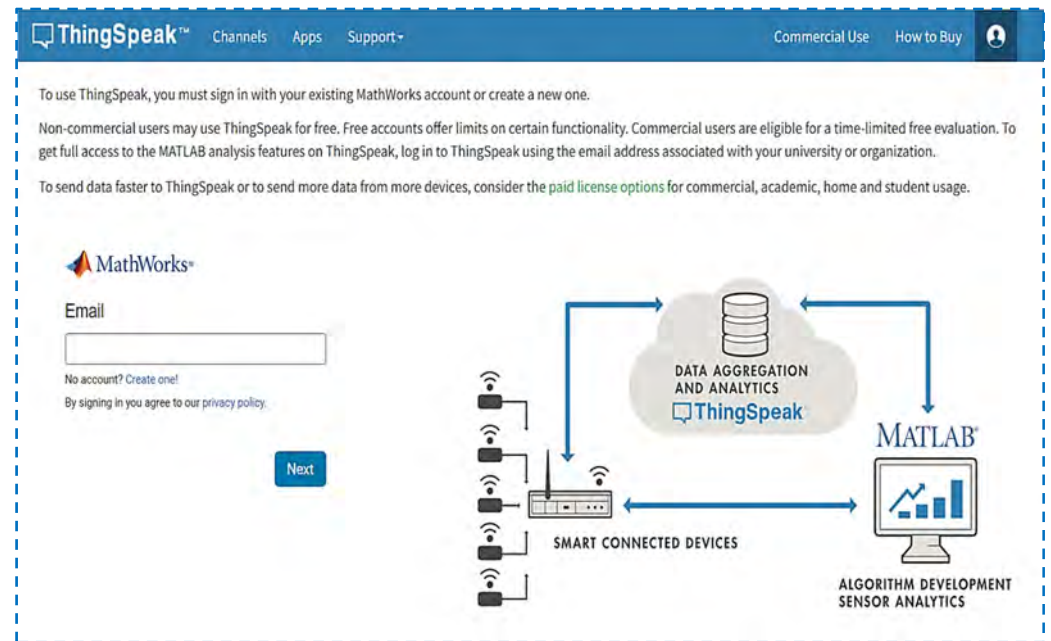


Figure 3. Platform for creating user interfaces (ThingSpeak platform).

MATLAB and the open-source IoT framework are used to model proposed communication architectures. For real-time cloud simulation, ThingSpeak was chosen because of the following advantages:

1. **Data aggregation, tracking, and analysis on the ThingSpeak Cloud platform.** The power profile is graphically depicted and monitored in real time in multiple ThingSpeak channels in the smart grid model.
2. **User authentication is enabled by login credentials, and every channel has its own ID. Each channel has two keys for the programming interface.** The API's read and write keys are generated at random. These keys enable the storage and retrieval of data from every channel over the Internet or a local area network.
3. **A communication network makes it possible for MATLAB and ThingSpeak to send and receive data over the Internet.**
4. **Data can be imported, exported, analyzed, and viewed on multiple platforms and fields at the same time.**

5. Proposed DSM Methodology

For purposes of residential load management, we divided home appliances into two categories. The first category consists of shiftable loads, such as vacuum cleaners, washing machines, etc., that can freely be shifted to operate at different times of day without negatively impacting customer convenience. The second type is non-shiftable loads such as electric vehicles, air conditioners, and water pumps, which cannot be operated in different time slots. Table 1 illustrates the rated information of both shiftable and non-shiftable residential loads. There are three water heaters, eight air conditioners, four electric vehicles, and two water pumps. All other appliances have only one unit. Table 2 shows the detailed operation hours and consumption energy of each appliance.



**Table 1.** Shiftable/non-shiftable residential Loads.

Shiftable/Non-Shiftable Appliances	Appliance Name	Energy Consumption (kWh)
Shiftable Appliances	Vacuum Cleaner (VC)	1
	Microwave Oven (MO)	1.8
	Washing Machine (WM)	2
	Water Heater (WH)	3.66 per unit
	Dish Washer (DW)	1.4
	Coffee Maker (CM)	1.6
Non-shiftable Appliances	Air Condition (AC)	12 per unit
	Electric Vehicle (EV)	5 per unit
	Water Pump (WP)	4 per unit

**Table 2.** Detailed operation hours and power consumption of shiftable/non-shiftable loads.

Operation Hour(s)	VC	MO	WM	WH	DW	CM	Operation Hour(s)	AC (Units)	EV (Units)	WP (Units)
1–2	ON	ON	ON	OFF	OFF	ON	1	5	2	2
2–4	OFF	ON	ON	OFF	OFF	ON	2	5	0	4
5	OFF	ON	ON	OFF	OFF	OFF	3–5	3	0	3
6	OFF	ON	OFF	OFF	ON	ON	6	2	2	2
7	ON	OFF	OFF	OFF	ON	ON	7	2	2	1
8	ON	ON	OFF	OFF	OFF	ON	8	3	4	0
9	ON	ON	OFF	OFF	OFF	OFF	9–11	8	0	2
10	ON	OFF	OFF	OFF	OFF	ON	11–13	8	4	0
11–13	OFF	OFF	OFF	OFF	OFF	ON	14	8	3	0
14	OFF	ON	OFF	OFF	ON	OFF	15	8	2	2
15	ON	OFF	ON	OFF	OFF	ON	16–17	8	0	0
16	ON	OFF	OFF	ON	OFF	OFF	18–19	2	0	0
17	OFF	ON	OFF	OFF	ON	OFF	20	2	0	2
18	OFF	ON	OFF	OFF	OFF	OFF	21	2	0	0
19	OFF	OFF	OFF	OFF	OFF	OFF	22–24	1	0	1
20	ON	ON	ON	OFF	OFF	ON				
21	OFF	ON	OFF	ON	OFF	OFF				
22	OFF	ON	ON	OFF	OFF	ON				
23	OFF	ON	OFF	OFF	OFF	OFF				
24	OFF	ON	OFF	OFF	ON	ON				

A flow chart illustrating the proposed optimal DSM strategy is shown in Figure 4. The first step is to conduct a survey to gather load data. Once the loads have been categorized, a load profile is created, which includes both the shiftable and non-shiftable appliances. Furthermore, the load curve is used to establish the durations of peak and off-peak periods. The amount of energy used in an hour is compared to the maximum allowed for that time period. The load-shifting technique reduces excessive energy consumption by redistributing it among various appliances in use at given time. The technique of load shifting is utilized if and only if the system has shiftable loads. We assume a two-day period to monitor the entire process. Loads can be met by either grid or SG resources once the optimization process is complete. If the energy consumption is less than the total energy of RERs, RERs are used to power the loads. Otherwise, the utility grid compensates for the energy deficit.

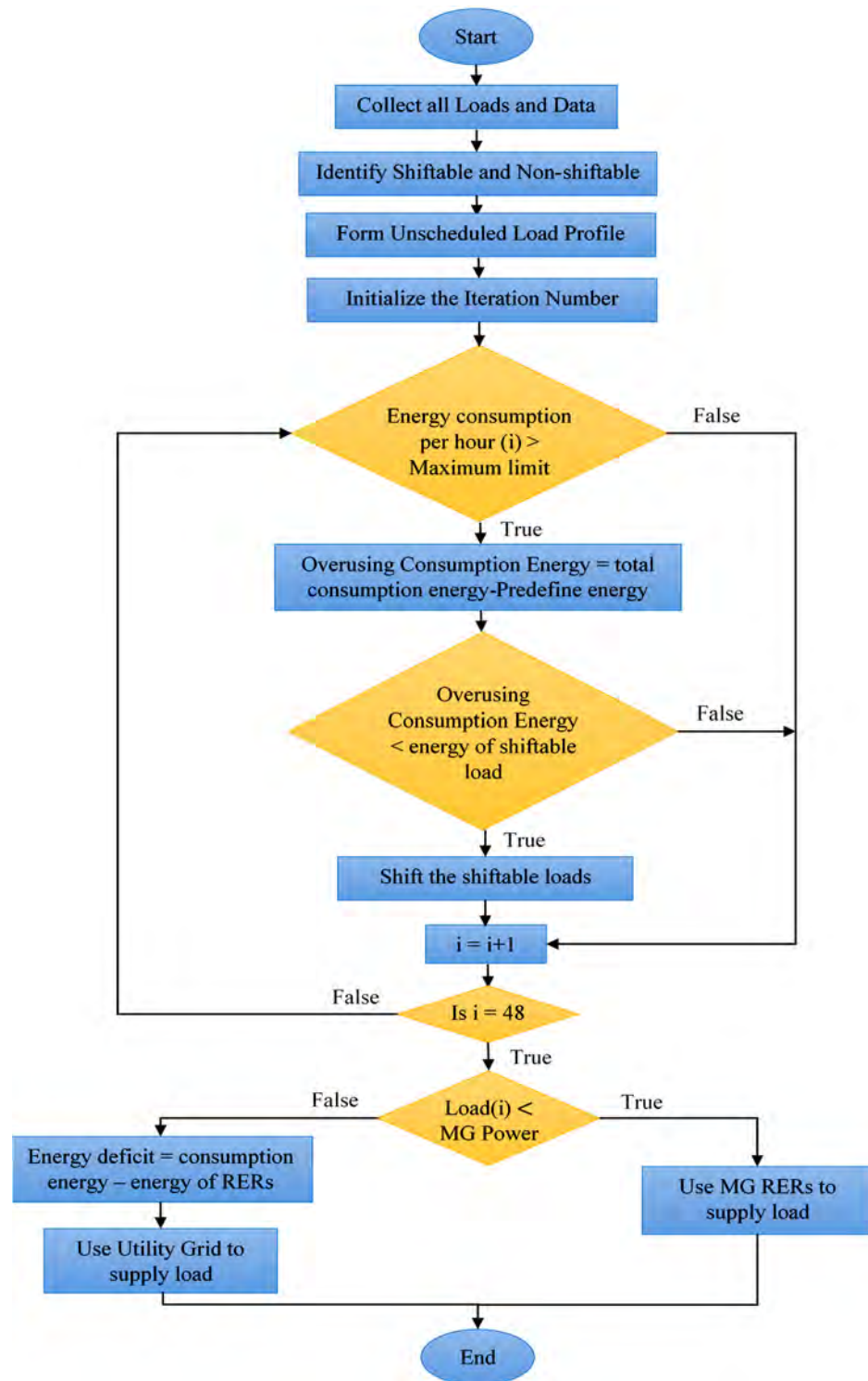


Figure 4. Flow chart of the optimal DSM strategy.

## 6. Problem Formulation

### 6.1. Mathematical Framework for Appliance Scheduling

On the basis of energy consumption, end-user preferences, operational hours, appliances can be categorized as either non-shiftable or shiftable. Shiftable appliances can be modified to operate on any time scale without affecting their performance. By shifting their operations to off-peak hours, energy consumption and costs can be reduced. The daily consumption cost of shiftable appliances ( $C_s$ ) is given by:

operations to off-peak hours, energy consumption and costs can be reduced. The daily consumption cost of shiftable appliances ( $C_S$ ) is given by:

$$C_S(t) = \sum_{t=1}^{24} \sum_{m=1}^{N_S} X_S(n,t) \times A_S(n,t) \times PR(t) = \sum_{t=1}^{24} E_S(t) \times PR(t) \quad (1)$$

where  $t$  is the time slot,  $n$  is the number of appliances,  $N_S$  represents the total number of shiftable appliances,  $A_S$  is the appliance's power consumption during time  $t$ ,  $E_S$  is the total energy consumption of shiftable appliances, and  $X_S$  denotes the ON/OFF state of shiftable appliances.

The load profiles of normally operated appliances, which are also referred to as fixed (non-shiftable) appliances and include the AC, WP, and EV, cannot be modified in any way. The daily cost of non-shiftable appliances ( $C_{NS}$ ) can be expressed as:

$$C_{NS}(t) = \sum_{t=1}^{24} \sum_{m=1}^{N_{NS}} X_{NS}(n,t) \times A_{NS}(n,t) \times PR(t) = \sum_{t=1}^{24} E_{NS}(t) \times PR(t) \quad (2)$$

where  $N_{NS}$  represents the total number of non-shiftable appliances,  $A_{NS}$  is the power consumption of non-shiftable appliances,  $E_{NS}$  is the total energy consumption of non-shiftable appliances, and  $X_{NS}$  denotes the ON/OFF state of non-shiftable appliances.

The total energy consumption ( $E(t)$ ) and cost ( $C(t)$ ) of all non-shiftable and shiftable appliances are given in Equations (3) and (4), respectively.

$$E(t) = E_{NS}(t) + E_S(t) \quad (3)$$

$$C(t) = C_{NS}(t) + C_S(t) \quad (4)$$

### 6.2. Objective Function

The proposed load-shifting-based DSM schedules shiftable loads so that the energy consumption curve is as close to optimal as possible. Additionally, time slots and movable loads are treated as variable components. Our goal is to minimize the user's electricity bill, in addition to lowering the peak energy consumption to improve the grid's efficiency. The following is the formulation of the minimization problem:

$$\text{Minimize : } \sum_{t=1}^{24} E(t) \times PR(t) = \sum_{t=1}^{24} (E_{NS}(t) + E_S(t)) \times PR(t) \quad (5)$$

where  $PR$  denotes the electricity price at the specified time ( $t$ ),  $X$  denotes the ON/OFF state of appliances, and  $E$  is the total energy consumption. The aggregate energy consumption of  $N$  appliances during time slot  $t$  is equal to or less than the maximum permissible output for energy consumption reduction. An appliance's maximum allowable delay is denoted by  $M_n = 24 - l_n$ , and the appliance's duration of operation is  $l_n$ .

### 6.3. Constraints

Constraints should be considered during the process of load scheduling. For example, the total amount of shiftable loads should exceed the total amount of shifted hourly loads. Otherwise, the inflated demand must be reined in. Additionally, shiftable loads have a limit of time shift, which can be advanced or delay within a permissible range. There must be more shifted appliances than there are shiftable appliances at time step  $t$ , as stipulated in Equation (6).

$$S(n,t) \leq \sum_{t=1}^{24} H(n,t) \quad \forall -T \leq t \leq T \quad (6)$$

where  $S$  and  $H$  denote shifted appliances and shiftable appliances, respectively, and  $T$  is the limit of time shift.

The load demand for scheduled and shifted loads in the entire day should equal the daily demand usage for loads prior to scheduling.

$$\text{Subject to } \sum_{t=1}^{24} \sum_{m=1}^M B(m, t) = \sum_{t=1}^{24} \sum_{m=1}^M A(m, t) \tag{7}$$

where  $B(m, t)$  is the total daily demand prior to the  $t$ -th hour of the  $m$ -th type of load shifting, and  $A(m, t)$  represents the overall daily demand after shifting for the  $t$ -th hour of the  $m$ -th load type.

### 7. Optimization Algorithms

Three metaheuristic optimization techniques for DSM are covered here. These algorithms are used in typical single building with nine different appliances (six shiftable and three non-shiftable appliances). The energy consumption patterns of various appliances necessitate distinct power ratings. Electricity involves four stages: production, transmission, distribution, and consumption. There are three main types of electricity consumers: households, businesses, and factories. To be clear, our primary objective is to improve the building power scheduling. Many scholars have presented various optimization strategies for DSM in residential areas. As such, we present optimization methods (SSA, BSOA, and CSO) in order to achieve optimal electrical usage. The concept of SSA is inspired by the foraging and predator avoidance behaviors of sparrows. The BSOA is a game-theoretic optimizer based on the principles of the orientation game. Players of BOSA’s orientation game, i.e., the searcher agents, move around the playground in response to the direction indicated by the referee. The CSO is an optimization algorithm based on the foraging behaviors of cockroach swarms. Using these algorithms, the shiftable appliances are shifted from peak to off-peak hours by comparing energy consumption with the unscheduled load profile, which helps to bring down the price of electricity because the price goes up gradually as peak use times get closer. The mathematical models and detailed explanations of the adopted algorithms are provided below.

#### 7.1. Sparrow Search Algorithm

Xue and Shen presented the sparrow search algorithm in (2020) [57]. The SSA is an algorithm for swarm intelligence optimization. The SSA is based on predator avoidance and feeding behavior of sparrow [57]. It simulates sparrow team foraging; those who seek better food are finders (discoverers), whereas others are followers. Simultaneously, a subset of the population conducts reconnaissance and early warning. If a threat is detected, they forgo food for safety. The matrix below represents the position of individual sparrows [57]:

$$X = \begin{bmatrix} x_{1,1} & x_{1,2} & \cdots & x_{1,d} \\ x_{2,1} & x_{2,2} & \cdots & x_{2,d} \\ \vdots & \vdots & \vdots & \vdots \\ x_{n,1} & x_{n,2} & \cdots & x_{n,d} \end{bmatrix} \tag{8}$$

where  $n$  denotes the number of sparrow, and  $d$  denotes the dimension of the variable under consideration. Then, the following vector can be used to represent the fitness values of all sparrows:

$$F(X) = \begin{bmatrix} f([x_{1,1} & x_{1,2} & \cdots & x_{1,d}]) \\ f([x_{2,1} & x_{2,2} & \cdots & x_{2,d}]) \\ \vdots & \vdots & \vdots & \vdots \\ f([x_{n,1} & x_{n,2} & \cdots & x_{n,d}]) \end{bmatrix} \tag{9}$$

where  $F(X)$  denote the sparrows’ fitness, and the value of each row represents a sparrow’s fitness. The discoverers are in charge of locating food and aiding the entire population in achieving increased fitness levels while prioritizing food acquisition throughout the search.

Thus, the discoverers can scour a much larger area for food than the participants. When a sparrow spots a predator, it begins singing as a warning signal. This means that if the alarm value exceeds the safety value, the finder directs the group to other secure foraging locations. The updated location of the sparrow finder in each iteration is expressed as follows [57]:

$$X_{i,j}^{t+1} = \begin{cases} X_{i,j}^t \cdot e^{-\left(\frac{i}{\alpha \cdot iter_{max}}\right)} & \text{for } R < ST \\ X_{i,j}^t + Q \times L & \text{for } R \geq ST \end{cases} \tag{10}$$

where  $X_{i,j}^t$  denotes the sparrow finder’s location;  $t$  denotes the current iteration;  $j = 1, 2, \dots, d$  denotes the dimensions of the  $i$ -th sparrow in iteration  $t$ ;  $iter_{max}$  denotes the constant with the maximum iterations;  $\alpha \in (0,1]$  denotes a random number;  $R \in [0,1]$  and  $ST \in [0.5,1]$  denote alarm and safety thresholds, respectively;  $Q$  is a normally distributed random number; and  $L$  is set to 1 if and only if every entry in a dimensioned matrix is a one.  $R < ST$  indicates that there are no dangers in the area, so the finder begins a thorough search;  $R \geq ST$  indicates that some sparrows have been attacked by predators, and all sparrows must flee as soon as possible for safety.

Individuals with lower energy levels are less likely to forage as part of the group. Some hungry newcomers are more likely to flee in search of additional energy. Entrants can always search for the finder while foraging, as the finder may obtain food or forage in the vicinity. Certain entrants may pay close attention to the finders for increased predation and food competition. Some entrants, on the other hand, pay closer attention to the finders if they notice the finder leaving their current location to compete for food. If they win, they receive the finder’s food right away. The following formula is used to update the positions of enrollees [57]:

$$X_{i,j}^{t+1} = \begin{cases} Q \times e^{-\left(\frac{X_{worst}^t - X_{i,j}^t}{i^2}\right)} & \text{for } i > \left(\frac{n}{2}\right) \\ X_p^{t+1} + \left|X_{i,j}^t - X_p^{t+1}\right| \times A^+ \times L & \text{Otherwise} \end{cases} \tag{11}$$

where  $X_{worst}^t$  is the current worst position in the search space;  $A^+$  is a random variable of dimension  $d$  with elements randomly distributed between  $[1,1]$ ; and  $A^+ = A^T(AA^T)^{-1}$ . If  $i$  is greater than  $\frac{n}{2}$ , the  $i$ -th entrant has a minimal fitness and is most likely to perish. Approximately 10% to 20% of the sparrow population is assumed to be danger-aware, which randomly produces the initial positions of the sparrows. The sparrows on the edge of the group rapidly fly to the secure area to find a better spot. The sparrows in the middle of the group relocate randomly to find other sparrows. The mathematical model of the scout is expressed as follows:

$$X_{i,j}^{t+1} = \begin{cases} X_{best}^t + \beta \times \left|X_{i,j}^t - X_{best}^t\right| & \text{for } f_i > f_g \\ X_{i,j}^t + K \times \left(\frac{\left|X_{i,j}^t - X_{worst}^t\right|}{(f_i - f_w) + \epsilon}\right) & \text{for } f_i = f_g \end{cases} \tag{12}$$

where  $X_{best}^t$  denotes the current optimal global location;  $\beta$  denotes the control parameter for step size in the form of random number normal distribution with a variance of “1” and a mean of “0”;  $K$  denotes the direction of sparrow movement in the form of a random number ( $\in [-1,1]$ );  $f$  denotes the fitness function of the optimization problem, where  $f_i$ ,  $f_g$ , and  $f_w$  denote the global current and best and worst sparrow fitness values, respectively; and  $\epsilon$  is the smallest constant required to prevent a zero division error. For simplicity’s sake,  $f_i > f_g$  indicates that sparrows are at the group’s edge, and  $X_{best}^t$  indicates that sparrows are around the center of the group; otherwise,  $f_i = f_g$  indicates that sparrows in the middle of the population know that there is a threat to their species.

Here, power consumption is managed by introducing the SSA into the DSM control strategy, taking into account the discoverer’s position based on the positions of shiftable

loads. The algorithm SSA manipulates the vertical and horizontal axes of the energy consumption pattern. The vertical axis represents the magnitude of energy consumption, whereas the horizontal axis represents the time of energy consumption. This algorithm determines the optimal energy consumption pattern that results in the lowest power cost based on maximum energy consumption and maximum time slot parameters. The chosen objective function to be minimized is shown in Equation (5).

The main steps of SSA are described in the Algorithm 1:

---

**Algorithm 1 SSA Steps**

---

*Step 1:* The utility’s ToU price, the daily demand profile, and the unscheduled load timing are all indications of input data that must be defined at the outset of the program.

*Step 2:* Input the control parameters  $R$ ,  $ST$ ,  $n$  and  $iter_{max}$ .

*Step 3:* Initialize a population with  $n$  sparrows using Equation (8).

*Step 4:* Calculate the initial fitness function, and determine the global best sparrow fitness value and global optimal location using Equations (5) and (9).

*Step 5:*  $t = 1$ .

*Step 6:* Rate the fitness values and assess the current worst and best evaluation.

*Step 7:*  $i = 1$ .

*Step 8:* Update the positions of producers, scroungers, and afraid sparrows using Equations (10)–(12).

*Step 9:* Last individual? yes > return to step 7, else > calculate the updated fitness values.

*Step 10:* If new  $x_{i,j}$  less than old  $x_{i,j}$  > update the sparrow positions and fitness value, else > return to 7.

*Step 11:* Last iteration?, yes > print the optimal solution, else > return to step 6.

---

**7.2. Binary Orientation Search Algorithm**

BOSA was proposed in (2019) [54] and simulates the rules of an orientation game. In this game, players move around the playground according to the referee’s instructions. The starting positions of the players are depicted in Equation (13) [54].

$$X_i = (x_i^1, \dots, x_i^d, \dots, x_i^n) \tag{13}$$

where  $x_i^d$  denotes the position of player  $i$  of dimension  $d$ , and  $n$  denotes the number of variables.

In each iteration, the player (P) with the best value of the fitness function is the referee (R), as described in Equation (14):

$$R = \begin{cases} \text{Maximization problem : location of } \max(f) \\ \text{Minimization problem : location of } \min(f) \end{cases} \tag{14}$$

The value of the fitness function is denoted by  $(f)$ .

A referee’s hand may or may not be moving in the same body direction. Players, on the other hand, must only take into consideration the referee’s hand. Equations (15) and (16) are used to simulate the direction [54]:

$$P_i = 0.8 + 0.2 \frac{t}{T} \tag{15}$$

$$\text{Orientation}_i^d = \begin{cases} \text{sign}(R^d - P_i^d) \text{ for } \text{rand} < P_i \\ -\text{sign}(R^d - P_i^d) \text{ otherwise} \end{cases} \tag{16}$$

At iteration  $t$  and maximum iteration  $T$ .

Although each player is required to move in the direction of the referee, a few players may not be able to do so. This problem is simulated in Equations (17) and (18) [54].

$$error = 0.2 \left( 1 - \frac{t}{T} \right) \tag{17}$$

$$x_i^d = \begin{cases} x_i^d + rand * Orientation_i^d * x_h^d \\ x_l^d + rand * (x_h^d - x_l^d) \end{cases} \tag{18}$$

where  $x_l^d$  and  $x_h^d$  are the lower and upper limits, respectively.

In discrete space, the dimensions of the particle position are denoted by the numbers “0” and “1” for each dimension. In any dimension, the movement of an agent corresponds to the change in its value from zero to one or vice versa. Therefore, the displacement in each dimension is determined as a probability function, and the player’s position is updated in response to this probability function. In BOSA, the probability function ( $dX^{j,d}$ ) is chosen to be restricted to the interval of [0–1]. The probability function is given in Equation (19) [54].

$$S(dX^{j,d}(t)) = \left| \tanh(dX^{j,d}(t)) \right| \tag{19}$$

Each player’s new position is simulated based on the probability function using Equation (20).

$$X^{j,d}(t+1) = \begin{cases} complement(X^{j,d}(t)) & \text{for } rand < S(dX^{j,d}(t)) \\ X^{j,d}(t) & \text{Otherwise} \end{cases} \tag{20}$$

The following procedures detail how to apply the BSOA-based proposed optimal DSM program to the investigated problem, taking into account the player positions based on the positions of the shiftable loads. This algorithm alters the axes of the energy consumption pattern. The vertical axis shows energy usage, whereas the horizontal axis shows time. Based on the adjusted parameters of maximum energy consumption and maximum time slots, this algorithm calculates the lowest-cost energy consumption pattern. In Algorithm 2, the steps involved in applying BSOA are as follow:

---

**Algorithm 2 BOSA Steps**

---

- Step 1: The utility’s ToU price, the daily demand profile, and the unscheduled load timing are all indications of input data that must be defined at the outset of the program.
  - Step 2: All of the BOSA settings in Table 2 should be set.
  - Step 3: The DSM objective (Equations (5) and (14)) can be minimized by randomly sampling a population.
  - Step 4: The player’s position is updated for every population inside the iteration range using Equations (19) and (20).
  - Step 5: Verify each population’s constraints.
  - Step 6: Repeat steps 3–5 until the stop condition is met.
- 

**7.3. Cockroach Swarm Optimization Algorithm (CSOA)**

CSO is derived from the foraging behavior of cockroaches, which includes swarming, scattering, and light evasion [58–60]. As a result, the CSOA employs a set of rules to mimic the collective behavior of cockroaches. The initial step of the algorithm is to generate a set of potential solutions. Initial solutions are typically generated at random in the search area. Additionally, the CSOA includes three different procedures for the purpose of solving various optimization issues during each iteration, including dispersing, ruthless behavior, and chase swarming. The strongest cockroaches in the chase-swarming process take the best local solutions ( $P_i$ ), create small swarms, and progress toward the global optimum in the new cycle ( $P_g$ ). Each individual ( $X_i$ ) in this procedure reaches its local optimum within its visibility range. Because individuals pursue their local optima in different ways,

it is possible for a cockroach in a small group to be the strongest by finding a better solution. A single cockroach’s local optimum exists within its own field of vision, and it seeks the best global solution [61]. Another procedure is for individuals to be dispersed. It is performed on a periodic basis to maintain cockroach diversity. In the search space, each cockroach takes a random step. This process is analogous to the phenomenon of the weakest cockroaches being consumed in the absence of sufficient food [61]. The following is the CSOA model [62,63]:

(1) *Chase-Swarming Behavior:*

$$X_i = \begin{cases} X_i + step.rand.(P_i - X_i) & P_i \neq X_i \\ X_i + step.rand.(P_g - X_i) & P_i = X_i \end{cases} \tag{21}$$

where  $X_i$  denotes the cockroach position,  $step$  denotes a constant value,  $rand$  denotes a random number between 0 and 1,  $P_i$  denotes an individual’s best position, and  $P_g$  denotes the global optimum position. Consider:

$$P_i = Opt_j\{X_j, |X_i - X| \leq v\} \tag{22}$$

where the perception distance,  $v$  is constant,  $j = 1, 2, \dots, N$  and  $i = 1, 2, \dots, N$ . Consider:

$$P_g = Opt_i\{X_i\} \tag{23}$$

(2) *Dispersion Behavior:*

$$X_i = X_i + rand(1, D) \tag{24}$$

where the random vector  $rand(1, D)$  has  $D$  dimensions.

(3) *Ruthless Behavior:*

$$X_k = P_g \tag{25}$$

where  $k$  is a random non-zero integer between  $[1, N]$ .

In this paper, we introduce the CSO into the DSM control strategy to manage power consumption. As a result of this algorithm, the axis along which energy is used is shifted. Electricity consumption is shown vertically, with time displayed horizontally. This method determines the least expensive energy consumption pattern given user-specified maximum energy consumption and maximum time slots. The principal steps for using the proposed optimal DSM program based on CSO are outlined in Algorithm 3 as:

---

**Algorithm 3 CSOA Steps**

---

*Step 1:* Indicators of input data that must be defined at the outset of the program include the utility’s ToU price, the daily demand profile, and the unscheduled load timing.

*Step 2:* Set all parameters to their default values and initialize the cockroach swarm using uniformly distributed random numbers.

*Step 3:* Use Equations (22) and (23) to determine  $P_i$  and  $P_g$ , respectively.

*Step 4:* Use Equations (21), (24), and (25), to carry out chase swarming, dispersion behavior, and ruthless behavior, respectively.

*Step 5:* Loop until a predetermined condition is met.

---

**8. Performance Results**

The adopted algorithm-based system was developed and tested using MATLAB software (R2021b). The simulation program was executed on a laptop computer with an extendable 2.30 GHz processor and 32.00 GB RAM. The program is executed with control parameters of each adopted algorithm, which are illustrated in Table 3. These parameters are set in the following manner: some algorithms (such as SSA and CSO) cannot be stable before 500 iterations (a stable operation means the results are exactly the same at any time of running the code). The maximum intended shift time for every shiftable appliance is 4 h, and this parameter can be adjusted based on the appliance’s maximum desired shift time. The maximum energy consumption parameter can be set



to reflect the maximum intended energy consumption of the residential building. The maximum energy consumption for appliances is set at 100 kW. Lastly, the algorithm finds the optimal load pattern by rescheduling shiftable loads within a 4 h window and lowering peak consumption to less than the maximum desired value (100 kW), all based on the user’s preferences as set in the algorithm parameters. Figure 5 illustrates the ToU pricing pattern that was been adopted.

Table 3. CSO, SSA, and BOSA control parameters.

Populations Size	Maximum Iterations	Maximum Limit Allow	Max. Shift Time Slot
30	1000	100	4

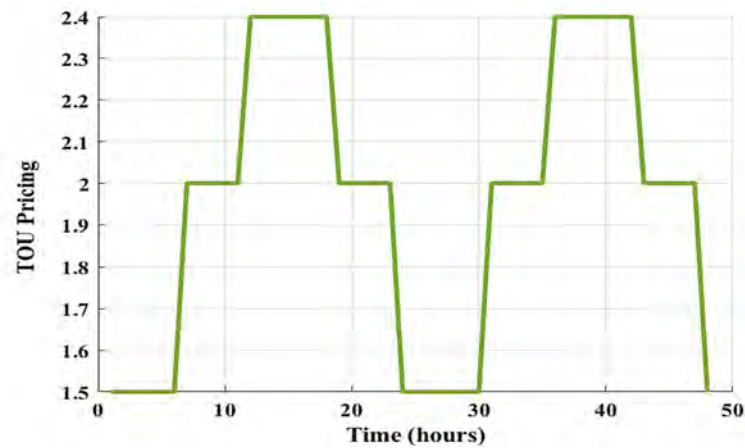
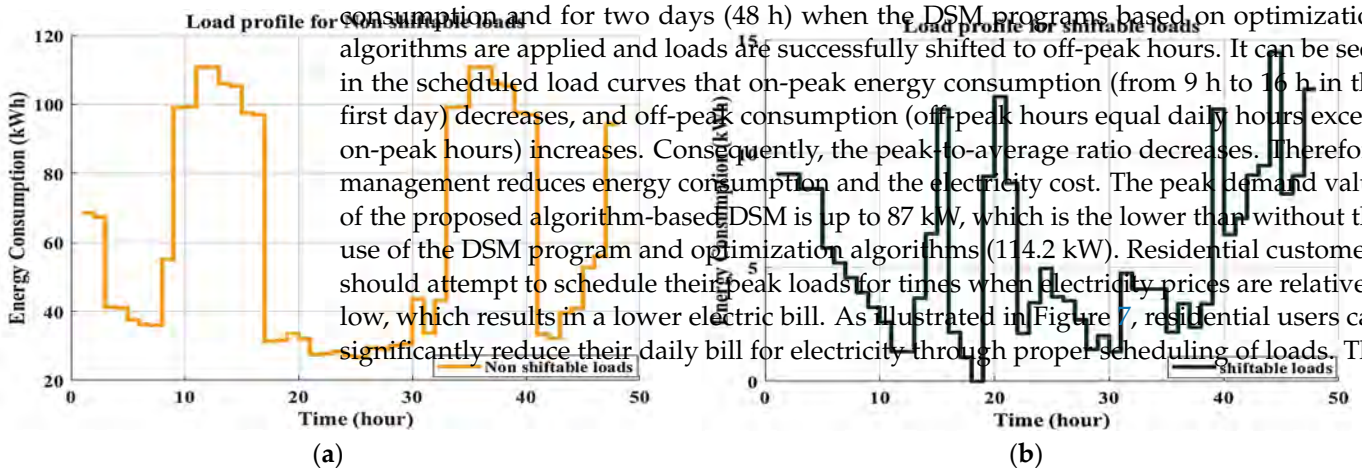


Figure 5. The adopted ToU signal.

The non-shiftable load profile mainly is based on the load data (Table 1) and is shown in Figure 6a. The only curve of shiftable loads is presented in Figure 6b. Figure 6c depicts the total load profile, which includes both shiftable and non-shiftable loads. The adopted virtual load data were assumed to be approximately simulated domestic actual load statistics in houses and residential structures. Therefore, they can be installed in homes or residential buildings. When the load data are input into an optimization method, a change is made to the time slot of the unschedulable shiftable load profile. To minimize the energy demand, RAR, and electricity cost, the proposed optimal DSM program only manipulates the non-scheduling shiftable load curve based on the maximum energy consumption and time shift hours according to Table 3. With this change, various appliances may be scheduled to run during off-peak hours rather than during peak hours, resulting in lower energy use. As the time intervals (horizon axis) shift, the magnitude of energy consumption is also altered, as peak consumption is shortened and peak-to-average energy is lowered.

Figure 7 illustrates the simulation results for the adopted residential area energy consumption, and for two days (48 h) when the DSM programs based on optimization algorithms are applied and loads are successfully shifted to off-peak hours. It can be seen in the scheduled load curves that on-peak energy consumption (from 9 h to 16 h in the first day) decreases, and off-peak consumption (off-peak hours equal daily hours except on-peak hours) increases. Consequently, the peak-to-average ratio decreases. Therefore, management reduces energy consumption and the electricity cost. The peak demand value of the proposed algorithm-based DSM is up to 87 kW, which is the lower than without the use of the DSM program and optimization algorithms (114.2 kW). Residential customers should attempt to schedule their peak loads for times when electricity prices are relatively low, which results in a lower electric bill. As illustrated in Figure 7, residential users can significantly reduce their daily bill for electricity through proper scheduling of loads. The



The non-shiftable load profile on an hourly basis based on the load data (Tables 1 and 2) is shown in Figure 6a. The hourly curve of shiftable loads is presented in Figure 6b. Figure 6c depicts the total load profile, which includes both shiftable and non-shiftable loads. The adopted virtual load data were assumed to be approximately simulated domestic actual load statistics in houses and residential structures. Therefore, they can be installed in homes or residential buildings. When the load data are input into an optimization method, a change is made to the time slot of the unschedulable shiftable load profile. The algorithm achieves very similar energy consumption and cost-saving results (all up to 16.3% savings). The peak demand is decreased below the maximum predetermined energy consumption limit in the scheduled curve, from 114.2 kW to 87 kW. In general, the DSM technique performs better as the number of controllable or shiftable appliances grows. The results prove that the proposed optimal DSM program effectively manages a number of residential loads in a residential area by shifting controllable loads in order to reduce peak energy consumption.

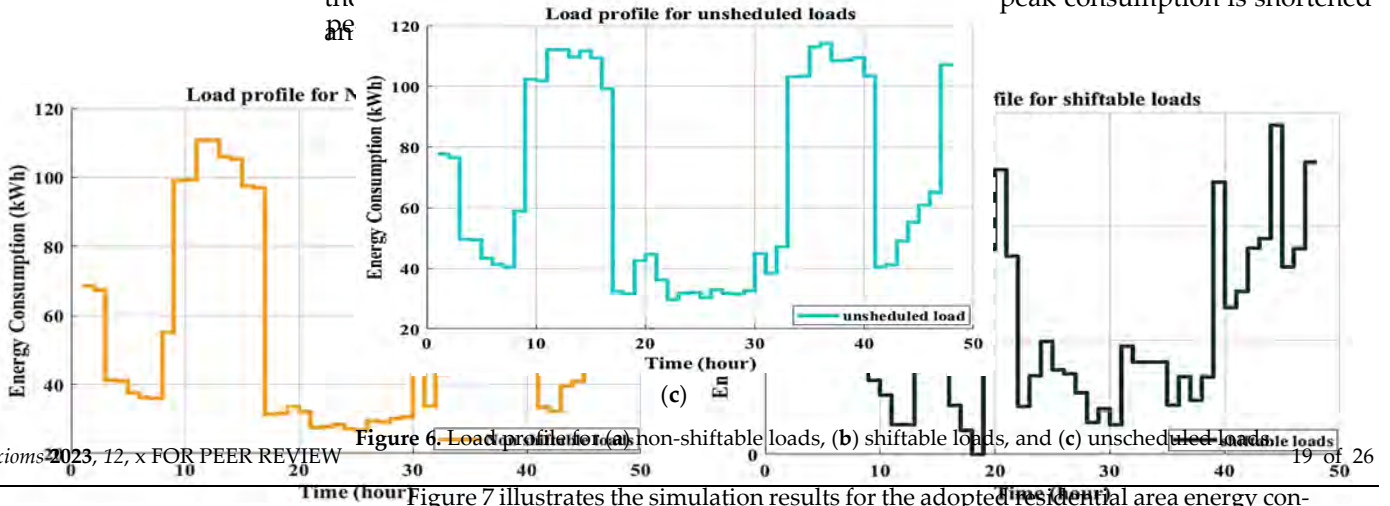
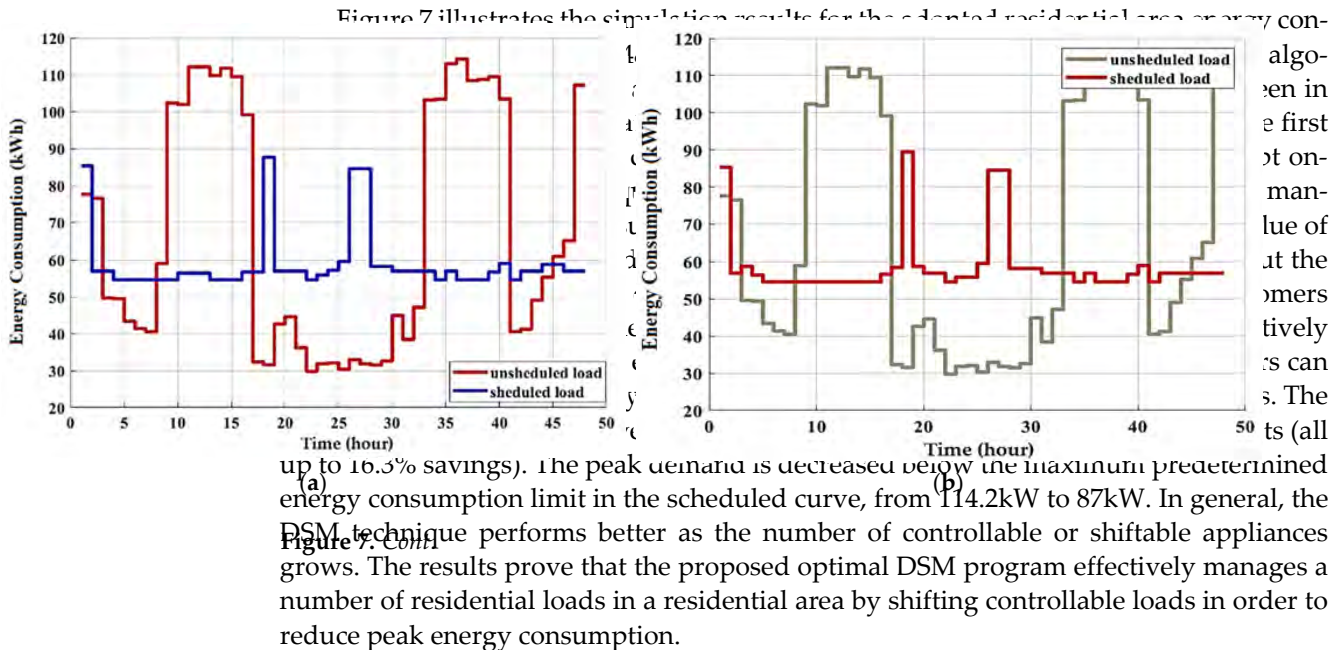


Figure 7 illustrates the simulation results for the adopted residential area energy consumption and for two days (48 h) when the DSM programs based on optimization algorithms are applied and loads are successfully shifted to off-peak hours. It can be seen in the scheduled load curves that on-peak energy consumption (from 9 h to 16 h in the first day) decreases, and off-peak consumption (off-peak hours equal daily hours except on-peak hours) increases. Consequently, the peak-to-average ratio decreases. Therefore, management reduces energy consumption and the electricity cost. The peak demand value of the proposed algorithm-based DSM is up to 87 kW, which is the lower than without the use of the DSM program and optimization algorithms (114.2 kW). Residential customers should attempt to schedule their peak loads for times when electricity prices are relatively low, which results in a lower electric bill. As illustrated in Figure 7, residential users can significantly reduce their daily bill for electricity through proper scheduling of loads. The adopted algorithms achieve very similar energy consumption and cost-saving results (all up to 16.3% savings). The peak demand is decreased below the maximum predetermined energy consumption limit in the scheduled curve, from 114.2 kW to 87 kW. In general, the DSM technique performs better as the number of controllable or shiftable appliances grows. The results prove that the proposed optimal DSM program effectively manages a number of residential loads in a residential area by shifting controllable loads in order to reduce peak energy consumption.



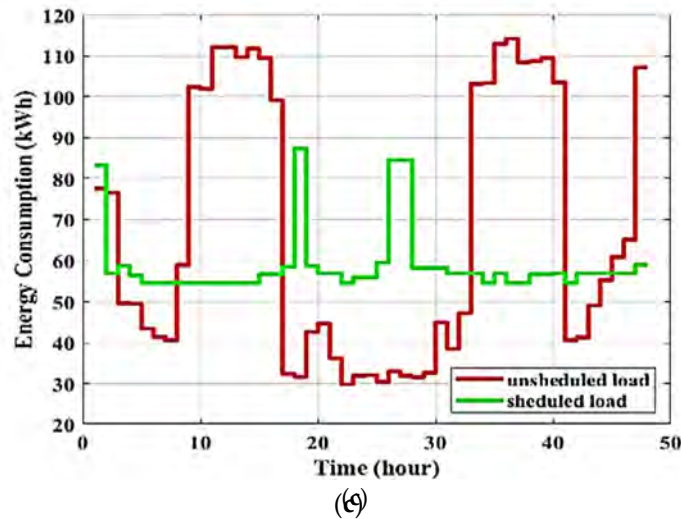


Figure 7. Unsheduled and sheduled loads using (a) BOSA (b) SSA, and (c) CSO.

Figure 8 illustrates the amount of power generated by the MG and the grid, the amount of power consumed by loads, and the costs associated with the grid. Figure 8a, c, e, g, assume that the MG supply power is set to 0%, 50%, 100%, and 150% of the total power consumed by the loads, respectively. Their costs are represented graphically in Figure 8b, d, f, h, respectively. As shown in Figure 8a, there is no MG power and all loads are supplied by the utility grid. In this case, the MG power is 0% of the total power, and the grid supplies the total power. In Figure 8b, the MG power is 50% of the total power, and the grid supplies the remaining 50%. In Figure 8c, the MG power is 100% of the total power, and the grid supplies the remaining 0%. In Figure 8d, the MG power is 150% of the total power, and the grid supplies the remaining -50%. Therefore, the grid supplies the deficit and its cost is shown in Figure 8e. There is no power supply deficit. Therefore, the utility grid supplies this deficit, and its cost is shown in Figure 8f. There is no power supply shortage in Figure 8g because the MG power is equal to the consumption power. Consequently, the total energy demand is met by MG resources. As the resource only in the final case shown in Figure 8h, no power is purchased from the utility grid. In the adopted MG, the utility grid, as the MG power is been expanded by 25% of the total consumption power. In the final case shown in Figure 8g, h, no power is purchased, but power is sold from the adopted MG to the utility grid, as the MG power is been expanded by 25% of the total consumption power.

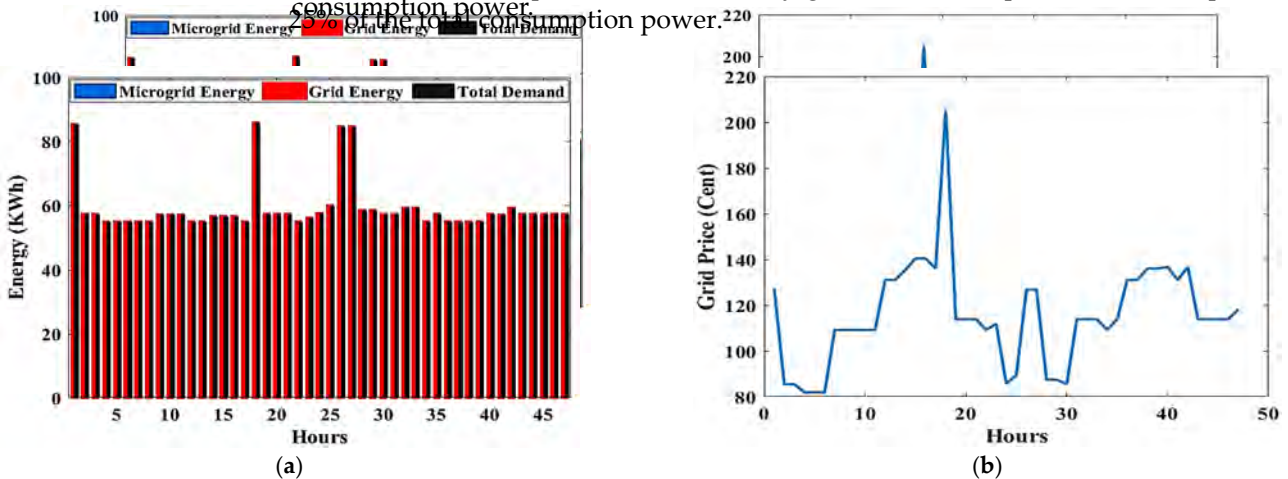
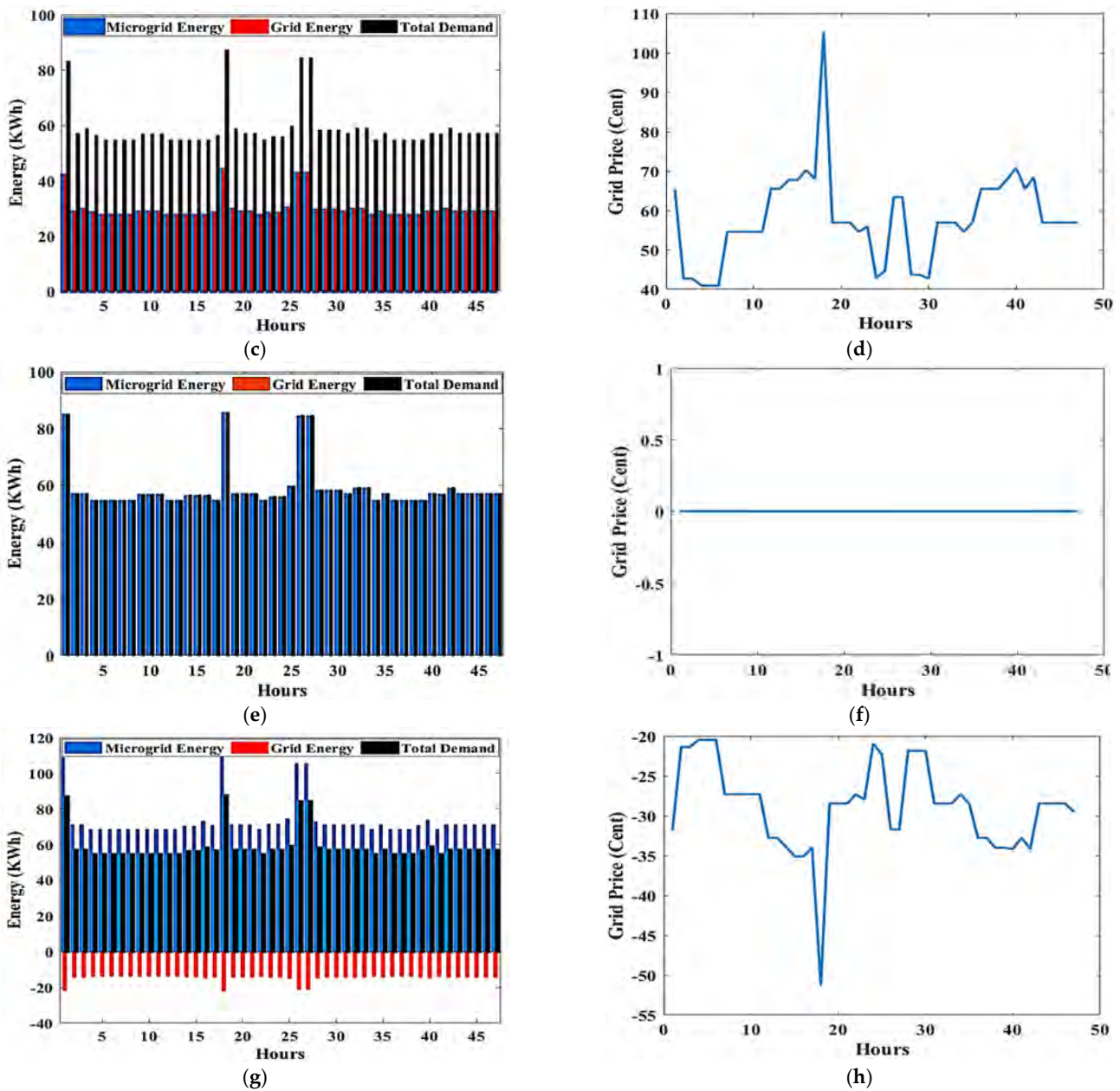


Figure 8. Cont.



**Figure 8.** The amount of power generated by the MG and the grid, the amount of power consumed by loads, and the grid costs with the MG supply power set to 0 (a,b), 0.5 (c,d), 1 (e,f), and 1.25 (g,h) from the total power consumed.

Figure 9 demonstrates the peak energy consumption and total electricity cost for both unscheduled and scheduled load profiles, illustrating the outcomes of the adopted algorithms, as well as GA, which is a commonly used algorithm in research studies. It can be observed that all algorithms yield similar results. The unscheduled peak energy consumption and cost are showcased as 114.2 kWh and 650.5 cents of USD, as indicated by black bars. With the proposed DSM, peak consumption energy is reduced to around 87 kWh by all algorithms, except for the BSOA (red bar), which can produce peak consumption of up to 85.8 kWh. The scheduled electricity costs are reduced to 5438 cents of USD. Figure 10 shows the peak amount of energy used and the total cost of electricity for both unscheduled and scheduled load profiles displayed on the ThingSpeak platform using the Energy Internet. As can be seen, the unscheduled peak energy consumption and cost are 114.2 kWh and 650.5 cents, respectively. After applying the proposed optimal DSM, the consumption energy drops to about 87 kWh, whereas the electricity costs drop to 5438

peak of consumption energy drops to about 87 kWh, whereas the electricity costs drop to 5438 cents of USD. The results indicate that the optimal DSM can properly address

the shiftable load in the presence or absence of EL. The convergence rates of the adopted algorithms are shown in Figure 11. The y-axis displays the value of the fitness versus time, whereas the x-axis depicts the iteration number. It is evident that the BSOA converges to the lowest cost compared to the other algorithms (up to 5438 cents of USD). In order to evaluate the robustness of the algorithms, a total of 20 independent runs were performed for each algorithm. Figure 12 demonstrates the mean of peak demand and the standard deviation for a total of 20 runs. As can be seen, the mean value of the CSO is the lowest (890.1 using a CSO-based DSM and 14.2 without DSM) in comparison with the other algorithms. Because the BSOA can reduce the peak demand to its smallest amount with the other algorithms, the BSOA algorithm is helpful in reducing the peak demand of 85.6 kWh, which is 54.38 cents of electricity. In this regard, the results in peak demand of 85.6 kWh, a cost of 5438.98 cents of USD, and 10.2% saving. Figure 13 illustrates the required computation time for each optimization algorithm. The elapsed time (ET) is computed based on the parameters of each algorithm, as shown in Table 3. It is clear that the BSOA and GA are superior in terms of computation time because they have shorter elapsed times (ET = 27.71 s for the BSOA and ET = 30.22 s for the GA). Finally, it can be stated that the BSOA is superior to the other algorithms in terms of peak energy demand reduction, cost minimization, robustness, and speed of computation. Finally, it can be stated that the BSOA is superior to the other algorithms in terms of peak energy demand reduction, cost minimization, robustness, and speed of computation.

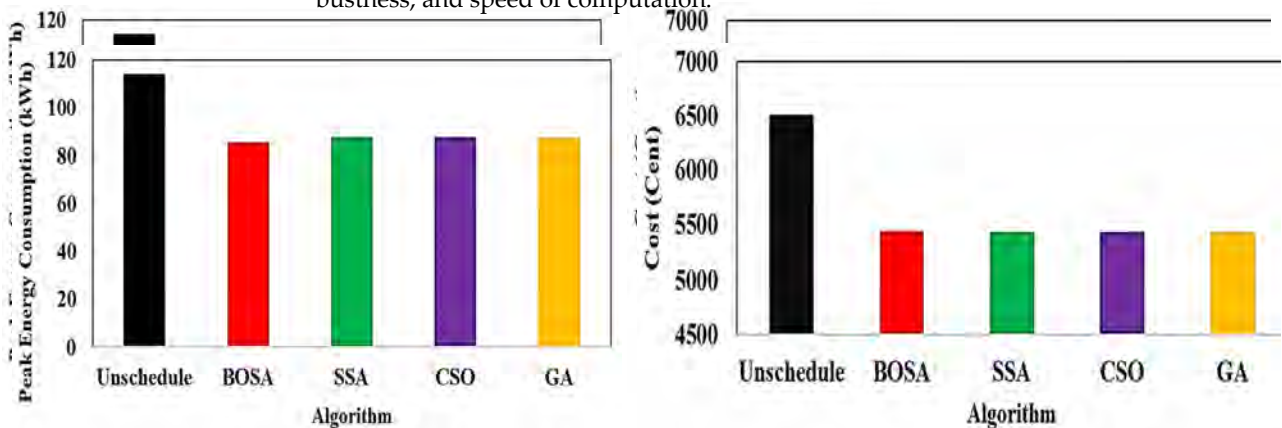


Figure 9. (a) Peak energy consumption and (b) electricity costs for both the unscheduled and scheduled load profiles. Figure 9. (a) Peak energy consumption and (b) electricity costs for both the unscheduled and scheduled load profiles.

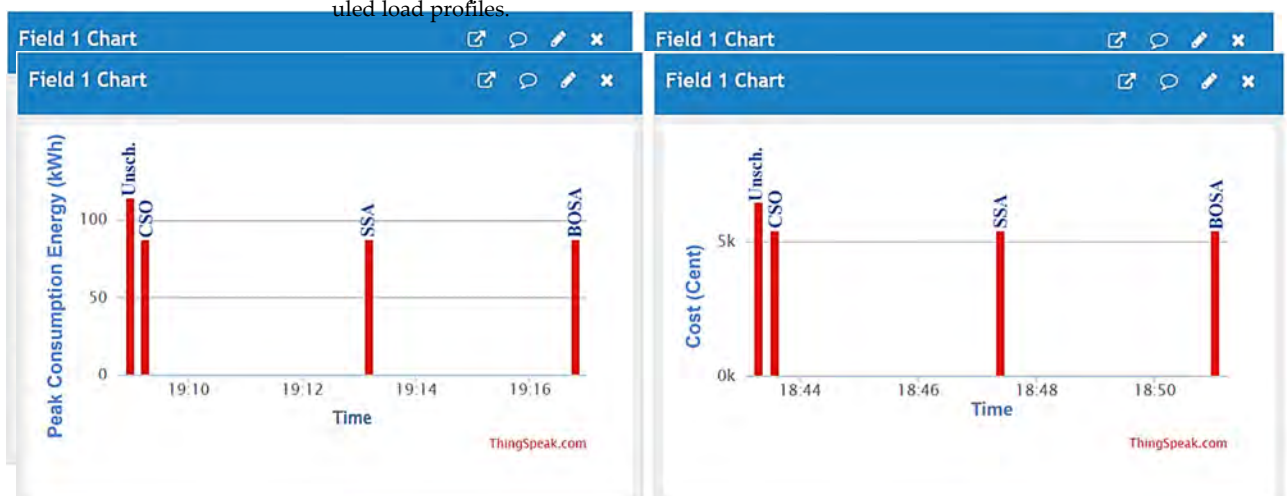


Figure 10. (a) Peak energy consumption and (b) electricity costs for both the unscheduled and scheduled load profiles displayed via ThingSpeak platform. Figure 10. (a) Peak energy consumption and (b) electricity costs for both the unscheduled and scheduled load profiles displayed via ThingSpeak platform.

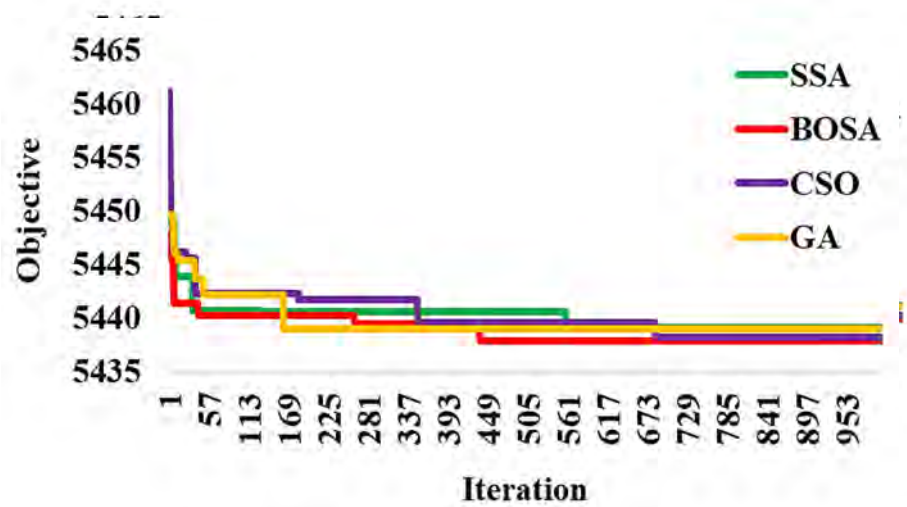


Figure 11. Convergence curves for BOSA, SSA, CSOA, and GA.  
Figure 11. Convergence curves for BOSA, SSA, CSOA, and GA.

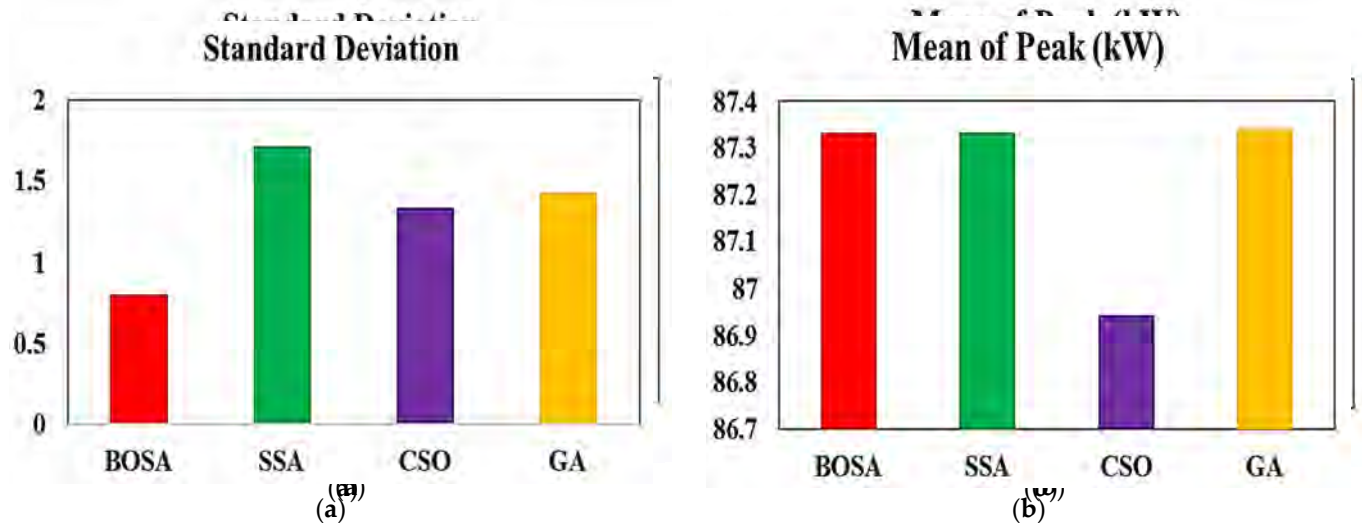


Figure 12. Standard deviation (a) and mean of peak values (b) using BOSA, SSA, CSO, and GA.  
Figure 12. Standard deviation (a) and mean of peak values (b) using BOSA, SSA, CSO, and GA.

Computation Time Chart of Optimization Algorithms



Figure 13. Elapsed times of the optimization algorithms in seconds.  
Figure 13. Elapsed times of the optimization algorithms in seconds.

## 9. Conclusions

DSM plays a crucial role in ensuring that electricity supply and demand are in balance. DSM aids in the maintenance of a reliable power system and the reduction in both electricity costs and PAR. In this study, we developed MATLAB-based optimization algorithms and an Energy Internet for residential users to reduce peak consumption of the load curve. This work has potential applications in the development of future SGs. Optimal DSM based on metaheuristic optimization algorithms was applied to a variety of residential controllable appliances. The proposed DSM program was optimized by recent optimizers of BOSA, SSA, and CSO using the load-shifting technique. The residential loads are primarily supplied by the SG's RERs, whereas the deficiency is compensated by the utility grid (grid is last priority). In addition, by using secure EI technology, the SG's energies are monitored properly. Total energy expenditures and peak energy consumption can be tracked in real time from anywhere. The proposed model indices, such as peak demand and electricity costs, ensure that the BOSA-based DSM outperforms other algorithms. Whereas the CSO algorithm has the smallest mean value of peak demand (86.61 kWh), the BOSA algorithm has the smallest deviation (i.e., standard deviation for BOSA = 0.8, SSA = 1.7 and CSO = 1.3), making it superior to the other algorithms in terms of electricity costs and savings (BOSA produced 5438.98 cent of USD cost (mean value) and 16.3% savings). Therefore, the BOSA technique is effective in lowering electricity bills and power consumption. Moreover, the results of the proposed approaches were compared to GA results. The GA produces nearly identical results to SSA and CSO in terms of mean peak demand and electricity cost, but the high standard deviation renders the GA inferior. In terms of computation time, the BOSA and GA are superior, owing to their shorter elapsed times (ET = 27.71 and 30.21 s, respectively).

The proposed system has one limitation: it is only applied to controllable appliances in order to minimize energy consumption using an optimal load-shifting DSM technique. It cannot reduce the amount of electricity used by manipulating non-controllable appliances with an optimal peak-clipping technique and operating non-shiftable appliances according to the priority of each appliance. In this paper, we propose recommendations for future research, including, in addition to the load-shift technique, the use of an optimal peak-clipping DSM program and running each appliance according to its priority in order to more efficiently cut power consumption.

**Author Contributions:** A.M.J.: original draft, software, methodology, and validation; B.H.J.: supervision, formal analysis, research resources, investigation, editing, and writing; B.H.J.: validation; B.-C.N.: visualization, project administration, funding acquisition; B.N.A.: editing, validation, and visualization. All authors have read and agreed to the published version of the manuscript.

**Funding:** This research was funded by “Gheorghe Asachi” Technical University of Iasi, Romania.

**Data Availability Statement:** Not applicable.

**Conflicts of Interest:** The authors declare no conflict of interest.

## References

1. Jasim, A.M.; Jasim, B.H.; Bureš, V. A novel grid-connected microgrid energy management system with optimal sizing using hybrid grey wolf and cuckoo search optimization algorithm. *Front. Energy Res.* **2022**, *10*, 960141. [[CrossRef](#)]
2. Álvaro, G. Optimization Trends in Demand-Side Management. *Energies* **2022**, *15*, 5961. [[CrossRef](#)]
3. Jasim, A.M.; Jasim, B.H.; Bureš, V.; Mikulecký, P. A New Decentralized Robust Secondary Control for Smart Islanded Microgrids. *Sensors* **2022**, *22*, 8709. [[CrossRef](#)] [[PubMed](#)]
4. Alhasnawi, B.N.; Jasim, B.H.; Esteban, M.D.; Guerrero, J.M. A Novel Smart Energy Management as a Service over a Cloud Computing Platform for Nanogrid Appliances. *Sustainability* **2020**, *12*, 9686. [[CrossRef](#)]
5. Alhasnawi, B.N.; Jasim, B.H.; Sedhom, B.E.; Hossain, E.; Guerrero, J.M. A New Decentralized Control Strategy of Microgrids in the Internet of Energy Paradigm. *Energies* **2021**, *14*, 2183. [[CrossRef](#)]
6. Ali, M.; Basil, H. Grid-Forming and Grid-Following Based Microgrid Inverters Control. *Iraqi J. Electr. Electron. Eng.* **2022**, *18*, 111–131.

7. Alhasnawi, B.N.; Jasim, B.H.; Siano, P.; Guerrero, J.M. A Novel Real-Time Electricity Scheduling for Home Energy Management System Using the Internet of Energy. *Energies* **2021**, *14*, 3191. [\[CrossRef\]](#)
8. Alhasnawi, B.N.; Jasim, B.H.; Rahman, Z.-A.S.A.; Guerrero, J.M.; Esteban, M.D. A Novel Internet of Energy Based Optimal Multi-Agent Control Scheme for Microgrid including Renewable Energy Resources. *Int. J. Environ. Res. Public Health* **2021**, *18*, 8146. [\[CrossRef\]](#)
9. Yan, Y.; Qian, Y.; Sharif, H.; Tipper, D. A survey on smart grid communication infrastructures: Motivations, requirements and challenges. *Communications Surveys Tutorials. IEEE* **2013**, *15*, 5–20.
10. Ma, R.; Chen, H.-H.; Huang, Y.-R.; Meng, W. Smart grid communication: Its challenges and opportunities. *Smart Grid. IEEE Trans.* **2013**, *4*, 36–46.
11. Jasim, A.M.; Jasim, B.H.; Neagu, B.-C. A New Decentralized PQ Control for Parallel Inverters in Grid-Tied Microgrids Propelled by SMC-Based Buck–Boost Converters. *Electronics* **2022**, *11*, 3917. [\[CrossRef\]](#)
12. Logenthiran, T.; Srinivasan, D.; Shun, T. Demand Side Management in Smart Grid using Heuristic Optimization. *IEEE Trans. Smart Grid* **2012**, *3*, 1244–1252. [\[CrossRef\]](#)
13. Yao, L.; Chang, W.-C.; Yen, R.-L. An iterative deepening genetic algorithm for scheduling of direct load control. *IEEE Trans. Power Syst.* **2005**, *20*, 1414–1421. [\[CrossRef\]](#)
14. Awais, M.; Javaid, N.; Shaheen, N.; Iqbal, Z.; Rehman, G.; Muhammad, K.; Ahmad, I. An Efficient Genetic Algorithm Based Demand Side Management Scheme for Smart Grid. In Proceedings of the 18th International Conference on Network-Based Information Systems (NBIS-2015), Taipei, Taiwan, 2–4 September 2015; IEEE: Washington, DC, USA, 2015. [\[CrossRef\]](#)
15. Jasim, A.M.; Jasim, B.H.; Kraiem, H.; Flah, A. A Multi-Objective Demand/Generation Scheduling Model-Based Microgrid Energy Management System. *Sustainability* **2022**, *14*, 10158. [\[CrossRef\]](#)
16. Usman, R.; Mirzania, P.; Alnaser, S.W.; Hart, P.; Long, C. Systematic Review of Demand-Side Management Strategies in Power Systems of Developed and Developing Countries. *Energies* **2022**, *15*, 7858. [\[CrossRef\]](#)
17. Jasim, A.M.; Jasim, B.H.; Mohseni, S.; Brent, A.C. Consensus-Based Dispatch Optimization of a Microgrid Considering Meta-Heuristic-Based Demand Response Scheduling and Network Packet Loss Characterization. *Energy AI* **2022**, *11*, 100212. [\[CrossRef\]](#)
18. Khan, A.R.; Mahmood, A.; Safdar, A.; Khan, Z.A.; Khan, N.A. Load forecasting, dynamic pricing and DSM in smart grid: A review. *Renew. Sustain. Energy Rev.* **2016**, *54*, 1311–1322.
19. Graditi, G.; Ippolito, M.; Telaretti, E.; Zizzo, G. Technical and economical assessment of distributed electrochemical storages for load shifting applications: An Italian case study. *Renew. Sustain. Energy Rev.* **2016**, *57*, 515–523. [\[CrossRef\]](#)
20. Flaim, T.; Levy, R.; Goldman, C. *Dynamic Pricing in a Smart Grid World*; NARUC: Washington, DC, USA, 2010.
21. Yaagoubi, N.; Mouftah, H. User-aware game theoretic approach for demand management. *IEEE Trans. Smart Grid* **2015**, *6*, 716–725. [\[CrossRef\]](#)
22. Zhang, D.; Li, S.; Sun, M.; O'Neill, Z. An optimal and learning based demand response and home energy management system. *IEEE Trans. Smart Grid* **2016**, *7*, 1790–1801. [\[CrossRef\]](#)
23. Song, L.; Xiao, Y.; van der Schaar, M. Demand side management in smart grids using a repeated game framework. *IEEE J. Sel. Areas Commun.* **2014**, *32*, 1412–1424. [\[CrossRef\]](#)
24. Costanzo, G.T.; Zhu, G.; Anjos, M.F.; Savard, G. A System Architecture for Autonomous Demand Side Load Management in Smart Buildings. *IEEE Trans. Smart Grid* **2012**, *3*, 2157–2165. [\[CrossRef\]](#)
25. Zhu, Z.; Tang, J.; Lambbotharan, S.; Chin, W.H.; Fan, Z. An Integer Linear Programming Based Optimization for Home Demand-Side Management in Smart Grid. In Proceedings of the IEEE PES Innovative Smart Grid Technologies (ISGT), Washington, DC, USA, 16–20 January 2012; pp. 1–5. [\[CrossRef\]](#)
26. Barth, L.; Ludwig, N.; Mengelkamp, E.; Staudt, P. A comprehensive modelling framework for demand side flexibility in smart grids. *Comput. Sci.—Res. Dev.* **2018**, *33*, 13–23. [\[CrossRef\]](#)
27. Kantarci, M.; Mouftah, H. Wireless Sensor Networks for Cost-Efficient Residential Energy Management in the Smart Grid". *IEEE Trans. Smart Grid* **2011**, *2*, 314–325. [\[CrossRef\]](#)
28. Agnetis, A.; de Pascale, G.; Detti, P.; Vicino, A. Load Scheduling for Household Energy Consumption Optimization. *IEEE Trans. Smart Grid* **2013**, *4*, 2364–2373. [\[CrossRef\]](#)
29. Samadi, P.; Wong, V.W.; Schober, R. Load scheduling and power trading in systems with high penetration of renewable energy resources. *IEEE Trans. Smart Grid* **2015**, *7*, 1802–1812. [\[CrossRef\]](#)
30. Ma, K.; Yao, T.; Yang, J.; Guan, X. Residential power scheduling for demand response in smart grid. *Int. J. Electric. Power Energy Syst.* **2016**, *78*, 320–325. [\[CrossRef\]](#)
31. Javaid, N.; Ullah, I.; Akbar, M.; Iqbal, Z.; Khan, F.A.; Alrajeh, N.; Alabed, M.S. An Intelligent Load Management System With Renewable Energy Integration for Smart Homes. *IEEE Access* **2017**, *5*, 13587–13600. [\[CrossRef\]](#)
32. Wu, Y.; Lau, V.K.N.; Tsang, D.H.K.; Qian, L.P.; Meng, L. Optimal Energy Scheduling for Residential Smart Grid with Centralized Renewable Energy Source. *IEEE Syst. J.* **2014**, *8*, 562–576. [\[CrossRef\]](#)
33. Rahim, S.; Javaid, N.; Ahmed, A.; Shahid, A.K.; Zahoor, A.K.; Nabil, A.; Umar, Q. Exploiting heuristic algorithms to efficiently utilize energy management controllers with renewable energy sources. *Energy Build.* **2016**, *129*, 452–470. [\[CrossRef\]](#)
34. Ogunjuyigbe, A.S.O.; Ayodele, T.R.; Akinola, O.A. User satisfaction-induced demand side load management in residential buildings with user budget constraint. *Appl. Energy* **2017**, *187*, 352–366. [\[CrossRef\]](#)



35. Ma, J.; Chen, H.H.; Song, L.; Li, Y. Residential load scheduling in smart grid: A cost efficiency perspective. *IEEE Trans. Smart Grid* **2016**, *7*, 771–784. [[CrossRef](#)]
36. Li, C.; Yu, X.; Yu, W.; Chen, G.; Wang, J. Efficient computation for sparse load shifting in demand side management. *IEEE Trans. Smart Grid* **2017**, *8*, 250–261. [[CrossRef](#)]
37. Shengan, S.; Manisa, P.; Saifur, R. Demand Response as a Load Shaping Tool in an Intelligent Grid With Electric Vehicles. *IEEE Trans. Smart Grid* **2011**, *2*, 624–631.
38. Yi, P.; Dong, X.; Iwayemi, A.; Zhou, C.; Li, S. Real-time Opportunistic Scheduling for Residential Demand Response. *IEEE Trans. Smart Grid* **2013**, *4*, 227–234.
39. Guo, Y.; Pan, M.; Fang, Y. Optimal Power Management of Residential Customers in the Smart Grid. *IEEE Trans. Parallel Distrib. Syst.* **2012**, *23*, 1593–1606. [[CrossRef](#)]
40. Yang, P.; Chavali, P.; Gilboa, E.; Nehorai, A. Parallel Load Schedule Optimization with Renewable Distributed Generators in Smart Grids. *IEEE Trans. Smart Grid* **2013**, *4*, 1431–1441. [[CrossRef](#)]
41. Alhasnawi, B.N.; Jasim, B.H.; Rahman, Z.-A.S.A.; Siano, P. A Novel Robust Smart Energy Management and Demand Reduction for Smart Homes Based on Internet of Energy. *Sensors* **2021**, *21*, 4756. [[CrossRef](#)]
42. Kinhekar, N.; Padhy, N.P.; Furong, L.; Gupta, H.O. Utility oriented demand side management using smart AC and micro DC grid cooperative. *IEEE Trans. Power Syst.* **2015**, *31*, 1151–1160. [[CrossRef](#)]
43. Babu, N.R.; Vijay, S.; Saha, D.; Saikia, L.C. Scheduling of Residential Appliances Using DSM with Energy Storage in Smart Grid Environment. In Proceedings of the 2nd ICEPE, Shillong, India, 1–2 June 2018; pp. 1–6.
44. Hasmat, M.; Smriti, S.; Yog, R.S.; Aamir, A. Applications of Artificial Intelligence Techniques in Engineering. *Springer Nat.* **2018**, *1*, 643. [[CrossRef](#)]
45. Srivastava, S.; Malik, H.; Sharma, R. Special issue on intelligent tools and techniques for signals, machines and automation. *J. Intell. Fuzzy Syst.* **2018**, *35*, 4895–4899. [[CrossRef](#)]
46. Waseem, M.; Lin, Z.; Liu, S.; Sajjad, I.A.; Aziz, T. Optimal GWCSO-based home appliances scheduling for demand response considering end-users comfort. *Electr. Power Syst. Res.* **2020**, *187*, 106477. [[CrossRef](#)]
47. Chang, H.-H.; Chiu, W.-Y.; Sun, H.; Chen, C.-M. User-centric multi-objective approach to privacy preservation and energy cost minimization in smart home. *IEEE Syst. J.* **2018**, *13*, 1030–1041.
48. Moon, S.; Lee, J. Multi-residential demand response scheduling with multi-class appliances in smart grid. *IEEE Trans. Smart Grid* **2016**, *9*, 2518–2528. [[CrossRef](#)]
49. Veras, J.M.; Silva, I.R.S.; Pinheiro, P.R.; Rabêlo, R.A.L.; Veloso, A.F.S.; Borges, F.A.S.; Rodrigues, J.J.P.C. A Multi-Objective Demand Response Optimization Model for Scheduling Loads in a Home Energy Management System. *Sensors* **2018**, *18*, 3207. [[CrossRef](#)]
50. Ayub, S.; Ayob, S.M.; Tan, C.W.; Ayub, L.; Bukar, A.L. Optimal residence energy management with time and device-based preferences using an enhanced binary grey wolf optimization algorithm. *Sustain. Energy Technol. Assess* **2020**, *41*, 100798. [[CrossRef](#)]
51. Albogamy, F.R.; Khan, S.A.; Hafeez, G.; Murawwat, S.; Khan, S.; Haider, S.I.; Basit, A.; Thoben, K.D. Real-Time Energy Management and Load Scheduling with Renewable Energy Integration in Smart Grid. *Sustainability* **2022**, *14*, 1792. [[CrossRef](#)]
52. Hafeez, G.; Alimgeer, K.S.; Wadud, Z.; Khan, I.; Usman, M.; Qazi, A.B.; Khan, F.A. An Innovative Optimization Strategy for Efficient Energy Management with Day-Ahead Demand Response Signal and Energy Consumption Forecasting in Smart Grid Using Artificial Neural Network. *IEEE Access* **2020**, *8*, 84415–84433. [[CrossRef](#)]
53. Philipo, G.H.; Kakande, J.N.; Krauter, S. Neural Network-Based Demand-Side Management in a Stand-Alone Solar PV-Battery Microgrid Using Load-Shifting and Peak-Clipping. *Energies* **2022**, *15*, 5215. [[CrossRef](#)]
54. Mohammad, D.; Zeinab, M.; Om, P.M.; Gaurav, D.; Vijay, K. BOSA: Binary Orientation Search Algorithm. *Int. J. Innov. Technol. Explor. Eng. (IJITEE)* **2019**, *9*, 5306–5310.
55. Ahmed, F.; Turki, M.A.; Hegazy, R.; Dalia, Y. Optimal energy management of micro-grid using sparrow search algorithm. *Energy Rep.* **2022**, *8*, 758–773. [[CrossRef](#)]
56. Ibidun, C.; Ademola, P. Binary Cockroach Swarm Optimization for Combinatorial Optimization Problem. *Algorithms* **2016**, *9*, 59. [[CrossRef](#)]
57. Xue, J.; Shen, B. A novel swarm intelligence optimization approach: Sparrow search algorithm. *Syst. Sci. Control Eng.* **2020**, *8*, 22–34. [[CrossRef](#)]
58. Chen, Z. Modified cockroach swarm optimization. *Energy Proc.* **2011**, *11*, 4–9.
59. Chen, Z.; Tang, H. Cockroach swarm optimization for vehicle routing problems. *Energy Procedia* **2011**, *13*, 30–35.
60. Cheng, L.; Wang, Z.; Yanhong, S.; Guo, A. Cockroach swarm optimization algorithm for TSP. *Adv. Eng* **2011**, *1*, 226–229. [[CrossRef](#)]
61. Joanna, K.; Marek, P. Cockroach Swarm Optimization Algorithm for Travel Planning. *Entropy* **2017**, *19*, 213.
62. ZhaoHui, C.; HaiYan, T. Cockroach swarm optimization. In Proceedings of the 2nd International Conference on Computer Engineering and Technology (ICCET '10), Chengdu, China, 16–18 April 2010; Volume 6, pp. 652–655.
63. Obagbuwa, I.; Adewumi, A. An Improved Cockroach Swarm Optimization. *Sci. World J.* **2014**, *2014*, 1–13. [[CrossRef](#)]

**Disclaimer/Publisher's Note:** The statements, opinions and data contained in all publications are solely those of the individual author(s) and contributor(s) and not of MDPI and/or the editor(s). MDPI and/or the editor(s) disclaim responsibility for any injury to people or property resulting from any ideas, methods, instructions or products referred to in the content.

Article

# An Advanced Decision Support Platform in Energy Management to Increase Energy Efficiency for Small and Medium Enterprises

Gheorghe Grigoraş \*  and Bogdan-Constantin Neagu 

Power Engineering Department, Gheorghe Asachi Technical University of Iasi, 700050 Iasi, Romania;  
bogdan.neagu@tuiasi.ro

\* Correspondence: ggrigor@tuiasi.ro

Received: 27 April 2020; Accepted: 15 May 2020; Published: 19 May 2020



**Abstract:** The paper presents a new vision on the energy consumption management in the case of the small and medium enterprises (SMEs), integrated into an advanced decision support platform, with technical and economic benefits on increasing the energy efficiency, with four modules for database management, profiling, forecasting, and production scheduling. Inside each module, artificial intelligence and data mining techniques were proposed to remove the uncertainties regarding the dynamic of technological flows. Thus, the data management module includes the data mining techniques, that extract the technical details on the energy consumption needed in the development of production scheduling strategies, the profiling module uses an original approach based on clustering techniques to determine the typical energy consumption profiles required in the optimal planning of the activities, the forecasting module contains a new approach based on an expert system to forecast the total energy consumption of the SMEs, and production scheduling module integrates a heuristic optimization method to obtain the optimal solutions in flattening the energy consumption profile. The testing was done for a small enterprise from Romania, belonging to the domain of trade and repair of vehicles. The obtained results highlighted the advantages of the proposed decision support platform on the decrease in the intensity of energy consumption per unit of product, reduction of the purchase costs, and modification of the impact for which energy bills have on the operational costs.

**Keywords:** energy management; energy efficiency; small and medium enterprises; artificial intelligence techniques; decision support platform

---

## 1. Introduction

Combating climate change is one of the five main themes of the Europe 2020 comprehensive strategy [1], adopted by the European Council in 2010, for smart, sustainable, and inclusive growth. The specific targets of the strategy consider that by 2020, greenhouse gas emissions to be reduced by 20%, 20% of electricity to be covered from renewable sources, and energy efficiency to be improved by 20%. However, the European Commission modified the targets set at the European Union (EU) level according to the document “Towards a Sustainable Europe by 2030” [2]. These targets refer to ensure at least 32% of the total energy consumption from renewable sources and energy efficiency of at least 32.5% in 2030, which will lead to exceeding the commitments made in within the framework of the Paris Agreement on climate change concerning to the reducing greenhouse gas emissions by at least 40% by 2030 compared to 1990 levels. If for the 2020 targets on greenhouse gas emissions and renewable energy, the EU is on track to achieve the target on the energy efficiency that may not be reached [3]. On 4 February 2020, Eurostat published a document [4] which stipulates that in 2018, the primary energy consumption in the EU was 4.9% above the efficiency target for 2020 and 22.0% away

away from the 2030 target, see Figure 1 adapted from [4]. It also highlights that since 1990, the primary energy consumption had a high variability between a maximum value recorded in 2006 with a gap of 15.2% from the 2020 target and a minimum value recorded in 2014 representing a difference of 4.9% from the 2020 target.



Figure 1: The primary energy consumption in the European Union (EU).

In December 2018, in the Official Journal of the European Union (L 328), three normative acts related to the “Clean Energy for All Europeans” legislative package, with effect on 24 December 2018, were published. EU Directive 2018/2002 on energy efficiency establishes a common framework for measures to promote energy efficiency throughout the Union, to ensure that its main objectives are reached at least 32.5% by 2030 and to pave the way for future efficiency gains energy after this date [5]. The European Energy Regulatory Authorities supports the small and medium enterprises (SMEs) to use energy efficiently, including through special schemes, in compliance with state aid regulations. The support schemes for SMEs were established, including, if they have entered into voluntary agreements, to cover the costs of an energy audit and the implementation of cost-effective recommendations made in the following energy audits [6]. The EU Directive 27/2012 on energy efficiency [7] represents the base through which the small and medium enterprises (SMEs) are encouraged to participate in the energy audit programs. However, the SMEs have no obligation to follow energy auditing programs, although Article 8 of this Directive stipulates that “the Member States must develop programs that encourage SMEs to undergo energy audits and to subsequently implement the recommendations from these audits”. Moreover, “the member States may establish aid schemes for SMEs, including where voluntary agreements have been concluded, to cover the costs of an energy audit and the recommendations of energy audits, the costs involved being high, if it is decided to implement the proposed measures” [7].

In this context, many industrial consumers become actively interested in the implementation of measures to reduce energy consumption because the energy efficiency is not only a tool to save money and resources but also a need for flexible adaptation to own needs.

Supporting SMEs and the promotion of energy efficiency measures are essential for economic progress because about 23 million European SMEs represent 98% of the total number of businesses. The majority of SMEs are microenterprises with less than 10 people, having an annual turnover of up to 2 million euros [8]. The share of SMEs with less than 250 persons is very high, approximately 99.79% [9].

see Table 1 and Figure 2 [9].

**Table 1.** Classification of small and medium enterprises (SMEs).  
**Table 1.** Classification of small and medium enterprises (SMEs).

SMEs' Type	SMEs' Type	Share (%)	Share (%)	Employees	Employees	Annual Turnover	
						Annual Turnover (mil. Euro)	Annual Turnover (mil. Euro)
Micro	Micro	92.13	92.13	0–9	0–10	<2	<2
	Micro	92.13	92.13	0–10	0–10	<2	<2
Small	Small	6.61	6.61	11–49	10–49	<10	<10
	Small	6.61	6.61	11–49	10–49	<10	<10
Medium	Medium	1.05	1.05	50–250	50–250	>50	>50
	Medium	1.05	1.05	50–250	50–250	>50	>50

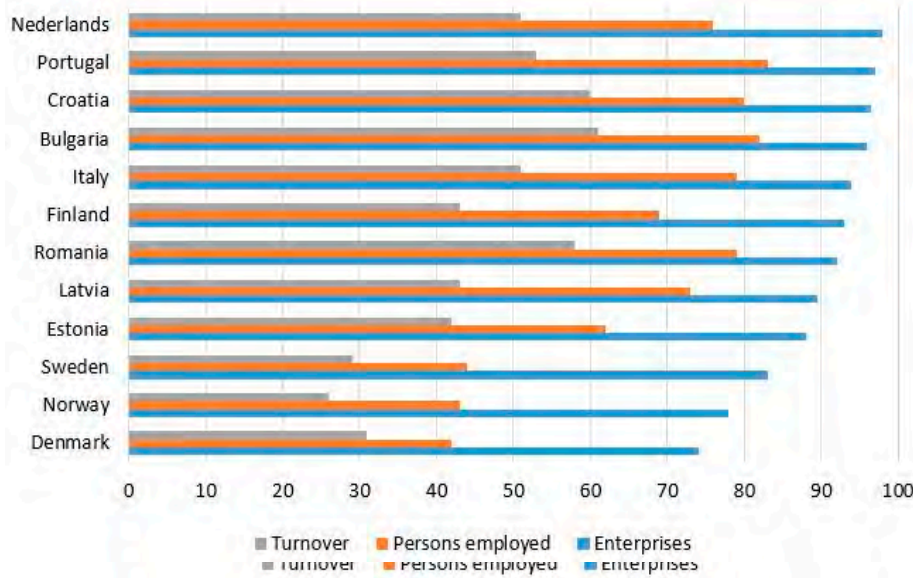


**Figure 2.** The number of SMEs, employees, and turnover, in 2015.  
**Figure 2.** The number of SMEs, employees, and turnover, in 2015.

Most activities of the SMEs are in the following fields: trade/repair of vehicles and motorcycles (32%), professional/scientific/technical (10%), transport and storage (10%), construction and manufacturing (10%), and others (38%), see Figure 3.

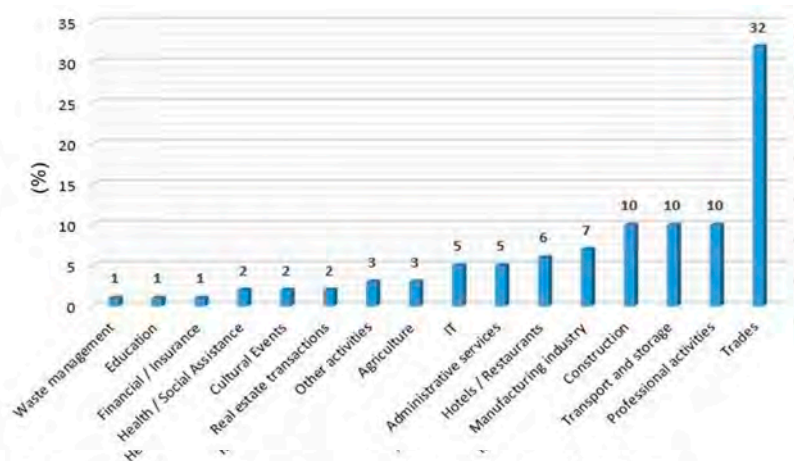


**Figure 3.** The share of SMEs according to the activity field.  
**Figure 3.** The share of SMEs according to the activity field.  
**Figure 3.** The share of SMEs according to the activity field.

In these conditions, SMEs represent one of the biggest potentials of energy saving, not fully exploited at present. The modern technologies available today, regarding the monitoring and control tools of energy consumption, have the potential to save at least 40% of energy consumption. The analyses have highlighted the significant energy savings, available at each point of the consumption chain if energy efficiency measures are implemented. Only one SME can save an amount of electricity equivalent to that of 1000 private houses [8]. In the case of investments, there are hidden costs whose share can be quite high for SMEs. Thus, for the large industrial consumers, energy efficiency measures can be quite high for SMEs. Thus, for the large industrial consumers, energy efficiency measures

share can be quite high for SMEs. Thus, for the large industrial consumers, energy efficiency measures require investments and resources. Their application could reduce the energy consumption with a certain percent, which is recovered with a very high probability because the energy bill is of thousands of euros. However, the allocation of financial resources is very difficult in the case of the SMEs due to the investments, which should lead to saving energy with a similar percent. Thus, the recovery must do from the benefits of energy saving, this being several hundred euros in most cases. In these conditions, more SMEs cannot allocate financial resources to purchase equipment or services [9,10].

Another aspect encountered in the case of many SMEs refers to the fact that there is not a relationship between the energy department, which takes care of the operation and maintenance of equipment and installations and the financial department, which pays the energy bills. In this case, there are no bonuses from the management staff to encourage the employees to save energy, this being a fixed component, without paying much attention, in the final cost of the final products, without the energy department to be responsible for it [11].

In addition, it is important to know whether SMEs are showing interest or make certain efforts to apply current management standards or moreover, how many of the SMEs seek to meet the requirements of an integrated management system. Most of the SMEs have implemented the following management systems: Quality Management System (ISO 9001), Environmental Management System (ISO 14001), and Health and Safety Management System (ISO OHSAS 18001) [12]. Regarding the Energy Management System ISO 50001 [13], published in 2018, it does not define the specific performance criteria associated with the SMEs' energy consumption and energy efficiency. Instead, a management model is proposed to influence the development and implementation of energy policy to achieve the targets and action plans, considering both legislation and information from the analysis and management of energy consumption. The standard describes the final target, but not how it can be achieved, and does not allow SMEs to understand clearly its position on the process to achieve this final target. Implementation of the ISO 50001 system alone is not enough for the SMEs, because it is necessary to follow the consumption indicators with the purpose of rational energy utilization, to fulfil the targets of the management system efficiency. Thus, the production planning based on an efficient energy use strategy, following ISO 50001, should consider monitoring the energy consumption and measures for increasing the energy efficiency.

In these conditions, SMEs have needed software products to monitor and control the consumption and to identify solutions that allow the adoption of measures to increase energy efficiency.

Thus, a decision support platform is proposed, having the modules with characteristics that differentiate it and offer more advantages compared to the other approaches which treated the energy management at the SMEs, whatever the industrial activity branch:

- (i) *The data management module* is based on the data mining technique that extracts the technical details on energy consumptions used to develop production scheduling strategies. It allows the analysis of large size databases regarding the daily, monthly, and yearly energy consumption or technical and operating characteristics for equipment and installations. In addition, it ensures the interface between the application modules, having a query that follows the correlation between energy consumption, economic indicators (the turnover, production value, personnel costs, and total purchases with goods and services), and costs.
- (ii) *The profiling module* integrates an original approach based on clustering techniques to determine the typical energy consumption profiles (TECPs) assigned to different activities necessary for establishing the type of tariffs that will lead to the reduction of energy bills and optimal planning of the activities.
- (iii) *The forecasting module* contains a new approach that uses an expert system based on the rules *If-Then* to forecast the energy consumption of each installation and equipment. The total energy consumption at the SME level is obtained through the aggregated process of all individual energy consumptions associated with each equipment and installation.

- (iv) *The production scheduling module* includes a novel approach based on the combinatorial optimization for daily consumption programming, which uses a fast searching algorithm to find the optimal solutions in the admissible set. The algorithm uses the status (on or off), type (programmable or non-programmable), working period, the number of operating cycles, and dependence (within the activities) of the equipment and installations as input data, determining the optimal solutions regarding the flattening of daily energy consumption profile with the benefits on the cost of energy bills.

The remainder of the paper is structured as follows. Section 2 presents a review on the treated topic highlighting the advantages of the proposed decision support platform. Section 3 details the characteristics of the developed decision support platform, highlighting the advantages of the proposed approaches inside of each module. The obtained results in testing of the platform at a small enterprise, from a representative field (the trade and repair of vehicles), are presented in Section 4. Section 5 highlights the conclusions and future works.

## 2. Literature Review

The various approaches were developed by companies in software applications for the management and analysis of energy consumption.

The software application developed in [14] allows the management, analysis, and control of energy consumption. Some disadvantages can be highlighted: an optimal consumption programming module according to the equipment and installations for an analysis contour is not developed, the forecasting module is missing, and the application domain is only for the large industrial consumers. The software tool developed in [15] allows, also, the management of energy consumption at large industrial consumers, without the forecasting and optimal production scheduling modules. The software product [16] has implemented energy consumption control and forecasting modules. The disadvantage refers to the fact that it only does short-term forecasting of the consumption, without considering the medium- or long-term forecasting. The software solution presented in [17] allows the acquisition, monitoring, management, and analysis of all types of consumption. The data analysis is presented for different consumption points, in tabular form, graphical representations, or brief reports, respectively maps. The disadvantages refer to the lack of energy consumption forecasting and the optimal scheduling modules. The solution identified in [18] envisages a software tool that allows management based on the energy balances for industrial consumers. The measures with major investments are proposed, without a deeper analysis of energy consumption, forecasting, and production scheduling. A management solution, which considers the analysis and control of the energy consumptions, is developed in [19], but with a lack of the consumption forecasting and production scheduling modules to obtain a streamline of the technological process and reducing the costs at the energy bills.

In addition, there are the patented approaches and systems for energy management. An energy management system applied to the large industrial consumers, which offers a complete knowledge of the energy consumption corresponding to their installations, is presented in the reference [20]. The system consists of two modules to analyse energy consumption and communicate with data acquisition points. However, it does not include energy efficiency modules based on energy consumption forecasting and production scheduling. Another system is developed in [21] to schedule the equipment to work at certain time intervals when the energy tariff is low. The energy storage system uses batteries and alternative energy sources that work to sell electricity to the distribution network operator during certain periods in favourable cost conditions. However, this system refers strictly to residential consumers and office buildings that have available renewable sources and storage units.

In addition, regarding software tools based on the statistical processing of input data and classical forecasting and optimization methods, there are researches carried out within European projects to propose new innovative approaches and methodologies. The main targets are to develop decision-making strategies to fulfil European goals regarding energy efficiency. The project “A holistic framework for supporting SMEs in increasing energy efficiency—SMEmPower Efficiency” [22]

focuses on increasing the energy savings in SMEs, being involved in eight countries from the main geographical regions of Europe: West (Spain), Central (Germany), South (Italy), North (Great Britain), and Eastern and Southern Europe (Romania, Slovenia, Greece, and Cyprus). The project supposes the development of the tools referring to a web platform for energy analysis, a tool for monitoring, and an instrument for measurement and verification. The SME Program for Energy Efficiency through Delivery and Implementation of the Energy Audits (SPEEDIER) program, a European project in the H2020 framework program, was officially launched on June 18 and 19, 2019. The project aims to address the obstacles encountered by SMEs in terms of expertise and resources when conducting energy audits and implementing recommended energy-saving measures [23].

In addition to research in projects, patents, and decision-making software products, there are also approaches published in journals and conferences that offer solutions for increasing energy efficiency at the SMEs. A comprehensive presentation on energy management for SMEs based on automatic meter reading (AMR) systems and an energy manager, which applies the energy efficiency recommendations, is done in [24]. The paper considers that the AMR system is not available to SMEs and the classical meters are read only annually or quarterly. The authors consider in [25] that a rational decision-making process (DMP) based on a databases management (DBM) is imperative for a real application of energy efficiency measures, which should also consider a schedule and optimization steps (SOS). Two typical load profiles for SME energy demand are found in [26] using a Smart Meter database, one for operation process, which includes the peak load, and other for the inactivity time. The two forecasted load profiles are improved using a Gaussian mixture technique. The E-learning platform presented in [27] contains practical tools for energy efficiency improvement on the SMEs' level.

On the other hand, some studies propose various approaches to minimize energy consumption. Some studies consider that a successful key for energy efficiency programs is the outreach of all SMEs personal: staff, employees, customers, guests [28], or energy audits [29,30]. However, the optimization of the operating parameters represents a no-cost strategy which can be implemented by SMEs to achieve real energy efficiency [31,32]. The various barriers encountered in increasing the SMEs' energy efficiency were investigated in [33–36]. Thus, six most important barriers were identified in [33] for the SMEs belonging to the ferrous material industry, namely, the government energy policy, the financial-economic problem, the managerial-organizational process, the technological factors, the quality of the workforce, the raw material, and the used fuel. The barriers are linked because they are interdependent. According to [36], the main drawback consists of restricted access to capital corroborated with a lack of information and low priority.

One way to develop a plan to improve energy efficiency (PIEE) is the use of new approaches and modern technologies to minimize energy consumption [37]. This PIEE should also be a priority for the SMEs [38]. Reorganization of production, modernization of technologies, and introduction of efficient equipment lead to the growth of industrial production. With the inclusion of these measures in the SMEs' sector, the reduction of consumed resources and energy, simultaneous with decreasing the cost, will appear. Optimal management of SMEs implies the aspects of the energy efficiency and environmental investments, with results on the increase of energy savings and reduction of greenhouse gas (GHG) emissions [39–41]. The energy management methodology adapted to each SMEs proposed in [42] is focused on the individual level of a triggering practice to increase energy efficiency. In this context, internal capabilities were used as a minimal resource required for energy management implementation.

Evidence of the high economic potential was highlighted in the case of active energy management in SMEs [43,44] and the implementation of a barrier's taxonomy regarding the adoption of energy-efficiency measures [45]. In addition, recent studies concluded that increasing energy efficiency could use the lean management concept at the SMEs level [46–48]. The lean refers to create more value for consumers with fewer resources [46]. Besides this concept, the intelligent energy management concept was also applied to buildings in the last period [49–51]. A detailed review of the studies

that developed data-driven building energy consumption prediction models based on the intelligent algorithms (machine learning) is presented in [51].

A brief description of the literature is presented in Table 2 to highlight the advantage of our new

vision on energy consumption management, proposed as an advanced decision support platform, with technical and economic benefits on increasing energy efficiency.

Table 2. Comparison between proposed approach and the literature.

Number of Reference	Database Management	Consumption Profiling	Consumption Forecasting	Schedule and Optimization	Cost Analysis	Decision-Making
[24,42,47]	Yes	No	No	No	No	Yes
[24,42,47]	Yes	No	No	No	No	Yes
[25,27,30]	Yes	Yes	Yes	No	No	Yes
[25,27,30]	Yes	No	No	Yes	No	Yes
[26]	Yes	Yes	Yes	No	Yes	Yes
[28,29]	Yes	No	No	Yes	No	Yes
[28,29]	Yes	No	No	Yes	Yes	Yes
[31,32]	No	No	No	No	Yes	Yes
[33–35]	No	No	No	No	Yes	Yes
[33–35]	No	No	No	No	No	Yes
[36,41]	Yes	No	No	Yes	No	Yes
[36,41]	Yes	No	No	No	Yes	No
[37,38]	Yes	No	No	Yes	Yes	Yes
[39,40]	Yes	No	Yes	No	Yes	Yes
[39,40]	Yes	No	Yes	No	Yes	Yes
[43,47]	Yes	No	Yes	Yes	No	Yes
[43,47]	Yes	No	Yes	Yes	No	Yes
[44,46]	Yes	Yes	No	Yes	No	No
[44,46]	Yes	Yes	No	Yes	No	No
[45]	Yes	No	No	No	Yes	No
[45]	Yes	No	No	No	Yes	No
Proposed approach	Yes	Yes	Yes	Yes	Yes	Yes

It should be emphasized that there are also other references which solved the problem of minimal management, but their proposed approaches are similar to those presented in the table.

### 3. The Structure of the Decision Support Platform

Four interdependent modules associated with the steps used in an efficient management process are integrated into the platform, see Figure 4.

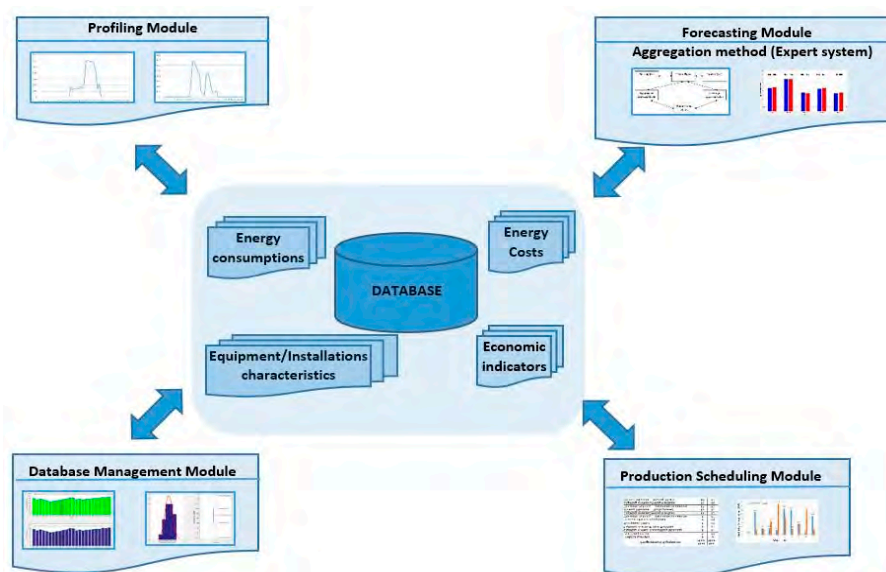


Figure 4. The structure of decision support platform.

The platform has applicability in the process of monitoring, control, and optimization of energy consumption, respectively cost reduction; it has the following features associated with efficient energy management: description and characterization of the SME through the characteristics of energy consumption by categories of industrial consumers, regardless of the field of activity of SMEs; the establishment of the correlations between energy consumptions, respectively consumption



The platform has applicability in the process of monitoring, control, and optimization of energy consumption, respectively cost reduction; it has the following features associated with efficient energy management: description and characterization of the SME through the characteristics of energy consumption by categories of industrial consumers, regardless of the field of activity of SMEs; the establishment of the correlations between energy consumptions, respectively consumption patterns; profiling and forecasting of energy consumption; and optimal production scheduling for flattening the energy consumption profile.

The platform allows the SME to manage the development of technological processes. Thus, the platform ensures the continuity of the technological processes, helping the SMEs to save money for purchases and updates. On the other hand, because the industrial processes are never static, the platform is built also to be adaptable. If the SMEs will adopt modern technologies and develop new processes to maintain their activity, the integration will be done easily on the database of the platform for new equipment and installations. At the least, the platform will be a common solution to the database of the platform for SME equipment and installations. Not least, the platform offers exclusive solutions, namely, what

Artificial intelligence based techniques were proposed inside each module of the platform to understand the evolution and trend of energy consumption and identify solutions which minimize the impact of the energy bills. The data management module is based on the data mining technique that extracts the technical details on energy consumptions used to develop production scheduling strategies; The profiling module integrates an original approach based on clustering techniques to determine the typical energy consumption profiles assigned to different activities; The forecasting module contains a new approach that uses an expert system to forecast the total energy consumption at the SME level; and The production scheduling module includes a novel approach based on the combinatorial optimization for daily consumption programming and determining the optimal solutions regarding the flattening of daily energy consumption profile with the benefits on the cost of energy bills.

All modules use procedures that allow the interaction between them, ensuring the communication of information and the synchronization of executions, to assist the Decision-Maker in the identification of the optimal solutions associated with an efficient management process. Details on each module are presented in the following subsections.

3.1. The Database

The database contains files with energy consumptions, costs from energy bills, equipment and installation associated with the technological flows from the SMEs and economic indicators. The working modules (consumption and cost analysis module, profiling module, forecasting module, and production scheduling module) of the platform will upload the data sequences recorded in the files with the matrix (consumption scheduling module) of the platform will upload the data sequences recorded in the files with the matrix associated with the data communication unit, then the energy consumption file includes fields associated with the calendar data (year, month, day from the month, and day from the week), representing the first four columns, and the energy consumptions (the following columns). The indices from 1 (January) to 12 (December) identify the months and from 1 (Monday) to 7 (Sunday) for the day from the week. Depending on the sampling step,  $m$ , (a quarter-hour, half-hour, and hour), the number of columns associated with the energy consumption can be 96, 48, and 24. All these data are accessed by all working modules from the matrix  $DW$ , having the size  $(N_W \times (4+m))$ , where  $N_W$  represents the number of records identified through days and  $m = \{24, 48, 96\}$ . A sequence from the energy consumption file, where  $m = 24$ , is presented in Figure 5.

Year	Month	Day from month	Day from week	Hour 1	Hour 2	Hour 3	Hour 4	Hour 5	Hour 6	Hour 7	Hour 8	Hour 9	Hour 10	Hour 11	Hour 12	Hour 13	Hour 14	Hour 15	Hour 16	Hour 17	Hour 18	Hour 19	Hour 20	Hour 21	Hour 22	Hour 23	Hour 24
2017	9	12	2	1.173	1.292	0.756	0.719	0.465	0.582	0.758	0.439	0.394	1.225	0.688	0.415	0.284	0.493	0.716	0.445	0.826	0.525	0.348	0.859	0.533	0.808	1.182	0.984
2017	9	13	3	1.283	1.199	0.929	0.877	0.516	0.671	0.943	0.561	0.774	1.276	0.871	0.616	0.678	0.491	0.536	0.331	0.406	0.648	0.938	1.123	0.916	1.400	1.204	0.987
2017	9	14	4	0.743	1.023	0.876	0.497	0.580	0.817	0.727	0.454	0.458	0.869	0.645	0.870	0.611	0.694	0.827	0.431	0.450	0.493	1.228	1.123	1.110	1.029	1.018	0.568

Figure 5. A sequence from the energy consumption file (SME with the smart meter installed).

The file has a different structure when the SME has a classic meter installed, containing only the calendar data and the daily energy consumption (which it reads at the end of working schedule the operating staff), such that the matrix  $DW$  has the size  $(N_W \times 5)$ .

The file energy costs include records associated with the calendar data (year and month) and the energy costs introduced in the database from the monthly bills. These costs are assigned to the monthly energy consumptions resulted from the aggregation of daily energy consumptions

The file has a different structure when the SME has a classic meter installed, containing only the calendar data and the daily energy consumption (which it reads at the end of working schedule the operating staff), such that the matrix  $DW$  has the size  $(N_W \times 5)$ .

The file energy costs include records associated with the calendar data (year and month) and the energy costs introduced in the database from the monthly bills. These costs are assigned to the monthly energy consumptions resulted from the aggregation of daily energy consumptions associated with the billed month. The same indices from 1 (January) to 12 (December) identify the months. All these data are accessed by the working modules from the matrix  $DC$ , having the size  $(N_C \times 3)$ , where  $N_C$  represents the number of records identified through months.

The file with the technical characteristics comprises the fields regarding the name of equipment or installations, rated power, and the number of working times. The number of fields for the working times will result after analysis of all operating regimes corresponding to each equipment and installation based on some detailed measurements, using the sampling steps with as small as possible size (1 or 5 s) to identify the working times with high accuracy. After this step, this file can be completed, and the data are accessed from the matrix  $DE$ , having the size  $(N_E \times R)$ , where  $N_E$  represents the number of records identified through equipment and installations associated with the activities of technological flows and  $R$  is the number of columns which can be different from one SME to another. The first two columns refer to equipment or installations and their rated power. The number of the next columns will result after the classification in categories of the working times associated with the operating regimes of equipment or installations.

The file with the economic indicators comprises the fields regarding the turnover, production value, personnel costs, and total purchases with goods and services. All these data are accessed from the matrix  $DI$ , having the size  $(N_I \times 4)$ , where  $N_I$  represents the number of records identified through months. This file can be optional inside the platform.

### 3.2. The Consumption and Cost Analysis Module

Decision-making implies the need to know the activities within the technological flow of an SME. The role of this module is to translate the user's queries into an optimized framework so that the Decision-Maker obtains the information about the energy consumptions over the requested period (year, month, week, and day), the energy costs, and evolution of the economic factors.

The analysis can be done on years, months, or days, choosing an analysed period. A period between 2 months (e.g., January and February) or a single month, for one or more years, can be used in the monthly analysis. The days (all, working, or weekend) from the same month, but different years or different months from the same year, can be selected to be used in the daily analysis. The data are uploaded from the energy consumption file.

The module presents the results through the graphical representations of the variables (energy consumption, energy cost, or economic indicators) or the statistical parameters calculated over the analysed period.

The statistical parameters refer to:

- *The mean* represents a synthesis expression in a single representative level of everything essential, typical, and objective in its occurrence, manifestation, and development of the analysed variable.

$$X_{mean} = \frac{\sum_{i=1}^n x_i}{n} \quad (1)$$

where:  $X_{mean}$ —mean of the analysed variable from the selected period, uploaded from the matrices  $DW$ ,  $DC$ ,  $DE$ , and  $DI$ ;  $x_i$ —value  $i$  of the analysed variable, uploaded from the matrices  $DW$ ,  $DC$ ,  $DE$ , and  $DI$ ;  $n$ —the number of records (rows) associated with the selected period.

- The *standard deviation* represents the most common parameter used to analyse the variation of a data set. The data with high homogeneity have a small value of the standard deviation.

$$\sigma = \sqrt{\frac{\sum_{i=1}^n (x_i - X_{mean})^2}{n}} \quad (2)$$

- The *median* is the value that divides the data set of the analysed variable (sorted in ascending or descending order) into two equal parts. If the series has an odd number of terms, then:

$$X_{median} = x_{\frac{n+1}{2}} \quad (3)$$

If the series has an even number of terms, then:

$$X_{median} = \frac{x_{\frac{n}{2}} + x_{\frac{n}{2}+1}}{2} \quad (4)$$

- *Quintiles* are position indicators that divide the data set into more parts with equal values. In the module, the quintiles are calculated as:

$$x_{\frac{1}{4}} = Q_1; x_{\frac{2}{4}} = Q_2 = X_{median}; x_{\frac{3}{4}} = Q_3; x_{\frac{4}{4}} = Q_4 \quad (5)$$

where  $Q_1, Q_2, Q_3,$  and  $Q_4$  are quintiles and divide the data set into four equal parts  $n/4$ .

The Decision-Maker will analyse the characteristics of the first quintile with the lowest energy consumption and the fourth quintile with the highest energy consumption.

### 3.3. The Profiling Module

#### 3.3.1. Working Assumptions

The module contains an original clustering-based method to estimate the typical energy consumption profiles. Different sampling steps (a quarter-hour, half-hour, or hour), which lead to 96, 48, or 24 values of energy consumption, depending on the setting of the smart meter installed to each SME, can characterize the daily energy consumption profiles. The assumption related to the approximation of hourly consumption was adopted in the profiling process for energy consumption [52]. According to this assumption, the energy consumption characteristics are unknown, but the TECPs can be used. This situation is encountered at the small consumers from the category of micro, small, and medium-sized enterprises, which absorbs a maximum power up to 100 kW. The shape of these profiles is also influenced by season, the category of equipment or installations, and the activity type [52]. However, a high number of energy consumption profiles can create complex issues in the identification of the consumption patterns.

The proposed method can arrange the energy consumption profiles in representative groups (consumption patterns), based on certain similarities. A typical energy consumption profile (TECP) will correspond to each consumption pattern, such that each SME can have one or more TECPs, depending on the activity type (e.g., small, medium, and high).

#### 3.3.2. Clustering-Based Method in Profiling Process

Clustering represents a special process to group the data recorded in the matrix  $DW$  on the columns associated with the energy consumptions given by the sampling step (24, 48, or 96), represented by

clusters.

The stages of the clustering process are shown in Figure 6.

*Extract the energy consumptions from matrix DW:* It refers to values the energy consumption from the columns of matrix DW subject to the clustering process and recorded in the vectors  $W_i, i = 1, \dots, p$ .  
*Data pre-processing:* Due to various random factors, the energy consumption profiles can contain abnormal, deviation, unrepresentative, noisy, strange, anomalous, or missing data. It is very important to detect and repair or eliminate the anomalous or abnormal values before the use of the  $p$  daily profiles introduced as vectors  $W_i, i = 1, \dots, p, m = \{24, 48, 96\}$ . If all energy consumption profiles from matrix DW are considered, then  $p = N_W$ . A statistic-based data mining technique is applied to solve these problems [53].

*Data normalization:* The normalization process uses the hourly values of energy consumption from each vector  $W_i, i = 1, \dots, p$ , a suitable normalizing factor represented by the average consumption, the maximum value of consumption, or the total energy consumption over the analysed period. This process is mandatory because all data must be brought in the range  $[0, 1]$  in the clustering process.

The vectors associated with the energy consumption profiles  $W_i, i = 1, \dots, p, m = \{24, 48, 96\}$ , are merged into different clusters, according to the distance calculated between each of them. Finally, one or more clusters (also called groups, patterns, models, classes, or categories) will be obtained in function by the spatial location of the characteristics of vectors  $W_i, i = 1, \dots, p$ . The characteristics of vectors will be closer to the common centre of the cluster they belong, compared to centres of consumption  $j$  from the record  $i$ , and  $\sum_i w_{ij}$  — the energy consumption over the analysed period, other clusters.

The stages of the clustering process are shown in Figure 6. identical with working schedule.

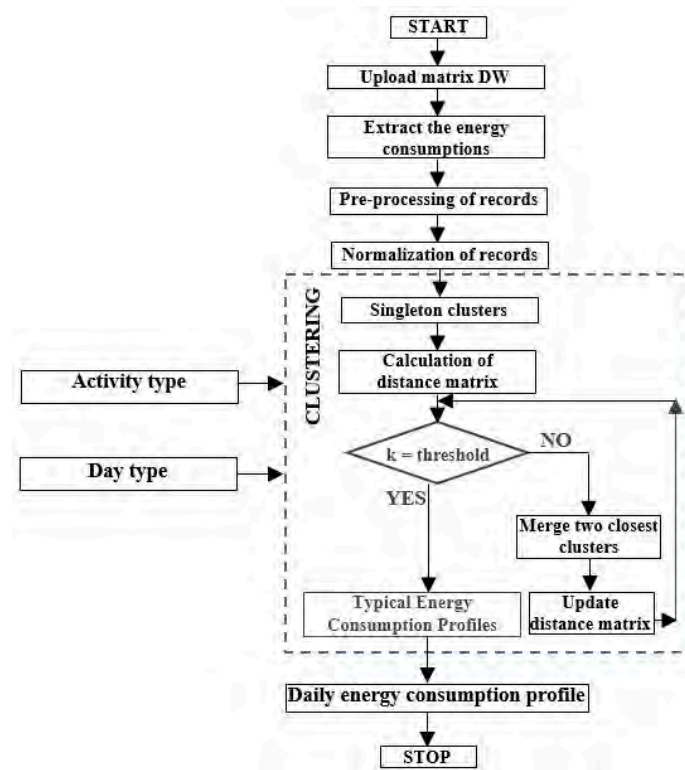


**Figure 6.** The steps completed to obtain the typical energy consumption profiles (TECPs).

*Extract the energy consumptions from matrix DW:* It refers to values the energy consumption from the columns of matrix DW subject to the clustering process and recorded in the vectors  $W_i, i = 1, \dots, p$ .  
*Data pre-processing:* Due to various random factors, the energy consumption profiles can contain abnormal, deviation, unrepresentative, noisy, strange, anomalous, or missing data. It is very important to detect and repair or eliminate the anomalous or abnormal values before the use of the energy consumption profile in the profiling process. A statistic-based data mining technique is applied to solve these problems [53].

*Data normalization:* The normalization process uses the hourly values of energy consumption from each vector  $W_i, i = 1, \dots, p$ , a suitable normalizing factor represented by the average consumption,

the maximum value of consumption, or the total energy consumption over the analysed period. This process is mandatory because all data must be brought in the range [0, 1] in the clustering process.

$$w_{i,j}^{norm} = \frac{w_{i,j}}{\sum_i w_{i,j}}; i = 1, \dots, p; j = 1, \dots, m, m = \{24, 48, 96\} \tag{7}$$

where  $w_{i,j}^{norm}$ —normalized value of the energy consumption  $j$  from the record  $i$ ,  $w_{i,j}$ —the energy consumption  $j$  from the record  $i$ , and  $\sum_i w_{i,j}$ —the energy consumption over the analysed period, identical with working schedule.

*The clustering process:* The clustering process can be carried out in several ways, depending on the methods chosen by the Decision-Maker. Inside of each method, a distance is chosen to determine the similarity between vectors  $W_i, i = 1, \dots, p$ , associated with the energy consumption profiles. Many measurement systems use different distances in the clustering process, but from them, the Euclidean distance is the most used. Thus, the distance, in the case of two vectors  $W_r$  and  $W_s$ , is calculated with the relation:

$$d(W_r^{norm}, W_s^{norm}) = \sqrt{(W_r^{norm} - W_s^{norm})(W_r^{norm} - W_s^{norm})^t}, r \neq s \tag{8}$$

All clustering methods should lead, in principle, to representative clusters, indifferently by the input data. There are cases when these clusters could not be obtained. Using another method represent an alternative to obtain better results than previous cases to identify a solution. The quality of the results can be the best when the separation of the elements leads to the well-defined clusters or less good when a membership degree to one of the clusters is associated.

*Extraction of TECPs:* A TECP will be assigned to each cluster, calculated as the mean of normalized energy consumptions associated with each profile.

$$\bar{w}_{j,k} = \frac{\sum_{l=1}^{N_k} w_{l,j}^{norm}}{N_k}; j = 1, \dots, m, m = \{24, 48, 96\}, k = 1, \dots, C_k \tag{9}$$

where  $C_k$  is the number of clusters resulted from the clustering process;  $\bar{w}_{j,k}$  represents the mean normalized value  $j$  of the energy consumption associated with the TECP corresponding to the cluster  $k, k = 1, \dots, C_k; l$  is the index of the energy consumption profiles, from the matrix  $W$ , associated with the cluster  $k$  in the clustering process; and  $N_k$  is the number of the energy consumption profiles associated with the cluster  $k$  in the clustering process.

The representativeness of the mean can be evaluated based on the variation coefficient:

$$v_{j,k} = \frac{\sigma_{j,k}}{\bar{w}_{j,k}} \cdot 100 \quad (\%); j = 1, \dots, m, m = \{24, 48, 96\}, k = 1, \dots, C_k \tag{10}$$

$$\sigma_{j,k} = \sqrt{\frac{\sum_{l=1}^{N_k} (w_{l,j}^{norm} - \bar{w}_{j,k})^2}{N_k}}; j = 1, \dots, m, m = \{24, 48, 96\}, k = 1, \dots, C_k \tag{11}$$

where  $v_{j,k}$  is the variation coefficient which indicated the confidence degree in the mean and  $\sigma_{j,k}$  represents the standard deviation for the normalized energy consumption  $j$  associated with the TECP corresponding to the cluster  $k$ .

A value very close to 0 of  $v_{j,k}$  leads to a high confidence degree in the mean, which means that the clusters are very representative and homogenous.

Appl. Sci. 2020, 10, 3503

The proposed method in this module uses an expert system that considers aggregation rules for the energy consumption of equipment and installations for each activity associated with the technological flow.

### 3.4. Forecasting Consumption Module

If for the SMEs, following the detailed analysis of the technological processes, the technical characteristics of operating periods are mainly SME energy consumption forecasting provides the primary information identified, making regarding the based for planning methods associated with the system (ES) can be developed energy consumption forecasting module. Figure 7 presents the flowchart of the proposed process. Inappropriate if the number of records is small then, the estimation errors can be high and can lead to additional operating or investment cost. On the other hand, energy consumption forecasting plays an important role in the development of economic strategies for SMEs. The decision-making in the different periods (short and long) is related to the planning and development of the industrial processes require a good knowledge of the energy consumption of each activity and technological flow. The technical parameters of each equipment or installation should be experienced a Decision-Making represents the way to understand all energy consumption characteristics (knowledge base and inference rules) try to model the Decision-Making process to establish the model accessible expert system. The framework of aggregation rules for the energy consumption of equipment and installations for each activity associated with the technological flow. The expert system interface (HMI) performs communication. The explanation of reasoning's module for the SMEs, following the detailed analysis to justify and explain processes regarding the characteristic of the operating periods. The number of operating cycles associated with each equipment or installation were identified, then an aggregation-based forecasting method knowledge, an expert system (ES) can be developed to estimate the daily energy consumption. Figure 7 presents the flowchart of the proposed method. In Figure 7, the following variables were used:  $n_a$  and  $n_e$  for equipment and installation number of priorities,  $M$  for the total number of equipment and installations associated with the activity problem, for the total number of activities.

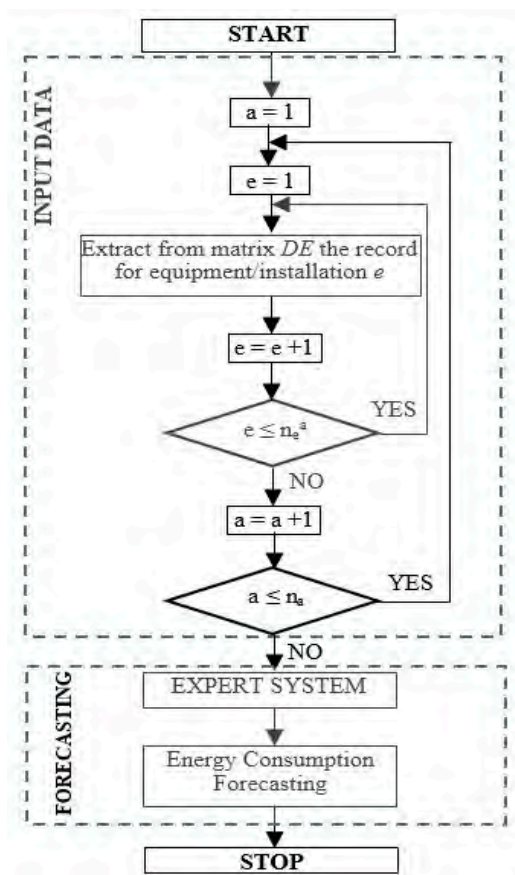


Figure 7. The flowchart of expert system-based aggregated method.

An ES is a powerful tool used in the proposed method, having the following main components: database, knowledge base, and inference rules. It can identify the solutions to the difficult problem regarding the energy consumptions of the equipment and installations in various operating regimes that require the extensive experience of a Decision-Maker.

The last two components (knowledge base and inference rules) try to model the Decision Makers' experience to establish the set of admissible solutions. The framework of an expert system is shown in Figure 8 [55].

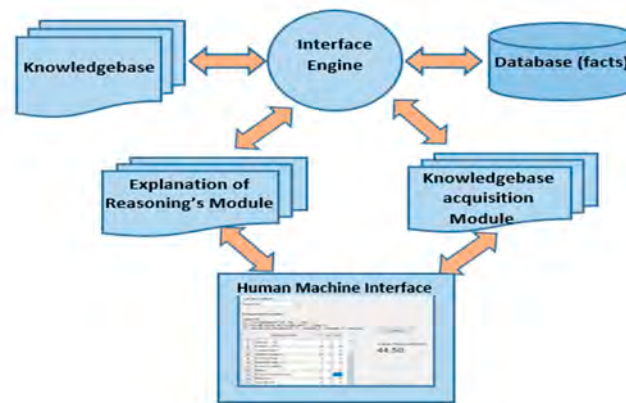


Figure 8. The framework of the expert system.

Human-machine interface (HMI) performs communication. The explanation of reasoning's module performs as the main function, the necessity to justify and explain the stages regarding the reasoning of the expert system. The demonstration of the necessity inside the ES can be done in the initial phase (development), confirming the correctness of acquiring and using knowledge, and in the final phase quantifying the importance and the result of the taken actions. The database is used to build inference rules. The inference engine determines which inference rules are fulfilled and taken over in the order of priorities. A code, written in the form of rules, will convert the knowledge base to solve the problem.

Two matrices are the basis of the expert system. The first matrix, Equipment and Installations' Matrix (EIM), contains the equipment and installations' characteristics initialized with the input data corresponding to the scheduled activities from the next days. The rated power, working times, according to the type of daily activity (e.g., small, medium, and high) and the absorbed power in the steady-state regime, for each equipment or installation, represent the elements in this matrix.

The second matrix, Decision-Making Matrix (DMM), has a high importance in decision-making. The information about the operating modes (on/off), using 1 or 0, the operating cycles, and the working times (reduced, normal, and long), identified through the numbers 1, 2, and 3, for each equipment or installation introduced in matrix EIM, are recorded in this matrix.

Based on the information contained in the two matrices, the rules of the expert systems with the logical structure

If  $\langle \text{equipment or installation } e \text{ is on} \rangle$  and  $\langle \text{working time is reduced} \rangle$  and  $\langle \text{number of cycles is } n_c \rangle$  then  $\langle \text{forecasted consumption is } W_f \rangle$

The information about the operating modes (on/off), using 1 with the operating cycles, and the working times (reduced, normal, and long) identified through the numbers 1, 2, and 3, for each equipment or installation introduced in matrix EIM, are recorded in this matrix.

Based on the information, contained in the two matrices, the rules of the expert systems with the logical structure

### 3.5. Production Scheduling Module

If  $\langle \text{equipment or installation } e \text{ is on} \rangle$  and  $\langle \text{working time is reduced} \rangle$  and  $\langle \text{number of cycles is } n_c \rangle$

The minimization of costs with energy bills and flattening of the consumption profile and the optimal scheduling of activities associated with the technological flows, through the reallocating of the equipment or installations in the hours, can be done with appropriate strategies are developed. Because the main objective is to reduce energy consumption, the main challenge facing the SMEs today, obtaining scheduling of the activities associated with the technological flows represents a traditional factor oriented, towards increasing energy efficiency. The production schedule can lead to positive effects on energy conservation, improving the technical and economic performance of the SMEs, and enhancing competitiveness, respectively [56].

#### 3.5.1. Mathematical Model

Considering the above aspects, a mathematical model, and the combinatorial optimization method to obtain the optimal scheduling frameworks of activities associated with the technological flows through modification of working time sequence corresponding to the programmable

### 3.5. Production Scheduling Module

The minimization of costs with energy bills and flattening of the consumption profile and the optimal scheduling of activities associated with the technological flows, through the reallocating of the equipment or installations in other hours, can be done if appropriate strategies are developed. Because these objectives represent the main challenges facing the SMEs today, optimum scheduling of the activities associated with the technological flows represents a direction vector oriented towards increasing energy efficiency. The production schedule can lead to positive effects on energy conservation, improving the technical and economic performance of the SMEs, and enhancing competitiveness, respectively [56].

#### 3.5.1. Mathematical Model

Considering the above aspects, a mathematical model, and the combinatorial optimization method to obtain the optimal scheduling frameworks of activities associated with the technological flows through modification of working time sequence corresponding to the programmable equipment or installations, is developed. The combinatorial optimization method is based on a fast heuristic search in the large admissible sets to obtain the optimal solution, represented by the time intervals in which the programmable equipment will work. The proposed method represents a useful decision-making tool in the choice of energy suppliers with the best offer of the energy cost and the identification of energy efficiency solutions.

The objective is the flattening of the energy consumption profile through the identification of the optimal solutions for the production scheduling of the SMEs, whatever may be the industrial activity branch.

The method considers the energy amount consumed by the equipment and installations which perform a certain activity inside a technological flow, from the moment they start working until their stopping after the associated task has been accomplished. Another aspect refers to the identification of the equipment and programmable installations. Those programmable installations and equipment, with high energy consumption, can be moved to work in the hourly periods with a small energy tariff or the reduced energy consumption without affecting the technological flow and having a minimum influence on the performance.

The flattening of the energy consumption profile is done for the work period when the activity is very intensive, moving the programmable equipment and installations in the hourly period with reduced activity. The mathematical expression of the objective function is [56]:

$$\min \sum_{h=1}^{T_H} c_{W,h} \cdot \left| \sum_{a=1}^{n_a} \sum_{e=1}^{n_e^a} w_{f,a,e,h} - \frac{C_T}{T} \right| \tag{12}$$

where

$$C_T = \sum_{a=1}^{n_a} C_{d,a} = \sum_{a=1}^{n_a} \sum_{e=1}^{n_e^a} c_{W,h} \cdot w_{f,a,e,h}, f = 1, \dots, n_p \tag{13}$$

$c_{W,h}$ —the energy cost at hour  $h$ ,  $h = 1, \dots, T_H$ ;  $T$ —analysis duration, usually is represented by the work schedule;  $w_{f,a,e,h}$ —the energy consumption of equipment or installation  $e$  necessary to execute the activity  $a$  and obtaining the final product  $f$ ;  $n_p$ —the total number of final products;  $n_a$ —the necessary activities to obtain the final product  $f$ ; and  $n_e^a$ —the number of equipment and installations used for the activity  $a$  to be carried out.

Due to the complexity of the industrial processes, the following technical constraints must be considered:



- the allocation of the equipment or installations to a technological flow to perform a task:

$$X_{f,a,e,h} = \begin{cases} 0 & \text{if } k \text{ does not work} \\ 1 & \text{if } k \text{ works} \end{cases} ; \tag{14}$$

$$h = 1, \dots, T_H, e = 1, 2, \dots, n_e^a, f = 1, 2, \dots, n_p, a = 1, 2, \dots, n_a$$

where  $X_{f,a,e,h}$  represents a decision variable for the allocation of the equipment or installations. Only if  $X_{f,a,e,h} = 1$ , then the equipment or installation  $e$  performs the activity  $a$ , to obtain the final product  $f$ , at the hour  $h$ .

- the working time of equipment or installation

$$T_{f,a,e}^{Start} - T_{f,a,e}^{Stop} \geq T_{f,a,e}; e = 1, 2, \dots, n_e^a, f = 1, 2, \dots, n_p, a = 1, 2, \dots, n_a \tag{15}$$

where  $T_{f,a,e}^{Start}$  and  $T_{f,a,e}^{Stop}$ —the start and stop hours, respectively, between which the equipment or installation  $e$  works to carry out the activity  $a$ , to obtain the final product  $f$  and  $T_{f,a,e}$ —the working time of the equipment or installation  $e$ .

- Phase sequence is considered because the activities associated with a technological flow for an equipment or installation  $e$ , to obtain the product  $f$ , should be finished before to start the next activities to process the product  $(f + 1)$  from another technological flow. This constraint takes into account that for any equipment and installation:

$$T_{(f+1),a,e}^{Stop} - T_{f,a,e}^{Stop} \geq T_{f,a,e}; e = 1, 2, \dots, n_e^a, f = 1, 2, \dots, n_p, a = 1, 2, \dots, n_a \tag{16}$$

Energy consumption balance between the total energy consumptions  $w_{f,a,e,h}$  of all equipment and installations  $e$  associated with the activities  $a$ , to obtain the products  $f$ , at the hour  $h$ , and the total energy consumption recorded by the general meter:

$$W_{T,h} = \sum_{a=1}^{n_a} \sum_{e=1}^{n_e^a} w_{f,a,e,h}; h = 1, \dots, T_H, e = 1, 2, \dots, n_e^a, f = 1, 2, \dots, n_p, a = 1, 2, \dots, n_a \tag{17}$$

### 3.5.2. The Steps of the Proposed Algorithm

The algorithm considers the following steps to obtain the proposed objective represented by the flattening of the energy consumption profile.

- *Step 1. Determine the working characteristics of equipment, installations, and systems*  
The records from the measurement database represents the base to determine the operating characteristics associated with the working time multiplied by the hourly energy consumption for each equipment, installation, and system. If two equipment are dependent and work together, the aggregate characteristic cumulates the working times.
- *Step 2. Initialization of the input data matrix*  
In the input data matrix (IDM) having the size  $(n_e \times 8)$ , where the total number of rows indicates all equipment and installations  $e, e = 1, \dots, n_e^a$ , associated with all activities  $a, a = 1, \dots, n_a$ , and the columns refers to the name of the equipment or installation, the characteristics relating to the operation mode (on or off), the working cycles, the working time, type (programmable or nonprogrammable), the dependency to work together with other equipment to obtain the final product  $f$ , and the start and stop working hours of the equipment, information are introduced.
- *Step 3. Optimization Process*  
Combinatorial optimization was implemented to obtain the optimal solution regarding the production scheduling, which leads to flattening of the energy consumption profile.

#### 4. Case Study

The testing of the platform, developed in MATLAB, was done by its implementation at an industrial consumer from the category of microenterprises (5–10 employees) in the most active field of SMEs (trade/repair of vehicles) from Romania [57].

##### 4.1. Database

The database includes the monthly energy consumptions and costs identified from energy bills, all equipment and installations associated with the technological flows from the SME, and those that provide the comfort (lighting system, heating system, or cooling system). The information for the analysed SME was available starting with 2018. A smart meter was installed at the beginning of 2019 in parallel with the settlement classic meter, to record and to communicate (wireless) the energy consumption profiles towards the software platform to test the profiling module. Thus, the availability of the profiles allowed calculation of the daily and monthly energy consumptions using an aggregation function implemented in the database module.

Table A1 from Appendix A presents the energy consumption and cost from monthly energy bills in the period 2018–2019 are presented in [57]. In addition, the daily energy consumptions, recorded in 2019 by the smart meter, are given in the attached Supplementary File. The technological processes contain activities relating to the tinsmith, mechanical repairs, and car dyeing. The equipment, installations, and systems associated with these activities, together with their rated powers ( $P_r$ ), are presented in Table 3.

**Table 3.** The electrical equipment/installations/systems recorded in the database.

No.	Equipment/Installation/System	$P_r$ (kW)
1	Dyeing installation	15.0
2	Air compressor system	11.0
3	Welding machine	6.20
4	Lighting system: tinsmithing department	1.20
5	Lighting system: repair department	0.75
6	Lighting system: dyeing installation	1.00
7	IT equipment—office	0.35
8	Other electric equipment	10.0
9	Vehicle lift	2.00
10	Gas boiler	12.0
	<b>Total installed power</b>	<b>59.5</b>

##### 4.2. The Consumption and Cost Analysis

The analysis can be done on years, months, or days, choosing an analysed duration. At the level of 2018, the total energy consumption was by 26.09 MWh/year, and the total cost, 23,479 RON, with an average value of 2.17 MWh/month and 1957 RON/month, respectively. A deeper analysis was done at the level of months. The information on the dispersion of the data regarding the energy consumptions was obtained based on a boxplot.

A boxplot represents a graph that indicates how the values are spread out. In Figure 9, the boxplot of the monthly energy consumption from 2018 was shown. The analysis of the boxplots shows that the median energy consumption for all months from 2018 is 1743.5 kWh. The minimum value is 1247 kWh recorded in August, and the maximum value is 5124 kW (February), plotted with “+” in the figure. The months with higher values, over the quintile  $Q_3$  (represented with a blue horizontal line), identified in the graph with the magenta colour and the outliers, like the month February with the red colour, were analysed.

boxplot of the monthly energy consumption for all months from 2018 is 1743.5 kWh. The minimum value is 1247 kWh recorded in August, and the maximum value is 5124 kWh (February), plotted with "+" in the figure. The months with higher values, over the quintile  $Q_3$  (represented with a blue horizontal line), are identified in the graph with the magenta colour and the outliers, like the month February with the red colour, were analysed.

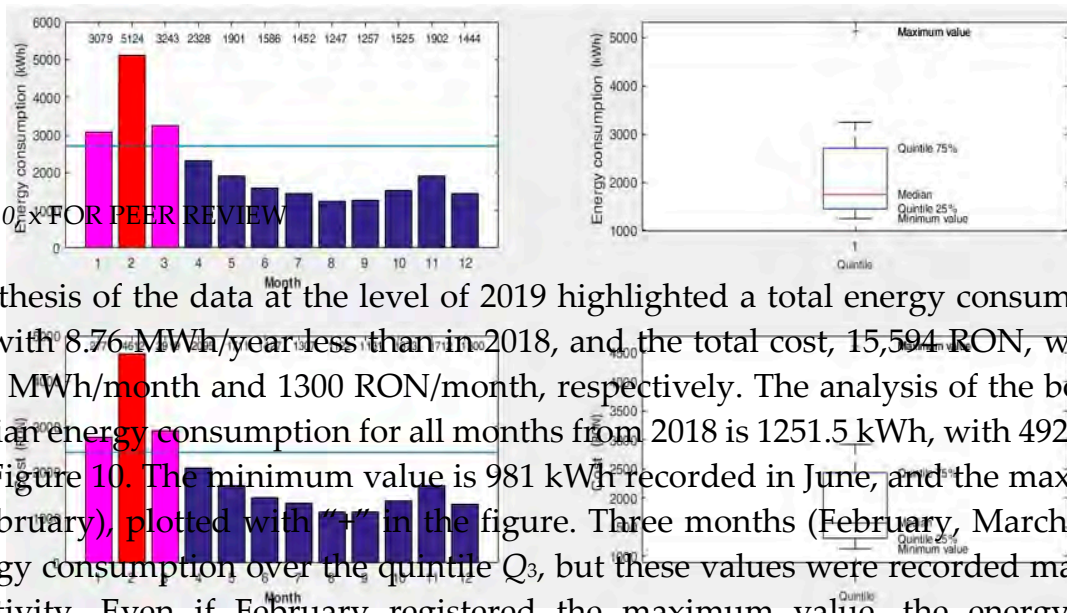


Figure 9. The boxplot of the monthly energy consumption from 2018.

The synthesis of the data at the level of 2019 highlighted a total energy consumption by 17.33 MWh/year, with 8.76 MWh/year less than in 2018, and the total cost, 15,594 RON, with an average value of 1.44 MWh/month and 1300 RON/month, respectively. The analysis of the boxplot showed that the median energy consumption for all months from 2018 is 1251.5 kWh, with 492 kWh less than in 2018, see Figure 10. The minimum value is 981 kWh recorded in June, and the maximum value is 2496 kWh (February), plotted with "+" in the figure. Three months (February, March, and October) had the energy consumption over the quintile  $Q_3$ , but these values were recorded mainly due to an intensive activity. Even if February registered the maximum value, the energy consumption decreased with 2628 kWh less than in 2018, which means that the new heating system is efficient.

Concerning to January, February, and March, the analysis of the weather conditions and the performance of the electric heating system (energy consumption in 2018) has been indicated that the heating system was inefficient. The data for 2019 showed that the energy consumption decreased in the three months due to make the replacement of the electric heating system with a gas boiler. For Figure 10.

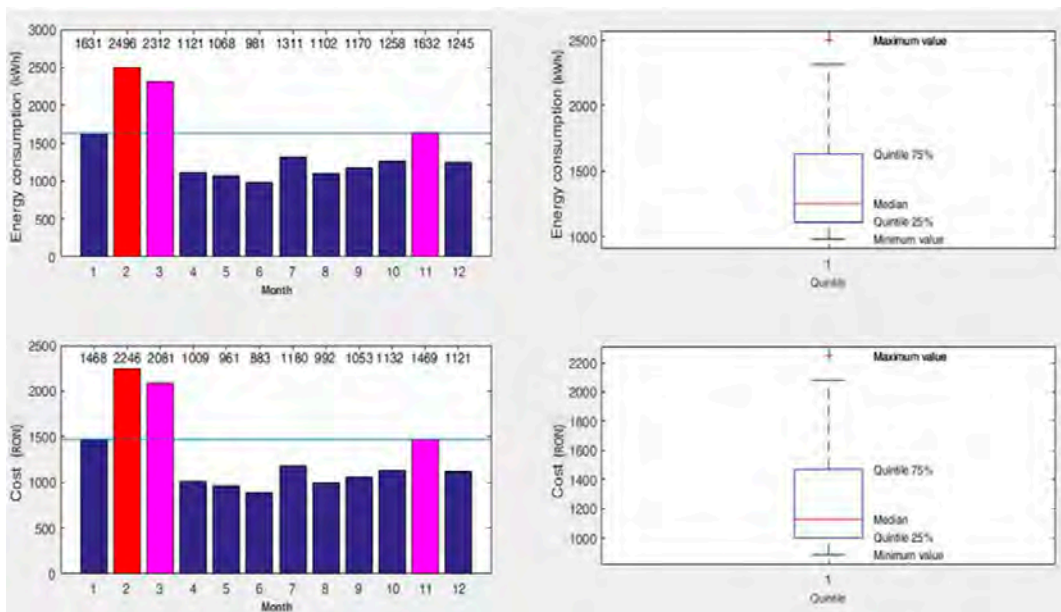


Figure 10. The boxplot of the monthly energy consumption from 2019.

The synthesis of the data at the level of 2019 highlighted a total energy consumption by 17.33 MWh/year, with 8.76 MWh/year less than in 2018, and the total cost, 15,594 RON, with an average value of 1.44 MWh/month and 1300 RON/month, respectively. The analysis of the boxplot showed that the median energy consumption for all months from 2018 is 1251.5 kWh, with 492 kWh less than in 2018, see Figure 10. The minimum value is 981 kWh recorded in June, and the maximum value is 2496 kWh (February), plotted with "+" in the figure. Three months (February, March, and

October) had the energy consumption over the quintile  $Q_3$ , but these values were recorded mainly due to an intensive activity. Even if February registered the maximum value, the energy consumption decreased with 2628 kWh less than in 2018, which means that the new heating system is efficient. Table 4 presents the comparative situation from both years.

**Table 4.** Comparison on the statistical results obtained from 2018 to 2019.

Variable	Mean (kWh)		Standard Deviation (kWh)		Confidence Degree (%)		Quintile $Q_1$ (kWh)		Quintile $Q_2$ (kWh)		Quintile $Q_3$ (kWh)		Quintile $Q_4$ (kWh)	
	2018	2019	2018	2019	2018	2019	2018	2019	2018	2019	2018	2019	2018	2019
Consumption	2274	1444	1142	493	50.2	34.1	1488	1112	1744	1252	2704	1632	5124	2496
Cost	2047	1300	1028	444	50.2	34.1	1303	1001	1569	1127	2433	1469	4612	2246

Besides the annual analysis, the daily energy consumptions from each month of the year 2019, obtained from the aggregation of the hourly values from profiles recorded by the smart meter, were investigated. Table 5 shows the statistical results.

**Table 5.** The statistical results obtained for the daily energy consumptions from each month of the year 2019.

Month	Mean (kWh)	Standard Deviation (kWh)	Confidence Degree (%)	Quintile $Q_1$ (kWh)	Quintile $Q_2$ (kWh)	Quintile $Q_3$ (kWh)	Quintile $Q_4$ (kWh)
January	77.7	29.5	38.0	56.8	77.0	95.8	145.0
February	124.8	22.4	17.9	109.0	127.5	145.0	157.0
March	107.7	19.6	18.2	96.0	110.0	122.0	141.0
April	58.6	18.6	31.7	49.0	51.0	70.0	97.0
May	50.9	8.4	16.5	46.0	50.0	57.0	68.0
June	49.1	13.2	26.9	40.5	47.5	60.5	72.0
July	57.0	13.3	23.3	45.0	56.0	63.0	83.0
August	50.1	7.1	14.3	44.0	49.5	56.0	63.0
September	58.5	10.7	18.3	50.5	56.0	67.5	78.0
October	54.7	13.2	24.2	47.5	57.0	63.5	76.0
November	77.7	8.1	10.4	72.0	79.0	84.0	90.0
December	69.2	10.4	15.0	68.0	72.5	75.0	80.0

The analysis of the results highlighted that the mean and median (represented by the quintile  $Q_2$ ) have the values approximately equal in the case of most months, with a higher difference for April. In addition, the confidence degree is high (between 10% and 20%) and moderate (between 20% and 30%) in most months, which means that the daily energy consumptions have the values close. However, there are two exceptions represented by January and April, where the confidence degree is weak.

All these analyses helped the Decision-Maker to understand the trend of the energy consumption from each month, season, or year, comparing the records from different selected periods, such that to develop the strategies, which to take into account by these characteristics, regarding the planning of production.

### 4.3. The Profiling Process

The profiling process used the daily energy consumption profiles, recorded with the help of smart meter during the year 2019. The sampling step has been set to a quarter-hour due to the dynamic of activities associated with the technological flow. The database has records for 250 days without the holidays and weekend days. These were normalized using daily energy consumption. To identify what is the best method to be used in the clustering process, the module has used the testing function based on the cophenetic correlation coefficient (CC). The Ward method, highlighted in red, led to the best performances in the case of this database, for which CC is equal with 0.840, see Figure 11. The results can be displayed if the Decision-Maker requests this information. The characteristics represented

to identify what is the best method to be used in the clustering process, the module has used the testing function based on the cophenetic correlation coefficient (CC). The Ward method, highlighted in red, led to the best performances in the case of this database, for which CC is equal with 0.840, see Figure 11. The results can be displayed if the Decision-Maker requests this information. The characteristics represented through the statistical variables (mean, standard deviation, and confidence degree in mean) of the daily energy consumption for the clusters obtained with the Ward method are presented in Table 6.

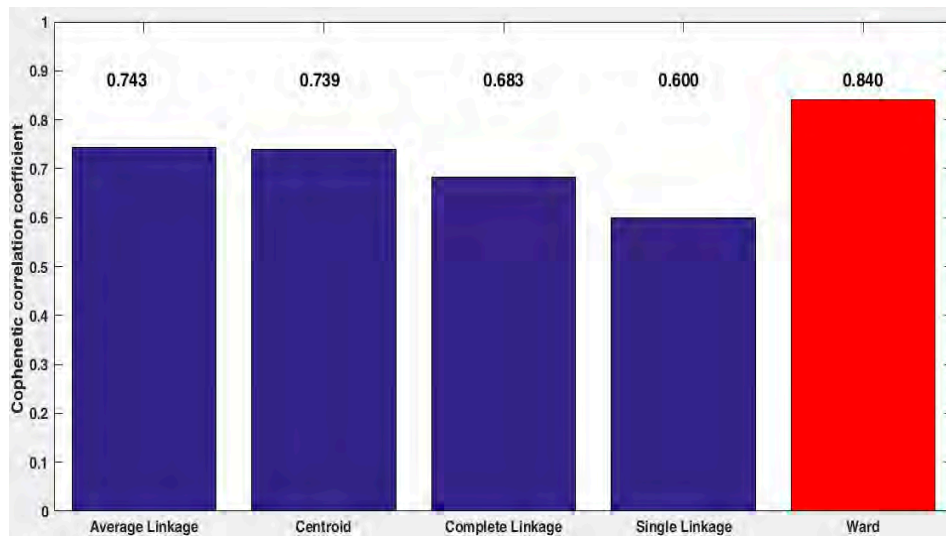


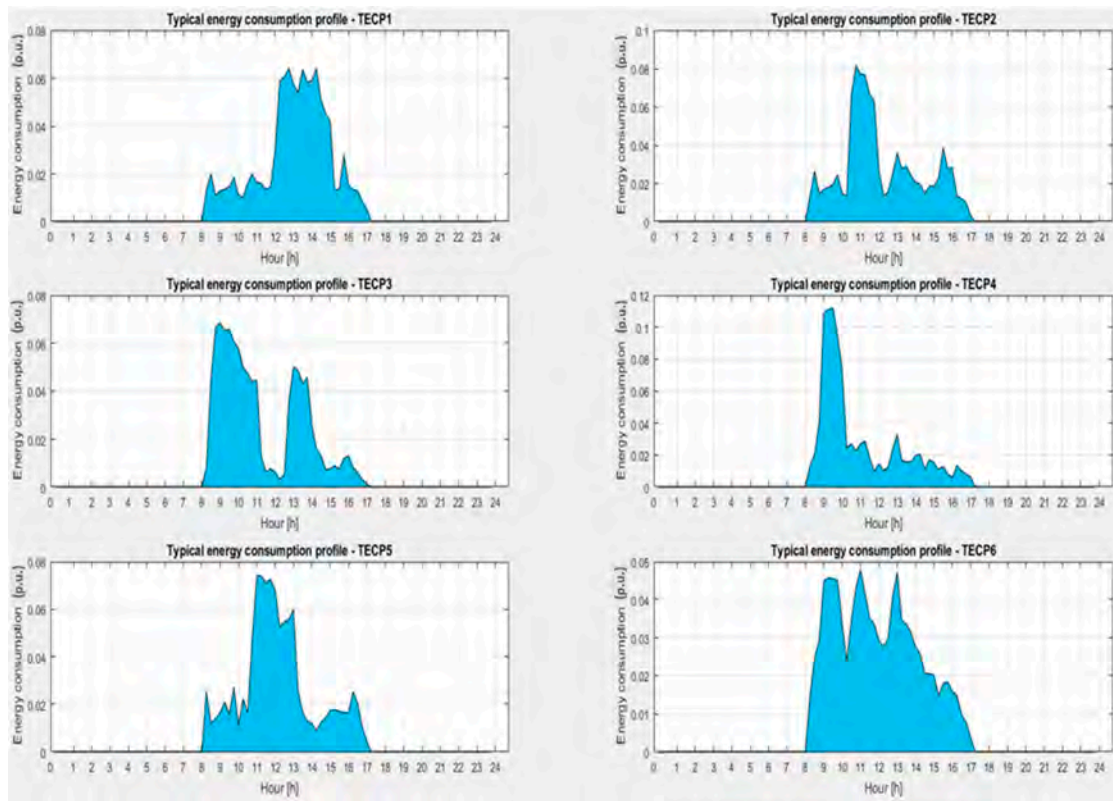
Figure 11. The cophenetic correlation coefficient associated with the clustering hierarchical methods.

Table 6. The results of the profiling process.

Cluster	Number of Profiles	Mean (kWh)	Standard Deviation (kWh)	Confidence Degree (%)
C1	14	99.4	3.8	3.8
C2	20	121.6	6.9	5.6
C3	85	55.6	5.3	9.5
C4	51	40.5	6.3	15.5
C5	71	75.9	6.0	8.7
C6	147.0	147.0	6.9	4.7

The profiles have been obtained based on the averaging process of the profiles assigned with each cluster. Figure 12 presents the TECPs, and the hourly values are indicated in Table A2 from Appendix A. Because the working schedule is 9 h (between 8.00 a.m. and 5.00 p.m.), the other values from TECPs are 0.

The dyeing installation cannot continuously operate during the 9 h of the working schedule. It can work with the two phases (dyeing and drying) at most two working cycles in a day if the vehicle is completely dyed, requiring a longer time, or at most three complete working cycles, if only various components of the vehicle are dyed. However, there are days when the other combinations between the working cycles can be met or when the second phase is missing (drying is done naturally, at ambient temperature, when it is over 20 °C, and the installation is no longer used for another dyeing phase). These operating regimes influence the intensity of the activities, three categories being identified: Small (the energy consumption is up to 75 kWh, clusters C3 and C4), medium (the energy consumption is between 75 and 100 kWh, clusters C1 and C5), and high (the energy consumption is up to 100 kWh, clusters C2 and C6). Table 7 presents the measurement of the intensity for each month. This information appears as a report for the decision-making, which can identify details on the activity from each month.



**Figure 12.** The typical energy consumption profiles associated with each cluster.

**Table 7.** The measurement of the intensity in each month, in (%).  
 The profiles have been obtained based on the averaging process of the profiles assigned with each cluster. Figure 12 represents the TECPs and the hourly values are indicated in Table A2 from Appendix A. Because the working schedule is 9 h (between 8:00 a.m. and 5:00 p.m.), the other values from C1-TECPs are 0.

Intensity	Jan	Feb	Mar	Apr	May	Jun	Jul	Aug	Sep	Oct	Nov	Dec
Small	10	40	48	0	0	0	0	0	0	0	0	0
C3—small	10	0	5	50	67	35	48	55	60	57	10	6
C4—small	19	0	0	20	29	50	30	45	13	26	9	6
C6—high	3	5	2	2	2	2	2	2	2	2	2	2
Medium	57	25	43	5	15	22	23	17	30	17	90	89
High	14	75	52	0	0	0	0	0	0	0	0	0
Total	100	100	100	100	100	100	100	100	100	100	100	100

It can be observed that a small intensity (over 70% of the days, in each month) has recorded in May, June, July, August, September, and October. In addition, the activity in January, November, and December had moderate intensity (over 50% of the days, in each month), and in February and March have recorded a high intensity (over 50% of the days, in each month). March is the month where medium and high intensities are very close (43% and 57%, respectively).

#### 4.4. The Energy Consumption Forecasting

To test the expert system-based method from the forecasting module, the working time and operating characteristics of the equipment and installations were identified based on the analysis of current and voltage measurements done for 1 month, in 2019, with the power analyser Chauvin Arnoux, using a sampling step by 5 s.

To test the expert system-based method from the forecasting module, the working time and operating characteristics of the equipment and installations were identified based on the analysis of current and voltage measurements done for 1 month, in 2019, with the power analyser Chauvin Arnoux, using a sampling step by 5 s.

The measurement equipment was installed in the general electric panel on the main feeder and secondary cables, which feeds each local electric panel. As an example, the consumption profile assigned to a day from the analysed period, recorded on the main feeder, with the identification of different equipment and installations, on which it operates, is presented in Figure 13. The main operations (tinsmith, mechanical repair and car dyeing) highlighted with red circles, associated with the activities of the technological processes, are identified inside the profile through the equipment and installations (air compressor, welding machine, and dyeing machine) with the starting and drying phases and relayed phases), related with the working time. The work on the following factors: the body factors (the body types (M/H/S/L), the equipment (variable, couple convertible, capacitor, thick or soft), the material and the number of components which compose the body which must be dyed.

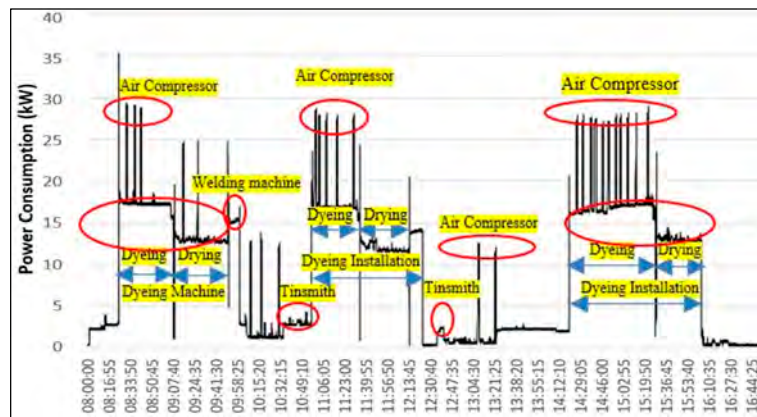


Figure 13. The consumption sampled at 5s in a day with high intensity of the activity.

The analysis of working time corresponding to each equipment and installation led to the following following shares from the total energy consumption: 50.1% dyeing installation, 20.5% air compressor, lighting system, 7.2% other electric equipment (vehicle lift, welding machine, hammer drills, blowers, etc.), and 5.9% reception office, see Figure 14.

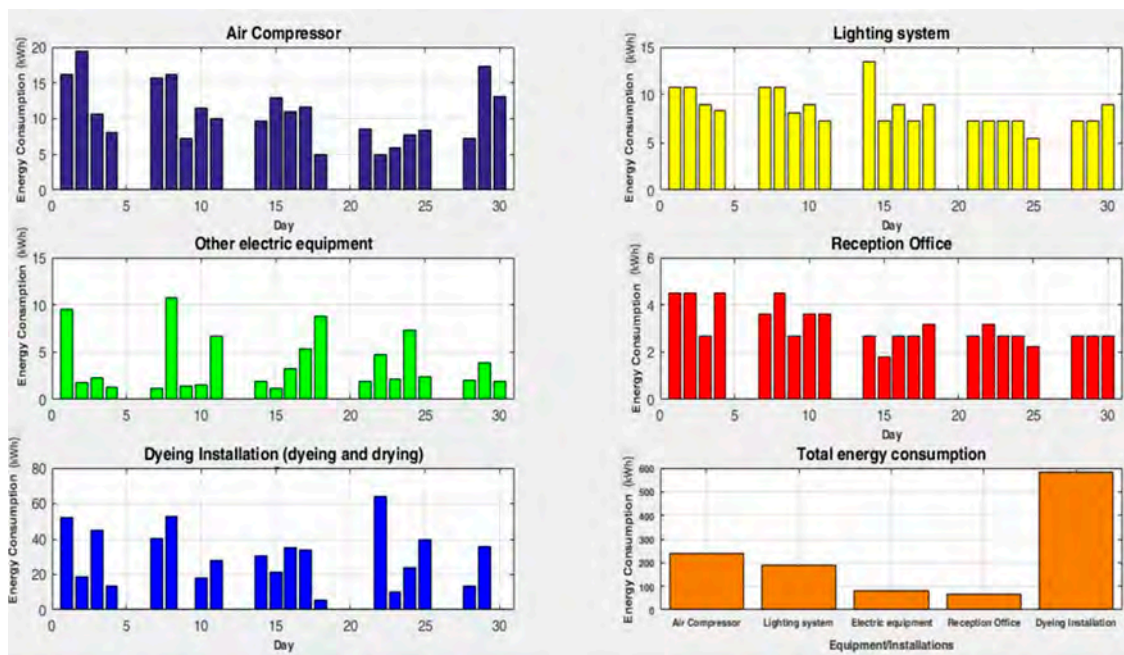


Figure 14. Daily electricity consumption for each equipment and installation in analysed period.

In the weekend periods, or when the equipment or installations did not operate, there is no energy consumption.

In addition, all profiles led to the division of the energy consumptions in three categories (small, medium, and high) considering the working time (reduced, normal, and long) for each equipment and installation, depending on the factors listed above, see Table 8. The first eight positions of the

In the weekend periods, or when the equipment or installations did not operate, there is no energy consumption.

In addition, all profiles led to the division of the energy consumptions in three categories (small, medium, and high) considering the working time (reduced, normal, and long) for each equipment and installation, depending on the factors listed above, see Table 8. The first eight positions of the table correspond to the phases of dyeing installation, which have operating regimes with different values of working times and energy consumptions according to the components (doors, tailgates, fenders, bumpers, etc.) or the whole body of the car.

**Table 8.** The working time and energy consumption of each equipment and installation depending on the intensity of activity.

No.	Equipment and Installation	Working time (Minutes/Hours)			Energy Consumption (kWh)		
		Reduced	Normal	Long	Small	Medium	High
1	Dyeing installation—dyeing phase/R1	90/1.5	120/2	150/2.5	18.75	25.00	31.25
2	Dyeing installation—dyeing phase/R2	90/1.5	120/2	150/2.5	17.25	23.00	28.75
3	Dyeing installation—dyeing phase/R3	42/0.7	60/1	72/1.2	8.75	12.50	15.00
4	Dyeing installation—dyeing phase/R4	42/0.7	60/1	72/1.2	8.05	11.50	13.80
5	Dyeing installation—dyeing phase/R5	42/0.7	60/1	72/1.2	9.94	14.20	17.04
6	Dyeing installation—drying phase/R1	36/0.6	45/0.75	54/0.9	6.72	8.40	10.08
7	Dyeing installation—drying phase/R2	36/0.6	45/0.75	54/0.9	6.3	7.87	9.45
8	Dyeing installation—drying phase/R3	36/0.6	45/0.75	54/0.9	7.5	9.375	11.25
9	Air compressor	51/0.85	66/1.1	81/1.35	8.84	11.44	14.04
11	Welding machine	6/0.1	18/0.3	30/0.5	0.27	0.81	1.35
12	Lighting system—tinsmith building	180/3	420/7	540/9	1.62	3.78	4.86
13	Lighting system—repair building	180/3	420/7	540/9	0.96	2.24	2.88
14	Lighting system—dyeing installation	60/1	120/2	180/3	1.10	2.20	3.30
15	Reception office	0/0	0/0	540/9	0.00	0.00	2.70
16	Various electric equipment	60/1	120/2	180/3	1.00	2.00	3.00
17	Vehicle elevator	1.2/0.02	3.6/0.06	6/0.1	0.04	0.12	0.20

This information helps the Decision-Maker to complete the equipment and installations matrix (EIM) associated with the system expert-based aggregation method.

The Decision-Maker can complete the matrix taken into account the type of operations for each programmed car in the next day. Thus, the information introduced in the matrix depends on the intensity of activity (small, medium, and high) considering the working time (reduced, normal, and long) and energy consumption associated with each equipment and installation and the number of working cycles, if some operations can be repeated to various time intervals.

Figure 15 and Table 9 present the results obtained after testing of the method for a week (16–20 September, where the activity type and the percentage errors are specified. The errors were calculated with the relation:

$$Error = \left| \frac{W_R - W_f}{W_R} \right| \cdot 100, (\%) \tag{18}$$

where  $W_R$  is the real energy consumption and  $W_f$  is the forecasted energy consumption.

**Table 9.** The obtained results using the proposed method.

Day	Monday	Tuesday	Wednesday	Thursday	Friday	Total
Intensity	Small	Medium	Small	Small	Small	
$W_f$ (kWh)	56.88	<b>79.23</b>	45.55	54.85	44.35	280.86
$W_R$ (kWh)	58.31	<b>77.91</b>	43.98	56.2	45.23	281.54
Error (%)	2.45	<b>1.69</b>	3.80	2.40	1.95	0.24



activity, highlighted with bold in Table 9, are presented in Table 10, where the grey cells belong to the Decision-Making Matrix (DMM), and the signification of the rules associated with the expert system being:

**If** (<Equipment or Installation  $k$  is On> **and** <working time is Reduced> **and** <operating cycles are  $Y$ >) **then** (Energy consumption ( $W_f$ ) is  $Z$ ).

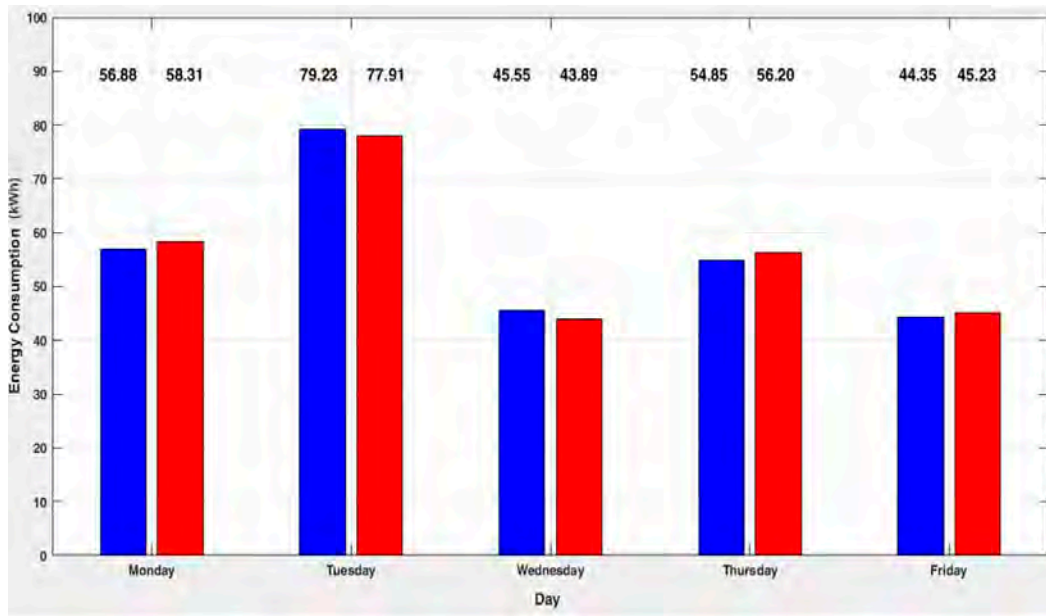


**Figure 15.** The comparison between the real (red) and forecasted (blue) energy consumptions.

It can be observed that the percentage errors are in the range [1.95, 3.80], and the mean absolute percentage error calculated on the analysed period (a week) is 0.24%. These values can be considered very satisfactory for the Decision-Maker in the situation in which the evolution of the activities associated with the technological process is dynamic and uncertainties regarding the execution of specific operations, such as tinsmith and mechanical repairs for each programmed car, can occur. Details about the energy consumption forecasting for the day with the medium intensity of the activity, highlighted with bold in Table 9, are presented in Table 10, where the grey cells belong to the Decision-Making Matrix (DMM), and the signification of the rules associated with the expert system being:

**If** (<Equipment or Installation  $k$  is On> **and** <working time is Reduced> **and** <operating cycles are  $Y$ >) **then** (Energy consumption ( $W_f$ ) is  $Z$ ).

**Table 10.** The Decision Matrix and forecasted energy consumption for Tuesday.

No.	Equipment or Installation	Operating Modes	Working Time	Operating Cycles	$W_f$ (kWh)
1	Dyeing installation—dyeing operation/R1	On	Reduced	2	37.5
2	Dyeing installation—drying operation/R1	On	Reduced	2	13.44
3	Air compressor	On	Long	1	14.04
4	Welding machine	On	Reduced	1	0.27
5	Lighting system—tinsmithing department	On	Long	1	4.86
6	Lighting system—repair department	On	Long	1	2.88
7	Lighting system—dyeing installation	On	Reduced	1	1.1
8	Reception office	On	Long	1	2.7
9	Other electric equipment	On	Reduced	1	1
10	Vehicle elevator	On	Reduced	3	0.12
<b>Total—forecasted energy consumption</b>					<b>77.91</b>

The specific (for each equipment and installation) and total energy consumptions forecasted for Tuesday are highlighted with bold. The results obtained for the other days are presented in Tables A3–A6, Appendix A.

#### 4.5. Production Scheduling

The production scheduling for the next day is established by the Decision-Maker to flatten the energy consumption profile. The combinatorial optimization is used to achieve this objective considering the constraints presented in Section 3.5: the appropriate allocation of the equipment or installations to each activity associated with a technological flow, the working time of each equipment or installation, the phase sequences, and energy consumption balance.

The input data used in the optimization process are the following: the decision on the operating mode (on or off, quantified by 1 or 0), working time (reduced, normal, or long), see Table 8, working cycles (1, 2, or 3), the dependency between equipment, the start and stop working hours, and technical characteristics, see Table 3, which characterize every equipment and installation associated to each activity.

Table 11 presents the input data for the equipment and installations from Tuesday (presented in Section 4.4). The activities programmed in this day required mechanical revisions for three cars, dyeing and drying operations for various components of two cars, mechanical repairs for two cars requiring welding and sheet metal straightening operations, and dyeing preparation for three cars. The optimal solution, presented in Table 12 and Figure 16, has been accepted by the Decision-Maker to ensure continuity of the technological flow.

**Table 11.** The input data matrix (IDM).

No.	Equipment/Installation	Operating Mode	Programmable	Working Time	Operating Cycles	Dependency	Start Hour	Stop Hour
1	Dyeing installation—dyeing operation/R1	On	Yes	Reduced	2	3	8:00	17:00
2	Dyeing installation—drying operation/R1	On	Yes	Reduced	2	1	8:00	17:00
3	Dyeing installation—lighting system	On	No	Reduced	1	2	8:00	17:00
4	Welding machine	On	Yes	Reduced	1	0	8:00	17:00
5	Lighting system—tinsmithing department	On	No	Long	1	0	8:00	17:00
6	Lighting system—repair department	On	No	Long	1	0	8:00	17:00
7	Air compressor	On	No	Long	1	0	8:00	17:00
8	Reception office	On	No	Long	1	0	8:00	17:00
9	Other electric equipment	On	Yes	Reduced	1	0	8:00	17:00
10	Vehicle elevator	On	Yes	Reduced	3	0	8:00	17:00

**Table 12.** The optimal production scheduling for analysed day (Tuesday).

No.	Equipment/Installation	Start Hour	Stop Hour
1	Reception office	8:00	17:00
2	Lighting system—tinsmithing department	8:00	17:00
3	Lighting system—repair department	8:00	17:00
4	Dyeing installation—dyeing operation/R1	8:00	9:30
5	Vehicle elevator	8:05	8:10
6	Air compressor	9:00	17:00
7	Vehicle elevator	9:00	9:05
8	Dyeing installation—drying operation/R1	9:30	10:20
9	Vehicle elevator	10:00	10:05
10	Welding machine	13:00	13:10
11	Lighting system—dyeing installation	13:00	14:00
12	Other electric equipment	13:00	14:00
13	Dyeing installation—dyeing operation/R1	14:00	15:30
14	Dyeing installation—drying operation/R1	15:30	16:20

operation. Usually, for the first use of the dyeing installation, preparing the car is done at the end of the working schedule from the previous day. The dependency expresses the association with one equipment or installation identified through the number of the row in the matrix IDM.

Due to the high energy consumption of dyeing installation and the smaller energy consumptions of other equipment and installations, the flattening of the profile is not very obvious at first glance. However, the analysis of the results presented in Figures 16 and 17 indicates a satisfactory decrease, with 2.95 kWh (16.23%) of the peak value (highlighted with red colour in Figure 17) from 18.17 kWh (recorded at the hour 14) to 15.22 kWh (recorded at the hour 15), after application of the optimization process.

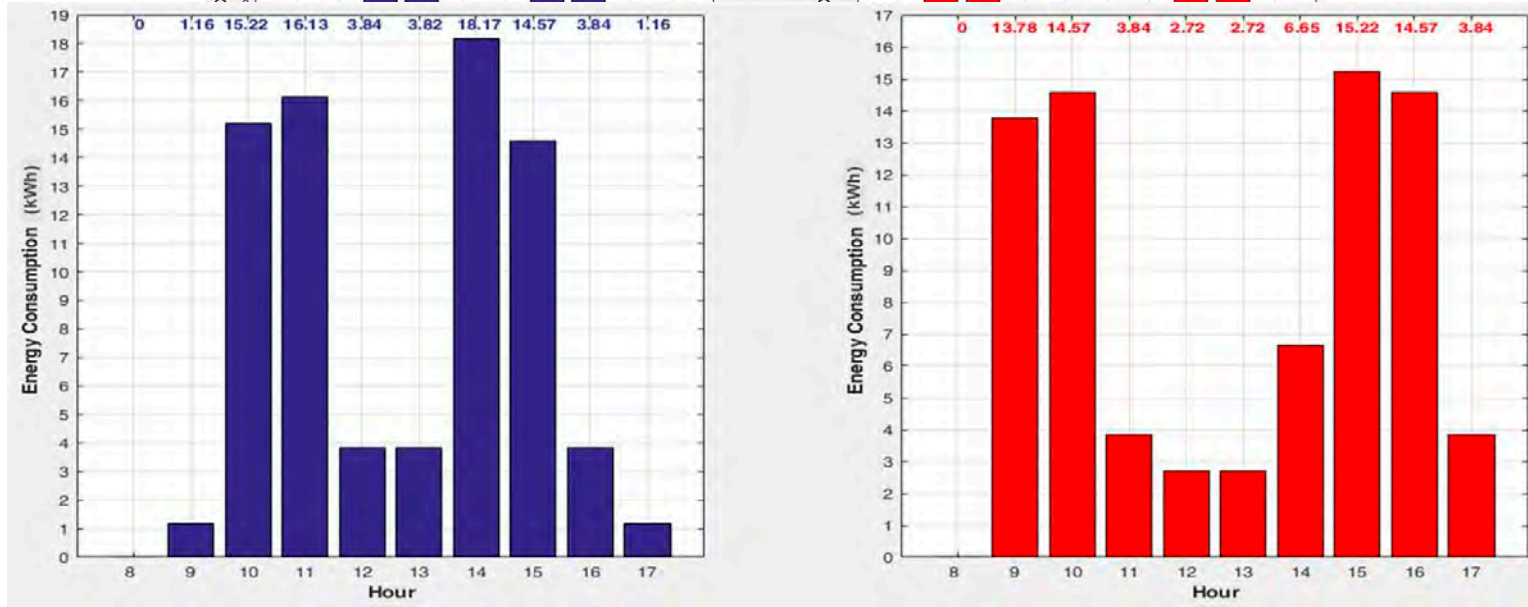


Figure 16. The real (blue) and optimal (red) hourly energy consumptions.

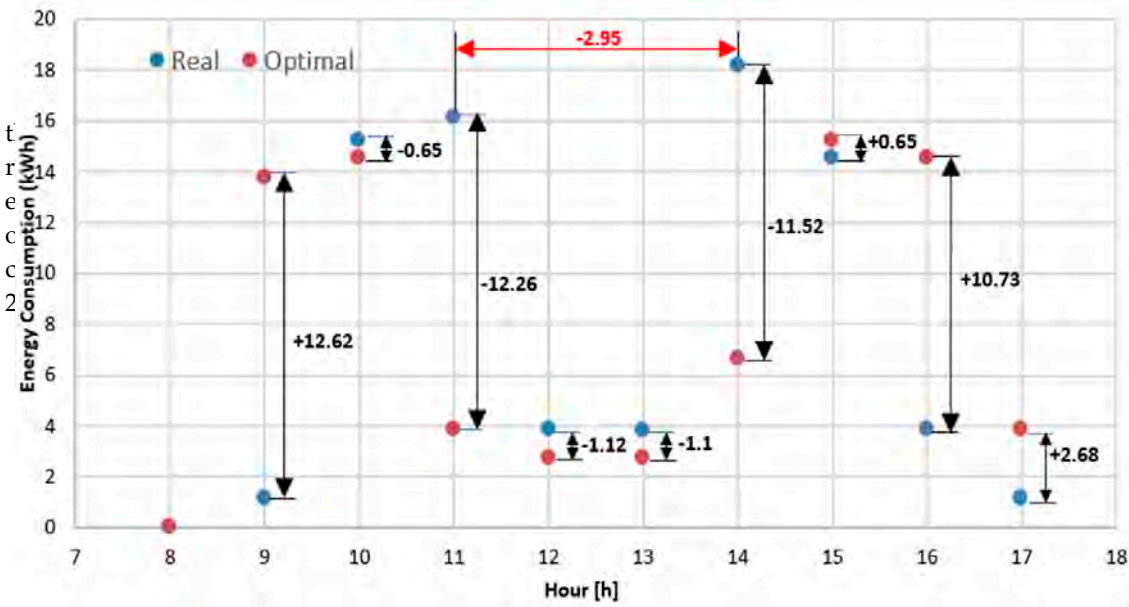


Figure 17. The differences between the real and optimal hourly energy consumptions.

In addition, the standard deviation of the energy consumption and the load factor can quantify the flattening of the energy consumption profile. Regarding the standard deviation, a decrease was recorded from 7.13 to 5.70 kWh. The load factor expresses a measure of the utilization rate, or efficiency of energy usage, being an indicator that quantifies how steady the energy consumption is over time. It represents the mean value of the energy consumption divided by the maximum energy consumption in a specified period (in our case, 1 day). The value of this indicator increased with 21.4%, from 0.42 to 0.51.

represents the mean value of the energy consumption divided by the maximum energy consumption in a specified period (in our case, 1 day). The value of this indicator increased with 21.4%, from 0.42 to 0.51.

## 5. Conclusions and Future Work

Supporting SMEs and the promotion of energy efficiency measures are essential for economic progress because, at the level of the European Union, the SMEs represent 98% of the total number of businesses. Many SMEs have expressed in the last period their interest in the implementation of measures to reduce energy consumption because the energy efficiency is not only a tool to save money and resources but also a need for flexible adaptation to the own needs. The SMEs have needed to implement this plan by software tools to monitor and control the consumption and to identify solutions that allow the adoption of measures to increase energy efficiency.

This paper presents a new vision on the energy consumption management at the SMEs, integrated into a decision support platform, with technical and economic benefits on increasing energy efficiency. The proposed platform has four modules which include Artificial Intelligence techniques (clustering-based unsupervised learning and expert systems) with characteristics that differentiate it and offer more advantages compared to the other similar products or approaches which treated the energy management at the SMEs: (i) *The data management module* is based on the data mining techniques that extract the technical details on the energy consumptions and cost used to develop production scheduling strategies. (ii) *The profiling module* uses an efficient profiling-based method based on clustering techniques to determine the typical energy consumption profiles (TECPs) assigned to different activity types necessary for establishing the type of tariffs that will lead to the reduction of energy bills and optimally planning of the activities. (iii) *The forecasting module* has implemented an original approach that uses an expert system based on the rules If-Then to forecast the energy consumption of each installation and equipment. The total energy consumption at the SME level is forecasted by aggregating all individual energy consumptions of the equipment and installations. (iv) *The production scheduling module* allows the flattening of the energy consumption profiles, using a fast searching algorithm to find the optimal solutions.

The platform can be successfully implemented, but with possible disadvantages (limitations) in the use of the platform at the maximum potential by some SMEs. The first refers to the profiling module, which can be used only if the SME has a smart meter with remote communication. The second is associated with the expert system, where the rules must be developed by qualified staff in energy management. The staff must know the technological processes, the operating regimes, and the characteristics of each equipment and installation very well. The third is linked by the forecasting module, where the same qualified staff must analyse the data from the current and measurements to determine the working times and associated energy consumptions. However, as stated, these three disadvantages are minimized by a qualified human resource, which can ensure efficient energy management to the SMEs using all functions of the platform.

The proposed decision support platform was tested at a small enterprise from Romania with the activity field of the repair of the vehicles. The obtained results demonstrate the ability of the platform to offer the support to the Decision-Maker in solving or understanding the following issues: the planning strategies of the SME based on the evolution of the energy consumption, the intensity of activities through the TECPs, the energy consumption forecasting for different periods (day, week, or month) depending on the scheduled activities, and the production scheduling such that the energy consumption profile to be as flat as possible.

The authors work to develop the decision support platform's functions, considering the particularities of the activities carried out at other SMEs, especially at the forecasting module, testing new methods which to consider the influence of the weather and economic factors, and at the production scheduling module through improving the mathematical model and testing new optimization algorithms.

Another direction considered by the authors refers to develop a new mathematical model which have the objective of the minimization of the energy cost considering the tariff differentiated by hourly zones and durations of energy use. This new model will be integrated into the production scheduling module, being useful for SMEs which have a schedule in three work shifts.

Additionally, the platform can support the implementation of the ISO 50001 standard through developing a new module, which to establish a link between improving energy efficiency, quantified through the results obtained using the other modules, and environmental impact reduction. Through identification of differences between the full application of the requirements from the ISO 50001 standard and the real level of implementation, the platform could provide a compact perspective on how energy management can be implemented in SMEs. In this context, the monitoring and control of energy efficiency indicators at the SME level lead to saving energy amounts and, consequently, to the reduction of greenhouse gas emissions, as the authors pointed in [58].

## 6. Patents

National Patent Application “Software Platform for Integrated Management and Control of Electric Energy and Natural Gas Consumption in Order to Increase Energy Efficiency in Small and Medium-Sized Enterprises”, Romania, 2018, RO132688A0.

**Supplementary Materials:** The following are attached to the paper and available online at <http://www.mdpi.com/2076-3417/10/10/3505/s1>: the excel file with title Daily Energy Consumptions-2019.

**Author Contributions:** Conceptualization, G.G. and B.-C.N.; methodology, G.G.; software, G.G.; validation, B.-C.N. and G.G.; formal analysis, B.-C.N.; investigation, G.G. and B.-C.N.; data curation, B.-C.N.; writing—original draft preparation, G.G. and B.-C.N.; writing G.G. and B.-C.N.; and supervision, G.G. All authors have read and agreed to the published version of the manuscript.

**Funding:** This research received no external funding.

**Acknowledgments:** This paper was realized with the support of national project PN-III-P2-2.1-CI-2017-0190, financed by the Romanian Government.

**Conflicts of Interest:** The authors declare no conflicts of interest.

## Nomenclature and Indices

$a$	The index for activity
$\sigma$	The standard deviation value for a data set
Error	The forecasting error, in (%)
$v_{j,k}$	The variation coefficient associated with the normalized energy consumption $j$ from the TECP corresponding to the cluster $k$
AMR	Automatic meter reading
CC	Cophenetic correlation coefficient
$C_k$	The number of clusters
$c_W$	The energy cost at hour
DBM	Databases management,
DMP	Decision-making process
DC	Matrix with energy costs
DE	Matrix with technical characteristics of equipment and installations
DI	Matrix with economic indicators
DMM	Matrix used in decision-making process
DW	Matrix with hourly energy consumptions
$e$	The index for equipment an installation
EIM	Matrix of equipment and installations' characteristics
ES	Expert system

EU	European Union
$f$	The index for the final product
GHG	Greenhouse gas
$h$	The index for hour
HMI	Human-machine interface
$i$	The index for daily profiles records
IDM	The input data matrix
$j$	The index for a normalized value
$k$	The index for clusters
$l$	The index for energy consumption profiles
RON	The Romanian currency (1 EUR(€) $\approx$ 4.8 RON)
$m$	The sampling step (24, 48, 96)
$n$	The number of records (rows) associated with the selected period.
$n_a$	The necessary activities to obtain the final product
$N_C, N_I$	The number of records from matrices DC and DI identified through months
$n_e^a$	The total number of equipment and installations associated with the activity $a$
$N_E$	The number of records form matrix DE identified through equipment and installations associated with the activities of technological flows
$n_p$	The total number of final products
$N_k$	The number of the energy consumption profiles associated with the cluster $k$
$N_W$	The number of records identified through days
$p$	The number of daily energy consumption profiles
$P_r$	The rated power of equipment or installations, in (kW)
PIEE	Plan to improve energy efficiency
SMEs	Small and medium enterprises
SM	Smart meter
SOS	Schedule and optimization steps
TECPs	Typical energy consumption profiles
$T$	Analysis duration (represented by the work schedule)
$T_H$	Maximum number of hours
$T_{f,a,e,h}^{Start}$	The start hours when the equipment works for final product $f$ , in activity $a$
$T_{f,a,e,h}^{Stop}$	The stop hours when the equipment works for final product $f$ , in activity $a$
$T_{f,a,e}$	The working time of the equipment or installation $e$ necessary to execute the activity $a$ and obtaining the final product $f$
$W$	Matrix with daily energy consumption profiles
$W^{norm}$	Matrix with daily normalized energy consumption profiles
$W_f$	The forecast energy consumption, in (kWh)
$W_R$	The real energy consumption, in (kWh)
$W_r, W_s$	Vector with daily profiles
$W_T$	Energy consumption balance
$\bar{w}_{j,k}$	The mean normalized value $j$ from the TECP associated with cluster $k$
$w_{i,j}^{norm}$	The normalized energy consumption on the column $j$ of the record $i$ from matrix $W^{norm}$ ;
$w_{i,j}$	The energy consumption on the column $j$ of the record $i$ from matrix $W$ ;
$w_{f,a,e,h}$	The energy consumption of equipment or installation $e$ necessary to execute the activity $a$ and obtaining the final product $f$ , at hour $h$
$x_i$	Value $i$ of the analysed variable for a period
$x_{Q1-xQ4}$	Quantiles
$X_{f,a,e,h}$	The decision variable for the allocation of the equipment or installation $e$ necessary to execute the activity $a$ and obtaining the final product $f$ , at hour $h$
$X_{mean}$	Mean of the analysed variable for a period
$X_{median}$	Median value for a data set

Appendix A

**Table A1.** The energy consumptions and costs in period 2018–2019 for the analysed SME.

Year	Month	Energy Consumption (kWh)	Energy Cost (RON)
2018	January	3079	2771.1
2018	February	5124	4611.6
2018	March	3243	2918.7
2018	April	2328	2095.2
2018	May	1901	1710.9
2018	June	1586	1427.4
2018	July	1452	1306.8
2018	August	1247	1122.3
2018	September	1257	1131.3
2018	October	1525	1372.5
2018	November	1902	1711.8
2018	December	1444	1299.6
2019	January	1631	1467.9
2019	February	2496	2246.4
2019	March	2312	2080.8
2019	April	1121	1008.9
2019	May	1068	961.2
2019	June	981	882.9
2019	July	1311	1179.9
2019	August	1102	991.8
2019	September	1170	1053
2019	October	1258	1132.2
2019	November	1632	1468.8
2019	December	1245	1120.5

**Table A2.** The typical energy consumption profiles, with a sampling size by quarter-hour, (kW/kWh).

Time	TECP1	TECP2	TECP3	TECP4	TECP5	TECP6
8.00	0	0	0	0	0	0
8.15	0.013393	0.013546	0.00824	0.013743	0.025376	0.01486
8.30	0.020021	0.026507	0.044887	0.020557	0.011842	0.024762
8.45	0.010969	0.014523	0.066527	0.040442	0.014045	0.029301
9.00	0.012846	0.017007	0.068519	0.109211	0.016504	0.044817
9.15	0.013507	0.017882	0.065193	0.111	0.021013	0.045719
9.30	0.014613	0.019347	0.065672	0.111922	0.015827	0.045476
9.45	0.018536	0.024541	0.060686	0.094925	0.027276	0.045193
10.00	0.011187	0.014812	0.057842	0.073206	0.011177	0.033645
10.15	0.010126	0.013406	0.049854	0.02452	0.022393	0.02406
10.30	0.016103	0.066158	0.04727	0.027263	0.016385	0.034636
10.45	0.019867	0.081688	0.044046	0.022762	0.047602	0.043193
11.00	0.016438	0.077147	0.044217	0.027246	0.074112	0.047832
11.15	0.01608	0.076673	0.012813	0.028857	0.073863	0.041657
11.30	0.013209	0.066332	0.006438	0.01836	0.071153	0.035098
11.45	0.014794	0.063396	0.007748	0.010106	0.072508	0.03371
12.00	0.029751	0.027441	0.006127	0.014857	0.068217	0.029279
12.15	0.058908	0.013544	0.003259	0.010266	0.052588	0.027713
12.30	0.060449	0.015448	0.005241	0.012511	0.054677	0.029665
12.45	0.064205	0.024973	0.03567	0.02365	0.055576	0.040815
13.00	0.057353	0.035752	0.049937	0.03318	0.059907	0.047226
13.15	0.054069	0.027779	0.048676	0.016543	0.025673	0.034548
13.30	0.063544	0.029028	0.043144	0.015834	0.016856	0.033681
13.45	0.05829	0.023955	0.04559	0.015996	0.012796	0.031325
14.00	0.058978	0.020694	0.026417	0.020015	0.01208	0.027637
14.15	0.064176	0.019569	0.01603	0.020568	0.008919	0.025853
14.30	0.050953	0.014842	0.013367	0.01153	0.012401	0.020619
14.45	0.045234	0.018562	0.007353	0.017264	0.014335	0.020549
15.00	0.042431	0.018399	0.00761	0.015332	0.017352	0.020225
15.15	0.013158	0.022855	0.008893	0.01117	0.017748	0.014765
15.30	0.013661	0.038599	0.007585	0.012979	0.017039	0.017972
15.45	0.027921	0.027516	0.011979	0.008311	0.01638	0.018421
16.00	0.015231	0.028079	0.01317	0.005874	0.01638	0.015747
16.15	0.013393	0.013546	0.00824	0.013743	0.025376	0.01486
16.30	0.012846	0.012007	0.00619	0.010211	0.020504	0.009817
16.45	0.00846	0.010007	0.00319	0.008211	0.010504	0.007817
17.00	0.00546	0.003071	0.00119	0.006211	0.004504	0.003817

**Table A3.** The Decision Matrix and forecasted energy consumption for Monday.

No.	Equipment or Installation	Operating Modes	Working Time	Operating Cycles	$W_f$ (kWh)
1	Dyeing installation—dyeing operation/R4	On	Reduced	1	8.05
2	Dyeing installation—dyeing operation/R4	On	Long	1	13.80
3	Dyeing installation—drying operation/R2	On	Long	1	9.45
3	Air compressor	On	Reduced	1	8.84
4	Welding machine	Off	–	–	–
5	Lighting system—tinsmithing department	On	Long	1	4.86
6	Lighting system—repair department	On	Long	1	2.88
7	Lighting system—dyeing installation	On	Long	1	3.30
8	Reception office	On	Long	1	2.70
9	Other electric equipment	On	Long	1	3
10	Vehicle elevator	Off	–	–	–
<b>Total—forecasted energy consumption</b>					<b>56.88</b>

**Table A4.** The Decision Matrix and forecasted energy consumption for Wednesday.

No.	Equipment or Installation	Operating Modes	Working Time	Operating Cycles	$W_f$ (kWh)
1	Dyeing installation—dyeing operation/R4	On	Long	1	13.80
2	Dyeing installation—drying operation/R1	On	Normal	1	7.87
3	Air compressor	On	Normal	1	11.44
4	Welding machine	Off	–	–	–
5	Lighting system—tinsmithing department	On	Long	1	4.86
6	Lighting system—repair department	On	Long	1	2.88
7	Lighting system—dyeing installation	On	Reduced	1	1.10
8	Reception office	On	Long	1	2.70
9	Other electric equipment	On	Reduced	1	1.00
10	Vehicle elevator	Off	–	–	–
<b>Total—forecasted energy consumption</b>					<b>45.65</b>

**Table A5.** The Decision Matrix and forecasted energy consumption for Thursday.

No.	Equipment or Installation	Operating Modes	Working Time	Operating Cycles	$W_f$ (kWh)
1	Dyeing installation—dyeing operation/R4	On	Normal	1	11.50
2	Dyeing installation—dyeing operation/R4	On	Reduced	1	8.05
3	Dyeing installation—drying operation/R2	On	Normal	1	7.87
3	Air compressor	On	Normal	1	11.44
4	Welding machine	On	Long	1	1.35
5	Lighting system—tinsmithing department	On	Long	1	4.86
6	Lighting system—repair department	On	Long	1	2.88
7	Lighting system—dyeing installation	On	Normal	1	2.20
8	Reception office	On	Long	1	2.70
9	Other electric equipment	On	Normal	1	2.00
10	Vehicle elevator	Off	–	–	–
<b>Total—forecasted energy consumption</b>					<b>54.85</b>

**Table A6.** The Decision Matrix and forecasted energy consumption for Friday.

No.	Equipment or Installation	Operating Modes	Working Time	Operating Cycles	$W_f$ (kWh)
1	Dyeing installation—dyeing operation/R4	On	Normal	1	11.50
2	Dyeing installation—drying operation/R2	On	Normal	1	7.87
3	Air compressor	On	Normal	1	11.44
4	Welding machine	Off	–	–	–
5	Lighting system—tinsmithing department	On	Long	1	4.86
6	Lighting system—repair hall	On	Long	1	2.88
7	Lighting system—dyeing department	On	Reduced	1	1.1
8	Reception office	On	Long	1	2.7
9	Other electric equipment	On	Normal	1	2.0
10	Vehicle elevator	Off	–	–	–
<b>Total—forecasted energy consumption</b>					<b>44.35</b>

## References

1. European Commission, Europe. A European Strategy for Smart, Sustainable and Inclusive Growth, Brussels. 2020. Available online: <https://ec.europa.eu/eu2020/pdf/COMPLET%20EN%20BARROSO%20%20%2020007%20-%20Europe%202020%20-%20EN%20version.pdf> (accessed on 25 April 2020).



2. European Commission. Towards a Sustainable Europe by 2030. Available online: [https://ec.europa.eu/info/publications/towards-sustainable-europe-2030\\_en](https://ec.europa.eu/info/publications/towards-sustainable-europe-2030_en) (accessed on 25 April 2020).
3. Sánchez Nicolás, E. Why Is EU off Track for 2020 Energy Efficiency Target? Available online: <https://euobserver.com/energy/147407> (accessed on 9 May 2020).
4. Eurostat, Energy Consumption in 2018. Primary and Final Energy Consumption still 5% and 3% away from 2020 Targets. Available online: <https://ec.europa.eu/eurostat/documents/2995521/10341545/8-04022020-BP-EN.pdf/39dcc365-bdaa-e6f6-046d-1b4d241392ad> (accessed on 9 May 2020). (In Romanian).
5. Pineaudit. SMES and the EU Directive 27/2012 on Energy Efficiency. Available online: <http://pineaudit.eu/ro/stiri-si-evenimente/direttiva.aspx> (accessed on 25 April 2020).
6. Romanian Government. Public Bodies and SMEs, Encouraged to Use Energy Efficiently. Available online: <https://www.gov.ro/ro/guvernul/sedinte-guvern/organismele-publice-i-imm-incurajate-sa-utilizeze-efficient-energia> (accessed on 25 April 2020). (In Romanian)
7. The EU Directive 27/2012 on Energy Efficiency, Brussels. 25 October 2012. Available online: <https://eur-lex.europa.eu/legal-content/EN/TXT/HTML/?uri=CELEX:32012L0027&from=EN> (accessed on 25 April 2020).
8. KeysFin. SME STUDY—Small and Medium Enterprises in Romania. Available online: <https://www.keysfin.com/#/Pages/News/NewsDetails&title=studiu-imm-uri-din-romania> (accessed on 25 April 2020). (In Romanian).
9. Papadopoulos, G.; Rikama, R.; Alajääskö, P.; Salah-Eddine, Z.; Airaksinen, A.; Luomaranta, H. Statistics on Small and Medium-Sized Enterprises. Available online: [https://ec.europa.eu/eurostat/statistics-explained/index.php?title=Statistics\\_on\\_small\\_and\\_medium-sized\\_enterprises](https://ec.europa.eu/eurostat/statistics-explained/index.php?title=Statistics_on_small_and_medium-sized_enterprises) (accessed on 25 April 2020).
10. Frédéric Simon. Europe Eyes ‘Big Bang’ in Power Savings from Industry, SMEs. Available online: <https://www.euractiv.com/section/energy/news/europe-eyes-big-bang-in-power-savings-from-industry-smes/> (accessed on 25 April 2020).
11. Engine, Energy Efficient Technologies for Industry and Best Practice. Available online: [http://www.engine-sme.eu/fileadmin/SME-Uploads/D15/ENGINE\\_WP5\\_D15\\_EN.pdf](http://www.engine-sme.eu/fileadmin/SME-Uploads/D15/ENGINE_WP5_D15_EN.pdf) (accessed on 25 April 2020).
12. Ionascu, M.; Ionascu, I.; Sacarin, M.; Minu, M. Exploring the impact of ISO 9001, ISO 14001 and OHSAS 18001 certification on financial performance: The case of companies listed on the Bucharest Stock Exchange. *Am. Econ. J.* **2017**, *19*, 166–180.
13. International Organization for Standardization, ISO 50001. Energy Management. Available online: <https://www.iso.org/standard/69426.html> (accessed on 10 May 2020).
14. Schneider Electric. PowerLogic Power Monitoring System. Available online: <https://www.se.com/ww/en/product-category/4100-power-monitoring-and-control/> (accessed on 25 April 2020).
15. Siemens. SIMATIC Energy Management. Available online: <https://new.siemens.com/global/en/products/automation/industry-software/automation-software/energymanagement/simatic-energy-manager-pro.html> (accessed on 25 April 2020).
16. ABB. Energy Management Software. Available online: <http://new.abb.com/cpm/energy-manager> (accessed on 25 April 2020).
17. ELSACO. Elsaco Meter Management System. Available online: [http://www.elsaco.com/wp-content/uploads/2012/12/elsaco\\_articol\\_d3\\_romaqua.pdf](http://www.elsaco.com/wp-content/uploads/2012/12/elsaco_articol_d3_romaqua.pdf) (accessed on 25 April 2020). (In Romanian).
18. Quartz-Matrix, e-Net. Available online: <https://www.quartzmatrix.ro/sistem-enet-monitorizare-energie-consumatori-industriali/> (accessed on 25 April 2020). (In Romanian).
19. Zucchetti. ZEnergy. Available online: <http://www.zucchettiromania.com/romania/cms/product/3273-zenergy.html> (accessed on 25 April 2020). (In Romanian).
20. Woolard, J.; Fong, D.; Dell’Era, P.; Gipson, K. Energy Management System and Method, Brevet US 6178362 B1. Available online: <https://patents.google.com/patent/US6178362B1/en> (accessed on 25 April 2020).
21. Miller, C.H. Optimized Energy Management System, Brevet US 7274975 B2. Available online: <http://www.google.com/patents/US7274975> (accessed on 25 April 2020).
22. The EU H2020 Research Project SMEmPower Efficiency. Available online: <https://smempower.com/> (accessed on 25 April 2020).
23. SME Program for Energy Efficiency through Delivery and Implementation of Energy Audits. Available online: <https://speedierproject.eu/2019/06/10/speedier-the-sme-program-for-energy-efficiency-through-delivery-and-implementation-of-energy/> (accessed on 25 April 2020).

24. Janda, K.B.; Bottrill, C.; Layberry, R. Learning from the “data poor”: Energy management in understudied organizations. *J. Prop. Invest. Financ.* **2014**, *32*, 424–442. [CrossRef]
25. Hampton, S.; Fawcett, T. *Challenges of Designing and Delivering Effective SME Energy Policy*; European Council for an Energy Efficient Economy: Stockholm, Sweden, 2017; Available online: [https://www.eceee.org/library/conference\\_proceedings/eceee\\_Summer\\_Studies/2017/1-foundations-of-future-energy-policy/challenges-of-designing-and-delivering-effective-sme-energy-policy/](https://www.eceee.org/library/conference_proceedings/eceee_Summer_Studies/2017/1-foundations-of-future-energy-policy/challenges-of-designing-and-delivering-effective-sme-energy-policy/) (accessed on 25 April 2020).
26. Lee, T.E.; Haben, S.A.; Grindrod, P. Modelling the electricity consumption of small to medium enterprises. In *European Consortium for Mathematics in Industry*; Springer: Basel, Switzerland, 2014; pp. 341–349.
27. Wajer, B.H.; Helgerud, S.H.E.; As, N.E.P. Energy Management and Benchmarking in Small and Medium Enterprises. *New Energy Perform. ACEEE* **2007**, *6*, 48–59.
28. Trombley, D. *One Small Step for Energy Efficiency: Targeting Small and Medium-Sized Manufacturers*; American Council for an Energy Efficient Economy: Washington, DC, USA, 2014. Available online: <https://www.nist.gov/system/files/documents/2017/04/28/ACEE.pdf> (accessed on 25 April 2020).
29. Fleitera, T.; Schleich, J.; Ravivanpong, P. Adoption of energy-efficiency measures in SMEs—An empirical analysis based on energy audit data. *Energy Policy* **2012**, *51*, 863–875. [CrossRef]
30. Bröckl, M.; Illman, J.; Oja, L.; Vehviläinen, I. *Energy Efficiency in Small and Medium Sized Enterprises*; Nordic Council of Ministers: Copenhagen, Denmark, 2014.
31. Yin, K.H. Dynamic Optimisation for Energy Efficiency of Injection Moulding Process. Ph.D. Thesis, University of Nottingham, Nottingham, UK, 2015.
32. Kähkönen, S.; Vakkilainen, E.; Laukkanen, T. Impact of Structural Changes on Energy Efficiency of Finnish Pulp and Paper Industry. *Energies* **2019**, *12*, 3689. [CrossRef]
33. Soepardi, A.; Pratikto, P.; Santoso, P.B.; Tama, I.P.; Thollander, P. Linking of Barriers to Energy Efficiency Improvement in Indonesia’s Steel Industry. *Energies* **2018**, *11*, 234. [CrossRef]
34. Haraldsson, J.; Johansson, M.T. Barriers to and Drivers for Improved Energy Efficiency in the Swedish Aluminium Industry and Aluminium Casting Foundries. *Sustainability* **2019**, *11*, 2043. [CrossRef]
35. Johansson, I.; Mardan, N.; Cornelis, E.; Kimura, O.; Thollander, P. Designing Policies and Programmes for Improved Energy Efficiency in Industrial SMEs. *Energies* **2019**, *12*, 1338. [CrossRef]
36. Henriques, J.; Catarino, J. Motivating towards energy efficiency in small and medium enterprises. *J. Clean. Prod.* **2016**, *139*, 42–50. [CrossRef]
37. Melnik, A.; Ermolaev, K. Strategy Context of Decision Making for Improved Energy Efficiency in Industrial Energy Systems. *Energies* **2020**, *13*, 1540. [CrossRef]
38. Melnik, A.N.; Ermolaev, K.A. An optimization approach to program development for energy saving and energy efficiency enhancement at enterprises. *Econ. Anal. Theory Pract.* **2019**, *18*, 200–216. [CrossRef]
39. Hrovatin, N.; Dolšak, N.; Zorić, J. Factors impacting investments in energy efficiency and clean technologies: Empirical evidence from Slovenian manufacturing firms. *J. Clean. Prod.* **2016**, *127*, 475–486. [CrossRef]
40. Miao, C.; Fang, D.; Sun, L.; Luo, Q.; Yu, Q. Driving effect of technology innovation on energy utilization efficiency in strategic emerging industries. *J. Clean. Prod.* **2018**, *170*, 1177–1184. [CrossRef]
41. Meng, B.; Liu, Y.; Andrew, R.; Zhou, M.; Hubacek, K.; Xue, J.; Peters, G.; Gao, Y. More than half of China’s CO<sub>2</sub> emissions are from micro, small and medium-sized enterprises. *Appl. Energy* **2018**, *230*, 712–725. [CrossRef]
42. Thollander, P.; Paramonova, S.; Cornelis, E.; Kimura, O.; Trianni, A.; Karlsson, M.; Cagno, I.; Morales, I.; Navarro, J.P.J. International study on energy end-use data among industrial SMEs (small and medium-sized enterprises) and energy end-use efficiency improvement opportunities. *J. Clean. Prod.* **2015**, *104*, 282–296. [CrossRef]
43. Richert, M. An energy management framework tailor-made for SMEs: Case study of a German car company. *J. Clean. Prod.* **2017**, *164*, 221–229. [CrossRef]
44. Narasimha, C.; Nagesha, N. Energy efficiency in sustainable development of Small and Medium Enterprises: An empirical study. In Proceedings of the 2013 7th International Conference on Intelligent Systems and Control (ISCO), Coimbatore, India, 4–5 January 2013; pp. 487–491.
45. Trianni, A.; Cagno, E.; Worrell, E. Innovation and adoption of energy efficient technologies: An exploratory analysis of Italian primary metal manufacturing SMEs. *Energy Policy* **2013**, *61*, 430–440. [CrossRef]

46. Viesi, D.; Pozzar, F.; Federici, A.; Crema, L.; Mahbub, M.S. Energy efficiency and sustainability assessment of about 500 small and medium-sized enterprises in Central Europe region. *Energy Policy* **2017**, *105*, 363–374. [CrossRef]
47. Dey, P.K.; Malesios, C.; De, D.; Chowdhury, S.; Abdelaziz, F.B. The Impact of Lean Management Practices and Sustainably-Oriented Innovation on Sustainability Performance of Small and Medium-Sized Enterprises: Empirical Evidence from the UK. *Br. J. Manag.* **2020**, *31*, 141–161. [CrossRef]
48. Dey, P.K.; Malesios, C.; De, D.; Chowdhury, S.; Abdelaziz, F.B. Could Lean Practices and Process Innovation Enhance Supply Chain Sustainability of Small and Medium-Sized Enterprises? *Bus. Strategy Environ.* **2019**, *28*, 582–598. [CrossRef]
49. Warren, P. The Potential of Smart Technologies and Micro-Generation in UK SMEs. *Energies* **2017**, *10*, 1050. [CrossRef]
50. Marinakis, V. Big Data for Energy Management and Energy-Efficient Buildings. *Energies* **2020**, *13*, 1555. [CrossRef]
51. Amasyali, K.; El-Gohary, N.M. A review of data-driven building energy consumption prediction studies. *Renew. Sustain. Energy Rev.* **2018**, *81*, 1192–1205. [CrossRef]
52. Grigoras, G.; Neagu, B.C.; Scarlatache, F.L. Influence of Sampling Size in Profiling Process of Electricity Consumption at Small and Medium Enterprises. In Proceedings of the 2018 International Conference and Exposition on Electrical and Power Engineering (EPE), Iasi, Romania, 18–19 October 2018.
53. Neagu, B.C.; Grigoras, G.; Scarlatache, F.L.; Schreiner, C.; Ciobanu, R. Patterns discovery of load curves characteristics using clustering based data mining. In Proceedings of the 11th IEEE International Conference on Compatibility, Power Electronics and Power Engineering (CPE-POWERENG), Cadiz, Spain, 4–6 April 2017.
54. Grigoras, G.; Neagu, B.C. Energy Consumption Forecasting to Small and Medium Enterprises Using a Hybrid Method. In Proceedings of the 2018 International Symposium on Fundamentals of Electrical Engineering (ISFEE), Bucharest, Romania, 1–3 November 2018.
55. Grigoras, G.; Neagu, B.C.; Ivanov, O. Aggregate Method based on Expert System for Electricity Consumption Forecasting of Small and Medium Enterprises. In Proceedings of the 2019 11th International Symposium on Advanced Topics in Electrical Engineering (ATEE), Bucharest, Romania, 28–30 March 2019.
56. Grigoras, G.; Neagu, B.C.; Ivanov, O. An Efficient Approach for Flattening the Electricity Consumption Profile at Small and Medium Enterprises. In Proceedings of the 2019 8th International Conference on Modern Power Systems (MPS), Cluj Napoca, Romania, 21–23 May 2019.
57. EFIENER. Integrated Control and Management Platform of Energy Carriers Flows for Increasing Energy Efficiency at SMEs. Available online: <http://www.gheorghe-grigoras.ieeia.tuiasi.ro/efiener.html> (accessed on 25 April 2020). (In Romanian).
58. Neagu, B.C.; Grigoras, G. Decision-Making Approach for Choosing of Electricity Supplier to Improve the Energy Efficiency. In Proceedings of the 2019 International Conference on Energy and Environment (CIEM), Timisoara, Romania, 17–18 October 2019; pp. 343–347.



© 2020 by the authors. Licensee MDPI, Basel, Switzerland. This article is an open access article distributed under the terms and conditions of the Creative Commons Attribution (CC BY) license (<http://creativecommons.org/licenses/by/4.0/>).

Power Systems

Bhargav Appasani  
Nicu Bizon *Editors*

# Smart Grid 3.0

Computational and Communication  
Technologies

 Springer

# **Power Systems**

Electrical power has been the technological foundation of industrial societies for many years. Although the systems designed to provide and apply electrical energy have reached a high degree of maturity, unforeseen problems are constantly encountered, necessitating the design of more efficient and reliable systems based on novel technologies. The book series Power Systems is aimed at providing detailed, accurate and sound technical information about these new developments in electrical power engineering. It includes topics on power generation, storage and transmission as well as electrical machines. The monographs and advanced textbooks in this series address researchers, lecturers, industrial engineers and senior students in electrical engineering.

**\*\*Power Systems is indexed in Scopus\*\***

Bhargav Appasani · Nicu Bizon  
Editors

# Smart Grid 3.0

Computational and Communication  
Technologies

 Springer

*Editors*

Bhargav Appasani  
School of Electronics Engineering  
Kalinga Institute of Industrial Technology  
Bhubaneswar, India

Nicu Bizon  
Faculty of Electronics Communications  
and Computers  
The National University of Science  
and Technology POLITEHNICA  
Bucharest, Pitești University Centre  
Pitești, Romania

ISSN 1612-1287

ISSN 1860-4676 (electronic)

Power Systems

ISBN 978-3-031-38505-6

ISBN 978-3-031-38506-3 (eBook)

<https://doi.org/10.1007/978-3-031-38506-3>

© The Editor(s) (if applicable) and The Author(s), under exclusive license to Springer Nature Switzerland AG 2023

This work is subject to copyright. All rights are solely and exclusively licensed by the Publisher, whether the whole or part of the material is concerned, specifically the rights of translation, reprinting, reuse of illustrations, recitation, broadcasting, reproduction on microfilms or in any other physical way, and transmission or information storage and retrieval, electronic adaptation, computer software, or by similar or dissimilar methodology now known or hereafter developed.

The use of general descriptive names, registered names, trademarks, service marks, etc. in this publication does not imply, even in the absence of a specific statement, that such names are exempt from the relevant protective laws and regulations and therefore free for general use.

The publisher, the authors, and the editors are safe to assume that the advice and information in this book are believed to be true and accurate at the date of publication. Neither the publisher nor the authors or the editors give a warranty, expressed or implied, with respect to the material contained herein or for any errors or omissions that may have been made. The publisher remains neutral with regard to jurisdictional claims in published maps and institutional affiliations.

This Springer imprint is published by the registered company Springer Nature Switzerland AG  
The registered company address is: Gewerbestrasse 11, 6330 Cham, Switzerland



# Foreword

This book discusses the recent developments in computational techniques and communication infrastructure that has led to the modernization of the smart grid.

It is obvious that now the smart grid represents an evolved version of the electrical grid, with improved monitoring and control capabilities, which continues to be improved in future implementations.

So, this book discusses emerging computational technologies, such as cloud computing, blockchain, deep learning, machine learning, big-data analytics, etc. along with the emerging communication technologies, such as the 5G, internet of things (IoT), etc., encompassing several applications, such as electric vehicles, wide-area monitoring systems, home automation, advanced metering infrastructure, etc., from the perspective of modernization of smart grid.

This book is the first of its kind on smart grid's upgrade to version 3.0, discussing the current status of emerging technologies and the utility of big data analytics, blockchain, cloud computing, deep learning IoT, etc., on the existing smart grid applications to infuse them with intelligence and make them proactive.

Thus, the content of this book is interdisciplinary, involving knowledge of electrical and electronics engineering, communication, signal processing, data analysis and artificial intelligence (machine learning, deep learning, etc.) and optimization. Therefore, the content of this book is addressed to students and specialists (researchers and engineers) in electrical engineering, power systems, communication, data scientists, and for industry personnel to develop grid with proactive intelligence and the techniques used in its design.

In conclusion, it is noteworthy that the content of the book chapters is presented gradually and theoretically in detail as necessary to understand the problems and

effective techniques for implementing the smart grid with proactive intelligence, being highly recommended for study in education and research.

May 2023

Prof. Dr. habil. Phatiphat Thounthong  
King Mongkut's University  
of Technology North Bangkok  
Bangkok, Thailand

# Preface

The power grid has come a long way since its inception, evolving from a simple system for delivering electricity to a complex and intelligent network. Today, we stand at the cusp of a new era in power grid systems—Smart Grid 3.0. This edited book, titled *Smart Grid 3.0: Computational and Communication Technologies*, comprising of 15 chapters, explores the advancements in computational and communication technologies that have paved the way for this next phase of evolution in the power grid.

The first chapter “[Smart Grid 3.0: Grid with Proactive Intelligence](#)” sets the stage by introducing the concept of Smart Grid 3.0, highlighting its key aspect of proactive intelligence. This chapter emphasizes the importance of emerging technologies like artificial intelligence, the Internet of Things, blockchain, big data, 5G, edge computing, and cloud computing in equipping the power grid with proactive intelligence. By gathering and analyzing real-time data, the grid can make informed decisions and take pre-emptive actions to optimize its performance.

The second chapter “[Blockchain for Energy Management: Smart Meters, Home Automation, and Electric Vehicles](#)” delves into the application of blockchain technology in energy management, particularly in the context of smart meters, home automation, and electric vehicles. The chapter explores the decentralized architecture of blockchain, its potential benefits in the energy sector, and how it can enable the creation of neighborhood microgrids and eliminate intermediaries between producers and consumers.

In the third chapter “[Engineering Applications of Blockchain Based Crowdsourcing Concept in Active Distribution Grids](#)”, the focus shifts to the concept of crowdsourcing in active distribution grids. The chapter explores how crowdsourcing can help mitigate energy scarcity and promote the selling of energy produced by small-scale distributed energy sources. It discusses the potential benefits for prosumers, distribution network operators, and consumers, highlighting the need for a comprehensive methodology to ensure efficient and sustainable energy provisioning.

The fourth chapter “[Machine Learning-Based Approaches for Transmission Line Fault Detection Using Synchrophasor Measurements in a Smart Grid](#)” addresses the

crucial issue of fault detection in transmission lines using synchrophasor measurements. The chapter highlights the role of machine learning-based approaches, such as K-Nearest Neighbour, Support Vector Machine, and Logistic Regression, in effectively detecting and classifying faults. Real-time implementation of these algorithms on a physical laboratory transmission line is presented, showcasing their effectiveness in ensuring the reliability and stability of transmission lines.

Power quality analysis takes the center stage in the fifth chapter “[Data Mining-Based Approaches in the Power Quality Analysis](#)”. The chapter discusses the challenges associated with maintaining high power quality in distribution networks and proposes the use of data mining techniques for power quality monitoring and analysis. By extracting relevant features from current and voltage measurements, these techniques can identify areas with power quality issues and assist decision-makers in improving the performance of electric distribution networks.

The sixth chapter “[Machine Learning and Deep Learning Approaches for Energy Management in Smart Grid 3.0](#)” focuses on the application of machine learning and deep learning approaches in energy management systems within smart grids. With the increasing complexity of energy systems, these techniques offer valuable tools for analyzing large amounts of data and optimizing energy usage. The chapter reviews various machine learning and deep learning algorithms, their critical applications, advantages, and disadvantages in the context of smart grids.

The seventh chapter “[Evolutionary Algorithms for Load Frequency Control of Renewable Microgrid](#)” explores load frequency control (LFC) in renewable microgrids. The chapter discusses the challenges posed by heavy fluctuations in voltage and frequency in islanded multi-microgrid systems. It introduces evolutionary algorithms such as Gravitational Search Algorithm, Particle Swarm Optimization, Teaching Learning-based Optimization, and Grey Wolf Optimization for optimizing the parameters of PID controllers, enhancing the dynamic performance of microgrids.

In the eighth chapter “[Agents-Based Energy Scheduling of EVs and Smart Homes in Smart Grid](#)”, the focus shifts to energy scheduling in smart grids, specifically for electric vehicles and smart homes. The chapter presents optimal energy scheduling techniques using agents-based approaches, enabling energy flow control and minimizing electricity costs. It highlights the integration of renewable energy sources, energy storage systems, and EV charging points in smart homes, emphasizing the benefits of energy management and optimization techniques.

In the ninth chapter “[Advanced Control Functionalities of Smart Grids from Communication and Computational Perspectives](#)”, the authors shed light on the sophisticated control schemes necessary to manage the complexity of Smart Grid 3.0. This chapter emphasizes the increasing requirements for communication and computational capabilities as control strategies become more advanced. It provides an overview of the advanced control functionalities of key components such as transmission and distribution systems, microgrids, distributed energy resources, and smart homes.

The tenth chapter “[Multistage PD-\(1+PI\) Controller Design for Frequency Control of a Microgrid Considering Demand Response Program](#)”, addresses the crucial issue

of load-frequency control in fully-renewable microgrids. The chapter presents a multistage controller design that combines Proportional Derivative (PD) and One + Proportional Integral (1+PI) controllers to ensure system stability and responsiveness. Furthermore, it explores the integration of demand response programs to compensate for the uncertainties and nonlinear variables inherent in microgrid operations.

The eleventh chapter is titled “[Solid State Transformer: Topologies, Design and Its Applications in a Smart Grid](#)”. The chapter highlights the significance of Solid State Transformers (SST) in enhancing the grid’s efficiency, monitoring, and control capabilities. It discusses the design process of SSTs, including power electronic converters and medium or high-frequency transformer design. The chapter also explores the role of SSTs in the Energy Internet as Energy Routers, showcasing their potential in improving reliability and power density.

The twelfth chapter “[Emerging Communication Technologies for V2X: Standards and Protocols](#)”, explores the integration of Electric Vehicles (EVs) into Intelligent Transportation Systems (ITS) and the Smart Grid. It examines the communication standards and protocols that enable EVs to interact wirelessly with the grid infrastructure and Road Side Units (RSUs). The chapter provides insights into existing communication protocols and emerging technologies, such as IEEE 802.11bd and New Radio (NR) V2X, designed to enhance reliability, low latency, and high throughput communications for autonomous vehicles and driving use cases.

The growing importance of the Internet of Things (IoT) in smart homes and smart cities is the focus of the thirteenth chapter “[Internet of Things for Smart Homes and Smart Cities](#)”. Titled “Internet of Things for Smart Homes and Smart Cities,” the chapter explains the architecture and enabling technologies of IoT. It explores the application of IoT in smart home environments, covering protocols, communication mediums, and important IoT-based services. Additionally, it delves into the concept of smart cities, discussing architecture and popular services enabled by IoT technology.

The fourteenth chapter “[Advancements in DC Microgrids: Integrating Machine Learning and Communication Technologies for a Decentralized Future](#)”, delves into the concept and components of DC microgrids. It explores different control strategies used in microgrids and highlights the advancements in machine learning and communication technologies that further enhance their efficiency and reliability. The chapter provides valuable insights into the decentralized future of DC microgrids and their contribution to a sustainable power system.

Lastly, the fifteenth chapter “[Advanced Communication and Computational Technologies in a Sustainable Urban Context: Smart Grids, Smart Cities and Smart Health](#)”, discusses the potential of modern communication and computational technologies in overcoming environmental and socio-economic challenges in cities and their potential applications in smart grids, smart cities, and smart health. The chapter emphasizes the need for a holistic approach to building sustainable and equitable cities, taking into account the environmental impacts beyond city boundaries.

The book as a whole addresses the critical role of computational and communication technologies in shaping the future of the electricity grid. Each chapter

provides unique insights into specific aspects of Smart Grid 3.0 and highlights the advancements, challenges, and opportunities presented by these technologies.

The editors and authors of this book have brought together their expertise and research to create a comprehensive resource for researchers, professionals, and students interested in the field of smart grids and energy systems. The interdisciplinary nature of the topics covered ensures that readers will gain a well-rounded understanding of the subject matter.

It is our hope that this book will serve as a valuable reference and guide for those seeking to navigate the complexities of Smart Grid 3.0. By exploring the advanced control functionalities, controller designs, communication protocols, and emerging technologies, readers will gain insights into the transformative potential of computational and communication technologies in creating a more sustainable and efficient energy future.

We would like to express our sincere gratitude to all the contributors who have shared their knowledge and expertise in this book. Their dedication and efforts have made this publication possible.

Lastly, we extend our appreciation to the readers for their interest in Smart Grid 3.0 and their commitment to advancing the field. We hope that the insights and knowledge shared in this book will inspire further research and innovation in the pursuit of a smarter and more sustainable energy ecosystem.

Bhubaneswar, India  
Pitești, Romania

Bhargav Appasani  
Nicu Bizon

# Contents

<b>Smart Grid 3.0: Grid with Proactive Intelligence</b> .....	1
Bhargav Appasani	
<b>Blockchain for Energy Management: Smart Meters, Home Automation, and Electric Vehicles</b> .....	23
Florentina Magda Enescu and Nicu Bizon	
<b>Engineering Applications of Blockchain Based Crowdsourcing Concept in Active Distribution Grids</b> .....	57
Bogdan-Constantin Neagu, Gheorghe Grigoras, and Florina Scarlatache	
<b>Machine Learning-Based Approaches for Transmission Line Fault Detection Using Synchrophasor Measurements in a Smart Grid</b> .....	77
Kunjabihari Swain, Ankit Anand, Indu Sekhar Samanta, and Murthy Cherukuri	
<b>Data Mining-Based Approaches in the Power Quality Analysis</b> .....	93
Gheorghe Grigoras, Bogdan-Constantin Neagu, and Florina Scarlatache	
<b>Machine Learning and Deep Learning Approaches for Energy Management in Smart Grid 3.0</b> .....	121
Amitkumar V. Jha, Bhargav Appasani, Deepak Kumar Gupta, Srinivas Ramavath, and Mohammad S. Khan	
<b>Evolutionary Algorithms for Load Frequency Control of Renewable Microgrid</b> .....	153
Nilesh Kumar Rajalwal and Deep Shekhar Acharya	
<b>Agents-Based Energy Scheduling of EVs and Smart Homes in Smart Grid</b> .....	185
Muhammad Waseem Khan, Guojie Li, Keyou Wang, Muhammad Numan, Linyun Xiong, Sunhua Huang, and Muhammad Azam Khan	

**Advanced Control Functionalities of Smart Grids from Communication and Computational Perspectives** ..... 221  
A. Paspatis, E. Pompodakis, I. Katsigiannis, and E. Karapidakis

**Multistage PD-(1+PI) Controller Design for Frequency Control of a Microgrid Considering Demand Response Program** ..... 241  
Hossein Shayeghi and Alireza Rahnama

**Solid State Transformer: Topologies, Design and Its Applications in a Smart Grid** ..... 275  
Selami Balci, Saban Ozdemir, Necmi Altin, and Ibrahim Sefa

**Emerging Communication Technologies for V2X: Standards and Protocols** ..... 301  
Yasin Kabalci and Ural Mutlu

**Internet of Things for Smart Homes and Smart Cities** ..... 331  
Nuri Kapucu and Mehmet Bilim

**Advancements in DC Microgrids: Integrating Machine Learning and Communication Technologies for a Decentralized Future** ..... 357  
Necmi Altin and Süleyman Emre Eyimaya

**Advanced Communication and Computational Technologies in a Sustainable Urban Context: Smart Grids, Smart Cities and Smart Health** ..... 389  
Patrick Moriarty



# Engineering Applications of Blockchain Based Crowdsourcing Concept in Active Distribution Grids



Bogdan-Constantin Neagu, Gheorghe Grigoras, and Florina Scarlatache

**Abstract** The future active distribution networks (ADNs) must ensure “smart” features like flexibility, accessibility, reliability, and high power quality for all consumers. Increased adoption of small-scale distributed energy sources (SSDES) helps decarbonise ADNs. In the present context, society must ensure the comprehensibility of the benefits stemming from smart electricity across the entirety of the population while concurrently ensuring that the provisioning process is achieved in an environmentally sustainable and efficient manner. Energy poverty is a lack of access to clean and affordable energy, resulting in soaring energy costs. The crowdsourcing concept, introduced by Surowiecki (The wisdom of crowds, Anchor, San Diego, CA, 2005), can be used to mitigate energy scarcity. It can be a useful tool for allowing the crowd to do community service within a specific geographic region. According to Romania’s Energy Regulation National Agency’s Order No. 228, launched on December 28, 2018, the prosumers can sell the energy-produced SSDES on the free market. More automated trading strategies aim to improve the benefits of peers who trade electricity in local community markets. The main aim is to quantify the distortion effects and introduce a stringent and comprehensive methodology integrating the distribution network operator (DNO), prosumers, and consumers. This chapter compares the ADNs cost saved by the households when prosumers move to increase their revenue, and the DNOs act to improve the benefits derived from an optimal network operation.

**Keywords** Renewable sources · Prosumers · Crowdsourcing concept · Transactive energy · Active distribution networks · Blockchain

---

B.-C. Neagu (✉) · G. Grigoras · F. Scarlatache  
Electrical Engineering Faculty, Power Engineering Department, “Gheorghe Asachi” Technical University of Iasi, Bd. Dimitrie Mangeron, No. 21-23, 700050 Iasi, Romania  
e-mail: [bogdan.neagu@tuiasi.ro](mailto:bogdan.neagu@tuiasi.ro)

G. Grigoras  
e-mail: [ggrigor@tuiasi.ro](mailto:ggrigor@tuiasi.ro)

F. Scarlatache  
e-mail: [florina.scarlatache@academic.tuiasi.ro](mailto:florina.scarlatache@academic.tuiasi.ro)

## Abbreviations

AND	Active distribution networks
SSDES	Small-scale distributed energy sources
DNO	Distribution network operator
PV	Photovoltaic
LV	Low voltage
SG	Smart grids
SM	Smart meter
P2P	Peer-to-peer
LMM	Local microgrid market
CES	Crowdsourcing energy systems
FCFS	First come first serve
MU	Monetary unit

## 1 Introduction

The increasing demand for electricity, coupled with the constraints imposed by global warming and climate change, necessitates exploring and utilising novel renewable energy resources with environmentally-friendly attributes. A result of this aim is the increasing number of SSDES. These green sources may instantly operate as ADN users (prosumers) with energy self-production. Significantly, there has been a remarkable surge in the adoption of solar photovoltaic panels (PVs) in recent years, driven by incentives provided by the European Union (EU) communities, including Romania (refer to [1]). This development substantiates the aforementioned concept and transforms it into an undeniable business reality. The base of bidirectional energy flows rising from the transactive energy in the local communities, as well as the need to decrease the power loss, led to changes in the ADN in Low Voltage (LV) grids, leading in the direction of a higher active and cost-effective Smart Grids (SGs).

Energy efficiency saves money and resources, representing a necessity for flexible adaptation to users' demands. Because electricity plays a fundamental role in modern lifestyles, users' load characteristics must reflect the people's lives at work and leisure.

The volume of available information necessary for the operation, management, planning, and security of the ADNs has gradually increased with technological development, requiring the introduction of the calculation technique and intelligent solutions [2]. Even if the prosumers have high benefits, their behavior is intermittent, so the DNOs must consider a comprehensive ADN planning strategy. Furthermore, they should be able to bind to the grid and operate independently (autonomously). The ADNs, which were created for cities, incorporate local energy supply to meet the specific demand of the customers. Active consumers and prosumers are identified in the framework of recent paradigms of energy independence, energy policy, and

distributive management. The ADN is viewed as a tool for constructing a coordinate system for SSDES fair integration, which will be an edifying challenge for DNOs that will require another operation plan. The prosumers make up the active cells of the ADNs, and each cell will supply installations to the DNO to maximize grid hosting power and execute SSRES in a successful and effective operating manner [3].

In our country, energy saving is improving as local suppliers (prosumers) with a rated capacity of up to 27 kilowatts create more electricity [4]. These funds are transferred to the supplier with whom a bilateral agreement has previously been negotiated [5].

Prosumer action must still be evaluated to store excess power during periods of low demand and transmit it when demand rises [6]. A recent report from the European Union’s Smart Grids Task Force [7] offers a specific mandate to develop a smart meter (SM) strategy to meet the needs of the emerging electricity market by adopting a flexible and adaptable measuring technology. As a result, the SM must ensure that useful information on the pattern of the prosumers’ generation is available [8].

The proliferation of SSDES changes the operating conditions and management requirements of the ADNs, which must now integrate new technologies and procedures. The SG principle has been applied in Romania on various scales and measures in recent years, with most of the hardware being tested and accepted but in isolation.

The presumption of a structure or unifying architecture of interfaces and protocols based on norms and standards is fundamental. As a result, a reference framework for data sharing between devices and ADNs must be specified, enabling the interaction of services, utilities, protocols, devices, and interfaces [9]. Figure 1 illustrates the transition from classical electricity grids to ADNs.

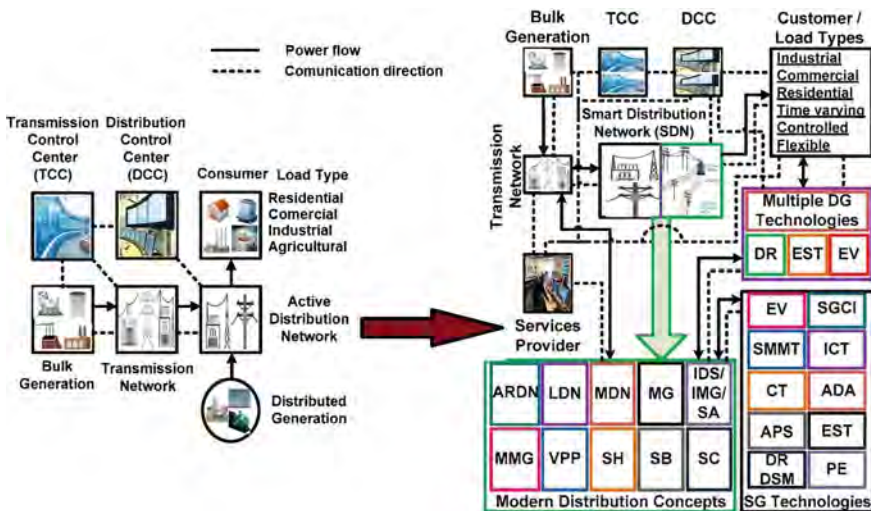


Fig. 1 The transition from classical grids to ADNs

The increasing number of prosumers with various distributed energy recourses promotes the P2P (peer-to-peer) electricity transaction in the SGs for less cost, more flexibility, lower carbon footprints, and higher reliability. Recent research on the prosumers' behavior in electric distribution systems has increased in recent years. A distributed privacy-preserving P2P energy transaction approach has been proposed to minimize the overall objective of renewable generation curtailment penalty, adjustment cost, and operation cost while satisfying linearized distribution network power flow, power line thermal, and voltage limit constraints.

The integration of prosumers into ADNs has become a serious concern in Romania in the last 2 years, with the national government pushing this practice using bonuses [1]. Figure 2 shows the overall quantity of over 3500 prosumers connected to Romanian DNOs' LV-ADN. [10]. The behavior of prosumers becomes a critical issue for aggregators, suppliers, and DNOs. This legal system provides prosumers with several benefits [1], including the following Fig. 2.

Law 184/2018 establishes a mechanism to encourage the share of renewables as a significant move forward in Romania's legislation of prosumer status as the following:

- prosumers with self-generation electricity units with a rated capacity of a maximum of 27 kW per individual home, residential blocks, residential, commercial, or industrial areas are covered by the scheme;
- electricity delivery operators must contact prosumers according to the regulatory authority's relevant regulations;
- prosumers can sell electricity surplus to suppliers with whom they have agreements at a price equivalent to the weighted medium price reported on the day-ahead market the previous year; suppliers with whom prosumers have a deal must take over the energy at the latter's order;

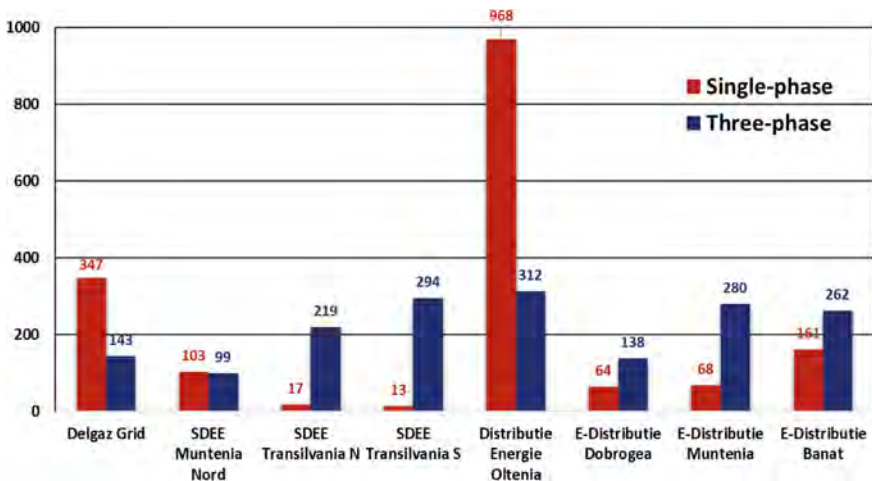


Fig. 2 The number of prosumers from each DSOs in Romania

- exemption from excise duties for prosumers for the volume of electricity produced from renewable sources for personal use and the surplus supply sold to suppliers;
- exemption of prosumers as individual citizens from the duty to purchase renewable certificates for electricity production and used for self-final use, beyond power plants technical losses, on an annual and quarterly basis;
- going to benefit from the service of regularization between the value of electricity delivered and the value of electricity used in the grid by electricity suppliers for which they have electricity supply deals.

According to the legislation, energy suppliers having agreements with prosumers ask to buy power at the weighted mean day-ahead spot price from the preceding year. As a result, the retailer gains from not paying the distribution system tariff because the prosumer will sell their extra energy on the market. The trading mechanism provides a basic approach, limiting both sides' options (consumers want to buy power at lower prices, and prosumers want to sell it).

By not encouraging prosumers to set custom sale rates, it ignores disparities in generation costs and installed power. There is no opportunity to stimulate local generation. Consumers are unable to purchase power directly from prosumers, limiting their ability to trade with specific prosumers [11].

More automated trading strategies aim to improve the benefits of peers who trade electricity in the local market of microgrids (LMM). A comprehensive methodology considering the DNOs and stakeholders, which to quantify the highlighted distortion effects, is proposed in the chapter. The authors will compare the ADNs cost saved by the households when prosumers move to increase their revenue, and the DNOs act to improve the benefits derived from an optimal ADNs operation.

## 2 Crowdsourcing Energy System

Crowdsourcing, a term first proposed in 2005 by James Surowiecki [12], can be used to alleviate energy poverty [13]. Crowdsourcing [14] is a new development in which users' ideas are combined with the mutual intelligence of the crowd [15]. To make these crowdsourced sensor cloud data accessible, developing a service-based solution is critical. It can also be an important way for the crowd to have a service-sharing community within a metropolitan region by allowing them to use their smartphones [16]. In this crowdsourced service community, consumers can benefit from the services of their neighbours. Since the crowd (i.e., service providers) is mobile, providing crowdsourced applications to customers is constrained by their spatial and temporal proximity, i.e., all service providers and users must be in the same geographic area simultaneously. Selecting and composing services from such a vast number of constantly evolving crowdsourced sensor cloud services to meet users' needs in real-time and dependent on spatiotemporal features is a major challenge. As a result, new spatial-temporal service collection and composition innovations

are important approaches for using spatial–temporal crowdsourcing as a forum for service provisioning.

A crowdsourced energy system (see Fig. 3) includes a plurality of distributed energy resources managed by crowdsources of the system, a power network to which the distributed energy resources are connected, and a system operator that manages energy trading transactions and energy delivery within the system. The system operator operating at least one computing device configured to obtain day-ahead peer-to-peer energy trading transaction requests from crowdsources for energy to be delivered from the distributed energy resources, estimate day-ahead energy load and solar forecasts, determine optimal power flow for the delivery of energy, and schedule delivery of energy from the distributed energy resources across the power network based upon the energy trading transaction requests, the estimated forecasts, and the determined optimal power flow [17]. It may be useful for allowing the general public to do community service within a certain geographic region.

Several billions of dollars have been spent on blockchain analysis in recent years to maximize its capacity and determine its appropriateness in various economic domains [1]. However, not all sectors can completely embrace blockchain technologies.

The current technological opportunities must be analyzed in each particular case, along with the challenges that end-users are confronted with and how a modern open architecture could provide value to them. Fortunately, the electricity sector is an excellent nominee for blockchain-based advancement. It integrates a complex supply chain with need to increase transparency and improve data management. It

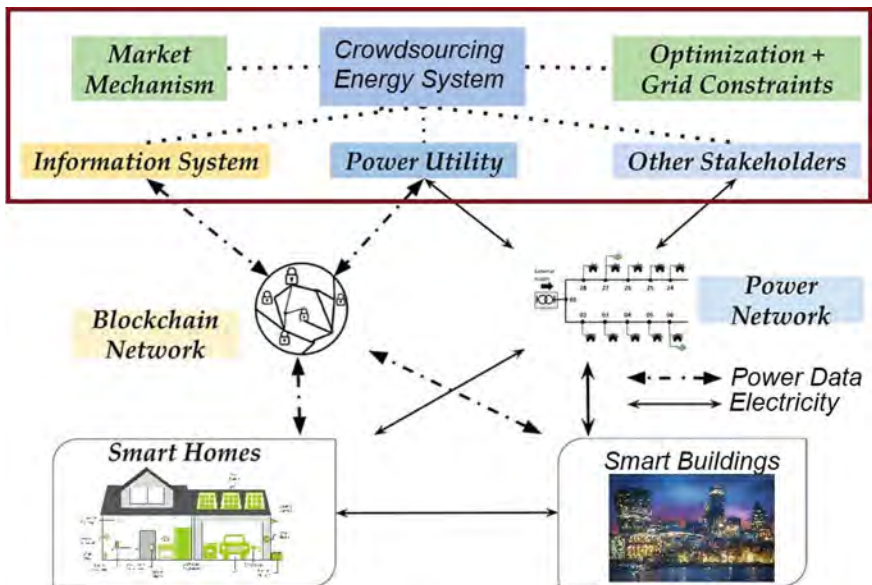


Fig. 3 A particular model for crowdsourcing energy system

also has a high-volume trade segment that will benefit from the immediate settlement. Blockchain's clarity and immutability will inspire business and customer end-users.

### 3 Blockchain Technology

A blockchain represents a decentralized (distributed) register of the number of transactions that occur in an ADN. This network is made up of nodes that are operated by different entities and use a cryptographic protocol to verify transactions. The protocol has an accuracy through which the data introduced in the register can't be reversed or altered. It is unchangeable, stable, and clear. More than that, the difference of blockchain is represented by the distributed software ledger of trusted and verified transactions which is structured in blocks and maintained by network nodes, see Fig. 4. Blockchain platforms are fully decentralized and distributed to the level of ADN nodes, making them difficult to hack and exploit by malicious actors [18].

A defining feature of blockchain technology is the immutability of the data. In simple terms, once the data are recorded and validated by the entire network and can no longer be modified. It is possible because the data related to any transaction is dispersed through the AND and verified to prevent fraud. Many projects have been undertaken to consider the potential synergies between the blockchain and the power system. Blockchain technology has the potential to solve various problems in the electricity sector and lead to the achievement of energy consumption goals, including compensating for financing gaps in different initiatives [19]. The transition to smart grids involves accepting challenges that need to be known and finding the most effective means to overcome them. Blockchain-based network technologies will result in structural improvements that will necessitate the participation of logistics and service providers, equipment suppliers, policymakers, and, last but not least,

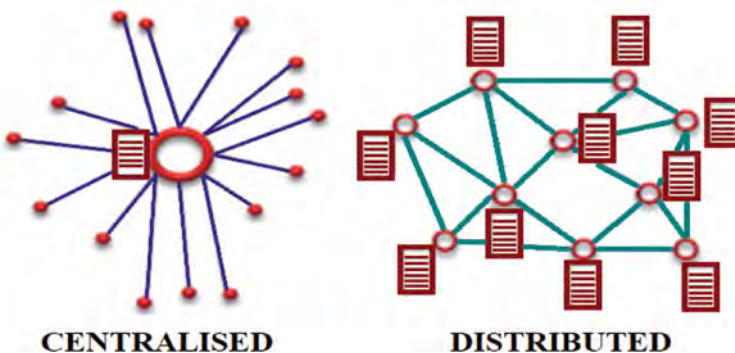


**Fig. 4** The comparison between centralised and distributed ledger of transaction for blockchain technology

final users. The power market has a lot of promise for blockchain implementation due to more challenges [11, 20, 21]:

Climate change and the need to incorporate clean energy sources have led to the advancement of technologies like PV panels and wind turbines, which are becoming more affordable. Their technical characteristics present opportunities to develop new actors represented by prosumers. Prosumers pose a threat to the existing configuration of electricity networks, posing technological problems for DNOs in maintaining energy balance. Nevertheless, electricity generation at the household level (typically with PV panels on the roof) represents a major potential for advancing blockchain technology-based architectures because it takes advantage of the distributed nature of electricity production and has a performance that no other paradigm can equal.

The creation of technologies that make the transition to AND was depicted in Fig. 1. Communications and networking components, inverters, bidirectional smart meters, and energy storage are all examples of technologies that have been implemented. As a result of this evolution, energy has become a more controllable, storable, and easily quantifiable substance. It is appropriate for trading across “smart” agreements. Local energy generation cooperatives founded by community residents oversee the development of energy communities. The ADN, which incorporates blockchain technology, maybe a workaround for providing the cleanest and cheapest electricity forms to the poorest customers and conserving resources by more responsible use. They achieve these goals by creating unity programs to lower vulnerable members’ electricity bills and supplying them with resources and training on reducing consumption. They still use the profits from electricity generation to help poor and low-income families improve their living conditions.

Introducing a blockchain-based prosumer network simplifies the design of exchange models, replacing intermediaries for electricity trading. There are many attempts to unlock the high potential that blockchain technology has in accelerating the transition to green energy. The immutability of data from the blockchain occurs due to the synergy of the three technologies: cryptographic keys, a distributed register, and a validation protocol. Records kept on a blockchain can be considered reliable, and the operator or aggregator cannot access them, see Fig. 5.

The transaction variables, such as sender, receiver, transaction value, and so on, are calculated in an ADN when a prosumer or an energy supplier and a prospective consumer agree to make an electricity transaction. Each transaction is secured and replicated through the entire network for data verification and storage on the local level. Each network member verifies, confirms, and saves the transaction data’s validity automatically. Thus, confidence is given by the network members who become witnesses and guarantors of each transaction. All information related to electricity transactions is mixed with identical information from all transactions in the network that takes place simultaneously to form a block. Subsequently, that block is added to a blockchain that brings together all the transactions ever made in the network publicly and transparently. Once added to the chain, the blocks and, implicitly all the transactions are no longer editable and become a detailed report of all the necessary elements to keep track of.



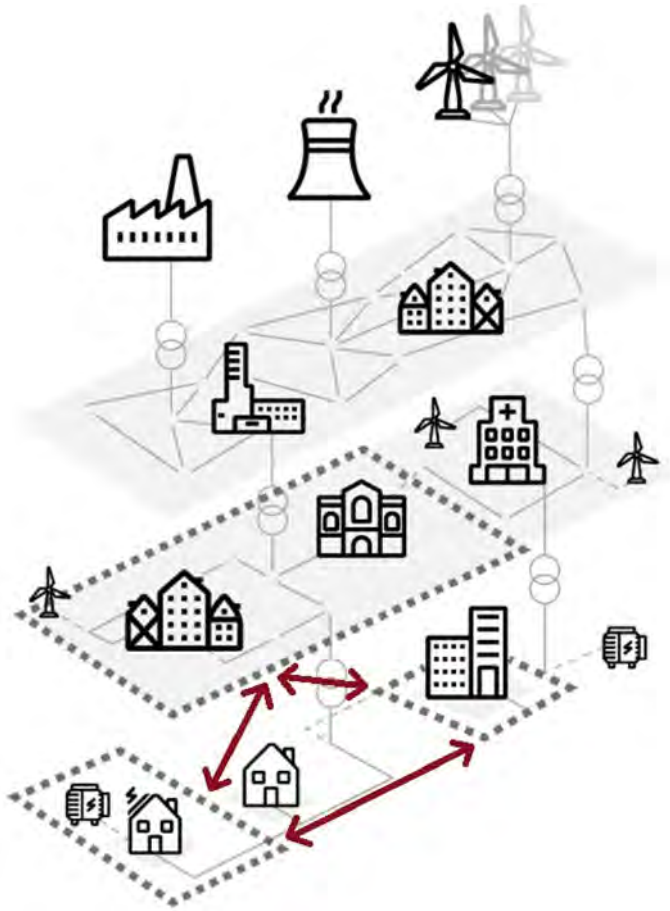


**Fig. 5** The transactive energy based on blockchain technology

Mathematical algorithms that assign a hash to each block verify its data. The hash is a collection of letters and numbers created from the related data from the transactions in a given block. The network periodically checks the hash value for each block in relation to the value of the previous block. In this way, it is impossible to any attempt to defraud data related to a transaction, as well as any attempt to cancel or reverse the transaction.

## 4 Enhanced Prosumers Trading Approach

### 4.1 Problem Formulation

This section explains the mathematical model for selling surplus energy generated by SSDES (residential solar panels) between peers in the local ADN markets—prosumers (*Pros*) and consumers (*Cons*). When “prosumers” are thought of as energy producers that sell their excess energy, they will sell the surplus of generated energy ( $W_{gp}$ ) if their consumptions ( $W_{oc}$ ) are less than their own generation.

Blockchain technology begins to function after this limit is met. If the energy demand ( $W_d$ ) volumes are greater than  $W_{gp}$ , the total prosumers offered energy ( $W_{of}$ ) is set by taking into account total produced power ( $W_g$ ) by prosumers as seen in the flowchart:

$$\sum_{k=1}^n W_{of}^{k,h} = \sum_{k=1}^n (U_g^{k,h} \cdot I_g^{k,h}) - \sum_{k=1}^n W_{oc}^{k,h} \quad (1)$$

$U_g$  and  $I_g$  for prosumer  $k$ , at hour  $h$ , is the operation voltage and current value. For the  $n$  lines, the total energy losses ( $\Delta W_T$ ) are calculated as:

$$\sum_{i=1}^n \Delta W_T^{i,h} = \sum_{i=1}^n R_l^{i,h} \cdot (I_l^{i,h})^2 + \sum_{i=1}^n (U_m^{i,h} \cdot I_m^{i,h}) \quad (2)$$

where  $R_l$  is the resistance,  $I_l$  are the current value for the  $i$  line, and  $U_m \cdot I_m$  is the miscellaneous energy loss.

After that, by subtracting the Eq. (2) from (1), the provided energy ( $W_{of}$ ) can be calculated as:

$$\sum_{i=1}^n W_{of}^{i,h} = \sum_{i=1}^n \Delta W_{gp}^{i,h} - \sum_{i=1}^n \Delta W_{oc}^{i,h} - \sum_{i=1}^n \Delta W_T^{i,h} \quad (3)$$

Energy Smart Contracts (Peer-to-Peer—P2P), representing the “translation” or “transposition” in the code of a contract to automatically verify the fulfilment of certain conditions and to automatically execute actions when the conditions are determined between the parties, are reached and verified [12].

### 4.2 The Blockchain-Based Crowdsourcing Algorithm Design for P2P Energy Transactions

A mathematical model is proposed for computing the hourly excess offered by prosumers to local consumers through Crowdsourcing Energy Systems. Table 1

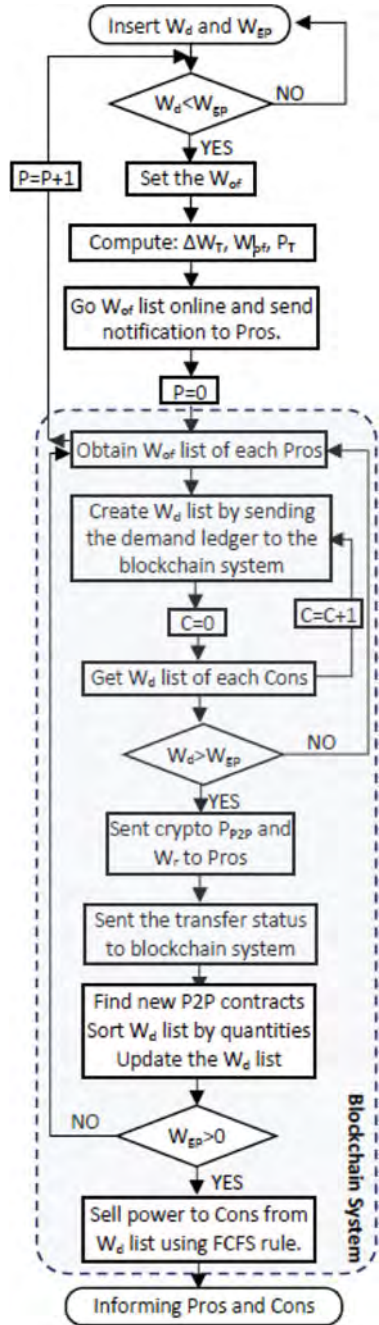
presents the pseudocode of the proposed approach. Also, Fig. 6 shows the flowchart of a blockchain-based prosumers energy trading system for peer-to-peer contracts. The total price for the  $W_{of}$  is determined through multiplication with the energy per unit price (PP2P), assured by negotiating process between Pros and Cons (from a local ADN) using P2P “smart” contracts. Following that, the Wof status for each available Pros is updated, and each  $P_{rs}$  is alerted by the blockchain method depicted in Fig. 6.

Consumers who have already signed a P2P deal tend to purchase electricity from the nearby  $P_{rs}$  when  $W_d$  is higher than  $W_{gp}$ . When a vendor and a client plan to do

**Table 1** The pseudocode of the proposed algorithm

<b>Step 1.</b> Input data details: consumer load profile (C), prosumer generation (G), and presumer price (PR)
<b>Step 2.</b> Initialize the acquisition quantities (A) and financial settlement (F)
<b>Step 3.</b> Initialize the unsold surplus (us): $us = 0$
<b>Step 4.</b> Start the P2P energy trading method based on blockchain texhnlology using a AND crowdsourcing energy system, Fig. III.9.6
4.1 for each hour: $h = 1 \dots 24$
for each presumer: $k = 1 \dots np$
compute surplus: $S(h, k): S(h, k) = G(h, k) - C(h, k)$
if $S(h, k) > 0$
surplus = $S(h, k)$ ;
4.2 build a temporary consumer priority (proce, length):
Distribute the surplus (srp):
set initial consumer index: $w = 0$ ;
while $srp > 0$ or $(w < nc)$
$k = k + 1$ ;
if the consumer has a P2P contract:
subtract the available surplus from its trading offer;
if the surplus exceeds the consumer contract quantity:
update the remaining surpkus;
the contract from consumer $w$ is fulfilled;
else
the contract from consumer $k$ is partially fulfilled and the surplus is depleted;
update matrix by subtracting from the served consumer demand the fulfilled contract;
update acquisition matrix A for hour $h$ according to the served consumer $k$ , serving prosumer ix an traded quantity
4.3 Update line the consumer load profile
4.4 Update the unsold surplus: $us = us + srp$ ;
<b>Step 5.</b> Compute the hourly and total electricity sold by prosumers to each consumer and the electricity traded hourly and daily by all prosumers, using matrices A and F

**Fig. 6** The energy trading approach based on P2P contracts in the blockchain environment



business together, they decide the factors, such as the receiver, sender, and transaction size, among other aspects. When Cons update their demand ledger status, the blockchain module generates a  $W_d$  list based on the necessary amount of energy,  $W_r$ , in order to compare both the  $W_d$  and  $W_{of}$  lists in the system. In addition, all inferred Pros and Cons receive a note informing them of the transaction status. The  $W_{of}$  would be moved from the  $\mu G$  (Pros) to the Cons if they comply with the transaction status. P2P crypto can be used as a virtual payment method. Another function of blockchain in our algorithm is to determine if the remaining electricity surplus in the AND satisfies the  $W_d$  list or if there are no prosumers willing to sell electricity. In this case, the sales can't be stored, so Cons would have to wait before sale deals become open. The Cons would then see advertisements for sale deals, and the blockchain system will sell power to customers based on the first come, first served (FCFS) concept. If  $W_{of}$  is greater than zero, or  $W_d$  from Cons persists, the algorithm begins. Finally, after the trade process is over, the Pros and Cons will be notified.

Blockchain technology enables stable anonymous purchases based on the FCFS theorem, which states that prosumers or market administrators have no control over trading partners and that purchasing deals are met regardless of quantity or price, with only the trading system's positioning moment taken into account. The algorithm reproduces this approach at each trading interval by randomly allocating each customer and prosumer preferences. In addition, since each offer's time index is special in the blockchain scheme, an embedded rule in the algorithm states that no two customers should have the same trading preferences. As a result, there is no need for a secondary requirement in this situation. Distributed algorithms have the potential to realize privacy-preserving P2P energy transactions since no party has direct access to all participants' private information. Figure 7 indicates the transaction mechanism.

A short comment must add regarding the proposed distributed algorithm-based information-exchanging, even if Step 4 from Table 1 has been treated extensively

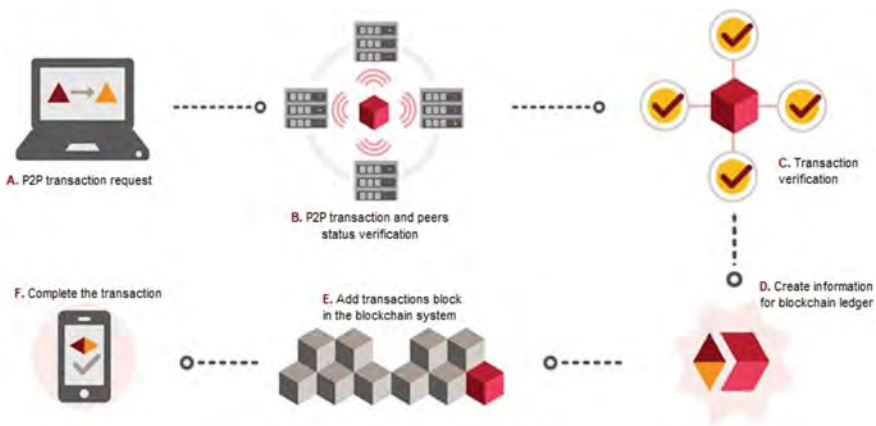


Fig. 7 The translation of the energy trading method on blockchain technology

in [18]. It refers to the fact that access to private information is not allowed by eavesdroppers. Thus, only six transaction steps (A, ..., F) are synthetically proposed, see Fig. 7.

First, if someone requests a transaction (step A), this transaction is broadcasted to a P2P crowdsourcing energy system (CES), characterized by ADN peers. In the second step (B), the CES peers validate the transaction and the user's status using the proposed FCFS algorithm. Step C applies blockchain technology when a verified transaction can involve cryptocurrency, smart contracts, records, or other transaction information. Once verified, the current transaction is combined with others to create a new information block for the ledger (Step D). The new blocks are added to the blockchain system (grey colour has been used in Fig. 6 to highlight it) in a permanent and unalterable way. The last step (F) is the complete confirmation of the transaction.

## 5 Case Study

The performance of the proposed distributed P2P energy transaction in the CES environment approach has been investigated through case studies in a 28-bus active distribution system belonging to a Romanian DNO (see Fig. 8), which provides 27 single-phase residential users with 4-wire three-phase power line (NFA2X 50 OL-AL + 3 × 70 mm<sup>2</sup>). The distance between the LV poles is between 36 and 42 m. The prosumers, seen on 6, 7, 15, 21, and 27 buses, want to sell their excess electricity to other ADN customers. The case study considers all consumers integrated into the local market, receiving electricity through smart P2P contracts from the prosumers. The consumption and generation profiles associated with the consumers and prosumers have been uploaded from the Smart Metering system [11].

The sampling step is by 1 h during a day. For considered prosumers, Table 2 shows the energy surplus available for trade in the considered interval. The transaction process would spread this surplus among customers or prosumers, as presented in the previous section.

Over the trading cycle, each prosumer's energy price is assumed to be stable. The average fixed price for customers to purchase energy (monetary unit—MU/kWh) from a traditional market operator is 0.72 MU/kWh, including taxes. In other words, the fixed price at which prosumers will sell electricity back to the grid has been set at 0.196 MU/kWh for 2021 (0.251 for 2020) [22], whereas local prosumer sale rates have been set at [0.40, 0.55] MU/kWh.

The study of Fig. 9 revealed that local generation accounts for 22.8% of usage between 06:00 and 18.00, with an hourly surplus that never exceeded demand in every selling cycle.

Via P2P contracts, prosumers sell all energy sums in the local ADN. Bus 1 is empty, and each prosumer cannot sell their excess energy, so it is sold on the market. The energy transaction considers the priority order as incentivising specific prosumers, based on the “close” tiers, technology, agreement, or social welfare enhancing in the crowdsourcing energy environment. The following study, applied in the case of an

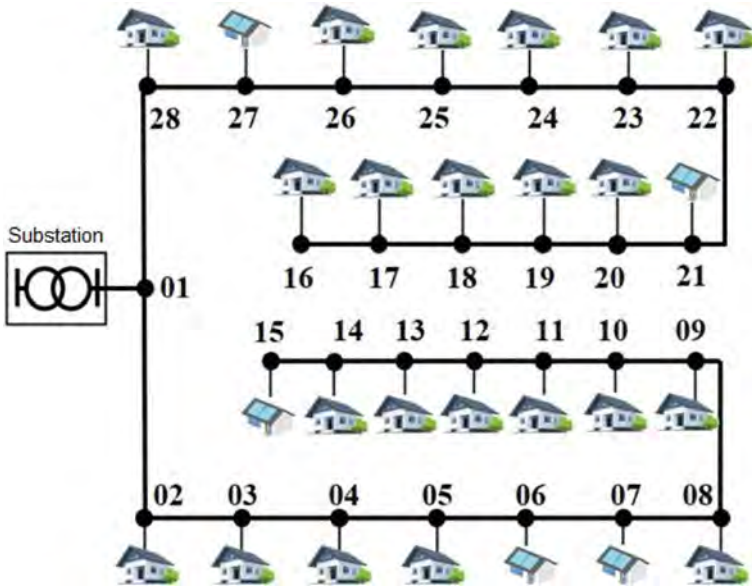


**Fig. 8** The diagram of a real active distribution network

**Table 2** Local generation (in kWh) and selling prices (in MU/kWh)

Hour	Prosumer Nodes				
	6	7	15	21	27
06	0.00	0.00	1.95	1.59	0.00
07	0.00	0.26	1.59	1.81	0.00
08	0.00	0.70	1.59	1.73	0.67
09	0.74	1.06	2.23	1.75	1.44
10	1.12	1.09	1.30	2.29	1.61
11	1.89	1.40	2.78	2.04	1.66
12	2.33	1.23	1.88	1.82	1.60
13	2.29	1.41	2.83	0.69	1.51
14	1.35	1.39	2.95	1.18	1.37
15	1.18	1.05	1.55	2.03	1.11
16	0.00	0.41	1.32	0.82	0.56
17	0.00	0.00	1.06	0.00	0.00
18	0.00	0.00	1.16	1.17	0.00
Total	10.90	9.99	24.17	18.90	11.51
Selling price	0.43	0.40	0.48	0.55	0.43

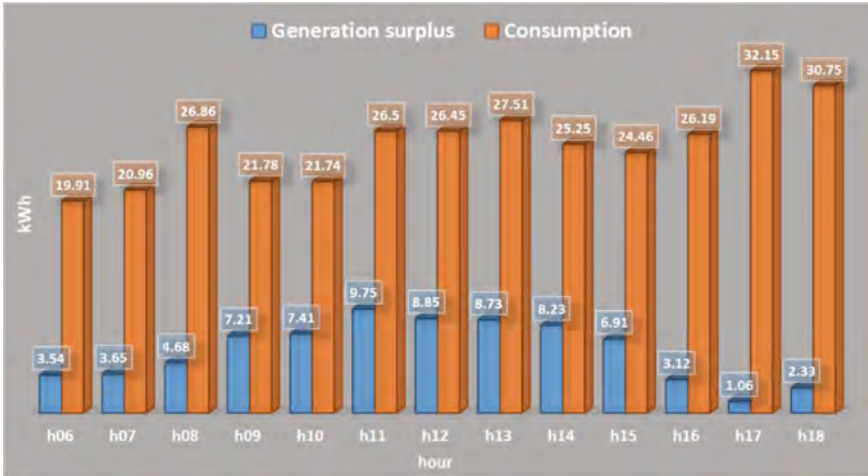


Fig. 9 Local generation and consumption, in kWh

emerging country, highlights the advantages of the proposed energy trading algorithm. The consumers’ money savings and increasing the market flexibility through “smart” contracts represent the main objectives of the algorithm.

Because the P2P contracts are already signed between peers based on the FCFS blockchain principle, it must be mention that only participant from bus 28 do not receive the electricity surplus, with insignificant daily electricity consumption.

Figure 10 shows the traded energy quantities from applying the proposed mathematical model. Moreover, Table 3 presents the daily electricity amounts from prosumers purchased by consumers.

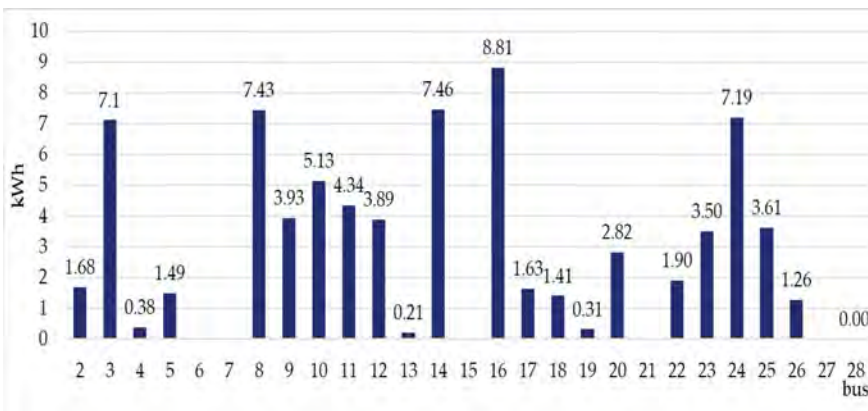


Fig. 10 The electricity achieved by the consumers in kWh



**Table 3** The traded prosumers excess and prices (in MU/kWh)

Bus	The electricity excess, in kWh					Total kWh	P2P price	Total cost/revenue	
	P6	P7	P15	P21	P27			for Cons	for Pros
2	0.860	0.000	0.000	0.176	0.641	1.678	0.743	1.208	0.329
3	0.000	1.154	2.962	1.394	1.599	7.109	3.338	5.118	1.393
4	0.378	0.000	0.000	0.000	0.000	0.378	0.163	0.272	0.074
5	0.000	0.000	0.181	0.749	0.559	1.489	0.739	1.072	0.292
8	0.244	1.048	0.603	2.761	2.773	7.430	3.525	5.350	1.456
9	0.000	0.002	2.046	0.773	1.106	3.927	1.884	2.827	0.770
10	2.295	1.356	0.122	1.361	0.000	5.133	2.336	3.695	1.006
11	1.845	0.745	1.130	0.620	0.000	4.340	1.975	3.125	0.851
12	0.000	0.645	2.572	0.668	0.000	3.885	1.860	2.797	0.761
13	0.150	0.056	0.000	0.000	0.000	0.206	0.087	0.148	0.040
14	1.116	0.691	2.141	2.140	1.372	7.460	3.551	5.371	1.462
16	1.917	1.632	1.634	3.631	0.000	8.814	4.259	6.346	1.728
17	0.000	1.331	0.294	0.000	0.000	1.625	0.674	1.170	0.319
18	0.000	0.263	1.144	0.000	0.000	1.407	0.654	1.013	0.276
19	0.000	0.298	0.017	0.000	0.000	0.315	0.127	0.227	0.062
20	0.000	0.000	1.100	1.722	0.000	2.822	1.475	2.032	0.553
22	0.412	0.000	1.136	0.000	0.353	1.901	0.874	1.369	0.373
23	0.000	0.410	3.090	0.000	0.000	3.500	1.647	2.520	0.686
24	0.000	0.000	2.430	1.649	3.108	7.187	3.410	5.174	1.409
25	0.742	0.368	1.242	1.260	0.000	3.612	1.755	2.601	0.708
26	0.940	0.000	0.324	0.000	0.000	1.264	0.560	0.910	0.248

The last columns correspond to the following indicators:

- the overall electricity bought by a customer;
- the tariff charged by consumers to prosumers for the surplus electricity achieved through the signed “smart” contracts;
- the imposed tariff that consumers could have paid to the ADN provider at 0.72 MU per one kilowatt;
- finally, the regulated price paid by prosumers to the grid aggregator at 0.196 MU per one kilowatt.

Figure 11 presents the prosumers’ financial benefits associated with the price paid for the consumers through the “smart” contracts and regulated price if the excess was deposited straight into the ADN. Consumers can also feel the effects of purchasing at a LMM. The variations between the standardized price, which customers must pay, and the P2P price used in the proposed algorithm, which is often smaller, are seen in Fig. 12.

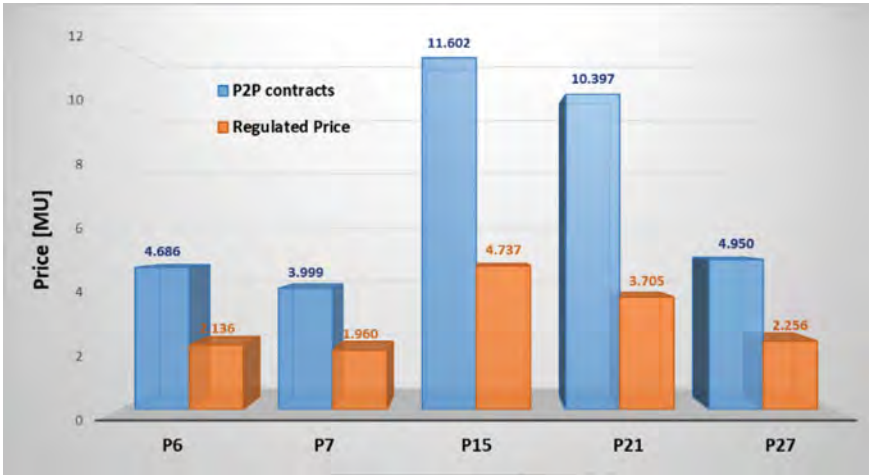


Fig. 11 The P2P and imposed tariff achieved by prosumers from LMM

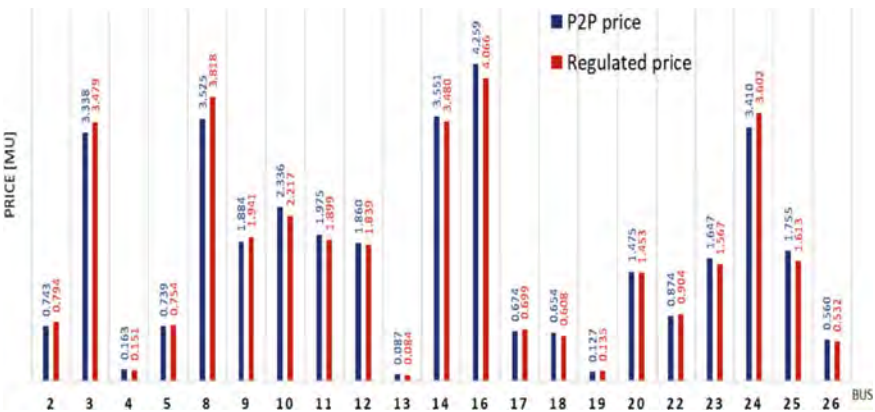


Fig. 12 The P2P and imposed tariff gained by the consumers

## 6 Conclusions

The use of a blockchain in the energy sector allows obtaining different advantages: provision of the local clearing process to run to reconcile planned and actual consumptions, as recorded by consumers' meters; reduction of transaction costs; local provision of ancillary services; local frequency and tension regulation; support of local production of electricity by renewable energy sources; provide a register of all energy transactions; tracing of green electricity. In the crowdsourcing energy systems, prosumers can sell the surplus to peers (both consumers and/or prosumers)

at a lower tariff than the imposed price, which is higher than the sale price of their electricity surplus to the network. In crowdsourcing energy systems, prosumers can sell electricity to prosumers at a lower price than the regulated tariff, which is higher than the sale price of their electricity surplus to the network. Testing the proposed trading mechanism has been done for the case with prosumers SSDES. If there is a surplus, the blockchain-based P2P contract solutions have proven to be the most convenient considering both energy quantity and price. Prosumers would pump excess electricity into the local DNO in the physical ADN, and customers would draw power similarly based on the power flow rule. The findings show that the DNOs benefit from optimal energy flows between prosumers and high-power-demand users. The proposed research, on the other hand, only included 24 daily trading hours, although the process may be used longer. A successful transaction depends on the proposed steady-state, with the following factors: prosumers' surplus and distance between users.

## References

1. The Romanian Parliament (2018) Law no. 184/2018 for approving the Government Emergency Ordinance no. 24/2017 regarding the modification and updating of Law no. 220/2008 for determining the incentive system for producing energy from renewable energy sources and the modification of other normative acts. Official Gazette, Part I, No. 635/20.07.2018
2. Lavin A, Gilligan-Lee CM, Visnjic A et al (2022) Technology readiness levels for machine learning systems. *Nat Commun* 13:6039
3. Espe E, Potdar V, Chang E (2018) Prosumer communities and relationships in smart grids: a literature review, evolution and future directions. *Energies* 11:2528
4. National Regulatory Authority for Energy (2018) The 228 order for the approval of the technical norm technical conditions for connection to the public electrical networks of the prosumers. National Regulatory Authority for Energy, Bucharest
5. Neagu BC, Grigoras G (2020) A fair load sharing approach based on microgrid clusters and transactive energy concept. In: 12th international conference on electronics, computers and artificial intelligence. Bucharest, Romania
6. Diahovchenko I, Kolcun M, Čonka Z, Savkiv V, Mykhailyshyn R (2020) Progress and challenges in smart grids: distributed generation, smart metering, energy storage and smart loads. *Iran J Sci Technol Trans Electr Eng* 44:1–15
7. European Smart Grids Task Force—Expert Group 3, Demand Side Flexibility—Perceived barriers and proposed recommendations, Final Report, Apr. 2019
8. Chicco G, Labate D, Notaristefano A, Piglione F (2020) Unveil the shape: data analytics for extracting knowledge from smart meters. *Energ Elettrica Suppl J* 96:1–16
9. Kazmi SA, Shahzad MK, Khan AZ, Shin R (2017) Smart distribution networks: a review of modern distribution concepts from a planning perspective. *Energies* 10:501
10. Neagu BC, Grigoras G (2020) A data-mining-based methodology to identify the behavioural characteristics of prosumers within active distribution networks. In: International symposium on fundamentals of electrical engineering 2020 (ISFEE), Bucharest
11. Neagu BC, Ivanov O, Grigoras G, Gavrilas M (2020) A new vision on the prosumers energy surplus trading considering smart peer-to-peer contracts. *Mathematics* 8:235
12. Surowiecki J (2005) *The wisdom of crowds*. Anchor, San Diego, CA
13. Neagu B-C, Ivanov O, Grigoras G, Gavrilas M, Istrate D-M (2020) New market model with social and commercial tiers for improved prosumer trading in microgrids. *Sustainability* 12:7265

14. Amour L, Dandoush A (2022) Crowdsourcing based performance analysis of mobile user heterogeneous services. *Electronics* 11:1011
15. Howe J (2006) The rise of crowdsourcing. *Wired Mag* 14(6):1–4
16. Mathew SS, El Barachi M, Kuhail MA (2022) CrowdPower: a novel crowdsensing-as-a-service platform for real-time incident reporting. *Appl Sci* 12:11156
17. Wang S, Taha AF, Wang J, Kvaternik K, Hahn A (2019) Energy crowdsourcing and peer-to-peer energy trading in blockchain-enabled smart grids. *IEEE Trans Syst Man Cybern B Cybern* **49**:1612–1623
18. Neagu BC, Grigoras G, Ivanov O (2019) An efficient peer-to-peer based blockchain approach for prosumers energy trading in microgrids. *International Conference on Modern Power Systems (MPS)*, Cluj Napoca
19. Unguru M (2018) Blockchain technology: opportunities for the energy sector. *EUROINFO* 2(1):53–58
20. Andoni M, Robu V, Flynn D, Abram S, Geach D, Jenkins D, McCallum P, Peacock A (2019) Blockchain technology in the energy sector: a systematic review of challenges and opportunities. *Renew Sustain Energy Rev* 100:143–174
21. Mika B, Goudz A (2020) Blockchain-technology in the energy industry: blockchain as a driver of the energy revolution? With focus on the situation in Germany. *Energy Syst* 12:285–355
22. <https://energyindustryreview.com/renewables/all-you-need-to-know-to-become-a-prosumer/>. Accessed 04 March 2021

Article

# Optimal Capacitor Bank Allocation in Electricity Distribution Networks Using Metaheuristic Algorithms

Ovidiu Ivanov \*, Bogdan-Constantin Neagu , Gheorghe Grigoras \*  and Mihai Gavrilas

Department of Power Engineering, Gheorghe Asachi Technical University of Iasi, 700050 Iasi, Romania; bogdan.neagu@tuiasi.ro (B.-C.N.); mgavrilas@yahoo.com (M.G.)

\* Correspondence: ovidiuivanov@tuiasi.ro (O.I.); ggrigor@tuiasi.ro (G.G.)

Received: 16 September 2019; Accepted: 1 November 2019; Published: 6 November 2019



**Abstract:** Energy losses and bus voltage levels are key parameters in the operation of electricity distribution networks (EDN), in traditional operating conditions or in modern microgrids with renewable and distributed generation sources. Smart grids are set to bring hardware and software tools to improve the operation of electrical networks, using state-of the art demand management at home or system level and advanced network reconfiguration tools. However, for economic reasons, many network operators will still have to resort to low-cost management solutions, such as bus reactive power compensation using optimally placed capacitor banks. This paper approaches the problem of power and energy loss minimization by optimal allocation of capacitor banks (CB) in medium voltage (MV) EDN buses. A comparison is made between five metaheuristic algorithms used for this purpose: the well-established Genetic Algorithm (GA); Particle Swarm Optimization (PSO); and three newer metaheuristics, the Bat Optimization Algorithm (BOA), the Whale Optimization Algorithm (WOA) and the Sperm-Whale Algorithm (SWA). The algorithms are tested on the IEEE 33-bus system and on a real 215-bus EDN from Romania. The newest SWA algorithm gives the best results, for both test systems.

**Keywords:** electricity distribution networks; optimal capacitor allocation; Genetic Algorithm; Particle Swarm Optimization; Bat Algorithm; Whale Algorithm; Sperm-Whale Algorithm

## 1. Introduction

Distribution Network Operators take into account the implementation of smart solutions to improve both the voltage level in the subordinate networks and the power factor, with the aim to maintain the balance between power generation and consumption while meeting the quality of supply standards and regulations.

In this context, the use of capacitor banks is an easy solution to be implemented with technical and economic benefits to the smart grid, maximizing the long-term return on investment as the network develops. An intelligent control of capacitor banks leads to improved energy efficiency and voltage level in the buses of distribution networks, resulting in an increase in the percentage of energy delivered to consumers [1].

The advantages of integrating capacitor banks in the flexible smart grid communication and control infrastructure are the increase of network energy efficiency and power quality improvement [2]. Thus, the technologies and modern techniques enable today the large-scale integration of capacitor banks managed with smart control algorithms.

In the literature, many methods have been proposed to solve the Optimal Capacitor Banks Allocation (OCBA) in distribution networks as a combinatorial optimization problem. These techniques

can be grouped in four main categories: numerical [3]; analytical [4]; heuristic [5–7]; and artificial intelligence, population based (Artificial Neural Networks, metaheuristics) [8,9]. An overview about the metaheuristics used for the problem of capacitor banks allocation is made in the following, highlighting their specific purpose. The OCBA solution for power losses or cost minimization is obtained using a genetic algorithm in [10,11], a fuzzy technique in [12] and an artificial neural network in [9]. Regarding the metaheuristics, a significant number of papers consider the joule loss minimization, voltage bus improvement, and total cost minimization. Thus, in [13–15] a Multi-Objective Particle Swarm Optimization (MOPSO) algorithm is proposed. For active power loss reduction using load flow computation, the branch and bound method is generally preferred, for its reduced computation time. For example, for the minimization of the total annual costs, the Crow Search Algorithm (CSA) is used in [16,17], the Particle Swarm Optimization (PSO) and hybrid PSO algorithm are adapted in [18–21], the Flower Pollination Algorithm (FPA) is preferred in [22,23], and an Improved Harmony Algorithm is chosen in [24]. On the other hand, the OCBA problem based on active power minimization was approached in [25,26] using the Bacterial Foraging Optimization Algorithm, the Intersect Mutation Differential Evolution (IMDE) Algorithm in [27], the Artificial Bee Colony (ABC) in [5,28] and the Ant Lion Optimization Algorithm in [29]. The improvement of the voltage profile carried out using the Symbiotic Organisms Search Algorithm (SOSA) in [30]. Another paper proposes the JAYA optimization algorithm [31] for power factor correction. For voltage profile improvement, the Oppositional Cuckoo Optimization Algorithm (OCO) was used in [32]. It must be mentioned that the authors' previous approaches regarding the OCBA problem used several metaheuristic algorithms, such as PSO, BOA, Fireworks Algorithm (FWA), and WOA [33].

A brief description of the papers that use metaheuristics in the CBA problem considering both objective functions (OF) and constraints (C) is presented in Table 1. The considered objective functions are: OF1, active power losses minimization; OF2, voltage profile improvement; OF3, voltage deviation minimization; OF4, cost minimization; OF5—net savings maximization; OF6, voltage stability improvement. The main constraints for the OCBA problem are a combination of the following: C1, bus voltage allowable limits; C2, current flow limits on the branches; C3, bus reactive allowable limits; C4, maximum stock of capacitors; C5, bus apparent power balance; C6, maximum number of transformer tap changer steps; C7, the total reactive power injected should not exceed the total reactive power demand; C8, power flow limits on the branches; and C9, bus power factor limits.

This paper is focused on a comparative study of several metaheuristic algorithms adapted for solving the OCBA problem with the objective of energy loss minimization in MV distribution networks. During the analysis, the well-known GA and PSO are tested against two newer metaheuristics that have seen previous uses in power engineering applications, the BOA and WOA, and another recent but much less used method, the SWA. The latter is shown to outperform all its predecessors, when tested on two MV distribution networks with different characteristics: the smaller IEEE 33—bus test network [5,13,25] and a larger 215—bus 20/0.4 kV distribution network from Romania. During the case study, the algorithms use the same initial population and fitness function. Results are shown regarding active power and energy losses and bus voltage levels, for which the best results are obtained with the SWA.

**Table 1.** Literature review regarding the capacitor allocation problem based on artificial intelligence.

Objective Function	Constraints									Test Network	References
	C1	C2	C3	C4	C5	C6	C7	C8	C9		
OF1	X	X	-	-	-	-	-	-	-	38 bus—Roy–Billinton Test System	[8]
	X	-	X	-	X	X	-	-	-	IEEE 30, 57, 118 and 300 bus	[10,27,29]
	X	-	X	-	X	-	-	-	-	IEEE 33 bus	[13]
	X	X	X	X	-	-	-	-	-	IEEE 33 and 94 bus	[14,15]
	X	X	X	-	X	X	-	-	-	IEEE 30 bus	[21]
	X	X	X	-	X	-	-	-	-	IEEE 33 and 85 bus	[25,28]
OF2	X	X	X	X	X	-	-	-	-	IEEE 33 and 119 bus	[5]
	X	-	-	-	-	-	-	-	-	IEEE 10, 23 and 34 bus	[12]
OF3	X	-	X	-	X	X	-	-	-	IEEE 22, 69, 85 and 141 bus	[32]
	X	-	X	-	X	X	-	-	-	IEEE 30, 57, 118 and 300 bus	[10,27]
OF4	X	X	X	-	X	X	-	-	-	IEEE 30 bus	[21]
	X	-	X	-	-	-	X	-	X	IEEE 10, 33 and 69 bus	[16,17,22,26]
	X	-	X	-	-	-	-	X	-	IEEE 10, 15 and 34 bus	[19]
	X	-	X	-	-	-	-	-	-	IEEE 30 and 85 bus	[20]
	X	-	X	-	-	-	-	-	-	IEEE 33, 34, 69 and 85 bus	[23,27]
OF5	X	-	X	-	X	-	X	-	X	IEEE 85 and 118 bus	[24]
	X	-	-	-	X	-	-	-	-	IEEE 28-bus	[11]
OF6	X	-	-	-	-	-	-	-	-	IEEE 9-bus	[30]
	X	-	X	-	-	X	X	-	-	IEEE 30 bus	[18]
	X	-	X	-	X	X	X	-	-	IEEE 30, 57 and 118 bus	[27]
	X	-	X	-	X	-	-	-	-	IEEE 30, 118 and 300 bus	[29]

## 2. Metaheuristic Algorithms

Metaheuristics are a special class of algorithms that can be used to solve search and optimization problems. As described in [34], they are approximate, usually non-deterministic methods that aim to search for solutions near the global optimum, exploring this space through a partly guided and partly random search. While the main disadvantage of metaheuristics is the uncertainty of reaching the global optimal solution, their advantages lie in not being problem-specific (allowing the flexibility of applying the same solving principle to several types of problems) and having intuitive mathematical models, borrowing concepts and approaches from the natural world, rather than from theoretical mathematical models. This contributes to their accessibility for a wider range of users. Most modern metaheuristics are population-based, starting from an initial group of solutions, called ‘population’, generated randomly, and refining it in an iterative process, according to a set of specific steps, until a stopping criterion is met. The performance of each individual from the population is assessed by computing its fitness function. The basic block diagram of a population-based metaheuristic algorithm (PMA) is depicted in Figure 1, where the steps common to all algorithms are represented with white boxes, and the part specific to each algorithm, delimited by symbols (A) and (B) is presented in gray.

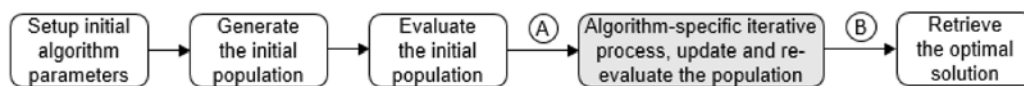


**Figure 1.** The basic flowchart of a population-based metaheuristic algorithm.

The initial parameters are partially common to all algorithms, such as population size  $N$  or maximum number of iterations  $maxit$ , and partially specific to each algorithm, such as the mutation rate  $rmut$  for the Genetic Algorithm (GA) or inertia value  $w$  for the Particle Swarm Optimization (PSO). An individual from a population with  $N$  members, denoted in the following as

$$X_i = [x_1, x_2, \dots, x_m], \quad i = 1 \dots N \quad (1)$$

is encoded as a vector with length  $m$ , and element types and values dictated by the problem that needs to be solved. It usually represents an input parameter combination or a possible solution for the problem, which must satisfy all the constraints of the optimization model. The fitness evaluation of each population member requires the decoding of the information contained in the solution that it represents, solving the problem and evaluating the results. The optimality degree of the solution is assessed with the fitness function value associated to the respective population member. For a population with  $N$  members,  $X_i, i = 1, \dots, N$ ,  $N$  fitness functions will be computed and ranked.

The (A) to (B) section from Figure 1 consists of several steps, which describe each specific metaheuristic algorithm. While in the figures accompanying Sections 2.1–2.5 are presented all the details specific to each algorithm, delimited by (A) to (B), Table 2 summarizes their main steps, emphasizing their particularities.



**Table 2.** The metaheuristic algorithms used in the paper for solving the OCBA problem.

Algorithm	Main Steps
Genetic Algorithm (GA)	Selection, crossover, mutation, using the entire population
Particle Swarm Optimization (PSO)	Speed and position update, using the entire population, and exploration followed by exploitation of the search space
The Bat Optimization Algorithm (BOA)	Speed and position update, frequency adaptation, and local search in each iteration, using the entire population, exploration followed by exploitation
The Whale Optimization Algorithm (WOA)	Continuous choice between three search methods: exploration, encircling, and spiral attack, using the entire population
The Sperm Whale Algorithm (SWA)	Population divided in subgroups that perform the search independently, using dominant crossover in each subgroup

Among the various metaheuristic algorithms available in the literature, those from Table 2 were chosen taking into account the following reasoning: the genetic algorithm and the particle swarm optimization are the best known and widely used metaheuristics, with numerous applications in power systems, which makes them a valid basis for comparison. The bat algorithm and the whale optimization algorithm are newer algorithms, previously used by the authors in solving similar optimization problems and shown to improve the quality of the results, compared with GA and PSO [35,36]. On the other hand, the sperm whale algorithm is a novelty in solving optimization problems in the power systems field. The results from the case study will show that the SWA outperforms the previous algorithms, making it a viable new alternative for solving optimization problems related to power systems applications.

The best-known PMAs are the genetic algorithm and the particle swarm optimization, which also describe two fundamental search principles used by metaheuristic algorithms: the evolutionary and performance-based patterns.

### 2.1. Genetic Algorithms

The Genetic Algorithm (GA), proposed in [37], is probably the best-known metaheuristic algorithm. In the GA, population members are named ‘chromosomes’, and their elements are ‘genes’. The search and optimization mechanisms use Darwinist natural evolution, based on perpetuation through genetic material exchange and mutation inside a population of same-species individuals, across a significant number of generations (iterations).

For finding new and improved solutions for an optimization problem, the GA relies on changing the population by using in each iteration the three main genetic operators (Figure 2):

- Selection: From the existing population, whole individuals are selected based on their performance, expressed by the fitness function. The better-adapted individuals are favored for surviving. In the standard GA, the population size is constant. Thus, the lesser adapted individuals, which are discarded, are replaced by clones of the survivors.
- Crossover: Pairs of parent chromosomes exchange a number of genes, the resulting offspring having new characteristics, possibly resulting in better solutions for the problem.
- Mutation: Randomly generated variations on gene values, resulting in chromosomes with minor structural changes, simulating genetic mutations of real living organisms.

- **Mutation:** Randomly generated variations on gene values, resulting in chromosomes with minor structural changes, simulating genetic mutations of real living organisms. 6 of 36

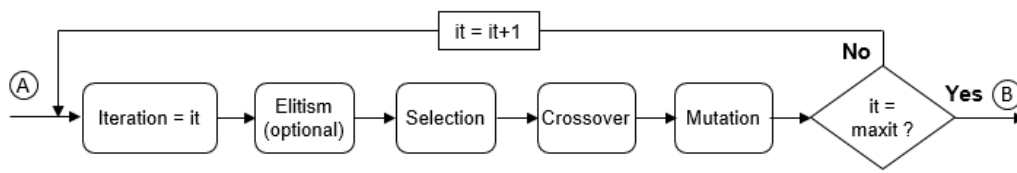


Figure 2. The flowchart of a GA iteration.

Optionally, an elitist procedure can also be incorporated in the GA, which ensures the preservation of the best-found optimal solution and its fitness function across generations.

The literature offers a high variety of selection [38] and crossover [39] types, which together with the user-chosen crossover and mutation rates provide significant customization possibilities, making the GA a flexible problem-solving tool.

In this paper, the tournament selection method was used, which draws randomly  $p$  members from the existing population, out of which retains the best  $q$ , according to their fitness function. The procedure is repeated until a new population of size  $N$  is created.

The method of choice for the crossover operator was the uniform crossover, illustrated in Figure 3. Two parents are randomly chosen from the population and, for each gene, a random number is generated. The parents swap the genes only if the generated random number exceeds a customizable threshold  $tr$ .

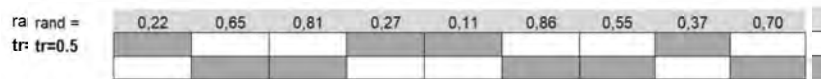


Figure 3. The uniform crossover.

2.2. Particle Swarm Optimization

2.2. Particle Swarm Optimization

On the other hand, the PSO algorithm [40] uses a different search method, based on variable travel speeds and its position shifting in the search space. Each individual (‘particle’) from the population (‘swarm’) changes its speed in each iteration based on its current distance from the reference compound. The best solution found so far, presented as a leader, and the best position for each particle, the particle itself, are compared with the GA, the PSO mechanism, presented in Figure 4, is very simple, requiring for each particle  $j, j = 1..N$ , only the computation of its new speed and position:

$$sp_j^{(it)} = w \cdot sp_j^{(it-1)} + 2 \cdot rnd_1 \cdot (x_{j,best}^{(it)} - x_{j,crt}^{(it)}) + 2 \cdot rnd_2 \cdot (leader^{(it)} - x_{j,crt}^{(it)}) \tag{2}$$

$$x_j^{(it+1)} = x_j^{(it)} + sp_j^{(it)} \tag{3}$$

$$x_j^{(it+1)} = x_j^{(it)} + sp_j^{(it)} \tag{3}$$

followed by the update of each particle’s best position and the change of the leader position, if better solutions are found. The particle speeds are initialized with low random values, which would not influence the search direction.

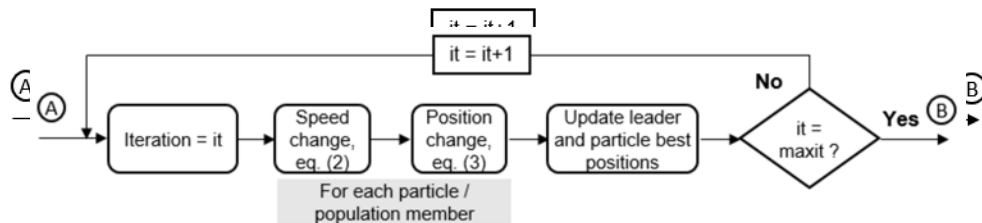


Figure 4. The flowchart of a PSO iteration.

In Equations (2) and (3),  $sp_j^{(it)}$  and  $sp_j^{(it-1)}$  are the speed of particle  $x_j (j = 1 \dots N)$  in the previous  $(it - 1)$  and current  $(it)$  iteration,  $rnd_1$  and  $rnd_2$  are random vectors,  $x_{j,best}^{(it)}$  and  $x_{j,crt}^{(it)}$  are the best personal

and the current position of particle  $x_j$ ,  $leader^{(it)}$  is the position of the leader in iteration  $it$ , and  $x_j^{(it)}$  is the position of particle  $x$  in the current iteration. The factor  $w$  from Equation (2) is an inertia term, which decreases over the iteration count, larger initial values encouraging exploration, and smaller final values enabling the exploitation or local search around the best-known optimal solution.

It should be noted that while the GA explores the search space using crossover to make random changes of the information that is already present in the population, the mutation probability being much smaller, PSO changes randomly the speed of each particle element, moving it in the direction of the leader and personal best position.

The newer metaheuristic methods used in this paper, while sharing the natural inspiration of GA and PSO, combine elements found in the two algorithms and increase the number of input parameters and the complexity of their mathematical model in order to improve their optimization performance. They are the Bat Optimization Algorithm (BOA), Whale Optimization Algorithm (WOA) and Sperm-Whale Algorithm (SWA).

### 2.3. The Bat Optimization Algorithm

Bats hunt for prey using echolocation. In the initial search stage, they emit high amplitude/low frequency ultrasound impulses, with low emission rate (10–20 imp/sec), decoding in real time the reflected waves in order to identify the approximate position of the prey. When a potential target is identified, the bat increases the pulse rate up to 200 imp/sec, and the pulse frequency, which enables it to search accurately the space separating it from the prey, identifying the obstacles in its path and precisely locating the victim and its movement pattern.

The bat optimization algorithm [41] uses the PSO principle of changing the speed and position of the population members (here called ‘bats’), but the speed update formula is more elaborated, considering the principle of raising the signal frequency and pulse rate as the bats are getting close to the prey, i.e., to the optimal solution. The basic flowchart of a BOA iteration is depicted in Figure 5.

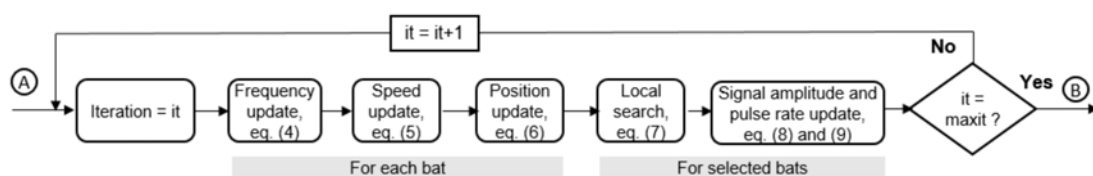


Figure 5. The flowchart of a BOA iteration.

The bats’ speeds are initialized in the same manner as in the PSO algorithm but are accompanied by the initial signal amplitude,  $A_j$ , maximum pulse rate,  $r_{j,max}$  and random pulse frequency  $f_j \in [f_{min}, f_{max}]$ ,  $j = 1, \dots, N$ .

In each iteration  $it$ , every bat from the population performs three operations:

- Frequency update:

$$f_j = f_{\min} + rnd \cdot (f_{\max} - f_{\min}) \quad (4)$$

- Speed update, with an equation inspired from (2):

$$sp_j^{(it)} = w \cdot sp_j^{(it-1)} + f_j \cdot rnd_1 \cdot (x_{j,crt}^{(it)} - x_{j,best}^{(it)}) \quad (5)$$

- Position update, identical to the formulation from (3):

$$x_j^{(it+1)} = x_j^{(it)} + sp_j^{(it)} \quad (6)$$

The BOA also includes a local search. The best individuals from the population are randomly moved in the search space, with

$$x_j^{(it+1)} = x_j^{(it+1)} + pp \cdot \bar{A}, \quad j = 1 \dots M, \quad M < N \quad (7)$$

where  $\bar{A}$  is the average bat amplitude for iteration  $it$  and  $pp \in [-1, 1]$ .

The new bat positions computed with Equations (4) to (7) are accepted in the population with random probability and only if the newly obtained position is better than the previous.

At the end of each iteration, if a bat improves its position, its signal amplitude is decreased:

$$A_j^{(it+1)} = \alpha \cdot A_j^{(it)} \quad (8)$$

and its pulse emission rate increases:

$$r_j^{(it+1)} = r_j^{(it)} \cdot (1 - e^{-\gamma \cdot it}) \quad (9)$$

where  $\alpha \in (0, 1)$  and  $\gamma > 0$ .

This behavior, much like the inertia term for PSO, increases the probability of performing local searches when the iteration count is nearing  $itmax$ .

#### 2.4. The Whale Optimization Algorithm

The hunting behavior of humpback whales is the source of inspiration for the Whale Optimization Algorithm (WOA). The whales hunt in groups, and when they find their prey, consisting of schools of krill or small fish near the water surface, they attack it from below using two maneuvers: encircling and spiraling.

The WOA uses a population of vector solutions ('whales'), which are hunting for prey independently, guiding their search by following a reference individual, usually their leader, i.e., the whale closest to the problem solution ('food'), according to its fitness function.

During the algorithm, whales use initially encircling, then spiral attack, in the same way PSO and BOA use the broad exploration and the exploitation of the search space near the optimal solution.

In each iteration  $it$ , the encircling performed by each whale  $j$  from the population is described by [42]:

$$x_j^{(it+1)} = reference^{(it)} - A \cdot D_1 \quad (10)$$

where

$$A = 2 \cdot a \cdot rnd_1 - a \quad (11)$$

$$D_1 = |C \cdot reference^{(it)} - x^{(it)}|, \quad C = 2 \cdot rnd_2 \quad (12)$$

The coefficient  $a$  from equation (11) is a scalar value decreasing during the iterative from a positive value to 0. The  $(\cdot)$  sign denotes the element-by-element multiplying of vectors, and  $||$ , an absolute value.

For the extreme values of  $a = 0$  and  $a = 1$ , equations (10) to (12) show that position  $x_j^{(it+1)}$  will always lie between  $x_j^{(it)}$  and  $reference^{(it)}$ , thus moving any whale towards the reference solution used to guide the population. If values larger than 1 are given to  $a$ , factor  $A$  from (11) will also increase, moving the whales beyond the target and exploring a possibly uncharted portion of the search space.

If the reference position is  $reference^{(it)} = leader^{(it)}$ , the leader from the current iteration, when  $A$  decreases, whales get closer to the leader, encircling the prey or the optimal solution. If another whale is used as reference,  $reference^{(it)} = random(x^{(it)})$ , the search will shift towards its path, simulating the exploration of the sea in search for food performed by real whales.

The spiral attack phase is described by an equation that combines oscillatory and exponentially varying components:

$$x_j^{(it+1)} = D_2 \cdot e^{b \cdot l} \cdot \cos(2 \cdot \pi \cdot l) + leader^{(it)} \quad (13)$$

with

$$D_2 = |leader^{(it)} - x_j^{(it)}| \tag{14}$$

In equation (13),  $b$  is a constant, and  $l$  is a random value from the  $[-1, 1]$  interval [42].

The initially large, then gradually decreasing values of  $a$ , so that first  $|A| > 1$ , then  $|A| < 1$ ,  $|A| \rightarrow 0$ , first move the whales away from the leader in exploration, then encourage encircling, followed by spiral attack. If  $p$  denotes a random number, the general equation for changing the position of a whale follows as:

$$x_j^{(it+1)} = \begin{cases} reference^{(it)} - A \cdot D_1, & \text{if } p \geq 0.5 \\ D_2 \cdot e^{bl} \cdot \cos(2 \cdot \pi \cdot l) + leader^{(it)} & \text{if } p < 0.5 \end{cases} \tag{15}$$

The flowchart of a WOA iteration is presented in Figure 6.

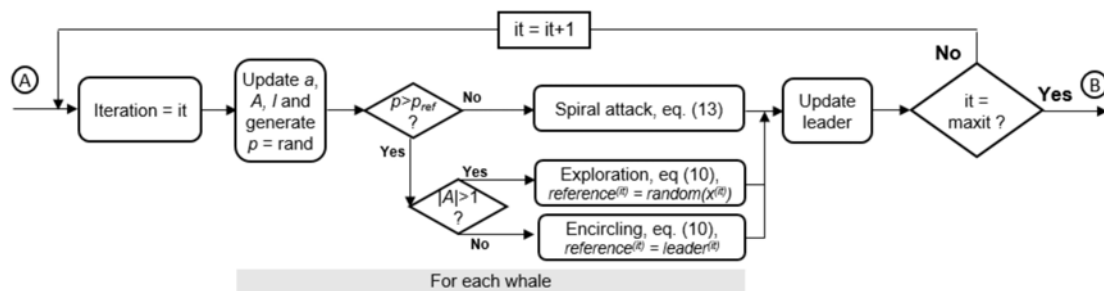


Figure 6. The flowchart of a WOA iteration.

WOA has two specific parameters that can be tuned for better performance: coefficient  $a$  from Equation (11) and constant  $b$  from (13).

### 2.5. The Sperm-Whale Algorithm

The search used by the SWA mimics the hunting behavior of sperm whales, which live alone or in small groups at the bottom of the sea and must come to the surface to hunt and breathe [43]. In each iteration, the population of the SWA is split into smaller search groups consisting in uniformly distributed better and worse adapted members ('sperm whales'). Consequently, the search for the optimal solution occurs independently in each group. First, the sperm whales change their position from the bottom of the sea to the surface. This step is simulated only for the worst adapted member of the group, for which the opposite position is computed. The positions of the leader and of the worst individual in a group  $g$ ,  $leader^{(g,it)}$  and  $worst^{(g,it)}$ , are used to compute an in-between distance  $dist^{(g,it)}$ :

$$dist^{(g,it)} = worst^{(g,it)} + w \cdot leader^{(g,it)} \tag{16}$$

The reflex position of  $worst^{(g,it)}$  is then computed with Equation (17).

$$reflex^{(g,it)} = worst^{(g,it)} + 2 \cdot (dist^{(g,it)} - worst^{(g,it)}) = 2 \cdot dist^{(g,it)} - worst^{(g,it)} \tag{17}$$

The newly computed individual  $reflex^{(g,it)}$  will replace  $worst^{(g,it)}$  only if its fitness function is better. At the beginning of the iterative process, when the inertia  $w$  from Equation (16) is large, the individual will search beyond  $leader^{(g,it)}$  (exploration phase, Figure 7a). As  $w$  decreases, the search will focus between  $worst^{(g,it)}$  and  $leader^{(g,it)}$ , exploiting the search space around the known optimal solution (Figure 7b).

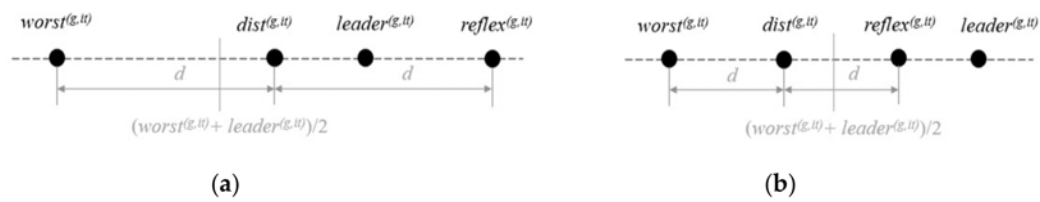


Figure 7. Reflex search in the SWA algorithm: (a) exploration, (b) exploitation.

In the second stage, a Good Gang is formed within the group, gathering the best gg individuals ranked according to their fitness function. Every Good Gang member performs several local searches in which its elements  $k$  are displaced randomly, within a small radius  $r$ :

$$x_{j,k} = \pm r \cdot x_{j,k}, \quad j = 1 \dots gg \tag{18}$$

The original Good Gang members are replaced only if better sperm-whale positions are found during the local search.

Finally, the best Good Gang member from the group (the dominant sperm-whale) performs genetic crossover with all other group individuals. One of the two resulting children is chosen randomly to replace the worst of the two parents.

At the end of the iteration, the groups are reunited in the final population, which will repeat the search process until the stopping criterion of the algorithm is met. The basic flowchart of a SWA iteration is presented in Figure 8.

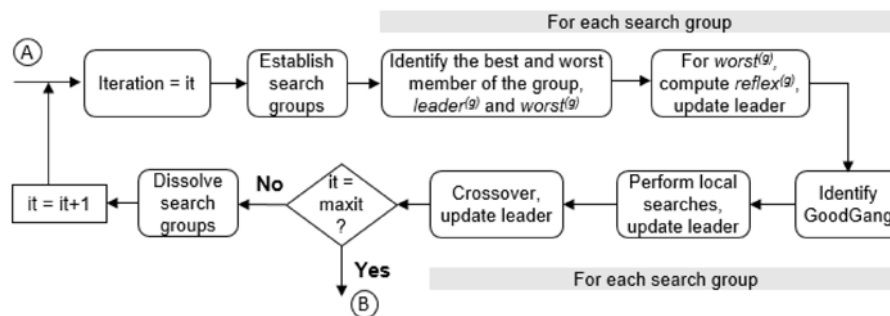


Figure 8. The flowchart of a SWA iteration.

The SWA offers several tuning options for the user. The population size, number of search groups within the population, the inertia  $w$  and its decrement, the Good Gang size and number of local searches for its members, the local search radius  $r$ , and the crossover method can be adjusted for better performance.

### 3. The Implementation of the Optimal Reactive Compensation for Loss Minimization Problem

The five metaheuristic algorithms presented in the previous chapter were run in an implementation of the Optimal Capacitor Banks Allocation (OCBA) problem for active energy loss minimization. The approach used in this paper is stated as follows: Find the optimal buses in an EDN where capacitor banks (CB) should be installed and the amount of reactive load compensation in each bus, with the objective of operating the EDN with minimal active power and energy losses for the interval of a typical day. For an EDN with  $NN$  buses (nodes) and  $NB$  branches, the mathematical expression of the objective function of the OCBA problem was defined as:

$$\Delta P[\%] = \sum_{h=1}^{24} \Delta P_h / \left( \sum_{h=1}^{24} \sum_{bus=1}^{NN} P_{b,h} + \sum_{h=1}^{24} \Delta P_h \right) * 100 = \min \tag{19}$$

The mathematical model of the fitness function considered the following constraints:

Cr1. The available CB stock cannot be exceeded:

$$\sum_{bus=1}^{NN} NCB_{bus} \leq stock_{CB} \tag{20}$$

Cr2. The compensation level in each bus cannot exceed the reactive bus load (avoid reversed reactive power flows):

$$NCB_{bus} \cdot q_{CB} \leq Q_{bus}, \quad bus = 1 \dots NN \tag{21}$$

Cr3. Branch current flows after compensation cannot exceed the branch rated current:

$$I_{br} \leq I_{max,br}, \quad br = 1 \dots NB \tag{22}$$

Cr4. Bus voltages after compensation cannot exceed the maximum allowed value:

$$U_{bus} \leq U_{max,bus}, \quad bus = 1 \dots NN \tag{23}$$

In Equations (19) to (22),  $\Delta P[\%]$  is the percent active power loss in the EDN over 24 h,  $\Delta P_h$  is the active power loss in the EDN at hour  $h$ ,  $NCB_{bus}$  is the number of CBs installed in a generic bus;  $q_{CB}$  is the reactive power rating of a CB,  $Q_{bus}$  is the reactive load of a generic bus,  $stock_{CB}$  is the CB stock;  $I_{br}$  is the current flow on a generic branch  $br$ ,  $I_{max,br}$  is the rated current of branch  $br$ ,  $U_{bus}$  is the voltage of a generic bus after compensation, and  $U_{max,bus}$  is the maximum bus voltage allowed in a generic bus.

All the algorithms tested in the case study used the same solution encoding for their population members. They were generated as vectors of the type described by Equation (1), with integer numbers and length equal to the number of buses in which compensation was possible in the network. The significance of the value of a generic element represented the number of CBs placed in the bus to which it was designated. All the algorithms started in the first iteration with the same population, generated randomly but considering constraint Cr2 of maximum allowed number of CBs in each bus and Cr1, the maximum CB stock (Figure 9).

	bus 1	bus 2	bus 3	...	bus M-1	bus M
max. allowed in bus	5	0	3		2	4
actual compensation	3	0	1		2	2

Figure 9. The encoding of the solutions used by the OCBA problem.

The fitness of the optimal solutions was assessed in all the algorithms using the objective function (19), which also considered the constraints from Equations (20) to (23). The methodology employed for calculating the fitness of each solution is described in Figure 10.

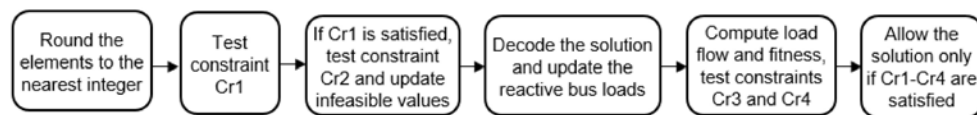


Figure 10. Fitness computation and solution validation for the OCBA problem.

By applying any of the equations (2) to (18) or by genetic crossover and mutation, the changes undergone by population members can result in their invalidation because of

- Non-integer values, leading to invalid number of CBs installed in a bus;
- Values exceeding the interval  $[0, NCB_{bus}]$  allowed by the constraint Cr2;
- Violation of constraint Cr1, by exceeding the available CB stock;
- Solutions otherwise valid but which lead to the violation of the constraints Cr3 or Cr4.

Thus, every newly generated population member, for each algorithm, must pass through a validation procedure before being allowed in the population created for the next iteration.

If constraint Cr1 is not satisfied, the solution is always discarded as unfeasible. If the constraint Cr2 is not fulfilled, the solution is modified by setting the unfeasible values to the nearest allowed value, using for each element  $x_j$  from Figures 1 and 9 the following correction:

$$x_j = \begin{cases} 0, & \text{if } x_j = 0 \\ NCB_j, & \text{otherwise} \end{cases} \quad (24)$$

For each population member, the active power losses used in equation (19) are computed with the Newton–Raphson load flow (LF) algorithm, which is slower, but generally considered more accurate than the branch-and-bound methods preferred in the analysis of distribution networks. The LF algorithm also provides the results required for checking the constraints Cr3 and Cr4, bus voltage and branch current flow limits. Prior to computing the LF, the compensation solution is simulated subtracting from the bus reactive loads the CB injection for each compensated bus, according to the population member/solution being tested.

#### 4. Results

The OCBA problem was solved using the metaheuristics presented in Section 2, with the aim of comparing the performance of the newer algorithm designs, BOA, WOA, and SWA against the two well established methods, GA and PSO. For comparison purposes, all the algorithms had a common representation for the members of the population, illustrated in Figure 9, and the same fitness function, active power and energy loss minimization, computed with Equation (19) and subjected to the constraints given by Equations (20) to (23), Section 3. The initial parameters used for the algorithms are presented in Table 3.

Since for all algorithms there was no improvement for the optimal solution beyond generation 350, the graphical representations of the results will be limited to the first 360 generations.

Two test networks were used to validate the comparison: the smaller sized IEEE 33-bus MV radial voltage distribution system (Figure 11) and a larger 215-bus MV EDN from a residential area of a major city from Romania (Figure 12).

Synthetic data regarding the physical characteristics for the IEEE 33-bus system is given in Table 4. The system does not include MV/LV transformer data; thus, the active power losses computed by the algorithms do not include transformer losses. The extended data regarding branch characteristics (connecting buses, type line or transformer, electrical parameters resistance and reactance, maximum branch current) is provided in Appendix A, Table A1. For the active and reactive bus loads, the study uses a custom representation consisting of daily 24-h profiles, described below.

For this particular test system, the literature provides only a set of instantaneous active and reactive bus loads. In this paper, these values were used as reference, in conjunction with a set of typical load profiles (TLP) provided in the Supplementary Materials attached to the paper, to create 24-h profiles. The TLPs considered several types of loads, residential, industrial, and their distribution in the network is summarized in Table 5.



**Table 3.** The initial parameters used for the metaheuristic algorithms.

<b>Common Parameters for All the Algorithms:</b>
Population size: 40, Number of generations: 500
<b>GA</b>
Selection method: tournament—keep best 2 from a random draw of 4 Crossover method: uniform at threshold 0.5 Mutation: random Crossover and mutation rates: 0.9/0.1
<b>PSO</b>
Inertia: 0.9 decreasing to 0.4, linear descent
<b>BOA</b>
Initial amplitude: 1 Initial pulse emission rate: 0.3 Amplitude attenuation rate: 0.7 Pulse emission increase rate: 0.3 Pulse frequency domain: $[-0.9, 1.2]$
Number of bats used for local search: dynamic. If a randomly generated number is greater than the bat's pulse emission rate, the bat is selected for local search in the current iteration.
<b>WOA</b>
Coefficient $a$ : decreasing from 3 to 0, linear descent Coefficient $l$ : random Coefficient $b$ : 1
<b>SWA</b>
Number of search groups: 4 Good Gang size: half of the search group size, rounded to the nearest integer Number of searches performed by each Good Gang member: 10 Local search radius: 1 Crossover type: uniform

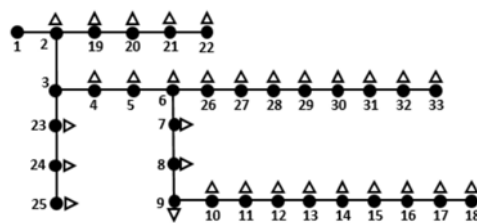


**Figure 11.** The IEEE 33-bus test system.

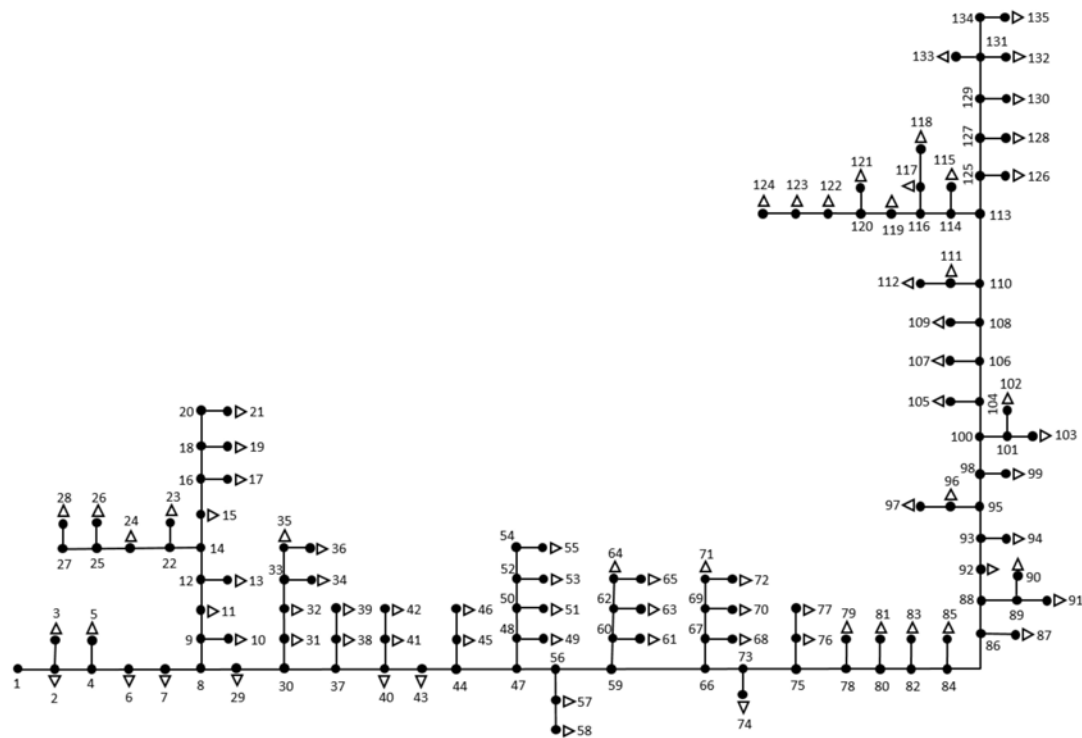


Figure 12. The residential 215-bus EDN.

Table 4. The physical characteristics of the IEEE 33-bus system.

Number of Buses	Transformer Rated Power/Number	Feeder Type	Feeder Cross-Section (mm <sup>2</sup> )	Total Length(km)
12.66 kV: 33	None	Unknown <sup>(1)</sup>	Unknown <sup>(1)</sup>	Unknown <sup>(1)</sup>

<sup>(1)</sup> Only the total resistance and reactance is known for each branch

Table 5. The TLP categories used for the IEEE 33 -bus system and their bus distribution.

TLP Category	Bus
Residential	4, 5, 6, 7, 8, 9, 10, 11, 12, 13, 14, 15, 16, 17, 18
Industry	2, 3, 19, 20, 21, 22, 23, 24, 25
Commercial	26, 27, 28, 29, 30, 31, 32, 33

The second test system used in the case study is a much larger EDN, consisting of 135 MV buses to which 80 loads are connected through MV/LV transformers. For simplicity, the transformers are omitted in Figure 12, together with the corresponding 80 bus numbers for the transformer LV busbars (from 136 to 215). A summary of the transformer rated power, together with the feeder and bus general information, is given in Table 6. The electrical parameters of the branches are given in Appendix A, Table A2. For this network, the bus loads were also modelled as 24-h daily profiles, being measured by the smart metering infrastructure installed by the local distribution utility for a typical working day.

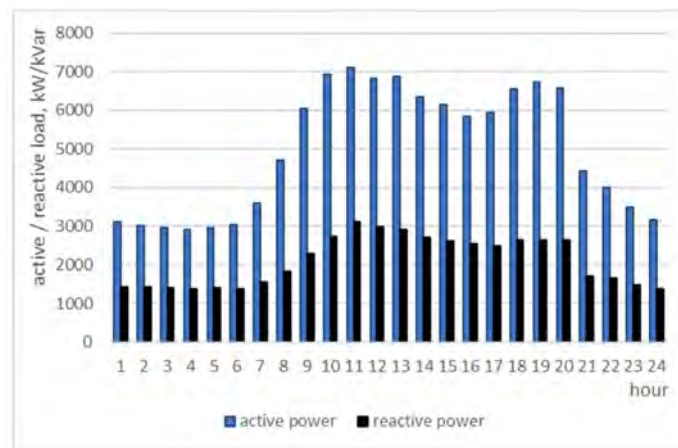
**Table 6.** The physical characteristics of the 215-bus EDN.

Number of Buses	Transformer Rated Power/Number	Feeder Type	Feeder Cross-Section (mm <sup>2</sup> )	Total Length (km)
20 kV: 135 (1–135) 0.4 kV: 80 (136–215)	63 kVA: 33; 100 kVA: 14	Cable	3 × 95	2.5
	160 kVA: 15, 250 kVA: 15		3 × 120	84.45
	400 kVA: 3		3 × 150	3.2

Because a 24-h voltage profile was not available for the 215-bus network, the voltage reference for the slack bus was recommended by the distribution utility at the value of 1.06 pu. For the IEEE 33-bus system, the setpoint was 1 pu (nominal voltage). The slack bus for both networks is bus 1, and all the other buses are modeled as PQ (consumer) buses.

#### 4.1. Results for the IEEE 33-Bus System

The first step of the study was the choice of the maximum CB stock used for optimization. For this purpose, the load profile of the network for 24 h, given in Figure 13, was analyzed. Since the purpose was to test the performance of each algorithm, the CB stock was set at  $70 \times 7.5$  kVar units, which would ensure a maximum of 525 kVar of VAR compensation, about half of the minimal value of the reactive load, occurring at night hours. In this way, the number of possible CB allocation variants is maximized, while reducing the investment cost.

**Figure 13.** The active and reactive load profiles of the IEEE 33-bus test system—hourly values.

The GA, PSO, BOA, WOA, and SWA were run using this CB stock, the initial parameters from Table 3, and the same initial population. The solution identified by each algorithm, compared with the reference case (no reactive power compensation), and their corresponding fitness functions (percent losses) are presented in Table 7. The first line of Table 7 also presents the maximum number of CBs that can be allocated in each bus, computed according to the minimal reactive power load, so that constraint Cr2 would be always fulfilled. The same results are displayed graphically in Figure 14. In Figure 15, the parallel evolution of the fitness function of each algorithm over the first 350 generations is presented, on a typical run, emphasizing the fact that the SWA and BOA obtain the solutions corresponding to the lowest loss values, followed by the PSO, GA, and BAT.

**Table 7.** The OCBA solutions found by the metaheuristic algorithms for the IEEE 33-bus system.

Bus	2	3	4	5	6	7	8	9	10	11	12	13	14	15	16	17	18
CB																	
limit	3	2	4	0	0	6	3	1	4	0	6	4	4	0	0	0	14
Reference	0	0	0	0	0	0	0	0	0	0	0	0	0	0	0	0	0
GA	1	1	1	0	0	1	1	1	2	0	5	1	2	0	0	0	13
PSO	0	0	0	0	0	4	0	1	0	0	0	4	4	0	0	0	14
BAT	0	2	4	0	0	3	1	1	1	0	6	4	3	0	0	0	2
WOA	0	0	0	0	0	0	0	1	0	0	1	4	4	0	0	0	14
SWA	0	0	0	0	0	0	0	0	0	0	4	4	4	0	0	0	14
Bus	19	20	21	22	23	24	25	26	27	28	29	30	31	32	33	CB Used	Fitness
CB																	
limit	6	1	17	2	3	7	5	0	0	0	3	39	4	5	0	143	N/A
Reference	0	0	0	0	0	0	0	0	0	0	0	0	0	0	0	0	5.482
GA	1	1	1	1	1	1	1	0	0	0	1	27	4	2	0	70	4.982
PSO	0	1	0	0	0	0	0	0	0	0	3	39	0	0	0	70	4.947
BAT	0	1	0	1	3	7	2	0	0	0	2	24	2	1	0	70	5.038
WOA	0	1	0	0	0	0	0	0	0	0	0	39	1	5	0	70	4.939
SWA	0	0	0	0	0	0	0	0	0	0	0	35	4	5	0	70	4.934

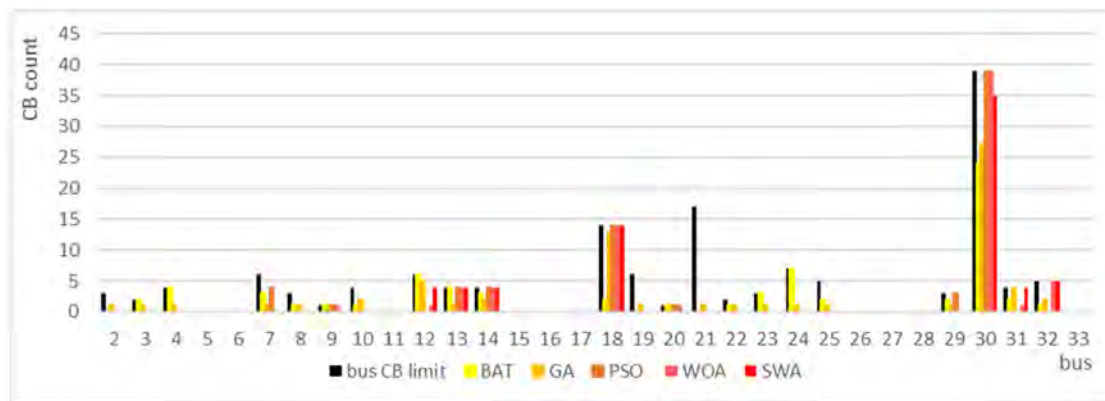


**Figure 14.** The number of CBs allocated in the buses of the IEEE 33-bus system by each algorithm.

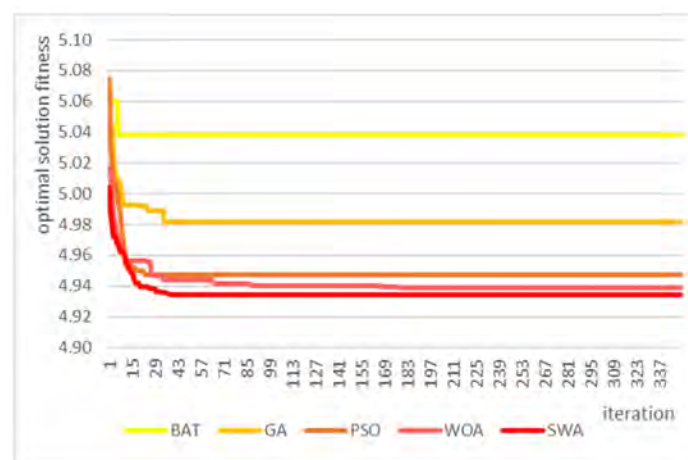


**Figure 15.** The fitness of the optimal solution found by the metaheuristic algorithms after 360 iterations, for the IEEE 33-bus system.

The results from Table 7 and Figure 14 show that the best fitness function values are obtained when maximum compensation is applied at buses 18 (feeder end), 29–32 (feeder end), and 12–14, while for other buses with compensation potential, such as 21–25, where the reactive load is high, no capacitor banks are allocated. All the algorithms use the entire CB stock available, with differences in the buses chosen for compensation and number of CBs allocated to each bus.

The results regarding the active power losses, for each hour and algorithm, compared with the reference case are plotted in Figure 16 and presented in Table 8. Table 9 gives the loss reduction in percent, against the reference case, for which the total values are represented in Figure 17. The loss reduction ranges between 6.55% and 16.78%, depending on the algorithm and network load. The improvement is higher in off-peak hours, and the best results are obtained with SWA (8.17% to 16.78%), with a global value of 10.51% over 24 h. PSO, WOA, and SWA are the closest to the optimal solution.

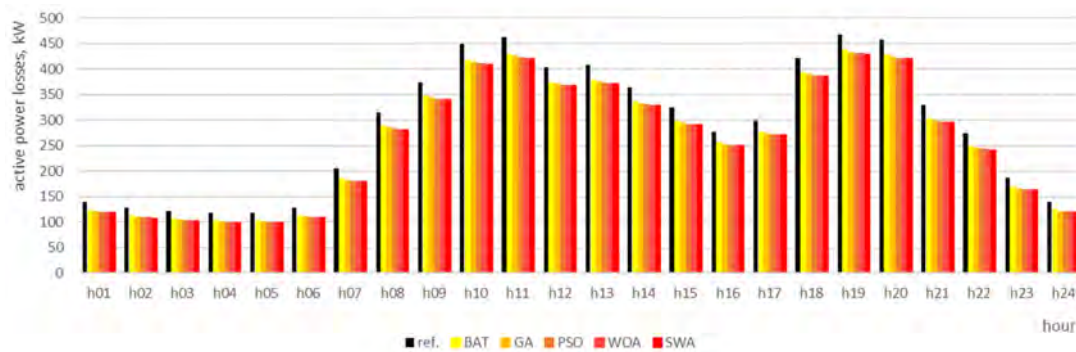


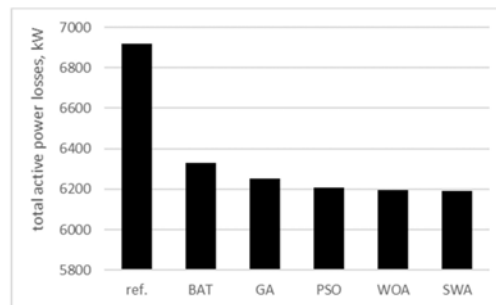
**Figure 16.** Hourly active power losses in the IEEE 33-bus system, for each algorithm.

**Table 8.** Hourly and total active power losses in the IEEE 33-bus system, in kW, for each algorithm.

Hour	Ref.	BAT	GA	PSO	WOA	SWA
h01	140.04	122.53	120.22	118.98	118.74	118.51
h02	128.61	111.53	109.32	108.14	107.93	107.70
h03	122.58	105.89	103.74	102.65	102.45	102.22
h04	119.17	102.76	100.65	99.59	99.39	99.17
h05	118.50	102.35	100.31	99.31	99.13	98.90
h06	128.54	112.25	110.25	109.23	109.04	108.82
h07	205.62	184.05	181.30	179.43	178.99	178.75
h08	314.56	287.82	284.37	281.89	281.25	280.98
h09	374.57	345.89	342.50	340.05	339.35	339.12
h10	448.92	416.40	412.92	410.21	409.41	409.15
h11	462.22	427.75	424.10	421.26	420.40	420.17
h12	404.06	373.11	370.05	367.81	367.11	366.87
h13	408.02	377.17	373.94	371.64	370.97	370.72
h14	364.61	335.05	331.31	328.94	328.27	328.03
h15	324.39	296.90	293.33	291.25	290.70	290.45
h16	277.75	254.32	251.42	250.06	249.70	249.46
h17	298.98	275.44	272.52	271.10	270.71	270.50
h18	421.48	391.95	388.02	385.68	385.03	384.78
h19	466.73	436.14	431.94	429.53	428.93	428.60
h20	458.26	427.14	422.83	420.32	419.70	419.36
h21	329.63	302.53	298.48	295.98	295.44	295.03
h22	273.68	248.43	244.68	242.37	241.88	241.51
h23	187.07	167.53	164.73	163.25	162.98	162.67
h24	139.61	123.09	120.90	119.80	119.60	119.37
total	6917.59	6328.03	6253.83	6208.47	6197.11	6190.86

**Table 9.** Hourly and total power loss reduction in the IEEE 33-bus system, in %, for each algorithm.

Hour	BAT	GA	PSO	WOA	SWA
h01	12.50	14.15	15.03	15.21	15.37
h02	13.28	15.00	15.91	16.08	16.26
h03	13.62	15.37	16.26	16.42	16.61
h04	13.77	15.54	16.43	16.60	16.78
h05	13.62	15.35	16.19	16.35	16.54
h06	12.67	14.22	15.02	15.17	15.34
h07	10.49	11.83	12.74	12.95	13.06
h08	8.50	9.60	10.39	10.59	10.67
h09	7.66	8.56	9.22	9.40	9.47
h10	7.24	8.02	8.62	8.80	8.86
h11	7.46	8.25	8.86	9.05	9.10
h12	7.66	8.42	8.97	9.15	9.20
h13	7.56	8.35	8.92	9.08	9.14
h14	8.11	9.13	9.78	9.97	10.03
h15	8.47	9.57	10.21	10.38	10.46
h16	8.44	9.48	9.97	10.10	10.18
h17	7.87	8.85	9.32	9.46	9.53
h18	7.00	7.94	8.49	8.65	8.71
h19	6.55	7.46	7.97	8.10	8.17
h20	6.79	7.73	8.28	8.41	8.49
h21	8.22	9.45	10.21	10.37	10.50
h22	9.23	10.60	11.44	11.62	11.76
h23	10.45	11.94	12.73	12.88	13.04
h24	11.83	13.40	14.19	14.33	14.49
total	8.52	9.60	10.25	10.42	10.51

**Figure 17.** The total active power loss reduction in the IEEE 33-bus system, in kW, for each algorithm.

Compared with the reference case, the best compensation solution found by the SWA leads to a loss reduction of 726.73 kW for the analyzed day, which, if it is extrapolated for a year, amounts to 265.26 MW loss saving. The difference between SWA and the second best result, given by WOA, is of 6.25 kW per day or 2.28 MW for an entire year. As Figure 16 shows, SWA achieves these savings mainly during two hours, at 19.00 and 24.00.

Reactive power compensation with capacitor banks is mainly used in EDN for voltage profile improvement, where specific networks configurations and load patterns lead to high voltage drops along the feeders. In the case of the IEEE 33-bus system, the nominal voltage setting for the slack bus and the load profiles from Appendix A lead, in the reference case without compensation, to the voltage profile described by Figure 18.

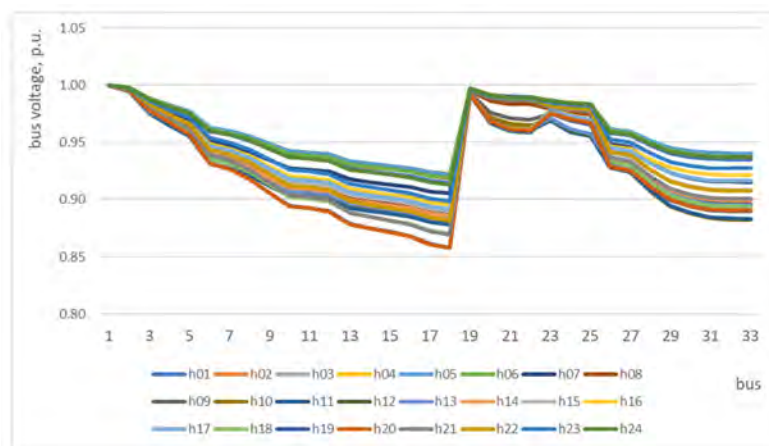


**Figure 18.** The bus voltages in the IEEE 33-bus system without compensation, for each hour from the analyzed day.

The values show voltage drops that exceed the lower limit of  $-10\%$  prescribed by the Romanian standards, in several buses located near the end of the main two supply paths, ending in buses 18 and 33. For bus 18, the voltage has the minimum value of 0.858 pu, at hours 19.00 and 20.00, while for bus 33, the minimum voltage is 0.882 pu, at hour 10.00.

The improvement of the voltages obtained hourly with each algorithm is depicted in Figure 19 for bus 18 and in Figure 20 for bus 33. The percent improvements over the reference values (no compensation) are given in Tables 10 and 11, respectively. Again, the SWA gives the best results, with the maximum voltage improvement. The minimum reference voltage value of 0.858 pu in bus 18 (hour 10.00) is raised by 1.65%, to 0.872 pu. However, the voltages remain below the 0.9 pu minimum allowed limit, for 10 h from the 24-h analysis interval. Better voltage regulation can be possible using a larger CB stock or raising the voltage in the reference bus, by changing the HV/MV transformer tap position from the substation at bus 1.

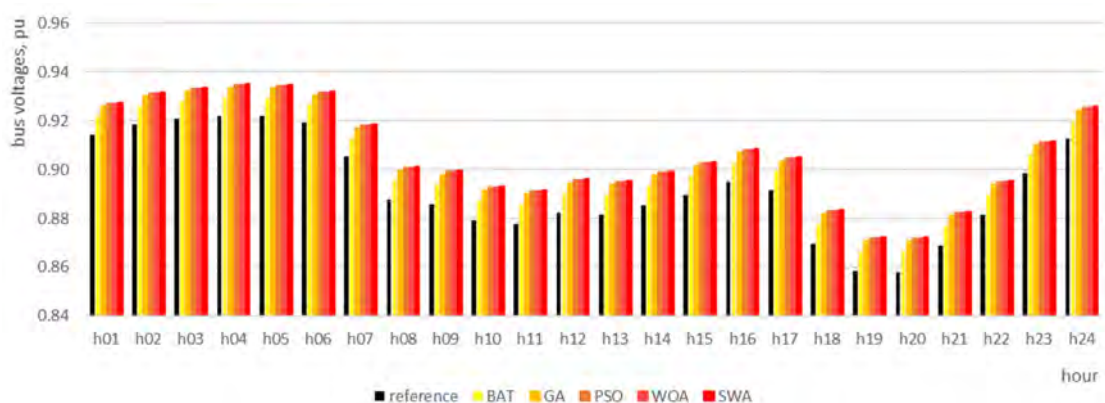


**Figure 19.** Voltage improvement after compensation for bus 18, the IEEE 33-bus system.



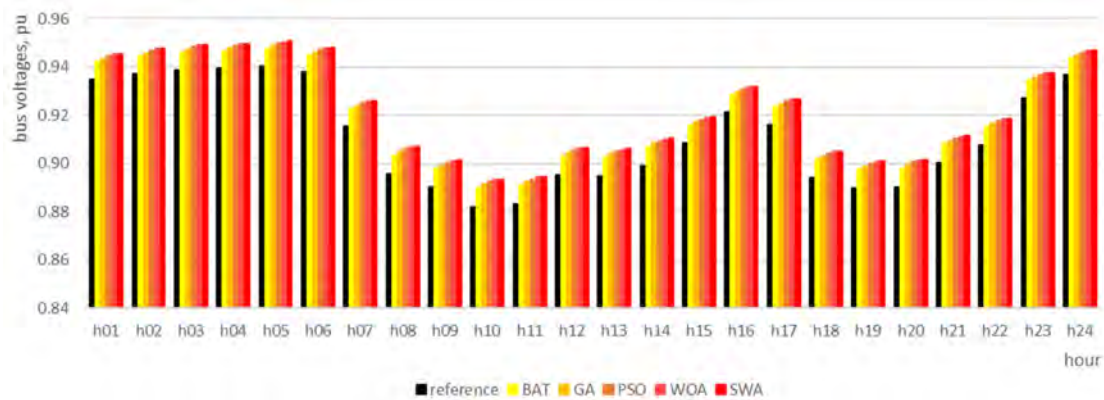


Figure 20. Voltage improvement after compensation for bus 33, the IEEE 33-bus system.

Table 10. Hourly reference voltage values for bus 18 and percent improvements after compensation, the IEEE 33-bus test system.

Hour	Voltage, pu		Improvement, %			
	Ref.	BAT	GA	PSO	WOA	SWA
h01	0.914	0.82	1.26	1.38	1.38	1.42
h02	0.919	0.81	1.25	1.37	1.37	1.41
h03	0.921	0.80	1.24	1.36	1.36	1.40
h04	0.922	0.80	1.23	1.36	1.36	1.40
h05	0.922	0.80	1.23	1.36	1.36	1.40
h06	0.919	0.80	1.24	1.36	1.36	1.40
h07	0.905	0.84	1.29	1.42	1.42	1.46
h08	0.888	0.88	1.35	1.48	1.48	1.53
h09	0.886	0.88	1.36	1.49	1.49	1.54
h10	0.879	0.90	1.38	1.52	1.52	1.56
h11	0.878	0.91	1.39	1.53	1.53	1.57
h12	0.882	0.89	1.37	1.50	1.50	1.55
h13	0.882	0.89	1.37	1.51	1.51	1.55
h14	0.885	0.89	1.36	1.50	1.50	1.54
h15	0.890	0.88	1.35	1.48	1.48	1.52
h16	0.895	0.86	1.32	1.45	1.45	1.50
h17	0.892	0.86	1.33	1.46	1.46	1.51
h18	0.870	0.92	1.41	1.55	1.55	1.60
h19	0.858	0.95	1.45	1.60	1.60	1.65
h20	0.858	0.95	1.45	1.60	1.60	1.65
h21	0.869	0.92	1.42	1.55	1.56	1.60
h22	0.882	0.89	1.37	1.51	1.51	1.55
h23	0.898	0.85	1.31	1.44	1.44	1.48
h24	0.913	0.82	1.26	1.38	1.39	1.43
minimum value, pu	0.858					
max. improvement, %		0.95	1.45	1.60	1.60	1.65

**Table 11.** Hourly reference voltage values for bus 33 and percent improvements after compensation, the IEEE 33-bus test system.

Hour	Voltage, pu	Improvement, %				
	Reference	BAT	GA	PSO	WOA	SWA
h01	0.935	0.78	0.91	1.02	1.10	1.11
h02	0.937	0.77	0.90	1.01	1.09	1.10
h03	0.939	0.77	0.90	1.01	1.09	1.10
h04	0.939	0.77	0.90	1.01	1.09	1.10
h05	0.940	0.77	0.90	1.01	1.08	1.10
h06	0.938	0.77	0.90	1.01	1.09	1.10
h07	0.915	0.82	0.96	1.08	1.16	1.17
h08	0.896	0.86	1.01	1.14	1.22	1.24
h09	0.890	0.88	1.02	1.15	1.24	1.25
h10	0.882	0.90	1.05	1.18	1.27	1.28
h11	0.883	0.90	1.05	1.18	1.27	1.28
h12	0.895	0.87	1.01	1.14	1.23	1.24
h13	0.895	0.87	1.01	1.14	1.23	1.24
h14	0.899	0.86	1.00	1.13	1.22	1.23
h15	0.908	0.84	0.98	1.10	1.19	1.20
h16	0.921	0.81	0.94	1.06	1.14	1.15
h17	0.916	0.82	0.96	1.07	1.16	1.17
h18	0.894	0.87	1.02	1.14	1.23	1.24
h19	0.890	0.88	1.03	1.15	1.24	1.26
h20	0.890	0.88	1.03	1.15	1.24	1.26
h21	0.900	0.85	1.00	1.12	1.21	1.22
h22	0.908	0.84	0.98	1.10	1.19	1.20
h23	0.927	0.79	0.93	1.04	1.12	1.14
h24	0.937	0.77	0.90	1.01	1.09	1.11
minimum value, p.u.	0.882					
max. improvement, %		0.90	1.05	1.18	1.27	1.28

The voltage improvements are smaller for bus 33, with a maximum of 1.28% with the SWA, but with three algorithms (SWA, PSO and WOA), the voltage levels are raised after compensation above the maximum  $-10\%$  deviation allowed by the regulations during 7 h (8.00, 9.00, 12.00, 13.00, 18.00, 19.00, and 20.00), only two hours remaining below this threshold (10.00 and 11.00), as it can be seen in Figure 20.

#### 4.2. Results for the 215-Bus Distribution Network

In this case, the CB stock used for compensation was chosen using the 24-h load profile of the network from Figure 21. In comparison with the IEEE 33-bus system, the minimum off-peak reactive load is reduced, while the number of buses available for compensation increases significantly, allowing a higher number of possible solutions. Thus, the CB stock was set at 90 units of 7.5 kVar each, providing a maximum of 675 kVar of reactive power. As the solutions from Figure 22 and Table 12 show, all the algorithms use the entire stock, with different bus allocation. The SWA provides the best solution (6.19% active power losses), followed by the PSO (6.21%). In Table 12, since the VAR compensation is performed at the LV side of the substation transformers, the bus numbers are given for both the MV buses denoted in Figure 12, and for their corresponding LV transformer busbars. In Figure 22, only the LV bus numbers are used, for better readability. Figure 23 presents the evolution of the fitness function of each metaheuristic algorithm over the first 360 generations, on a typical run.

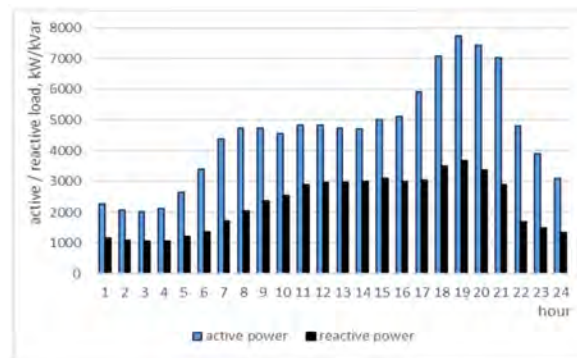


**Figure 21.** The active and reactive load profiles of the 215-bus network—hourly values.

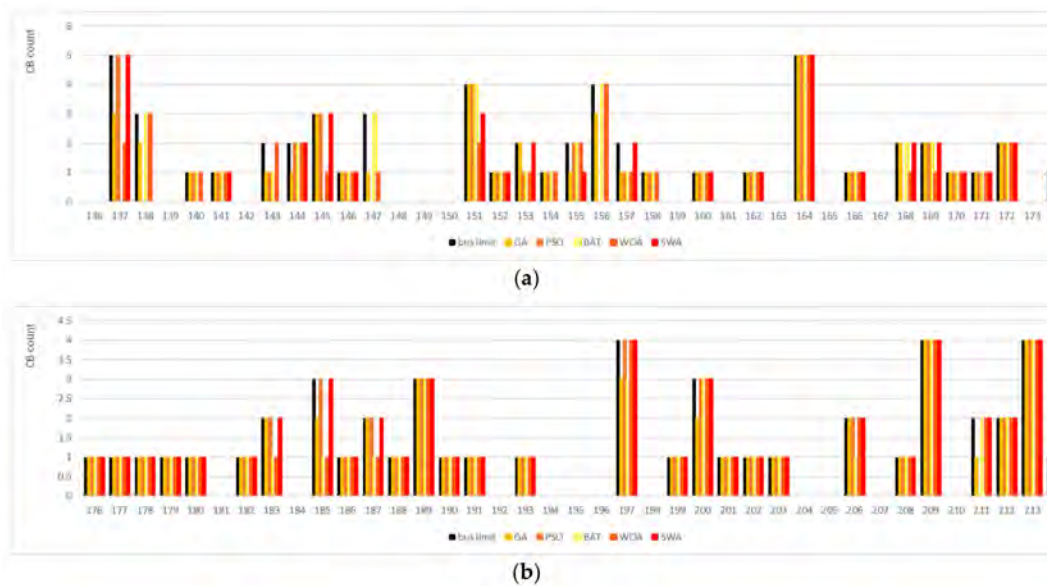


**Figure 22.** The number of CBs allocated in the buses of the 215-bus network by each algorithm: (a)—buses 136–175, (b)—buses 176–215.

For this network, as Figure 22 shows, the best two solutions (SWA, PSO) are mainly differentiated by the CB allocation at buses 151, LV side (28, MV side); 153 (31); 155 (34); 156 (35); and 157 (36), located at the beginning of the network, and having significant reactive power loads. This behavior is triggered by the use of the 90 CB stock, which is close to the maximum possible number of CBs that can be allocated for compensation, 107, and because of the sufficient stock, most of the buses can use the maximum possible CB allocation.

The comparison between the hourly active power losses computed by the Newton–Raphson algorithm for the reference case (no compensation) and the losses determined for each best compensation solution found by the metaheuristic algorithms is presented in Table 13 and Figure 24. Furthermore, Table 14 gives the percent reduction in losses obtained using the compensation solutions, while Figure 25 allows for an overview of the total losses obtained in each case, based on the values computed in Table 13.

**Table 12.** The OCBA solutions found by the metaheuristic algorithms for the 215-bus network.

MV Bus	2	3	5	6	7	10	11	13	15	17	19	21	23	24	26	28	29	31	32	34	35
LV Bus	136	137	138	139	140	141	142	143	144	145	146	147	148	149	150	151	152	153	154	155	156
bus limit	0	5	3	0	1	1	0	2	2	3	1	3	0	0	0	4	1	2	1	2	4
reference	0	0	0	0	0	0	0	0	0	0	0	0	0	0	0	0	0	0	0	0	0
GA	0	3	2	0	1	1	0	1	1	3	1	1	0	0	0	4	1	2	1	1	3
PSO	0	5	0	0	1	1	0	1	2	3	1	0	0	0	0	4	1	1	1	2	0
BAT	0	0	3	0	1	1	0	1	2	0	1	3	0	0	0	4	1	1	1	2	4
WOA	0	2	3	0	1	1	0	2	2	1	1	1	0	0	0	2	1	1	1	2	4
SWA	0	5	0	0	0	1	0	0	2	3	1	0	0	0	0	3	1	2	0	1	0
MV Bus	36	38	39	40	41	42	43	45	46	49	51	53	55	57	58	61	63	64	65	68	70
LV Bus	157	158	159	160	161	162	163	164	165	166	167	168	169	170	171	172	173	174	175	176	177
bus limit	2	1	0	1	0	1	0	5	0	1	0	2	2	1	1	2	0	1	1	1	1
reference	0	0	0	0	0	0	0	0	0	0	0	0	0	0	0	0	0	0	0	0	0
GA	1	1	0	1	0	1	0	5	0	1	0	2	2	1	1	2	0	1	1	1	1
PSO	1	1	0	1	0	1	0	5	0	1	0	0	2	1	1	2	0	1	1	1	1
BAT	1	1	0	1	0	1	0	5	0	1	0	2	2	1	1	2	0	1	1	1	1
WOA	1	1	0	1	0	1	0	5	0	1	0	1	1	1	1	2	0	1	1	1	1
SWA	2	0	0	1	0	1	0	5	0	1	0	2	2	1	1	2	0	1	1	1	1
MV Bus	71	72	74	76	77	79	81	83	85	87	90	91	92	94	96	97	99	102	103	105	107
LV Bus	178	179	180	181	182	183	184	185	186	187	188	189	190	191	192	193	194	195	196	197	198
bus limit	1	1	1	0	1	2	0	3	1	2	1	3	1	1	0	1	0	0	0	4	0
reference	0	0	0	0	0	0	0	0	0	0	0	0	0	0	0	0	0	0	0	0	0
GA	1	1	1	0	1	2	0	2	1	2	1	3	1	1	0	1	0	0	0	3	0
PSO	1	1	1	0	1	2	0	3	1	2	1	3	1	1	0	1	0	0	0	4	0
BAT	1	1	1	0	1	1	0	1	1	1	1	3	1	1	0	1	0	0	0	3	0
WOA	1	1	1	0	1	1	0	1	1	1	1	3	1	1	0	1	0	0	0	4	0
SWA	1	1	1	0	1	2	0	3	1	2	1	3	1	1	0	1	0	0	0	4	0
MV Bus	109	111	112	115	117	118	119	121	122	123	124	126	128	130	132	133	135				
LV Bus	199	200	201	202	203	204	205	206	207	208	209	210	211	212	213	214	215	CB Used	Fitness		
bus limit	1	3	1	1	1	0	0	2	0	1	4	0	2	2	4	1	3	107			
reference	0	0	0	0	0	0	0	0	0	0	0	0	0	0	0	0	0	0	6.8578		
GA	1	2	1	1	1	0	0	2	0	1	4	0	1	2	4	1	0	90	6.2385		
PSO	1	3	1	1	1	0	0	2	0	1	4	0	0	2	4	1	3	90	6.2050		
BAT	1	3	1	1	1	0	0	1	0	1	4	0	2	2	4	1	3	90	6.2278		
WOA	1	3	1	1	1	0	0	2	0	1	4	0	2	2	4	1	3	90	6.2175		
SWA	1	3	1	1	1	0	0	2	0	1	4	0	2	2	4	1	3	90	6.1910		

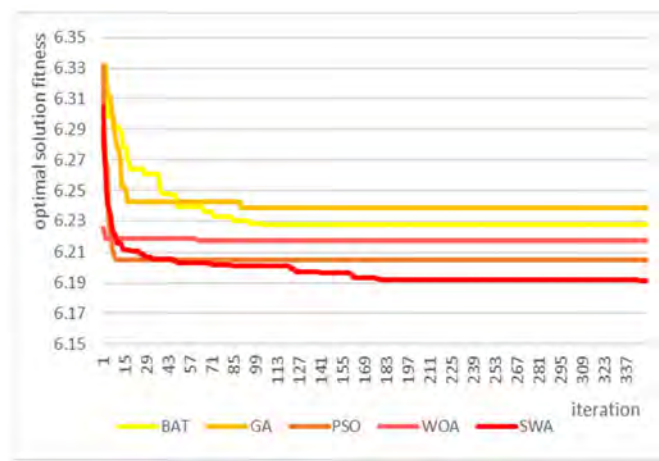


**Figure 23.** The fitness of the optimal solution found by the metaheuristic algorithms after 360 iterations, for the 215-bus network.

**Table 13.** Hourly and total active power losses in the 215-bus network, in kW, for each algorithm.

Hour	Ref.	BAT	GA	PSO	WOA	SWA
h01	67.331	55.673	55.609	55.539	55.583	55.305
h02	56.182	45.636	45.575	45.517	45.541	45.319
h03	53.214	43.113	43.053	43.000	43.016	42.817
h04	58.190	47.878	47.818	47.762	47.782	47.572
h05	90.377	77.534	77.467	77.382	77.446	77.109
h06	147.228	131.143	131.068	130.941	131.065	130.562
h07	245.758	223.025	223.059	222.583	222.867	222.029
h08	290.292	262.257	262.479	261.527	261.962	260.864
h09	303.227	270.552	271.077	269.405	270.026	268.696
h10	296.025	261.012	261.713	259.595	260.336	258.874
h11	354.181	312.943	313.922	311.078	312.050	310.247
h12	363.306	320.607	321.658	318.606	319.647	317.753
h13	352.690	310.099	311.147	308.090	309.134	307.242
h14	350.992	308.310	309.373	306.281	307.332	305.437
h15	394.674	349.439	350.570	347.313	348.428	346.400
h16	393.582	349.764	350.799	347.811	348.843	346.908
h17	505.757	458.845	459.845	456.827	457.938	455.824
h18	741.209	680.993	682.464	678.467	679.882	677.100
h19	892.805	825.937	827.555	823.210	824.773	821.637
h20	795.742	736.564	737.748	734.379	735.670	732.945
h21	672.197	623.613	624.385	621.999	622.971	620.808
h22	304.238	280.233	280.128	279.887	280.171	279.245
h23	194.076	175.399	175.315	175.153	175.327	174.688
h24	122.607	107.163	107.100	106.949	107.055	106.594
total	8045.88	7257.73	7270.93	7229.30	7244.84	7211.97



Figure 24. Hourly active power losses in the IEEE 33-bus system, for each algorithm.

Table 14. Hourly and total power loss reduction in the 215-bus network, in %, for each algorithm.

Hour	BAT	GA	PSO	WOA	SWA
h01	17.31	17.41	17.51	17.45	17.86
h02	18.77	18.88	18.98	18.94	19.33
h03	18.98	19.09	19.19	19.16	19.54
h04	17.72	17.82	17.92	17.89	18.25
h05	14.21	14.28	14.38	14.31	14.68
h06	10.92	10.98	11.06	10.98	11.32
h07	9.25	9.24	9.43	9.31	9.66
h08	9.66	9.58	9.91	9.76	10.14
h09	10.78	10.60	11.15	10.95	11.39
h10	11.83	11.59	12.31	12.06	12.55
h11	11.64	11.37	12.17	11.90	12.40
h12	11.75	11.46	12.30	12.02	12.54
h13	12.08	11.78	12.65	12.35	12.89
h14	12.16	11.86	12.74	12.44	12.98
h15	11.46	11.17	12.00	11.72	12.23
h16	11.13	10.87	11.63	11.37	11.86
h17	9.28	9.08	9.67	9.45	9.87
h18	8.12	7.93	8.46	8.27	8.65
h19	7.49	7.31	7.80	7.62	7.97
h20	7.44	7.29	7.71	7.55	7.89
h21	7.23	7.11	7.47	7.32	7.64
h22	7.89	7.92	8.00	7.91	8.22
h23	9.62	9.67	9.75	9.66	9.99
h24	12.60	12.65	12.77	12.68	13.06
total	9.80	9.63	10.15	9.96	10.36

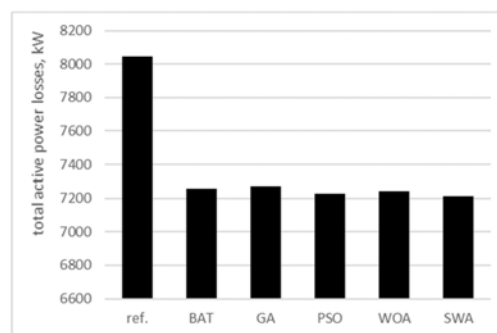
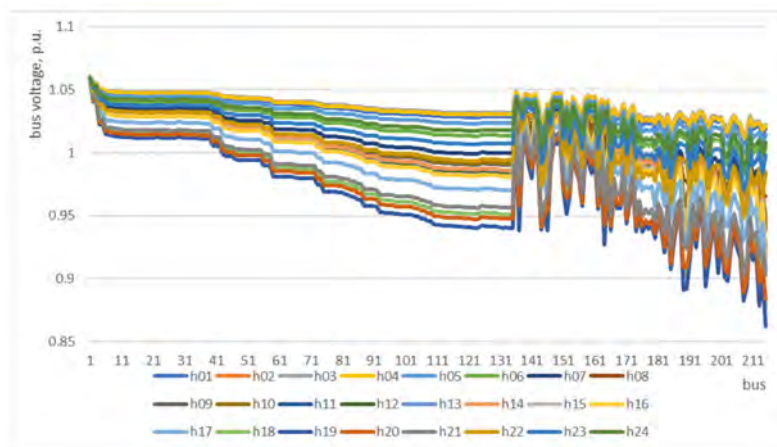


Figure 25. The total active power loss reduction in the 215-bus network, in kW, for each algorithm.

The best CB allocation solution, obtained with the SWA, achieves a loss reduction of 833.91 kW or 10.36% for the entire network, in 24 h, which amounts to 304.38 MW in an entire year. The next best

solution, found with the PSO algorithm, achieves only 816.58 kW (10.15%). The difference between the two solutions is of 17.33 kW in the analyzed day, or 6.32 MW in a year. The improvement over the IEEE 33-bus system regarding the loss reduction can be attributed to the presence of the MV/LV transformers.

The bus voltage levels for all 24 h and buses from the 215-bus network are presented in Figure 26. The length of the main feeder and the bus loadings lead to low voltage levels at the last buses on the main supply path, with values below the 0.9 pu limit at the LV side. At the MV side, the voltages are inside the allowed range, varying from 1.060 pu in the slack bus to 0.940 pu.



**Figure 26.** The bus voltages in the 215-bus network without compensation, for each hour from the analyzed day.

Figures 27 and 28 depict the effect of VAR compensation on the voltages at bus 135 (MV) and 215 (LV). By allocating the available CB stock according to the solutions found by the five metaheuristic algorithms, the bus voltages increase with maximum 1.36%, as shown in Table 15 for bus 215 (LV). This increase is not sufficient for raising the lowest voltage values above the desired limit of 0.9 pu. Since the CB stock is near the maximum allowed reactive load compensation which fulfills constraint Cr2 specified by the optimization model, an alternative solution is to change the MV/LV transformer tap settings in the affected buses.

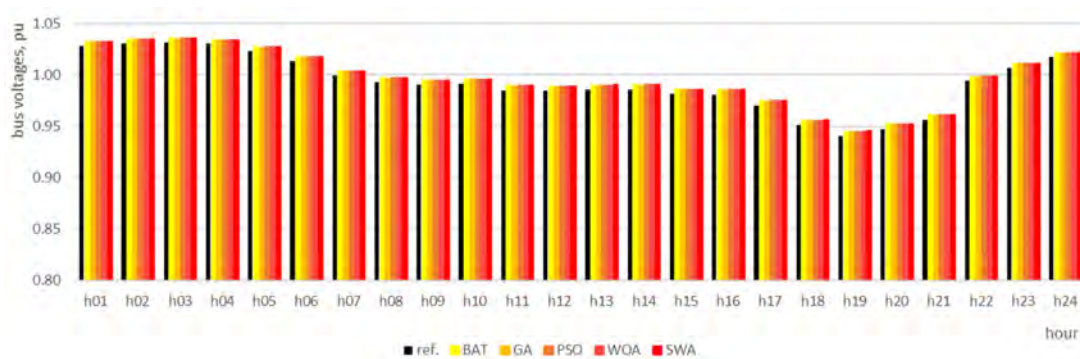


**Figure 27.** Voltage improvement after compensation for bus 135, medium voltage, the 215-bus network.



**Figure 28.** Voltage improvement after compensation for bus 215, low voltage, the 215-bus network.

**Table 15.** Hourly reference voltage values for bus 215 and percent improvements after compensation, the 215-bus network.

Hour	Voltage, pu		Improvement, %				
	Ref.	BAT	GA	PSO	WOA	SWA	
h01	1.019	0.86	0.36	0.86	0.87	0.88	
h02	1.022	0.85	0.35	0.86	0.86	0.87	
h03	1.022	0.85	0.35	0.86	0.86	0.87	
h04	1.021	0.86	0.35	0.86	0.86	0.87	
h05	1.014	0.87	0.36	0.87	0.88	0.89	
h06	1.004	0.89	0.37	0.89	0.90	0.91	
h07	0.983	0.94	0.39	0.94	0.95	0.96	
h08	0.965	0.99	0.41	0.99	0.99	1.01	
h09	0.948	1.04	0.43	1.04	1.04	1.06	
h10	0.940	1.06	0.45	1.07	1.07	1.09	
h11	0.922	1.12	0.47	1.13	1.13	1.15	
h12	0.917	1.14	0.48	1.15	1.15	1.16	
h13	0.918	1.14	0.48	1.14	1.15	1.16	
h14	0.918	1.14	0.48	1.14	1.15	1.16	
h15	0.911	1.16	0.49	1.17	1.17	1.18	
h16	0.916	1.14	0.48	1.15	1.15	1.17	
h17	0.905	1.17	0.49	1.18	1.18	1.20	
h18	0.876	1.28	0.54	1.28	1.29	1.30	
h19	0.863	1.33	0.57	1.33	1.34	1.36	
h20	0.884	1.24	0.53	1.25	1.25	1.27	
h21	0.903	1.17	0.50	1.17	1.18	1.19	
h22	0.985	0.93	0.39	0.94	0.94	0.95	
h23	0.998	0.90	0.38	0.91	0.91	0.92	
h24	1.008	0.88	0.37	0.89	0.89	0.90	
minimum value, pu	0.863						
max. improvement, %		1.33	0.57	1.33	1.34	1.36	

## 5. Discussions and Conclusions

The reactive power flow in the active electricity distribution networks has an important influence on the bus voltage level and the active power losses. Therefore, in order to control the reactive power absorbed by consumers, their consumption must be characterized by a power factor approximately equal to the neutral value (0.9 in Romania). Optimal allocation of reactive sources in the electricity distribution networks is made for power losses reduction, power factor correction and/or voltage profile improvement.

The optimization model considered in the paper has as main objective the optimal allocation of capacitor banks (CBs) in the medium voltage networks to minimize the power/energy losses, taking into account the technical restrictions imposed by the available CB stock, the compensation



level in each bus, branch current flows, and bus voltages. This is very useful for distribution network operators that install now large amounts of capacitor banks (CB) in the distribution networks. In order to optimize the location of these CBs, the used test networks (the IEEE 33-bus system and a real 215-bus EDN from Romania) were modelled considering the MV lines, the MV/LV transformers from the electric distribution substations, where available, and the MV and LV buses. The different algorithms (Genetic Algorithm (GA), Particle Swarm Optimization (PSO), Bat Optimization Algorithm (BOA), Whale Optimization Algorithm (WOA) and Sperm-Whale Algorithm (SWA)) were tested to see which would be the best to solve the problem of capacitor bank allocation. The study, made using the IEEE 33-bus system, highlighted the fact that the SWA leads to the best results compared to the other algorithms. Compared with the reference case, the best compensation solution found by the SWA leads to a loss reduction of 726.73 kW for the analyzed day, which, if it is extrapolated for a year, amounts to 265.26 MW loss saving. The difference between SWA and the second best result, given by WOA, is of 6.25 kW per day or 2.28 MW for an entire year. In the case of the voltage level, an improvement was observed on the entire electricity distribution network, in all nodes, also obtained with the help of SWA. The minimum reference voltage value in bus 18 (the farthest node), at hour 10.00, was increased by 1.65%.

Moreover, the algorithms were tested in a real electricity distribution network (215-bus EDN) from Romania. The best CB allocation solution, obtained again with the SWA, achieves a loss reduction of 833.91 kW or 10.36% for the entire network, in 24 h, which amounts to 304.38 MW in an entire year. The next best solution, found with the PSO algorithm, achieves only 816.58 kW (10.15%). The difference between the two solutions is of 17.33 kW in the analyzed day, or 6.32 MW in a year. The solutions found led to an increase of the voltage in the farthest node (215) with maximum 1.36%.

Based on the obtained results, it can be affirmed that the use of capacitor banks is an easy solution to be implemented with technical and economic benefits to the electricity distribution networks that maximizes long-term return on investment as the network develops. An intelligent control of capacitor banks leads to improved energy efficiency and voltage level in the buses of electricity distribution networks, resulting in an increase in the percentage of energy delivered to consumers. Amongst the tested algorithms, the SWA finds the best compensation solutions, which can lead to significant additional loss savings and shorter investment recovery times.

**Supplementary Materials:** The following are available online at <http://www.mdpi.com/1996-1073/12/22/4239/s1>, file IEEE33\_load\_data.xls, active and reactive load profiles for the IEEE-33bus test system, and file EDN215\_load\_data.xls, active and reactive load profiles for the 215-bus distribution network.

**Author Contributions:** Conceptualization, O.I., B.-C.N. and G.G.; methodology, O.I. and G.G.; software, O.I. and B.-C.N.; validation, B.-C.N. and G.G.; formal analysis, M.G.; investigation, O.I. and B.-C.N.; data curation, B.-C.N.; writing—original draft preparation, O.I. and B.-C.N.; writing—B.-C.N., G.G. and M.G.; supervision, M.G.

**Funding:** This research received no external funding.

**Conflicts of Interest:** The authors declare no conflict of interest.

## Appendix A

**Table A1.** Branch parameters for the IEEE 33-bus system.

Bus 1	Bus 2	I <sub>max</sub> , A	Type <sup>1</sup>	Resistance, Ω	Reactance, Ω
1	2	420	1	0.092	0.047
2	3	420	1	0.493	0.251
3	4	420	1	0.366	0.186
4	5	420	1	0.381	0.194
5	6	420	1	0.819	0.707
6	7	420	1	0.187	0.619
7	8	420	1	0.711	0.235
8	9	420	1	1.03	0.74

Table A1. Cont.

Bus 1	Bus 2	I <sub>max</sub> , A	Type <sup>1</sup>	Resistance, Ω	Reactance, Ω
9	10	420	1	1.044	0.74
10	11	420	1	0.197	0.065
11	12	420	1	0.374	0.124
12	13	420	1	1.468	1.155
13	14	420	1	0.542	0.713
14	15	420	1	0.591	0.526
15	16	420	1	0.746	0.545
16	17	420	1	1.289	1.721
17	18	420	1	0.732	0.574
19	20	420	1	1.504	1.356
2	19	420	1	0.164	0.157
20	21	420	1	0.41	0.478
21	22	420	1	0.709	0.937
23	24	420	1	0.898	0.709
24	25	420	1	0.896	0.701
26	27	420	1	0.284	0.145
27	28	420	1	1.059	0.934
28	29	420	1	0.804	0.701
29	30	420	1	0.508	0.259
3	23	420	1	0.451	0.308
30	31	420	1	0.975	0.963
31	32	420	1	0.311	0.362
32	33	420	1	0.341	0.53
6	26	420	1	0.203	0.103

<sup>1</sup> Branch type can be 1—line; 2—transformer.

Table A2. Branch parameters for the 215-bus distribution network.

Bus 1	Bus 2	I <sub>max</sub> , A	Type	Resistance, Ω	Reactance, Ω
1	2	235	1	0.80625	0.314159
2	3	315	1	0.1051	0.061104
2	4	295	1	0.7701	0.358142
4	5	295	1	0.00154	0.000716
4	6	295	1	0.30804	0.143257
6	7	295	1	0.021306	0.009909
7	8	295	1	0.021306	0.009909
8	9	295	1	0.272102	0.126543
8	29	295	1	0.056474	0.026264
9	10	295	1	0.02567	0.011938
9	11	295	1	0.213061	0.099086
11	12	295	1	0.115515	0.053721
101	102	295	1	0.141185	0.065659
101	103	295	1	0.02567	0.011938
104	105	295	1	0.02567	0.011938
104	106	295	1	0.361947	0.168327
106	107	295	1	0.02567	0.011938
106	108	295	1	0.2567	0.119381
108	109	295	1	0.05134	0.023876
108	110	295	1	0.467194	0.217273

Table A2. Cont.

Bus 1	Bus 2	Imax, A	Type	Resistance, $\Omega$	Reactance, $\Omega$
110	111	295	1	0.115515	0.053721
110	113	295	1	0.12835	0.05969
12	13	295	1	0.07701	0.035814
12	14	295	1	0.019253	0.008954
111	112	295	1	0.041072	0.019101
113	114	295	1	0.2567	0.119381
113	125	295	1	0.07701	0.035814
114	115	295	1	0.173273	0.080582
114	116	295	1	0.035938	0.016713
116	117	295	1	0.369648	0.171908
116	119	295	1	0.07701	0.035814
117	118	295	1	0.202793	0.094311
119	120	295	1	0.562173	0.261443
120	121	295	1	0.15402	0.071628
120	122	295	1	0.110381	0.051334
122	123	295	1	0.187391	0.087148
123	124	295	1	0.187391	0.087148
125	126	295	1	0.038505	0.017907
125	127	295	1	0.169422	0.078791
127	128	295	1	0.02567	0.011938
127	129	295	1	0.064175	0.029845
129	130	295	1	0.20536	0.095504
129	131	295	1	0.361947	0.168327
14	15	295	1	0.097546	0.045365
14	22	295	1	0.035938	0.016713
131	132	295	1	0.120649	0.056109
131	133	295	1	0.17969	0.083566
131	134	295	1	0.2567	0.119381
134	135	295	1	0.033371	0.015519
15	16	295	1	0.15402	0.071628
16	17	295	1	0.15402	0.071628
16	18	295	1	0.019253	0.008954
18	19	295	1	0.17969	0.083566
18	20	295	1	0.019253	0.008954
20	21	295	1	0.02567	0.011938
22	23	295	1	0.351679	0.163551
22	24	295	1	0.248999	0.115799
24	25	295	1	0.23103	0.107442
25	26	295	1	0.071876	0.033427
25	27	295	1	0.392751	0.182652
27	28	295	1	0.10268	0.047752
29	30	295	1	0.038505	0.017907
30	31	295	1	0.071876	0.033427
30	37	295	1	0.056474	0.026264
31	32	295	1	0.123216	0.057303
32	33	295	1	0.087278	0.040589
33	34	295	1	0.192525	0.089535
33	35	295	1	0.071876	0.033427
35	36	295	1	0.351679	0.163551
37	38	295	1	0.10268	0.047752
37	40	295	1	0.318308	0.148032
39	38	309	1	0.46244	0.268858
40	41	295	1	0.41072	0.191009
40	43	295	1	0.403019	0.187427
42	41	295	1	0.12835	0.05969

Table A2. Cont.

Bus 1	Bus 2	Imax, A	Type	Resistance, $\Omega$	Reactance, $\Omega$
43	44	295	1	0.084711	0.039396
44	45	295	1	0.33371	0.155195
44	47	295	1	0.189958	0.088342
45	46	295	1	0.02567	0.011938
47	48	295	1	0.238731	0.111024
47	56	295	1	0.338844	0.157582
48	49	295	1	0.17969	0.083566
48	50	295	1	0.238731	0.111024
50	51	295	1	0.288788	0.134303
50	52	295	1	0.040045	0.018623
52	53	295	1	0.07701	0.035814
52	54	295	1	0.10268	0.047752
54	55	295	1	0.23103	0.107442
56	57	295	1	0.05134	0.023876
56	59	295	1	0.659719	0.306808
57	58	295	1	0.10268	0.047752
59	60	295	1	0.043639	0.020295
59	66	295	1	0.084711	0.039396
60	61	295	1	0.02567	0.011938
60	62	295	1	0.074443	0.03462
62	63	295	1	0.441524	0.205335
62	64	295	1	0.028237	0.013132
64	65	295	1	0.17969	0.083566
66	67	295	1	0.17969	0.083566
66	73	295	1	0.467194	0.217273
67	68	295	1	0.10268	0.047752
67	69	295	1	0.120649	0.056109
69	70	295	1	0.02567	0.011938
69	71	295	1	0.210494	0.097892
71	72	295	1	0.02567	0.011938
73	74	295	1	0.02567	0.011938
73	75	295	1	0.467194	0.217273
75	76	295	1	0.64175	0.298451
75	78	295	1	0.021306	0.009909
76	77	295	1	0.30804	0.143257
78	79	295	1	0.15402	0.071628
78	80	295	1	0.084711	0.039396
80	81	295	1	0.02567	0.011938
80	82	295	1	0.12835	0.05969
82	83	295	1	0.10268	0.047752
82	84	295	1	0.189958	0.088342
84	85	295	1	0.23103	0.107442
84	86	295	1	0.2567	0.119381
86	87	295	1	0.05134	0.023876
86	88	295	1	0.5134	0.238761
88	89	295	1	0.07701	0.035814
88	92	295	1	0.084711	0.039396
89	90	295	1	0.02567	0.011938
89	91	295	1	0.02567	0.011938
92	93	295	1	0.5134	0.238761
93	94	295	1	0.02567	0.011938
93	95	295	1	0.084711	0.039396
95	96	295	1	0.07701	0.035814
95	98	295	1	0.12835	0.05969
96	97	295	1	0.053907	0.02507

Table A2. Cont.

Bus 1	Bus 2	Imax, A	Type	Resistance, $\Omega$	Reactance, $\Omega$
98	99	295	1	0.084711	0.039396
98	100	295	1	0.064175	0.029845
100	101	295	1	0.07701	0.035814
100	104	295	1	0.12835	0.05969
2	136	1000	2	0.06	0.082
3	137	1000	2	0.011	0.037
5	138	1000	2	0.011	0.037
6	139	1000	2	0.011	0.037
7	140	1000	2	0.011	0.037
10	141	1000	2	0.019	0.036
11	142	1000	2	0.06	0.082
102	195	1000	2	0.04	0.05
103	196	1000	2	0.06	0.082
105	197	1000	2	0.011	0.037
107	198	1000	2	0.06	0.082
109	199	1000	2	0.011	0.037
111	200	1000	2	0.006	0.023
112	201	1000	2	0.011	0.037
115	202	1000	2	0.06	0.082
117	203	1000	2	0.06	0.082
118	204	1000	2	0.06	0.082
119	205	1000	2	0.06	0.082
13	143	1000	2	0.019	0.036
121	206	1000	2	0.011	0.037
122	207	1000	2	0.06	0.082
123	208	1000	2	0.06	0.082
124	209	1000	2	0.019	0.036
126	210	1000	2	0.06	0.082
128	211	1000	2	0.019	0.036
130	212	1000	2	0.019	0.036
132	213	1000	2	0.006	0.023
133	214	1000	2	0.06	0.082
135	215	1000	2	0.019	0.036
15	144	1000	2	0.06	0.082
17	145	1000	2	0.04	0.05
19	146	1000	2	0.06	0.082
21	147	1000	2	0.011	0.037
23	148	1000	2	0.06	0.082
24	149	1000	2	0.06	0.082
26	150	1000	2	0.06	0.082
28	151	1000	2	0.019	0.036
29	152	1000	2	0.06	0.082
31	153	1000	2	0.04	0.05
32	154	1000	2	0.019	0.036
34	155	1000	2	0.019	0.036
35	156	1000	2	0.011	0.037
36	157	1000	2	0.04	0.05
38	158	1000	2	0.011	0.037
39	159	1000	2	0.019	0.036
40	160	1000	2	0.019	0.036
41	161	1000	2	0.04	0.05
42	162	1000	2	0.06	0.082
43	163	1000	2	0.019	0.036
45	164	1000	2	0.006	0.023
46	165	1000	2	0.06	0.082
49	166	1000	2	0.06	0.082
51	167	1000	2	0.06	0.082

Table A2. Cont.

Bus 1	Bus 2	I <sub>max</sub> , A	Type	Resistance, Ω	Reactance, Ω
53	168	1000	2	0.04	0.05
55	169	1000	2	0.04	0.05
57	170	1000	2	0.019	0.036
58	171	1000	2	0.06	0.082
61	172	1000	2	0.011	0.037
63	173	1000	2	0.06	0.082
64	174	1000	2	0.06	0.082
65	175	1000	2	0.06	0.082
68	176	1000	2	0.06	0.082
70	177	1000	2	0.04	0.05
71	178	1000	2	0.06	0.082
72	179	1000	2	0.06	0.082
74	180	1000	2	0.06	0.082
76	181	1000	2	0.06	0.082
77	182	1000	2	0.04	0.05
79	183	1000	2	0.04	0.05
81	184	1000	2	0.06	0.082
83	185	1000	2	0.04	0.05
85	186	1000	2	0.04	0.05
87	187	1000	2	0.011	0.037
90	188	1000	2	0.011	0.037
91	189	1000	2	0.011	0.037
92	190	1000	2	0.06	0.082
94	191	1000	2	0.04	0.05
96	192	1000	2	0.019	0.036
97	193	1000	2	0.04	0.05
99	194	1000	2	0.019	0.036

## References

1. T&D World Magazine. Capacitor Bank Control Adapts to Evolving Challenges of Smart Grid. Available online: <https://www.tdworld.com/test-monitor-amp-control/capacitor-bank-control-adapts-evolving-challenges-smart-grid> (accessed on 15 July 2019).
2. Cooper Power Series. Smart Grid Ready Capacitor Bank Control Delivers Automation and Efficiency. Available online: <https://www.eaton.com/content/dam/eaton/products/utility-and-grid-solutions/grid-automation-systems/capacitor-bank-control/cbc-8000-capacitor-bank-control/cbc-8000-capacitor-bank-pa916001en.pdf> (accessed on 15 July 2019).
3. Hogan, P.M.; Rettkowski, J.D.; Bala, J.L. Optimal capacitor placement using branch and bound. In Proceedings of the 37th Annual North American Power Symposium, Ames, IA, USA, 25 October 2005; pp. 84–89.
4. Grainger, J.; Lee, S. Optimum Size and Location of Shunt Capacitors for Reduction of Losses on Distribution Feeders. *IEEE Trans. Power Appar. Syst.* **1981**, *3*, 1105–1118. [CrossRef]
5. Muthukumar, K.; Jayalalitha, S. Optimal placement and sizing of distributed generators and shunt capacitors for power loss minimization in radial distribution networks using hybrid heuristic search optimization technique. *Int. J. Electr. Power Energy Syst.* **2016**, *78*, 299–319. [CrossRef]
6. Segura, S.; Romero, R.; Rider, M.J. Efficient heuristic algorithm used for optimal capacitor placement in distribution systems. *Int. J. Electr. Power Energy Syst.* **2010**, *32*, 71–78. [CrossRef]
7. Biagio, M.A.; Coelho, M.A.; Franco, P.E.C. Heuristic for solving capacitor allocation problems in electric energy radial distribution networks. *Pesquisa Oper.* **2012**, *32*, 121–138. [CrossRef]
8. Bakker, E.; Deljou, V.; Rahmani, J. Optimal Placement of Capacitor Bank in Reorganized Distribution Networks Using Genetic Algorithm. *Int. J. Comp. App. Techn. Res. (IJCATR)* **2019**, *8*, 2319–8656. [CrossRef]
9. Ozgonenel, O.; Karagol, S. A novel generation and capacitor integration technique for today's distribution systems, *Turk. J. Elec. Eng. Comp. Sci.* **2017**, *25*, 2434–2443. [CrossRef]

10. Villa-Acevedo, W.; López-Lezama, J.; Valencia-Velásquez, J. A novel constraint handling approach for the optimal reactive power dispatch problem. *Energies* **2018**, *11*, 2352. [[CrossRef](#)]
11. Rahmani-andebili, M. Simultaneous placement of DG and capacitor in distribution network. *Electr. Power Syst. Res.* **2016**, *131*, 1–10. [[CrossRef](#)]
12. Bhattacharya, S.K.; Goswami, S.K. A new fuzzy based solution of the capacitor placement problem in radial distribution system. *Expert Syst. Appl.* **2009**, *36*, 4207–4212. [[CrossRef](#)]
13. Kumar, M.; Nallagownden, P.; Elamvazuthi, I. Optimal Placement and Sizing of Renewable Distributed Generations and Capacitor Banks into Radial Distribution Systems. *Energies* **2017**, *10*, 811. [[CrossRef](#)]
14. Zeinalzadeh, A.; Mohammadi, Y.; Moradi, M.H. Optimal multi objective placement and sizing of multiple DGs and shunt capacitor banks simultaneously considering load uncertainty via MOPSO approach. *Int. J. Electr. Power Energy Syst.* **2015**, *67*, 336–349. [[CrossRef](#)]
15. Sharaf, A.M.; El-Gammal, A.A. Optimal selection of capacitors in distribution networks for voltage stabilization and loss reduction. In Proceedings of the 2010 IEEE Electrical Power & Energy Conference, Halifax, NS, Canada, 25–27 August 2010; pp. 1–5.
16. Díaz, P.; Pérez-Cisneros, M.; Cuevas, E.; Avalos, O.; Gálvez, J.; Hinojosa, S.; Zaldivar, D. An improved crow search algorithm applied to energy problems. *Energies* **2018**, *11*, 571. [[CrossRef](#)]
17. Montazeri, M.; Askarzadeh, A. Capacitor placement in radial distribution networks based on identification of high potential busses. *Int. Trans. Elec. Energy Syst.* **2019**, *29*, e2754. [[CrossRef](#)]
18. Jiang, F.; Zhang, Y.; Zhang, Y.; Liu, X.; Chen, C. An Adaptive Particle Swarm Optimization Algorithm Based on Guiding Strategy and Its Application in Reactive Power Optimization. *Energies* **2019**, *12*, 1690. [[CrossRef](#)]
19. Elsheikh, A.; Helmy, Y.; Abouelseoud, Y.; Elsherif, A. Optimal capacitor placement and sizing in radial electric power systems. *Alex. Eng. J.* **2014**, *53*, 809–816. [[CrossRef](#)]
20. Arulraj, R.; Kumarappan, N. Optimal economic-driven planning of multiple DG and capacitor in distribution network considering different compensation coefficients in feeder's failure rate evaluation. *Eng. Sci. Technol. Int. J.* **2019**, *22*, 67–77. [[CrossRef](#)]
21. Sahli, Z.; Hamouda, A.; Bekrar, A.; Trentesaux, D. Reactive Power Dispatch Optimization with Voltage Profile Improvement Using an Efficient Hybrid Algorithm. *Energies* **2018**, *11*, 2134. [[CrossRef](#)]
22. Abdelaziz, A.Y.; Ali, E.S.; Elazim, S.A. Flower pollination algorithm and loss sensitivity factors for optimal sizing and placement of capacitors in radial distribution systems. *Int. J. Electr. Power Energy Syst.* **2016**, *78*, 207–214. [[CrossRef](#)]
23. Tamilselvan, V.; Jayabarathi, T.; Raghunathan, T.; Yang, X.S. Optimal capacitor placement in radial distribution systems using flower pollination algorithm. *Alex. Eng. J.* **2018**, *57*, 2775–2786. [[CrossRef](#)]
24. Ali, E.S.; Elazim, S.A.; Abdelaziz, A.Y. Improved Harmony Algorithm for optimal locations and sizing of capacitors in radial distribution systems. *Int. J. Electr. Power Energy Syst.* **2016**, *79*, 275–284. [[CrossRef](#)]
25. Devabalaji, K.R.; Ravi, K.; Kothari, D.P. Optimal location and sizing of capacitor placement in radial distribution system using bacterial foraging optimization algorithm. *Int. J. Electr. Power Energy Syst.* **2015**, *71*, 383–390. [[CrossRef](#)]
26. Kishore, C.; Ghosh, S.; Karar, V. Symmetric fuzzy logic and IBFOA solutions for optimal position and rating of capacitors allocated to radial distribution networks. *Energies* **2018**, *11*, 766. [[CrossRef](#)]
27. Khodabakhshian, A.; Andishgar, M.H. Simultaneous placement and sizing of DGs and shunt capacitors in distribution systems by using IMDE algorithm. *Int. J. Electr. Power Energy Syst.* **2016**, *82*, 599–607. [[CrossRef](#)]
28. Dixit, M.; Kundu, P.; Jariwala, H.R. Incorporation of distributed generation and shunt capacitor in radial distribution system for techno-economic benefits. *Eng. Sci. Technol. Int. J.* **2017**, *20*, 482–493. [[CrossRef](#)]
29. Mouassa, S.; Bouktir, T.; Salhi, A. Ant lion optimizer for solving optimal reactive power dispatch problem in power systems. *Eng. Sci. Technol. Int. J.* **2017**, *20*, 885–895. [[CrossRef](#)]
30. Baysal, Y.A.; Altas, İ.H. Power quality improvement via optimal capacitor placement in electrical distribution systems using symbiotic organisms search algorithm. *Mugla J. Sci. Technol.* **2017**, *3*, 64–68. [[CrossRef](#)]
31. Helmy, W.; Abbas, M.A.E. Optimal sizing of capacitor-bank types in the low voltage distribution networks using JAYA optimization. In Proceedings of the 9th International Renewable Energy Congress (IREC), Hammamet, Tunisia, 20–22 March 2018; pp. 1–5.
32. Sultana, S.; Roy, P.K. Capacitor Placement in Radial Distribution System Using Oppositional Cuckoo Optimization Algorithm. *Int. J. Swarm Intel. Res. (IJSIR)* **2018**, *9*, 64–95. [[CrossRef](#)]

33. Neagu, B.C.; Ivanov, O.; Gavrilas, M. A comprehensive solution for optimal capacitor allocation problem in real distribution networks. In Proceedings of the Conference on Electromechanical and Power System (SIELMEN), Iasi, Romania, 11–13 October 2017; pp. 565–570.
34. Blum, C.; Roli, A. Metaheuristics in Combinatorial Optimization: Overview and Conceptual Comparison. *ACM Comp. Surv.* **2003**, *35*, 268–308. [[CrossRef](#)]
35. Neagu, B.C.; Ivanov, O.; Georgescu, G. Reactive Power Compensation in Distribution Networks Using the Bat Algorithm. In Proceedings of the International Conference and Exposition on Electrical and Power Engineering, Iasi, Romania, 20–22 October 2016; pp. 711–714.
36. Neagu, B.C.; Ivanov, O.; Gavrilas, M. Voltage profile improvement in distribution networks using the whale optimization algorithm. In Proceedings of the International Conference on Electronics, Computers and Artificial Intelligence (ECAI 2017), Targoviste, Romania, 29 June–1 July 2017.
37. Holland, J.H. *Adaptation in Natural and Artificial Systems: An Introductory Analysis with Applications to Biology, Control and Artificial Systems*; University of Michigan Press: Ann Arbor, MI, USA, 1975.
38. Jebari, K. Selection Methods for Genetic Algorithms. *Int. J. Emerg. Sci.* **2013**, *3*, 333–344.
39. Umbarkar, A.J.; Sheth, P.D. Crossover Operators in Genetic Algorithms: A Review. *ICTACT J. Soft Comput.* **2015**, *6*, 1083–1092.
40. Kennedy, J.; Eberhart, R.C. Particle Swarm Optimization. In Proceedings of the ICNN'95—International Conference on Neural Networks, Perth, WA, Australia, 27 November–1 December 1995; IEEE: Piscataway, NJ, USA, 1995.
41. Yang, X.S. A New Metaheuristic Bat-Inspired Algorithm. In *Nature Inspired Cooperative Strategies for Optimization (NISCO 2010)*; Cruz, C., González, J.R., Krasnogor, N., Pelta, D.A., Terrazas, G., Eds.; Springer: Berlin, Germany, 2010; pp. 65–74.
42. Mirjalili, S.; Lewis, A. The Whale Optimization Algorithm. *Adv. Eng. Soft.* **2016**, *95*, 51–67. [[CrossRef](#)]
43. Ebrahimi, A.; Khamsehchi, E. Sperm whale algorithm: An effective metaheuristic algorithm for production optimization problems. *J. Nat. Gas. Sci. Eng.* **2016**, *29*, 211–222. [[CrossRef](#)]



© 2019 by the authors. Licensee MDPI, Basel, Switzerland. This article is an open access article distributed under the terms and conditions of the Creative Commons Attribution (CC BY) license (<http://creativecommons.org/licenses/by/4.0/>).



Article

# Optimal Phase Load Balancing in Low Voltage Distribution Networks Using a Smart Meter Data-Based Algorithm

Gheorghe Grigoraş <sup>1,\*</sup> , Bogdan-Constantin Neagu <sup>1</sup> , Mihai Gavrilăş <sup>1</sup>, Ion Trîstiu <sup>2</sup> and Constantin Bulac <sup>2</sup>

<sup>1</sup> Department of Power Engineering, “Gheorghe Asachi” Technical University of Iasi, 700050 Iasi, Romania; bogdan.neagu@tuiasi.ro (B.-C.N.); mgavril@tuiasi.ro (M.G.)

<sup>2</sup> Department of Power System, “Politehnica” University of Bucharest, 060042 Bucharest, Romania; itristiu@upb.ro (I.T.); constantin.bulac@upb.ro (C.B.)

\* Correspondence: ggrigor@tuiasi.ro or ghgrigoras@yahoo.com; Tel.: +04-0232-278-683

Received: 21 February 2020; Accepted: 3 April 2020; Published: 8 April 2020



**Abstract:** In the electric distribution systems, the “Smart Grid” concept is implemented to encourage energy savings and integration of the innovative technologies, helping the distribution network operators (DNOs) in choosing the investment plans which lead to the optimal operation of the networks and increasing the energy efficiency. In this context, a new phase load balancing algorithm was proposed to be implemented in the low voltage distribution networks with hybrid structures of the consumption points (switchable and non-switchable consumers). It can work in both operation modes (real-time and off-line), uploading information from different databases of the DNO which contain: The consumers’ characteristics, the real loads of the consumers integrated into the smart metering system (SMS), and the typical load profiles for the consumers non-integrated in the SMS. The algorithm was tested in a real network, having a hybrid structure of the consumption points, on a by 24-h interval. The obtained results were analyzed and compared with other algorithms from the heuristic (minimum count of loads adjustment algorithm) and the metaheuristic (particle swarm optimization and genetic algorithms) categories. The best performances were provided by the proposed algorithm, such that the unbalance coefficient had the smallest value (1.0017). The phase load balancing led to the following technical effects: decrease of the average current in the neutral conductor and the energy losses with 94%, respectively 61.75%, and increase of the minimum value of the phase voltage at the farthest pillar with 7.14%, compared to the unbalanced case.

**Keywords:** phase load balancing; smart meters; dynamic optimization; real-time implementation; low voltage electric distribution networks

## 1. Introduction

The three-phase electric distribution networks (EDN) are designed and built to operate in symmetrical and balanced regimes on all phases with all elements (lines, transformers, and not least the distributed generation sources) having identical electrical parameters. In these regimes, the symmetrical current and voltage systems in each node of the system have equal values of the magnitudes of the voltage and currents on each phase, with a phase shift by 120 degrees. But, an ideal system of the currents and voltages is practically impossible to be met in the real operation conditions of the EDN because of the emergence of imbalances created mainly by the constructive conditions of some network elements (lines and transformers) or the supply of the single-phase (1-P) consumers. Thus, the operating regimes become asymmetric (unbalanced), the symmetry loss of the voltage and current systems [1].

The main causes of the imbalances in an EDN can be grouped into the following categories [2]:

- Constructive imbalances. These appear because of the spatial arrangement of the phase conductors, at the electrical lines, and the arrangement of the windings on the three columns of the ferromagnetic core, at the power transformers.
- Functional imbalances. These are created by 1-P consumers. They are connected between two phases or between a phase and the neutral point. Many of them are represented by domestic and tertiary consumers supplied from the low-voltage (LV) network, which shall constitute the absorbed power (up to 100 kVA). Also, there are 1-P industrial consumers. They have high absorbed powers being connected to electric medium voltage (MV) networks. The representative 1-P industrial consumers are the following: the welding installations, with absorbed powers between 100 kVA and 3 MVA, the 1-P arc furnaces, and the electric stations that supply power the railway traction network).

The current unbalances causes many issues at all voltage levels of the electric distribution networks [3]. The issues caused by current unbalance and the effects on the voltage unbalance are presented in Figure 1, adapted after [3].

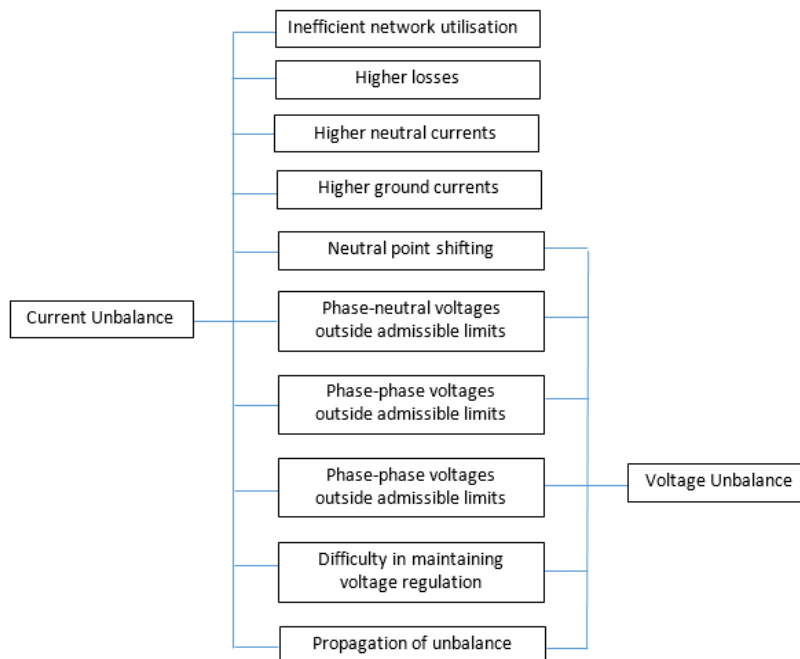


Figure 1. The issues caused by the current unbalances [3].

It can be observed that the current and voltage unbalances cannot be separately treated. In this context, the voltage unbalances could take as current unbalances, with economic and technical losses for both for both consumers (users and DNO). Concerning the mitigation measures, the current unbalances can be easier solved by the DNO. The main advantage of current balancing refers to the minimization of the current flow in the neutral conductor with benefits on the decrease of the total losses in the EDN [1].

Several phase load balancing (PLB) mechanisms are found in the literature. The PLB problem was solved in [4] using the branch and bound algorithm. The aforementioned approach uses real data of customer power demand in different periods to minimize the value of unbalance factor and customer power demand in different periods to minimize the value of unbalance factor and find the optimal three-phase load balance in an EDN. The PLB approach used in [5] considers the reallocation of the customers to reduce the phase load imbalance in the EDN. The other approaches use different automatic three-phase load balancing devices [6–8]. The solutions for the PLB model were obtained using various techniques and technical measures: Hierarchical Petri nets [9], LV the feeder reconfiguration [10,11],

or switching the consumers on the three phases [12–14]. The PLB problem was solved with particular metaheuristic algorithms in [15–17]. A PLB mechanism was proposed in [18] to be used at the MV/LV power transformer level. A particular approach, based on the optimal placement of a decentralized and autonomous battery storage system, was developed in [19,20]. A different formulation of the PLB optimization problem is presented in [21] which follows the implementation of a commutation system, with two-phase thyristor parallel contactor structure, or based on the power-line communication (PLC) and supervisory control and data acquisition (SCADA) technologies in [22,23], and not based on smart meters [24,25]. Another category of the published papers [26–28] regards the PLB problem at the active distribution networks (smart grids) level, using heuristic or metaheuristic methods. Moreover, an automatic phase load balancing device [29], a shunt passive compensator [30], or a controlled active filter [31] were proposed. Also, a controller was proposed in [31] to switch the connected 1-P loads from one phase to another based on an algorithm with a minimum count of loads adjustment.

To highlight the originality of the proposed algorithm, a brief description of the literature is presented in Table 1, based on four main characteristics: The network type, the location of PLB operation, the used algorithm, and the operation mode. Other papers from the literature indeed solve the PLB problem, but they coincide with those presented in Table 1. The objective functions refer to the minimization of unbalance factor at the pillar level or supply point (electric distribution substation).

Table 1. A comparative state-of-the-art between proposed method and the literature.

Number of Reference	Type of Network		Location of PLB		Type of Algorithm	Operation Mode	
	Real	Fictive (Test)	Pillar (P)/ Consumer (C)	Supply Point		Real-Time	Off-Line
[4,27]	Yes	Yes	No	Yes	Heuristic	No	Yes
[5,17,28]	Yes	No	No	Yes	Metaheuristic	No	Yes
[6,21,24]	No	Yes	No	No	Experimental	No	Yes
[7,8,26]	No	Yes	No	Yes	Heuristic	No	Yes
[9,10]	Yes	No	No	Yes	Heuristic	No	Yes
[12,13]	No	Yes	Yes	No	Metaheuristic	No	Yes
[14,29]	No	Yes	Yes	No	Experimental	Yes	No
[15,16]	No	Yes	No	Yes	Metaheuristic	No	Yes
[18,32]	No	No	No	Yes	Heuristic	No	Yes
[19,20]	Yes	No	Yes	No	Heuristic	No	Yes
[23]	No	Yes	No	No	Heuristic	Yes	No
[30,31]	No	Yes	Yes	Yes	Metaheuristic	No	Yes
Proposed approach	Yes	No	Yes	Yes	Heuristic	Yes	Yes

Regardless of the algorithm used and the locations (networks) proposed for the PLB process, each consumer should have a smart phase load balancing system (SPLBS) integrated in the SMS, containing a smart meter and an automatic phase load balancing device (APBD) [27], see Figure 2. 4 of 28

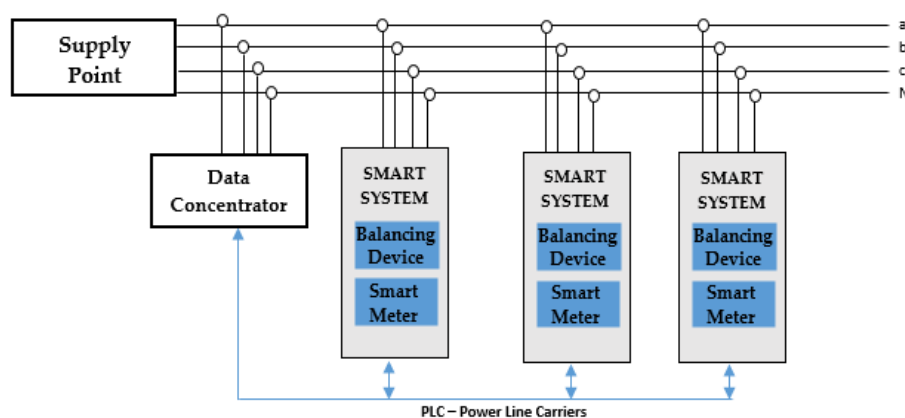


Figure 2. The structure of a smart phase load balancing system (SPLBS) installed at the consumers integrated in the smart metering system (SMS).

Currently, the technical solution developed by the producers is available to be implemented by the DNOs in the EDN with a high unbalanced degree [33,34]. The solution will be introduced by the DNOs only on basis of a feasibility analysis to justify the investment.

The system contains the following main components: data concentrators, smart phase load

Currently, the technical solution developed by the producers is available to be implemented by the DNOs in the EDN with a high unbalanced degree [33,34]. The solution will be introduced by the DNOs only on basis of a feasibility analysis to justify the investment.

The system contains the following main components: data concentrators, smart phase load balancing systems (SPLBS) placed to the consumers integrated into the SMS, and communication lines. The real-time data communication occurs through power line communication (PLC) wiring from the SPLBS to data concentrators and through various communication channels from the data concentrators to a central database. The use of open standard communication protocols plays a very important role in connecting SPLBS to the data concentrators. Such an approach avoids the massive investment in equipment that is not interoperable and cannot log or generate errors in the data transmission when purchased from different suppliers [35].

The analysis should identify in each stage the associated cost to implement the PLB. The main stages refer to the identification of a feasible technology, the planning of assembly at consumers, the commissioning of the system, the integration in the SMS, testing the communication with data concentrator from the supply point, and the maintenance plan [27].

Compared to the approaches from the literature, the proposed algorithm has the following advantages:

- It can be implemented in the EDNs with hybrid structures of the consumption points (switchable and non-switchable 1-P consumers). The three-phase (3-P) consumers, having identical loadings on the three phases, are not considered in the algorithm, belonging to the non-switchable consumers' category.
- It can work in both operation modes (real-time and off-line), uploading information from different databases of the DNO. The consumers' characteristics (connecting pillar, allocated phase, consumption sector and class, integration in the SMS, identification number of the meter) are extracted based on the identification number of the supply point. The value of consumption and operating status of phase load balancing device (PLBD) are uploaded from the database of the SMS if the meter is integrated, or from the typical load profiles (TLPs) database if the consumer has a standard energy meter (non-integrated in the SMS).
- The convergence is rapid because of the fast recognition of the EDN topology with the help of a structure vectors-based algorithm. The optimal solutions for PLB are found at the level of each pillar such that the global solution obtained for the level of the supply point will be also optimal.

The paper has a structure organized as follows: Section 2 details the stages of the proposed PLB algorithm, accompanied by the implementation procedure. Section 3 presents the results obtained in the case of a real EDN belonging a DNO from the north-eastern of Romania and a comparison with other three algorithms to demonstrate the accuracy of the proposed algorithm. Section 4 highlights the conclusions and the future works.

## 2. The Proposed PLB Algorithm

The proposed algorithm can be implemented at the level of data concentrator from the supply point (electric distribution substation) to work in the real-time mode or to the decision-making central level (DMCL) of DNO for the off-line work mode helping to identify the EDNs with a high unbalanced degree and to determine the optimal solutions to decrease it. The real-time implementation in the soft architecture of the data concentrator from the supply point (SP) involves the installation of a SPLBS at the level of each consumer, as indicated in Figure 2. Also, the algorithm can be implemented in the EDN with standard and smart meters.

The PLB algorithm has the following steps:

central level (DMCL) of DNO for the off-line work mode helping to identify the EDNs with a high unbalanced degree and to determine the optimal solutions to decrease it. The real-time implementation in the soft architecture of the data concentrator from the supply point (SP) involves the installation of a SPLBS at the level of each consumer, as indicated in Figure 2. Also, the algorithm can be implemented in the EDN with standard and smart meters. 5 of 29

The PLB algorithm has the following steps:

**Step 1. Identification of topology for the EDN.**

The topology is identified using a two structure vectors-based algorithm [36]. The algorithm leads to the systematization of the topology, grouping the branches into vicinity levels relative to the supply point (the electric distribution substation). For an EDN with 9 nodes and 8 branches, the branches are grouped in three vicinity levels, starting from the supply point (SP): Level 1 – 1 branch (B2); Level 2 – 2 branches (B3 and B4), and Level 3 – 5 branches (B5, B6, B7, B8, and B9); see Figure 3. The recognition of each branch is based on the input and end nodes (pillars), being numbered relative to the end node. The input and end nodes of branches are recorded in the vectors  $B_i$  and  $B_e$ , considered as input data of the algorithm.

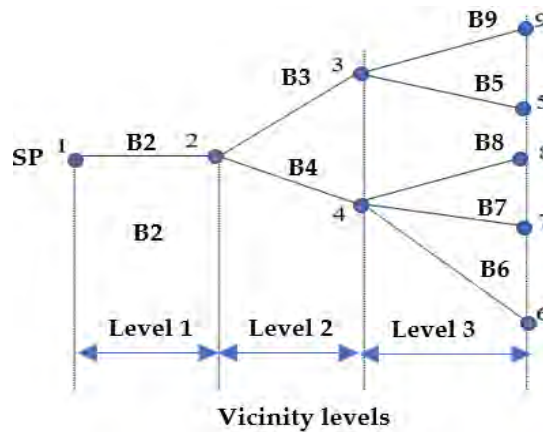


**Figure 3.** Grouping the branches into vicinity levels.

Considering these aspects, the topology of the EDN can be described using two integer vectors, TV1 and TV2. The vector TV1 contains the number of branches from each vicinity level and the vector TV2 includes all branches in the order of the vicinity levels. The elements of vectors TV1 and TV2 are presented in Table 2.

**Table 2.** The elements of topology vectors.

TV1	TV1	LL1	LL2	L3	L3
TV2	TV2	B1	B2, B3	B5, B6, B7, B8, B9	B8, B9

**Step 2. Upload the input data sequence**

The algorithm uploads from the database of the DNO a data sequence that is stored in the input vectors. This input data sequence is formed from the following fields, see Figure 4:

- **Supply point:** Each electric distribution substation has an identification number that allows the algorithm to allocate correct data from the database to all consumers supplied from this point.
- **Connecting pillar:** The connecting pillar is recorded in the database to identify the position of each consumer in the network. Also, this information is very important in the calculus of a steady-state regime to evaluate the performance of the PLB measure through reducing the power/energy losses and improving the voltage level at the consumers. The vector associated with this field is noted with  $CP$ , having the size  $(N_C \times 1)$ , where  $N_C$  represents the total number of consumers from the EDN.
- **Branching Phase:** Each 1-P consumer is allocated by the DNO at one of the phases  $ph = \{a, b, c\}$ , and the 3-P consumers are connected at all three phases  $ph = \{a, b, c\}$ . The records regarding this information are found in the vector  $PB$  with the size  $(N_C \times 1)$ .

2002814771	3	a	1	4	1	111069
----	-	-	-	-	-	-
2002814771	4	c	1	3	0	111075

Figure 4. The input data sequence of the algorithm.

- Consumption Sector. The information is used to assign the consumer to the following consumption sectors: domestic, non-domestic, commercial, and industrial. The records for this information have the identification code derived from the 4-database (1) 2 (non-domestic), 3 (commercial), and 4 (industrial) included in the vector  $PI$  with the size  $(N_c \times 1)$  in the database to identify the position of each consumer in the network. Also, this information is allocated to each consumer in the calculation of the DNO. As an example, a Romanian DNO has a classification in five consumption classes for consumers from the domestic sector [36]:  $\leq 400$  kWh (first class), range [400 kWh, 1250 kWh] (second class), range [1250 kWh, 2500 kWh] (third class), range [2500 kWh, 3500 kWh] (the fourth class), and range [2500 kWh, 3500 kWh] (the fifth class). This information is loaded in the vector  $CC$ , having the size  $(N_c \times 1)$ .
- Branching Phase. Each 1- $\varphi$  consumer is allocated by the DNO at one of the phases  $ph = \{a, b, c\}$ , and the 3- $\varphi$  consumers are connected at all three phases  $ph = \{a, b, c\}$ . The records regarding this information are found in the vector  $PB$  with the size  $(N_c \times 1)$ .
- Integration in SMS. Currently, not all consumers from the LV distribution networks are integrated into the smart metering system. In this case, the value 1 (if it is integrated) and 0 (otherwise) will be recorded in the database. If the meter is integrated into the SMS, it can communicate to the central system information about the currents or active and reactive powers, which will record them in the database (see Figure 5).
- Consumption Sector. The information is used to assign the consumer to the following consumption sectors: domestic, non-domestic, commercial, and industrial. The records for this information have the identification numbers from 1 to 4: 1 (domestic), 2 (non-domestic), 3 (commercial), and 4 (industrial) included in the vector  $CS$  with the size  $(N_c \times 1)$ .

- Consumption class. More consumption classes are allocated to each consumption sector by the DNO. As an example, a Romanian DNO has a classification in five consumption classes for consumers from the domestic sector [36]:  $\leq 400$  kWh (first class), range [400 kWh, 1250 kWh] (second class), range [1250 kWh, 2500 kWh] (third class), range [2500 kWh, 3500 kWh] (the fourth class), and range [2500 kWh, 3500 kWh] (the fifth class). This information is loaded in the vector  $CC$ , having the size  $(N_c \times 1)$ .
- Integration in SMS. Currently, not all consumers from the LV distribution networks are integrated into the smart metering system. In this case, the value 1 (if it is integrated) and 0 (otherwise) will be recorded in the database. If the meter is integrated into the SMS, it can communicate to the central system information about the currents or active and reactive powers, which will record them in the database (see Figure 5).

2002814771	3	a	1	4	1	111069
----	-	-	-	-	-	-
2002814771	4	c	1	3	0	111075

Figure 4. The input data sequence of the algorithm.

SERIAL_NUMBE	SAMPLE	Hour 00	Hour 01	Hour 02	Hour 03	Hour 04	Hour 05	Hour 06	Hour 07	Hour 08	Hour 09	Hour 10	Hour 11	Hour 12	Hour 13	Hour 14	Hour 15	Hour 16	Hour 17	Hour 18	Hour 19	Hour 20	Hour 21	Hour 22	Hour 23
000953000117408	21.12.2017	0.333	0.335	0.338	0.343	0.341	0.642	0.483	0.262	0.127	0.254	0.104	0.082	0.061	0.101	0.173	0.153	0.239	0.418	0.360	0.433	0.250	0.102	0.122	0.095
000953000118517	21.12.2017	0.003	0.003	0.003	0.003	0.003	0.003	0.004	0.003	0.003	0.003	0.003	0.003	0.004	0.003	0.003	0.003	0.003	0.004	0.003	0.003	0.003	0.003	0.003	0.004
000953000118687	21.12.2017	0.201	0.166	0.209	0.178	0.171	0.205	0.615	0.795	0.212	0.152	0.277	0.231	0.263	0.073	0.056	0.041	0.146	0.599	0.452	0.300	0.376	0.301	0.264	0.175

Figure 5. The sequence of the power active recorded in the database.

- Connecting pillar. The connecting pillar is recorded in the database to identify the position of each consumer in the network. Also, this information is very important in the calculus of a steady-state regime to evaluate the performance of the RLB measure through reducing the energy losses and improving the voltage level at the consumer. The vector associated with this field is stored with 1 if it is classified by the algorithm in the category of switchable consumers, recorded in the value 1 in the database. Otherwise, when the consumer is integrated into the SMS and RLB is in the EDN is 0, or has a standard meter, it cannot be allocated on other phase and will be classified in the set of non-switchable consumers, recording the value 0 in the database. The algorithm will record these values in the vectors  $AI$  (for integration mode) and  $BS$  (for the RLB status), having the size  $(N_c \times 1)$ . Also, for the non-switchable consumers because of the missing data from the consumption point, the algorithm will use the hourly values from the typical load profiles (TLPs) allocated in function by Consumption sector (vector  $CS$ ) and Consumption class (vector  $CC$ ) for this status. Concerning the TLPs, these are defined by the DNO for all consumers which are not integrated in the SMS and are determined for each consumption sector (domestic, non-domestic, commercial, and industrial) having common characteristics regarding the consumption classes, days (weekend or working), and seasons (springer, summer, autumn, or winter). Finally, each consumer will have an assigned TLP, depending on the above characteristics. The profiling process to obtain the TLPs presented in [36].
- Integration in SMS. Currently, not all consumers from the LV distribution networks are integrated into the smart metering system. In this case, the value 1 (if it is integrated) and 0 (otherwise) will be recorded in the database. If the meter is integrated into the SMS, it can communicate to the central system information about the currents or active and reactive powers, which will record them in the database (see Figure 5).

SERIAL_NUMBE	SAMPLE	Hour 00	Hour 01	Hour 02	Hour 03	Hour 04	Hour 05	Hour 06	Hour 07	Hour 08	Hour 09	Hour 10	Hour 11	Hour 12	Hour 13	Hour 14	Hour 15	Hour 16	Hour 17	Hour 18	Hour 19	Hour 20	Hour 21	Hour 22	Hour 23
000953000117408	21.12.2017	0.333	0.335	0.338	0.343	0.341	0.642	0.483	0.262	0.127	0.254	0.104	0.082	0.061	0.101	0.173	0.153	0.239	0.418	0.360	0.433	0.250	0.102	0.122	0.095
000953000118517	21.12.2017	0.003	0.003	0.003	0.003	0.003	0.003	0.004	0.003	0.003	0.003	0.003	0.003	0.004	0.003	0.003	0.003	0.003	0.004	0.003	0.003	0.003	0.003	0.003	0.004
000953000118687	21.12.2017	0.201	0.166	0.209	0.178	0.171	0.205	0.615	0.795	0.212	0.152	0.277	0.231	0.263	0.073	0.056	0.041	0.146	0.599	0.452	0.300	0.376	0.301	0.264	0.175

switching options increases, leading to a solution very close to the optimal solution (in the ideal case, it is equal with 1.00).

The values of the hourly loads for all consumers are recorded in the matrix  $IC$ , with the size  $(N_C \times H)$ .

- *Serial number.* Each consumer is recognized in the database through the serial number of meter installed (smart or standard). The information is recorded in the vector  $SN$ , having the size  $(N_C \times 1)$ .

### Step 3. The PLB procedure

The PLB procedure is characterized by a dynamic process which follows the minimization of unbalance degree (as close to 1) at the level of each pillar by allocation to other phases (e.g., phase  $a$  on phases  $b$  or  $c$ ) of the switchable consumers (with SPLBS installed). The procedure is based on the decomposition and coordination of the complex distribution networks. Decomposition considers the division of the distribution network into groups of pillars and to carry out optimization on the pillar level to obtain a minimum unbalance coefficient. At the level of each pillar will be determined the optimal solution considering all combinations between the allocations of the switchable consumers on the phases. The optimal solutions at the level of each pillar are obtained by coordination of the switchable consumers, such that the global optimal solution, represented by the unbalance coefficient at the level of the supply point, will be obtained. In other words, if the balancing solutions are optimal at the level of each pillar, then the global solution at the level of the supply point is also optimal.

To evaluate if an EDN is in an unbalanced regime, an unbalance coefficient is calculated. There are formulas proposed by the IEEE (The Institute of Electrical and Electronics Engineers) and NEMA (The National Equipment Manufacturer's Association) standards [37] for the voltage unbalance. But, there is no widespread agreement for the current unbalance. Thus, the negative and positive sequence components of the current can be used to evaluate the current unbalance [3]. This approach requires the decomposition of the current system into instantaneous positive, negative, and zero sequence components using phasor representation, which is not always possible. Easy evaluation of current unbalance in a node (pillar) of the EDN can be made based on an unbalance coefficient calculated based on the effective values of phase currents [27]. The value of this coefficient must be less than 1.1, agreed by the DNOs.

$$UC = \frac{1}{3} \cdot \left( \left( \frac{I_a}{I_{average}} \right)^2 + \left( \frac{I_b}{I_{average}} \right)^2 + \left( \frac{I_c}{I_{average}} \right)^2 \right) \quad (1)$$

where:  $UC$ —the unbalance coefficient;  $I_a, I_b, I_c$ —the currents on the phases  $a, b$ , and  $c$ ;  $I_{average}$ —the average value of the phase currents.

The mechanism of the proposed algorithm is explained for a particular case with 2 pillars and 5 consumers, see Figure 6. For the switchable consumers, the initial phase has a yellow color, the optimal phase has a red color, and the phase of non-switchable consumers has a blue color. The optimal phase is the initial phase when the yellow color is missing. It can be observed that one consumer (3) belongs to the non-switchable consumer category, and only two consumers (2 and 5), after applying the algorithm, switched from the phases  $\{a, a\}$  to the phases  $\{c, b\}$ . Consumers 1, 4, and 6 maintained the allocations on the phases  $\{b, c, a\}$ .

The analysis of the obtained results highlighted that a final value of UC very close by 1 (1.006) can be reached starting from an initial high value (1.636), switching only 2 consumers on other phases.

after applying the algorithm, switched from the phases {a, a} to the phases {c, b}. Consumers 1, 4, and 6 maintained the allocations on the phases {b, c, a}.

The analysis of the obtained results highlighted that a final value of UC very close by 1 (1.006) can be reached starting from an initial high value (1.636), switching only 2 consumers on other phases.

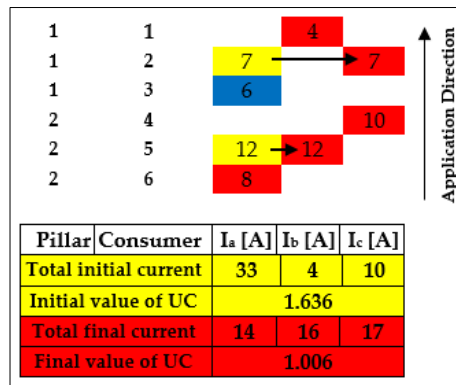


Figure 6. The mechanism of proposed algorithm and the obtained results.

The minimization of unbalance coefficient (UC) at each busbar  $h = 1, \dots, H$ , and each pillar  $p = 1, \dots, N_p$  represents the objective of the IEB problem:

$$\min UC^{(p),h} \quad p = 1, \dots, N_p; h = 1, \dots, H \tag{2}$$

where:  
where:

$$UC^{(p),h} = \frac{1}{3} \cdot \left( \left( \frac{I_a^{(p),h}}{I_{average}^{(p),h}} \right)^2 + \left( \frac{I_b^{(p),h}}{I_{average}^{(p),h}} \right)^2 + \left( \frac{I_c^{(p),h}}{I_{average}^{(p),h}} \right)^2 \right) \tag{3}$$

$$I_a^{(p),h} = I_{a,ns}^{(p),h} + I_{a,s}^{(p),h} + I_a^{(d),h}; p = 1, \dots, N_p; p \neq d \tag{4}$$

$$I_b^{(p),h} = I_{b,ns}^{(p),h} + I_{b,s}^{(p),h} + I_b^{(d),h}; p = 1, \dots, N_p; p \neq d \tag{5}$$

$$I_c^{(p),h} = I_{c,ns}^{(p),h} + I_{c,s}^{(p),h} + I_c^{(d),h}; p = 1, \dots, N_p; p \neq d \tag{6}$$

$$I_{a,ns}^{(p),h} = I_{a,ns}^{(p),h} + I_{a,ns}^{(p),h} \left( \sum_{j=1}^{N_p} I_{a,ns,j}^{(p),h} \right); p = 1, \dots, N_p; p \neq d \tag{7}$$

$$I_{b,ns}^{(p),h} = I_{b,ns}^{(p),h} + I_{b,ns}^{(p),h} \left( \sum_{j=1}^{N_p} I_{b,ns,j}^{(p),h} \right); p = 1, \dots, N_p; p \neq d \tag{8}$$

$$I_{c,ns}^{(p),h} = I_{c,ns}^{(p),h} + I_{c,ns}^{(p),h} \left( \sum_{j=1}^{N_p} I_{c,ns,j}^{(p),h} \right); p = 1, \dots, N_p; p \neq d \tag{9}$$

$$I_{a,s}^{(p),h} = I_{a,s}^{(p),h} + I_{a,s}^{(p),h} \left( \sum_{l=1}^{N_{c,ns}} I_{a,s,l}^{(p),h} \right) \tag{10}$$

$$I_{b,s}^{(p),h} = I_{b,s}^{(p),h} + I_{b,s}^{(p),h} \left( \sum_{l=1}^{N_{c,ns}} I_{b,s,l}^{(p),h} \right) \tag{11}$$

$$I_{c,s}^{(p),h} = I_{c,s}^{(p),h} + I_{c,s}^{(p),h} \left( \sum_{o=1}^{N_{c,ns}} I_{c,s,o}^{(p),h} \right) \tag{12}$$

$$I_{c,s}^{(p),h} = \sum_{o=1}^{N_{c,ns}} I_{c,s,o}^{(p),h} \tag{13}$$



$$N_{C,ns}^{(p)} = N_{a,ns}^{(p),h} + N_{b,ns}^{(p),h} + N_{c,ns}^{(p),h} \tag{14}$$

$$N_{C,s}^{(p)} = N_{a,s}^{(p),h} + N_{b,s}^{(p),h} + N_{c,s}^{(p),h} \tag{15}$$

$$N_C^{(p),h} = N_{C,ns}^{(p),h} + N_{C,s}^{(p),h} \tag{16}$$

where:  $UC^{(p),h}$ —the unbalance coefficient calculated at the pillar  $p$  and hour  $h$ ;  $I_a^{(p),h}, I_b^{(p),h}, I_c^{(p),h}$ —the currents on the phases  $a, b,$  and  $c,$  at the pillar  $p$  and hour  $h$ ;  $I_{average}^{(p),h}$ —the average value of the phase currents, at the pillar  $p$  and hour  $h$ ;  $I_{a,ns}^{(p),h}, I_{b,ns}^{(p),h}, I_{c,ns}^{(p),h}$ —the total current of the non-switchable consumers on the phases  $a, b,$  and  $c,$  at the pillar  $p$  and hour  $h$ ;  $I_{a,s}^{(p),h}, I_{b,s}^{(p),h}, I_{c,s}^{(p),h}$ —the total current of the switchable consumers on the phases  $a, b,$  and  $c,$  at the pillar  $p$  and hour  $h$ ;  $I_{a,s}^{(d),h}, I_{b,s}^{(d),h}, I_{c,s}^{(d),h}$ —the currents on the phases  $a, b,$  and  $c,$  at the pillar  $d$  (located downstream by pillar  $p$ ), and hour  $h$ ;  $I_{a,ns,j}^{(p),h}$ —the current of the non-switchable consumer  $j$  connected on the phase  $a,$  at the pillar  $p,$  and hour  $h$ ;  $I_{b,ns,k}^{(p),h}$ —the current of the non-switchable consumer  $k$  connected on the phase  $b,$  at the pillar  $p,$  and hour  $h$ ;  $I_{c,ns,l}^{(p),h}$ —the current of the non-switchable consumer  $l$  connected on the phase  $c,$  at the pillar  $p,$  and hour  $h$ ;  $I_{a,s,m}^{(p),h}$ —the current of the switchable consumer  $m$  connected on the phase  $a,$  at the pillar  $p,$  and hour  $h$ ;  $I_{b,s,n}^{(p),h}$ —the current of the switchable consumer  $n$  connected on the phase  $b,$  at the pillar  $p,$  and hour  $h$ ;  $I_{c,s,o}^{(p),h}$ —the current of the switchable consumer  $o$  connected on the phase  $c,$  at the pillar  $p,$  and hour  $h$ ;  $N_{a,ns}^{(p),h}, N_{b,ns}^{(p),h}, N_{c,ns}^{(p),h}$ —the number of the non-switchable consumers connected on the phases  $a, b,$  and  $c,$  at the pillar  $p,$  and hour  $h$ ;  $N_{a,s}^{(p),h}, N_{b,s}^{(p),h}, N_{c,s}^{(p),h}$ —the number of the switchable consumers connected on the phases  $a, b,$  and  $c,$  at the pillar  $p,$  and hour  $h$ ;  $N_{C,ns}^{(p),h}$ —the total number of the non-switchable consumers connected at the pillar  $p,$  and hour  $h$ ;  $N_{C,s}^{(p),h}$ —the total number of the switchable consumers connected at the pillar  $p,$  and hour  $h$ ;  $N_C^{(p),h}$ —the total number of the consumers connected at the pillar  $p,$  and hour  $h$ ;  $N_p$ —the total number of the pillars;  $H$ —the analyzed time period.

The implementation procedure of the mathematical model (2)–(16) is presented in Figure 7a,b, and the details are given in Table 3.

**Table 3.** The implementation procedure of the proposed phase load balancing (PLB) algorithm.

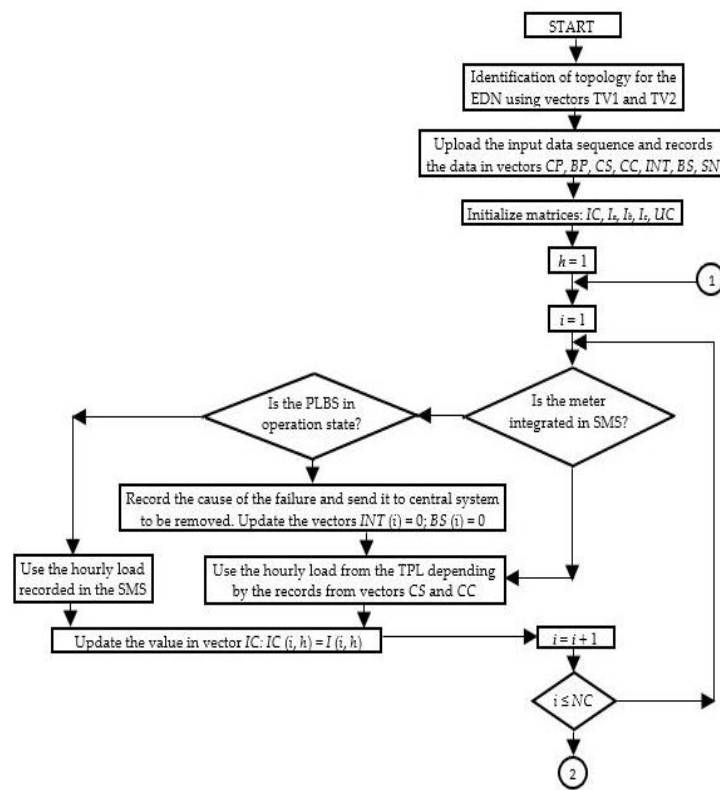
Steps of PLB Algorithm Based on the Smart Meter Data
<p><b>Step 1. Identification of the topology</b> for the EDN based on the vectors TV1 and TV2, built with the vectors <math>B_i</math> and <math>B_e</math> which contain the input and end nodes (pillars) assigned each branch.</p>
<p><b>Step 2. Upload the input data sequence</b> from the database of the DNO corresponding to the SP of EDN: Store the information in the vectors: <math>CP, BP, CS, CC, INT, BS,</math> and <math>SN</math>.                      Determine the number of consumers supplied: <math>NC = \text{length}(SN)</math>;                      Initialize the matrices <math>IC \in \mathbb{R}^{(Nc \times H)}, I_a, I_b,</math> and <math>I_c \in \mathbb{R}^{(Np \times H)},</math> and <math>UC \in \mathbb{R}^{(Np \times H)}</math>                      for each hour <math>h, h = 1 \dots H</math>                      Set initial consumer index: <math>i = 0</math>;                      while <math>i \leq N_C</math>                      Increase consumer index: <math>i = i + 1</math>;                      if <math>INT(i, h) = 1</math>                      if <math>BS(i, h) = 1</math>                      Update <math>IC(i, h)</math> with the value recorded on the line <math>SN(i)</math> and column <math>h</math> of the consumption matrix loaded from the SMS;                      else                      Send a warning message to the central system on the failure/missing communication of PLBD to be repaired as soon as possible;                      Update <math>IC(i, h)</math> with the assigned value from the TLP depending the records from the vectors <math>CS(i)</math> and <math>CC(i),</math> day (weekend or working), and season (springer, summer, autumn, or winter);                      else                      Update <math>IC(i, h)</math> with the assigned value from the TLP depending the records from the vectors <math>CS(i)</math> and <math>CC(i),</math> day (weekend or working), and season (springer, summer, autumn, or winter);</p>

Table 3. Cont.

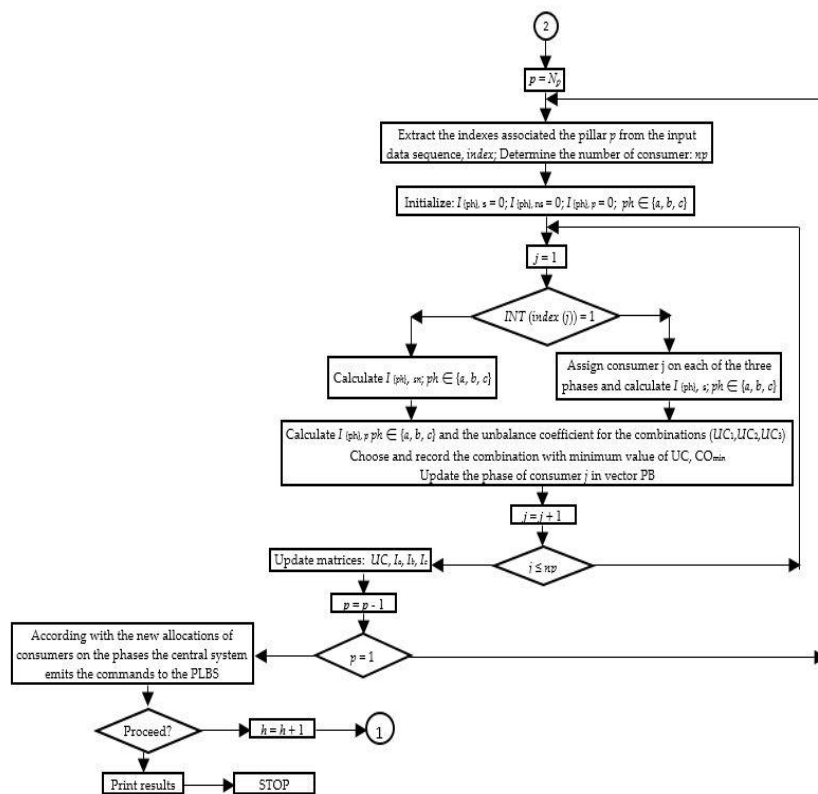
Steps of PLB Algorithm Based on the Smart Meter Data
<p><b>Step 3. The PLB sequence</b> at the level of each pillar:</p> <p>Set initial pillar index: <math>p = Np</math>;</p> <p>while (<math>p \geq 1</math>) and (<math>p \leq N_p</math>)</p> <p style="padding-left: 20px;">Initialize the vector <i>index</i>;</p> <p style="padding-left: 20px;">Find the index corresponding to pillar <math>p</math> in vector <math>CP</math>, and store in vector <i>index</i>;</p> <p style="padding-left: 20px;">Determine the number of consumers connected at the pillar <math>p</math>: <math>n_p = \text{length}(\textit{index})</math>;</p> <p style="padding-left: 20px;">Initialize the sums of phase currents corresponding to:</p> <p style="padding-left: 40px;">switchable consumers: <math>I_{as} = 0, I_{bs} = 0, I_{cs} = 0</math>;</p> <p style="padding-left: 40px;">non-switchable consumers: <math>I_{ans} = 0, I_{bns} = 0, I_{cns} = 0</math>;</p> <p style="padding-left: 40px;">all consumers: <math>I_{ap} = 0, I_{bp} = 0, I_{cp} = 0</math>;</p> <p style="padding-left: 20px;">Set initial consumer index: <math>j = 0</math>;</p> <p>while <math>j \leq n_p</math></p> <p style="padding-left: 20px;">Increase consumer index: <math>j = j + 1</math>;</p> <p style="padding-left: 20px;">if (<math>INT(\textit{index}(j)) = 0</math>) and (<math>BP(\textit{index}(j)) = \{a\}</math>)</p> <p style="padding-left: 40px;">Update sum of current to non-switchable consumers on the phase a:</p> <p style="padding-left: 60px;"><math>I_{ans} = I_{ans} + IC(\textit{index}(j))</math>;</p> <p style="padding-left: 40px;">if <math>BP(\textit{index}(j)) = \{b\}</math></p> <p style="padding-left: 60px;">Update sum of current to non-switchable consumers on the phase b:</p> <p style="padding-left: 80px;"><math>I_{bns} = I_{bns} + IC(\textit{index}(j))</math>;</p> <p style="padding-left: 40px;">else</p> <p style="padding-left: 60px;">Update sum of current to non-switchable consumers on the phase c:</p> <p style="padding-left: 80px;"><math>I_{cns} = I_{cns} + IC(\textit{index}(j))</math>;</p> <p style="padding-left: 20px;">if (<math>INT(\textit{index}(j)) = 1</math>) and (<math>BS(\textit{index}(j)) = 0</math>)</p> <p style="padding-left: 40px;">Changing the category of consumer <math>j</math> from switchable in non-switchable;</p> <p style="padding-left: 20px;">if (<math>BP(\textit{index}(j)) = \{a\}</math>)</p> <p style="padding-left: 40px;">Update sum of current to non-switchable consumers on the phase a:</p> <p style="padding-left: 60px;"><math>I_{ans} = I_{ans} + IC(\textit{index}(j))</math>;</p> <p style="padding-left: 40px;">if <math>BP(\textit{index}(j)) = \{b\}</math></p> <p style="padding-left: 60px;">Update sum of current to non-switchable consumers on the phase b: <math>I_{bns} = I_{bns} + IC(\textit{index}(j))</math>;</p> <p style="padding-left: 40px;">else</p> <p style="padding-left: 60px;">Update sum of current to non-switchable consumers on the phase c: <math>I_{cns} = I_{cns} + IC(\textit{index}(j))</math>;</p> <p style="padding-left: 20px;">if (<math>INT(\textit{index}(j)) = 1</math>) and (<math>BS(\textit{index}(j)) = 1</math>)</p> <p style="padding-left: 40px;">Assigning the consumer <math>j</math> on each of the three phases:</p> <p style="padding-left: 60px;">case <i>Combination 1 – allocation of the consumer j on the phase a</i></p> <p style="padding-left: 80px;">Compute the fictive sum of phase currents to switchable consumers:</p> <p style="padding-left: 100px;"><math>I_{asf1} = I_{as} + IC(\textit{index}(j)); I_{bsf1} = I_{bs}; I_{csf1} = I_{cs}</math>;</p> <p style="padding-left: 80px;">Compute the fictive sum of the phase currents to all consumers:</p> <p style="padding-left: 100px;"><math>I_{apf1} = I_{ans} + I_{asf1}; I_{bpf1} = I_{bns} + I_{bsf1}; I_{cpf1} = I_{cns} + I_{csf1}</math>;</p> <p style="padding-left: 80px;">Compute the average value of the phase currents, <math>I_{average1}</math> (rel. (3))</p> <p style="padding-left: 80px;">Compute the <math>UC_1</math> (rel. (2));</p> <p style="padding-left: 60px;">case <i>Combination 2 – allocation of the consumer j on the phase b</i></p> <p style="padding-left: 80px;">Compute the fictive sum of phase currents to switchable consumers:</p> <p style="padding-left: 100px;"><math>I_{asf2} = I_{as}; I_{bsf2} = I_{bs} + IC(\textit{index}(j)); I_{csf2} = I_{cs}</math>;</p> <p style="padding-left: 80px;">Compute the fictive sum of the phase currents to all consumers:</p> <p style="padding-left: 100px;"><math>I_{apf2} = I_{ans} + I_{asf2}; I_{bpf2} = I_{bns} + I_{bsf2}; I_{cpf2} = I_{cns} + I_{csf2}</math>;</p> <p style="padding-left: 80px;">Compute the average value of the phase currents, <math>I_{average2}</math>, (rel. (3));</p> <p style="padding-left: 80px;">Compute the <math>UC_2</math> (rel. (2));</p>

Table 3. Cont.

Steps of PLB Algorithm Based on the Smart Meter Data
<p>case <i>Combination 3 – allocation of the consumer j on the phase c</i></p> <p>Compute the fictive sum of phase current to switchable consumers:  <math>I_{asf3} = I_{as}; I_{bsf3} = I_{bs}; I_{csf3} = I_{cs} + IC</math> (<i>index (j)</i>);</p> <p>Compute the fictive sum of the phase currents of all consumers:  <math>I_{apf3} = I_{ans} + I_{asf3}; I_{bpf3} = I_{bns} + I_{bsf3}; I_{cpf3} = I_{cns} + I_{csf3}</math>;</p> <p>Compute the average value of the phase currents, <math>I_{average3}</math> (rel. (3));</p> <p>Compute the <math>UC_3</math> (rel. (2));</p> <p>Determine the minimum value of <math>UC</math>: <math>\min(UC_1, UC_2, UC_3)</math>;</p> <p>Store the number of combination with <math>UC_{min}</math>, <math>CO_{min}</math>, corresponding to one of the three phase:</p> <p>if <math>CO_{min} = 1</math></p> <p>Update in the vector <math>PB</math> the phase <math>a</math>: <math>PB(index(j)) = \{a\}</math>;</p> <p>Update the sum of phase currents to switchable consumers:  <math>I_{as} = I_{asf1}; I_{bs} = I_{bsf1}; I_{cs} = I_{csf1}</math>;</p> <p>Update the sum of phase currents to all consumers:  <math>I_{ap} = I_{apf1}; I_{bp} = I_{bpf1}; I_{cp} = I_{cpf1}</math>;</p> <p>if <math>CO_{min} = 2</math></p> <p>Update in the vector <math>PB</math> the phase <math>b</math>: <math>PB(index(j)) = \{b\}</math>;</p> <p>Update the sum of phase currents to switchable consumers:  <math>I_{as} = I_{as2}; I_{bs} = I_{bsf2}; I_{cs} = I_{csf2}</math>;</p> <p>Update the sum of phase currents to all consumers:  <math>I_{ap} = I_{apf2}; I_{bp} = I_{bpf2}; I_{cp} = I_{cpf2}</math>;</p> <p>else</p> <p>Update in the vector <math>PB</math> the phase <math>c</math>: <math>PB(index(j)) = \{c\}</math>;</p> <p>Update the sum of phase currents to switchable consumers:  <math>I_{as} = I_{as3}; I_{bs} = I_{bsf3}; I_{cs} = I_{csf3}</math>;</p> <p>Update the sum of phase currents to all consumers:  <math>I_{ap} = I_{apf3}; I_{bp} = I_{bpf3}; I_{cp} = I_{cpf3}</math>;</p> <p>Update the value of unbalanced coefficient <math>UC(p, h) = UC_{min}</math>;</p> <p>Update the value of phase currents <math>I_a(p, h) = I_{ap}</math>, <math>I_b(p, h) = I_{bp}</math>, and <math>I_c(p, h) = I_{cp}</math>;</p> <p>Decrease pillar index: <math>p = p - 1</math>;</p> <p>According with the new allocations from vector <math>PB</math> the central system emits the instructions at each PLBD;</p> <p>Increase hour index: <math>h = h + 1</math>;</p> <p>Print results: <math>UC, I_a, I_b, I_c</math>.</p>



(a)



(b)

Figure 7. (a) The flowchart of the proposed algorithm (the first step—identification of the topology and second step—upload the input data sequence). (b) The flowchart of the proposed algorithm (the third step—PLBS sequence).

### 3. Case Study

#### 3. Case Study

The proposed PLB algorithm was tested in the case of a real LV EDN from a rural area, located in northeastern Romania. The structure of the network is presented in Figure 8. The structure of the network is presented in Figure 8. This network was chosen because of the very complex structure (88 pillars, a total length of 3.52 km, and many lateral branches) and the high number of consumers (163 consumers). Generally, the LV distribution networks have an average length by 1.2 km, with approximately 30 pillars, and an average number of consumers by 60 consumers [38,39]. The values of the characteristics (length, poles, and consumers) of the considered network are about three times higher than the average values. The EDN is supplied from a point (SP), through a power transformer 20/0.4 kV. The numbering of pillars is real, given by the DNO from this distribution area, beginning with Pillar 8. The distance between two successive pillars is 0.04 km, stipulated in Romanian technical normative [40]. The technical characteristics of the branches are presented in Table 4, where  $r_0$  and  $x_0$  represent the specific resistance and reactance. If the reactance is not known, an estimation technique can be used [41].

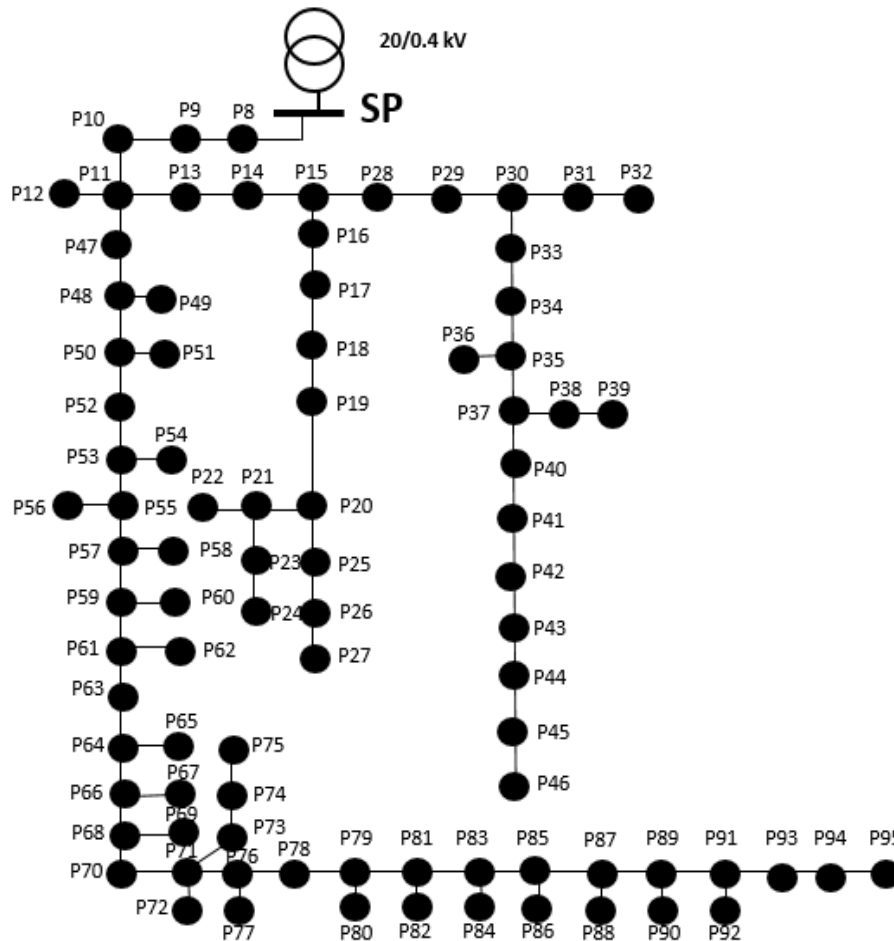


Figure 8. The structure of analyzed electric distribution network (EDN).

Table 4. The technical characteristics of the branches.

Branch	Type Conductor	Cross-Section of Phase Conductors [mm <sup>2</sup> ]	Cross-Section of Neutral Conductor [mm <sup>2</sup> ]	Length [km]	$r_0$ [Ω/km]	$x_0$ [Ω/km]
SP-11	Classic	50	50	0.160	0.61	0.298
11-15	Classic	50	50	0.160	0.61	0.298
11-95	Classic	50	50	1.960	0.61	0.298
15-27	Classic	35	35	0.480	0.871	0.055

**Table 4.** The technical characteristics of the branches.

Branch	Type Conductor	Cross-Section of Phase Conductors [mm <sup>2</sup> ]	Cross-Section of Neutral Conductor [mm <sup>2</sup> ]	Length [km]	r <sub>0</sub> [Ω/km]	x <sub>0</sub> [Ω/km]
SP-11	Classic	50	50	0.160	0.61	0.298
11–15	Classic	50	50	0.160	0.61	0.298
11–95	Classic	50	50	1.960	0.61	0.298
15–27	Classic	35	35	0.480	0.871	0.055
15–39	Classic	35	35	0.480	0.871	0.055
37–46	Classic	25	25	0.280	1.235	0.319
Total		50	50	2.280	0.61	0.298
		35	35	0.960	0.871	0.055
		25	25	0.280	1.235	0.319
Total				3.520		

From the database of the DNO, the information about the characteristics of the consumers from this EDN based on the identification number of the SP was uploaded. The format of the input data was presented in Section 2, see Figure 4. The characteristics of the consumers are presented synthetically in Table 5. Detailed information regarding the connected pillars, the branching phase, and the consumption sector are given in Table A1 from Appendix A.

**Table 5.** Synthesis on the characteristics of the consumers from the analyzed EDN.

Consumer' Type		Initial Phase				Consumption SECTOR			
1-P	3-P	a	b	c	abc	I	II	III	IV
161	2	42	72	47	2	161	2	-	-

It can be observed that the vast majority of consumers (98.8%) have a 1-P branching with the following initial allocation: 25.8% on phase *a*, 44.2% on phase *b*, and 28.8% on phase *c*. Only 1.2% of the consumers have 3-P branching. Regarding the consumption sector, 98.8% of the consumers belong to the domestic sector, and only 1.2% are from the non-domestic sector.

From all consumers, 114 1-P consumers, representing 70.8%, are integrated into the SMS with the possibility to have PLBD installed. They will be considered from the switchable consumers' category in our algorithm. The algorithm imports for each consumer  $i$ ,  $i = 1, \dots, N_c$ , according to the serial number of meter recorded in the vector  $SN$ , the hourly load from the database of SMS for the analyzed period  $H$ . In our case study, the period  $H$  corresponds to a winter working day with hourly records  $h$ ,  $h = 1, \dots, 24$ , see the supplementary file which contains the active and reactive power profiles. The other 47 1-P consumers are considered as non-switchable consumers due to the standard meters, non-integrated in the SMS. For these consumers, the algorithm uses TLPs according to the information stored in the vectors  $CS$ , associated with the consumption sector, and  $CC$ , associated with the consumption class.

The phase currents ( $I_a$ ,  $I_b$  and  $I_c$ ) and neutral current ( $I_0$ ) in the SP (on the 0.4 kV side) were determined considering all load profiles, using the calculations of steady-state regime, see Table 6 and Figure 9). The used algorithm is an improved version of the forward/backward sweep-based algorithm, developed in [36], to calculate the steady-state regimes to three-phase LV distribution networks in the balanced and unbalanced regime.

**Table 5.** Synthesis on the characteristics of the consumers from the analyzed EDN.

**Table 6.** The currents in the conductors of the first branch, SP—Pillar 8, initial case.

Consumer Type	Initial Phase			Consumption SECTOR				
	$I_a$ [A]	$I_b$ [A]	$I_c$ [A]	I	II	III	UC	
1	16.77	42.72	48.71	49.47	161	31.84	-	1.29
2	14.01	46.55	18.64	30.49	1.29			1.30
3	18.36	44.40	17.45	28.29	1.29			1.29
4	13.55	43.94	17.99	28.43	1.28			1.28
5	12.38	36.47	16.98	22.15	1.23			1.23
6	16.73	41.58	19.49	23.59	1.18			1.18
7	19.53	49.37	20.93	24.97	1.17			1.17
8	18.05	53.57	21.70	33.83	1.26			1.26
9	19.21	61.57	23.16	40.52	1.30			1.30
10	17.44	58.17	20.53	39.28	1.33			1.33
11	17.94	61.76	21.40	42.20	1.35			1.35
12	17.87	60.11	22.55	40.18	1.32			1.32
13	17.01	63.07	20.21	41.18	1.33			1.33
14	15.98	54.16	21.22	35.84	1.33			1.33
15	18.38	61.07	22.53	40.77	1.32			1.32
16	21.55	66.87	25.80	43.34	1.29			1.29
17	21.31	59.27	25.14	36.19	1.23			1.23
18	21.22	51.86	23.97	29.41	1.26			1.26
19	25.66	67.08	27.08	32.46	1.17			1.17
20	27.69	68.53	31.57	39.04	1.19			1.19
21	24.83	69.17	30.67	41.72	1.22			1.22
22	17.12	53.18	23.17	33.45	1.26			1.26

It can be observed that the most major class of consumers (98.8%) have a 1-P branching with the following initial allocation: 25.8% on phase *a*, 44.2% on phase *b*, and 28.8% on phase *c*. Only 1.2% of the consumers have 3-P branching. Regarding the consumption sector, 98.8% of the consumers belong to the domestic sector, and only 1.2% are from the non-domestic sector.

From all consumers, 114 (9.5%) consumers, representing 70.8%, are integrated into the SMS with the possibility to have PLBD installed. They will be considered from the switchable consumers' category in our algorithm. The algorithm imports for each consumer  $i, i = 1, \dots, N_c$ , according to the serial number of meter recorded in the vector *SN*, the hourly load from the database of SMS for the analyzed period *H*. In our case study, the period *H* corresponds to a winter working day with hourly records  $h, h = 1, \dots, 24$ , see the supplementary file which contains the active and reactive power profiles. The other 4751-P consumers are considered as non-switchable consumers due to the standard meters, non-integrated in the SMS. For these consumers, the algorithm uses TEPs according to the information stored in the vectors *CS*, associated with the consumption sector, and *CC*, associated with the consumption class.

The phase currents ( $I_a, I_b$  and  $I_c$ ) and neutral current ( $I_0$ ) in the SP (on the 0.4 kV side) were determined considering all load profiles, using the calculations of steady-state regime, see Table 6 and Figure 9). The used algorithm is an improved version of the forward/backward sweep-based algorithm, developed in [36], to calculate the steady-state regimes to three-phase LV distribution networks in the balanced and unbalanced regime.

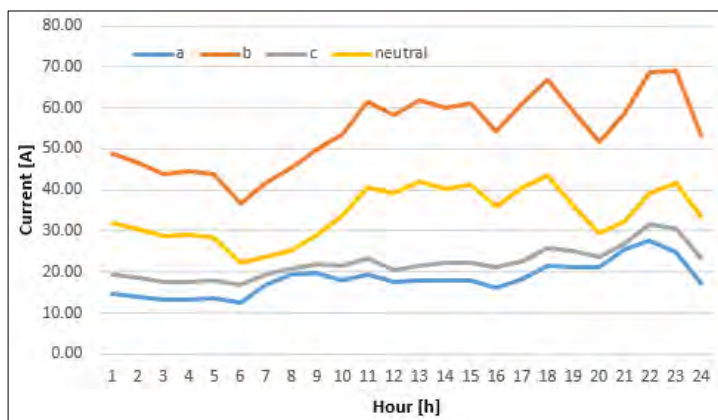


**Figure 9.** The currents in the conductors of the first branch, SP—Pillar 8, initial case.

The analysis of the obtained results highlights a high difference between the phase currents and an important current in the neutral conductor (exceeds the current on the phases *a* and *b*), which leads to an unbalanced degree beyond the threshold (1.1) imposed by the DNO. The *UC* is in the range [1.17, 1.35], having an average value of 1.26.

Also, the current unbalance leads to higher power/energy losses because of current flows in the neutral conductor and a significant voltage unbalance, as shown in Table 7 and Figure 10. The losses in the neutral conductor represent an important percent (37%) of the total energy losses such that the PLB measure must be implemented.

Table 7. The energy losses calculated in the initial case, [kWh].

Hour	Main Conductors				Branching Conductors				Total
	a	b	c	Neutral	a	b	c	Neutral	
1	0.03	14.54	19.17	0.43	0.003	0.014	0.001	1.32	1.14
2	0.03	0.49	0.10	0.39	0.003	0.013	0.001	0.011	1.04
3	0.02	15.43	17.91	0.35	0.002	0.011	0.001	1.33	0.92
4	0.02	16.44	16.99	0.51	0.002	0.012	0.001	1.31	0.93
5	0.02	17.44	18.38	0.35	0.002	0.011	0.001	1.32	0.93
6	0.02	0.31	0.08	0.25	0.002	0.006	0.001	0.006	0.67
7	0.04	18.41	21.55	0.52	0.005	0.007	0.001	1.29	0.90
8	0.05	19.50	21.31	0.58	0.007	0.008	0.001	1.23	1.08
9	0.05	20.59	21.27	0.46	0.007	0.012	0.001	1.18	1.27
10	0.04	0.66	0.13	0.52	0.005	0.017	0.001	0.015	1.40
11	0.05	21.87	25.66	0.58	0.006	0.025	0.001	1.17	1.81
12	0.04	22.77	20.69	0.60	0.005	0.025	0.001	1.19	1.58
13	0.04	23.86	24.83	0.68	0.005	0.029	0.001	1.22	1.77
14	0.04	0.82	0.14	0.65	0.005	0.025	0.001	0.020	1.71
15	0.04	24.85	17.12	0.67	0.005	0.026	0.001	1.26	1.76
16	0.04	0.67	0.13	0.53	0.004	0.019	0.001	0.015	1.40
17	0.05	0.85	0.15	0.67	0.005	0.026	0.001	0.021	1.76
18	0.06	1.04	0.19	0.82	0.007	0.028	0.002	0.024	2.17
19	0.06	0.84	0.18	0.66	0.007	0.017	0.002	0.017	1.78
20	0.06	0.86	0.16	0.51	0.007	0.011	0.001	0.013	1.43
21	0.10	0.10	0.10	0.10	0.012	0.014	0.002	0.018	1.89
22	0.10	0.10	0.10	0.10	0.012	0.014	0.002	0.018	1.89
23	0.08	1.17	0.27	0.93	0.009	0.021	0.002	0.021	2.51
24	0.04	0.66	0.15	0.53	0.004	0.014	0.001	0.012	1.42
Total	1.13	16.93	3.48	13.34	0.130	0.408	0.028	3.370	35.81

The analysis of the obtained results highlights a high difference between the phase currents and an important current in the neutral conductor (exceeds the current on the phases *a* and *b*), which leads to an unbalanced degree beyond the threshold (1.1) imposed by the DNO. The *UC* is in the range [1.17, 1.35], having an average value of 1.26.

Also, the current unbalance leads to higher power/energy losses because of current flows in the neutral conductor and a significant voltage unbalance, as shown in Table 7 and Figure 10. The losses in the neutral conductor represent an important percent (37%) of the total energy losses such that the PLB measure must be implemented.

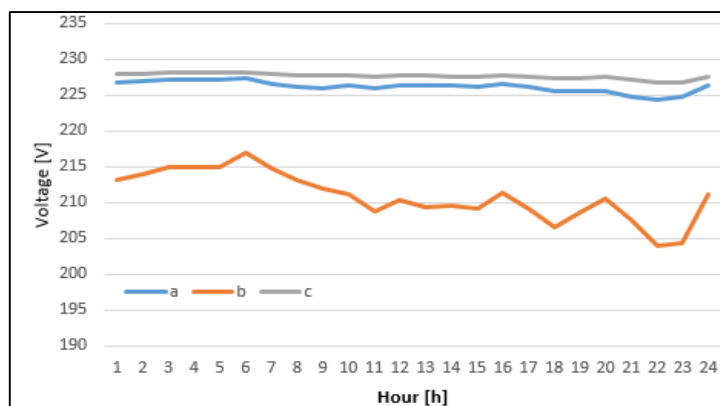


Figure 10. Exemplification of the voltage unbalance at the farthest pillar (P95).

After the application of the proposed algorithm at each hour  $h = 1, \dots, 24$ , the current unbalance was significantly reduced, see Table 8. The average value of *UC* decreased at 1.0017. It can be observed that the current in the neutral conductor decreased with 94%, from the average value of 34.08 A at 2.07 A. This aspect is highlighted in Figure 11. The effects are felt at the level of power/energy losses, see Table 9, and the voltage quality, see Figure 12.



Hour	$I_a$ [A]	$I_b$ [A]	$I_c$ [A]	$I_0$ [A]	$U_G$	$U_C$	$U_D$	$U_E$	$U_F$	Losses
5	0.02	0.44	0.09	0.35	0.002	0.011	0.001	0.010	0.010	0.93
6	0.02	0.31	0.08	0.25	0.002	0.006	0.001	0.006	0.006	0.67
7	0.04	0.41	0.11	0.32	0.005	0.007	0.001	0.008	0.008	0.90
8	0.05	0.50	0.12	0.38	0.007	0.009	0.001	0.011	0.011	1.08
9	0.05	0.59	0.14	0.46	0.007	0.012	0.001	0.013	0.013	1.27
10	0.04	0.66	0.13	0.52	0.005	0.017	0.001	0.015	0.015	1.40
11	0.05	0.87	0.15	0.68	0.006	0.025	0.001	0.021	0.021	1.81
12	0.04	0.77	0.14	0.60	0.005	0.025	0.001	0.020	0.020	1.58
13	0.04	0.86	0.16	0.75	0.005	0.82	0.029	0.30001	1.00023	1.77
14	0.04	0.82	0.14	0.65	0.005	0.24	0.025	0.0001	1.00020	1.71
15	0.04	0.85	0.14	0.78	0.005	0.19	0.026	0.0001	1.00021	1.76
16	0.04	0.67	0.13	0.50	0.004	0.21	0.019	0.21001	1.00015	1.40
17	0.05	0.85	0.15	0.67	0.005	1.14	0.026	1.14001	1.0006	1.76
18	0.06	1.04	0.19	0.87	0.007	28.31	0.028	3.58001	1.0042	2.17
19	0.06	0.84	0.13	0.66	0.007	0.54	0.017	4.59002	1.00517	1.78
20	0.06	0.66	0.16	0.51	0.007	31.81	0.011	1.10001	1.0003	1.43
21	0.09	0.87	0.21	0.65	0.012	34.53	0.014	0.22001	1.0000	1.89
22	0.10	1.18	0.29	0.93	0.012	32.23	0.019	1.26002	1.00022	2.55
23	0.08	1.17	0.27	0.93	0.009	33.29	0.021	0.77002	1.0001	2.51
24	0.04	0.66	0.15	0.52	0.004	33.40	0.014	0.76001	1.00012	1.42
Total	1.13	16.93	33.78	13.48	0.136	37.77	0.408	0.64028	1.00970	35.81

After the application of the proposed algorithm at each hour  $h=1, \dots, 24$ , the current unbalance was significantly reduced, see Table 8. The average value of  $U_G$  decreased from 1.0017. It can be observed that the current in the neutral conductor decreased with 4.4%, from the average value of 34.08 A at 2.07 A. This aspect is highlighted in Figure 11. The effects are felt at the level of power/energy losses, see Table 9, and the voltage quality, see Figure 12.

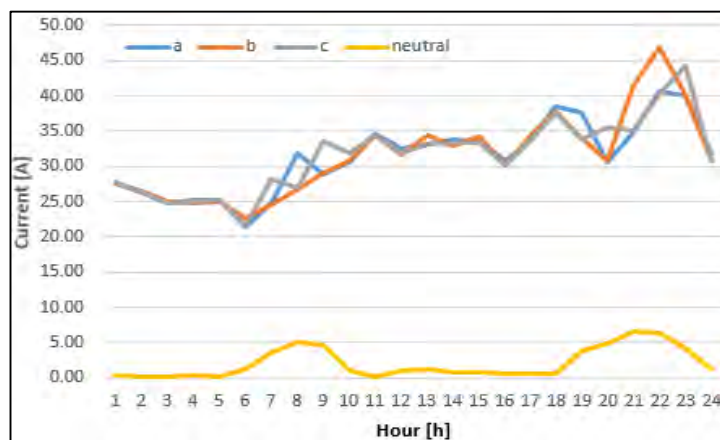
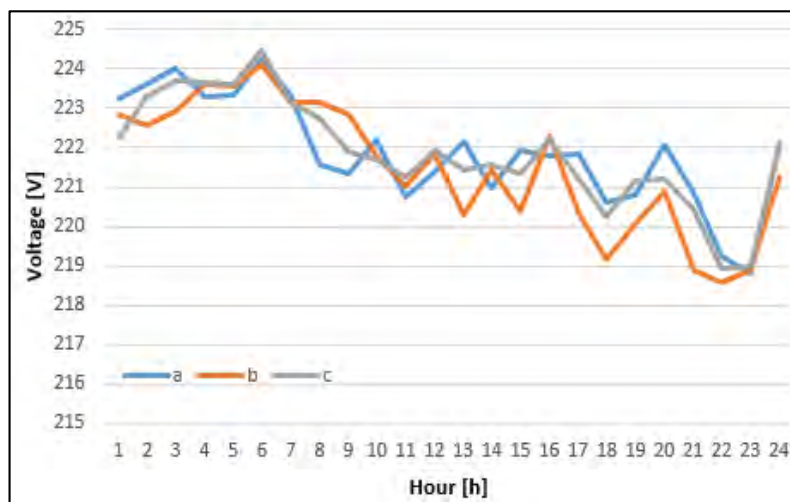


Figure 11. The currents in the conductors of the first branch, SP-Pillar 8, with the proposed algorithm.

The results were compared with other algorithms to emphasize the accuracy of the smart meter data-based proposed algorithm (SMD): from heuristic (the minimum count of loads adjustment (MCLA) algorithm [32]) and metaheuristic (particle swarm optimization (PSO) algorithm [28] and genetic algorithm (AG) [17]) categories. The computational times needed to obtain the solution are presented in Table 10 for each algorithm. The algorithms with a Matlab implementation were run on a computer Intel Core i5, 3.10 GHz, 4GB RAM, WIN 10 64-bit operating system.

**Table 9.** The energy losses calculated with the data obtained using the proposed algorithm, [kWh].

Hour	Main Conductors				Branching Conductors				Total
	a	b	c	Neutral	a	b	c	Neutral	
1	0.12	0.13	0.14	0.01	0.00	0.01	0.01	0.01	0.43
2	0.11	0.13	0.12	0.01	0.00	0.01	0.01	0.01	0.39
3	0.10	0.12	0.10	0.01	0.00	0.01	0.00	0.01	0.35
4	0.12	0.10	0.10	0.01	0.01	0.01	0.00	0.01	0.35
5	0.11	0.11	0.10	0.01	0.01	0.00	0.00	0.01	0.35
6	0.08	0.08	0.08	0.00	0.00	0.00	0.00	0.01	0.26
7	0.11	0.11	0.13	0.01	0.00	0.00	0.01	0.01	0.37
8	0.17	0.12	0.13	0.01	0.01	0.00	0.00	0.01	0.45
9	0.17	0.13	0.18	0.01	0.01	0.00	0.01	0.01	0.52
10	0.15	0.17	0.17	0.01	0.01	0.01	0.01	0.01	0.54
11	0.22	0.20	0.20	0.01	0.01	0.01	0.01	0.02	0.68
12	0.19	0.16	0.17	0.01	0.01	0.01	0.01	0.02	0.59
13	0.17	0.23	0.19	0.02	0.01	0.02	0.01	0.02	0.66
14	0.21	0.19	0.18	0.01	0.01	0.01	0.01	0.02	0.64
15	0.17	0.22	0.19	0.01	0.01	0.01	0.01	0.02	0.65
16	0.17	0.15	0.16	0.01	0.01	0.01	0.01	0.01	0.52
17	0.17	0.22	0.20	0.01	0.01	0.01	0.01	0.02	0.66
18	0.23	0.27	0.24	0.01	0.01	0.01	0.01	0.02	0.82
19	0.22	0.22	0.19	0.01	0.01	0.01	0.01	0.02	0.69
20	0.16	0.18	0.20	0.01	0.00	0.01	0.01	0.01	0.58
21	0.21	0.29	0.22	0.02	0.00	0.02	0.01	0.02	0.78
22	0.28	0.35	0.32	0.02	0.00	0.02	0.01	0.02	1.01
23	0.30	0.28	0.32	0.01	0.01	0.01	0.01	0.02	0.96
24	0.16	0.18	0.16	0.01	0.00	0.01	0.01	0.01	0.54
Total	4.09	4.34	4.18	0.26	0.15	0.20	0.19	0.36	13.76



**Figure 12.** Improvement of voltage quality at the conductors (P95) after applying the proposed algorithm.

**Table 10.** Comparison between the computational times.

**Table 8.** The currents in the conductors of the first Branch, S1, after the proposed algorithm.

Hour	Algorithm		Computational Times (Seconds)		
	$I_a$ [A]	$I_b$ [A]	$I_c$ [A]	$I_0$ [A]	UC
1	27.56	27.50	27.82	0.398	1.0000
2	26.25	26.53	26.37	0.241	1.0000
3	24.88	25.03	24.82	0.19	1.0000
4	25.29	24.88	24.99	0.36	1.0000
5	25.22	25.01	25.21	0.21	1.0000
6	21.47	22.69	21.65	1.14	1.0006
7	24.77	24.68	28.31	3.58	1.0042
8	31.90	26.76	26.93	5.06	1.0070

The values from the table correspond to 24 h. It can be observed that the lowest values were obtained for the heuristic methods (SMD and MCLA) and higher values for the metaheuristic methods (PSO and GA). Even if the computational time of MCLA is lower than SMD, this does not guarantee that effects will be better in the evaluation of the UC coefficient, the current in the neutral conductor (and implicit on the energy losses), or the voltage at the level of each pillar.

Regarding the UC coefficient, the obtained value with the proposed algorithm is identical with AG (1.0017) at the SP level, being smaller than in the case of MCLA and PSO, as shown in Figure 13.

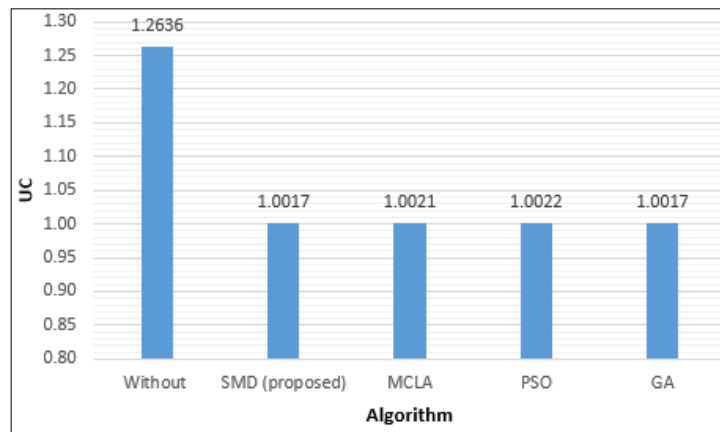


Figure 13. Comparison between the average values of UC at the SP level calculated with different algorithms.

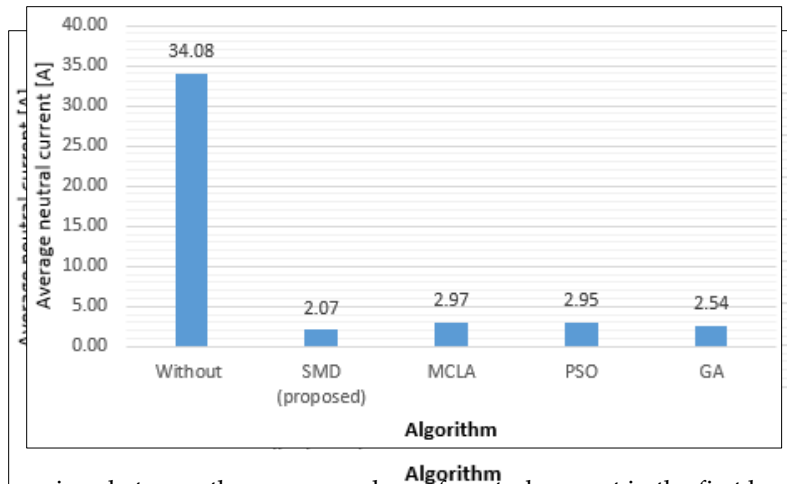
Also, a comparison with the mathematical programming models, proposed by Arias et al. in [4] and Zhu et al. in [42], was done considering the UC coefficient. The UC coefficient was reduced from 1.17 to 1.07 (a reduction with 9.4%) using the Branch and Bound algorithm (BBA) proposed [4], in the case of a test radial network without lateral branches. The reduced integer programming (RIP) had a reduction of the UC coefficient from 1.086 to 1.005 (a reduction with 8.4%) for a test network with 5 nodes [42]. The results are indicated in Table 11.

Table 11. Comparison with the linear programming models.

No.	No.	Algorithm	Characteristics of EDN	UC <sub>initial</sub>	UC <sub>final</sub>	Improvement [%]
1	1	SMD (Proposed)	real/complex/88 nodes/163 consumers	1.26	1.0017	25.8
2	1	BBA	fictive/complex/88 nodes/163 consumers	1.17	1.07	9.4
3	1	(Proposed)	fictive/radial with 2 lateral branches/6 nodes	1.086	1.005	8.0
2	2	BBA	fictive/radial without lateral branches/5 nodes	1.17	1.07	9.4
3	3	MIP	fictive/radial with 2 lateral branches/6 nodes	1.086	1.005	8.0

The results confirm the advantages of the proposed algorithm compared with the mathematical programming algorithms. Also, the accuracy of the SMD algorithm was demonstrated in the case of a real complex EDN, compared with the other algorithms, which were tested using fictive EDNs, with simple topologies (radial).

The results confirm the advantages of the proposed algorithm compared with the mathematical programming algorithms. Also, the accuracy of the SMD algorithm was demonstrated in the case of a real complex EDN, compared with the other algorithms obtained which were tested using SMD, MIP, PSO, and GA) topologies (radial). To highlight the effect on the decrease of the current in the neutral conductor (and implicit on the energy losses) and on the voltage quality at the level of each pillar, the steady-state regimes were calculated, having as input data the load matrices obtained with each algorithm (SDM, MCLA, PSO, and GA). The average value of the current in the neutral conductor, on the first branch, is shown in Figure 14, for each algorithm. It can be observed that the smallest value was obtained by applying the proposed algorithm (2.07 A), with 22.7% better than GA.



**Figure 14.** Comparison between the average values of neutral current in the first branch, SP-Pillar 8, calculated with different algorithms.  
**Figure 14.** Comparison between the average values of neutral current in the first branch, SP-Pillar 8, calculated with different algorithms.

Regarding the energy losses, Table 12 presents the values calculated on the phase and neutral conductors in the branching and main conductors. The analysis of the results indicates smaller energy losses in the branching and proposed algorithm. The analysis of the results indicates smaller energy losses in the branching and proposed algorithm compared to the other algorithms, as shown in Tables 12 and 15. The proposed algorithm is compared by the other algorithms in the case of the energy losses in the phase and neutral conductors. The difference from the energy losses is higher with 19.01% than in the case of AG. The difference from the MCLA algorithm is higher, with 19.01%.

**Table 12.** Comparison between the energy losses calculated with different algorithms, [kWh].

Algorithm	Main Conductors				Branching Conductors				Total	ΔΔW [%]
	a	b	c	Neutral	a	b	c	Neutral		
Without	1.13	15.23	3.48	13.34	0.13	0.41	0.03	0.36	35.81	
SMD (proposed)	4.03	4.93	4.18	0.26	0.13	0.21	0.03	0.38	13.76	61.57
SMD (proposed)	4.09	4.34	4.18	0.26	0.13	0.20	0.19	0.36	13.76	61.57
W/MCLA	4.14	6.23	4.98	4.32	0.33	0.05	0.16	0.36	20.57	42.56
SMD (proposed)	4.04	4.43	4.18	0.30	0.23	0.20	0.15	0.36	13.86	61.57
MCLA	4.36	6.22	4.98	4.31	0.34	0.05	0.21	0.36	14.19	60.37
PSO	4.44	4.43	3.77	0.32	0.23	0.17	0.15	0.36	13.86	61.30
GA									14.19	60.37

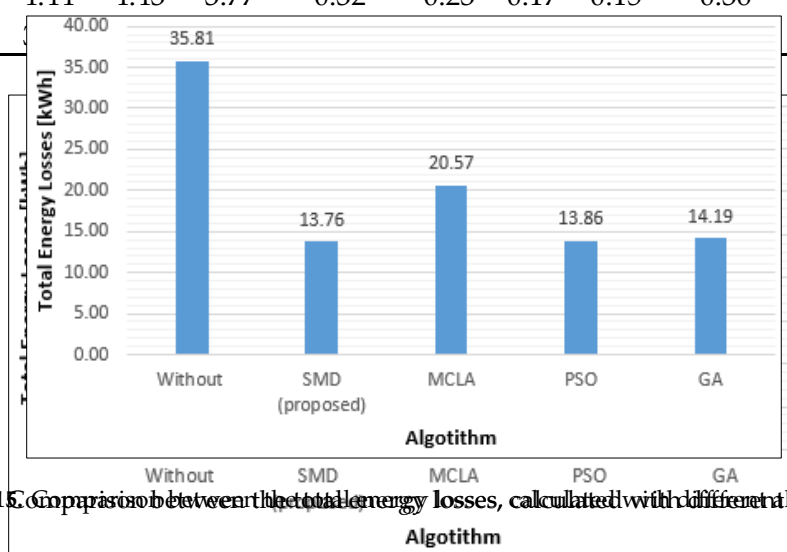


**Figure 15.** Comparison between the total energy losses, calculated with different algorithms.

Also, the saving-energy (ΔΔW), given in percent, are indicated in Table 12. The calculation relation is the following:

$$\Delta\Delta W = \left| \frac{\Delta W_{initial} - \Delta W_{algorithm}}{\Delta W_{initial}} \right| \cdot 100, [\%] \quad (17)$$

where algorithm is SMD, MCLA, PSO, and GA.

$$\Delta\Delta W = \left| \frac{\Delta W_{initial} - \Delta W_{algorithm}}{\Delta W_{initial}} \right| \cdot 100, [\%] \quad (17)$$

Also, the saving-energy ( $\delta\Delta W$ ), given in percent, are indicated in Table 12. The calculation relation is the following:

$$\delta\Delta W = \left| \frac{\Delta W_{initial} - \Delta W_{algorithm}}{\Delta W_{initial}} \right| \cdot 100, [\%] \tag{17}$$

where *algorithm* is SMD, MCLA, PSO, and GA.

The voltage quality was evaluated at the level of the farthest pillar (P95), and the results are presented in Table 13. The minimum values are highlighted with bold to be easily identified in the analysis. It can be observed that the phase voltages are between the admissible limits (rated voltage  $\pm 10\%$ , where the rated voltage is 230 V). Small differences between the phase voltages, in the range [0.13V, 0.36 V], were obtained in the case of the proposed algorithm, with an improvement of value on phase *b* of 14.58 V (7.15%). The biggest differences, in the range [5.59 V, 12.9 V], were obtained in the case of the MCLA algorithm.

**Table 13.** The minimum value of the phase voltages at the level of the farthest pillar (P95).

Algorithm	Phase		
	a	b	c
Without	224.33	<b>204.00</b>	226.71
SMD (proposed)	218.81	<b>218.58</b>	218.94
MCLA	218.90	<b>211.59</b>	224.49
PSO	<b>218.19</b>	219.03	218.55
GA	219.41	<b>217.28</b>	219.07

The detailed results for each algorithm are presented in Tables A2–A5 from Appendix B.

#### 4. Conclusions

In the paper, a PLB algorithm was proposed having the following advantages: It can be implemented in the EDNs with hybrid structures of the consumption points (switchable and non-switchable consumers); it can work in both operation modes (real-time and off-line), uploading information from different databases of the DNO which contain the consumers’ characteristics, real loads of the consumers integrated into the SMS, and loads from the TLPs for the consumers non-integrated in the SMS; the convergence is rapid because of the fast recognition of EDN topology with the help of a structure vectors based-algorithm.

The testing of the algorithm was made in a real rural EDN from the northeastern region of Romania, having a hybrid structure of the consumption points (114 1-P consumers (70.8%) are integrated into the SMS with the possibility to have SPLBS, the other consumers having standard meter). The obtained results were analyzed and compared with other algorithms from the heuristic category (minimum count of loads adjustment (MCLA) algorithm) and the metaheuristic category (particle swarm optimization (PSO) and genetic algorithm (AG)).

The best performances were recorded for the proposed algorithm, obtaining the smallest value of the unbalance coefficient (1.0017), in comparison with MCLA (1.0022) and PSO (1.0021) algorithms. The same value (1.0017) was also obtained in the case of AG. The average value of the current in the neutral conductor decreased with 94% from the average value of 34.08 A (initial case) at 2.07 A. This value is smaller with 22.70% than AG, 42.51% than PSO, and 43.47% than MCLA. The energy losses decreased with 61.75% compared to the initial case using the data obtained with the proposed algorithm. This value is smaller by 0.20% than AG, 0.27% than PSO, and 19.01% than MCLA.

The proposed solution can be introduced by the DNOs to ensure the transition toward the smart grids, but only on the basis of a feasibility analysis, to justify the investment. Also, the DNOs must take into account that the proposed algorithm cannot have very high efficiency in networks with many not integrated consumers into the SMS, for which the TLPs must be associated. Within the proposed algorithm, they belong to the category of non-switchable consumers, so that the number of switching

options will be limited. The transition process should be mainly implemented in the “hot” areas where there are EDNs without or with small number of non-switchable consumers, leading to a solution very close to the optimal solution (in the ideal case, it is equal with 1.00).

The authors work now at an improved variant of the proposed algorithm, which considers the weight of each switchable consumer at the unbalance degree. The main objective is the determination of the optimal number of PLBD, which minimizes the unbalance coefficient and the investment costs.

**Supplementary Materials:** The following are available online at <http://www.mdpi.com/2227-7390/8/4/549/s1>.

**Author Contributions:** G.G. proposed the implementation methodology, mathematical modeling, validation, and writing—original draft preparation B.-C.N. implemented the software, data curation, and validation; C.B. and I.T. improved the methodology, performed simulations, and writing; M.G. performed simulations, and reviewed the manuscript. All authors discussed the results and have agreed with the structure of the paper. All authors have read and agreed to the published version of the manuscript.

**Funding:** This research received no external funding.

**Conflicts of Interest:** The authors declare no conflict of interest.

## Nomenclature

0	Neutral conductor
1-P	Single-phase consumer
3-P	Three-phase consumer
EDN	Electric distribution network
LV	Low voltage
TLP	Typical load profile
DNO	Distribution network operator
SMS	Smart metering system
SMD	Smart meter data
PLB	Phase load balancing
PLC	Power-line communication
SCADA	Supervisory control and data acquisition
APLBD	Automatic phase load balancing device
SPLBS	Smart phase load balancing system
DMCL	Decision-making central level
PSO	Particle swarm optimization
AG	Genetic algorithm
MCLA	Minimum count of loads adjustment
$H$	The analyzed time period, [hours]
$B_i$	Vector of the input nodes of branches
$B_j$	Vector of the end nodes of branches
$a, b, c$	The phases of the EDN
$abc$	3-P consumer in the input data files
{ph}	The set of phases $\{a, b, c\}$
TV1	Topology vector containing the number of branches from each vicinity level
TV2	Topology vector containing the branches placed in the order of the vicinity levels
SP	Supply Point
$N_C$	The total number of consumers from the EDN
$CP$	Vector of the connected pillars, size $(N_C \times 1)$
$PB$	Vector of the branching phase, size $(N_C \times 1)$
$CS$	Vector of the consumption sector of the consumers, size $(N_C \times 1)$

CC	Vector of the consumption class of the consumers from a certain consumption sector, size ( $N_C \times 1$ )
INT	Vector of the integration mode in the SMS, size ( $N_C \times 1$ )
BS	Vector of the PLBD status, size ( $N_C \times 1$ )
IC	Vector of the hourly loads for all consumers, size ( $N_C \times H$ )
SN	Vector of the serial numbers corresponding the smart meters, size ( $N_C \times 1$ )
$r_0$	Specific resistance, [ $\Omega/\text{km}$ ]
$x_0$	Specific reactance, [ $\Omega/\text{km}$ ]
UC	The unbalance coefficient
$I_a, I_b, I_c$	The currents on the phases $a, b$ , and $c$ , [A]
$I_{average}$	The average value of the phase currents, [A]
$h$	The current hour ( $h = 1, \dots, H$ )
$N_p$	The number of pillars from the EDN
$p$	The analyzed current pillar ( $p = 1, \dots, N_p$ )
$d$	Pillar located downstream by pillar $p$
$UC^{(p),h}$	The unbalance coefficient calculated at the pillar $p$ and hour $h$
index	Vector of the indices corresponding to pillar $p$ in vector $CP$
$I_a^{(p),h}$	The current on the phase $a$ , at the pillar $p$ and hour $h$ , [A]
	The current on the phase $b$ , at the pillar $p$ and hour $h$ , [A]
$I_c^{(p),h}$	The current on the phase $c$ , at the pillar $p$ and hour $h$ , [A]
$I_{a,ns}^{(p),h}$	The total current of the non-switchable consumers on the phase $a$ , pillar $p$ and hour $h$ , [A]
$I_{b,ns}^{(p),h}$	The total current of the non-switchable consumers on the phase $b$ , pillar $p$ and hour $h$ , [A]
$I_{c,ns}^{(p),h}$	The total current of the non-switchable consumers on the phase $c$ , pillar $p$ and hour $h$ , [A]
$I_{a,s}^{(p),h}$	The total current of the switchable consumers on the phase $a$ , pillar $p$ and hour $h$ , [A]
$I_{b,s}^{(p),h}$	The total current of the switchable consumers on the phase $b$ , pillar $p$ and hour $h$ , [A]
$I_{c,s}^{(p),h}$	The total current of the switchable consumers on the phase $c$ , pillar $p$ and hour $h$ , [A]
$I_a^{(d),h}$	The currents on the phase $a$ , pillar $d$ , and hour $h$ , [A]
$I_b^{(d),h}$	The currents on the phase $b$ , pillar $d$ , and hour $h$ , [A]
$I_c^{(d),h}$	The currents on the phase $c$ , pillar $d$ , and hour $h$ , [A]
$j$	Index of the non-switchable consumer connected on the phase $a$ , pillar $p$ , and hour $h$
$k$	Index of the non-switchable consumer connected on the phase $b$ , pillar $p$ , and hour $h$
$l$	Index of the non-switchable consumer connected on the phase $c$ , pillar $p$ , and hour $h$
$m$	Index of the switchable consumer connected on the phase $a$ , pillar $p$ , and hour $h$
$n$	Index of the switchable consumer connected on the phase $b$ , pillar $p$ , and hour $h$
$o$	Index of the switchable consumer connected on the phase $c$ , pillar $p$ , and hour $h$
$N_{a,ns}^{(p),h}$	The number of the non-switchable consumers connected on the phase $a$ , pillar $p$ , and hour $h$
$N_{b,ns}^{(p),h}$	The number of the non-switchable consumers connected on the phase $b$ , pillar $p$ , and hour $h$
$N_{c,ns}^{(p),h}$	The number of the non-switchable consumers connected on the phase $c$ , pillar $p$ , and hour $h$
$N_{a,s}^{(p),h}$	The number of the switchable consumers connected on the phase $a$ , pillar $p$ , and hour $h$
$N_{b,s}^{(p),h}$	The number of the switchable consumers connected on the phase $b$ , pillar $p$ , and hour $h$
$N_{c,s}^{(p),h}$	The number of the switchable consumers connected on the phases $c$ , pillar $p$ , and hour $h$
$N_{C,ns}^{(p),h}$	The total number of the non-switchable consumers connected at the pillar $p$ , and hour $h$
$N_{C,s}^{(p),h}$	The total number of the switchable consumers connected at the pillar $p$ , and hour $h$
$N_C^{(p),h}$	The total number of the consumers connected at the pillar $p$ , and hour $h$
$I_{a,ns,j}^{(p),h}$	The current of the non-switchable consumer $j$ ( $j = 1, \dots, N_{a,ns}^{(p),h}$ ), [A]
$I_{b,ns,k}^{(p),h}$	The current of the non-switchable consumer $k$ ( $k = 1, \dots, N_{b,ns}^{(p),h}$ ), [A]
$I_{c,ns,l}^{(p),h}$	The current of the non-switchable consumer $l$ ( $l = 1, \dots, N_{c,ns}^{(p),h}$ ), [A]
$I_{a,s,m}^{(p),h}$	The current of the switchable consumer $m$ ( $m = 1, \dots, N_{a,s}^{(p),h}$ ), [A]
$I_{a,s,n}^{(p),h}$	The current of the switchable consumer $n$ ( $n = 1, \dots, N_{b,s}^{(p),h}$ ), [A]
$I_{a,s,o}^{(p),h}$	The current of the switchable consumer $o$ ( $o = 1, \dots, N_{c,s}^{(p),h}$ ), [A]
$\delta\Delta W$	The percentage error, [%]





**Appendix B**

**Table A2.** Comparison between the hourly UC calculated with different algorithms at the SP level.

Hour	Without	SMD (Proposed)	MCLA	PSO	GA
1	1.2949	1.0000	1.0001	1.0017	1.0010
2	1.2965	1.0000	1.0005	1.0023	1.0009
3	1.2923	1.0000	1.0007	1.0024	1.0007
4	1.3016	1.0000	1.0012	1.0026	1.0011
5	1.2837	1.0000	1.0010	1.0029	1.0007
6	1.2265	1.0006	1.0005	1.0023	1.0003
7	1.1840	1.0042	1.0017	1.0010	1.0027
8	1.1700	1.0070	1.0042	1.0021	1.0046
9	1.2036	1.0050	1.0040	1.0004	1.0017
10	1.2630	1.0003	1.0022	1.0007	1.0000
11	1.3041	1.0000	1.0039	1.0018	1.0007
12	1.3339	1.0002	1.0031	1.0029	1.0019
13	1.3485	1.0003	1.0026	1.0040	1.0028
14	1.3209	1.0001	1.0028	1.0028	1.0016
15	1.3313	1.0001	1.0027	1.0031	1.0023
16	1.3078	1.0001	1.0012	1.0030	1.0013
17	1.3198	1.0001	1.0025	1.0030	1.0021
18	1.2881	1.0001	1.0018	1.0010	1.0006
19	1.2344	1.0025	1.0011	1.0001	1.0003
20	1.1843	1.0049	1.0029	1.0025	1.0032
21	1.1691	1.0070	1.0040	1.0053	1.0058
22	1.1867	1.0051	1.0031	1.0028	1.0032
23	1.2241	1.0024	1.0021	1.0007	1.0008
24	1.2562	1.0004	1.0005	1.0008	1.0001

**Table A3.** Comparison between the hourly neutral currents calculated with different algorithms, the first branch (SP-Pillar 8).

Hour	Without	SMD (Proposed)	MCLA	PSO	GA
1	31.84	0.30	0.56	2.42	1.87
2	30.49	0.24	1.23	2.68	1.72
3	28.58	0.19	1.40	2.60	1.42
4	29.20	0.36	1.81	2.71	1.74
5	28.43	0.21	1.67	2.85	1.39
6	22.15	1.14	1.06	2.21	0.87
7	23.59	3.58	2.27	1.75	2.85
8	24.97	5.06	3.90	2.79	4.10
9	29.18	4.59	4.07	1.34	2.66
10	33.83	1.10	3.11	1.70	0.30
11	40.52	0.22	4.57	3.07	1.98
12	39.28	0.91	3.78	3.67	2.92
13	42.20	1.26	3.67	4.49	3.80
14	40.18	0.77	3.73	3.76	2.85
15	41.18	0.76	3.68	3.98	3.39
16	35.84	0.68	2.19	3.52	2.34
17	40.77	0.64	3.59	3.96	3.33
18	43.34	0.63	3.39	2.58	1.89
19	36.19	3.72	2.49	0.74	1.37
20	29.41	4.79	3.68	3.39	3.90
21	32.43	6.61	4.97	5.71	6.03
22	39.04	6.46	5.02	4.75	5.12
23	41.72	4.29	3.99	2.30	2.44
24	33.45	1.24	1.53	1.90	0.79

**Table A4.** Comparison between the hourly power losses calculated with different algorithms, [kWh].

Hour	SMD (Proposed)			MCLA			PSO			GA		
	a	b	c	a	b	c	a	b	c	a	b	c
1	0.40	0.03	0.43	0.60	0.03	0.63	0.40	0.03	0.43	0.43	1.68	2.11
2	0.36	0.03	0.39	0.54	0.03	0.57	0.37	0.03	0.39	0.39	1.52	1.91
3	0.32	0.02	0.35	0.48	0.02	0.50	0.33	0.02	0.35	0.35	1.35	1.70
4	0.33	0.02	0.35	0.48	0.02	0.50	0.33	0.02	0.36	0.35	1.36	1.71
5	0.33	0.02	0.35	0.49	0.02	0.51	0.33	0.02	0.36	0.35	1.38	1.73
6	0.25	0.01	0.26	0.40	0.01	0.41	0.25	0.01	0.26	0.26	1.08	1.35
7	0.35	0.02	0.37	0.55	0.02	0.57	0.35	0.02	0.37	0.37	1.51	1.88
8	0.43	0.03	0.45	0.67	0.03	0.70	0.42	0.03	0.45	0.45	1.85	2.30
9	0.48	0.03	0.52	0.74	0.03	0.77	0.48	0.03	0.51	0.52	2.06	2.58
10	0.50	0.04	0.54	0.75	0.04	0.78	0.51	0.04	0.54	0.54	2.11	2.64
11	0.63	0.05	0.68	0.91	0.05	0.96	0.64	0.05	0.69	0.68	2.59	3.27
12	0.54	0.05	0.59	0.83	0.05	0.88	0.55	0.05	0.60	0.59	2.35	2.94
13	0.60	0.06	0.66	0.92	0.06	0.97	0.61	0.06	0.67	0.66	2.60	3.25
14	0.59	0.05	0.64	0.84	0.05	0.89	0.60	0.05	0.64	0.64	2.42	3.05
15	0.60	0.05	0.65	0.86	0.05	0.91	0.61	0.05	0.66	0.65	2.46	3.11
16	0.49	0.04	0.52	0.71	0.04	0.75	0.49	0.04	0.53	0.52	2.02	2.55
17	0.61	0.05	0.66	0.87	0.05	0.92	0.62	0.05	0.67	0.66	2.50	3.16
18	0.76	0.06	0.82	1.12	0.06	1.18	0.77	0.06	0.82	0.82	3.18	3.99
19	0.65	0.04	0.69	1.01	0.04	1.05	0.65	0.04	0.69	0.69	2.79	3.48
20	0.55	0.03	0.58	0.89	0.03	0.92	0.55	0.03	0.58	0.58	2.42	3.00
21	0.73	0.04	0.78	1.15	0.04	1.19	0.73	0.04	0.77	0.78	3.16	3.94
22	0.96	0.05	1.01	1.58	0.05	1.64	0.96	0.05	1.01	1.01	4.29	5.31
23	0.91	0.05	0.96	1.48	0.05	1.53	0.91	0.05	0.96	0.96	4.02	4.98
24	0.51	0.03	0.54	0.80	0.03	0.83	0.51	0.03	0.54	0.54	2.20	2.73

**Table A5.** Comparison between the hourly phase voltages calculated with different algorithms, at the level of the farthest pillar P95, [V].

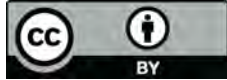
Hour	SMD (Proposed)			MCLA			PSO			GA		
	a	b	c	a	b	c	a	b	c	a	b	c
1	223.25	222.85	222.25	223.28	219.05	225.96	222.50	222.46	223.38	223.81	221.64	222.90
2	223.62	222.55	223.27	223.55	219.75	226.08	222.87	222.78	223.78	224.12	222.13	223.18
3	224.01	222.94	223.69	223.91	220.40	226.29	223.28	223.20	224.17	224.45	222.65	223.54
4	223.29	223.60	223.67	223.79	220.47	226.25	223.20	223.17	224.18	224.47	222.60	223.47
5	223.33	223.55	223.59	223.82	220.35	226.26	223.30	223.07	224.10	224.35	222.57	223.55
6	224.24	224.12	224.45	224.80	221.03	226.94	224.38	223.89	224.55	224.75	223.43	224.63
7	223.33	223.16	223.14	223.26	219.58	226.72	223.09	223.16	223.38	223.64	222.57	223.42
8	221.59	223.17	222.75	222.20	218.58	226.65	222.23	222.67	222.60	222.95	221.91	222.65
9	221.36	222.83	221.88	221.84	218.08	226.07	221.69	222.03	222.35	222.69	221.29	222.08
10	222.22	221.81	221.69	221.95	218.13	225.57	221.54	221.62	222.55	222.90	220.91	221.90
11	220.73	221.02	221.25	220.94	217.16	224.83	220.43	220.62	221.95	222.37	219.82	220.81
12	221.37	221.86	221.91	223.84	216.11	225.09	221.04	221.36	222.74	223.15	220.59	221.39
13	222.15	220.28	221.45	223.49	215.53	224.75	220.57	220.86	222.45	222.89	220.05	220.93
14	220.97	221.41	221.57	221.44	217.53	224.91	220.80	220.86	222.29	222.72	220.05	221.18
15	221.95	220.37	221.35	221.37	217.39	224.85	220.71	220.76	222.20	222.70	219.83	221.14
16	221.78	222.27	222.22	222.47	218.35	225.39	221.77	221.59	222.89	223.26	220.89	222.11
17	221.85	220.34	221.23	221.31	217.20	224.85	220.73	220.63	222.06	222.56	219.66	221.19
18	220.60	219.18	220.24	220.17	215.27	224.49	219.58	219.62	220.82	221.41	218.47	220.14
19	220.78	220.07	221.17	220.96	215.62	225.34	220.40	220.60	221.03	221.63	219.37	221.01
20	222.07	220.89	221.23	221.49	216.34	226.24	221.15	221.66	221.38	221.99	220.40	221.80
21	220.83	218.92	220.42	221.29	214.22	224.53	219.60	220.66	219.91	220.66	219.12	220.39
22	219.25	218.58	218.94	218.90	211.59	225.06	218.19	219.03	218.55	219.41	217.28	219.07
23	<b>218.81</b>	218.91	218.98	219.75	212.05	224.71	218.55	219.04	219.11	219.98	217.33	219.38
24	222.11	221.24	222.09	222.58	217.10	225.67	221.60	221.57	222.27	222.74	220.64	222.06

## References

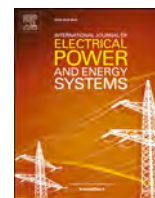
1. Toader, C.; Porumb, R.; Bulac, C.; Tristiu, I. A perspective on current unbalance in low voltage distribution network. In Proceedings of the 9th International Symposium on Advanced Topics in Electrical Engineering (ATEE), Bucharest, Romania, 7–9 May 2015; pp. 741–746.
2. Chembe, D.K. Reduction of Power Losses Using Phase Load Balancing Method in Power Networks. In Proceedings of the World Congress on Engineering and Computer Science (WCECS 2009), San Francisco, CA, USA, 20–22 October 2009; Volume 1.
3. Beharrysingh, S. Phase Unbalance on Low-Voltage Electricity Networks and Its Mitigation Using Static Balancers. Ph.D. Thesis, Loughborough University, Loughborough, UK, 2014. Available online: <https://dspace.lboro.ac.uk/dspace-jspui/handle/2134/16252> (accessed on 1 February 2020).
4. Arias, J.; Calle, M.; Turizo, D.; Guerrero, J.; Candelo-Becerra, J.E. Historical Load Balance in Distribution Systems Using the Branch and Bound Algorithm. *Energies* **2019**, *12*, 1219. [[CrossRef](#)]
5. Homae, O.; Najafi, A.; Dehghanian, M.; Attar, M.; Falaghi, H. A practical approach for distribution network load balancing by optimal re-phasing of single phase customers using discrete genetic algorithm. *Int. Trans. Electr. Energy Syst.* **2019**, *29*, e2834. [[CrossRef](#)]
6. Li, Y.; Gong, Y. Design of Three Phase Load Unbalance Automatic Regulating System for Low Voltage Power Distribution Grids. In *MATEC Web of Conferences*; EDP Science: Les Ulis, France, 2018; Volume 173, p. 02040.
7. Safitri, N.; Shahnia, F.; Masoum, M. Coordination of single-phase rooftop PVs in unbalanced three-phase residential feeders for voltage profiles improvement. *Aust. J. Electr. Electron. Eng.* **2016**, *13*, 77–90. [[CrossRef](#)]
8. Siti, M.W.; Jimoh, A.A.; Nicolae, D.V. Distribution network phase load balancing as a combinatorial optimization problem using fuzzy logic and Newton–Raphson. *Electr. Power Syst. Res.* **2011**, *81*, 1079–1087. [[CrossRef](#)]
9. Sicchar, J.R.; Da Costa, C.T., Jr.; Silva, J.R.; Oliveira, R.C.; Oliveira, W.D. A Load-Balance System Design of Microgrid Cluster Based on Hierarchical Petri Nets. *Energies* **2018**, *11*, 3245. [[CrossRef](#)]
10. Siti, M.W.; Jimoh, A.A.; Nicolae, D.V. LV self balancing distribution network reconfiguration for minimum losses. In Proceedings of the IEEE Bucharest Power Tech, Bucharest, Romania, 28 June–2 July 2009; pp. 1–6.
11. Esfandeh, M.A. Load Balancing Using a Best-Path-Updating Information-Guided Ant Colony Optimization Algorithm. *J. Nov. Res. Electr. Power* **2019**, *7*, 37–45.
12. Kalesar, B.M. Customers swapping between phases for loss reduction considering daily load profile model in smart grid. In Proceedings of the CIRED Workshop 2016, Helsinki, Finland, 14–15 June 2016; pp. 1–4.
13. Shahnia, F.; Wolfs, P.J.; Ghosh, A. Voltage Unbalance Reduction in Low Voltage Feeders by Dynamic Switching of Residential Customers among Three Phases. *IEEE Trans. Smart Grid* **2014**, *5*, 1318–1327. [[CrossRef](#)]
14. Bao, G.; Ke, S. Load Transfer Device for Solving a Three-Phase Unbalance Problem Under a Low-Voltage Distribution Network. *Energies* **2019**, *12*, 2842. [[CrossRef](#)]
15. Rios, M.A.; Castaño, J.C.; Garcés, A.; Molina-Cabrera, A. Phase Balancing in Power Distribution Systems: A heuristic approach based on group-theory. In Proceedings of the IEEE Milan Power Tech, Milan, Italy, 23–27 June 2019; pp. 1–6.
16. Mahendran, G.; Govindaraju, C. Flower Pollination Algorithm for Distribution System Phase Balancing Considering Variable Demand. *Microprocess. Microsyst.* **2020**. [[CrossRef](#)]
17. Ivanov, O.; Neagu, B.C.; Gavrilas, M.; Grigoras, G.; Sfintes, C. Phase Load Balancing in Low Voltage Distribution Networks Using Metaheuristic Algorithms. In Proceedings of the International Conference on Electromechanical and Energy Systems (SIELMEN), Craiova, Romania, 9–11 October 2019; pp. 1–6.
18. Ali, B.; Siddique, I. Distribution system loss reduction by automatic transformer load balancing. In Proceedings of the International Multi-topic Conference (INMIC), Lahore, Pakistan, 24–26 November 2017; pp. 1–5.
19. Fäßler, B.; Schuler, M.; Kepplinger, P. Autonomous, Decentralized Battery Storage Systems for Load Balancing in Low Voltage Distribution Grids. In Proceedings of the 7th International Symposium on Energy, Manchester, UK, 14 August 2017.
20. Faessler, B.; Schuler, M.; Preißinger, M.; Kepplinger, P. Battery Storage Systems as Grid-Balancing Measure in Low-Voltage Distribution Grids with Distributed Generation. *Energies* **2017**, *10*, 2161. [[CrossRef](#)]

21. Liu, X.; Jia, J.; Wang, J. Research of Three-Phase Unbalanced Treatment in Low-Voltage Distribution Network Based on New Commutation Switch. *World J. Eng. Technol.* **2019**, *7*, 10–17. [CrossRef]
22. Kharche, R.; Diwane, A.; Bhalerao, B.; Jhadhav, A.; More, S.M.; Shinde, G.H. Automatic Load Balancing and Phase Balancing By PLC and SCADA. In Proceedings of the International Conference on New Frontiers of Engineering, Management, Social Science and Humanities, Pune, India, 27 May 2018; pp. 174–179.
23. Kardam, N.; Ansari, M.A. Farheen, Communication and load balancing using SCADA model based integrated substation. In Proceedings of the International Conference on Energy Efficient Technologies for Sustainability, Nagercoil, India, 10–12 April 2013; pp. 1256–1261.
24. Pasdar, A.; Mehne, H.H. Intelligent three-phase current balancing technique for single-phase load based on smart metering. *Int. J. Electr. Power Energy Syst.* **2011**, *33*, 693–698. [CrossRef]
25. Bordagaray, A.G.; Prado, J.G.; Vélez, M. Optimal Phase Swapping in Low Voltage Distribution Networks Based on Smart Meter Data and Optimization Heuristics. In *Harmony Search Algorithm: Proceedings of the 3rd International Conference on Harmony Search Algorithm (ICHSA 2017)*; Springer: Singapore, 2017; Volume 514, p. 283.
26. Pires, V.; Santos, N.M.; Cordeiro, A.; Sousa, J.L. Balancing LV Distribution Networks in the Context of the Smart Grid. *Int. J. Smart Grid* **2019**, *3*, 42–53.
27. Grigoras, G.; Gavrilas, M.; Neagu, B.C.; Ivanov, O.; Triștiu, I.; Bulac, C. Efficient Method to Optimal Phase Load Balancing in Low Voltage Distribution Network. In Proceedings of the Int. Conf. on Energy and Environment (CIEM), Timisoara, Romania, 17–18 October 2019; pp. 323–327.
28. Ivanov, O.; Grigoras, G.; Neagu, B.C. Smart Metering based Approaches to Solve the Load Phase Balancing Problem in Low Voltage Distribution Networks. In Proceedings of the International Symposium on Fundamentals of Electrical Engineering (ISFEE), Bucharest, Romania, 1–3 November 2018; pp. 1–6.
29. Tung, T.A.; Son, T.T. Current unbalance reduction in low voltage Distribution networks using automatic phase balancing device. *Vietnam J. Sci. Technol.* **2017**, *55*, 108–119. [CrossRef]
30. Tung, N.X.; Fujita, G.; Horikoshi, K. Phase loading balancing by shunt passive compensator. In Proceedings of the 2009 Transmission & Distribution Conference & Exposition: Asia and Pacific, Seoul, Korea, 26–30 October 2009; pp. 1–4.
31. Siti, M.W.; Nicolae, D.V.; Jordaan, J.A.; Jimoh, A.A. Distribution Feeder Phase Balancing Using Newton-Raphson Algorithm-Based Controlled Active Filter. In Proceedings of the International Conference on Neural Information Processing, Kitakyushu, Japan, 13–16 November 2007; Springer: Berlin/Heidelberg, Germany; pp. 713–720.
32. Zheng, Y.; Zou, L.; He, J.; Su, Y.; Feng, Z. Fast Unbalanced Three-phase Adjustment based on Single-phase Load Switching. *Telekomnika Indones. J. Electr. Eng.* **2013**, *11*, 4327–4334.
33. Novatek-Electro. Available online: <https://novatek-electro.com/en/products/phase-selector-switch/universal-automatic-electronic-phase-switch-pef-301.html> (accessed on 1 February 2020).
34. Henderieckx, H. Smart Metering Device with Phase Selector. Available online: <https://patents.google.com/patent/US20120078428A1/en> (accessed on 1 February 2020).
35. Grigoras, G. *Impact of Smart Meter Implementation on Saving Electricity in Distribution Networks in Romania. Chapter in Book: Application of Smart Grid Technologies Case Studies in Saving Electricity in Different Parts of the World*; Academic Press: London, UK, 2018; pp. 313–346.
36. Grigoras, G.; Neagu, B.-C. Smart Meter Data-Based Three-Stage Algorithm to Calculate Power and Energy Losses in Low Voltage Distribution Networks. *Energies* **2019**, *12*, 3008. [CrossRef]
37. Pillary, P.; Manyage, M. Definitions of voltage unbalance. *IEEE Power Eng. Rev.* **2001**, *21*, 50–51. [CrossRef]
38. Romanian Energy Regulatory Authority. Report on the Performance Indicators for Electric Transmission, System and Distribution Services and the Technical State of Electric Transmission and Distribution Networks in 2018 (in Romanian), Romania. 2019. Available online: <https://www.anre.ro/ro/energie-electrica/rapoarte/rapoarte-indicatori-performanta> (accessed on 1 February 2020).
39. Baričević, T.; Skok, M.; Majstrović, G.; Perić, K.; Brajković, J. South East European Distribution System Operators Benchmarking Study. Available online: <https://www.usea.org/sites/default/files/SEE%20DSO%20Benchmarking%20Study%202008%20-%202015%20-%20final.pdf> (accessed on 1 February 2020).
40. Romanian Energy Regulatory Authority. Normative for the Design of the Electrical Networks of Public Distribution-PE 132/2003. 2003. Available online: <https://www.anre.ro/ro/legislatie/norme-tehnice/normative-tehnice-energetice-nte> (accessed on 1 February 2020).

41. Han, S.; Kodaira, D.; Han, S.; Kwon, B.; Hasegawa, Y.; Aki, H. An Automated Impedance Estimation Method in Low-Voltage Distribution Network for Coordinated Voltage Regulation. *IEEE Trans. Smart Grid* **2016**, *7*, 1012–1020. [[CrossRef](#)]
42. Zhu, J.; Chow, M.Y.; Zhang, F. Phase Balancing using Mixed-Integer Programming. *IEEE Trans. Power Syst.* **1998**, *13*, 1487–1492.



© 2020 by the authors. Licensee MDPI, Basel, Switzerland. This article is an open access article distributed under the terms and conditions of the Creative Commons Attribution (CC BY) license (<http://creativecommons.org/licenses/by/4.0/>).



## Passive anti-Islanding protection for Three-Phase Grid-Connected photovoltaic power systems

Ioan Viorel Banu<sup>a,b,\*</sup>, Fadila Barkat<sup>c</sup>, Marcel Istrate<sup>b</sup>, Josep M. Guerrero<sup>d</sup>, George Culea<sup>a</sup>, Petru Livinti<sup>a</sup>, Justina G. Motas<sup>b</sup>, Bogdan Neagu<sup>b</sup>, Dragos Andrioaia<sup>a</sup>

<sup>a</sup> The Department of Power Engineering and Computer Science, Faculty of Engineering, "Vasile Alecsandri" University of Bacau, Bacau 600115 Romania

<sup>b</sup> "Gheorghe Asachi" Technical University of Iasi, Iasi 700050 Romania

<sup>c</sup> Semiconductors and Functional Material Laboratory, Faculty of Technology, University of Amar Telidji, Laghouat 03000, Algeria

<sup>d</sup> The Villum Center for Research on Microgrids (CROM), AAU Energy, Aalborg University, 9220 Aalborg East, Denmark

### ARTICLE INFO

#### Keywords:

DC-link voltage  
Distributed energy resources  
Grid-connected PV systems  
Islanding detection  
Solar power generation

### ABSTRACT

This paper presents the performances of a new passive anti-islanding protection with minimal switching losses for three-phase grid-connected photovoltaic power systems. The novelty of the proposed strategy consists of five conventional passive relays, which are as follows: over/under current, over/under voltage, over/under frequency, rate of change of frequency, and dc-link voltage-based anti-islanding methods. Integrating these methods in a synergistic way reduces the limitations of each method, while combining the strengths and benefits of each method in islanding detection. As such, the dc-link voltage-based method consists in supervising the dc-link voltage in voltage source converters to reduce the voltage stress and increase performance. The performance in islanding prevention is determined by the detection time of islanding operation mode. The proposed anti-islanding protection was simulated under complete disconnection of the photovoltaic inverter from the electrical power system, as well as under grid faults as required by new grid codes.

### 1. Introduction

For suitable performance, the grid-connected photovoltaic (PV) power systems designs should consider the behavior of the electrical networks. Because the distributed energy resources (DERs) are increasing, their behavior must become more interactive [1]. The PV inverters design is influenced by the grid requirements, including the anti-islanding requirement which is the most challenging [2,3]. Developing sensitive and reliable anti-islanding prevention methods is vital to support the integration of DERs into the electrical networks and smart grids (SGs) and avoid unnecessary tripping of DERs [3].

Islanding or loss of grid or loss-of-mains [3] happens when a portion of the electric power system (EPS) that contains both loads and DERs remains energized while separated from the rest of the EPS [4]. Also, according to [5], an island is a portion of an EPS area energized just by one or several local DERs via the corresponding point of common coupling (PCC) whereas that portion of an EPS area is separated electrically from the rest of the EPS area [6].

#### 1.1. Motivation and incitement

Islanding for PV systems appears when the utility grid is disconnected and the PV inverter continues to operate with local loads during the utility outage [2,6]. The islanding operation can be unintentional or intentional [5,6,7]. An intentional islanding operation is planned whereas an unintentional islanding operation is unplanned [5]. An unintentional islanding operation can take place when a portion of the EPS area is separated accidentally from the rest of the EPS area and the DERs continue to supply power [5].

The difference between controlled and uncontrolled islanding operation mode must be made. Also, it is necessary to distinguish between short-time islanding operation mode and sustained or long-time islanding operation mode [8]. Islanding operation is desired if the PV distributed power generation systems (DPGSs) are present, and the service of local customers must be provided even without grid connection. Undesired islanding represents a danger to network maintenance personnel [2,8].

According to the grid codes, the DERs are required to quickly detect the unintentional islanding and immediately disconnect the grid in maximum two seconds (s) [2,6,9,10]. This rule should be applied to all

\* Corresponding author.

E-mail addresses: [ionut.banu@ub.ro](mailto:ionut.banu@ub.ro), [ibanu@tuiasi.ro](mailto:ibanu@tuiasi.ro), [ibanu86@yahoo.com](mailto:ibanu86@yahoo.com) (I.V. Banu).

<https://doi.org/10.1016/j.ijepes.2023.108946>

Received 16 July 2022; Received in revised form 27 October 2022; Accepted 3 January 2023

Available online 11 January 2023

0142-0615/© 2023 Elsevier Ltd. All rights reserved.

## Nomenclature

### Abbreviations/Acronyms

ac	Alternating Current
dc	Direct Current
DERs	Distributed Energy Resources
DG	Distributed Generation
DPGSs	Distributed Power Generation Systems
DSO	Distribution System Operator
EPS	Electric Power System
FDZ	Fault Detection Zone
FRT	Fault-Ride Through
LVRT	Low Voltage Ride-Through
MPPT	Maximum Power Point Tracking
NDZ	Non-Detection Zone
OC	Overcurrent Protection
OF	Over Frequency Protection
OUC	Over/Under Current Protection
OUF	Over/Under Frequency Protection
OUV	Over/Under Voltage Protection
OV	Overvoltage Protection
PCC	Point of Common Coupling
PLL	Phase-Locked Loop
PV	Photovoltaic
PWM	Pulse Width Modulation
RMS	Root Mean Square
ROCOF	Rate of Change of Frequency Protection
s	seconds

STCs	Standard Test Conditions
THD	Total Harmonic Distortion
TSO	Transmission System Operator
UC	Undercurrent Protection
UF	Under Frequency Protection
UV	Undervoltage Protection
VSC	Voltage Source Converter

### Variable/Parameter

$f$	Frequency
$f_n$	Grid frequency
$I_a, I_b, I_c$	Normalized three-phase primary grid currents
$P$	Active power
$P_n$	Nominal power
$Q$	Reactive power
$t$	Time
$V$	Voltage
$V_a, V_b, V_c$	Normalized three-phase primary grid voltages
$V_m$	Grid phase voltage amplitude
$L$	Inductor of the LC grid filter
$C_{dc}$	DC-link capacitor (two in series)
$L_1$	Boost inductor
$f_{sw}$	Switching frequency boost converter
$\omega$	Angular frequency
$V_{dc}$	dc-link voltage
$V_{dc,ref}$	Reference dc-link voltage
$V_{nom,dc}$	Nominal dc bus voltage
$V_{dc,m}$	Measured dc-link voltage

DPGSs with PVs [4]. After disconnecting the embedded generator, in some scenarios it can keep supplying the local connected loads or eventually a small part of the power grid determined by grid topology and its capacity [3].

One of the greatest challenging issues of DERs protection is the islanding detection sensitivity, which keeps the system stable to frequency excursions and external faults. To achieve the islanding protection in specific circumstances, i.e., failure to form a stable island, can be enough to use a combination of over/under voltage (OUV) and over/under frequency (OUF) protections [3].

As the PV systems become more competitive, reliable islanding detection becomes of utmost importance. New islanding detection solutions are required since the limitations of the existing techniques can finally put a barrier to the DERs integration into the energy networks [3]. To scale down the cost and to make the PV systems more efficient, the PV inverters must contain effective and reliable anti-islanding algorithms [11].

### 1.2. Literature review

In view of the inverter-resident detection [2,7,12], the anti-islanding techniques can be passive [13], active [14], and hybrid methods [15,16]. The passive methods are based on monitoring the parameters of the electric network which usually changes under islanding operation mode (frequency, phase, amplitude,  $P$ ,  $Q$ , or harmonics). Therefore, the passive islanding methods imply the use of controls or relays to avoid the unintentional islanding [5].

The active methods [15,17], which are not widely utilized in the present because of power quality issues [3], are based on small disturbances in the PCC to produce a detectable change in system parameters by the passive anti-islanding methods [2]. More innovative anti-islanding methods were reported, especially active techniques based on frequency and voltage drift, grid impedance estimation, and phase-locked loop (PLL) [2]. There are also artificial intelligence techniques

like [18,19], and [20], hybrid anti-islanding methods like [15,21], and [22], anti-islanding methods for distributed generations (DGs) [23,24] or anti-islanding methods for PV-based microgrids (MGs) [25,26].

Standard low-cost methods for islanding detection, such as OUV and OUF protection relays protect the consumers equipment and serve as passive inverter-resident anti-islanding methods [27,28]. These methods can be software procedures implemented in the PV inverter. The OUF protection disconnects the grid-connected PV inverters if the frequency at the PCC between the grid and the customer is outside the set boundaries [27]. The OUF thresholds for disconnection of DERs and PV power systems from the grid are defined by the IEEE Std 1547–2003 [6]. The most widely used passive anti-islanding method for DERs is the rate of change of frequency (ROCOF), which is based on the local voltage waveform monitoring of the PV inverters [3].

Reference [29] presents an analysis on several passive anti-islanding protections in various islanding scenarios for PV systems [30], in which it was revealed that the dc-link voltage rises significantly during islanding operation and transient grid faults [29]. The rise detection can be implemented in the PV power inverters controls. Results in an elegant solution for islanding prevention realized in the inverter control by supervising the dc-link voltage. Then, the dc-link voltage-based method is implemented, analyzed, and compared with OUF and ROCOF relays in different islanding scenarios in [30]. The dc-link voltage-based method has also been used in a hybrid anti-islanding detection method to trigger multiple PV inverters in [15].

### 1.3. Contribution and paper organization

The scope of the paper is to improve the anti-islanding protection into the large three-phase grid-connected PV power systems focusing on islanding detection time.

The paper aims to devise, test, and analyze a passive solution of anti-islanding protection strategy for three-phase grid connected PV power systems.

The objective of the paper is to create a new passive anti-islanding strategy for large three-phase grid-connected PV systems.

The previous studies with passive methods in real power grid systems are rare and not sufficient. Therefore, it is necessary strong research to investigate the impact of passive methods when they are applied to large three-phase grid-connected PV systems to give a clear idea for the network problems and to eliminate the islanding situation in the system. And in this time, the given solutions are the passive methods [31,32]. The main drawback of passive methods is large NDZ which results in failure to detect islanding and wrong detection, whereas the disconnection happens basically from their values. The main drawback of active and hybrid filters is disturbing the power quality. A solution to avoid these problems can be to add another kind of anti-islanding detection methods in parallel with them.

Passive methods have certain specifications which are not similar to other kinds of islanding detection methods, like active methods, hybrid filters, artificial intelligence methods, and others. These specifications are why passive methods are always present even if other active methods are used or not. There is the choice to add or remove active methods, but there is no such option for passive methods. The passive methods are always present in any grid-connected system. It is therefore essential and very necessary to carry out in-depth research with passive methods to choose the appropriate or convenient strategy.

This paper presents improvements to previous works [29,30]. The main contribution of this paper compared to [29] and [30] is the introduction of a detailed anti-islanding protection with all studied passive relays which combine the advantages of each method in islanding detection. The results are presented more clearly in parallel for all relays to confirm the performance and efficiency of the proposed method. In [29] and [30] the passive methods are independently studied. The advantage of the proposed strategy with respect to the [29], and [30] is combining the studied passive methods synergistically in a single anti-islanding strategy.

The main contribution and novelty of the proposed anti-islanding strategy consists of combining five well-known passive protection methods to cover most of the islanding detection possibilities. That made it a novel and improved strategy studied under different conditions and scenarios to show its performance and limitations.

Currently, due to the fault ride-through (FRT) requirements of the new grid codes imposed on the anti-islanding methods of the PV power systems, they cannot disconnect from the power grid under certain circumstances because of supportability and stability issues. Therefore, the performance of the proposed anti-islanding protection under FRT operation is considered.

This paper introduces a new passive anti-islanding protection method with reduced voltage stress for three-phase grid-connected PV power systems based on various conventional passive methods from literature. All analyzed methods are individually modeled and validated in the MATLAB and Simulink environment. The focus of the paper is on the performance of the grid-connected PV systems under islanding operation which occurs between the PCC and the rest of the EPS under various grid faults required by current grid codes [10]. The proposed method is justified by the introduction of a simple, reliable, and very fast method for detection of the islanding operating mode of PV systems in a short time and without power quality concerns.

Finally, to justify the efficiency of the suggested method, a 100-kW three-phase grid-connected PV system equipped with different conventional passive anti-islanding methods like over/under current (OUC), OUV, OUF, ROCOF, and dc-link voltage-based method is simulated in different islanding conditions and the reaction times for all these methods are measured through the simulation and compared. The considered scenarios evaluate the performances of the proposed anti-islanding protection for grid-connected PV power systems in case of analysis depending on islanding detection time. The paper shows under which islanding conditions the suggested anti-islanding protection is the most effective, including the FRT requirements. The data/dataset files

related to the paper are available on IEEE DataPort [33].

The main contribution of the paper is analyzing the performances of a passive anti-islanding strategy for PV systems considering islanding detection times and the behavior of frequency, ROCOF, and DC-Link voltage-based method under islanding operation mode. Moreover, the analysis of non-detection zone (NDZ) and fault detection zone (FDZ) and the performance under grid faults and no islanding conditions and FRT operation are also studied. The proposed strategy is tested and analyzed in different conditions and islanding scenarios. The impact of the proposed anti-islanding detection strategy on the power quality in terms of total harmonic distortion (THD) is also given.

The drawbacks and gaps in the literature are the lack of a complete passive anti-islanding strategy with more methods working together. The proposed strategy aims at filling these gaps by combining more passive methods to cover most of the possibilities of developing new passive anti-islanding strategies.

The paper is organized as follows. First Section of the paper reviews various passive anti-islanding methods for DERs and PV systems. The grid-connected PV power system and the suggested passive anti-islanding protection are described in Section 2. Section 3 presents and discusses the results of islanding operation mode detected by the proposed anti-islanding protection with analyzed methods concerning the islanding detection times in each case and scenario. Finally, the conclusions are presented in the last Section of the paper.

## 2. Materials and methods

This section presents the simulation setup which comprises the grid-connected PV power system and its proposed passive anti-islanding protection, including the model parameters and simulation data collection methodology. To replicate the work, the simulation model is available open access at [33].

### 2.1. Grid-Connected PV power system

The detailed Simulink model [33] of the 100-kW three-phase grid-connected PV power system used in the simulations is presented in Fig. 1 [34]. The simulation model was developed based on [35]. The PV system includes the anti-islanding relay protection on the 20 kV bus. The PV solar array, formed by 330 SunPower modules [36] generates in standard test conditions (STCs) of 1000 W/m<sup>2</sup> solar irradiance, 25° solar cell temperature, 1.5 air mass, and ASTM G173-03 standard spectrum of solar insolation a maximum power of 100.7 kW and 273.5 V, while at 250 W/m<sup>2</sup> provides 22.6 kW and 252.4 V [29,30]. The characteristics of PV modules are taken from NREL System Advisor Model [35,36]. Manufacturer specifications for one PV module measured under STCs are given in [29].

The 100-kW PV Array is connected to a standard 20-kV utility grid (20-kV distribution feeder and 110-kV equivalent transmission systems) with the main frequency of 50 Hz through a 100-kVA 260 V/20 kV three-phase coupling transformer via a two-stage PV inverter with a 5 kHz dc-dc step-up (boost) power converter and a 2 kHz three-phase three-level voltage source converter (VSC). The dc-dc step-up converter increases the dc voltage to 500 V from 272 V PV maximum natural voltage. The Maximum Power Point Tracking (MPPT) control system controls the dc-dc boost converter [30] using a variant subsystem, as in [37], with incremental conductance MPPT algorithm, as described in [38] which automatically changes and optimizes the switching duty cycle of the power converter to extract maximum available power and generate the required voltage [29]. The boost converter independently controls the MPPT and the VSC controls the dc-link voltage for the power grid connection [39].

The three-phase PV inverter sets the dc-link voltage at 500 V [35]. The three-phase three-level VSC converter converts from 500 Vdc to 260 Vac while maintaining unity power factor [35]. The VSC filter which contains the 25 μH inductor  $L$  and the 10-kvar capacitor bank  $C$  filters



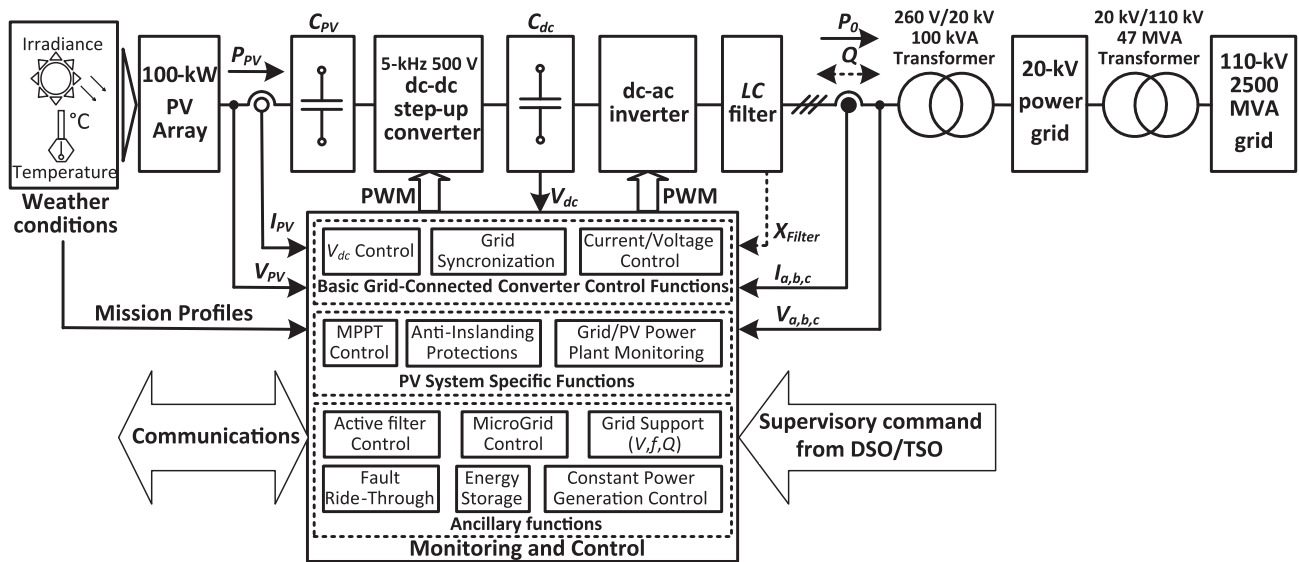


Fig. 1. 100-kW Grid-Connected PV Power System.

the harmonics produced by the PV inverter [29,35]. The system parameters are listed in Table 1 [33,40].

2.2. Proposed passive anti-Islanding protection

The implemented passive anti-islanding protection is given in Fig. 2. The investigated anti-islanding methods are triggered only once during simulation. The trip signals are not connected to the three-phase circuit breaker on the 20 kV side of the PCC of the grid-connected PV system to activate as many as possible relays and compare their islanding detection times.

The conventional over/under current, voltage, frequency, ROCOF, and dc-link voltage-based anti-islanding methods used in the proposed method are presented in the next sections.

2.2.1. Current, Voltage, and frequency relays

The conventional OUC, OUV, and OUF relays for anti-islanding protection of grid-connected PV systems are depicted in Figs. 3 – 5. These relays operate on the same principle by measuring the three-phase current, three-phase voltage, or the system frequency parameters and comparing them with some thresholds. The minimum and maximum current and voltage thresholds blocks in Fig. 3 and Fig. 4 output either the minimum or the maximum elements of the inputs. The models shown in these Figs. work very fast in real-time [29].

The OUF protection continuously checks the frequency in the PV inverter and compares its value with certain default thresholds [29]. The frequency is measured using the PLL [29,30]. The input vector of the discrete three-phase PLL block contains the  $V_a$ ,  $V_b$ , and  $V_c$  normalized three-phase primary grid voltages and the output represents the estimated frequency (Hz)  $f = \omega/(2\pi)$ .

Table 1  
Parameters of the 100-kW double-stage three-phase PV system.

Parameter	Symbol	Value
Nominal power	$P_n$	100 kW
Grid phase voltage amplitude	$V_m$	20 kV
Grid frequency	$f_n$	50 Hz
Inductor of the LC grid filter	$L$	250 $\mu$ H
DC-link capacitor (two in series)	$C_{dc}$	24 mF
Boost inductor	$L_1$	5 mH
Switching frequency boost converter	$f_{sw}$	5 kHz

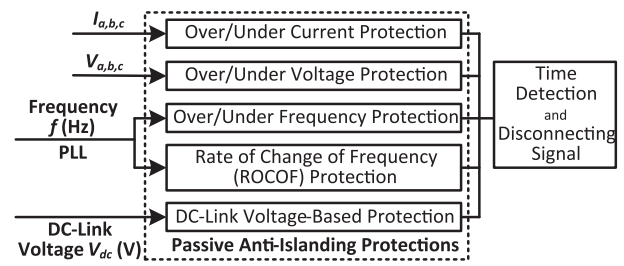


Fig. 2. Suggested Passive anti-Islanding Protection for PV Systems.

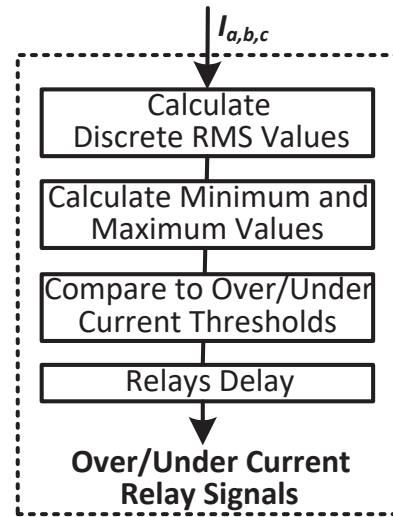


Fig. 3. Over/under current protection.

2.2.2. ROCOF relay

The ROCOF method is presented in Fig. 6. The ROCOF protection from [29] and [41] measures the frequency and terminal voltage parameters in the PV inverter. In this work, the ROCOF protection measures only the frequency parameter of the PV inverter to calculate the discrete derivative ROCOF which is compared with a ROCOF threshold. In this paper, the ROCOF threshold is set at 12 Hz/s. The ROCOF relay is activated when the ROCOF threshold is exceeded and the PV inverter

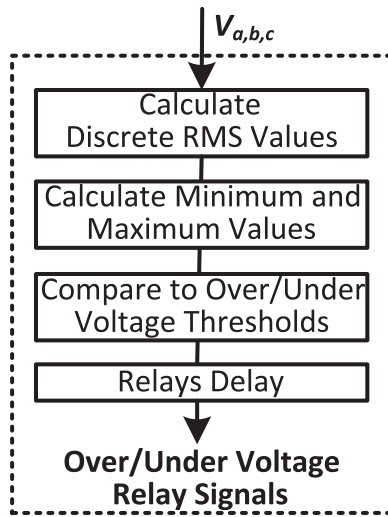


Fig. 4. Over/under voltage protection.

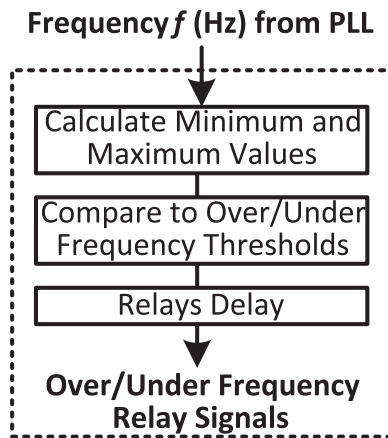


Fig. 5. Over/under frequency protection.

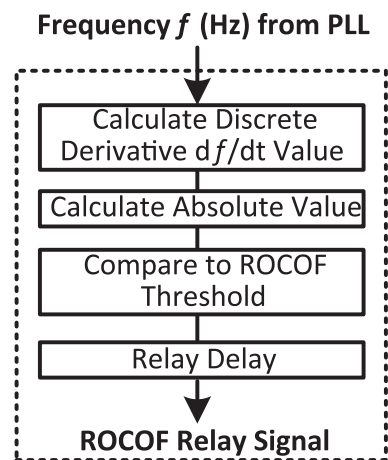


Fig. 6. ROCOF protection.

disconnects the utility grid [30].

### 2.2.3. DC-Link Voltage-Based method

The DC-Link Voltage-Based method consists in supervising the dc-link voltage of the grid converters, which rises significantly during

islanding operation mode [30] and transient grid faults [30,40], as shown in [29]. The rise detection of dc-link voltage can be realized in the main control of the VSC converter of the three-phase PV power inverters [30].

The dc-link voltage-based anti-islanding protection is shown in Fig. 7. The operating principle of the dc-link voltage-based anti-islanding techniques is very simple and easy to implement. The dc-link voltage-based method has a dc-link voltage  $V_{dc}$  input, which is the output voltage of the dc-dc boost converter. If the dc-link voltage trip threshold is exceeded, then the method is activated [30].

The dc-link voltage,  $V_{dc,m}$  is estimated by the VSC main controller of the PV system. The reference dc-link voltage  $V_{dc,ref}$  is set at 500 V, which is the nominal dc bus voltage  $V_{nom,dc}$ . The optimal trip threshold of the dc-link voltage-based method was set at 10 % of normal dc-link voltage  $V_{nom,dc}$  based on experiments and justified by operating with a low dc-link voltage to reduce the power converter switching losses, as stated in [42]. After several simulations, it was observed that the islanding detection time increases in direct proportion to the increasing the dc-link voltage threshold [30].

Other advantages of the protection scheme from Fig. 3 to Fig. 7 are the introduction of operating principles and detailed implementation of these basic passive methods from literature used synergistically in the proposed strategy to facilitate de anti-islanding protection into the PV power system.

The proposed anti-islanding protection is a combination of all previously presented passive anti-islanding relays, where the dc-link voltage-based method detects the islanding mode in all conditions with reduced switch voltage stress and without affecting the electric power quality, as is detailed in the following results in next section.

### 2.3. Data collection methodology

This section presents how the simulation data was generated from the used model to determine the performances of the proposed method under certain islanding conditions.

The 100-kW grid-connected PV system from Fig. 1, equipped with the proposed passive anti-islanding protection was simulated in MATLAB and Simulink environment during 0.4 s at 1000 W/m<sup>2</sup> irradiance level and 25 °C in various islanding scenarios. Dynamic simulation cases involve opening the three-phase circuit breaker (see Fig. 1) on the 110 kV grid side, which led to an islanding condition, and different grid faults (short-circuits) appearing at 5 km away from the PCC of the PV system [34]. The islanding operation mode takes place when the circuit breaker on the 110 kV grid side is opened at the time  $t = 0.1$  s. The circuit breaker disconnects the power grid from the rest of EPS during 150 ms, where the locally produced power was lower than the local

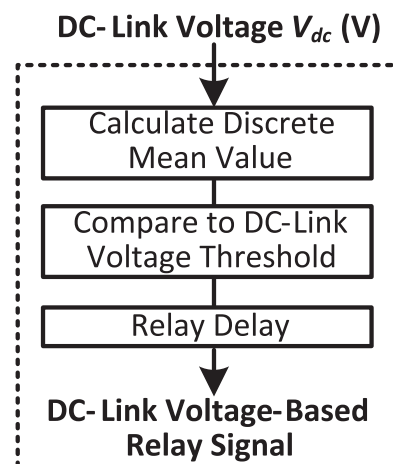


Fig. 7. DC-link voltage-based anti-islanding method.

connected loads.

An encoder was used to measure the trip status and trip time of each relay of the proposed strategy. The obtained results were achieved by recording independently the relays status and time detection of islanding operation for each relay of the proposed passive anti-islanding protection in each studied case (islanding operation, grid faults and no islanding condition, and FRT operation).

The implemented grid-connected PV system and all proposed models are independently validated in MATLAB/Simulink and can be used to verify the results in software based simulations and hardware in the loop simulations.

### 3. Results of islanding operation mode and discussion

The results under these islanding scenarios which includes the performances of the proposed anti-islanding protection under various load scenarios and the detection times of islanding methods are presented and assessed in the following sections. The islanding mode results in perturbations of the currents, voltages, power, and frequency of the electrical network. After the islanding operation mode or three-phase grid faults, the current increases, voltage decreases, and frequency shifts. The islanding detection times of analyzed cases are presented in Fig. 8 and Fig. 11, respectively.

#### 3.1. Studied islanding operation cases

The three studied islanding cases are: (i) the islanding operation mode because of the opening of the three-phase circuit breaker on 110-kV grid side, (ii) grid faults and no islanding condition, and (iii) islanding mode under FRT operation.

##### 3.1.1. Test case 1: Opening the Three-Phase circuit breaker

The detection times of the proposed passive anti-islanding strategy in case 1 are compared next.

3.1.1.1. *Islanding detection times of the proposed strategy.* Fig. 8 depicts graphically the islanding detection times (ms) of all methods discussed in this paper for the test case 1 in all considered scenarios. The performance of the dc-link voltage-based method is emphasized by comparing favorably its islanding detection time with those of all studied methods. As can be noted from Fig. 8, during islanding mode the undervoltage

(UV), overcurrent (OC), dc-link voltage-based, ROCOF, under frequency (UF), and over frequency (OF) protections are activated in the same order in all analyzed scenarios.

Comparing the islanding detection time performance of the analyzed anti-islanding methods, the fastest protection was the undervoltage method. The longest islanding detection time was obtained by the frequency relays. The scenario with the smallest detection times is the local load greater than the local PV power generation (scenario 1). The under-frequency protection is activated only in this scenario. The over-frequency protection is activated in scenarios 1 and 2. The OUF protection has the preset thresholds limits imposed by the grid codes, resulting in late detection of the islanding operation mode of PV systems. The overvoltage protections did not detect the islanding operation mode in this islanding case.

3.1.1.2. *Behavior of frequency and ROCOF under islanding.* Fig. 9 depicts the frequency and ROCOF ( $df/dt$ ) variations during islanding operation mode of the grid-connected PV system [30]. From Fig. 9 it can be observed the effect of islanding mode on the frequency of PV systems. During islanding operation mode, the frequency decreases quickly. Fast change in frequency involves a noticeable variation of ROCOF [30]. As can be seen from Fig. 9, the optimal value of the ROCOF threshold limit which is exceeded after the islanding mode is 12 Hz/s [29]. The minus sign indicates a decrease in grid frequency [30].

3.1.1.3. *Behavior of DC-Link voltage under islanding.* A direct comparison between the dc-link voltage and frequency for resistive loads is illustrated in Fig. 10 [30]. The dc-link voltage variation is detected faster than frequency variation due to the fact that it has a larger slope and range during islanding operation [30].

3.1.1.4. *Performance of DC-Link Voltage-Based method during islanding scenarios.* As shown in Fig. 10, the dc-voltage rises significantly in islanding operation mode without dc-link voltage-based protection in all three scenarios and implicitly the power losses on the switching devices of the PV inverter are significantly increased [43]. Thus, with dc-link voltage-based anti-islanding method activated in 14.6 – 23.2 ms, as shown in Fig. 8, the overall reliability of the PV power system is improved [43] by dc voltage level limitation to keep the switching losses down [42], which results in a lower mean junction temperature [43] and operating with the reference for the controlled dc-link voltage at 10 %

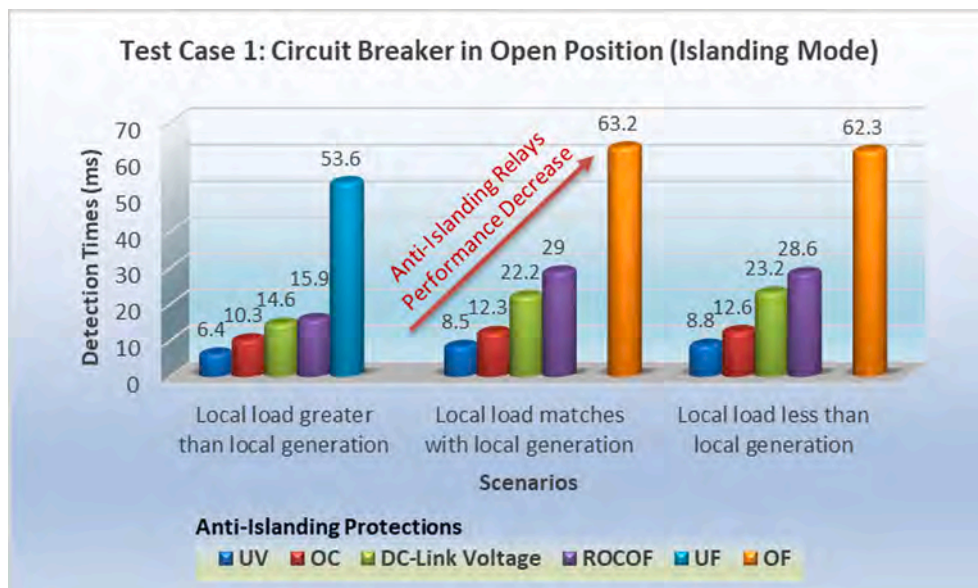


Fig. 8. Detection times of the analyzed anti-islanding methods in case study 1.

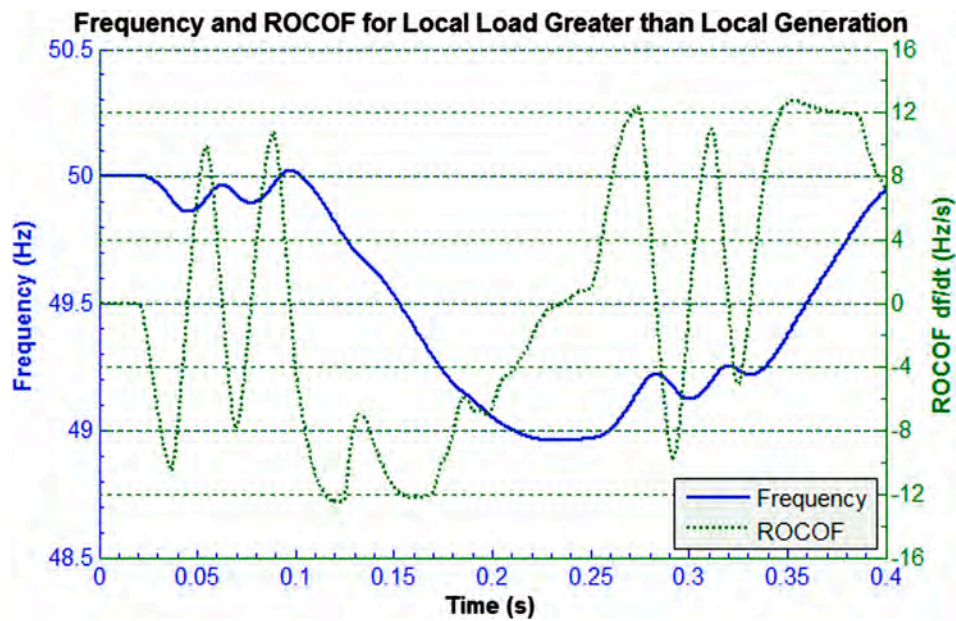


Fig. 9. Frequency and its ROCOF in PCC during islanding mode [30].

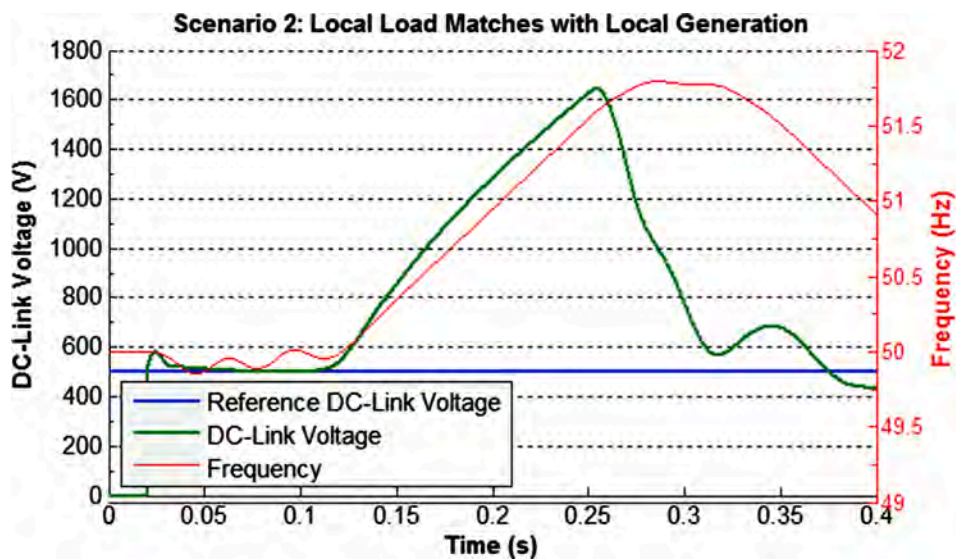


Fig. 10. DC-Link Voltage and frequency variations [30].

higher than the natural dc-link voltage [42] (which means that the dc-link voltage threshold is equal to 550 Vdc).

Fig. 9 and Fig. 10 provide with respect to the anti-islanding protection the information concerning the effect of islanding mode on the behavior of frequency, ROCOF and DC-Link voltage-based methods, and respectively the effect of islanding mode on the variation given by the studied methods to know if the passive methods can detect these changes in terms of islanding detection time. As can be noted from those figures, it can be concluded that the studied methods perform very well under islanding mode.

3.1.2. Test case 2: Performances under grid faults (No Islanding)

This test case presents the performance of the proposed anti-islanding protection under grid faults with no islanding scenario.

A number of grid faults such as three-phase-to-ground faults, phase-to-phase and phase-to-phase-to-ground faults, and single-phase-to-ground faults lasting for 150 ms have been simulated in the 20-kV power grid of the PV system at 5 km away from the PCC at the time

(t) = 0.1 s [40,34]. The results are depicted in Fig. 11. During grid faults and no islanding scenario more anti-islanding relays detect an abnormal situation, as shown in Fig. 11.

3.1.3. Test case 3: Islanding detection times during grid faults (FRT Operation)

This islanding test case presents the performance of the proposed anti-islanding protection under FRT operation. Therefore, in this test case the three-phase circuit breaker on the 110 kV grid side is simulated in an open position with grid faults.

The comparison of islanding detection times in test case 3 under islanding operation and different short-circuit grid faults are depicted in Fig. 12. The best performances have also been obtained by the overcurrent and undervoltage protections, as observed in the first test case. The overvoltage protection is activated in phase-to-phase-to-ground and three-phase-to-ground faults scenarios. The longest detection time was obtained by the under frequency relay. The undercurrent (UC) and OF protection did not detect the islanding mode in FRT operation.

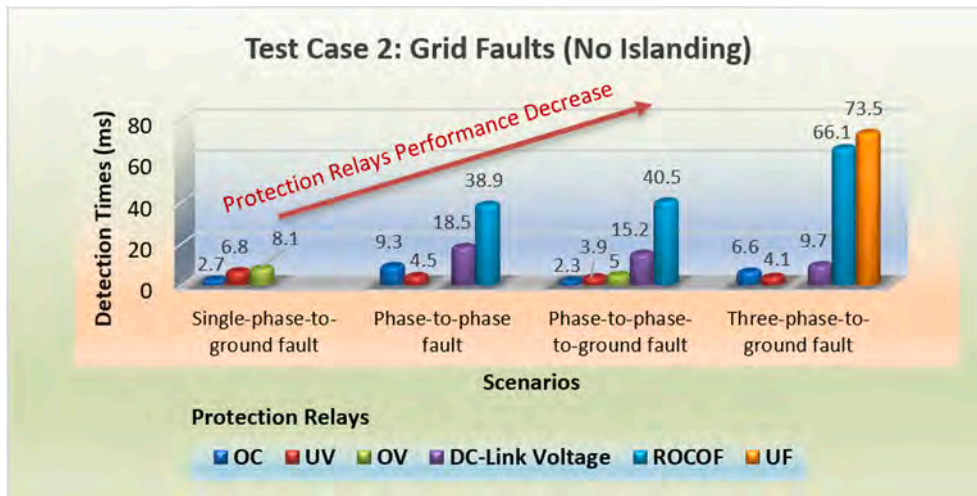


Fig. 11. Detection times under different grid faults (no islanding).

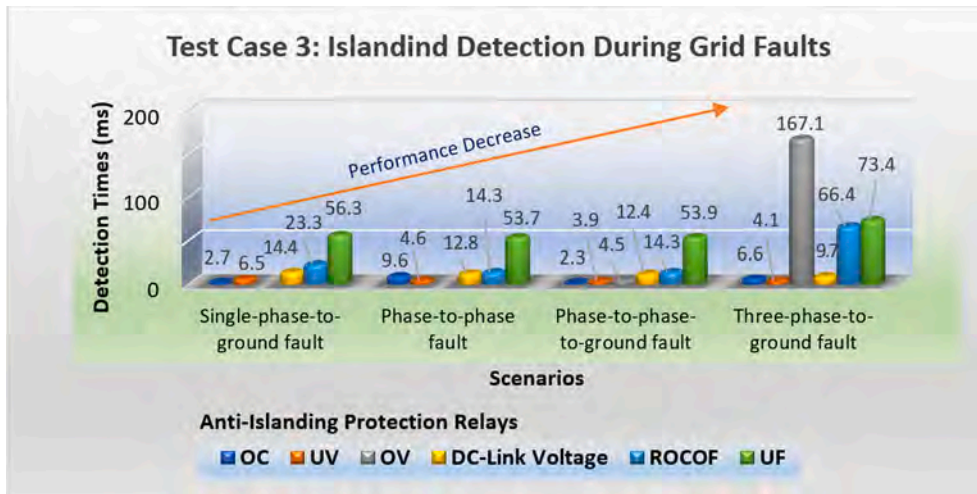


Fig. 12. Islanding detection times in case study 3 (islanding mode under different grid faults).

The dc-link voltage-based method under FRT operation has good islanding detection times (better than ROCOF and under frequency methods) and limits the dc-link voltage of the PV inverter to a safe level during grid faults through its islanding detection and disconnecting the PV inverter from the grid. The performance of the ROCOF method under three-phase faults is like the under frequency method.

Due to the fact that the simulation results under grid faults with and no islanding operation are very close, the PV inverters should incorporate a fast grid fault detection (i.e., monitoring system) to improve the islanding detection and performance of the entire system under FRT.

**3.1.3.1. Performance of proposed protection during islanding and FRT operations.** For proper and successful operation of the proposed anti-islanding protection and to not disconnect the PV inverter during FRT, it should have the following settings according to the islanding detection times in Fig. 8 and Fig. 11.

- 1) OC: 10.3 – 12.6 ms/2.7 – 9.6 ms (islanding detection/FRT) and 2.3 – 9.3 ms (grid fault)
- 2) UC: no islanding detection time
- 3) UV: 6.4 – 8.8 ms/3.9 – 6.5 ms (islanding detection/FRT) and 4.1 – 6.8 ms (grid fault)
- 4) OV: 15.9 – 29 ms/4.5 – 167.1 ms (islanding detection/FRT) and 5 – 8.1 ms (grid fault)

- 5) DC-Link: 14.6 – 23.2 ms/9.7 – 14.4 ms (islanding detection/FRT) and 9.7 – 18.5 ms (grid fault)
- 6) ROCOF: 15.9 – 29 ms/14.3 – 66.4 ms (islanding detection/FRT) and 38.9 – 66.1 ms (grid fault)
- 7) UF: 53.6 ms/53.7 – 73.4 ms (islanding detection/FRT) and 73.5 ms (grid fault)
- 8) OF: 63.2 ms (islanding detection)

When the detection times are higher than the specified ones defined in Fig. 11, the PV inverter should not disconnect to the utility grid and inject reactive power to support the grid during FRT and low voltage ride-through (LVRT) [44].

The proposed passive anti-islanding protection identifies and distinguishes between islanding operation mode and grid faults, like short-circuits depending on the detection time of the events. To minimize the unintentional islanding operation mode and grid fault effects and to meet the grid codes requirements, the anti-islanding protections must be installed at points where islanding operating mode can occur. Therefore, the obtained results are useful for selecting these points and designing the anti-islanding protection devices for three-phase grid-connected PV systems.

### 3.2. Discussion of obtained results and main achievements

Overall, the suggested passive anti-islanding protection confirmed its performance and functionality under islanding operating mode and FRT operation. As for the dc-link voltage-based relay, it is suitable for anti-islanding protection of PV power systems and can be used instead of ROCOF and frequency relays or in combination with active methods like in [15] since it has small detection time and low switch voltage stress, is effective in islanding detection, and easy to implement.

The proposed protection has good and acceptable THD in terms of their impacts on the power quality [14,45].

#### 3.2.1. Comparison with other reported anti-islanding methods

The proposed strategy has fast islanding detection times in comparison with other simple passive [29,41] and active methods [46,47], or hybrid strategies [19,48]. The suggested method also results in low switching losses in power converters for PV systems [49].

The proposed anti-islanding strategy results in a small NDZ and FDZ compared with other reported strategies [15,25].

The proposed anti-islanding protection has a low computational burden and operation time [22] compared with other passive [50] and intelligent methods [51].

## 4. Conclusions

In this paper, a novel passive anti-islanding protection with reduced switching losses for double-stage three-phase grid-connected photovoltaic power systems was introduced. The islanding detection time of the proposed method is compared in various cases and scenarios, including under fault ride-through operation case.

The investigation revealed that using the suggested protection results in significantly better performance in terms of islanding detection times. Additionally, the proposed anti-islanding protection can detect the islanding mode during grid faults. The proposed anti-islanding protection makes the difference between islanding operation mode and fault ride-through operation required by new grid codes depending on the detection time of the abnormal event. The proposed anti-islanding protection can increase the resilience of the electric grid and power system resilience, as it can operate in both the islanding mode and the fault ride-through mode.

It can be concluded that the proposed anti-islanding protection can be suitable for islanding detection of photovoltaic systems under different scenarios since it has small detection time and reduced voltage stress, is effective, and easy to implement.

### CRedit authorship contribution statement

**Ioan Viorel Banu:** Conceptualization, Methodology, Software, Writing – original draft, Visualization, Investigation, Writing – review & editing. **Fadila Barkat:** Writing – review & editing, Validation. **Marcel Istrate:** Supervision, Project administration, Resources, Writing – original draft, Writing – review & editing. **Josep M. Guerrero:** Supervision, Funding acquisition, Writing – review & editing. **George Culea:** Formal analysis, Writing – review & editing, Software, Validation, Data curation. **Petru Livinti:** Formal analysis, Writing – review & editing. **Justina G. Motas:** Writing – review & editing. **Bogdan Neagu:** Writing – review & editing, Validation. **Dragos Andrioaia:** Software, Validation, Data curation, Writing – review & editing.

### Declaration of Competing Interest

The authors declare that they have no known competing financial interests or personal relationships that could have appeared to influence the work reported in this paper.

### Data availability

Data will be made available on request.

### Acknowledgements

This work was supported by VILLUM FONDEN under the VILLUM Investigator Grant (no. 25920): Center for Research on Microgrids (CROM); [www.crom.et.aau.dk](http://www.crom.et.aau.dk).





### References

- [1] Rekioua D, Matagne E. Optimization of photovoltaic power systems, modelization. Simulation and Control Springer 2012. <https://doi.org/10.1007/978-1-4471-2403-0>.
- [2] Teodorescu R, Liserre M, Rodríguez P. Grid converters for photovoltaic and wind power systems. John Wiley & Sons Ltd 2011. <https://doi.org/10.1002/9780470667057>.
- [3] CIGRE Working Group B5.34, "The Impact of Renewable Energy Sources and Distributed Generation on Substation Protection and Automation," CIGRE, Aug. 2010.
- [4] IEEE Std 929-2000, IEEE recommended practice for utility interface of photovoltaic (PV) systems, IEEE, 2000, doi: [10.1109/IEEESTD.2000.91304](https://doi.org/10.1109/IEEESTD.2000.91304).
- [5] IEEE Std 1547.2-2008, IEEE Application Guide for IEEE Std 1547™, IEEE Standard for Interconnecting Distributed Resources with Electric Power Systems, IEEE, 2008, doi: [10.1109/IEEESTD.2008.4816078](https://doi.org/10.1109/IEEESTD.2008.4816078).
- [6] IEEE Std 1547-2003, Standard for Interconnecting Distributed Resources with Electric Power Systems, IEEE, 2003, doi: [10.1109/IEEESTD.2003.94285](https://doi.org/10.1109/IEEESTD.2003.94285).
- [7] M, Ciobotaru, V, Agelidis, R, Teodorescu, "Accurate and less-disturbing active anti-islanding method based on PLL for grid-connected PV Inverters," in 2008 IEEE Power Electron. Specialists Conf., Rhodes, Greece, 2008, pp. 4569-4576, doi: [10.1109/PESC.2008.4592685](https://doi.org/10.1109/PESC.2008.4592685).
- [8] Bollen M, Hassan F. Integration of distributed generation in the power system. Wiley-IEEE Press 2011. <https://doi.org/10.1002/9781118029039>.
- [9] IEEE Std 1547.1-2005, IEEE standard conformance test procedures for equipment interconnecting distributed resources with electric power systems," IEEE, 2005, DOI: [10.1109/IEEESTD.2005.96289](https://doi.org/10.1109/IEEESTD.2005.96289).
- [10] Standard Conformance Test Procedures for Equipment Interconnecting Distributed Energy Resources with Electric Power Systems and Associated Interfaces, IEEE 1547.1-2020, 2020, doi: [10.1109/IEEESTD.2020.9097534](https://doi.org/10.1109/IEEESTD.2020.9097534).
- [11] Pyps IEA. Utility aspects of grid connected photovoltaic power systems. Report IEA PVPS 1998;T5-01:1998.
- [12] Edhura KN, Ahmad K, Selvaraj J, Rahim NA. "A review of the islanding detection methods in grid-connected PV inverters." *Renewable and Sustainable Energy Reviews* 2013;21:756-66. <https://doi.org/10.1016/j.rser.2013.01.018>.
- [13] De Mango F, Liserre M, Dell'Aquila A, Pigazo A. Overview of anti-islanding algorithms for PV systems. Part I: passive methods. In: in 2006 12<sup>th</sup> Int. Power Electron. and Motion Control Conf; 2006. p. 1878-83. <https://doi.org/10.1109/EPEPEMC.2006.4778679>.
- [14] De Mango F, Liserre M, Dell'Aquila A. Overview of anti-islanding algorithms for PV systems. Part II: active methods. In: in 2006 12<sup>th</sup> Int. Power Electron. and Motion Control Conf; 2006. p. 1884-9. <https://doi.org/10.1109/EPEPEMC.2006.4778680>.
- [15] F, Barkat, A, Cheknane, J. M, Guerrero, A, Lashab, M, Istrate, I. V, Banu, "Hybrid islanding detection technique for single-phase grid-connected photovoltaic multi-inverter systems," *IET Renew. Power Gener.*, vol. 14, no. 18, pp. 3864-3880, ISSN 1752-1416, 20 Jan. 2021, doi: [10.1049/iet-rpg.2019.1183](https://doi.org/10.1049/iet-rpg.2019.1183).
- [16] Pal D, Panigrahi BK. Small signal stability analysis oriented design of hybrid anti-islanding protection technique based on active disturbance injection. *IEEE Syst J* March 2022;16(1):1448-59. <https://doi.org/10.1109/JSYST.2021.3050468>.
- [17] Shamsheh MB, Inzunza R, Ambo T. A novel islanding detection technique based on positive-feedback negative sequence current injection. *IEEE Trans Power Electron* July 2022;37(7):8611-24. <https://doi.org/10.1109/TPEL.2022.3146342>.
- [18] Khamis A, Shareef H, Mohamed A, Bizkevelci E. Islanding detection in a distributed generation integrated power system using phase space technique and probabilistic neural network. *Neurocomputing* 2015;148:587-99. <https://doi.org/10.1016/j.neucom.2014.07.004>.
- [19] Kong X, Xu X, Yan Z, Chen S, Yang H, Han D. Deep learning hybrid method for islanding detection in distributed generation. *Appl Energy* 2018;210:776-85. <https://doi.org/10.1016/j.apenergy.2017.08.014>.
- [20] Ahmadipour M, Hizam H, Othman ML, Radzi MAM, Murthy AS. Islanding detection technique using Slantlet Transform and Ridgelet Probabilistic Neural Network in grid-connected photovoltaic system. *Appl Energy* 2018;231:645-59. <https://doi.org/10.1016/j.apenergy.2018.09.145>.
- [21] Mlakić D, Baghaee HR, Nikolovski S. Gibbs phenomenon-based hybrid islanding detection strategy for VSC-Based Microgrids Using Frequency Shift,  $THD_U$ , and  $RMS_U$ . *IEEE Trans Smart Grid* 2019;10(5):5479-91. <https://doi.org/10.1109/TSG.2018.2883595>.
- [22] Mlakić D, Baghaee HR, Nikolovski S. A novel ANFIS-based islanding detection for inverter-interfaced microgrids. *IEEE Trans Smart Grid* 2019;10(4):4411-24. <https://doi.org/10.1109/TSG.2018.2859360>.

- [23] Nikolovski S, Baghaee HR, Mlakić D. Islanding detection of synchronous generator-based DGs using Rate of Change of Reactive Power. *IEEE Syst J* 2019;13(4): 4344–54. <https://doi.org/10.1109/JSYST.2018.2889981>.
- [24] Marchesan G, Maresch K, Cardoso G, de Moraes AP, Muraro MR. Distributed Synchronous generation ride-through enhancement by anti-islanding protection blocking. *Electr Power Syst Res* 2021;196:107232. <https://doi.org/10.1016/j.epsr.2021.107232>.
- [25] Baghaee HR, Mlakić D, Nikolovski S, Dragičević T. Anti-Islanding Protection of PV-Based Microgrids Consisting of PHEVs Using SVMs. *IEEE Trans Smart Grid* 2020;11(1):483–500. <https://doi.org/10.1109/TSG.2019.2924290>.
- [26] Bakhshi-Jafarabadi R, Sadeh J. New voltage feedback-based islanding detection method for grid-connected photovoltaic systems of microgrid with zero non-detection zone. *IET Renew Power Gener* 2020;14(10):1710–9. <https://doi.org/10.1049/iet-rpg.2019.1174>.
- [27] Pvpis IEA. Evaluation of islanding detection methods for photovoltaic utility-interactive power systems. Task V, Report IEA-PVPS March 2002;T5–09:2002.
- [28] Y, Zhihong, A, Kolwalkar, Y, Zhang, D, Pengwei, R, Walling, “Evaluation of anti-islanding schemes based on nondetection zone concept,” *IEEE Trans. Power Electron.*, vol. 19, no. 5, pp. 1171–1176, Sept. 2004, doi: [10.1109/TEPEL.2004.833436](https://doi.org/10.1109/TEPEL.2004.833436).
- [29] I. V, Banu, M, Istrate, D, Machidon, R, Pantelimon, “A study on anti-islanding detection algorithms for grid-tied photovoltaic systems,” in *Int. Conf. Optimization Elect. and Electron. Equipment (OPTIM)*, IEEE, pp. 655–660, Bran, Romania, 2014. doi: [10.1109/OPTIM.2014.6850940](https://doi.org/10.1109/OPTIM.2014.6850940).
- [30] I. V, Banu, M, Istrate, “Islanding prevention scheme for grid-connected photovoltaic systems in Matlab/ Simulink,” in *49th Int. Universities’ Power Eng. Conf. (UPEC)*, IEEE, Cluj-Napoca, Romania, pp. 1-6, 2-5 Sept. 2014. doi: [10.1109/UPEC.2014.6934698](https://doi.org/10.1109/UPEC.2014.6934698).
- [31] Nale R, Biswal M, Kishor N. A passive communication based islanding detection technique for AC microgrid. *Int J Electr Power Energy Syst* 2022;137:107657. <https://doi.org/10.1016/j.ijepes.2021.107657>.
- [32] Song G, Cao B, Chang L. “A passive islanding detection method for distribution power systems with multiple inverters”, *IEEE J Emerg Sel Top Power Electron* Oct. 2022;10(5):5727–37. <https://doi.org/10.1109/JESTPE.2022.3165631>.
- [33] I. V, Banu, M, Istrate, April 4, 2021, “Passive Anti-Islanding Protection for Three-Phase Grid-Connected Photovoltaic Systems”, IEEE Dataport, doi: <https://dx.doi.org/10.21227/Op56-1844>.
- [34] I. V, Banu, “Research on Integration of Photovoltaic Sources into the Power Grid,” Ph.D. dissertation (in Romanian), Faculty Elect. Eng., Tech. Univ. Iasi, Iasi, Romania, 2015. doi: [10.13140/RG.2.1.2742.7041/1](https://doi.org/10.13140/RG.2.1.2742.7041/1). (Supervisor: M. Istrate).
- [35] The MathWorks Inc. *Detailed Model of a 100-kW Grid-Connected PV Array* [Online]. Available: <https://www.mathworks.com/help/physmod/sps/examples/detailed-model-of-a-100-kw-grid-connected-pv-array.html>. [Accessed 11 March 2021].
- [36] <https://sam.nrel.gov/> - NREL System Advisor Model.
- [37] Banu IV, Beniugă R, Istrate M. Comparative analysis of the perturb-and-observe and incremental conductance MPPT methods. In: in 2013 *8th Int. Symp. Advanced Topics in Elect. Eng.* Bucharest, Romania: (ATEE), IEEE; 2013. p. 1–4. <https://doi.org/10.1109/ATEE.2013.6563483>.
- [38] I. V, Banu, M, Istrate, “Modeling of maximum power point tracking algorithm for PV systems,” in 2012 *Int. Conf. and Exp. Elect. and Power Eng. (EPE)*, IEEE, Iasi, Romania, pp. 953–957, 25–27 Oct. 2012. doi: [10.1109/ICEPE.2012.6463577](https://doi.org/10.1109/ICEPE.2012.6463577).
- [39] Reddy KN, Agarwal V. Utility-interactive hybrid distributed generation scheme with compensation feature. *IEEE Trans Energy Convers* 2007;22(3):666–73. <https://doi.org/10.1109/TEC.2006.878247>.
- [40] I. V, Banu, M, Istrate, “Study on Three-Phase Photovoltaic Systems under Grid Faults,” in 2014 *Int. Conf. and Expo. Elect. and Power Eng. (EPE)*, IEEE, pp. 1132–1137, Iasi, Romania, 16–18 Oct. 2014. doi: [10.1109/ICEPE.2014.6970086](https://doi.org/10.1109/ICEPE.2014.6970086).
- [41] Samaroo KO. Methodology of selection, setting and analysis of anti-islanding protection for distribution generation system. Department of Electrical Engineering: University of Guyana; 2012.
- [42] Liserre M, Blaabjerg F, Dell’Aquila A. Step-by-step design procedure for a grid-connected three-phase PWM voltage source converter. *Int J Electron* 2004;91(8): 445–60. <https://doi.org/10.1080/00207210412331306186>.
- [43] Yang Y, Enjeti P, Blaabjerg F, Wang H. Wide-scale adoption of photovoltaic energy: grid code modifications are explored in the distribution grid. *IEEE Ind Appl Mag* Sept.-Oct. 2015;21(5):21–31. <https://doi.org/10.1109/MIAS.2014.2345837>.
- [44] Talha M, Raihan SRS, Rahim NA. A Grid-tied PV Inverter with sag-severity-independent low-voltage ride through, reactive power support, and islanding protection. *J Mod Power Syst Clean Energy* Nov. 2021;9(6):1300–11. <https://doi.org/10.35833/MPCE.2021.000319>.
- [45] Bakhshi-Jafarabadi R, Ghazi R, Sadeh J. Power quality assessment of voltage positive feedback based islanding detection algorithm. *J Modern Power Systems Clean Energy* July 2020;8(4):787–95. <https://doi.org/10.35833/MPCE.2018.000509>.
- [46] Ropp ME, Begovic M, Rohatgi A. Analysis and performance assessment of the active frequency drift method of islanding prevention. *IEEE Trans Energy Convers* Sept. 1999;14(3):810–6. <https://doi.org/10.1109/60.790956>.
- [47] Lopes LAC, Sun H. Performance assessment of active frequency drifting islanding detection methods. *IEEE Trans Energy Convers* March 2006;21(1):171–80. <https://doi.org/10.1109/TEC.2005.859981>.
- [48] Seyedi M, Taher SA, Ganji B, Guerrero JM. A hybrid islanding detection method based on the rates of changes in voltage and active power for the multi-inverter systems. *IEEE Trans Smart Grid* July 2021;12(4):2800–11. <https://doi.org/10.1109/TSG.2021.3061567>.
- [49] Priyadarshi N, Padmanaban S, Kiran Maroti P, Sharma A. An Extensive Practical Investigation of FPM-based MPPT for Grid Integrated PV system under variable operating conditions with anti-islanding protection. *IEEE Syst J* June 2019;13(2): 1861–71. <https://doi.org/10.1109/JSYST.2018.2817584>.
- [50] Reddy VR, Sreeraj ES. A feedback-based passive islanding detection technique for one-cycle-controlled single-phase inverter used in photovoltaic systems. *IEEE Trans Ind Electron* 2020;67(8):6541–9. <https://doi.org/10.1109/TIE.2019.2938464>.
- [51] Kim MS, Haider R, Cho GJ, Kim CH, Won CY, Chai JS. Comprehensive review of islanding detection methods for distributed generation systems. *Energies* Mar. 2019;12(5):837. <https://doi.org/10.3390/en12050837>.

## Article

# Contributions to Power Grid System Analysis Based on Clustering Techniques

Gheorghe Grigoraş<sup>1,\*</sup>, Maria Simona Raboaca<sup>2,3,4</sup> , Catalin Dumitrescu<sup>5,\*</sup> , Daniela Lucia Manea<sup>6</sup>,  
Traian Candin Mihaltan<sup>7</sup>, Violeta-Carolina Niculescu<sup>2,\*</sup> , and Bogdan Constantin Neagu<sup>1,\*</sup> 

- <sup>1</sup> Department of Power Engineering, “Gheorghe Asachi” Technical University of Iasi, 700050 Iasi, Romania
  - <sup>2</sup> National Research and Development Institute for Cryogenic and Isotopic Technologies—ICSI Rm. Vâlcea, Uzinei Street, No. 4, P.O. Box 7 Râureni, 240050 Ramnicu Valcea, Romania
  - <sup>3</sup> Faculty of Electrical Engineering and Computer Science, Stefan cel Mare University of Suceava, 720229 Suceava, Romania
  - <sup>4</sup> Doctoral School Polytechnic, University of Bucharest, 060042 Bucharest, Romania
  - <sup>5</sup> Department Telematics and Electronics for Transports, University “Politehnica” of Bucharest, 060042 Bucharest, Romania
  - <sup>6</sup> Faculty of Civil Engineering, Technical University of Cluj-Napoca, Constantin Daicoviciu Street, No. 15, 400020 Cluj-Napoca, Romania
  - <sup>7</sup> Faculty of Building Services Engineering, Technical University of Cluj—Napoca, Bd. 21 Decembrie 1989, No. 128-130, 400604 Cluj-Napoca, Romania
- \* Correspondence: ggrigor@ee.tuiasi.ro (G.G.); catalin.dumitrescu@upb.ro (C.D.); violeta.niculescu@icsi.ro (V.-C.N.); bogdan.neagu@tuiasi.ro (B.C.N.)

**Abstract:** The topic addressed in this article is part of the current concerns of modernizing power systems by promoting and implementing the concept of smart grid(s). The concepts of smart metering, a smart home, and an electric car are developing simultaneously with the idea of a smart city by developing high-performance electrical equipment and systems, telecommunications technologies, and computing and infrastructure based on artificial intelligence algorithms. The article presents contributions regarding the modeling of consumer classification and load profiling in electrical power networks and the efficiency of clustering techniques in their profiling as well as the simulation of the load of medium-voltage/low-voltage network distribution transformers to electricity meters.

**Keywords:** smart grid; clustering techniques; pattern clustering; power distribution planning; regression algorithms



**Citation:** Grigoraş, G.; Raboaca, M.S.; Dumitrescu, C.; Manea, D.L.; Mihaltan, T.C.; Niculescu, V.-C.; Neagu, B.C. Contributions to Power Grid System Analysis Based on Clustering Techniques. *Sensors* **2023**, *23*, 1895. <https://doi.org/10.3390/s23041895>

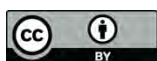
Academic Editors: Ching-Hung Lee and Lian-Wang Lee

Received: 17 December 2022

Revised: 4 February 2023

Accepted: 4 February 2023

Published: 8 February 2023



**Copyright:** © 2023 by the authors. Licensee MDPI, Basel, Switzerland. This article is an open access article distributed under the terms and conditions of the Creative Commons Attribution (CC BY) license (<https://creativecommons.org/licenses/by/4.0/>).

## 1. Introduction

A few of the changes and problems the world’s population is currently facing are related to the climate, electricity, food, water, transport, utilities, health, education, administration, and industry. Cities use 75% of the energy produced and are answerable for 80% of all dioxide emissions, although they only cover 2% of the planet’s surface. Future cities will need to adapt in order to counteract the effects of factors such as environmental change, population expansion, and social mobility, together with migration, human conflicts and unfairness, economic globalization, technological advancements, food, water, and energy vulnerability, geostrategic shifts, etc. Future cities must manage infrastructure and resources more intelligently to meet people’s needs both now and, in the future, as the world becomes increasingly “urban” [1,2].

Mobility is at the core of modern society when the aforementioned factors are considered. Over the next 20 years, there will be a lot of changes in this area as global auto markets and the transportation industry are reshaped by electrification, shared mobility, vehicle networking, and autonomous vehicles. This transformation is supported by technological advancement and other crucial variables, such as legislative directives pointing these two sectors in the direction of low-carbon solutions and increased fuel efficiency [3–6].



In the medium and long term, automakers and major EV operators are ensuring that the decarbonization goals are treated to a higher standard. Around the world, there are currently more than 7 million electric vehicles (EVs) in use, and other aspects of road transportation, such as the freight industry, are being electrified.

The electric vehicle is not a recent invention; it first emerged alongside internal combustion engine vehicles. Electric cars outperformed all other car types between 1890 and 1900. Because they were less noisy and polluted than cars with internal combustion engines, they significantly increased in popularity at the beginning of the 20th century. However, the short battery life of electric automobiles meant that their owners could travel great distances.

In recent years, technological advancements and concerns related to climate change have progressively sparked the resurgence of electric automobiles. The transformation from internal combustion to electric engines, which is now occurring in the automotive area, represents the most significant change. To adjust to changing market conditions, automakers have undertaken massive financial investments and unforeseen alliances [7–9].

EVs have been more and more popular in recent years due to their capacity to provide a variety of benefits, including [9]:

- Energy efficiency: Electric vehicles use less energy than vehicles powered by traditional internal combustion engines (ICEs).
- Electric mobility improves energy security because the road transportation industry is so reliant on petroleum-based fuels. Additionally, electricity may be created using a range of materials and fuels and is frequently produced locally.
- Air pollution: Since electric vehicles produce no emissions, they are an excellent solution to the issue of air pollution, particularly in densely populated regions and those nearby, where many citizens can be exposed to dangerous toxins from transit vehicles.
- Greenhouse gas (GHG) emissions: Combined with a progressive increase in the production of low-carbon energy, increasing electric mobility can result in considerable reductions in GHG emissions from the transportation infrastructure when compared to other traditional vehicles. Additionally, electric vehicles can behave according to the integration of renewable energy, which is often unpredictable for generating electricity, and offer flexible services for power systems.
- Noise reduction: Electric vehicles, especially those with two or three wheels, are quieter than ICE vehicles.

Industrial advancement: Given the relevance of energy storage for the switch to “clean” electricity, electric vehicles also have the capability of storing generated energy. In essence, battery technology, one of the fundamental factors in industrial competitiveness, is a possible facilitator for the significant reduction in cost in the electric car industry.

In many cities across the world today, one can find personal automobiles, common transport, car sharing, taxis, municipal parking lots, two- and three-wheeled machines (mainly electric scooters), as well as an expanding number of commercial and freight vehicle sectors. The proposed study topic fits within the background and is related to actual policies in the decarbonization of transportation areas, minimization of urban pollution, and the integration of EVs into electrical systems [10–12].

This study’s objectives were to analyze the impact and potential effects of integrating many EVs into the power network, as the efficiency could be influenced in both positive and negative ways by the need to charge all these EVs, as well as suggest several strategies and measures to integrate them. The article discusses the effects of integrating electric vehicles into the electric distribution networks and analyses those effects from a technical standpoint in terms of how they affect urban electric distribution networks and how that affects changes in electricity usage.

One challenge is connected to energy management, the impact of which may be reduced if the charging of EVs is achieved outside the peak period, which is likely to occur when big fleets of electric vehicles are incorporated into power networks. Electric vehicles (EVs) can be viewed from the perspective of electrical networks as either basic tasks

(with continuous consumption) or using the Vehicle-to-Grid (V2G) idea, where storage devices plan recharging intervals or they can inject grid energy using their energy storage devices [9,10]. In the case of a significant uptake of EVs, it will be important to coordinate their functioning both as a potential source of revenue and as a new aggregator that affects the electrical network by managing demand.

If EVs are gathered or aggregated, they can contribute to the balancing process by lowering grid usage or injecting electricity into the grid as needed by helping to coordinate the load.

The article is organized in the following way: a presentation of the clustering methods used in this study is first given; electrical load profiling, load-type profiles correlated with low voltage (LV) consumers, and a distribution network loading simulation are discussed along with the results obtained, and then the conclusions are presented.

In recent years, technological developments in the energy domain, including the introduction of smart meters and the transition to the concept of “Smart Grids”, have provided transmission and distribution operators with opportunities to forecast the load required by the system, modeling consumers to take into account their behavior, for the prevention of unplanned outages, the optimal load planning of generating units, etc. [13]. In these cases, operators must manage a lot of data and perform complex analyses in order to make the best decisions regarding the optimal planning and operation of electricity networks. For the efficient management of large databases, there are two aspects that need to be considered: data extraction (data analysis to obtain specific knowledge, patterns, or models) and database management (data storage, processing, and querying). Both related concepts are crucial in the energy networks’ decision-making process [14]. The choice of technology and the organization of installation, processing, and maintenance operations are the first steps in the adoption of smart metering systems. These technologies mark a significant development in the interaction between users and network operators. If consumer-mounted smart meters were totally integrated into a modern metering infrastructure and data were adapted, then distribution operators (ODs) could have access to full monitoring, which would make it easier to estimate the state of distribution networks [15–17].

The transition to the “Smart Grids” concept can lead to the implementation of smart monitoring and remote communications equipment necessary for optimal power systems operation and planning that will lead to maximizing economic benefits and minimizing the environmental impact. The phrase “Smart Grids” represents a hyperbole that involves the management of the EEA without the intervention of the human factor. The key components of this idea include two-way communication with consumers and all other market participants, as well as digital control of the energy transmission and distribution network. This smart infrastructure will enable various energy services, markets, integrated distributed energy sources, and control systems. The world economy in the future will be supported by the smart grid. It suggests that, in many respects, electricity generation, transmission and distribution companies, regulators, and institutions, indeed, all levels of government, face a real challenge in terms of the energy sector which is the driving force behind the world economy [18–22].

Starting from the aspects highlighted above, the efficient solution to many problems related to the management of the electric power system goes through the elaboration of solutions based on one form or another of artificial intelligence. Artificial Intelligence (AI) techniques aim to create intelligent computing systems, systems based on the characteristics of human intelligence: reasoning, ability to learn, solve and communicate, systems for problems for which there is no classical computational algorithm. Over time, with the development of AI techniques, hybrid algorithms have been developed and perfected, such as fuzzy logic-controlled neural networks, fuzzy genetic algorithms or expert systems, and artificial neural networks generated by genetic algorithms or neuro systems, having already proven their effectiveness [23–25].

Because an AI system has more complex tasks to solve, the knowledge that needs to be represented in it increases (facts, rules and heuristics of the field, general concepts, and

theories). In general, a system may work well, in line with the goal set by the knowledge provided, but any move outside its competence causes its performance to decline rapidly. This phenomenon is also called the fragility of knowledge [26].

Several machine learning techniques are presented in the studied literature, including supervised and unsupervised approaches that have been utilized for energy consumption level predictions. Among the unsupervised learning techniques, clustering is considered one of the most frequently applied techniques in data mining and machine learning. Clustering involves partitioning objects with similar patterns under observation into different groups. A vast number of works on clustering electricity usage patterns have been presented by researchers. The article [27] generated a typical load profile from data measured with automatic meter reading systems, then performed cluster analysis using three clustering algorithms, specifically, the hierarchical, k-means, and fuzzy c-means algorithms. In [28], classified daily load curves in industrial parks, which can be regarded as micro-grids from the energy network perspective using SOM, then exploited k-means to obtain a number of clusters, and [29] demonstrated the possibility of applying disaggregation techniques on smart meter data via fuzzy c-means clustering. Similar work is in [30], where they utilized the k-means algorithm to group residential houses with similar hourly electricity use profiles, and in [31] where they proposed a method to characterize medium voltage electricity consumers by using several clustering algorithms. In order to choose the best one among the typical load profiles, they measured the performance of the clustering algorithms in terms of eight clustering validity indices. To deal with the scalability and computational complexity of the power consumption profiling process, the authors of [32] proposed a multi-layered clustering method for power consumption profiling. First, they acquired local power consumption profiles using k-means, considering clusters with a low number of patterns as abnormal power consumption behavior. In the second stage, a global power consumption profile was derived from the local ones. Furthermore, Refs. [33,34] applied an improved k-means algorithm with particle swarm optimization (PSO) to open residential buildings datasets to divide their electricity consumption in an entire region into different levels. The authors of [35] developed a methodology in which one-dimensional time series smart meter data were reshaped to two-dimensional arrays called load profile images. After performing image processing techniques on those images, they derived the class load image profiles via clustering algorithms. In addition, [36] partitioned customers into electricity user groups based on similar electricity usage behavior with the SOM, k-means, and hierarchical clustering algorithms. Similar to group electricity consumption profiles, the authors of [37] investigated a shape-based clustering method.

The discussed literature reveals several limitations of the employed techniques from various perspectives of energy consumption prediction. The literature lacks focus on capturing the recognizable patterns in building smart sensing data, which has a limited number of features. These features can be represented in low-dimensional feature space and may affect the overall performance of data analytic tasks. Many of the existing techniques enquire about the number of clusters to differentiate among distinct categories of data. In addition, the presentation of energy consumption for data analysts and common individuals is a common problem that has not been tackled effectively in the existing literature.

Therefore, based on the above-mentioned problems in household energy predictions, this paper presents a new framework with the following main contributions:

- There is not a lot of energy consumption data obtained from smart sensors for residential buildings, and the presence of missing data is a difficult problem in statistical analysis. Less than 1% of missing data can be considered a common problem, and between 1 and 5% can be considered a solvable problem. If the percentage is greater than 5%, difficulties may arise in solving the respective problems. Thus, if the values are between 5 and 15%, the problem requires the application of sophisticated solution methods, and if the value exceeds 15%, the problem may have difficulties in interpretation. Finding recognizable patterns in such data is very difficult, which affects the performance of electricity consumption analysis. To solve this problem, five

hierarchical clustering methods were used in the clustering process: average distance (Average Method), the center of gravity (Centroid Method), minimum distance (Single Linkage Method), maximum distance (Complete Linkage Method), and Ward, which were the basis for obtaining the load-type profiles presented in the article. Based on the clustering methods used, we propose a method based on load-type profiles which is more robust, reduces calculation errors for off-peak time/peak time, requires less computation volume, and converts small model representations from data with reduced dimensions in high-level representations, comparable to using large databases.

- Clustering algorithms require an input parameter to divide data into multiple clusters. This article, by using the method of simultaneous layers in the hierarchical clustering process, average distance (Average Method), the center of gravity (Centroid Method), minimum distance (Single Linkage Method), maximum distance (Complete Linkage Method), and Ward, obtained an adaptive grouping to organize large data.
- After dividing the data into several clusters, the regression model based on first- and second-degree polynomials for every consumption class was applied, performing a predictive statistical analysis on the data to determine which buildings had a high, medium, and low level of energy consumption.

## 2. Materials and Methods

### 2.1. Clustering Techniques

The use of clustering algorithms allows for the spatial distribution of characteristic vectors to be used as a basis for grouping input data. Each element connected with a set of data will be characterized by a vector whose components are represented by the representative qualities or attributes of the vector in order to examine the similarity or differences between them and to categorize them. The determination of the characteristic/attribute number and their definition requires a deeper analysis of the database designed on the available information and considering the expertise of specialists [38,39]. The vectors connected to the input data are grouped throughout the clustering phase based on the estimated distance between each of them. Depending on the analyzed topic, the clustering process will result in one or more clusters (groups, patterns, models, or classes), which describe the spatial position of the qualities taken into account for the process' elements. Within each cluster, the elements are closer to a common center when compared to other centers belonging to

Sensors 2023, 23, x FOR PEER REVIEW

other groups. This aspect is exemplified in Figure 1.

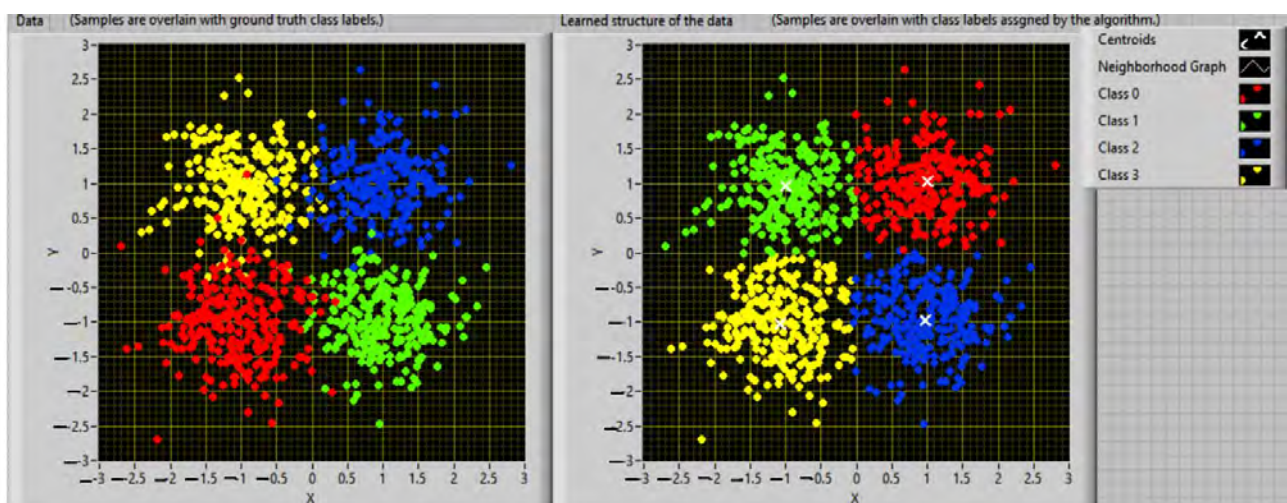


**Figure 1.** Example of clustering processing.

In Figure 1, the elements, represented by vectors with two characteristics  $(x_i, y_i)$ ,  $i = 1, N$ , (where  $N$  is the maximum number of elements of the database subjected to the clustering procedure) were assembled using a similarity principle defined by the distance calculated between vectors. In this mode, two or more components can be associated with the same pattern if the distance between them is smaller in relation to the distance from the elements of another cluster. Finally, each cluster will be characterized by a representative element, determined by mediating the characteristics of the elements that make up the cluster.

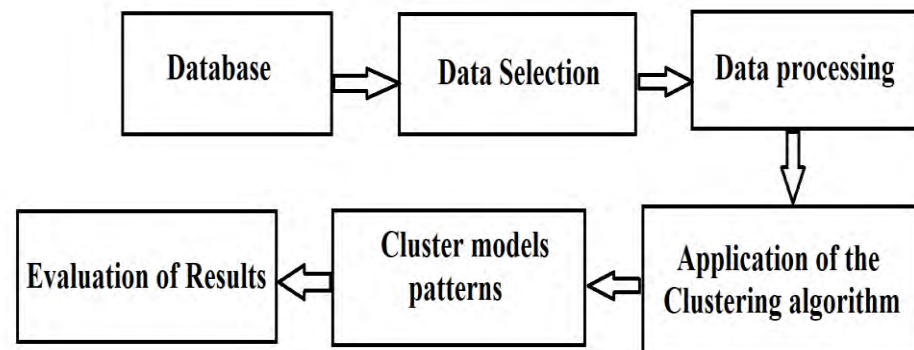
**Figure 1.** Example of clustering processing.

In Figure 1, the elements, represented by vectors with two characteristics  $(x_i, y_i)$ ,  $i = 1, \dots, N$  (where  $N$  is the maximum number of elements of the database subjected to the clustering procedure) were assembled using a similarity principle defined by the distance calculated between vectors. In this mode, two or more components can be associated with the same cluster if the distance between them is smaller in relation to the distance from the elements of another cluster. Finally, each cluster will be characterized by a representative element, determined by mediating the characteristics of the elements that make up the cluster [40].

## 2.2. Stages of the Clustering Procedure

### 2.2. Stages of the Clustering Procedure

Clustering processes can be applied in various domains in order to group unlabeled components. These domains already involve various assumptions, terms, or techniques, related to clustering procedure phases, as a function of the addressed problems. The steps that must be covered are described below and represented in Figure 2 [40].

**Figure 2.** Clustering process phases.**Figure 2.** Clustering process phases.

Step 1. The components subjected to the clustering procedure must be established.

In this phase, it is necessary to consider the option from the database that is best suited to the aim of the problem. The type and size of the attributes available for the clustering procedure can be chosen.

Step 2. The attributes/characteristics of the components subjected to the process must be extracted.

Step 2. The attributes/characteristics of the components subjected to the process must be extracted. The identification of the most useful and important characteristics must be achieved. During this process, one or more component transformations can be accomplished to obtain new dominant attributes.

Step 3. A similarity measure must be defined. Usually, the similarity can be determined by measuring the distance connecting adjacent items. Once a vector has been attributed to each component, this length may indicate how similar two elements are. The literature has defined several different distance measurement techniques, with Euclidean distance being the most used.

Step 4. This phase represents the actual clustering procedure. It can be achieved in various modes depending upon the techniques chosen by the decisional factor. All clustering techniques should conduct several clusters for any input data set. If no clusters resulted from the process, other techniques can be applied in order to obtain the desired results. The obtained results can be “clear”, meaning that the separation of the components is achieved in well-defined clusters, or they can be “fuzzy”, meaning that each component has a degree of dependence on each cluster.

Step 5. The results must be extracted. For this, an accurate interpretation of the results is necessary so that their rendering can be achieved in a simple way that is easy to interpret by the decisional factor. In this scenario, either from the point of view of automatic analysis (where a computational system can perform further data processing effectively) or from the perspective of a human, simplicity is required (the representation used for results is easier to understand by decision makers). The extraction of the results from the clustering method is a brief illustration of each cluster using representative components.

Step 6. Evaluation of results. An assessment of the clustering procedure is taken into account when analyzing the validity of the outcomes (represented by clusters), and this evaluation often employs an optimization criterion. This impartial analysis examines

whether the outcomes are accurate. If a cluster does not occur unintentionally or for other reasons, it is validated.

### 2.3. Clustering Methods

Next, certain terms will be defined and the notions that will be used will be briefly described in the next section.

The element  $x^j$ ,  $j = 1, \dots, N$  (where  $N$  is the total number of elements), is a unique object used in the clustering process. It is usually represented by an  $n$ -dimensional vector  $x^j = [x_1^j \ x_2^j \ \dots \ x_n^j]$ .

Scalar components  $x_i^j$ ,  $i = 1, \dots, n$ , are called characteristics/attributes of the vector  $x^j$  and are established by the decision maker.

The distance between vectors is a metric in the space of the attributes  $x_i^j$ ,  $i = 1, \dots, n$ , corresponding to input vectors  $x^j$ ,  $j = 1, \dots, N$ , and used to determine the similarity between elements. The most used is the Euclidean distance.

For a database  $X$ , consisting of the vectors  $x^j$ ,  $j = 1, \dots, N$ , with  $n$  characteristics,  $x^j = [x_1^j \ x_2^j \ \dots \ x_n^j]$ , different distances between vectors can be defined. Thus, if two vectors  $x^r$  and  $x^s$  are taken into account, the distance can be calculated with the relation:

$$d(x^r, x^s) = \sqrt{(x^r - x^s)(x^r - x^s)^t} \quad (1)$$

There are several ways to classify clustering methods in the literature. The most used classifications are given in [40,42]: hierarchical methods and the K-means method.

Hierarchical clustering methods can be subdivided, according to their meaning, into methods of agglomeration and division. In the case of agglomeration methods, for example, we start from the  $k$  clusters, each containing a single element  $x^j$ ,  $j = 1, \dots, N$ , and by successive mergers, form a single cluster, containing all  $N$  elements. In the case of division methods, the direction of deployment is inverse, i.e., starting from a single cluster containing all the  $x^j$ ,  $j = 1, \dots, N$  elements, we reach  $k$  clusters, each containing a single element  $x^j$ . Agglomeration techniques are usually used more frequently. As shown above, in the hierarchical spatial grouping, an agglomeration process goes through a series of mergers/couplings of groups/classes,  $P_n, P_{n-1}, \dots, P_1$ . The first,  $P_n$ , consists of  $n$  "groups" with a single element/object, and the last  $P_1$  includes a single group having all  $n$  elements/objects. At each stage, the method couples two close groups (at the first level, of course, this means the coupling of two elements/objects that are close to each other (in distance), since at the initial stage, each group has an element) [40,43].

The clustering process can be illustrated as a two-dimensional diagram named a dendrogram. These methods are suitable for small tables, having a few hundred rows. The desired number of clusters can be chosen after the proper shaft is designed by imposing a threshold [30,40].

The difference among the agglomeration techniques is given by the method for defining the distance between the clusters.

Considering two clusters,  $C_r$  and  $C_s$ , containing  $n_r$  and  $n_s$  elements, the average distance  $d(C_r, C_s)$  is calculated on an Euclidean distance base:

$$d(x_r^f, x_s^h) = \sqrt{\sum_{k=1}^N (x_{rk}^f - x_{sk}^h)^2} \quad (2)$$

can be expressed through the relation:

$$d(C_r, C_s) = \frac{1}{n_r n_s} \sum_{f=1}^{n_r} \sum_{h=1}^{n_s} d(x_r^f, x_s^h) \quad (3)$$

Starting from the above-mentioned, the most used hierarchical clustering methods are briefly presented below.

$$d(x_r^f, x_s^h) = \sqrt{\sum_{k=1}^N (x_{rk}^f - x_{sk}^h)^2} \quad (2)$$

can be expressed through the relation:

$$d(C_r, C_s) = \frac{1}{n_r n_s} \sum_{f=1}^{n_r} \sum_{h=1}^{n_s} d(x_r^f, x_s^h) \quad (3)$$

Starting from the above-mentioned, the most used hierarchical clustering methods are briefly presented below.

The following figure shows the result obtained by applying the hierarchical clustering algorithm (Figure 3).

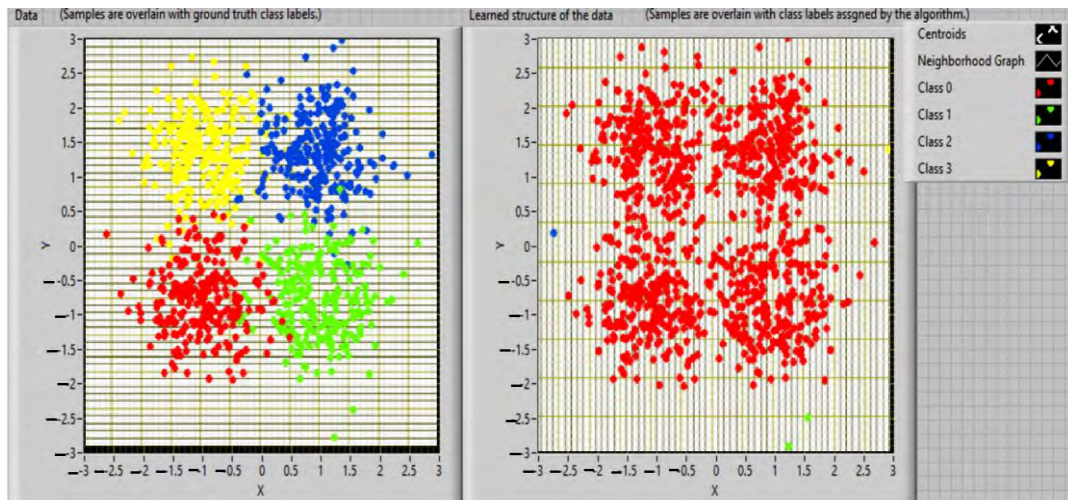


Figure 3. The representation of hierarchical clustering algorithms.

a. Minimum distance method (minimum method)

This method is the simplest, being based on the minimum distance, also known as the method of the closest neighbor, such as the distance between the clusters represents the distance between the closest items:

$$d(C_r, C_s) = \min\{d(f, h)\} \quad (4)$$

where the  $f$  component is attributed to the  $C_r$  cluster and the element  $h$  to cluster  $C_s$ . In this case, the distance is calculated between each possible pair of elements  $(f, h)$ . The minimum value is the distance between the cluster  $C_r$  and  $C_s$ . In other words, the distance between two clusters is given by the shortest link value. At every stage of the clustering process, the  $C_r$  and  $C_s$  clusters, for which  $d(C_r, C_s)$  is minimal, will be coupled. A graphical interpretation of the minimum distance between the clusters is shown in Figure 4.

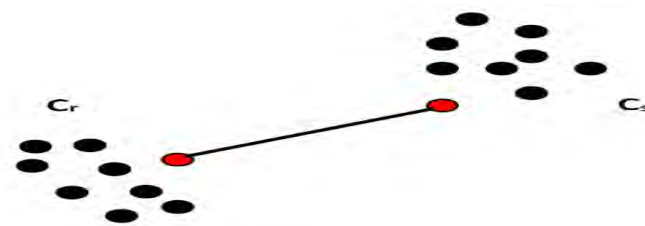


Figure 4. A representation of the minimum distance between two clusters.

b. Maximum distance method (maximum method)

This method, also known as the farthest neighbor method, is based on distance maximum, being the opposite of the minimum method. In this technique, the distance  $d(C_r, C_s)$  is calculated using the equation:

$$d(C_r, C_s) = \max\{d(f, h)\} \quad (5)$$

where the  $f$  element is attributed to the  $C_r$  cluster and the  $h$  element to the cluster  $C_s$ . In such a case, the distance between two clusters is given by the longest link value. At each phase of the spatial hierarchical grouping, the clusters  $C_r$  and  $C_s$  for which  $d(C_r, C_s)$  is maximum will be coupled. Figure 5 presents a graphical interpretation of the distance between the clusters.







#### f. K-means method

This method involves a simple and easy mechanism to classify the input data set into several  $K$  clusters ( $K$  fixed a priori). The basic plan implies defining  $K$  centers of *weight*, one by one for each group. These centers of *weight* must be rationally fixed because different locations lead to different results. The best choice is to fix them, if possible, as far apart as possible from each other. The next step is to take each element of the input data set and link it with the closest center of *weight*. The first grouping stage ends when there are no more ungrouped items. At this point, it is mandatory to recalculate new  $K$  centers of the groups arising from the previous phase. The process continues until the positions of the new centers no longer change significantly.

The objective of the method is to minimize an objective function (quadratic error function) given by the expression:

$$J = \sum_{k=1}^K \sum_{l=1}^{n_k} \|x_l^k - c_k\|^2 \quad (9)$$

where  $\|x_l^k - c_k\|^2$  is the distance measured between point  $x_l^k$ ,  $l = 1, \dots, n_k$ , where  $n_k$  is the total number of components of the  $k$  cluster, and the center of the group  $c_k$ ,  $k = 1, \dots, K$ .

#### 2.4. Validation of Results

The evaluation of the results obtained from the clustering process is the main concern of cluster validation. At this stage, the density, size and shape, separation of clusters, and robustness of classification were examined. The literature mentions the following tests to validate the clustering process [39,40,44,45]:

- External tests—data not included in the basic ranking are compared with the categorization results of the input data.
- Internal tests—only input data are utilized to evaluate the classification's quality; each cluster's separate validation is carried out using this test.
- Relative tests—this approach takes into account several classifications of the database, the results being analyzed using the same clustering method, but with various input data.

Internal cluster validation tests are more common and effective in real-world settings. Testing based on the creation of a global silhouette index of clusters is one of them and is also one of the most popular. This test determines the average shape width for each cluster, the median shape width of each element, and the average shape width of the entire collection of input data. With this method, each cluster might have a "shape" that is based on comparing its separation and density. The clustering procedure is then validated using the shape's average width, and the ideal cluster number will also be set using the same information.

$$GSI = \frac{1}{N_k} \sum_{k=1}^K F_k \quad (10)$$

$F_k$ , the local silhouette coefficient, is calculated using the relation:

$$F_k = \frac{1}{r_k} \sum_{l=1}^{r_k} f_l \quad (11)$$

$f_l$ , the silhouette width coefficient for element  $l$ , is calculated by:

$$f_l = \frac{b_l - a_l}{\max\{b_l, a_l\}} \quad (12)$$

where  $a_l$  is the average distance from element  $l$  and the elements from cluster  $k$  and  $b_l$  is the minimum median distance from component  $l$  and the components in the closest cluster  $k$ .

In Equation (12), if the element  $l$  is unique inside a cluster, then  $f_l = 0$ . The literature proposes the following explanation of the GSI coefficient [38,40]:

- 0.71 to 1.00 (a strong structure was highlighted);
- 0.51 to 0.70 (a reasonable structure was obtained);
- 0.26 to 0.50 (the structure is weak and might be artificial);
- <0.25 (no substantial structure was noticed).

Verifying the clustering process quality is one of the main steps in analyzing the inherent database characteristics. Its purpose is to evaluate the results of the process clustering and select the schema that best fits the elements in the database.

### 2.5. Electric Load Profiling

The loads from the nodes within the electrical networks range in consumption time and place. Consequently, distribution operators (ODs) need details regarding the load of fed consumers so that they will be able to optimally plan and operate the network and ensure proper power supply and operation modes, load management, and proper billing [40,46–48]. The load demanded by consumers depends on various parameters such as:

- Consumer type: consumption type, with/without electric heating, or size of the building;
- Time factor: time of day, weekday, and month;
- Climatic factors: humidity, temperature, cloudiness, wind speed, etc.;
- Other electrical charges related to the analyzed load.

For a certain consumer, his behavior is determined by a load profile correlated with the electricity consumption for each interval. The accessibility of this data is dependent on the type of consumer. In general, small consumers (such as residential ones) have an uncertain behavior, because the implementation of smart metering on a large scale would lead to large investments whose recovery time from their energy consumption would be too long. For these consumers, there is only the consumption of electricity at certain periods of time each year. For large consumers (such as industrial consumers), the installation of smart meters is facilitated by advantages related to billing (done every month) and high electricity consumption (justifying the investment by the fact that the detailed recording of consumption allows for the application of differentiated tariffs varying with consumption period).

In the traditional strategy for a distribution system plan, load profiles are employed to evaluate the maximum necessary load, in correlation with the simultaneity coefficient of the consumers coupled to the network node. Despite the fact that this strategy is appropriate, some major disadvantages arise:

- There are inherent inaccuracies, due to the simultaneity coefficients, which must be highlighted;
- The energy consumption and losses calculation does not have an increased precision;
- The voltage within the network nodes from various hours is not known;
- The load profiles of nodes having arbitrary variations in power requirement cannot be accurately modeled or evaluated.

Utilizing modern techniques of load analysis, load forecasts and the calculation of power and energy losses (for any period) can be achieved. The use of load profiles has some advantages [40,49]:

- It is not necessary to estimate or calculate concurrency coefficients, as load profiles already include the information;
- The energy consumption and power/energy losses calculation can be correctly achieved at any point within the network;
- The main voltage and charging are known for any period;
- The optimal position of the transformer plot can be determined, both for the peak load period, as well as for other times of the day;
- The effect of overloading or increasing the load is modeled more accurately than in the traditional method.

Medium voltage (MV) and low voltage (LV) networks, mainly urban ones, have many nodes even if only the nodes where electric distribution substations (EDSs) are located are taken into account. Thus, monitoring the system consumption for every node can become overwhelming, sometimes virtually impossible. This is practically overcome if, in the organization studies corresponding to the networks, the load-type profiles are associated with the node groups.

### 2.6. Load-Type Profiles Correlated with Nodes in Electrical Distribution Networks

This paragraph presents an approach based on hierarchical clustering techniques (presented in Section 2) for calculating the load-type profiles (LTP) correlated with nodes' high voltage (HV) and medium voltage (MV) electrical distribution networks. Through knowledge of the load profile of the nodes, the OD can clarify the procedure for estimating the requirement in a certain sector.

In this respect, it is mandatory to understand the daily loading profiles. The load diagram of the nodes must be reconstructed by applying the standard load profile and daily demand. This standard profile is characterized by 24 or 48 load values.

The type and season influence the shape of load profiles. Because many profile responsibilities are correlated with various nodes of the network and may complicate the problem, they must be grouped into clusters, taking into consideration some similarities among them. For every cluster, the typical load profile can be established.

In this sense, all the measurements performed must be processed, by arrangement and normalization, using a convenient normalization factor (average power, peak power, or more frequently, the energy consumption of the studied period):

$$p_i^h = \frac{P_i^h}{\sum_{h=1}^T P_i^h}, i = 1, \dots, N \quad (13)$$

where  $p_i^h$  is the normal value of the power in  $i$  node at  $h$  hour,  $P_i^h$  is the real value of the power in  $i$  node at  $h$  hour, and  $\sum_{h=1}^T P_i^h$  is the total energy consumption in the interval  $T$  (24 h).

It is worth mentioning that after the clustering procedure is applied, clusters can be acquired as coherent and representative so that the diagrams within the same cluster are similar [40,49,50]. In the end, every cluster will be related to a typical task profile, estimated using the graphs median.

$$m_{C_k}^h = \frac{\sum_{i=1}^{N_{C_k}} p_i^h}{N_{C_k}}; h = 1, \dots, 24; k = 1, \dots, N_K \quad (14)$$

where  $N_K$  is the cluster numbers derived from the node's classification in concordance with the absorbed load (active power) and  $N_{C_k}$  is the node number from each cluster  $C_k$ ,  $k = 1, \dots, N_K$ .

### 2.7. Load-Type Profiles Correlated to Low-Voltage Consumers

In recent years, distribution operators have increasingly used smart metering systems (Smart Metering System) to monitor the electricity consumption of consumers. The development of these systems begins with technology selection and planning for installation, operation, and maintenance. In general, the implementation of residential or non-residential consumer categories is quite discrete in the case of many countries in the European Union. Currently, there are two alternative solutions to solve the problem of metering electricity consumption for consumers.

The first solution envisages the installation of smart meters for all consumers, being expensive and uneconomical, but the most accurate. The second solution envisages the continued use of traditional meters and the attachment of load-type profiles to the monthly energy consumption, which is then distributed over days and hours.

For large consumers, in the category of industrial ones, the presence of smart meters is necessary for several reasons: invoicing is done every month, the consumption of electricity is high (which implies rapid amortization of the investment), and it provides a detailed recording of consumption necessary for the process of invoicing.

This section presents an algorithm for determining the type of load profiles associated with LV consumers according to the category of energy consumption in which they fall. Consumption categories are identified from historical information and can be updated following changes in consumer behavior.

The algorithm phases are [40]:

Phase 1. In this phase of load analysis and database formation, a representative specimen must be identified from the crowd of consumers who have installed smart meters and the sampling step for the purchase of load schedules must be described. Consequently, a database with the registered load program and the consumer category is created.

Phase 2. Technical problems in the pre-processing of the data may affect the quality of the database in real cases of monitoring consumer charges, requiring many meters spread over a large geographic region over an extended period. The most relevant and frequent problems are communication issues, interruptions, meter failure, and, occasionally, the irregular behavior of individual consumers. These issues will influence the records of the database, appearing as null values or exceeding a particular threshold set by the connection notice. Such records must be identified and working techniques must be applied to obtain the missing data, resulting in the substitution of missing or equal to zero data with some estimated values so the database can be made ready to obtain clusters.

Phase 3. The database with records of load schedules must be divided into clusters of consumption, defined by the consumer's type: residential, commercial, or industrial.

Phase 4. This phase represents the clustering procedure. A hierarchization of clusters is achieved, taking into consideration the daily consumers' energy consumption within every consumption macro-category. In this respect, the K-media clustering technique is applied. For every cluster, the representative load profile is determined by applying the average of the load graphs' hourly values.

Phase 5. Task-type profiles must be assigned. For every customer's class, a typical task profile is assigned as a function of the activity macro-category to which the consumption belongs.

The suggested algorithm was evaluated using a database with 296 load diagrams. After the macro-categories were divided, 147 consumers were distributed in the residential consumers class, 97 in the commercial consumers class, and 52 in the industrial consumers class.

The utilization of the k-means clustering technique within every activity macro-category resulted in five clusters within the residential consumers class and three clusters within the commercial and industrial consumers ones.

Using these standard profiles, consumers can be better delineated in connection with load modification than the standard profiles correlated to the complete activity macro-category. This detail can be emphasized if a correlation is achieved between the load-type profiles of every activity macro-category and the load-type profiles linked to these macro-categories (Figure 7).

The change in consumers' energy consumption determines important problems in the planning of activities associated with the technological procedure, in terms of adopting the optimal power supply and operation solutions. Solving these issues can be efficiently achieved by utilizing consumption profiles correlated to energy carriers.

This section proposes a perspective based on clustering methods for the determination of load-type profiles for electric vehicle charging networks. The standard profile's forms, which take into account both the type of electrical equipment or installations supplied and the time of year the survey is conducted, represent the specifics of how consumers use electricity.

category resulted in five clusters within the residential consumers class and three clusters within the commercial and industrial consumers ones.

Using these standard profiles, consumers can be better delineated in connection with load modification than the standard profiles correlated to the complete activity macro-category. This detail can be emphasized if a correlation is achieved between the load-type profiles of every activity macro-category and the load-type profiles linked to these macro-categories (Figure 7).

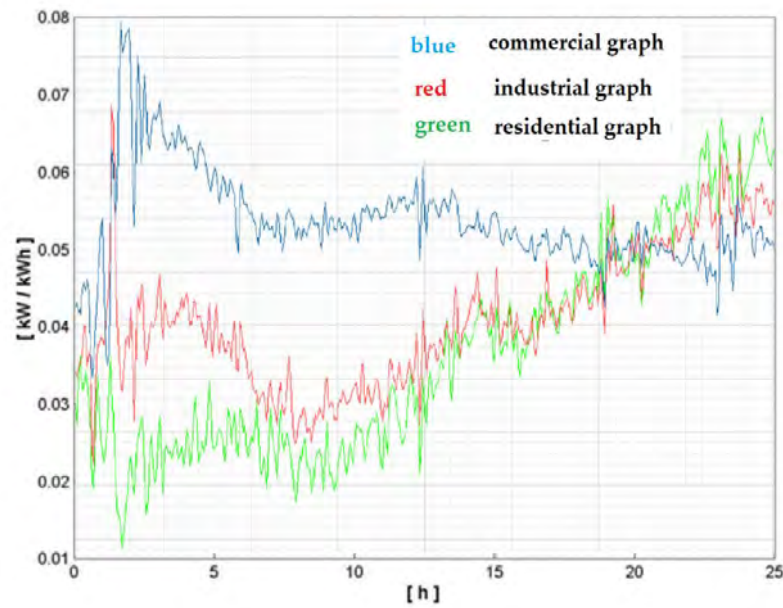


Figure 7. Load-type profiles of activity macro-categories.

The methodology proposed for the load profiling process for electrical vehicles as industrial consumers is presented in Figure 8. The methodological procedure, in terms of adopting the optimal power supply and operation solutions. Solving these issues can be effi-

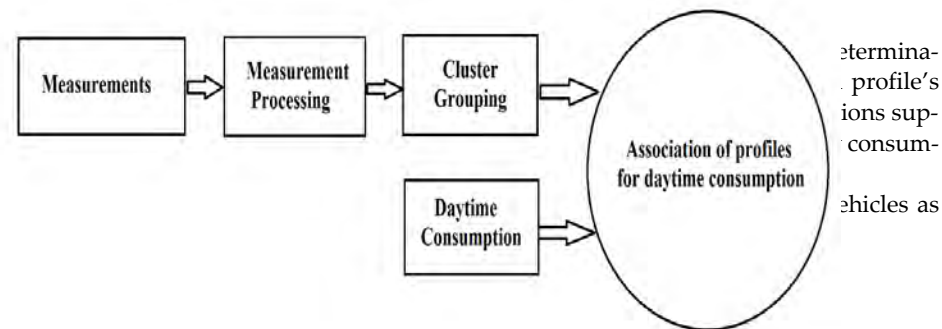


Figure 8. Scheme for the determination of load-type profiles in electric vehicles considered as industrial consumers.

The importance of every phase from Figure 7 is the same as for all profiling procedures that are operated with clustering methods from the previous paragraphs.

2.8. Distribution Network Loading Simulation

In the distribution network, the basic component represents the loading simulation of MV/LV transformers. Because tens of thousands of transformers are positioned in the distribution matrix, their hourly load is hard to determine, due to the many distribution networks, including current and voltage sensors mounted in devices, transformers, and MV connections unequipped with recording meters with transmission capacity, remote, real-time recording, and load level. Consequently, it is hard to identify those transformers operating at overload or to estimate the loads of MV connections intended for transfer between distributors without a simulation.

The most effective route to evaluate a load of transformers, without performing real measurements, is represented by the utilization of simulation programs, with some of the following elements being taken into consideration [40]:

- 1.1. The number of consumers coupled to every transformer;
2. The consumer type;
3. The annual energy consumption for every consumer;
4. Task type diagrams correlated with every consumer class;
5. Software able to calculate the load of transformers.

It must be emphasized that, when a load of transformers is estimated, the maximum and hourly active powers (within low voltage/medium voltage side) are computed on peak days and varying typical intervals (winter, summer, average working days of the

4. Task type diagrams correlated with every consumer class;
5. Software able to calculate the load of transformers.

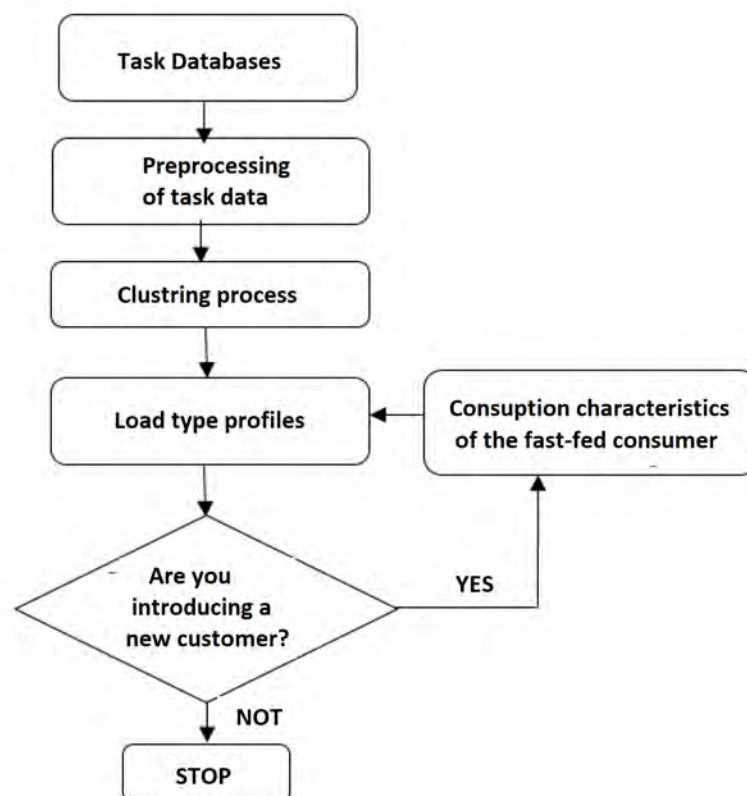
It must be emphasized that, when a load of transformers is estimated, the maximum and hourly active powers (within low voltage/medium voltage side) are computed on peak days and varying typical intervals (winter, summer, average working days of the week, etc.).

### 2.9. MV/LV Distribution Transformers Load Simulation by Clustering Procedure

The database structure that is necessary to simulate the load of the distribution transformers in the MV/LV substations includes:

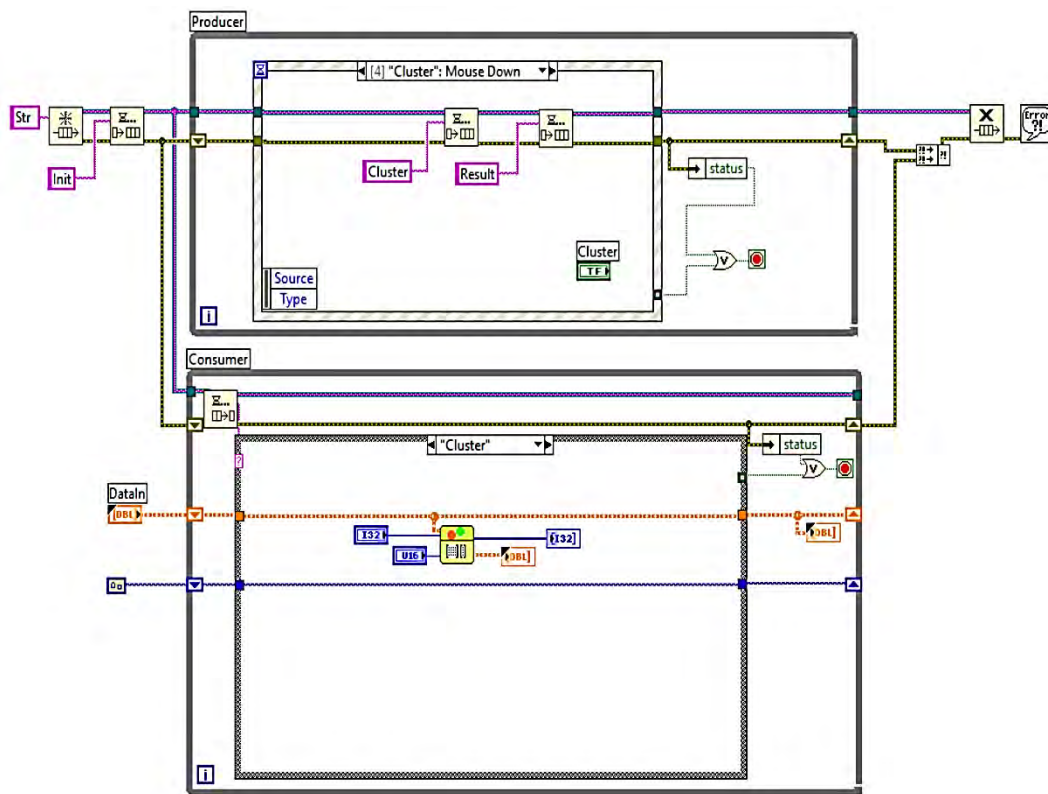
- The LV database having a “consumer link-substation (CS)” (number and class of consumers from every transformer in CS);
- Basic profiles containing task-type profiles for all consumers classes;
- A consumption database containing data on the annual energy consumption and consumer class.

In order to establish the typical load profiles correlated with consumers in LV networks, a database is required to include as many registered load diagrams as possible, representing all consumption categories. The decisional procedure of associating a typical task profile with a certain consumer constitutes a complicated problem. Consequently, a load profiling algorithm using clustering methods has been suggested for residential and non-residential consumers. Figure 9 shows the implementation diagram for determining load type profiles for residential and non-residential LV consumers [40] and the software pseudocode. In the following figures, the software implementation for the proposed algorithm is represented. The software development was carried out in the LabVIEW programming language developed by National Instruments.

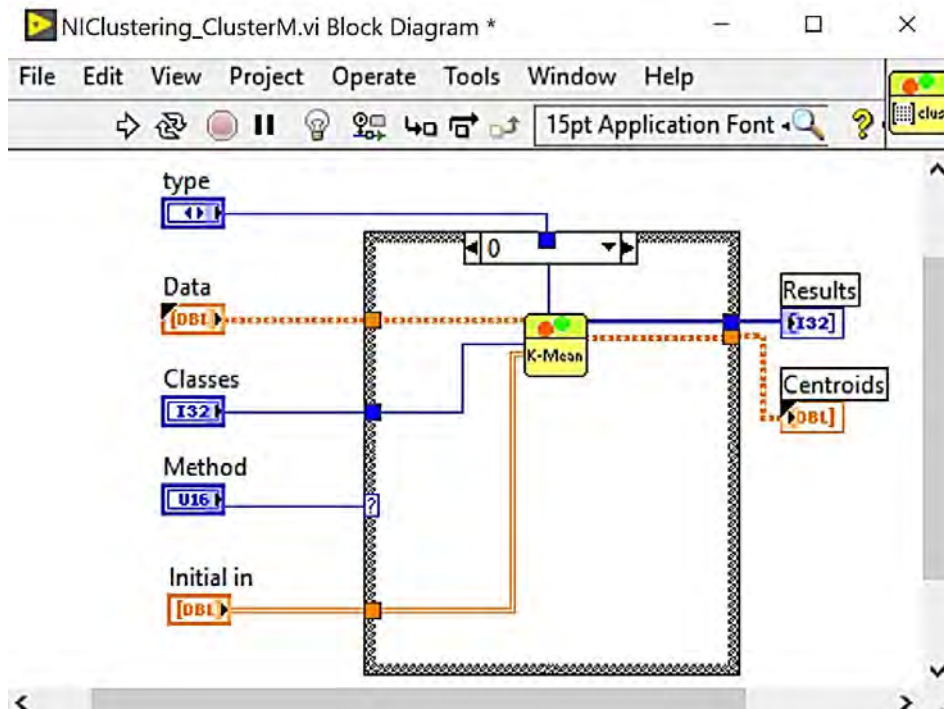


(a)

Figure 9. Cont.



(b)



(c)

Figure 9. Cont.

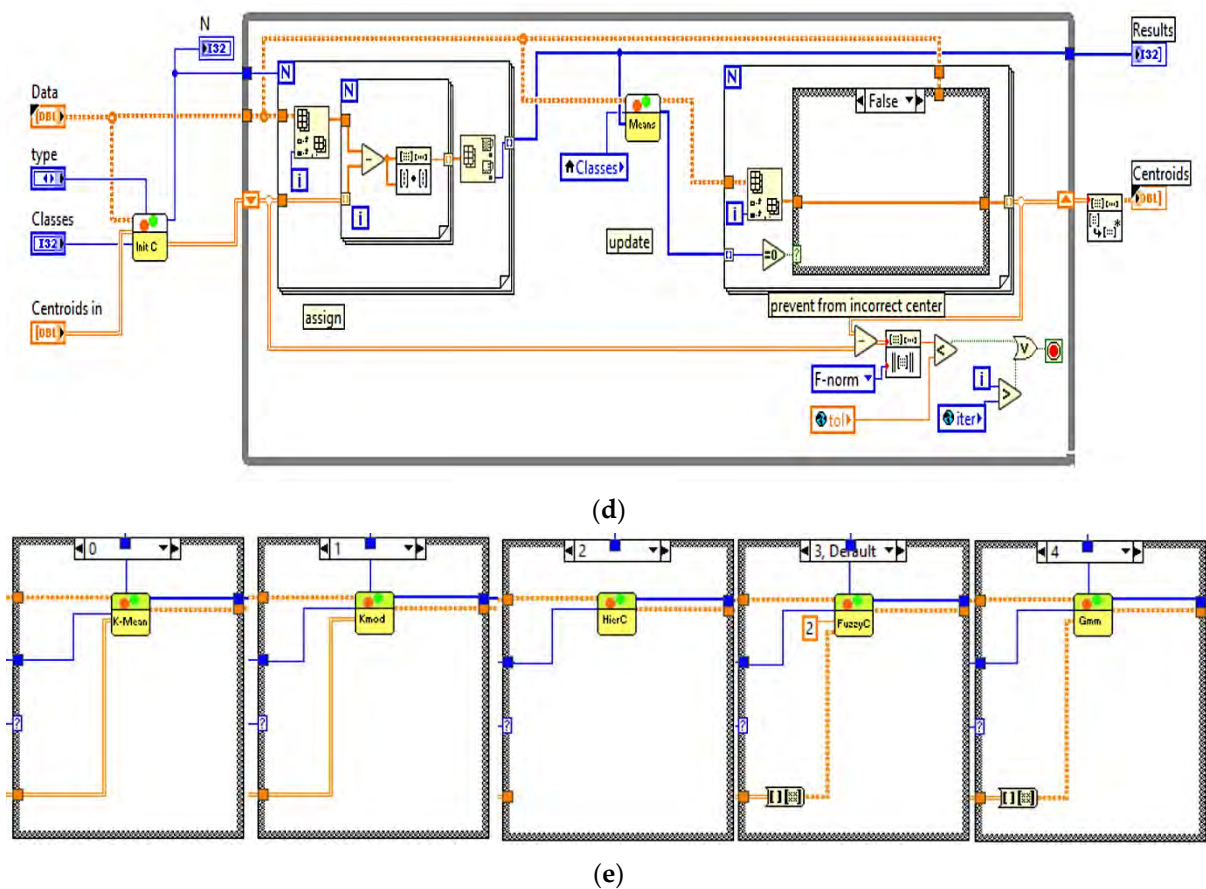


**Figure 9.** Implementation diagram for determining the load-type profiles for residential and non-residential LV (a) consumers and the software pseudocode: (b) is master code, (c) implementation code for k-means, (d) implementation code for hierarchical cluster and (e) represent software modules for all clustering methods.

### 3. Results

An important issue in the optimal operation and planning of electric distribution networks by electric companies is the estimation of the maximum load of consumers. This problem occurs especially with home consumers. The decision to determine the optimal number of consumption categories within the same class of consumers and the estimation of the maximum load is a complex problem. Therefore, an improved regression method with clustering techniques is presented. Within the proposed method, to define the consumption categories of consumers, a classification can be made considering the monthly energy consumption and the maximum load (data obtained from the recorded load graphs). After identifying the consumption category, the maximum load of each user is estimated using a regression model corresponding to each consumption class. The proposed advantage of the application of the data exploration cluster techniques is to determine total models/patterns/categories of patterns/patterns of consumption.

The contributions to modeling loads in electrical networks, the effectiveness of clustering techniques in the profiling and the load simulation for MV/LV distribution transformers using clustering procedures are highlighted in the study.

#### 3.1: Estimating the Maximum Load of LV Users (Consumers) Using Clustering Techniques

The estimation of the maximum load of users is a key parameter in the effective operation and planning of electricity distribution networks by energy providers. This problem occurs especially in household consumers, but also in the integration of electric vehicle charging. From analyzing the built databases and using data exploration techniques, load



patterns/models can be identified that can be extrapolated to other potential consumers such as electric vehicle charging networks.

The decision to estimate the appropriate number of consumption categories within the same consumer class and the maximum burden is a complex issue. Thus, a customized regression method using clustering techniques is presented.

The monthly energy consumption, as well as the maximum load, can be classified using the suggested approach to determine the consumption groups of users (data obtained from the recorded load graphs). After determining the consumption category, a regression pattern matching every consumption class is used to estimate the maximum load of each consumer. The main benefit of the suggested approach is the data exploration utilizing clustering techniques to produce models, trends, and consumption categories that would aid in consumer modeling.

Its stages are presented below [40]:

Stage 1. Database. For consumers in the selected pilot area where smart meters have been installed, the load graphs for the analyzed time period are recorded. For each consumer, the variables that characterize the consumption category (maximum load, monthly and annual energy) are extracted.

Stage 2. Data pre-processing. All records from the database are analyzed, and those that contain missing values, equal to zero or atypical, are subjected to the process of treatment with missing data techniques. After all processing, the data are used to classify consumption categories.

Stage 3. Data exploration process. The first step in this stage is the use of clustering techniques in order to obtain consumption categories according to the maximum load and monthly energy consumption. The K-media technique is utilized for the clustering process. Then, a regression model is built for each consumption category to estimate the maximum load related to consumers.

Step 4. Estimation of peak load. The regression models obtained in Stage 3 are used to estimate the maximum load absorbed by the monitored consumers by means of classical meters.

The structure of the database includes information on the type of consumers (residential, industrial, commercial, and public) and their daily/monthly/annual consumption respective to the maximum load absorbed. This information can be obtained using smart meters. The information acquired is represented by the load curves that describe the consumer's behavior during the day. The processing of the load curves allows us to determine the data on energy consumption respective to the maximum load absorbed by each consumer. For the method implementation, the database was split in two, a working base and a testing base. The application of the working base will lead to mathematical regression models able to conduct the estimation of the maximum load for each type of consumer within the same category of energy consumption. Energy consumption categories are then acquired using the K-average clustering procedure for each consumer type (residential, industrial, commercial, and public). The outcomes of the clustering technique are confirmed using a group quality assessment, based on the shape coefficient. The method is then tested to estimate the maximum load absorbed by consumers belonging to the testing base.

The method was applied using an initial database containing records of load schedules for 1160 household consumers located in a countryside region over a one-month period. For each consumer, the characteristic variables related to the peak load ( $P_{\max}$ ) and monthly energy consumption ( $W_{\text{luna}}$ ) were extracted.

In Stage 2, the analysis of load graphs and characteristic variables led to the elimination of 15 consumers due to zero energy consumption. Thus, in the next phase, the database consisted only of the associated information for 1145 consumers. This base was split in two, a working and a testing base. The size of the working and testing bases varies in the literature and primarily depends on the total amount of records in the original database. The split between the two bases ranges from 90/10 to 60/40. In this instance, the working

the literature and primarily depends on the total amount of records in the original database. The split between the two bases ranges from 90/10 to 60/40. In this instance, the database contained 814 consumers (representing 66 percent of the database), leaving the testing database with the remaining customers (331 consumers, 33 percent of the database).

In Stage 3, the data exploration process was initialized through the K-media clustering method to obtain the consumption categories in which the consumers in the work base will be integrated.

The first phase of the K-average method consisted of the determination of the maximum cluster number (consumption categories) with the relation:

$$C_{k \max} = \sqrt{N} = \sqrt{841} = 29 \tag{15}$$

Then, for each  $K = 2, \dots, 29$ , the K-averages technique was applied. For the clustering process initiated for the K value of the number of clusters, the quality of the grouping process was estimated by calculating the global silhouette index (GSI). The values of the shape index obtained for each  $K = 2, \dots, 29$  are represented in Figure 10. This grouping is the best result of the clustering technique since the GSI has the greatest value for  $K = 5$ . The results for the global silhouette index (GSI = 0.775) show that the clustering technique was quite effective. The graphical representation of the clusters obtained in the case  $K_{opt} = 5$  is illustrated in Figure 11.

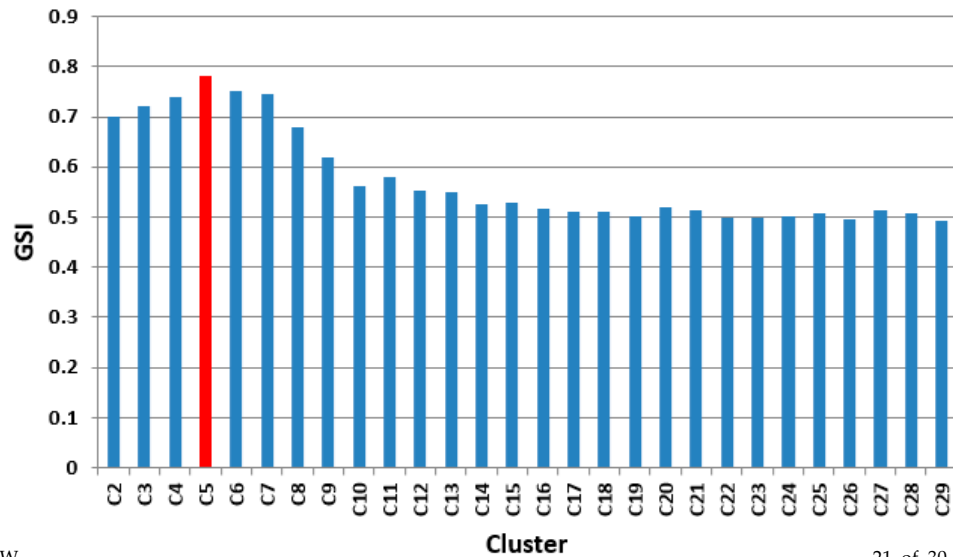


Figure 10. GSI values for cluster ranges between C2 and C29.

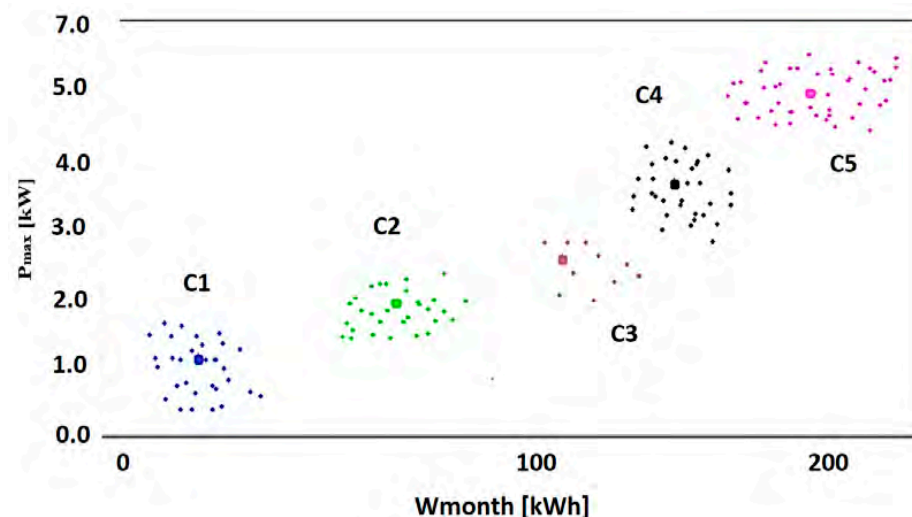


Figure 11. Graphical representation of clusters for the case  $K_{opt} = 5$ .

The characteristic variables represented by the mean values ( $m$ ) and the dispersion ( $\sigma$ ) corresponding to the maximum load ( $P_{max}$ ) and the monthly energy ( $W_{month}$ ) for each cluster (consumption category) are summarized in Table 1.

Figure 11. Graphical representation of clusters for the case  $K_{optim} = 5$ .

The characteristic variables represented by the mean values ( $m$ ) and the dispersion ( $\sigma$ ) corresponding to the maximum load ( $P_{max}$ ) and the monthly energy ( $W_{month}$ ) for each cluster (consumption category) are summarized in Table 1.

Table 1. Statistical variables of the characteristic variables associated with the consumption categories.

Consumption Class	Number of Consumers	$P_{max}$ (kW)		$W_{month}$ (kWh)	
		$m_m$	$\sigma$	$m_m$	$\sigma$
C1	31	151	0.32	192.20	13.66
C2	104	106	0.13	115.62	11.83
C3	387	43	0.09	307.00	12.93
C4	279	87	0.17	88.64	11.83
C5	12	4.78	0.92	252.96	19.70

The analysis of data from each consumption category indicated a correlation between the maximum load and the monthly energy consumption that can be mathematically modeled by applying regression models. In Figures 12–14, regression models are represented based on first- and second-degree polynomials for every consumption class.

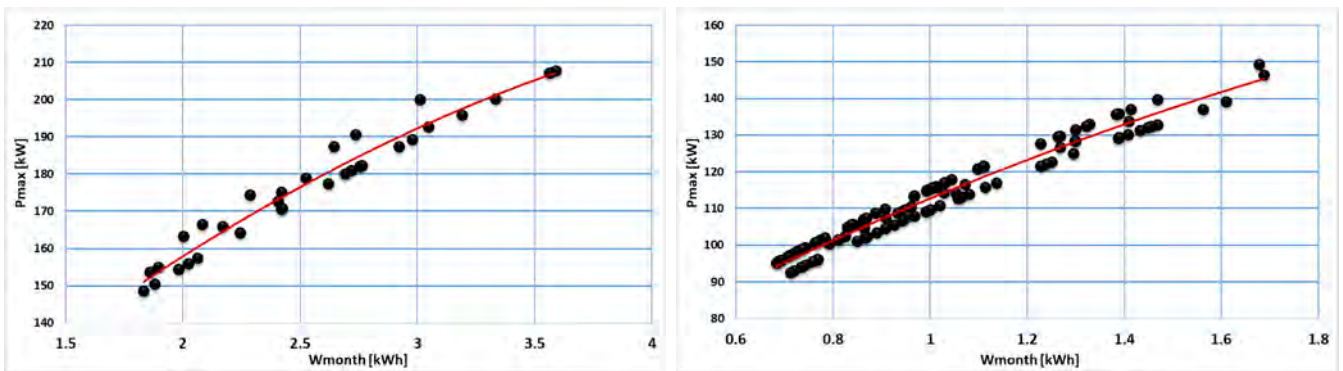


Figure 12. Regression models correlated to consumption class C1 (a) and C2 (b).

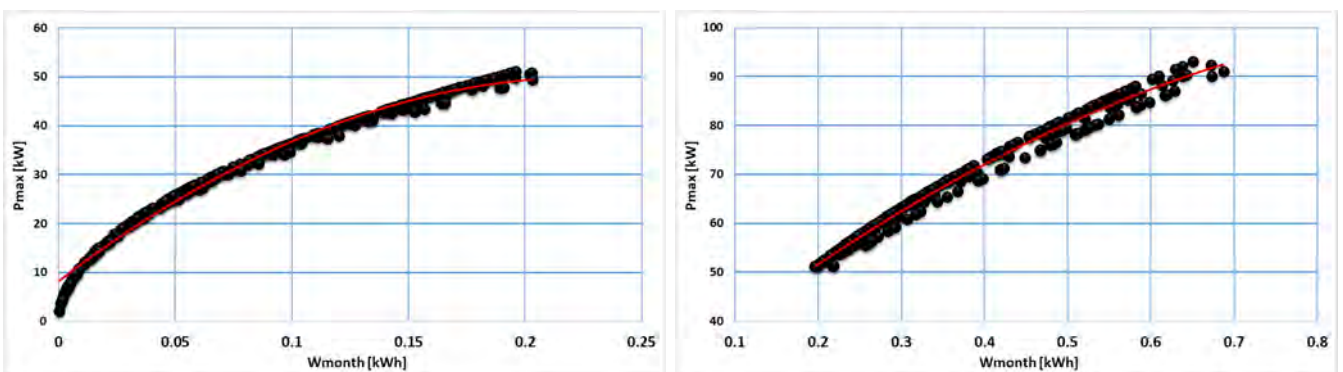


Figure 13. Regression models associated with consumption class C3 (a) and C4 (b).

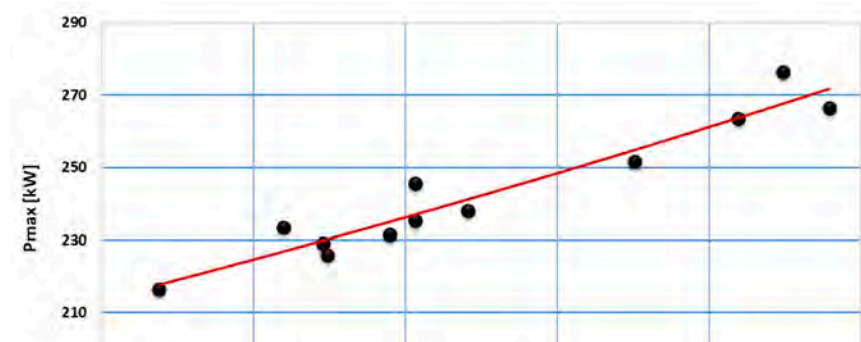


Figure 13. Regression models associated with consumption class C3 (a) and C4 (b).

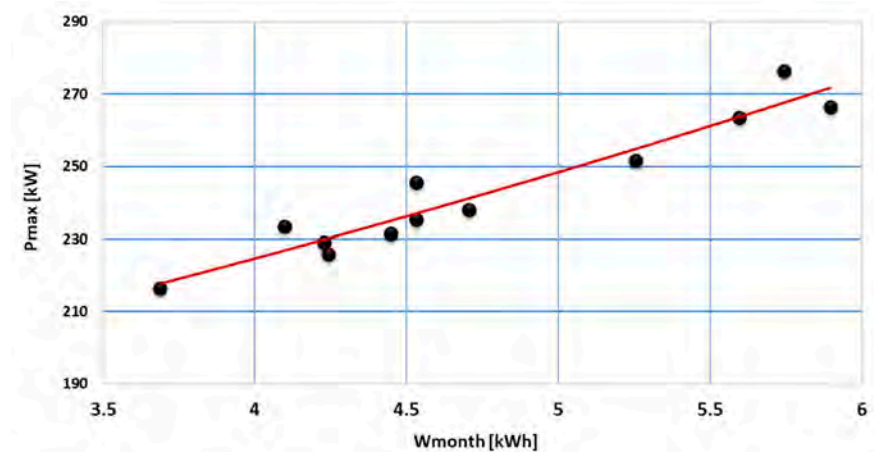


Figure 14. Regression models associated with consumption class C5.

Regression models based on the degree III polynomial led to a better approximation than the degree I polynomial. Thus, regression models based on the degree III polynomial were adopted to determine the  $P_{max}$  ( $W_{month}$ ) dependence; coefficients of the regression models determined for each consumption class are summarized in Table 2.

Table 2. Regression model coefficients associated with consumption categories.

Consumption Class	$a (\times 10^{-5})$	$a (\times 10^{-5})$	$b (\times 10^{-3})$	$b (\times 10^{-3})$	$c$	$c$
C1 C1	13	13	22	22	2.6	2.6
C2 C2	6.2	6.2	3.1	3.1	0.7	0.7
C3 C3	7.3	7.3	0.023	0.023	0.00008	0.00008
C4 C4	8.2	8.2	0.45	0.45	0.027	0.027
C5 C5	15	15	105	105	17	17

In Stage 4, for all consumers in the test base, the maximum load is estimated by applying the regression model of the consumption class associated with every consumer, depending on the monthly energy consumed.

Figure 15 presents the real and forecasted values associated with the maximum consumer tasks within the test base, assembled according to the consumption class.

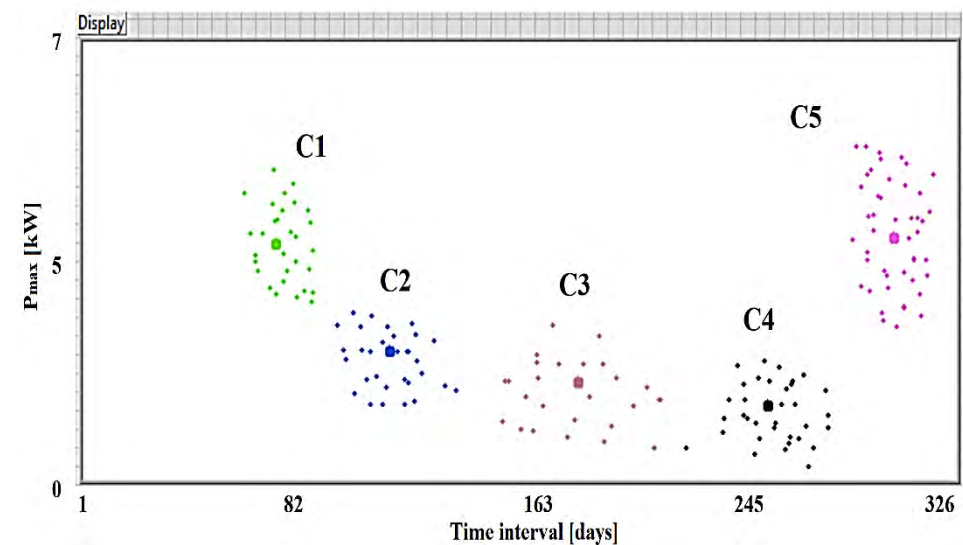


Figure 15: Real and estimated maximum load values of the clustering testing base (C1–C5 represent the clusters used for the analysis).

Of the 331 testing base consumers, 206 (approximately 62%) forecast errors were  $\leq 3\%$ , 77 (approximately 23%) errors were between 3 and 7%, and 48 (approximately 15%) errors were between 7 and 10% (Figure 16); thus, the average estimation error in the testing base was 4.01%. This value is reasonable in the context that most consumers do not



**Figure 15.** Real and estimated maximum load values of the clustering testing base (C1–C5 represent the clusters used for the analysis).

Of the 331 testing base consumers, 206 (approximately 62%) forecast errors were  $\leq 3\%$ , 77 (approximately 23%) errors were between 3 and 7%, and 48 (approximately 15%) errors were between 7 and 10% (Figure 16); thus, the average estimation error in the testing base was 4.01%. This value is reasonable in the context that most consumers do not have permanent monitoring.

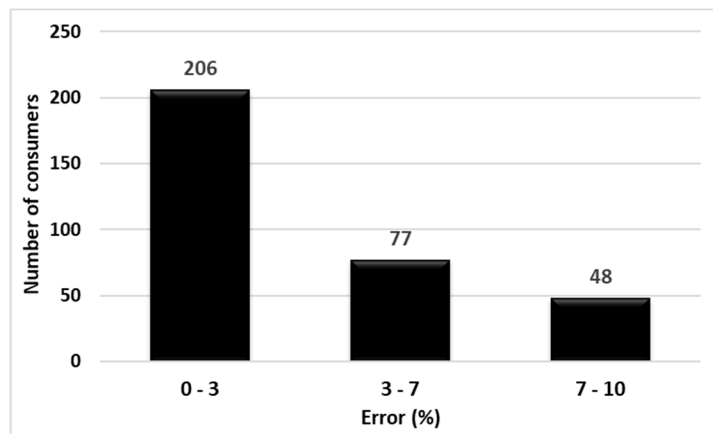


**Figure 16.** Classification of maximum load forecast errors for testing base consumers.

### 3.2. Simulation of a Load of MV/LV Distribution Transformers by Clustering Procedure Application

The future power supply networks of electric vehicles will be powered by medium and low-voltage networks.

The following algorithm is suggested for simulating the load of the distribution transformers from the MV/LV transformation stations [40].

Phase 1. Database: representative consumers with smart meters will be sorted out from the database. Typical load diagrams will be recorded for every consumer, then, the main characteristic variables will be detached, i.e., minimum ( $P_{min}$ ) and maximum active power ( $P_{max}$ ), daily energy ( $W_z$ ), and consumption class.

Phase 2. Pre-processing load diagrams: all records involving missing data or values will be excluded or subjected to processing. After being pre-processed and reduced, the results will be applied to obtain the classification into consumption categories (clusters) using the clustering procedure.

Phase 3. The division into consumption macro-categories: the database with the records of load schedules will be split into clusters described by the consumer’s type: residential, commercial, and industrial.

Phase 4. Clustering procedure: a clustering technique will be applied for load-type profile determination to determine the optimum results. In the end, a typical load profile for each consumption class will be obtained by applying the average of the hourly values for the load diagrams.

Phase 5. Determining the load profiles: a typical load profile will be attributed to every consumer’s class, depending on their consumption class.

Phase 6. Estimating the load of the MV/LV transformer: a simulation protocol will then be proposed based on the Equation [40]:

$$P^h = \sum_{k=1}^{C_k} n_k W_{med k} p_k^h + \sqrt{\sum_{k=1}^{C_k} n_k (W_{med k} \sigma_k^h)^2}, h = 1, \dots, 24 [kW] \quad (16)$$

where:

$P^h$  is the MV/LV transformer load from the transformer station at  $h$ , (kW);

$n_k$  is the consumer number, where  $k$  is the consumption class;

$W_{med k}$  is the average energy consumption, where  $k$  is the consumption class, (kWh);

$p_k^h$  is the hourly coefficient of transformation for energy consumed by the consumers, (kW/kWh);

$\sigma_k$  is the standard deviation of the power distribution necessary to the cluster consumption (kW/kWh);

$C_k$  is the cluster number (consumption class) correlated to the consumer's feed.

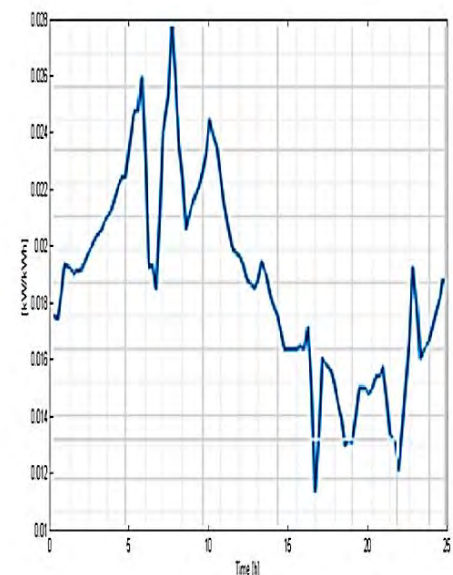
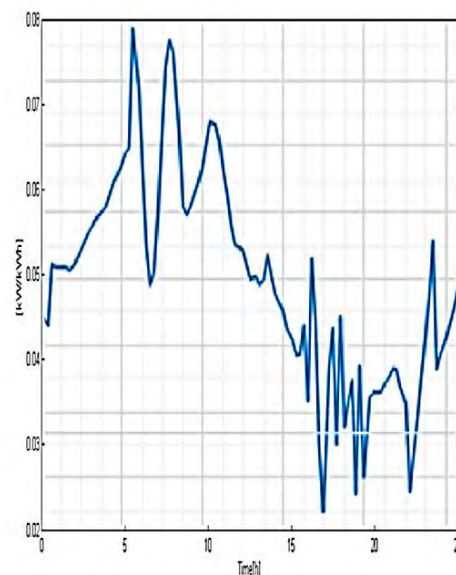
The weight center technique was applied to evaluate the load-type profiles through a database containing 180 load curves registered by smart meters from residential consumers in a distribution system from the LV pilot.

To evaluate the representative load profiles, the gravity center was applied, taking into consideration the scattering of the LV pilot located in a region from Romania [40]. Every load graph is set by 48 hourly values correlated with consumer behavior over one day. Missing load curves or abnormal values of zero throughout the day must be eliminated from the procedure, with only 144 consumers remaining eligible. The clustering procedure resulted in five consumption classes (clusters) (Table 3).

**Table 3.** Consumption class characteristics.

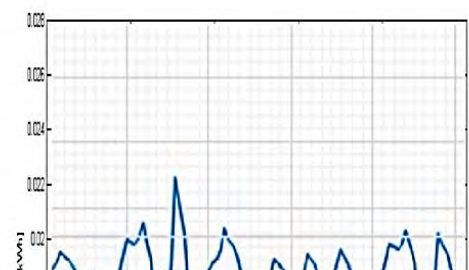
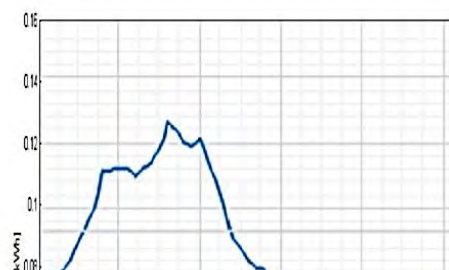
Consumption Class	Number of Consumers	$P_{\max}$ (kW)		$P_{\min}$ (kW)		W (kWh)	
		m	$\sigma$	m	$\sigma$	m	$\sigma$
C1	15	0.21	0.02	0.06	0.01	3.41	0.82
C2	5	0.51	0.05	0.02	0.02	4.35	1.20
C3	22	0.46	0.12	0.03	0.01	2.98	0.54
C4	30	0.04	0.06	0.02	0.03	0.25	0.43
C5	72	0.17	0.06	0.03	0.02	1.95	0.41

It can be observed that the most representative class of consumption is C5 (50% of the total consumer number), the least representative being C2 (only 3.5%). The load-type profiles correlated to every cluster (consumption class) are depicted in Figures 17–19 and the consumer distribution is presented in Figure 20.



**Figure 17.** Load-type profile related to C1 and C2 consumption classes.

**Figure 17.** Load-type profile related to C1 and C2 consumption classes.



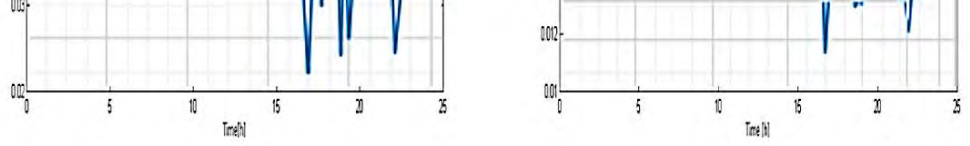


Figure 17. Load-type profile related to C1 and C2 consumption classes.

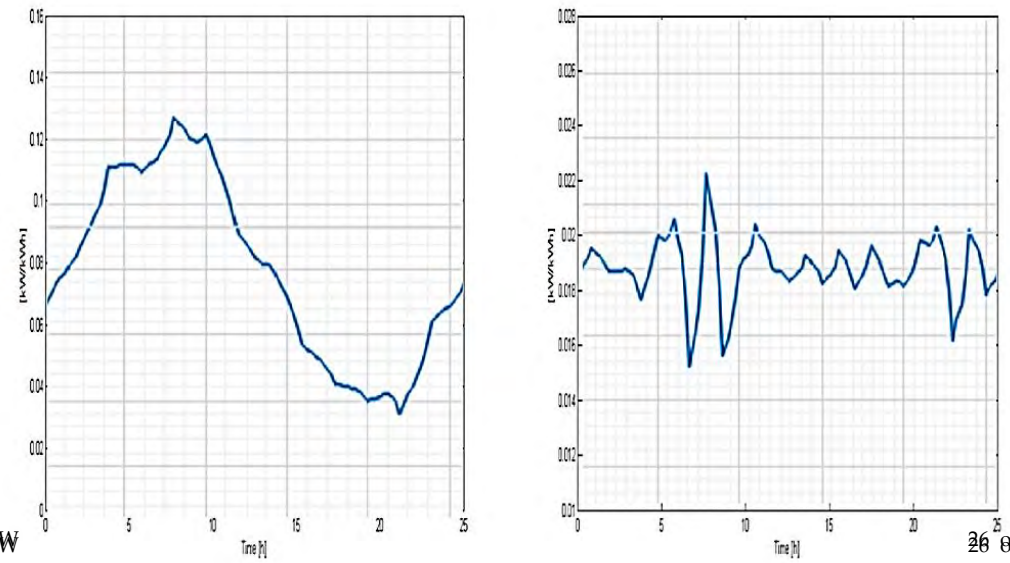


Figure 18. Load-type profile related to C3 and C4 consumption classes.

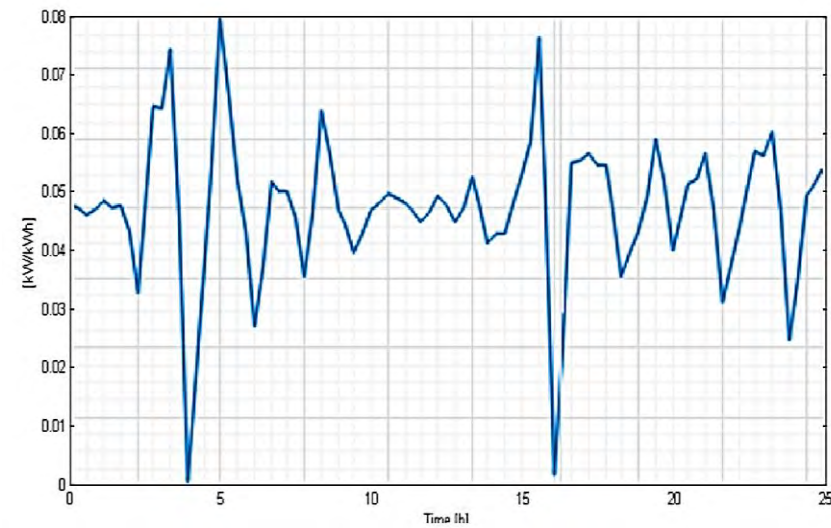


Figure 19. Load-type profile related to C5 consumption class.

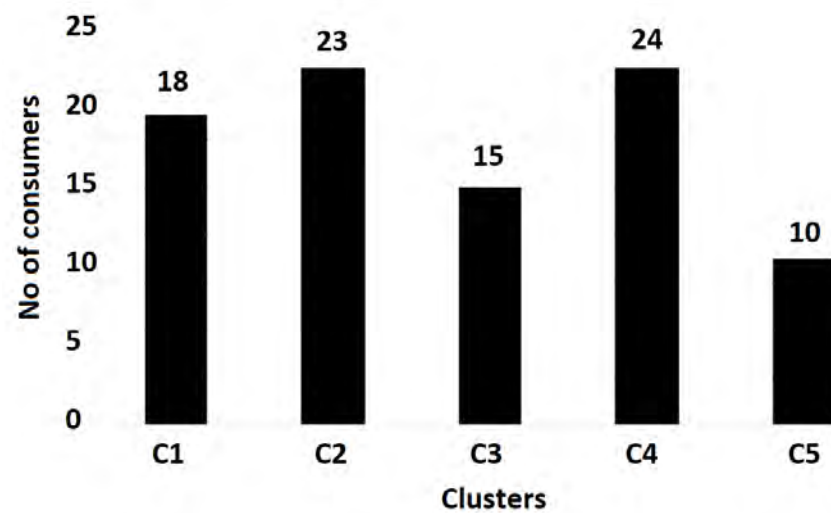


Figure 20. Consumer associations resulting from the testing base.

#### 4. Discussion

Numerical simulations related to the methodologies, algorithms, and calculation programs developed in this paper have shown that the intelligent distribution of consumers in Smart Grid distribution systems can help smooth the charging curve that can lead to lower electricity prices and facilitate the integration of renewable energy sources, resulting in a much safer and more economical operation of Smart Grid networks. The authors in [37,38] perform an analysis of data extraction techniques from the perspectives of different technical approaches to achieve consumer profiles using direct clustering, indirect clustering, clustering evaluation criteria, and customer segmentation. The article [39] presents an approach to the consumer profile from the perspective of time series, and in [38], the issue discussed is approached with the Bayes model and k-means clustering. As can be seen from the literature, clustering algorithms are frequently used in the energy field for profiling consumers. The method proposed in this article combines grouping algorithms by clustering techniques and evaluation criteria for the clustering results using the regression algorithm with second-order polynomials (logistic regression). By separating consumer behaviors, the relationship between them can be simplified. The use of hierarchical clusters (hierarchical classification) can significantly reduce the influence of external factors (e.g., region, weather, time, day, and social activities) on classifier performance. The results of the case study showed that the model proposed in this paper achieves a better classification of electricity consumption. In addition, the technique presented in this article contributes to an overall improvement in the profiling of consumers, as the proposed method achieves a better classification using fewer training samples. The performance of the results presented suggests that the proposed data-based model can be used as an effective tool in real-time. The idea of load demand variability is key information for the load monitoring control unit, thus the proposed task prediction models will help energy management. Based on a more accurately forecasted load demand, different optimization techniques for demand response applications can be developed. In addition, the classification of the model proposed in this paper depends on the completeness and reliability of the data. By combining these two algorithms in the next stage, we plan to develop a supervised machine learning algorithm that will automatically determine the profile of consumers based on historical data and data acquired in real-time (data mining).

#### 5. Conclusions

Following the proposed study that formed the basis of this article, some conclusions can be made:

- Urban areas have significant issues in several areas, including the economy, water supply, energy, buildings transit, environmental protection, and basic services as a result of the phenomenon known as “global urbanization”.
- Municipalities are encouraged to employ smart ideas and try various smart infrastructure approaches in order to address these problems, thereby becoming the future smart cities or “Smart Cities”.
- Urban transportation issues are a key component of the Smart City idea, and the approximately 7.2 million electric passenger and freight vehicles demonstrate that electrification of the transportation sector is the undeniable future of mobility.
- The restrains in regulations on the use of conventional fossil fuels in Europe and China caused the automotive industry to quickly realign to multiple EV and BEV models, with more than 442 new products being available at this moment, leading to an 87% drop in Lithium-Ion battery prices, per kWh, between 2010 and 2019. These factors all have contributed to the rapid growth of the number of EVs. When considering the above-mentioned factors, electric vehicles have emerged as one of the primary solutions for decarbonizing the transportation industry and using renewable energy sources to generate electricity. Their impact on electrical networks, however, cannot be disregarded. The quest for low-emission mobility around the globe is expected to drive a major increase in the electrification of road transportation in the next decades.



The volume of the world's electricity demand may shift as a result of the rise in electric vehicles, posing serious problems for the infrastructure supporting electricity production, transmission, and distribution.

- The integration of too many EVs will significantly impact the electric power systems; however, by coordinating EV charging, flexibility services in the electric power network can be achieved, and the required investments in infrastructure can be kept to a minimum level.

Future study directions suggested to continue the research outlined in this paper include:

- Participation of EVs or charging stations equipped with converters that use power electronics in reactive power regulation services for EVs.
- Offering support services by coordinating EV charging via LV power grids.
- Variations in the voltage level caused by EV fleets since it is equal to the electrical charge throughout the steady state operation or photovoltaic renewable energy sources while supplying energy to the grid.
- Analysis of hybrid solutions utilizing battery energy storage systems for the necessary integration of ultra-fast charging stations with capacities of up to 350 kW in metropolitan electricity networks.

**Author Contributions:** Conceptualization, G.G., M.S.R., C.D. and V.-C.N.; Data curation, G.G., C.D., D.L.M. and B.C.N.; Formal analysis, G.G., C.D., D.L.M., T.C.M., V.-C.N. and B.C.N.; Funding acquisition, M.S.R.; In-vestigation, G.G., C.D., D.L.M., T.C.M. and V.-C.N.; Methodology, G.G., M.S.R., C.D., T.C.M. and B.C.N.; Project administration, G.G., M.S.R. and B.C.N.; Resources, M.S.R.; Software, M.S.R., T.C.M. and B.C.N.; Supervision, G.G. and B.C.N.; Validation, G.G., M.S.R., T.C.M. and B.C.N.; Visualization, G.G., C.D., D.L.M., V.-C.N. and B.C.N.; Writing—original draft, M.S.R., C.D. and V.-C.N.; Writing—review and editing, G.G., M.S.R., D.L.M., V.-C.N. and B.C.N. All authors have read and agreed to the published version of the manuscript.

**Funding:** This research was funded by “Gheorghe Asachi” Technical University of Iasi, Romania. This paper was partially supported by UEFISCDI Romania and MCI through BEIA project AutoDecS, AISTOR, Hydro3D, PREVENTION, DAFCC, EREMI, FinSESCO, CREATE and by Europe research and innovation program under grant agreement No. 101084323 (BLOW).

**Institutional Review Board Statement:** Not applicable.

**Informed Consent Statement:** Not applicable.

**Data Availability Statement:** Not applicable.

**Acknowledgments:** This work is supported by Ministry of Research, Innovation, Digitization from Romania by the National Plan of R&D, Project PN 1911, Subprogram 1.1, Contract No. 19PFE/30.12.2021.

**Conflicts of Interest:** The authors declare no conflict of interest.

## References

1. Institute of Communication & Computer Systems of the National Technical University of Athens ICCS-NTUA. *Study on Cost Benefit Analysis of in EU Member States Smart Metering Systems*; European Commission, Final Report; Institute of Communication & Computer Systems of the National Technical University of Athens ICCS-NTUA: Athina, Greece, 2015.
2. IEA Secretariat Energy Efficiency Working Party, Proposal for an International Energy Association Initiative to Promote Energy-Efficient Distribution Transformers. Available online: <http://www.copperinfo.com/energy/transformers.proposal.html> (accessed on 12 January 2023).
3. McDonald, J. Adaptive Intelligent Power Systems: Active Distribution Networks. *Energy Policy* **2008**, *36*, 4346–4351. [CrossRef]
4. ANRE. *Rapoarte de Evaluare a Potențialului de Creștere a Eficienței Energetice a Rețelelor de Energie Electrică și Gaze Naturale, în ceea ce Privește Transportul, Distribuția, Gestiunea Sarcinii și Interoperabilitatea, Precum și Racordarea Capacităților de Producere, Inclusiv a Microgeneratoarelor*; Evaluation Report of the Romanian Energy Agency: Romania, 2014.
5. Iordache, M.; Conecini, I. *Electric Power Quality (in Romanian)*; Ed. Tehnica: Bucharest, Romania, 1997.
6. ANRE. Standardul de Performanță Pentru Serviciul de Distribuție a Energiei Electrice. Available online: <https://www.anre.ro/ro/energieelectrica/legislatie/norme-tehnice/standarde-de-performanta1387201290> (accessed on 14 January 2023).
7. Charalampopoulos, C.; Psomopoulos, C.; Ioannidis, G.C. *Implementing the E.U. Ecodesign Directive on Distribution Transformers*; IET MedPower Conference: Athens, Greece, 2014.

8. International Energy Agency—Global EV Outlook 2020, June 2020. Available online: <https://www.iea.org/reports/global-ev-outlook-2020> (accessed on 13 January 2023).
9. Lopes, J.A.P.; Soares, F.J.; Almeida, P.M.R. Integration of Electric Vehicles in the Electric Power System. *Proc. IEEE* **2011**, *99*, 168–183.
10. Degefa, M.Z.; Millar, R.J.; Koivisto, M.; Humayun, M.; Lehtonen, M. Load Flow Analysis Framework for Active Distribution Networks Based on Smart Meter Reading System. *Engineering* **2013**, *5*, 1–8.
11. Loughlin, F.M.; Duffy, A.; Conlon, M. *Analyzing Domestic Electricity Smart Metering Data Using Self Organizing Maps*; CIRED Workshop: Lisbon, Portugal, 29–30 May 2012.
12. Leite, D.R.V.; Lamin, H.; de Albuquerque, J.M.C.; Camargo, I.M.T. Regulatory Impact Analysis of Smart Meters Implementation in Brazil. In Proceedings of the Innovative Smart Grid Technologies (ISGT), Washington, DC, USA, 13–14 February 2012.
13. Richardson, D.B. Electric Vehicles and the Electric Grid: A Review of Modeling Approaches, Impacts and Renewable Energy Integration. In *Renewable and Sustainable Energy Reviews*; Elsevier: Amsterdam, The Netherlands, 2012; Volume 19, pp. 247–254.
14. Li, W.; Li, Y.; Deng, H.; Bao, L. Planning of Electric Public Transport System under Battery Swap Mode. *Sustainability* **2018**, *10*, 2528. [[CrossRef](#)]
15. Radu, A.T.; Eremia, M.; Toma, L. Optimal Electrical Vehicle Charging Strategy for Operating Conditions Improvement in Distribution Electrical Grid. In Proceedings of the International Conference on Condition Monitoring, Diagnosis and Maintenance—CMDM 2017, (4th Edition), Bucharest, Romania, 21 September 2017.
16. Jain, A.K.; Murty, M.N.; Flynn, P.J. Data Clustering: A Review. Available online: [www.cermics.enpc.fr/~jkeriven/vision/articles](http://www.cermics.enpc.fr/~jkeriven/vision/articles) (accessed on 13 January 2023).
17. Mutanen, A.; Ruska, M.; Repo, S.; Järventausta, P. Customer Classification and Load Profiling Method for Distribution Systems. *IEEE Trans. Power Deliv.* **2011**, *26*, 1755–1763.
18. Guo, Z.; Wang, Z.J.; Kashani, A. Home Appliance Load Modeling from Aggregated Smart Meter Data. *IEEE Trans. Power Syst.* **2014**, *in press*.
19. Piacentini, R. Modernizing Power Grids with Distributed Intelligence and Smart Grid-Ready Instrumentation. In Proceedings of the Innovative Smart Grid Technologies (ISGT), Washington, DC, USA, 13–14 February 2012.
20. Turker, H.; Radu, A.; Bacha, S.; Frey, D.; Richer, J.; Lebrusq, P. Optimal charge control of electric vehicles in parking stations for cost minimization in V2G concept. In Proceedings of the 2014 International Conference on Renewable Energy Research and Application (ICRERA), Milwaukee, WI, USA, 17 March 2014; pp. 945–951.
21. Eremia, M.; Shahidehpour, M. (Eds.) *Electrical Power System Dynamics. Modeling, Stability, and Control*; John Wiley&Sons: Hoboken, NJ, USA, 2013.
22. Fidalgo, J.N.; Matosb, M.A.; Ribeiro, L. A new clustering algorithm for load profiling based on billing data. *Electr. Power Syst. Res.* **2012**, *82*, 27–33.
23. Hussein, T. *Mouftah, Melike Erol-Kantarci, Sameh Sorour, Connected and Autonomous Vehicles in Smart Cities*; CRC Press: Boca Raton, FL, USA, 2020; Volume 516, p. 242. ISBN 9780367350345.
24. Rigas, E.S.; Ramchurn, S.D.; Bassiliades, N. Managing Electric Vehicles in the Smart Grid Using Artificial Intelligence: A Survey. *IEEE Trans. Intell. Transp. Syst.* **2015**, 16–25. [[CrossRef](#)]
25. Marijana, Z.; Mitrović, S.; Has, A. Machine learning based system for managing energy efficiency of public sector as an approach towards smart cities. *Int. J. Inf. Manag.* **2021**, *58*, 102074. [[CrossRef](#)]
26. Howell, S.; Rezgui, Y.; Hippolyte, J.L.; Jayan, B.; Li, H. Towards the next generation of smart grids: Semantic and holonic multiagent management of distributed energy resources. *Elsevier J. Renew. Sustain. Energy Rev.* **2017**, *77*, 193–214. [[CrossRef](#)]
27. Kim, Y.-I.; Ko, J.-M.; Choi, S.-H. Methods for generating TLPs (typical load profiles) for smart grid-based energy programs. In Proceedings of the 2011 IEEE Symposium on Computational Intelligence Applications in Smart Grid (CIASG), Paris, France, 11–15 April 2011; pp. 1–6.
28. Hernandez, L.; Baladron, C.; Aguiar, J.; Carro, B.; Sánchez-Esguevillas, A. Classification and clustering of electricity demand patterns in industrial parks. *Energies* **2012**, *5*, 5215–5228. [[CrossRef](#)]
29. Ford, V.; Siraj, A. Clustering of smart meter data for disaggregation. In Proceedings of the 2013 IEEE Global Conference on Signal and Information Processing, Austin, TX, USA, 3–5 December 2013; pp. 507–510.
30. Rhodes, J.D.; Cole, W.J.; Upshaw, C.R.; Edgar, T.F.; Webber, M.E. Clustering analysis of residential electricity demand profiles. *Appl. Energ.* **2014**, *135*, 461–471. [[CrossRef](#)]
31. Ramos, S.; Duarte, J.M.; Duarte, F.J.; Vale, Z. A data-mining-based methodology to support MV electricity customers’ characterization. *Energy Build.* **2015**, *91*, 16–25. [[CrossRef](#)]
32. Al-Jarrah, O.Y.; Al-Hammadi, Y.; Yoo, P.D.; Muhaidat, S. Multi-layered clustering for power consumption profiling in smart grids. *IEEE Access* **2017**, *5*, 18459–18468.
33. Cai, H.; Shen, S.; Lin, Q.; Li, X.; Xiao, H. Predicting the energy consumption of residential buildings for regional electricity supply-side and demand-side management. *IEEE Access* **2019**, *7*, 30386–30397. [[CrossRef](#)]
34. Nordahl, C.; Boeva, V.; Grahn, H.; Netz, M.P. Profiling of Household Residents’ Electricity Consumption Behavior Using Clustering Analysis. In Proceedings of the International Conference on Computational Science, Faro, Portugal, 12–14 June 2019; pp. 779–786.

35. Park, K.-J.; Son, S.-Y. A Novel Load Image Profile-Based Electricity Load Clustering Methodology. *IEEE Access* **2019**, *7*, 59048–59058.
36. Rasanen, T.; Voukantsis, D.; Niska, H.; Karatzas, K.; Kolehmainen, M. Data-based method for creating electricity use load profiles using large amount of customer-specific hourly measured electricity use data. *Appl. Energ.* **2010**, *87*, 3538–3545.
37. Wen, L.; Zhou, K.; Yang, S. A shape-based clustering method for pattern recognition of residential electricity consumption. *J. Clean. Prod.* **2019**, *212*, 475–488.
38. Rousseeuw, P.J. Silhouettes: A Graphical Aid to the Interpretation and Validation of Cluster Analysis. *J. Comput. Appl. Math.* **1987**, *20*, 53–65. [[CrossRef](#)]
39. Yatskiv, I.; Gusarova, L. The Methods of Cluster Analysis Results Validation. In Proceedings of the International Conference RelStat'04, Latvia, Riga, 13–15 October 2005; pp. 75–80.
40. Grigoras, G. Contributions on the Use of Artificial Intelligence in Supervision and Control of the Power Systems. Habilitation Thesis, “Gheorghe Asachi” Technical University of Iasi, Iasi, Romania, 2019. Available online: [https://doctorat.tuiasi.ro/doc/Teze\\_abilitare/IEEIA/Grigoras/Teza\\_abilitare\\_Gheorghe\\_Grigoras.pdf](https://doctorat.tuiasi.ro/doc/Teze_abilitare/IEEIA/Grigoras/Teza_abilitare_Gheorghe_Grigoras.pdf) (accessed on 13 January 2023).
41. Gerbec, D.; Gasperic, S.; Simon, I.; Gubina, F. Hierarchic Clustering Methods for Consumers Load Profile Determination. In Proceedings of the 2nd Balkan Power Conference, Belgrad, Yugoslavia; 2002; pp. 9–15.
42. Gordon, A.D. *Classification*, 2nd ed.; Chapman & Hall: New York, NY, USA, 1999.
43. Clustering: An introduction. Available online: [www.elet.polimi.it/upload/matteucc/Clustering/tutorial\\_html](http://www.elet.polimi.it/upload/matteucc/Clustering/tutorial_html) (accessed on 13 January 2023).
44. Seppälä, A. Load Research and Load Estimation in Electricity Distribution. Available online: <https://cris.vtt.fi/en/publications/load-research-and-load-estimation-in-electricity-distribution-dis> (accessed on 13 January 2023).
45. Carter-Brown, C.G. Load profile modeling for integrated energy planning. In Proceedings of the Domestic Use of Electrical Energy Conference, Rome, Italy, 1999; pp. 13–18.
46. Nazarko, J.; Zalewski, W. The Fuzzy Regression Approach to Peak Load Estimation in Power Distribution Systems. *IEEE Trans. Power Syst.* **1999**, *14*, 809–814.
47. Wang, Y.; Chen, Q.; Kang, C.; Zhang, M.; Wang, K.; Zhao, Y. Load Profiling and Its Application to Demand Response: A Review. *Tsinghua Sci. Technol.* **2015**, *20*, 117–129.
48. Leong, H.; Jung, J.; Kang, B. Development of Operational Strategies of Energy Storage System Using Classification of Customer Load Profiles under Time-of-Use Tariffs in South Korea. *Energ. J.* **2020**, *13*, 1723. [[CrossRef](#)]
49. Issi, F.; Kaplan, O. The Determination of Load Profiles and Power Consumptions of Home Appliances. *Energ. J.* **2018**, *11*, 607. [[CrossRef](#)]
50. Wen, Z.; Li, P.; Lang, X.; Shen, X.; Cao, M.; Hua, X. Hierarchical classification method of electricity consumption industries through TNPE and Bayes, Measurement and Control. *J. Sage Pub.* **2021**, *54*, 346–359. [[CrossRef](#)]

**Disclaimer/Publisher’s Note:** The statements, opinions and data contained in all publications are solely those of the individual author(s) and contributor(s) and not of MDPI and/or the editor(s). MDPI and/or the editor(s) disclaim responsibility for any injury to people or property resulting from any ideas, methods, instructions or products referred to in the content.